Volume 22 · Issue 2
April 2025

Asian Journal of WATER, ENVIRONMENT AND POLLUTION

ISSN: 0972-9860 (Print)
ISSN: 1875-8568 (Online)

ACCSCIENCE PUBLISHING

WSSET
World Society of Sustainable Energy Technologies

Asian Journal of Water, Environment and Pollution

Print ISSN: 0972-9860
Online ISSN: 1875-8568

Asian Journal of Water, Environment and Pollution is an international, peer-reviewed, academic Open Access journal. It aims to publish high-quality, original research and practical solutions across a wide range of topics that address global environmental challenges. These include water availability and pollution management, global warming and climate adaptation, solid and liquid waste management, mining impacts and environmental degradation, renewable energy integration, energy access and sustainability, and policy analysis focused on social equity. The journal also covers infrastructure development, transnational water body pollution, energy storage and conversion, low-carbon and zero-energy buildings, and sustainable transport systems.

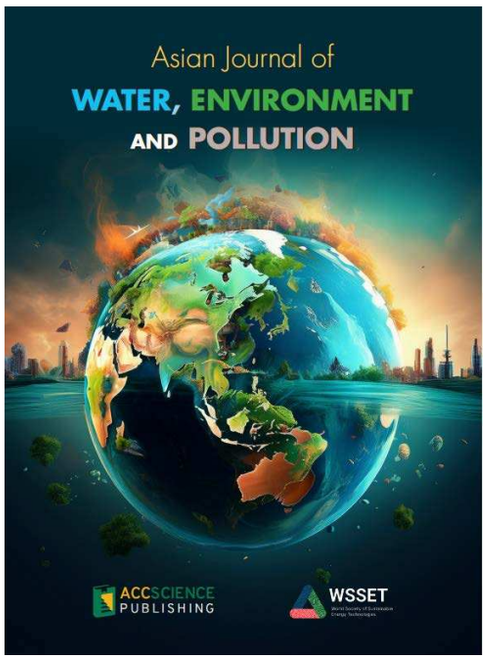

About the Publisher

AccScience Publishing is a publishing company based in Singapore. We publish a range of high-quality, open-access, peer-reviewed journals and books from a broad spectrum of disciplines.

Contact Us

Managing Editor
ajwep.office@accscience.sg

AccScience Publishing
8 Burn Road, #15-03 Trivex, Singapore 369977.

Volume 22 • Issue 2 • April 2025
ISSN 0972-9860 (print) ISSN 1875-8568 (online)

Asian Journal of Water, Environment and Pollution

Editor-in-Chief
Saffa Riffat
University of Nottingham, Nottingham, UK

ACCSCIENCE PUBLISHING
Access Science Without Barriers

Full issue copyright © 2025 AccScience Publishing
All rights reserved. Without permission in writing from the publisher, this full issue publication in its entirety may not be reproduced or transmitted for commercial purposes in any form or by any means, electronic or mechanical, including photocopying, recording, or any information storage and retrieval system. Permissions may be sought from ajwep.office@accscience.sg.

Article copyright © Respective Author(s)
See articles for copyright year. All articles in this full issue publication are open-access. There are no restrictions in the distribution and reproduction of individual articles, provided the original work is properly cited. However, permission to reuse copyrighted materials of an article for commercial purposes is applicable if the article is licensed under Creative Commons Attribution-NonCommercial License. Check the specific license before reusing.

ASIAN JOURNAL OF WATER, ENVIRONMENT AND POLLUTION

ISSN: 0972-9860 (print)
ISSN: 1875-8568 (online)

Editorial and Production Credits

Publisher: AccScience Publishing
Managing Editor: Irene Zhao
Production Editor: Samyuktha Balakrishnan
Article Layout and Typeset: Sinjore Technologies (India)

For all advertising queries, contact ajwep.office@accscience.sg.

Supplementary file

Supplementary files of articles can be obtained at https://accscience.com/journal/AJWEP/22/2.

Disclaimer

AccScience Publishing is not liable to the statements, perspectives, and opinions contained in the publications. The appearance of advertisements in the journal shall not be construed as a warranty, endorsement, or approval of the products or services advertised and/or the safety thereof. AccScience Publishing disclaims responsibility for any injury to persons or property resulting from any ideas or products referred to in the publications or advertisements. AccScience Publishing remains neutral with regard to jurisdictional claims in published maps and institutional affiliations.

Asian Journal of Water, Environment and Pollution

Editorial Board

Editor-in-Chief

Saffa Riffat, *UK*

Executive Editor

Upaka Rathnayake, *Ireland*

Associate Editors

Ziwei Chen, *UK*

James Riffat, *UK*

*Editorial Board Members**

Mardiana Idayu Ahmad, *Malaysia*
Khalil Ahmad, *Pakistan*
Awais Ahmad, *Pakistan*
Amit Awasthi, *India*
Rohit B. Meshram, *India*
Abubakr Bahaj, *UK*
Michele Bottarelli, *Italy*
Salvatore Carlucci, *Cyprus*
Constantinos Cartalis, *Greece*
Yulong Ding, *UK*
Muhammad Ehsan, *Mexico*
Daniele Fattorini, *Italy*
Francesco Fiorito, *Australia*
Gagné François, *Canada*
Qiulai He, *China*
Jie Ji, *China*
Nadeem Ahmad Khan, *India*
Ali Kilicarslan, *Turkey*
Chee Kong YAP, *Malaysia*
Katarzyna Kubiak-Wójcicka, *Poland*
Angui Li, *China*
Qiang Li, *China*
Tapas Mallick, *UK*
Edward Ng, *China*
Armando Oliveira, *Portugal*
Mohammad Oves, *Saudi Arabia*
Maulin P Shah, *India*
Ashok Pandey, *India*
Pradhan Parth Sarthi, *India*
Gang Pei, *China*
Richard Powell, *UK*
Ram Prasad, *India*
Namal Rathnayake, *Japan*
K. Srinivas Reddy, *India*
Prakash Sarangi, *India*
Li Shao, *UK*
Kwok Wai Tham, *Singapore*
Chi-Hwa Wang, *Singapore*
Ruzhu Wang, *China*
Liu Wen, *China*
Yuying Yan, *UK*
Hongxing Yang, *China*
Yi Yang, *China*
Weiming Zhang, *China*
Lizhi Zhang, *China*
Xudong Zhao, *UK*
Tianshou Zhao, *China*
Chengyun Zhou, *China*
Yingxin Zhu, *China*
Muhammad Zubair, *Pakistan*
Walter Timo de Vries, *Germany*

Youth Editorial Board Member

Mingming Ge, *China*

ACCSCIENCE PUBLISHING

Volume 22 | Issue 2 | April 2025 | Page 1 – 215 |

Asian Journal of Water, Environment and Pollution

https://accscience.com/journal/AJWEP

CONTENTS

REVIEW ARTICLE

1 **Traditional knowledge in soil management and water conservation: Perspectives from the agrodiverse state of Uttar Pradesh, India**
Himanshu Sahu, Pooja Purohit, Arun Pratap Mishra, Amit Kumar, Purnendu Sardar, Bojan Đurin, Upaka Rathnaya

ORIGINAL RESEARCH ARTICLES

19 **Enhancing swimming pool hygiene: A robotic approach to debris removal and water quality monitoring**
Hemalatha Senthilmahesh, Kiran Mayee Adavala, Thilagam Thangamariappan, Pullela S. V. V. S. R. Kumar, Ramesh Tumaati, Muthuvairavan Pillai Nagapp

32 **Testing the ability of *Vetiveria zizanioides* plants to bind cadmium and its influence on soil microbial diversity**
Aida Abdali Dehdezi, Ebrahim Alaei, Pejman Azadi, Mahmoud Shavandi, Seyed Amir Mousavi

43 **Method validation and its application to gas chromatography-mass spectrometry analysis of dimethyl methylphosphonate in OPCW proficiency testing**
Faris Rudi, Nor Kartini Abu Bakar, Noor Azilah Mohd Kasim, Mohd Nor Faiz Norrrahim, Wan Elyn Amira Wan Adnan

51 **Groundwater contamination with heavy metals: A case study in Hebron, Palestine**
Waseem Al-Tamimi, Fadoua Hamzaoui-Azaza, Marwan Ghanem, Rachida Bouhlila

64 **Geospatial flood modeling and risk assessment of floodplain villages along the Barak River, Northeast India**
Shanku Ghosh, Chakkaravarthi Prakasam

87 **Assessment of surface water quality impacted by upstream artisanal mining in Prek Te area, Cambodia**
Vibol Sao, Chan Oeurn Chey, Socheata Korng, Eang Chorney, Kyoung-Woong Kim

97 **Integrated modeling of socioeconomic and hydrological factors for adaptive drought response in the Kowsar Dam basin, Iran**
Ali Ghasemi, Seyed Nematollah Mosavi, Bahaeddin Najafi

114 **Utilization of treated wastewater from sewage treatment plants as a replacement for potable water in concrete mix**
Jitin Vasudeva, Mrunmyee Manjari Sahoo, Jaspreet Singh

125 **Natural radioactivity and radiation risks of soils in Ali Al-Sharqi and Kumait, Iraq**
Zahraa A. Ismail AL-Sudani, Sawsan Sherif, Mazin Mohammed

140 **Water scarcity in Asian nations and the path to resilience**
Muhammad Khalid Anser, Muhammad Zaheer Akhtar, Syed Tahir Hussain Shah, Muhammad Azhar Khan, Khalid Zaman

152 **An enhanced renewable energy integration system with improved power system stability** *Vemireddy Suryanarayana Reddy, Busireddy Hemanth Kumar*

168 **Topographic and watershed analysis of Haditha Dam Basin using geographic information system and remote sensing for water management**
Nabaa Isam Ali, Salwan Sabbar Al-Hasnawi

184 **Mitigating the impacts of climate change: A case study of the city of Tshwane, South Africa** *Odirile Sefolo, Ilesanmi Daniyan, Kemlall Ramdass, Oluwatoyin Esther Akinbowale, Humbulani Simon Phuluwa*

204 **Wastewater treatment using recycled automobile tires**
Liudmyla Melnik, Olha Rybalova, Olena Bryhada, Oleksii Ilinskyi, Anton Matsak, Bohdan Tsym

Asian Journal of Water, Environment and Pollution. Vol. 22, No. 2 (2025), pp. 1-18.
doi: 10.36922/AJWEP025060035

REVIEW ARTICLE

Traditional knowledge in soil management and water conservation: Perspectives from the agrodiverse state of Uttar Pradesh, India

Himanshu Sahu[1,2,3], Pooja Purohit[1,2], Arun Pratap Mishra[4]*, Amit Kumar[5], Purnendu Sardar[6], Bojan Đurin[7], and Upaka Rathnayake[8]*

[1]Department of Animal Ecology and Conservation Biology, Wildlife Institute of India, Dehradun, Uttarakhand, India
[2]Research and Development, Bhomya Foundation, Dehradun, Uttarakhand, India
[3]Academy of Scientific and Innovative Research (AcSIR), Ghaziabad, Uttar Pradesh, India
[4]Department of Forestry and Remote Sensing, Earthtree Enviro Private Limited, Shillong, Meghalaya, India
[5]Department of Habitat Ecology, Wildlife Institute of India, Dehradun, Uttarakhand, India
[6]Department of Physical Geography and Ecosystem Science (INES), Centre for Advanced Middle Eastern Studies, Lund University, Lund, Sweden
[7]Department of Civil Engineering, University North, Varazdin, Croatia
[8]Department of Civil Engineering and Construction, Faculty of Engineering and Design, Atlantic Technological University Sligo, Sligo, Ireland
***Corresponding authors:** Arun Pratap Mishra (arunpratap7371@gmail.com);
Upaka Rathnayake (upaka.rathnayake@atu.ie)

Received: February 4, 2025; 1st revised: March 11, 2025; 2nd revised: March 20, 2025; 3rd revised: March 26, 2025; Accepted: March 27, 2025; Published online: April 21, 2025

Abstract: Soil management is a crucial aspect of sustainable agriculture, and traditional knowledge has played a pivotal role in shaping practices that maintain soil health over time. This study examines the significance of traditional soil management techniques used in Uttar Pradesh, India, and assesses their effectiveness in addressing modern agricultural challenges. The primary objective of this analysis is to investigate how indigenous practices, such as crop rotation, intercropping, organic manure application, and traditional water conservation techniques, contribute to soil fertility and sustainability. By examining these traditional methods, the study aims to assess their potential for integration with contemporary agricultural practices to enhance overall soil health and agricultural productivity. A comprehensive analysis of existing literature was conducted to synthesize findings from various studies on traditional soil management practices in Uttar Pradesh. The analysis highlights the mechanisms by which these practices affect soil properties and fertility and identifies the strengths and limitations associated with their use. The findings reveal that traditional methods offer significant benefits, including enhanced soil structure, improved nutrient availability, and increased moisture retention. However, challenges such as limited adoption of modern technologies and varying regional practices are also noted. The integration of traditional knowledge with modern techniques is evaluated as a means to address these challenges and optimize soil management strategies. This analysis bridges the gap between traditional knowledge and contemporary agricultural practices, providing valuable insights for policymakers, researchers, and practitioners. The study underscores the importance of integrating traditional soil management practices with modern approaches to foster sustainable agriculture in Uttar Pradesh and similar regions.

Keywords: Crop rotation; Indigenous practices; Organic manuring; Soil fertility; Soil management; Sustainable agriculture; Traditional knowledge

1. Introduction

Soil management is a keystone of sustainable agriculture, influencing not only crop productivity but also broader ecosystem functions and resilience.[1,2] Effective soil management practices are crucial for maintaining soil fertility, preventing soil degradation, and ensuring food security, particularly in regions that rely heavily on agriculture for their livelihoods.[3,4] In the contemporary discourse on sustainable agriculture, traditional knowledge has emerged as a crucial component of soil management strategies, particularly in developing countries where access to modern agricultural technologies may be limited or economically unfeasible.[5,6]

Traditional knowledge refers to the cumulative form of knowledge, practices, and beliefs developed by indigenous and local communities over centuries, often transmitted verbally across generations.[7,8] This knowledge is deeply rooted in the cultural and ecological contexts of these communities, offering time-tested solutions for soil management that are adapted to specific local conditions.[9,10] In India, a country with a rich agricultural heritage, traditional soil management practices have been integral to sustaining agricultural productivity and ensuring environmental sustainability.[11,12] These practices encompass a range of techniques, including crop rotation, intercropping, organic manure application, water conservation, and agroforestry, all of which contribute to the long-term health of soils.[13]

Uttar Pradesh, one of India's most agriculturally significant states, presents a diverse agroecological landscape that includes the fertile Gangetic plains, the arid Bundelkhand region, and the humid Terai region. Each region has developed unique traditional soil management practices that are finely tuned to local environmental conditions and agricultural needs.[14-17] For instance, in the Gangetic plains, traditional crop rotation systems involving cereals and legumes have been demonstrated to maintain soil fertility and reduce the need for synthetic fertilizers.[18,19] In Bundelkhand, a region prone to drought, traditional water harvesting techniques, such as the construction of check dams and contour bunding, have played a crucial role in preventing soil erosion and sustaining agriculture under challenging climatic conditions.[20-22]

Despite the proven benefits of these traditional practices, the Green Revolution of the 1960s and 1970s marked a significant shift in agricultural practices across India, including Uttar Pradesh. The widespread adoption of high-yielding varieties (HYVs), chemical fertilizers, and pesticides has led to substantial increases in crop productivity but also introduced new challenges, such as soil degradation, loss of biodiversity, and increased environmental pollution.[23,24] These changes have raised concerns about the sustainability of modern agricultural practices and have prompted a renewed interest in integrating traditional knowledge with contemporary soil management strategies.[25,26]

Recent studies have highlighted the importance of traditional knowledge in promoting sustainable soil management and enhancing the resilience of agricultural systems in the face of climate change.[27,28] Traditional practices, such as the use of organic manure and crop residues, have been found to improve soil structure, increase organic matter content, and enhance microbial activity, all of which are crucial for maintaining soil health.[1,29-31] Moreover, these practices often employ low-input methods that reduce dependence on external inputs, making them particularly relevant for resource-poor farmers in regions such as Uttar Pradesh.[32-34]

The integration of traditional knowledge with modern soil management techniques offers a promising pathway for achieving sustainable agriculture in Uttar Pradesh. Such integration can enhance the effectiveness of soil conservation efforts, reduce the environmental impact of farming, and improve the livelihoods of smallholder farmers.[35,36] However, this approach also presents challenges, including the need to document and validate traditional practices, overcome institutional barriers, and address the erosion of traditional knowledge in the face of rapid socioeconomic changes.[8,37]

Considering the aforementioned aspects in view, the current communication aims to provide a comprehensive analysis of the role of traditional knowledge in soil management in Uttar Pradesh, with a focus on its relevance, challenges, and potential for integration with modern agricultural practices. By synthesizing existing literature and examining case studies from various regions of Uttar Pradesh, this article aims to contribute to the ongoing discourse on sustainable agriculture and the preservation of traditional knowledge in the context of contemporary challenges.[13,38,39] The findings of this analysis are expected to inform policy recommendations and guide future research efforts aimed at enhancing the sustainability of soil management practices in India and beyond.

2. Methods

2.1. Study area

This study focuses on Uttar Pradesh, India, a state known for its agricultural diversity and rich traditional knowledge in soil and water conservation. Uttar Pradesh is located

in northern India, covering an area of 243,286 km^2, making it the fourth-largest state in the country. The state lies between 23°52'N and 31°28'N latitude and 77°3'E and 84°39'E longitude, bordered by Uttarakhand and Nepal to the north, Bihar to the east, Madhya Pradesh to the south, and Rajasthan, Haryana, and Delhi to the west. The sub-tropical climate in Uttar Pradesh features summer heat, monsoon precipitation, and a mild winter season, while annual rainfalls reach 990 mm but vary between different areas. The four primary waterways of Uttar Pradesh consist of the Ganga, Yamuna, Gomti, and Ghagra, which serve essential functions for irrigation and water management. The state spans nine agroclimatic zones, which extend from Terai in the northern end to Bundelkhand in the southern portion and exhibit different soil characteristics, together with unique cultivation practices and water preservation priorities.[176]

2.2. Systematic review

For this review, we performed a systematic literature search from various database sources, including Web of Science, Scopus, and Google Scholar, using keywords or combinations of words, such as "traditional knowledge," "indigenous knowledge," "soil management," "water conservation," "agriculture in Uttar Pradesh," and "agricultural practices in north India." Our original search revealed over 200 articles, which were screened by title and abstract to determine eligibility. We applied inclusion criteria based on studies on traditional soil and water conservation practices for Uttar Pradesh published in peer-reviewed journals or credible sources. Studies that were not empirical, not regional, or did not analyze traditional practices were excluded. Based on the above criteria, we included a total of 50 published articles for detailed analysis. The data extraction aimed to identify relevant traditional practices, efficacy, cultural importance, and the applicability of conventional practices to modern conservation strategies. The findings were synthesized to highlight the most prevalent soil and water conservation methods used in Uttar Pradesh and their potential integration with contemporary approaches. This methodology ensures a comprehensive understanding of traditional knowledge in soil and water conservation, contributing valuable insights for sustainable agricultural practices in the state.

3. Traditional soil management practices

3.1. Traditional knowledge and soil management

Traditional knowledge in soil management encompasses a diverse array of practices deeply intertwined with the cultural and ecological contexts of specific regions.[40,41] These practices, which have been developed and refined over centuries, include crop rotation, intercropping, organic manuring, and water conservation techniques.[42] They are tailored to local environmental conditions and contribute significantly to soil health and sustainability. This section provides an in-depth analysis of these traditional practices, emphasizing their scientific foundations and relevance to contemporary soil management challenges. A comprehensive flowchart of the soil management process is presented in Figure 1 and Table 1.

3.2. Crop rotation and intercropping

A traditional agricultural method is crop rotation, which entails planting several crops in succession in the same field throughout different growing seasons.[43,44] This practice enhances soil fertility and structure by alternating crops with varying nutrient requirements and root structures.[45-47] Traditional crop rotation systems often include a combination of cereals, legumes, and root crops. For instance, in Uttar Pradesh, rotations involving wheat, rice, and pulses are typical.[48]

Crop rotation offers numerous well-documented benefits, including healthier soils, improved crop yields, and better pest and disease management. Leguminous crops, such as pulses, fix atmospheric nitrogen in the soil, reducing the need for synthetic fertilizers and improving soil nitrogen levels.[49-51] In addition, rotation helps in disrupting pest and disease cycles, thereby reducing the need for chemical pest control.[24] Scientific studies have demonstrated that crop rotation can enhance soil organic matter content and improve soil structure, thereby contributing to overall soil health (Figure 2).[52-54]

Intercropping, the practice of growing two or more crops simultaneously in the same field, complements crop rotation by enhancing biodiversity and reducing the risk of soil depletion.[36] This practice can optimize resource use, as different crops may utilize soil nutrients, water, and light in complementary ways.[55,56] In Uttar Pradesh, intercropping systems often involve combinations, such as maize and legumes, which can improve soil nitrogen content and reduce pest populations.[57-60] Intercropping has been demonstrated to enhance soil fertility and productivity by increasing soil microbial diversity and activity.[61,62] Furthermore, this practice can help mitigate soil erosion by providing ground cover and reducing runoff.[56]

3.3. Organic manuring

Organic manuring involves the application of organic materials, such as compost, animal dung, and green

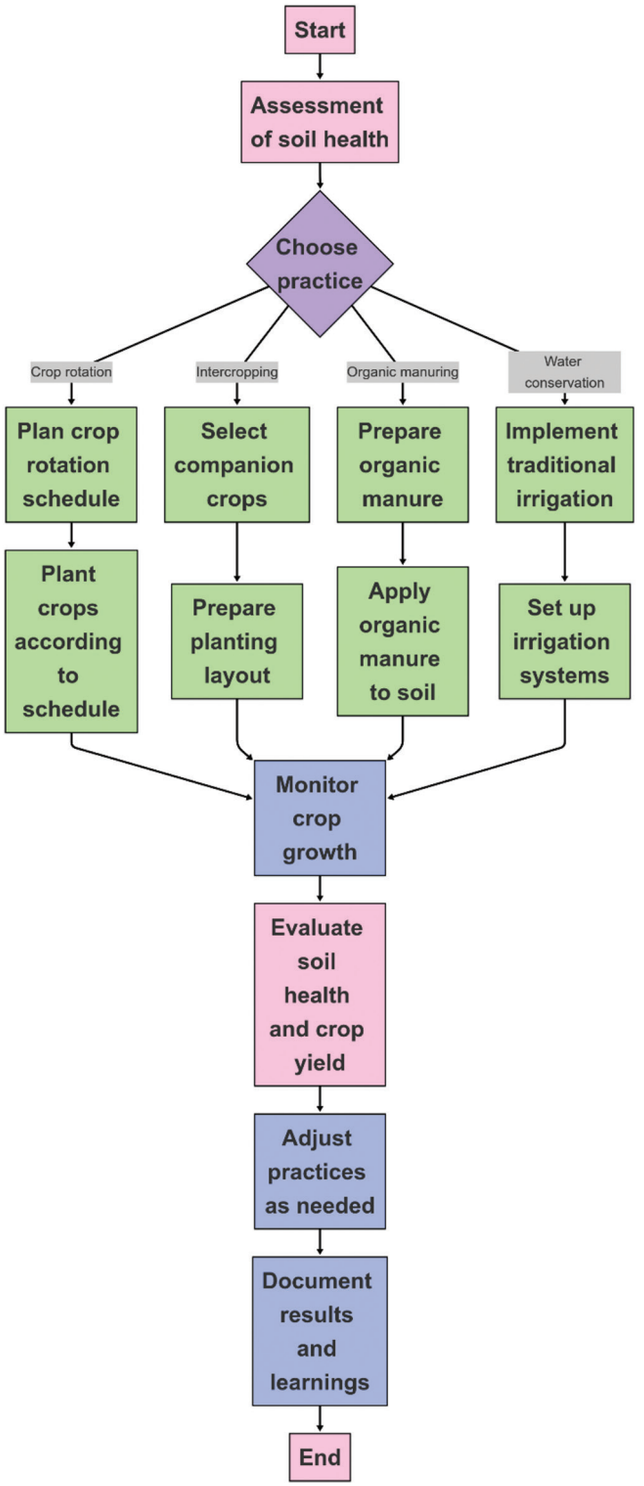

Figure 1. Decision-making process for implementing traditional soil management practices

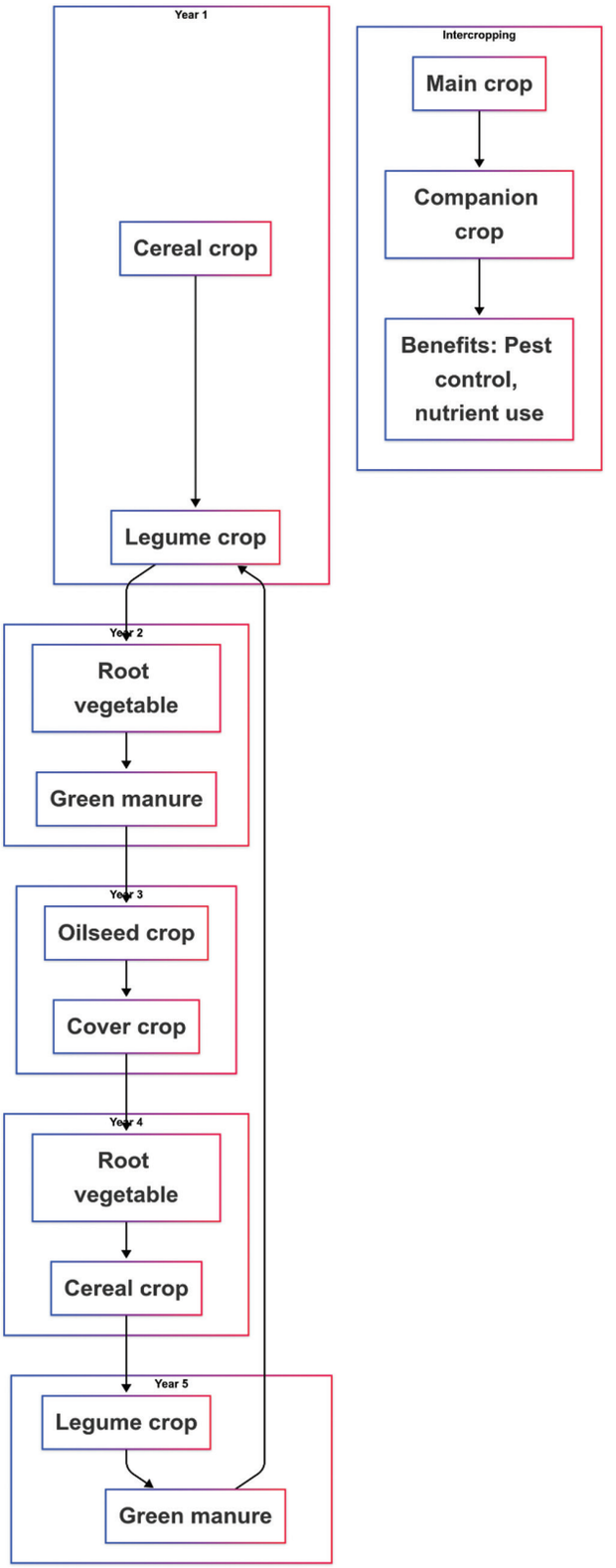

Figure 2. Crop rotation and intercropping pattern in India

manure, to improve soil fertility and structure.[63] This practice has been a mainstay of conventional soil management in Uttar Pradesh and many other regions.[64,65] A process flowchart of organic manuring is presented in Figure 3.

Compost and animal dung are rich in essential nutrients and organic matter, which enhance soil fertility

Table 1. Aspects of traditional soil management practices and modern techniques

Aspect	Traditional soil management practices	Modern techniques	References
Nutrient levels	Crop rotation: Enhances soil nutrient balance; reduces soil depletion	Chemical fertilizers: Quick nutrient supply but can lead to soil degradation	[118,148]
	Organic manuring: Increases organic matter and soil fertility	Precision agriculture: Optimizes nutrient application based on soil and crop needs, reducing excess use	[149,150]
	Intercropping: Enhances nutrient availability through complementary plant interactions	N/A	[150,151]
Soil erosion rates	Crop rotation: Helps reduce erosion by maintaining ground cover	Conventional tillage: Can increase erosion risk due to soil disturbance	[32]
	Organic manuring: Improves soil structure, reducing erosion	No-till farming: Reduces erosion by maintaining soil cover and structure	[152]
	Water conservation techniques: Methods like bunding reduce runoff and erosion	Contour plowing: Helps in reducing soil erosion by aligning plowing with the land's contour	[153,154]
Soil structure	Organic manuring: Improves soil texture and structure; increases moisture retention	Chemical amendments: Can improve soil texture but may degrade over time	[155,156]
	Crop rotation: Enhances soil structure by varying root types and depths	Soil health management: Incorporates practices to maintain and improve soil structure through minimal disturbance and organic inputs	[157]
	Intercropping: Diverse root systems improve soil structure	N/A	[158]
Yield outcomes	Crop rotation: Can increase yields over time by maintaining soil health	High-yield varieties: Generally lead to higher yields but may require more inputs	[159,160]
	Organic manuring: Often results in improved long-term yields due to enhanced soil fertility	Precision agriculture: Enhances yield by optimizing inputs and practices tailored to specific needs	[161]
	Intercropping: Increases overall yield by optimizing resource use	Green revolution technologies: Increased yields through improved varieties and chemical inputs	[162]
Sustainability	Crop rotation: Reduces dependency on chemical inputs and maintains soil health	Integrated pest management: Reduces reliance on chemical pesticides and promotes ecological balance	[25,142,163]
	Organic manuring: Promotes long-term soil health and reduces environmental impact	Sustainable intensification: Aims to increase productivity while minimizing environmental impacts	[164]
	Water conservation: Sustainable use of water resources	Technological innovations: Enhance sustainability through precise management and reduced resource use	[165,166]

Abbreviation: N/A: Not available.

by increasing the soil's nutrient-holding capacity and promoting microbial activity.[66,67] The use of compost improves soil structure, water-holding capacity, and nutrient availability, thereby supporting plant growth and reducing the need for synthetic fertilizers.[68-70] Similarly, animal dung serves as a valuable source of nitrogen, phosphorus, and potassium, which are essential for plant growth and development.[71,72]

Green manure, which involves incorporating cover crops such as legumes into the soil, enhances soil fertility and structure.[49,73,74] Green manure crops can fix atmospheric nitrogen, improve soil organic matter,

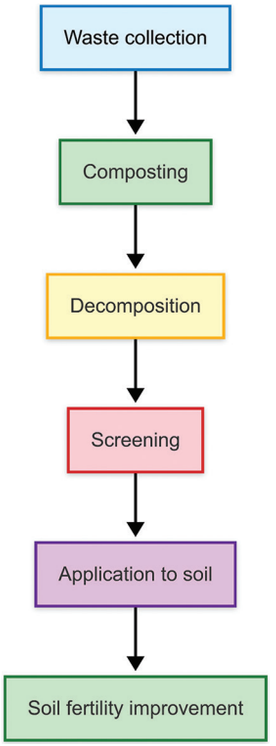

Figure 3. Process flowchart of organic manuring

and increase microbial biomass.[74] The incorporation of green manure into the soil also helps reduce soil erosion and promote nutrient cycling.[50,65]

3.4. Water conservation techniques

Traditional water conservation techniques have been employed in various regions to manage water resources effectively and prevent soil erosion.[75] These techniques are fundamental in water-scarce areas and regions prone to soil erosion, such as Bundelkhand in Uttar Pradesh.[20,76] Rainwater harvesting, contour bunding, check dams, percolation tanks, and step wells are standard methods that help with water storage, groundwater replenishment, and runoff reduction.[77] In addition to improving the amount of water available for everyday consumption and agriculture, these techniques are vital for maintaining livelihoods in regions vulnerable to drought.[78,79] To further enhance water conservation and climate change resilience, contemporary adaptations of these age-old practices are being combined with cutting-edge irrigation techniques and research methodologies.

Bunds, embankments, and check dams are traditional water conservation structures designed to capture and store runoff water, reducing soil erosion and promoting soil moisture retention.[80-83] These structures help control water flow, prevent the loss of valuable topsoil, and maintain soil fertility.[83] These structures play a crucial role in regulating water flow, preventing flash floods, and enhancing groundwater recharge.[84] Bunds, widely spread in agrarian landscapes, retain water flow and facilitate longer infiltration times while reducing crop loss from rapid runoff.[85] Check dams, the step-like barriers built across the streams and small rivers in arid regions, effectively trap sediments and regulate the velocity of the streams and also meet irrigation needs during the dry periods.[86]

In areas such as Bundelkhand and Rajasthan, these traditional practices play a crucial role in mitigating the effects of drought, enhancing soil fertility, and supporting rural livelihoods.[73] Bunds and check dams can play a crucial role in achieving long-term water security and sustainable agriculture when utilized in conjunction with contemporary principles of water management.

Terracing is another traditional technique used to manage water flow and reduce soil erosion on sloped land.[7,87] By creating level areas on sloped fields, terracing reduces runoff and encourages water infiltration, which helps maintain soil moisture and fertility.[88,89] This practice is particularly beneficial in areas with high rainfall and steep slopes, where soil erosion is a major concern.[90,91] By stabilizing slopes, terracing also improves soil fertility, enhances crop yields, and supports sustainable farming practices in challenging terrains.[92]

In contemporary applications, terracing can be utilized in conjunction with modern solutions, including stone bunds, vegetative buffer strips, and contour plowing, to enhance overall water retention and soil conservation.[93] It remains a key adaptation strategy in regions vulnerable to climate change, which is fundamental for sustaining agriculture and ensuring food security in the long term.[94]

3.5. Distribution of traditional soil management practices

Traditional soil management practices in India, including organic manure application, crop rotation, and intercropping, are crucial for promoting sustainable agriculture and maintaining soil health.[95] Organic manuring utilizes natural materials, such as compost and animal manure, to enhance soil fertility, while crop rotation replenishes nutrients and controls pests by alternating crops, often incorporating nitrogen-fixing legumes.[96] Intercropping, the practice of growing multiple crops together, enhances biodiversity and resource use.[97] Organic manuring is the most widely

used method, followed by crop rotation, covering approximately 30 million hectares and contributing nearly 55% to the effectiveness of soil management.[98] Water conservation techniques, though harder to quantify in coverage, contribute 25% due to their importance in improving soil health.[99] Intercropping, practiced on roughly one million hectares, accounts for 20% of the overall impact.[100] Together, these methods reflect farmers' ecological knowledge, playing a significant role in sustainable agricultural systems and environmental conservation across India.[19] A distribution chart of various traditional soil management practices is presented in Figure 4.

3.6. Evolution of soil management practices

The evolution of soil management practices reflects a progression from early traditional methods to contemporary techniques aimed at enhancing soil fertility and sustainability.[101] Early traditional practices, dating back to the early 1900s, primarily involved basic crop rotation and organic manuring, which were essential for maintaining soil health in agrarian societies.[102,103] The introduction of essential organic fertilizers around 1920 marked the beginning of systematic efforts to improve soil fertility through the use of compost and green manure.[104] The mid-20th century witnessed the adoption of early modern agricultural practices, including the use of synthetic fertilizers and basic irrigation systems, which significantly transformed soil management.[105] By the 1970s, advanced traditional methods began to emerge, refining crop rotation and organic manuring techniques to enhance their effectiveness.[106] The 1980s introduced more sophisticated crop rotation techniques and the integration of pest management strategies, which further improved soil health.[107] The 1990s saw the adoption of integrated pest management, which aimed to balance pest control with minimal chemical use.[108] The turn of the millennium brought advancements in traditional methods, emphasizing sustainability and efficiency.[109] The 2010s marked the rise of precision agriculture, leveraging technology to optimize soil management practices.[110] Recent developments include advanced soil testing and monitoring technologies, which provide detailed insights into soil conditions and support more informed management decisions.[111] As of 2024, modern techniques continue to evolve, integrating cutting-edge technologies with traditional practices to foster more sustainable and productive soil management strategies.[112] A timeline of the evolution of soil management practices is presented in Figure 5.

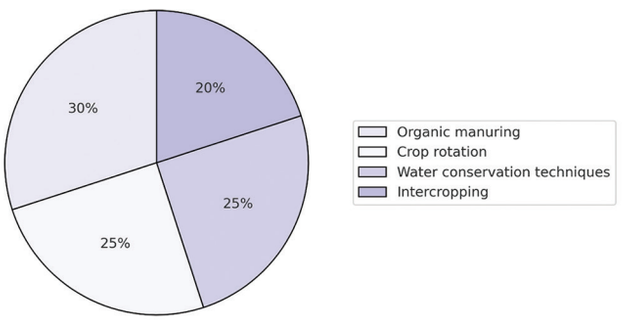

Figure 4. Distribution of traditional soil management practices

4. Case studies from Uttar Pradesh

Uttar Pradesh, with its diverse agroclimatic zones, showcases a variety of traditional soil management practices that reflect the region's rich agricultural heritage.[113] This section presents detailed case studies from three distinct areas within Uttar Pradesh, each highlighting the effectiveness of traditional practices tailored to local environmental conditions. A tabular representation of the current state of scholarly work is presented in Table 2.

4.1. The Bundelkhand region

The Bundelkhand region, characterized by its semi-arid climate and frequent droughts, has a long history of employing traditional water conservation techniques to combat soil erosion and sustain agriculture. Contour bunding is one such practice where embankments are constructed along the contour lines of slopes to capture and slow down runoff water. This method reduces soil erosion, enhances water infiltration, and contributes to improved soil moisture retention. Research indicates that contour bunding can significantly mitigate soil loss and improve crop yields in Bundelkhand.[21,28] In addition, the construction of small check dams, or *Nadi* dams, has proven effective in capturing runoff water and recharging groundwater levels. These check dams help stabilize water availability for irrigation, thereby increasing agricultural productivity.[114,115] Studies have demonstrated that these traditional water conservation practices in Bundelkhand have led to significant improvements in water availability and soil health.[20,21,116]

4.2. The Gangetic plains

In the Gangetic plains, known for their fertile alluvial soils, traditional practices, such as crop rotation and organic manuring, play a crucial role in maintaining soil fertility and productivity. Crop rotation, specifically the

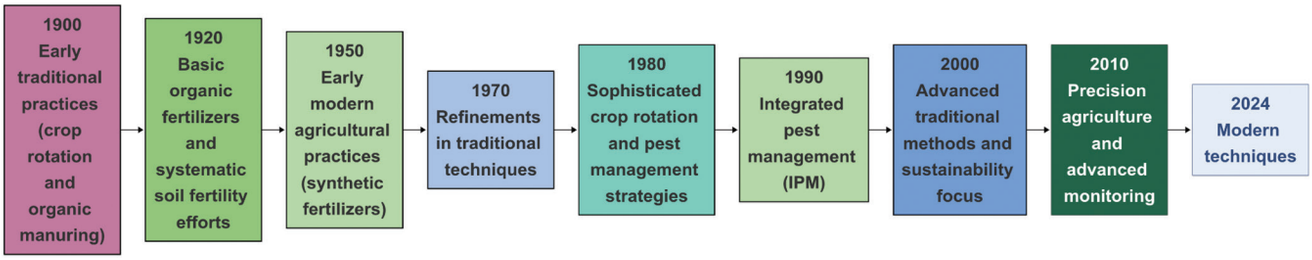

Figure 5. Timeline of the evolution of soil management practices

Table 2. Case studies on soil traditional management practices conducted in Uttar Pradesh

Case study	Location	Practice used	Results achieved	Observations	References
1	Village Nagla, Aligarh	Crop rotation	Increased soil fertility by 25%; reduced pest incidence by 30%	Effective in enhancing soil nutrient balance and pest control	[167]
2	Village Daryapur, Agra	Intercropping	Boosted crop yields by 20%; improved soil nutrient levels by 15%	Combined cultivation of legumes and cereals optimized soil fertility	[168,169]
3	Village Sadabad, Hathras	Organic manuring	Enhanced soil structure; increased crop productivity by 35%	Compost and green manure improved moisture retention and soil health	[170]
4	Village Kheri, Bulandshahr	Crop rotation + organic manuring	Reduced soil erosion by 40%; improved nutrient cycling by 30%	Integration of practices led to significant soil conservation and fertility	[117,171]
5	Village Rasoolpur, Etah	Traditional water conservation	Increased water retention by 25%; improved crop growth by 20%	Techniques, like bunding and check dams, were effective in semi-arid conditions	[172]
6	Village Raebareli, Raebareli	Crop rotation	Improved soil organic matter by 30%; decreased soil salinity	Rotation between legumes and cereals enhanced soil fertility	[11]
7	Village Mirzapur, Mirzapur	Organic manuring	Increased soil moisture by 20%; enhanced crop resilience	Organic manure application improved soil texture and moisture retention	[173]
8	Village Jalaun, Jalaun	Traditional water conservation	Reduced runoff by 30%; improved soil fertility	Traditional water management practices were effective in conserving water	[174]

rotation of rice with pulses, helps replenish soil nutrients and improve soil structure by breaking pest and disease cycles. This practice has been demonstrated to increase soil organic matter and nutrient availability, resulting in improved crop yields.[48,117] Organic manuring, involving the use of cow dung, compost, and other organic materials, is integral to soil management in this region. Organic manures enhance soil fertility by providing essential nutrients and stimulating microbial activity, which in turn supports sustainable agriculture.[118] Studies have demonstrated that organic manure results in better soil health and higher crop yields compared to chemical fertilizers.[119,120]

4.3. The Terai region

The Terai region, characterized by its heavy, clayey soils and high water table, employs unique traditional

practices, such as raised beds and organic mulching, to manage soil moisture and prevent waterlogging. Raised bed farming involves creating elevated planting beds to improve soil drainage and aeration, crucial for managing excessive moisture in clayey soils. This technique has been demonstrated to improve crop yields and soil health by preventing waterlogging and promoting root growth.[121,122] Organic mulching, the application of organic materials, such as straw or leaf litter, helps conserve soil moisture, prevent erosion, and add organic matter to the soil. Mulching has been effective in maintaining soil structure and increasing water-holding capacity, thus supporting sustainable agricultural practices in the Terai region.[123,124] Studies have highlighted that organic mulching improves soil fertility and promotes beneficial microbial activity, resulting in improved crop performance.[6,125]

5. Relevance of traditional knowledge in modern agriculture

Traditional knowledge, with its deep roots in cultural and ecological contexts, remains highly relevant in modern agriculture, particularly in the realm of soil management. Despite the rapid advancements in agricultural technology and scientific research, many traditional practices offer compelling advantages that align with contemporary needs for sustainability and environmental stewardship.

5.1. Environmental sustainability and resilience

Traditional soil management practices often emphasize environmental sustainability, a concept that is increasingly crucial in the face of climate change. Techniques, such as crop rotation, organic manuring, and water conservation, deeply embedded in traditional knowledge contribute to soil health and resilience. For instance, crop rotation, a common practice in traditional agriculture, helps maintain soil fertility by preventing nutrient depletion and disrupting pest and disease cycles.[126,127] This practice aligns well with modern concepts of sustainable agriculture, which advocate for reducing reliance on chemical inputs and enhancing soil biodiversity.[128]

5.2. Low-cost and resource-efficient practices

Many traditional soil management practices are notably low-cost and resource-efficient. Organic manuring, utilizing locally available materials such as compost and animal dung, reduces the dependency on synthetic fertilizers, which can be expensive and environmentally harmful.[1,129] These practices are not only cost-effective but also enhance soil health by improving its organic matter content and microbial activity.[6,37] This is particularly relevant for smallholder farmers in developing regions who may have limited access to modern agricultural inputs.

5.3. Cultural and local adaptation

Traditional knowledge is inherently adapted to local environmental conditions and cultural practices. For example, water conservation techniques, such as bunding and check dams, which have been used for centuries in regions like Bundelkhand, are tailored to the specific hydrological and soil conditions of the area.[130,131] These practices often integrate indigenous knowledge of local weather patterns, soil types, and water resources, making them highly relevant and effective for local contexts.[132]

5.4. Integration with modern technologies

Integrating traditional knowledge with modern agricultural technologies can offer synergistic benefits. For instance, the use of raised beds in the Terai region, a traditional practice for managing clayey soils, can be complemented with modern irrigation systems to optimize water use and crop productivity.[133] Similarly, combining traditional organic manuring practices with precision agriculture techniques can enhance soil fertility while minimizing environmental impacts.[134] This integration can lead to more sustainable and resilient agricultural systems.

5.5. Addressing climate change

As climate change continues to pose significant challenges to agriculture, traditional knowledge offers valuable insights into climate adaptation and mitigation. Practices such as intercropping and mulching, which have been used for centuries, help conserve soil moisture, reduce erosion, and improve soil fertility, thereby contributing to climate resilience.[135,136] These traditional practices can be instrumental in developing adaptive strategies for changing climatic conditions.

6. Challenges and opportunities for integration

Integrating traditional knowledge with modern agricultural practices involves navigating various challenges while seizing opportunities for enhanced soil management. The coexistence of these approaches can lead to innovative solutions that balance cultural heritage with technological advancement, promoting sustainable agricultural practices.

6.1. Challenges

6.1.1. Knowledge erosion

One of the primary challenges is the erosion of traditional knowledge due to the increasing adoption of modern agricultural practices. As farming becomes more mechanized and reliant on chemical inputs, conventional techniques, such as crop rotation, organic manuring, and water conservation, are often overlooked.[137,138] This shift results in a decline in the transmission of traditional knowledge across generations. Younger farmers, influenced by modern methods and lacking exposure to conventional practices, may not learn or use these time-tested techniques, leading to a loss of valuable agronomic wisdom.[139]

6.1.2. Lack of documentation

Traditional knowledge is frequently passed down orally, which can lead to its eventual loss if not systematically documented.[140] The absence of written records or formal documentation makes it challenging to study, validate, and integrate traditional practices into contemporary agricultural systems. This lack of documentation hinders efforts to scientifically evaluate and adapt conventional methods for modern use, risking the loss of effective soil management strategies.[141]

6.1.3. Policy and institutional barriers

Agricultural policies and institutional frameworks often prioritize modern agricultural techniques over traditional practices, presenting a significant challenge.[25,142,143] Policies that favor large-scale, industrial agriculture may not adequately support or recognize the benefits of traditional practices, resulting in insufficient resources, incentives, or support for integrating traditional knowledge. In addition, research and development funds are frequently allocated to modern technologies rather than to studying and reviving traditional methods.[134]

6.2. Opportunities

6.2.1. Revival of traditional practices

There is substantial potential to revive and promote traditional soil management practices through dedicated initiatives. Documenting traditional knowledge through research and community engagement can help preserve and enhance these practices.[139,144] Collaborative efforts involving researchers, practitioners, and local communities can facilitate the recording and dissemination of traditional techniques, ensuring their continued relevance and application in modern agriculture.[139]

6.2.2. Integration with modern techniques

Combining traditional soil management practices with modern technologies presents a promising approach to enhancing soil health and agricultural sustainability. Integrative approaches can leverage the strengths of both traditional and modern methods to address contemporary agricultural challenges.[128,145] For example, integrating traditional water conservation techniques with modern irrigation technologies can optimize water use and enhance soil fertility.[127] Such synergies can lead to more sustainable and effective soil management strategies.

6.2.3. Community-based approaches

Engaging local communities in the planning and implementation of soil management strategies can ensure the effective integration of traditional knowledge. Community-based approaches that involve local knowledge holders can enhance the relevance and acceptance of soil management practices.[146,147] By fostering collaboration between communities, researchers, and policymakers, it is possible to develop strategies that honor traditional knowledge while addressing modern agricultural needs.

6.2.4. Policy and institutional support

Advocating for policy and institutional changes to support traditional practices is crucial for their integration with modern techniques. Policy reforms that recognize and incentivize the use of conventional knowledge can create a more inclusive agricultural system.[137,143] Providing financial and technical support for research on traditional practices and their integration with modern technologies can facilitate the broader adoption of these practices.

In summary, while integrating traditional knowledge with modern agricultural practices presents challenges, including knowledge erosion, a lack of documentation, and policy barriers, it also offers significant opportunities. Reviving traditional practices, combining them with modern technologies, and involving communities in the integration process can lead to more sustainable and resilient soil management strategies. Addressing these challenges and leveraging the opportunities can enhance the effectiveness and sustainability of agricultural systems.

7. Conclusion

Integrating traditional knowledge with modern agricultural practices offers a pathway to more sustainable

and resilient soil management. Traditional practices, such as crop rotation, organic manuring, and water conservation techniques, have long demonstrated their effectiveness in maintaining soil health and productivity. However, the erosion of this knowledge, the lack of documentation, and policy barriers pose significant challenges to their integration with contemporary methods. To address these challenges, it is essential to revitalize and document traditional practices through collaborative efforts involving researchers, practitioners, and local communities. Integrating these practices with modern technologies can optimize soil management and enhance agricultural sustainability. Policymakers should support this integration by developing inclusive policies that recognize and incentivize traditional practices. Future research should focus on the practical applications of combined approaches and their impacts on soil health and productivity. By bridging traditional and modern practices, we can foster a more holistic approach to soil management that benefits both agriculture and the environment.

Acknowledgments

None.

Funding

None.

Conflict of interest

Upaka Rathnayake is an Editorial Board Member of this journal but was not in any way involved in the editorial and peer-review process conducted for this paper, directly or indirectly. Separately, other authors declared that they have no known competing financial interests or personal relationships that could have influenced the work reported in this paper.

Author contributions

Conceptualization: Himanshu Sahu, Pooja Purohit, Arun Pratap Mishra

Investigation: Himanshu Sahu, Pooja Purohit, Arun Pratap Mishra

Methodology: Himanshu Sahu, Pooja Purohit, Arun Pratap Mishra, Amit Kumar

Writing – original draft: Himanshu Sahu, Pooja Purohit, Arun Pratap Mishra, Amit Kumar, Purnendu Sardar

Writing – review & editing: All authors

Availability of data

Not applicable.

References

1. Lal R. Restoring soil quality to mitigate soil degradation. *Sustainability*. 2015;7(5):5875-5895. doi: 10.3390/su7055875
2. Montgomery DR. *Dirt: The Erosion of Civilizations, with a New Preface*. United States: University of California Press; 2012.
3. Brady NC, Weil RR. *The Nature and Properties of Soils*. United Kingdom: Pearson Education; 1996.
4. Powlson DS, Whitmore AP, Goulding KWT. Soil carbon sequestration to mitigate climate change: A critical re-examination to identify the true and the false. *Eur J Soil Sci*. 62(1):42-55. doi: 10.1111/j.1365-2389.2010.01342.x
5. Altieri MA. Linking ecologists and traditional farmers in the search for sustainable agriculture. *Front Ecol Environ*. 2004;2(1):35-42. doi: 10.2307/3868293
6. Berkes F. *Sacred Ecology*. London: Routledge; 2017.
7. Gadgil M, Berkes F, Folke C. Indigenous knowledge for biodiversity conservation. *Ambio*. 1993;22(2-3):151-156.
8. Nakashima D, Galloway McLean K, Thulstrup H, Ramos Castillo A, Rubis J, Traditional Knowledge Initiative. *Weathering Uncertainty: Traditional Knowledge for CLIMATE change Assessment and Adaptation*. Paris: UNESCO and Darwin, UNU; 2012.
9. Ramakrishnan PS. Ecology and Sustainable Development. Delhi: National Book Trust; 2001.
10. Sillitoe P. *Local Science vs. Global Science: An Overview. Approaches to Indigenous Knowledge in International Development*. Vol. 4. New York: Berghahn Books; 2007. p. 1-22.
11. Agrawal A. Dismantling the divide between indigenous and scientific knowledge. *Dev Change*. 1995;26(3):413-439. doi: 10.1111/j.1467-7660.1995.tb00560.x
12. Shiva V. *The Violence of the Green Revolution: Third World Agriculture, Ecology and Politics*. United Kingdom: Zed Books; 1991.
13. Thapa G, Gaiha R. *Smallholder Farming in Asia and the Pacific: Challenges and Opportunities. IFAD Conference on New Directions for Smallholder Agriculture.* Vol. 4; 2011. p. 25. doi: 10.1093/acprof: oso/9780199689347.003.0004
14. Kumar D, Yadav SR, Kaur R, Choudhary A, Meena BS. Soil fertility status and nutrient recommendations based on soil analysis of Jaisalmer district of western Rajasthan. *Asian J Soil Sci*. 2017;12(1):103-107.
15. Kumar M, Raina P, Sharma BK. Soil fertility appraisal

under dominant land use systems in north-eastern part of arid Rajasthan. *Ann Arid Zone*. 2011;50(1):11-15.
16. Gupta A, Singh UB, Sahu PK, *et al.* Linking soil microbial diversity to modern agriculture practices: A review. *Int J Environ Res Public Health*. 2022;19(5):3141. doi: 10.3390/ijerph19053141
17. Sangha KK. Modern agricultural practices and analysis of socio-economic and ecological impacts of development in agriculture sector, Punjab, India-A review. *Indian J Agric Res*. 2014;48(5):331-341. doi: 10.5958/0976-058X.2014.01312.2
18. Yadav MR, Parihar CM, Jat SL, *et al*. Long term effect of legume intensified crop rotations and tillage practices on productivity and profitability of maize vis-a-vis soil fertility in North-Western Indo-Gangetic Plains of India. *Legume Res Int J.* 2017;40(2):282-290. doi: 10.18805/lr.v0i0.7583
19. Ghosh PK, Hazra KK, Venkatesh MS, Nath CP, Singh J, Nadarajan N. Increasing soil organic carbon through crop diversification in cereal-cereal rotations of Indo-Gangetic plain. *Proc Natl Acad Sci India B Biol Sci*. 2019;89:429-440. doi: 10.1007/s40011-017-0953-x
20. Singh R, Singh RM, Singh KN, Kar SK. Hydrological assessment of Haveli-based traditional water harvesting system for the Bundelkhand Region, Uttar Pradesh, India. *Curr Sci*. 2023;125(1):43-51.
21. Singh R, Akuraju V, Anantha KH, *et al*. Traditional rainwater management (haveli cultivation) for building system level resilience in a fragile ecosystem of Bundelkhand region, Central India. *Front Sustain Food Syst*. 2022;6:826722. doi: 10.3389/fsufs.2022.826722
22. Gupta AK, Nair SS, Ghosh O, Singh A, Dey S. *Bundelkhand Drought: Retrospective Analysis and Way Ahead*. New Delhi: National Institute of Disaster Management; 2014. p. 148.
23. Pingali PL. Green revolution: Impacts, limits, and the path ahead. *Proc Natl Acad Sci*. 2012;109(31):12302-12308. doi: 10.1073/pnas.0912953109
24. Hazell P, Wood S. Drivers of change in global agriculture. *Philos Trans R Soc B Biol Sci*. 2008;363(1491):495-515. doi: 10.1098/rstb.2007.2166
25. Pretty J. Agricultural sustainability: Concepts, principles and evidence. *Philos Trans R Soc Lond B Biol Sci*. 2008;363(1491):447-465. doi: 10.1098/rstb.2007.2163
26. Altieri MA, Nicholls CI, Henao A, Lana MA. Agroecology and the design of climate change-resilient farming systems. *Agron Sustain Dev*. 2012;35(3):869-890. doi: 10.1007/s13593-015-0285-2
27. Lwoga ET, Ngulube P, Stilwell C. Managing indigenous knowledge for sustainable agricultural development in developing countries: Knowledge management approaches in the social context. *Int Inform Library Rev*. 2010;42(3):174-185. doi: 10.1016/j.iilr.2010.07.006
28. Pandey V, Mittal R, Sharma P. Documentation and application of indigenous traditional knowledge (ITK) for sustainable agricultural development. *Asian J Agric Extens Econ Sociol*. 2017;15(3):1-9. doi: 10.9734/AJAEES/2017/31481
29. Jat RA, Wani SP, Sahrawat KL. Conservation agriculture in the semi-arid tropics: Prospects and problems. *Adv Agron*. 2012;117:191-273. doi: 10.1016/B978-0-12-394278-4.00004-0
30. Das S, Chatterjee S, Rajbanshi J. Responses of soil organic carbon to conservation practices including climate-smart agriculture in tropical and subtropical regions: A meta-analysis. *Sci Total Environ*. 2022;805:150428. doi: 10.1016/j.scitotenv.2021.150428
31. Scopel E, Triomphe B, Affholder F, *et al*. Conservation agriculture cropping systems in temperate and tropical conditions, performances and impacts. A review. *Agron Sustain Dev*. 2013;33:113-130. doi: 10.1007/s13593-012-0106-9
32. Pimentel D, Burgess M. Soil erosion threatens food production. *Agriculture*. 2013;3(3):443-463. doi: 10.3390/agriculture3030443
33. Montgomery DR. Soil erosion and agricultural sustainability. *Proc Natl Acad Sci*. 2007;104(33):13268-13272. doi: 10.1073/pnas.0611508104
34. Tilman D, Balzer C, Hill J, Befort BL. Global food demand and the sustainable intensification of agriculture. Proc Natl Acad Sci. 2011;108(50):20260-20264. doi: 10.1073/pnas.1116437108
35. Altieri MA, Nicholls CI. Agroecology and the reconstruction of a post-COVID-19 agriculture. *J Peasant Stud.* 2020;47(5):881-898. doi: 10.1080/03066150.2020.1782891
36. Francis C, Lieblein G, Gliessman S, *et al*. Agroecology: The ecology of food systems. *J Sustain Agric*. 2003;22(3):99-118. doi: 10.1300/J064v22n03_10
37. Berkes F, Folke C. *Linking Social and Ecological Systems: Management Practices and Social Mechanisms for Building Resilience*. United Kingdom: Cambridge University Press; 2000. doi: 10.1017/CBO9780511526144
38. Pretty JN. The sustainable intensification of agriculture. *Nat Resour Forum*. 2009;21(4):247-256. doi: 10.1111/j.1477-8947.1997.tb00699.x
39. Pretty J, Bharucha ZP. *Sustainable Intensification of Agriculture: Greening the World's Food Economy* 1st ed. London: Routledge; 2018.
40. Kumar P, Choudhury D. Role of indigenous knowledge in agricultural soil reclamation without disturbing other ecosystems. In: *Bioremediation of Emerging Contaminants from Soils*. Netherlands: Elsevier; 2024.

p. 465-488.
doi: 10.1016/B978-0-443-13993-2.00021-9
41. Boerma D, Koohafkan P. Local knowledge systems and the management of dryland agro-ecosystems: Some principles for an approach. In: *GIAHS Background Document.* Rome: Food and Agriculture Organization of the United Nations; 2004.
42. Rietra R, Heinen M, Oenema O. A review of crop husbandry and soil management practices using meta-analysis studies: Towards soil-improving cropping systems. *Land*. 2022;11(2):255.
doi: 10.3390/land11020255
43. Liebman M, Dyck E. Crop rotation and intercropping strategies for weed management. *Ecol Appl*. 1993;3(1):92-122.
doi: 10.2307/1941795
44. Sumner DR. Crop rotation and plant productivity. In: *Handbook of Agricultural Productivity*. United States: CRC Press; 2018. p. 273-314.
45. Havlin JL, Kissel DE, Maddux LD, Claassen MM, Long JH. Crop rotation and tillage effects on soil organic carbon and nitrogen. *Soil Sci Soc Am J*. 1990;54(2):448-452.
doi: 10.2136/sssaj1990.03615995005400020026x
46. Van Eerd LL, Congreves KA, Hayes A, Verhallen A, Hooker DC. Long-term tillage and crop rotation effects on soil quality, organic carbon, and total nitrogen. *Can J Soil Sci.* 2014;94(3):303-315.
doi: 10.4141/cjss2013-093
47. Bansal S, Yin X, Sykes V, Lee J, Jagadamma S. Soil aggregate-associated organic carbon and nitrogen response to long-term no-till crop rotation, cover crop, and manure application. *Soil Sci Soc Am J*. 2021;85(6):2169-2184.
doi: 10.1002/saj2.20329
48. Singh G, Bhattacharyya R, Das TK, *et al*. Crop rotation and residue management effects on soil enzyme activities, glomalin and aggregate stability under zero tillage in the Indo-Gangetic Plains. *Soil Tillage Res*. 2018;184:291-300.
doi: 10.1016/j.still.2018.08.006
49. Giller KE. *Nitrogen Fixation in Tropical Cropping Systems*. England: CABI Publishing; 2001.
50. Hauggaard-Nielsen H, Mundus S, Jensen ES. Nitrogen dynamics following grain legumes and subsequent catch crops and the effects on succeeding cereal crops. *Nutr Cycling Agroecosyst*. 2009;84:281-291.
doi: 10.1007/s10705-008-9242-7
51. Chen B, Liu E, Tian Q, Yan C, Zhang Y. Soil nitrogen dynamics and crop residues. A review. *Agron Sustain Dev*. 2014;34:429-442.
doi: 10.1007/s13593-014-0207-8
52. Aziz I, Ashraf M, Mahmood T, Islam KR. Crop rotation impact on soil quality. *Pak J Bot*. 2011;43(2):949-960.
53. Neugschwandtner RW, Liebhard P, Kaul HP, Wagentristl H. Soil chemical properties as affected by tillage and crop rotation in a long-term field experiment. *Plant Soil Environ.* 2014;60(2):57-62.
doi: 10.17221/879/2013-PSE
54. Marriot EE, Wander MM. Total and labile soil organic matter in organic and conventional farming systems. *Soil Sci Soc Am J*. 2006;70(1):951-960.
doi: 10.2136/sssaj2005.0241
55. Lithourgidis AS, Dordas CA, Damalas CA, Vlachostergios DN. Annual intercrops: An alternative pathway for sustainable agriculture. *Aust J Crop Sci*. 2011;5(4):396-410.
56. Zou XX, Shi PX, Zhang CJ, *et al*. Rotational strip intercropping of maize and peanuts has multiple benefits for agricultural production in the northern agropastoral ecotone region of China. *Eur J Agron*. 2021;129:126304.
doi: 10.1016/j.eja.2021.126304
57. Layek J, Das A, Mitran T, *et al*. Cereal+ legume intercropping: An option for improving productivity and sustaining soil health. In: *Legumes for Soil Health and Sustainable Management.* Berlin: Springer; 2018. p. 347-386.
doi: 10.1007/978-981-13-0253-4_11
58. Ananda MR, Vaiahnav S, Naide PR, Aruna NV. Long term benefits of legume based cropping systems on soil health and productivity. An overview. *Int J Environ Climate Change*. 2022;12(9):299-315.
doi: 10.9734/ijecc/2022/v12i930767
59. Begam A, Mondal R, Dutta S, Banerjee H. Impact of cereal+ legume intercropping systems on productivity and soil health-a review. *Int J Bioresour Stress Manag*. 2020;11:274-286.
doi: 10.23910/1.2020.2109
60. Yang T, Siddique KH, Liu K. Cropping systems in agriculture and their impact on soil health-A review. *Glob Ecol Conserv*. 2020;23:e01118.
doi: 10.1016/j.gecco.2020.e01118
61. Mousavi SR, Eskandari H. A general overview on intercropping and its advantages in sustainable agriculture. *J Appl Environ Biol Sci*. 2011;1(11):482-486.
62. Ouma G, Jeruto P. Sustainable horticultural crop production through intercropping: The case of fruits and vegetable crops: A review. *Agric Biol J N Am*. 2010;1(5):1098-1105.
63. Bhunia S, Bhowmik A, Mallick R, Mukherjee J. Agronomic efficiency of animal-derived organic fertilizers and their effects on biology and fertility of soil: A review. *Agronomy*. 2021;11(5):823.
doi: 10.3390/agronomy11050823
64. Singh TB, Ali A, Prasad M, *et al*. *Role of Organic Fertilizers in Improving Soil Fertility. Contaminants in Agriculture: Sources, Impacts and Management.* Berlin: Springer; 2020. p. 61-77.
doi: 10.1007/978-3-030-41552-5_3
65. Roobroeck D, van Asten PJ, Jama B, Harawa R,

Vanlauwe B. *Integrated Soil Fertility Management: Contributions of Framework and Practices to Climate-Smart Agriculture*. CSA Practice Brief; 2015. Available from: https://hdl.handle.net/10568/69018 [Last accessed on 2025 Feb 01].
66. Weigelhofer G, Jirón TS, Yeh TC, Steniczka G, Pucher M. Dissolved organic matter quality and biofilm composition affect microbial organic matter uptake in stream flumes. *Water*. 2020;12(11):3246. doi: 10.3390/w12113246
67. Šimon T, Madaras M, Mayerová M, Kunzová E. Soil organic carbon dynamics in the long-term field experiments with contrasting crop rotations. *Agriculture*. 2024;14(6):818. doi: 10.3390/agriculture14060818
68. Stevenson FJ, Cole M. *Cycles of Soils: Carbon, Nitrogen, Phosphorus, Sulfur, Micronutrients*. United States: John Wiley & Sons; 1999.
69. Iqbal M, van Es HM, Hassan A, Schindelbeck RR, Moebius-Clune BN. Soil health indicators as affected by long-term application of farm manure and cropping patterns under semi-arid climates. *Int J Agric Biol*. 2014;16(2):242-250.
70. Rayne N, Aula L. Livestock manure and the impacts on soil health: A review. *Soil Syst*. 2020;4(4):64. doi: 10.3390/soilsystems4040064
71. Ramesh P, Raten Panwar N, Bahadur Singh A, Ramana S, Subba Rao A. Impact of organic-manure combinations on the productivity and soil quality in different cropping systems in central India. *J Plant Nutr Soil Sci*. 2009;172(4):577-585. doi: 10.1002/jpln.200700281
72. Lakshmi CSR, Sreelatha T, Rani TU, Rao SRK, Naidu NV. Effect of organic manures on soil fertility and productivity of sugarcane in north coastal zone of Andhra Pradesh. *Indian J Agric Res*. 2011;45(4):307-313.
73. Maitra S, Zaman A, Mandal TK, Palai JB. Green manures in agriculture: A review. *J Pharmacogn Phytochem*. 2018;7(5):1319-1327.
74. Iderawumi AM, Kamal TO. Green manure for agricultural sustainability and improvement of soil fertility. *Farm Manag*. 2022;7(1):1-8. doi: 10.31830/2456-8724.2022.FM-101
75. Mishra P, Rai A, Rai S. Agronomic measures in traditional soil and water conservation practices in the Sikkim Himalaya, India. *Am Res J Agric*. 2019;5(1):1-16.
76. Chaurasia PR, Chandra S. Bundelkhand water woes: Paradigm shift is needed in the strategy. *J Institut Eng Ser A*. 2021;102(1):335-345. doi: 10.1007/s40030-020-00496-8
77. Sivanappan RK. Rain water harvesting, conservation and management strategies for urban and rural sectors. In: *National Seminar on Rainwater Harvesting and Water Management*. Vol. 11. New Delhi, India: Institution of Engineers (India), Nagpur Local Centre, Nagpur in Association with UNESCO; 2006. p. 1.
78. Calow RC, MacDonald AM, Nicol AL, Robins NS, Kebede S. *The Struggle for Water: Drought, Water Security and Rural Livelihoods. BGS Technical Report*; 2006.
79. Enfors EI, Gordon LJ. Dealing with drought: The challenge of using water system technologies to break dryland poverty traps. *Glob Environ Change*. 2008;18(4):607-616. doi: 10.1016/j.gloenvcha.2008.07.006
80. Goyal RK, Gaur MK. Soil and Water Conservation Measures for Agricultural Sustainability in Arid Lands. In: *Natural Resources Management: Watershed-based Approach*. London: Intechopen; 2021. p. 57.
81. Rao BK, Annapurna S, Rani BR, *et al*. *Soil and Water Conservation Techniques in Rainfed Areas [E-book]*. Hyderabad: National Institute of Agricultural Extension Management (MANAGE) & Water and Land Management Training and Research Institute (WALAMTARI); 2022.
82. Mishra PK, Tripathi KP. Soil and water conservation research for land management in India. *Indian J Dryland Agric Res Dev*. 2013;28(1):1-18.
83. Bhatt R, Singh P, Kaur G. Soil Management Vis-à-Vis Carbon Sequestration in Relation to Land Use Cover/ Change in Terrestrial Ecosystem-A review. In: *Managing plant Production Under Changing Environment*. Berlin: Springer Nature Singapore Pte Ltd.; 2022. p. 43-78. doi: 10.1007/978-981-16-5059-8_3
84. Lucas-Borja ME, Piton G, Yu Y, Castillo C, Zema DA. Check dams worldwide: Objectives, functions, effectiveness and undesired effects. *Catena*. 2021;204:105390. doi: 10.1016/j.catena.2021.105390
85. Abiye W. Soil and water conservation nexus agricultural productivity in Ethiopia. *Adv Agric*. 2022;2022(1):8611733. doi: 10.1155/2022/8611733
86. Morris GL. Classification of management alternatives to combat reservoir sedimentation. *Water*. 2020;12(3):861. doi: 10.3390/w12030861
87. Gikonyo NW. *Smallholder Farmers' Household Savings and their Influence on Adoption of Climate Smart Agriculture Technologies in Nyando Basin, Kenya* (Doctoral Dissertation, University of Nairobi); 2022.
88. Widomski MK. Terracing as a measure of soil erosion control and its effect on improvement of infiltration in eroded environment. In: *Soil Erosion Issues in Agriculture*. London: Intechopen; 2011. p. 314-335.
89. Dorren L, Rey F. A review of the effect of terracing on erosion. In: Boix-Fayons C, Imeson A, editors. *Briefing Papers of the 2nd SCAPE Workshop*; 2004. p. 97-108.
90. Zhang H, Wei W, Chen L, Wang L. Effects of terracing on soil water and canopy transpiration of Chinese pine plantation in the Loess Plateau, China. *Hydrol Earth Syst Sci Discuss.* 2016;2016:1-30.

doi: 10.1016/j.ecoleng.2017.02.044
91. Leichenko R. Climate change and urban resilience. *Curr Opin Environ Sustain*. 2011;3(3):164-168. doi: 10.1016/j.cosust.2010.12.014
92. Chapagain T, Raizada MN. Agronomic challenges and opportunities for smallholder terrace agriculture in developing countries. *Front Plant Sci*. 2017;8:331. doi: 10.3389/fpls.2017.00331
93. Yousuf A, Lenz J, Dar EA. Measures to control soil erosion. In: *Watershed Hydrology, Management and Modeling*. United States: CRC Press; 2019. p. 77-97.
94. Branca G, Lipper L, McCarthy N, Jolejole MC. Food security, climate change, and sustainable land management. A review. *Agron Sustain Dev.* 2013;33:635-650. doi: 10.1007/s13593-013-0133-1
95. Patel SK, Sharma A, Singh GS. Traditional agricultural practices in India: An approach for environmental sustainability and food security. *Energy Ecol Environ*. 2020;5(4):253-271. doi: 10.1007/s40974-020-00158-2
96. Kumar A, Kadam S, Arif M, Meena R, Verma T. Legumes an alternative land use options for sustaining soil health. *Agric Food E-Newsl*. 2020;6:1-3.
97. Mala M, Mollah MMI, Baishnab M. Importance of intercropping for biodiversity conservation. *J Sci Technol Environ Inform*. 2020;10(2):709-716. doi: 10.18801/jstei.100220.71
98. Ali Q, Ashraf S, Kamran M, *et al*. Organic manuring for agronomic crops. In: *Agronomic Crops: Management Practices*. Vol. 2. Berlin: Springer; 2019. p. 163-193. doi: 10.1007/978-981-32-9783-8_10
99. Reicosky D. Conservation agriculture systems: Soil health and landscape management. In: *Advances in Conservation Agriculture*. England: Burleigh Dodds Science Publishing; 2020. p. 87-154.
100. Hong Y, Heerink N, Jin S, Berentsen P, Zhang L, van der Werf W. Intercropping and agroforestry in China-current state and trends. *Agric Ecosyst Environ*. 2017;244:52-61. doi: 10.1016/j.agee.2017.04.019
101. Hou D, Bolan NS, Tsang DC, Kirkham MB, O'Connor D. Sustainable soil use and management: An interdisciplinary and systematic approach. *Sci Total Environ.* 2020;729:138961. doi: 10.1016/j.scitotenv.2020.138961
102. Pushpanjali JS, Rejani R. Traditional knowledge for soil management India. *BEST Int J Humanit Art Med Sci.* 2013;1:39-44.
103. Occelli M, Mantino A, Ragaglini G, *et al*. Traditional knowledge affects soil management ability of smallholder farmers in marginal areas. *Agron Sustain Dev*. 2021;41:1-15.
104. Lotter DW. Organic agriculture. *J Sustain Agric*. 2003;21(4):59-128. doi: 10.1300/J064v21n04_06
105. Spiertz H. Agricultural sciences in transition from 1800 to 2020: Exploring knowledge and creating impact. *Eur J Agron*. 2014;59:96-106. doi: 10.1016/j.eja.2014.06.001
106. Shorrocks VM. *Conventional and Organic Farming: A Comprehensive Review through the Lens of Agricultural Science*. England: 5m Books Ltd.; 2017.
107. Hillocks RJ, Logan JWM, Riches CR, Russell-Smith A, Shaxson LJ. Soil pests in traditional farming systems in Sub-Saharan Africa-a review. Part 2. Management strategies. *Int J Pest Manage*. 1996;42(4):253-265. doi: 10.1080/09670879609372003
108. Kogan M, Bajwa WI. Integrated pest management: A global reality? *An Soc Entomol Bras.* 1999;28:1-25. doi: 10.1590/S0301-80591999000100001
109. Mol AP. *Globalization and Environmental Reform: The Ecological Modernization of the Global Economy*. United States: MIT Press; 2003. doi: 10.2307/798155
110. Charania I, Li X. Smart farming: Agriculture's shift from a labor intensive to technology native industry. *Internet Things*. 2019;9:100142. doi: 10.1016/j.iot.2019.100142
111. Nadporozhskaya M, Kovsh N, Paolesse R, Lvova L. Recent advances in chemical sensors for soil analysis: A review. *Chemosensors*, 2022;10(1):35. doi: 10.3390/chemosensors10010035
112. de Sousa RN, Grichar WJ. *Strategic Tillage and Soil Management: New Perspectives*. Germany: BoD-Books on Demand; 2024. doi: 10.5772/intechopen.111208
113. Sekhar M, Rastogi M, Rajesh CM, *et al*. Exploring traditional agricultural techniques integrated with modern farming for a sustainable future: A review. *J Sci Res Rep.* 2024;30(3):185-198. doi: 10.9734/jsrr/2024/v30i31871
114. Gao H, Ding Y, Zhao Q, Hrachowitz M, Savenije HH. The importance of aspect for modelling the hydrological response in a glacier catchment in Central Asia. *Hydrol Processes*. 2017;31(16):2842-2859. doi: 10.1002/hyp.11224
115. Garg KK, Singh R, Anantha KH, et al. Building climate resilience in degraded agricultural landscapes through water management: A case study of Bundelkhand region, Central India. *J Hydrol.* 2020;591:125592. doi: 10.1016/j.jhydrol.2020.125592
116. Parvizi H, Sepaskhah AR, Ahmadi SH. Effect of drip irrigation and fertilizer regimes on fruit yields and water productivity of a pomegranate (*Punica granatum* (L.) cv. Rabab) orchard. *Agric Water Manag*. 2014;146:45-56. doi: 10.1016/j.agwat.2014.07.005
117. Kumar R, Singh RR, Singh M, Kant L, Kumar Y. Physico-chemical and biological properties of soil under Sorghum-wheat farming system of Bulandshahr and Meerut Districts in Uttar Pradesh. *J Krishi Vigyan*.

2016;4(2):83-89.
118. Sahu H, Kumar U, Mariappan S, Mishra AP, Kumar S. Impact of organic and inorganic farming on soil quality and crop productivity for agricultural fields: A comparative assessment. *Environ Challenges*. 2024;15:100903. doi: 10.1016/j.envc.2024.100903
119. Yadav SK, Babu S, Yadav MK, Singh K, Yadav GS, Pal S. A review of organic farming for sustainable agriculture in Northern India. *Int J Agron*. 2013;2013(1):718145. doi: 10.1155/2013/718145
120. Shekhawat K, Rathore SS, Kandpal BK, Premi OP, Singh D, Chauhan BS. Crop establishment techniques affect productivity, sustainability, and soil health under mustard-based cropping systems of Indian semi-arid regions. *Soil Tillage Res*. 2016;158:137-146. doi: 10.1016/j.still.2015.12.008
121. Wang G, Zhang L, Zhuang Q, *et al*. Quantification of the soil organic carbon balance in the Tai-Lake paddy soils of China. *Soil Tillage Res*. 2016;155:95-106. doi: 10.1016/j.still.2015.08.003
122. Verma P, Bijalwan A, Dobriyal MJ, Swamy SL, Thakur TK. A paradigm shift in agroforestry practices in Uttar Pradesh. *Curr Sci.* 2017;112(3):509-516. doi: 10.18520/cs/v112/i03/509-516
123. Sinkevičienė A, Jodaugienė D, Pupalienė R, Urbonienė M. The influence of organic mulches on soil properties and crop yield. *Agron Res*. 2009;7(1):485-491.
124. Ngosong C, Okolle JN, Tening AS. Mulching: A sustainable option to improve soil health. In: *Soil Fertility Management for Sustainable Development*. Berlin: Springer; 2019. p. 231-249. doi: 10.1007/978-981-13-5904-0_11
125. Sagar L, Singh S, Sindhu L. Impact of mulching in improving soil properties and crop performance-an introspect. *Biosci Biotechnol Res Commun*. 2020;13(12):178-184.
126. Altieri MA. *Agroecology: The Science of Sustainable Agriculture*. United States: CRC Press; 2018. doi: 10.1201/9781315271683
127. Schneider UA, Havlík P, Schmid E, *et al*. Impacts of population growth, economic development, and technical change on global food production and consumption. *Agric Syst*. 2011;104(2):204-215. doi: 10.1016/j.agsy.2010.11.003
128. Gliessman SR. *Agroecology: The Ecology of Sustainable Food Systems*. 3rd ed. United States: CRC Press; 2015. doi: 10.1201/9781315468021
129. Wang Z, Hu Y, Wang R, *et al*. Soil organic carbon on the fragmented Chinese Loess Plateau: Combining effects of vegetation types and topographic positions. *Soil Tillage Res*. 2017;174:1-5. doi: 10.1016/j.still.2017.05.005
130. Kumar S, Srivastava RK, Singh AK, Kalra A, Tomar VKS, Bansal RP. Higher yields and profits from new crop rotations permitting integration of mediculture with agriculture in the Indo-Gangetic plains. *Curr Sci*. 2001;80:563-566.
131. Naresh RK, Rathore RS, Dwivedi A, *et al*. Bed planting system promotes crop diversification for improving livelihoods in western Uttar Pradesh, India. *Int J Curr Microbiol Appl Sci*. 2017;6(2):1580-1590. doi: 10.20546/ijcmas.2017.602.177
132. Nair PKR. *Agroforestry Systems in the Tropics. Forestry.* Berlin: Springer; 1989.
133. Chathuranika I, Khaniya B, Neupane K, Rustamjonovich KM, Rathnayake U. Implementation of water-saving agro-technologies and irrigation methods in agriculture of Uzbekistan on a large scale as an urgent issue. *Sustain Water Resour Manag.* 2022;8(5):1-16. doi: 10.1007/s40899-022-00746-6
134. Shafi U, Mumtaz R, García-Nieto J, Hassan SA, Zaidi SAR, Iqbal N. Precision agriculture techniques and practices: From considerations to applications. *Sensors*. 2019;19(17):3796. doi: 10.3390/s19173796
135. Aulakh CS, Sharma S, Thakur M, Kaur P. A review of the influences of organic farming on soil quality, crop productivity and produce quality. *J Plant Nutr*. 2022;45(12):1884-1905. doi: 10.1080/01904167.2022.2027976
136. Gurmu G. Soil organic matter and its role in soil health and crop productivity improvement. *Forest Ecol Manage*. 2019;7(7):475-483. doi: 10.14662/ARJASR2019.147
137. FAO. *The State of Food and Agriculture 2020. Overcoming Water Challenges in Agriculture*. Roma: FAO; 2020.
138. Partey ST, Zougmoré RB, Ouédraogo M, Campbell BM. Developing climate-smart agriculture to face climate variability in West Africa: Challenges and lessons learnt. *J Clean Prod*. 2018;187:285-295. doi: 10.1016/j.jclepro.2018.03.199
139. Berkes F, Colding J, Folke C. Rediscovery of traditional ecological knowledge as adaptive management. *Ecol Appl*. 2000;10(5):1251-1262. doi: 10.1890/1051-0761(2000)010[1251:ROTEKA]2.0.CO;2
140. Walker BG, Boersma PD, Wingfield JC. Physiological and behavioral differences in Magellanic penguin chicks in undisturbed and tourist-visited locations of a colony. *Conserv Biol.* 2005;19(5):1571-1577.
141. Sillitoe P, editor. *Local Science vs. Global Science: Approaches to Indigenous Knowledge in International Development*. Vol. 4. New York: Berghahn Books; 2009.
142. Umesha S, Manukumar HM, Chandrasekhar B. Sustainable agriculture and food security. In: *Biotechnology for Sustainable Agriculture*. United Kingdom: Woodhead Publishing; 2018. p. 67-92. doi: 10.1016/B978-0-12-812160-3.00003-9
143. Van der Ploeg JD. *The New Peasantries: Struggles for*

Autonomy and Sustainability in an era of Empire and Globalization. London: Routledge; 2012. doi: 10.4324/9781849773164

144. Chambers R, Thrupp LA, editors. *Farmer First: Farmer Innovation and Agricultural Research*. France: Karthala Editions; 1994.
145. Aliche EB, Oortwijn M, Theeuwen TP, Bachem CW, Visser RG, van der Linden CG. Drought response in field grown potatoes and the interactions between canopy growth and yield. *Agric Water Manag.* 2018;206:20-30. doi: 10.1016/j.agwat.2018.04.013
146. Ostrom E. *Governing the Commons: The Evolution of Institutions for Collective Action*. Cambridge: Cambridge University Press; 1990. doi: 10.1017/CBO9780511807763
147. Adade Williams P, Sikutshwa L, Shackleton S. Acknowledging indigenous and local knowledge to facilitate collaboration in landscape approaches-Lessons from a systema2 tic review. *Land*. 2020;9(9):331. doi: 10.3390/land9090331
148. Komatsuzaki M, Ohta H. *Soil Management Practices for Sustainable Agro-Ecosystems*. Vol. 2. Berlin: Springer-Verlag; 2007. p. 103-120. doi: 10.1007/s11625-006-0014-5
149. Robert PC. Precision agriculture: A challenge for crop nutrition management. In: *Progress in Plant Nutrition: Plenary Lectures of the XIV International Plant Nutrition Colloquium: Food Security and Sustainability of Agro-ecosystems through Basic and Applied Research*. Berlin: Springer Netherlands; 2002. p. 143-149. doi: 10.1023/A:1021171514148
150. Bongiovanni R, Lowenberg-DeBoer J. Precision agriculture and sustainability. *Precis Agric*. 2004;5:359-387. doi: 10.1023/B: PRAG.0000040806.39604.aa
151. Lal R. Soil degradation as a reason for inadequate human nutrition. *Food Secur*. 2009;1:45-57. doi: 10.1007/s12571-009-0009-z
152. Lal R. Enhancing ecosystem services with no-till. *Renew Agric Food Syst*. 2013;28(2):102-114. doi: 10.1017/S1742170512000452
153. Vach M, Hlisnikovský L, Javůrek M. The effect of different tillage methods on erosion. *Agriculture*. 2018;64(1):28-34. doi: 10.2478/agri-2018-0003
154. Wang Y, Zhang JH, Zhang ZH, Jia LZ. Impact of tillage erosion on water erosion in a hilly landscape. *Sci Total Environ*. 2016;551:522-532. doi: 10.1016/j.scitotenv.2016.02.045
155. Rabot E, Wiesmeier M, Schlüter S, Vogel HJ. Soil structure as an indicator of soil functions: A review. *Geoderma*. 2018;314:122-137. doi: 10.1016/j.geoderma.2017.11.009
156. Pachepsky YA, Rawls WJ. Soil structure and pedotransfer functions. *Eur J Soil Sci*. 2003;54(3):443-452. doi: 10.1046/j.1365-2389.2003.00485.x
157. Kay BD. Impact of tillage on soil structure and function. *Soil Tillage Res.* 2001;61(1-2):59-65.
158. Reganold JP, Wachter JM. Organic agriculture in the twenty-first century. *Nat Plants*. 2016;2:15221. doi: 10.1038/nplants.2015.221
159. Diacono M, Montemurro F. Long-term effects of organic amendments on soil fertility. *Sustain Agric Vol.* 2011;2:761-786. doi: 10.1007/978-94-007-0394-0_34
160. Bonanomi G, De Filippis F, Zotti M, *et al*. Repeated applications of organic amendments promote beneficial microbiota, improve soil fertility and increase crop yield. *Appl Soil Ecol*. 2020;156:103714. doi: 10.1016/j.apsoil.2020.103714
161. Kumar A, Kumar A, Cabral-Pinto MMS, *et al*. Lead toxicity: Health hazards, influence on food chain, and sustainable remediation approaches. *Int J Environ Res Public Health*. 2020;17(7):2179. doi: 10.3390/ijerph17072179
162. Evenson RE, Gollin D. Assessing the impact of the Green Revolution, 1960 to 2000. *Science*. 2003;300(5620):758-762. doi: 10.1126/science.1078710
163. Farooq M, Rehman A, Pisante M. Sustainable agriculture and food security. In: *Innovations in Sustainable Agriculture*. Berlin: Springer; 2019. p. 3-24. doi: 10.1007/978-3-030-23169-9_1
164. Altieri MA, Nicholls CI. *Agroecology: The Science of Sustainable Agriculture.* United States: CRC Press; 2021.
165. Fleming A, Vanclay F. Farmer responses to climate change and sustainable agriculture. A review. *Agron Sustain Dev*. 2010;30:11-19. doi: 10.1051/agro/2009028
166. Wall E, Smit B. Climate change adaptation in light of sustainable agriculture. *J Sustain Agric*. 2005;27(1):113-123. doi: 10.1300/J064v27n01_07
167. Malik N, Singh MK, Kumar A, Nain MS, Vashishtha P. Farmers' readiness for organic farming: A study of Aligarh District in Uttar Pradesh. *Indian J Extension Educ*. 2023;59(1):42-45. doi: 10.48165/IJEE.2023.59109
168. Kumar A, Chauhan S. Evaluation of intercropping system of mustard under Agra region. *J Rural Agric Res*. 2009;9(2):27-29.
169. Rohit JS, Kumar R. Enhancement of productivity and profitability through resource conserving technologies in Rainfed conditions in Agra. *IJCS*. 2019;7(5):2093-2097.
170. Singh S. Contribution of starter dose and seed inoculation in yield and economics of black gram under Hathras condition. *J Pharmacogn Phytochem*. 2021;10(1S):158-162.
171. Khan N, Parashari AK. Integrated crop-livestock farming system and its impact on livelihood and sustainability of poor farmers in Bulandshahr District, UP. *Int J*

Multidiscipl Res. 2023;5(6):1-15.
doi: 10.36948/ijfmr.2023.v05i06.9098

172. AICRP on SASUSW. In: Kaledhonkar MJ, Meena BL, editors. *Significant Technologies Along with Impact based on 50 Years of Salinity Research under ICAR-AICRP on Management of Salt Affected Soils & Use of Saline Water in Agriculture*. Haryana: ICAR-Central Soil Salinity Research Institute; 2022. p. 81.
173. Sharma PK, Kumar S. Management of soil physical environment in relation to plant growth. In: *Soil Physical Environment and Plant Growth: Evaluation and Management*. Cham: Springer International Publishing; 2023. p. 231-254.
doi: 10.1007/978-3-031-28057-3_9
174. Lata S. *Irrigation Water Management for Agricultural Development in Uttar Pradesh, India*. Berlin: Springer International Publishing; 2019.
doi: 10.1007/978-3-030-00952-6
175. Singh NJ, Kudrat M, Jain K, Pandey K. Cropping pattern of Uttar Pradesh using IRS-P6 (AWiFS) data. *Int J Remote Sens*. 2011;32(16):4511-4526.
doi: 10.1080/01431161.2010.489061

Asian Journal of Water, Environment and Pollution. Vol. 22, No. 2 (2025), pp. 19-31.
doi: 10.36922/ajwep.6564

ORIGINAL RESEARCH ARTICLE

Enhancing swimming pool hygiene: A robotic approach to debris removal and water quality monitoring

Hemalatha Senthilmahesh[1]*, Kiran Mayee Adavala[2], Thilagam Thangamariappan[3], Pullela S. V. V. S. R. Kumar[4], Ramesh Tumaati[5], and Muthuvairavan Pillai Nagappan[6]

[1]Department of Computer Science and Business Systems, Panimalar Engineering College, Poonamallee, Chennai, India
[2]CSE (AI&ML), Kakatiya Institute of Technology and Science, Warangal, India
[3]Department of Computer Science and Engineering, Vel Tech Rangarajan Dr. Sagunthala R&D Institute of Science and Technology, Chennai, India
[4]Department of Computer Science and Engineering, Aditya University, Surampalem, Andhra Pradesh, India
[5]Department of Computer Science and Engineering, R.M.K. Engineering College, Chennai, Tamil Nadu, India
[6]Department of Computer Science and Business Systems, R.M.D. Engineering College, Tiruvallur, Tamil Nadu, India
***Corresponding author:** Hemalatha Senthilmahesh (csbshod@pit.ac.in)

Received: November 26, 2024; Revised: February 6, 2025; Accepted: February 19, 2025; Published online: March 26, 2025

Abstract: The World Health Organization has underscored swimming as a significant exercise for attaining health, and it is also recognized as a competitive sport in many nations. Individuals across all age groups choose swimming as a means to enhance their fitness levels. Maintaining the cleanliness of the swimming pool is imperative to prevent the spread of waterborne diseases. Despite regular weekly or monthly maintenance, cleanliness is often compromised due to service provider limitations. In the contemporary landscape, artificial intelligence technologies are progressively assuming roles where human providers fall short. This article proposes the integration of ethical robots to augment cleaning services both within and around swimming pools. These waterproof robots are designed to navigate within the pool environment, efficiently collecting debris and waste into their attached receptacles. The deployment of such ethical robotics marks a significant advancement in swimming pool maintenance, promising enhanced efficiency and hygiene standards. This work presents the design and implementation of an autonomous swimming pool cleaning robot, integrating multiple functional units: Power, sensor, wireless communication, motor, and water quality monitoring. After the power is on, the robot starts calibrating its sensors and establishes a connection with a remote human-machine interface to transmit the initial operational status. By utilizing advanced image processing algorithms, specifically color moments, the robot identifies and classifies floating debris while continuously monitoring water quality parameters. When debris is detected, the robot calculates its trajectory based on X and Y coordinates, adjusting its movement accordingly to collect the debris with a salvage net. It incorporates ultrasonic sensors for obstacle detection, employing a threshold-based avoidance algorithm to navigate around obstacles effectively. The cleaning process is repeated until the pool is cleared, after which the robot returns to its charging station, powering down non-essential systems in preparation for the next cycle. This study highlights the efficiency and effectiveness of robotic automation in pool maintenance, demonstrating significant advancements in the integration of robotics, sensor technology, and real-time data communication. The findings contribute valuable insights into future developments in robotic cleaning systems and their applications in various environments.

Keywords: Robotic pool cleaning; Autonomous maintenance; Obstacle handling; Battery optimization; Underwater visibility; Environmental factors; IoT integration; Real-time monitoring

1. Introduction

Swimming is a physical activity with numerous health benefits. It is an excellent full-body workout that can improve cardiovascular health, muscle strength, flexibility, and endurance. Swimming is also low-impact, making it suitable for people of all ages and fitness levels.[1] One of the significant advantages of swimming is its positive impact on mental health. Studies have shown that swimming can reduce symptoms of anxiety and depression by promoting the release of mood-enhancing endorphins Cox *et al*.[2] In addition, the rhythmic nature of swimming can induce a meditative state, helping to reduce stress, Halliwell and Grogan.[3] Swimming is also a crucial life skill. According to the World Health Organization,[4] drowning is one of the leading causes of accidental death worldwide, particularly among children. Learning to swim can significantly reduce the risk of swimming-related fatality risk, as it equips individuals with essential skills to stay safe in and around water.

If not properly maintained, swimming pools may pose health risks to the users. One significant concern is the risk of waterborne infections, which can occur due to pathogens such as *Cryptosporidium*, *Escherichia coli*, and *Legionella*. These pathogens can lead to gastrointestinal illnesses, skin infections, or respiratory issues, particularly in poorly disinfected pools.[5] Chlorine is a common disinfectant used to reduce microbial contamination, but its usage necessitates proper management as high levels of chlorine and chloramines can cause respiratory irritation and eye irritation and exacerbate conditions such as asthma.[6] In addition to chemical exposure, swimmer's ear (otitis externa) is a common issue that results from water trapped in the ear canal, which promotes bacterial growth and infection.[7] Another risk is skin irritation or rashes, which can develop from prolonged exposure to pool chemicals or from certain microbes present in inadequately treated pools.

Several functional issues of the swimming pools may occasionally limit their usability and diminish users' satisfaction. Some of these common problems include ineffective circulation systems, inadequate water filtration, and poor temperature regulation, all of which can affect pool cleanliness and comfort. Inefficient circulation systems can lead to uneven chemical distribution, resulting in certain areas of the pool becoming a hotspot for bacteria or algae growth, while inadequate filtration allows for the accumulation of debris and contaminants, making the pool unpleasant or unsafe to use.[8] In addition, pools without proper temperature control may make the water either too cold or too warm, deterring usage and creating potential safety risks, especially for young children and the elderly.[9]

Swimming pool robots, developed to automate pool maintenance and improve efficiency, have undergone significant advancements since their inception in the early 1980s. The first-generation pool robots primarily relied on basic suction technology and required manual control. With the advancements in technology, however, the 1990s saw the introduction of more sophisticated models with enhanced navigation capabilities that enable autonomous cleaning of pool floors and walls.

Swimming pool maintenance robots are autonomous devices Lee[10] that efficiently clean and maintain pool surfaces, reducing the need for manual effort. These robots are equipped with motors, wheels or tracks, and advanced sensors that allow them to navigate the pool floor and walls while avoiding obstacles. They use suction mechanisms to collect debris, which is trapped in filters, and many models also feature rotating brushes that scrub the pool surfaces to loosen dirt and algae. These robots feature straightforward operation: Users can plug the device in or utilize models with built-in batteries, place it in the pool, and set automated cleaning cycles. Some models even allow for remote or app-based control, enabling customization of cleaning modes and schedules. As the robot moves across the pool, it vacuums debris while its filtration system ensures that only clean water is returned to the pool. After each cycle, the filter can be easily removed, emptied, and rinsed in a bid to simplify the maintenance process. These robots are energy-efficient and time-saving and often complete the cleaning task better than traditional methods, making them an ideal solution for pool owners looking for convenience and enhanced pool hygiene. In recent years, advancements in sensors, artificial intelligence (AI), and battery technology have enabled pool robots to become more efficient, energy-saving, and user-friendly. Today, features such as Wi-Fi connectivity and app-based controls are incorporated, allowing users to remotely operate and monitor their devices for optimal convenience.[11]

Topouzelis *et al.*[12] developed an autonomous transportation robot boat utilizing an unmanned surface vehicle (USV) for autonomous navigation on urban waterways. This invention, designed to facilitate transportation, features a modified structure that enhances portability. Similarly, Compa *et al.*[13] introduced a USV tailored for hydrographic surveys,

particularly effective for surveying and creating charts in near-shore shallow waters.

Traditional swimming pool maintenance predominantly relies on human labor, which, despite being effective, presents several challenges. Manual cleaning is labor-intensive, time-consuming, and inconsistent, as its effectiveness depends on human skill, availability, and fatigue. In addition, human-based cleaning often follows scheduled intervals (weekly or monthly), leading to potential lapses in hygiene between sessions. Pool maintenance personnel are also exposed to harmful chemicals, such as chlorine, which can cause respiratory and skin irritation over time.

In contrast, robotic pool cleaners offer numerous advantages. They provide higher efficiency by operating continuously or on demand, ensuring immediate removal of debris and contaminants. Unlike human cleaners, robotic systems execute predefined cleaning patterns with greater consistency, covering the entire pool uniformly while avoiding human error. These robots also contribute to safety improvements, as they eliminate the need for human workers to be in direct contact with pool chemicals and contaminated water. Moreover, robotic pool cleaners optimize energy and water consumption, reducing operational costs compared to traditional maintenance methods. A detailed comparison of these factors is crucial to highlight the long-term benefits of robotic solutions in swimming pool maintenance.

Most currently available robotic pool cleaner systems in the market rely on predefined path planning and basic suction mechanisms to operate. This work introduces an advanced robotic cleaner that integrates real-time debris classification using color moments, AI-enhanced navigation, and water quality monitoring. By incorporating ultrasonic-based obstacle avoidance and an Internet of Things (IoT)-enabled remote monitoring system, the proposed design offers a more adaptive and efficient cleaning solution. This article provides a detailed exploration of a swimming pool maintenance robot designed for detecting and cleaning pool surfaces while also assessing the chemical quality of the water to help prevent diseases among users. The structure of the article includes a survey of existing robotic technologies in Section 2, followed by a comprehensive description of the proposed swimming pool cleaning robot in Section 3. Section 4 illustrates the functionality of the algorithm employed in the robot, and the article concludes with a summary of the findings in Section 5.

2. Literature survey

This section reviews AI technology adopting modern algorithms such as machine learning, USV, Programmable Logic Controller (PLC), Vector Field Histogram (VFH), and Autonomous Surface Vehicle (ASV). For making a variety of robotic mechanisms to achieve water cleaning and maintenance. Table 1 summarizes various techniques for water monitoring and waste management, highlighting their merits, demerits, and potential future enhancements. Each entry provides insights into different robotic systems and technologies designed for specific applications, such as autonomous navigation, environmental monitoring, and waste collection.

Hasany *et al.*[14] developed an autonomous water surface-cleaning robot using USV technology with navigation capabilities. This robot is designed to autonomously clean small water bodies by collecting debris and garbage. It has the merit of being able to navigate and operate independently in small water environments. However, it has some limitations, such as a restricted operating time and a limited garbage-holding capacity. In addition, the robot's effectiveness has only been evaluated in smaller water bodies. Future enhancements could focus on extending battery life, increasing garbage capacity, and improving adaptability to larger water bodies. Chang *et al.*[15] introduced a water surface cleaning robot that also checks water quality, utilizing USV technology but without a mechanical design. This robot is capable of simultaneously cleaning the water surface and monitoring water quality. Its simplified design, which lacks mechanical components, is an advantage. However, the robot has limitations in terms of automation and path planning, making it less effective in complex environments. Future enhancements could include improving automation, refining path planning capabilities, and increasing adaptability for operation in a variety of environments.

Chen *et al.*[16] developed a semi-automatic drainage water cleaner that utilizes a mechanical cleaning mechanism controlled by a PLC. This device reduces the need for manual labor and minimizes the risks associated with cleaning hazardous drainage pipes by limiting human exposure to toxic gases. Although it provides significant safety benefits, the system is only semi-automatic. Future improvements could focus on achieving full automation and incorporating advanced sensors to detect hazardous gases, enhancing safety and efficiency. Jeon *et al.*[17] developed an automated sewage wastewater treatment system that utilizes a Siemens

Table 1. Summary of water cleaning methods

Authors	Invention	Technology used	Impact	Merits	Demerits	Future enhancement
Hasany *et al*.[14]	Autonomous water surface cleaning robot	USV with navigation	Cleans small water bodies autonomously	Autonomous navigation for small water bodies	Limited operating time, small garbage capacity, only able to navigate and evaluate small water bodies	Improve battery life, garbage capacity, and adaptability to larger water bodies
Chang *et al*.[15]	Water surface cleaning and water quality check robot	USV without mechanical design	Capable of checking water quality while cleaning	Simplified design without mechanical parts	Limited automation and path planning; challenges in adapting to complex environments	Enhanced automation, path planning, and adaptability to diverse environments
Chen *et al*.[16]	Semi-automatic drainage water cleaner	Mechanical cleaner with PLC controller	Reduces manual effort and risk in cleaning hazardous drainage pipes	Reduces human exposure to toxic gases	Semi-automatic, not fully autonomous	Full automation and advanced sensors for hazardous gas detection
Jeon *et al*.[17]	Automated sewage wastewater treatment system	Siemens PLC controller for various controls	Automates sewage water treatment and minimizes human labor in hazardous conditions	Cost-effective and efficient; reduces the risk of human loss	Potential for improved automation and efficiency	Integration of AI for real-time monitoring and control
Li *et al*.[18]	Watercolor isolated perception-oriented USV	ASV, data collection modules	Self-governing pathfinding, water quality measurement, weather monitoring, remote control	Multifunctional, robust water monitoring capabilities	Potential for limited coverage area based on battery life and module capabilities	Broader environmental monitoring and enhanced obstacle avoidance
Ferri *et al*.[19]	ASV for hydrocarbon and heavy metal measurement	ASV with miniaturized sensors, VFH+ML for collision avoidance	Measures hydrocarbon and heavy metal concentration	Small size, collision avoidance capabilities	May be limited in harsh conditions, requiring frequent sensor maintenance	Incorporating advanced machine learning for improved collision prediction
Madeo *et al*.[20]	Water environmental mobile observer	USV with sensors for salinity, oxygen, pH, etc.	Tracks various environmental parameters in water bodies	Versatile in monitoring different environmental parameters	Limited in scope for specific water parameters	Improved parameter detection and adaptability to different water bodies

(*Contd*...)

Table 1. (*Continued*)

Authors	Invention	Technology used	Impact	Merits	Demerits	Future enhancement
Cao *et al*.[21]	Intelligent USV for water quality monitoring	Autonomous system for monitoring turbidity, solids, and pH	Effective in shallow water environments, autonomous monitoring	High-resolution measurements, adaptive to coastal habitats	Limited to shallow waters; potential navigation issues in complex environments	Improved adaptability to diverse environments, expanded parameter monitoring
Kong *et al*.[22]	Smart water waste scrubbing robot system	Image module, motion control, YOLOv3 for trash detection	Efficiently detects and scrubs floating waste from water surfaces	Effective trash detection with YOLOv3; capable of real-time image processing	Limited in adaptability to diverse trash types and sizes	Integrating AI for distinguishing different types of waste
Ruangpayoongsak *et al*.[23]	Floating garbage scooper robot	Floating robot with trash collection capabilities	Efficient for collecting specific types of waste such as plastic bottles	Simple design, effective for small trash	Limited to specific trash types, not capable of handling submerged waste	Adaptability to handle a broader range of waste types
Cryer *et al*.[24]	ASV for coastal habitat monitoring	Sensors for conductivity, temperature, nitrate, etc.	Extends time-based and space-based water quality monitoring	Comprehensive water quality analysis in coastal habitats	Limited by proximity and sensor durability	Enhanced sensor durability and expanded coverage area

Abbreviations: AI: Artificial intelligence; ASV: Autonomous surface vehicle; ML: Machine learning; PLC: Programmable logic controller; VFH: Vector field histogram; USV: Unmanned surface vehicle.

PLC to manage various control functions. This system automates the treatment process, significantly reducing the need for human labor in potentially hazardous conditions. It is both cost-effective and efficient, offering substantial safety benefits by minimizing human exposure to risks. However, there is still room for improvement in terms of automation and efficiency. Future enhancements could include the integration of AI for real-time monitoring and control, which would further optimize the system's performance and responsiveness.

Li *et al.*[18] designed a Water Color Isolated Perception-Oriented USV equipped with autonomous navigation and data collection modules, which is capable of self-governing path searching, measuring water quality, monitoring weather conditions, and being remotely controlled. Its multifunctional design provides robust capabilities for comprehensive water monitoring. However, the system may face limitations in the coverage area due to constraints related to battery life and the capabilities of the data collection modules. Future enhancements could focus on expanding its use for broader environmental monitoring and improving obstacle avoidance to enhance operational efficiency and range. Ferri *et al.*[19] developed an ASV equipped with miniaturized sensors for measuring hydrocarbon and heavy metal concentrations in water. This ASV employs a VFH combined with machine learning for collision avoidance, enabling it to navigate effectively while collecting environmental data. The system's compact size and collision avoidance capabilities are key advantages. However, the ASV may be limited in harsh environmental conditions that would require frequent sensor maintenance. Future enhancements could include the integration of advanced machine learning algorithms to improve collision prediction and further enhance navigation accuracy.

Madeo *et al.*[20] developed a Water Environmental Mobile Observer, a USV equipped with sensors that measure various parameters, including salinity, oxygen, and pH levels. This USV is designed to monitor a range of environmental factors in water bodies,

providing versatile and comprehensive data collection capabilities. However, it may be limited in its scope, as it is optimized for specific water parameters. Future enhancements could focus on expanding the range of detectable parameters and adapting the system to function effectively across diverse water bodies for broader environmental monitoring. Cao *et al.*[21] developed an intelligent USV designed for water quality monitoring, specifically measuring parameters like turbidity, suspended solids, and pH levels. This autonomous system operates effectively in shallow water environments and provides high-resolution measurements, making it well-suited for coastal habitat monitoring. While it offers precise and adaptive monitoring, it is primarily limited to shallow waters and may encounter navigation challenges in more complex environments. Future improvements could focus on enhancing the system's adaptability to a wider range of environments and expanding its capabilities to monitor additional water quality parameters.

Kong *et al.*[22] introduced a smart water waste-scrubbing robot system that utilizes an image module, motion control, and YOLOv3 for trash detection. This system is highly effective at detecting and scrubbing floating waste from water surfaces, benefiting from YOLOv3's real-time image processing capabilities. While it excels in detecting trash efficiently, it may have limitations in adapting to diverse types and sizes of waste. Future enhancements could integrate AI for distinguishing between different types of waste and improve the robot's adaptability and effectiveness in various cleaning scenarios. Ruangpayoongsak *et al.*[23] developed a floating garbage scooper robot designed specifically for collecting certain types of waste, such as plastic bottles. This robot features a simple design and is effective for efficiently collecting small trash items from the water surface. However, it is limited to specific types of waste and may struggle to handle submerged debris. Future enhancements could focus on adapting the robot to manage a broader range of waste types, thereby improving its overall efficiency and effectiveness in cleaning various water environments. Cryer *et al.*[24] developed an ASV specifically for coastal habitat monitoring, equipped with sensors that measure conductivity, temperature, nitrate levels, and other key water quality parameters. This ASV enhances both time-based and space-based water quality monitoring, enabling comprehensive analysis of aquatic environments in coastal areas. However, its effectiveness is limited by the proximity of the sensors to the water body and concerns regarding sensor durability over time. Future improvements could focus on enhancing sensor durability and expanding the vehicle's coverage area to enable more extensive monitoring of coastal habitats.

Table 1 summarizes various robotic systems developed for water monitoring and waste management, highlighting their techniques, merits, demerits, and suggested future enhancements. Various methods exist for maintaining water bodies, including autonomous cleaning robots known for efficient navigation but limited by operating time and capacity, dual-function robots for cleaning and water quality monitoring, and semi-automatic drainage cleaners with potential AI enhancements for gas detection. In addition, automated sewage treatment systems could incorporate AI for real-time monitoring, while multifunctional USVs support environmental monitoring. ASVs aid in hydrocarbon measurement, and specialized robots, such as waste-scrubbing and garbage-scooping robots, improve trash detection and removal of object or particles. Overall, the table highlights the strengths and weaknesses of each system while suggesting future improvements to enhance efficiency and effectiveness in their respective applications.

Separately, this article presents a robot designed to effectively clean swimming pools while also monitoring water quality, addressing the health concerns associated with inadequate hygiene standards in pool environments. The proposed solution aims to enhance pool maintenance and ensure a safer swimming experience for users.

3. Proposed swimming pool robot

The motive of this study lies in our belief that proper maintenance of swimming pool cleanliness helps prevent diseases. Through a literature survey, we identified several modern technical components that could support the development of an AI robot designed to detect waste in swimming pools and assess water quality. The proposed swimming pool robot is engineered to enhance pool maintenance through effective cleaning and water quality monitoring, addressing concerns about hygiene standards. The proposed design of the robot, illustrated in Figure 1, includes several functional modules that outline the sequence of operations. Each and every functionality of the robot is designated as a unit, with specific components responsible for ensuring effective operation.

The proposed robot consists of five units: The power unit, sensor unit, wireless unit, motor unit, and water

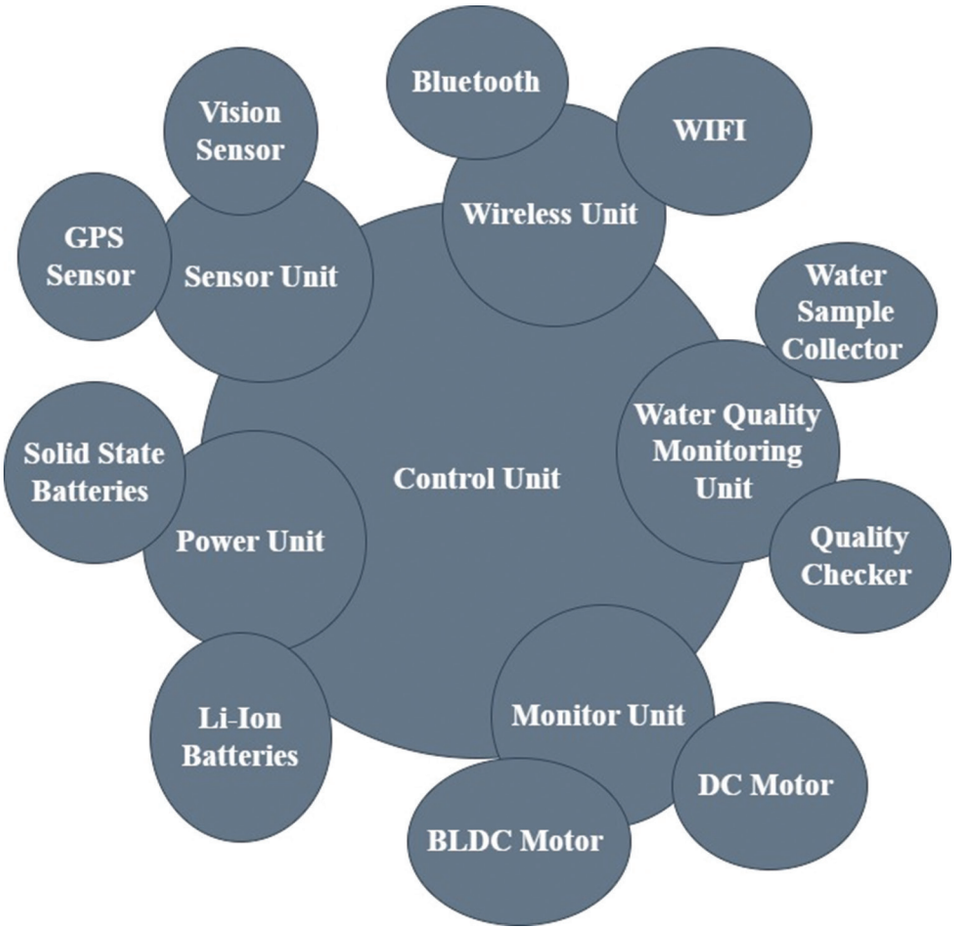

Figure 1. Swimming pool robot functional units
Abbreviations: BLDC: Brushless direct current motor; DC: Direct current; GPS: Global Positioning System.

quality monitoring unit. The power unit is essential for the robot's functionality, as it must operate both inside and outside the swimming pool. Therefore, a water-resistant power unit is selected. Solid-state and lithium-ion batteries are recommended due to their waterproofing capabilities. Regardless of the battery type, it is crucial to ensure that it is adequately sealed or housed in a waterproof compartment to prevent damage attributed to water exposure. In addition, weight considerations are important; for smaller aquatic vehicles, lightweight options such as lithium-ion or lithium-polymer batteries are prioritized. Finally, implementing battery management systems is essential to monitor battery health and prevent overcharging, especially for lithium-based batteries.

The sensor unit has two kinds of sensors: a GPS sensor that defines the boundary of the swimming pool and a vision sensor that identifies the objects in the pool. A high-resolution vision sensor and water surface cleaning equipment are packed inside the robot cleaning machine. In this case, the Pixy CMU Cam5 vision sensor is utilized. This sensor features a dual-core ARM Cortex-A72 processor capable of operating at a frequency of 1.5 GHz, which is widely used in DIY robotics, home automation, and research projects involving image processing. It also includes a unidirectional image sensor, 128k RAM, 2 MB flash memory, and various communication interfaces such as CAN, RS-232, UART, SPI, I2C, and USB. The vision sensor employs color moments[24] because this algorithm is useful in recognizing objects and classifying tasks to detect objects, specifically using a method known as the color-connected components algorithm. This algorithm was implemented on the ARM Cortex-A72 processor using JAVA. The color moments algorithm operates with high speed, efficiency, and reliability. In this context, statistical measures of color distribution were used in an image for filtering. The algorithm calculates the first

three moments (mean, variance, and skewness) of the color channels. These moments were used to classify and filter regions based on their color characteristics. These color pixels are derived from the image sensor and represent the primary parameters for color filtering. In general, the color of an object remains unchanged unless exposed to strong lighting conditions.

The integration of Wi-Fi and wireless communication units in swimming pool cleaning robots significantly enhances their functionality and user experience. These technologies allow users to remotely control and monitor the robot through a smartphone app, providing real-time feedback on performance, battery status, and maintenance needs. In addition, the wireless units facilitate the robot's connection to smart home systems, enabling voice control and automation as part of a broader home ecosystem. Enhanced navigation features supported by WiFi allow for efficient mapping of the pool area, optimizing cleaning paths and algorithms. Moreover, WiFi connectivity enables over-the-air software updates, ensuring that the robot benefits from the latest features and improvements. Overall, these advancements lead to greater convenience and efficiency in pool maintenance, making modern cleaning robots more user-friendly and effective in maintaining swimming pool cleanliness.

For assessing water quality in a swimming pool, various methods can be employed to monitor key parameters such as pH levels, chlorine concentration, and alkalinity. One common approach is using chemical testing kits, which involve reagents that react with the pool water to produce colorimetric results. Users can also opt for digital testers that provide precise measurements for various water quality indicators. For consistent monitoring, automated water quality systems can be installed to measure and transmit data in real time, alerting owners when parameters fall outside acceptable ranges. In addition, regular visual inspections can help assess clarity, while laboratory testing offers a more comprehensive analysis of contaminants. Maintaining water quality involves consistent testing and regular maintenance, which includes balancing chemicals and cleaning the pool. Resources such as the Centers for Disease Control and Prevention and Swim Art provide detailed guidance on the best practices for ensuring safe and clean swimming pool water.

Equipping a swimming pool cleaning robot with a water quality monitoring function significantly enhances its functionality and efficiency. This can be achieved by integrating sensors into the robot to measure key parameters such as pH, chlorine levels, and turbidity, allowing for real-time monitoring as the robot cleans. A wireless communication unit can transmit this data to a user interface, such as a Smartphone app, enabling users to monitor water quality remotely and receive alerts when parameters deviate from acceptable ranges. In addition, the integration of a microcontroller can process the sensor data to generate automated reports, tracking water quality trends over time. The robot can also optimize its cleaning paths based on sensor data, spending more time in areas that require additional attention. User interaction features allow for personalized maintenance strategies, enabling users to set desired water quality parameters and adjust cleaning schedules accordingly. Overall, this integration transforms the robot from a mere cleaning device into an intelligent water quality management system, promoting healthier swimming conditions and making pool maintenance more efficient.

The water surface cleaning system is equipped with two direct current and brushless direct current motor gear motors and salvage nets designed for collecting floating debris. The salvage net can be raised and lowered using bobbins, while the motors are controlled by a motor-driving module interfaced with an Arduino microcontroller. A vision sensor detects floating waste, specifically identifying objects as trash. This sensor is mounted on the front of the cleaning device, which employs an effective water surface cleaning algorithm to automatically track and collect waste. The device captures images in a coordinate system defined by ranges X (0-319) and Y (0-199). The direction of movement is determined by the X coordinates, allowing the robot to turn in various directions based on detected waste.

The control system of the USV consists of two Arduino microcontrollers operating at 16 MHz; one manages steering and obstacle avoidance, whereas the other handles navigation. The USV includes various modules directly connected to the control unit, including motion and water waste scrubbing modules. A GPS module is integrated for navigation, providing real-time coordinates for water sampling points. The USV is also equipped with ultrasonic sensors for obstacle detection, employing a threshold-based algorithm for collision avoidance. The vehicle uses a 6V battery and communicates with a remote human-machine interface via Bluetooth, allowing for the monitoring and control of its functions. This interface displays critical data such as trip time and movement trajectory, facilitating real-time updates and manual control options for the operator.

4. Swimming pool cleaning robot algorithm

The operational process of the swimming pool robot given in algorithm I, which begin with powering on the system and calibrating all sensors to ensure they function correctly.[20,25] It establishes a connection with a remote human-machine interface through the wireless unit to transmit initial status updates. The robot continuously monitors water quality parameters using its dedicated unit, sending alerts to the interface if any readings exceed acceptable limits. It then activates the sensor unit to scan the pool surface for floating debris, employing image processing algorithms such as color moments for identification and classification. Based on the sensor data, the robot determines the location and type of debris and calculates the trajectory toward it using X and Y coordinates. The motor unit adjusts its movement accordingly – turning left or right depending on the debris's position or moving straight ahead if the debris is directly in front. Once the debris is reached, the robot lowers its salvage net to collect it and then raises the net to return to its cleaning path. Throughout the operation, ultrasonic sensors detect obstacles, triggering a threshold-based avoidance algorithm that directs the robot to turn or reverse as necessary. The robot repeats the debris detection and cleaning cycle while continuously monitoring water quality. After completing the cleaning tasks, it returns to the charging station, powers down non-essential systems, and prepares for the next operational cycle.

This algorithm provides a structured approach to designing the swimming pool robot, enabling it to efficiently monitor and maintain water cleanliness while ensuring user safety through real-time communication and obstacle avoidance.

Algorithm I. Algorithm for swimming pool robot design

a. Power on the robot, calibrate sensors, and ensure all components are functioning correctly
b. Establish a connection with the remote human-machine interface using the wireless unit and transmit the initial status to the interface
c. Continuously measure water quality parameters using the water quality monitoring unit. If parameters exceed acceptable limits, send an alert to the human-machine interface
d. Activate the sensor unit to scan the pool surface for floating debris and use image processing algorithms (color moment) to identify and classify debris
e. Based on sensor data, determine the location and type of debris
f. If debris is detected, calculate the trajectory toward it using X and Y coordinates
g. Adjust the motor unit's movement accordingly:
  i. If debris is on the left, turn left (e.g., 30° or 15°)
  ii. If debris is straight ahead, move forward
  iii. If debris is on the right, turn right (e.g., 30° or 15°).
h. Lower the salvage net and use the motor unit to collect the identified debris
i. Raise the net once the debris is captured and return to the cleaning path
j. Utilize ultrasonic sensors to detect obstacles in the robot's path
k. Implement a threshold-based avoidance algorithm:
  i. If an obstacle is detected on the left, turn right
  ii. If an obstacle is detected on the right, turn left
  iii. If an obstacle is directly ahead, reverse or turn around.
l. Repeat the debris detection and cleaning process
m. Continuously monitor water quality throughout the operation
n. Once cleaning is completed, return to the charging station
o. Power down non-essential systems and prepare for the next operation cycle.

4.1. Comparison with manual cleaning

Robotic cleaning offers several advantages over traditional manual maintenance, which relies on human labor and comes with challenges such as being labor-intensive, time-consuming, and inconsistent due to variations in skill, availability, and fatigue.[10] In addition, manual cleaning is typically performed at scheduled intervals, such as weekly or monthly, which can result in lapses in hygiene between sessions.[9] In contrast, robotic cleaning systems provide enhanced efficiency by operating continuously or on demand, ensuring immediate removal of debris and contaminants.[11] They also offer greater consistency, as robots follow predefined algorithms and cleaning patterns, covering the entire pool area uniformly without missing spots.[12] Another significant advantage is safety, as pool maintenance personnel are often exposed to chlorine and cleaning chemicals that may cause respiratory and skin issues, a risk that can be eliminated through automation.[6] Furthermore, modern robotic systems are designed for energy and resource optimization, reducing operational costs compared to employing human workers for frequent clean-ups.[19] Thus, robotic cleaning systems present a more efficient, reliable, and cost-effective solution for maintaining swimming pool hygiene.

4.2. Explicit problem statement

Maintaining swimming pools presents significant hygiene challenges if not managed properly. One

major issue is the accumulation of debris, including leaves, insects, and dirt, which not only compromises water quality but can also clog filtration systems.[25] In addition, inadequate cleaning can lead to the proliferation of waterborne diseases, as bacteria such as *E. coli* and *Legionella*, along with parasites such as *Cryptosporidium*, pose serious infection risks.[5] Traditional manual cleaning methods further contribute to inefficiencies, as they rely on human intervention, which can be inconsistent due to time constraints, human error, and resource limitations.[17] Another challenge is maintaining proper chemical balance because incorrect chlorine levels can cause skin irritation or allow bacterial growth, requiring constant monitoring.[4]

To address these challenges, the proposed autonomous robot offers a systematic and real-time solution. It continuously scans the pool for debris, adjusts its movement accordingly, and monitors water quality parameters.[21] Unlike manual methods that follow scheduled cleaning routines, this robotic system ensures proactive rather than reactive maintenance, resulting in a consistently clean and hygienic swimming environment.

4.3. Technical depth on navigation and control

The robot's navigation system is designed using a combination of sensor fusion and autonomous decision-making algorithms to ensure precise movement and obstacle avoidance. To achieve accurate localization, the system integrates Kalman filtering, which processes noisy GPS and vision sensor data, enhancing positional accuracy.[18] For obstacle avoidance, the potential field method is employed, where obstacles are modeled as repelling forces while the target cleaning area acts as an attractive force, allowing the robot to dynamically adjust its path.[20] In addition, if required, the *A search algorithm** can be used for path optimization, ensuring the most efficient route for systematic cleaning.[23] To enhance debris detection, the robot utilizes image processing techniques, specifically the color moments algorithm, which extracts statistical features such as mean, variance, and skewness from images to identify and classify floating debris in real time.[24] For improved classification accuracy, a machine learning model could be incorporated to differentiate between various debris types.[22] These advanced navigation and control techniques enable the robot to operate autonomously while adapting to dynamic environments, ensuring efficient and effective cleaning in diverse pool settings.

4.4. Cost analysis of robotic versus manual maintenance

The adoption of autonomous robots for pool maintenance marks a transition from labor-intensive to technology-driven cleaning. A cost comparison highlights the financial advantages of robotic cleaning over traditional manual methods.[26] While manual cleaning requires a low initial investment in hiring personnel, it incurs high recurring costs due to wages and potential health risks from chemical exposure. In contrast, robotic cleaning involves a higher upfront cost but significantly lower recurring expenses, limited to periodic maintenance and energy consumption. In addition, robotic systems operate continuously or on demand, ensuring superior consistency through predefined cleaning patterns, whereas manual cleaning is typically performed weekly or monthly and is prone to human error and fatigue.

4.5. Break-even analysis

Despite the higher initial investment, the long-term savings from robotic pool cleaners outweigh the costs associated with manual labor.[23] Autonomous systems reduce chemical usage, minimize filtration system wear, and require minimal human intervention, leading to enhanced cost efficiency. A case study comparing traditional maintenance expenses with robotic operations over multiple years could provide concrete evidence of the financial benefits of automation in pool cleaning.

Factor	Manual cleaning	Robotic cleaning
Initial investment	Low (hiring costs)	High (robot purchase)
Recurring costs	High (wages, chemical exposure)	Low (periodic maintenance, energy use)
Cleaning frequency	Weekly/Monthly	Continuous/ On-demand
Consistency	Variable (human error, fatigue)	High (predefined cleaning pattern)
Long-term savings	Low (ongoing wages)	High (one-time investment, minimal upkeep)

4.6. Deployment challenges and mitigation strategies

While robotic swimming pool cleaners offer significant advantages, their deployment presents several challenges that must be addressed for optimal performance and widespread adoption. One major technical limitation is battery life, as limited operational time necessitates

optimized power management to extend cleaning cycles.[27] In addition, obstacle handling remains a challenge, as floating debris moves unpredictably, requiring adaptive navigation strategies.[25] Another issue is underwater visibility, as high water turbidity can interfere with image recognition and debris detection, reducing cleaning efficiency.[28]

Environmental factors also impact robotic cleaning performance. An adaptable navigation feature tailored to various pool sizes and shapes is required to ensure thorough coverage.[1] Furthermore, weather conditions, especially in outdoor pools, introduce wind-driven debris that may affect cleaning effectiveness.[5]

User acceptance is another critical factor in the adoption of robotic cleaners. The high initial investment may deter potential users despite long-term cost savings.[15] In addition, the technical complexity of setup and maintenance may discourage users unfamiliar with automated systems.[5]

To overcome these challenges, future enhancements could include AI-powered debris classification, allowing the robot to identify and selectively remove different types of waste. IoT integration could enable smart pool management with real-time alerts and automated water quality adjustments. In addition, incorporating solar charging capabilities would enable sustainable operation, reducing dependence on external power sources. Addressing these challenges and implementing such advancements will ensure broader adoption and long-term efficiency of robotic pool cleaning systems.

5. Conclusion

This paper presents the design and implementation of a swimming pool cleaning robot equipped with a sophisticated integration of various units, including power, sensor, wireless, motor, and water quality monitoring systems. The robot effectively utilizes advanced algorithms for debris detection and obstacle avoidance, ensuring efficient cleaning operations while maintaining water quality. By employing image processing techniques and real-time data communication with a remote human–machine interface, the robot enhances operational efficiency and user interaction. Continuous monitoring and responsive actions enable the robot to adapt to changing environments, making it a valuable tool for maintaining clean swimming pool conditions. Overall, this work underscores the potential of robotic systems in automating pool maintenance tasks, leading to improved cleanliness and safety for users while also contributing to advancements in robotics and sensor technology. Further research could explore enhancements in navigation algorithms and the integration of more advanced machine learning techniques for even greater efficiency and adaptability. Future work will focus on the development of a functional prototype to validate the proposed design. Experimental evaluation will assess cleaning efficiency, navigation accuracy, and real-time water quality monitoring under varying environmental conditions.

Acknowledgments

None.

Funding

None.

Conflict of interest

All the authors declare they have no competing interests.

Author contributions

Conceptualization: Hemalatha Senthilmahesh
Data curation: Kiran Mayee Adavala
Investigation: Hemalatha Senthilmahesh
Methodology: Hemalatha Senthilmahesh
Resources: Thilagam Thangamariappan
Validation: Pullela S.V.V.S.R. Kumar
Visualization: Ramesh Tumaati
Writing–original draft: Hemalatha Senthilmahesh
Writing–review & editing: Muthuvairavan Pillai Nagappan

Availability of data

Not applicable.

References

1. American Heart Association. *Benefits of Swimming*; 2021. Available from: https://www.heart.org/en/healthy-living/fitness/fitness-basics/swimming [Last accessed on 2025 Mar 04].
2. Cox C, Fitzgerald A, Williams D. The impact of swimming on mental health: A systematic review. *J Health Psychol*. 2019;24(6):787-795. doi: 10.1177/1359105317718921
3. Halliwell E, Grogan S. Swimming and mental well-being: A phenomenological study. *Psychol Sport Exerc*. 2017;31:1-9.

doi: 10.1016/j.psychsport.2017.03.001
4. World Health Organization. *Drowning*; 2020. Available from: https://www.who.int/news-room/fact-sheets/detail/drowning [Last accessed on 2025 Mar 04].
5. Centers for Disease Control and Prevention. *Healthy Swimming: Pool-Related Illnesses and Injuries*; 2022. Available from: https://www.cdc.gov/healthywater/swimming/swimmers/rwi.html [Last accessed on 2025 Mar 04].
6. Environmental Protection Agency. *Swimming Pool Chemicals and Health Risks*; 2019. Available from: https://www.epa.gov/chemical-research/swimming-pool-chemicals-and-health-risks [Last accessed on 2025 Mar 04].
7. Mayo Clinic. *Swimmer's Ear: Causes, Symptoms, and Treatment*; 2021. Available from: https://www.mayoclinic.org/diseases-conditions/swimmers-ear/symptoms-causes/syc-20351682 [Last accessed on 2025 Mar 04].
8. American Society of Civil Engineers. *Swimming Pool Functionality and Maintenance: Best Practices for Optimal Operation*; 2021. Available from: https://www.asce.org/publications/swimming-pool-functionality [Last accessed on 2025 Mar 04].
9. National Swimming Pool Foundation. *Swimming Pool and Spa Operations: Addressing Common Challenges*; 2018. Available from: https://www.nspf.org/resources/swimming-pool-spa-operations [Last accessed on 2025 Mar 04].
10. Lee J. *The ultimate Guide to Swimming Pool Maintenance Robots: Benefits and How They Work*; 2022. Available from: https://www.pooltechjournal.com/swimming-pool-maintenance-robots [Last accessed on 2024 Oct 12.
11. Pool and Spa News. *Evolution of Swimming Pool Robots: From Basic Suction to Intelligent Navigation*; 2023. Available from: https://www.poolspanews.com/technology/evolution-of-swimming-pool-robots [Last accessed on 2025 Mar 04].
12. Topouzelis K, Papakonstantinou A, Garaba SP. Detection of floating plastics from satellite and unmanned aerial systems (Plastic Litter Project). *Int J Appl Earth Obs Geoinf*. 2019;79:175-183.
doi: 10.1016/j.jag.2019.03.011
13. Compa M, March D, Deudero S. Spatio-temporal monitoring of coastal floating marine debris in the Balearic Islands from sea-cleaning boats. *Mar Pollut Bull*. 2019;141:205-214.
doi: 10.1016/j.marpolbul.2019.02.050
14. Hasany SN, Zaidi SS, Sohail SA, Farhan M. An Autonomous Robotic System for Collecting Garbage Over Small Water Bodies. In: *Proceedings of the 2021 6th International Conference on Automation, Control and Robotics Engineering (CACRE)*, Dalian, China; 2021. p. 81-86.
15. Chang HC, Hsu YL, Hung SS, Ou GR, Wu JR, Hsu C. Autonomous water quality monitoring and water surface cleaning for unmanned surface vehicles. *Sensors (Basel)*. 2021;21(4):1102.
doi: 10.3390/s21041102
16. Chen J, Du C, Zhang Y, Han P, Wei W. A clustering-based coverage path planning method for autonomous heterogeneous UAVs. *IEEE Trans Intell Transp Syst.* 2021;99:1-11.
doi: 10.1109/TITS.2021.3066240
17. Jeon CW, Kim HJ, Yun C, Han X, Kim JH. Design and validation testing of a complete paddy field-coverage path planner for a fully autonomous tillage tractor. *Biosyst Eng*. 2021;208:79-97.
doi: 10.1016/j.biosystemseng.2021.05.005
18. Li Y, Tian L, Li W, *et al*. Design and experiments of a water color remote sensing-oriented unmanned surface vehicle. *Sensors (Basel)*. 2020;20(7):2183.
doi: 10.3390/s20072183
19. Ferri G, Manzi A, Fornai F, Ciuchi F, Laschi C. The HydroNet ASV, a small-sized autonomous catamaran for real-time monitoring of water quality: From design to missions at sea. *IEEE J Ocean Eng*. 2015;40(3):710-726.
doi: 10.1109/JOE.2014.2362392
20. Madeo D, Pozzebon A, Mocenni C, Bertoni D. A low-cost unmanned surface vehicle for pervasive water quality monitoring. *IEEE Trans Instrum Meas*. 2020;69(4):1433-1444.
doi: 10.1109/TIM.2019.2963515
21. Cao H, Guo Z, Wang S, Cheng H, Zhan C. Intelligent wide-area water quality monitoring and analysis system exploiting unmanned surface vehicles and ensemble learning. *Water (Basel)*. 2020;12(3):681.
doi: 10.3390/w12030681
22. Kong H, Wang X, Li T. Smart Water Waste Scrubbing Robot System Using YOLOv3 for Trash Detection. In: *IEEE Transactions on Automation Science and Engineering*. United States: IEEE; 2022.
23. Ruangpayoongsak N, Sumroengrit J, Leanglum M. A floating waste scooper robot on the water surface. In: *Proceedings of the 2017 17th International Conference on Control, Automation and Systems (ICCAS)*, Jeju, Korea; 2017. p. 1543-1548.
doi: 10.23919/ICCAS.2017.8206078.
24. Cryer S, Carvalho F, Wood T, *et al*. Evaluating the sensor-equipped autonomous surface vehicle C-worker 4 as a tool for identifying coastal ocean acidification and changes in carbonate chemistry. *J Mar Sci Eng*. 2020;8(11):939.
doi: 10.3390/jmse8110939.
25. Gupta A, Sharma S. Smart water quality monitoring system: A survey. Int *J Environ Sci Technol*. 2022;19(6):4735-4746.
doi: 10.1007/s13762-021-03495-x
26. Lee J. *The Ultimate Guide to Swimming Pool Maintenance Robots: Benefits and How they Work*;

2022. Available from: https://www.pooltechjournal.com/swimming-pool-maintenance-robots [Last accessed on 2025 Mar 04].
27. Dzhafarov RM, Panchenko AA. Color moments for the recognition of color images. *J Imaging*. 2022;8(4):116. doi: 10.3390/jimaging8040116
28. Sharma A, Choudhary R. Robotics and automation in water treatment and water quality management. *J Clean Prod*. 2021;308:127333. doi: 10.1016/j.jclepro.2021.127333

Asian Journal of Water, Environment and Pollution. Vol. 22, No. 2 (2025), pp. 32-42.
doi: 10.36922/AJWEP025040021

ORIGINAL RESEARCH ARTICLE

Testing the ability of *Vetiveria zizanioides* plants to bind cadmium and its influence on soil microbial diversity

Aida Abdali Dehdezi[1], Ebrahim Alaei[2]*, Pejman Azadi[3], Mahmoud Shavandi[4], and Seyed Amir Mousavi[5]

[1]Department of Horticulture, Science and Research Branch, Islamic Azad University, Tehran, Iran
[2]Environment and Biotechnology Research Division, Research Institute of Petroleum Industry, Tehran, Iran
[3]Department of Genetic Engineering, Agricultural Biotechnology Research Institute of Iran, Agricultural Research, Education and Extension Organization, Karaj, Iran
[4]Ecology and Environmental Pollution Control Research Group, Research Institute of Petroleum Industry, West Blvd. of Azadi Sport Complex, Tehran, Iran
[5]Department of Plant Biotechnology, National Institute of Genetic Engineering and Biotechnology, Tehran, Iran
***Corresponding author**: Ebrahim Alaei (alaiee@ripi.ir)

Received: January 22, 2025; Revised: February 19, 2025; Accepted: February 28, 2025 Published Online: March 27, 2025

Abstract: Phytoremediation is an environmentally friendly and cost-effective approach for the remediation of heavy metals from contaminated environments. However, its effectiveness can be influenced by various factors, particularly the structure and diversity of soil microbial communities, which play a crucial role in enhancing or hindering the phytoremediation process. In this study, the remediation of cadmium-contaminated soil was investigated through the cultivation of *Vetiveria zizanioides*, examining its effects on the diversity of soil microbial communities. The concentration of Cd in roots and leaves reached more than 600 mg/kg DW and 400 mg/kg DW, respectively, at 60 mg/kg Cd treatment. Next-generation sequencing was used to characterize the soil microbial community. It was shown that the increased Cd contaminant from 20 mg/kg to 60 mg/kg of soil noticeably reduced the microbial count. A significant increase in species numbers was observed in the clean soil containing the *V. zizanioides* plants. In addition, soil samples from Cd-contaminated soil showed a considerable change in microbial structure at the genus level with the *Sphingomonas* bacteria becoming the most dominant genus against Cd-contamination.

Keywords: Phytoremediation; Cadmium remediation; Soil microbial composition; Soil contamination; *Vetiveria zizanioides*; *Sphingomonas*

1. Introduction

Soil is a vital component of ecosystems and significantly contributes to the sustainability of human populations. Over the years, researchers have been investigating methods for the prevention and treatment of contaminated soils, with significant progress made since 1985. Soil contamination with various inorganic and organic pollutants has led to the degradation of vast areas of urban and agricultural land worldwide.[1] Industrial activities, particularly from sectors such as mining and petroleum, have been identified as major contributors to the release of toxic heavy metals (HMs) into the soil, negatively affecting soil fertility, microbial activity, and agricultural productivity.[2] As this contamination becomes a pervasive global issue, it is

crucial that we address the challenges in soil degradation to safeguard food security and human health.[3,4] It is important to note that contamination of the lithosphere has been aggravated in the past decade due to rapid industrialization, with petroleum and mining industries being the primary contributors.[5]

Among various contaminants, HMs such as zinc, cadmium, arsenic (As), and lead are of particular concern due to their carcinogenic and mutagenic properties, and their removal from ecosystems is imperative.[6] Consequently, the urgency for environmental protection and the development of effective remediation techniques has increased.[7,8] In recent years, several remediation technologies—including physical,[9,10] chemical,[11] and biological[12,13] approaches – have been considerably applied to treat HM contamination. Traditional remediation methods, such as chemical techniques involving immobilization, soil washing, and vitrification, are often expensive and not feasible for large-scale applications.[1] As such, there is an urgent need for cost-effective, eco-friendly, and sustainable alternatives.[14] Biological methods, particularly phytoremediation, offer a promising solution to this challenge.[15] Phytoremediation involves the adsorption of contaminants, such as HMs, in plant roots and leaves.[16] This process can be further divided into various mechanisms such as phytostabilization, phytoextraction, phytovolatilization, rhizofiltration, and others, which enable plants to remove, stabilize, or degrade pollutants.[17] Among the various plant species used in phytoremediation, *vetiver* stands out due to its remarkable characteristics. Vetiver, previously identified as *Vetiveria zizanioides* Nash, has been reclassified as *Chrysopogon zizanioides* (L.) Roberty, known for its tall, fast-growing perennial nature and deep root system that can extend 3 – 4 m into the soil, which is particularly effective at remediating contaminated sites. This grass can tolerate a wide range of harsh environmental conditions, including high concentrations of HMs, making it an ideal candidate for phytoremediation in various contaminated environments.[18,19]

In addition, microbes play a key role in most of the Earth's biogeochemical cycles and are crucial to the functioning of virtually all ecosystems. Certain microorganisms in the rhizosphere form symbiotic relationships with plants, suggesting that phytoextraction, supported by plant growth-promoting bacteria, could be an effective approach to improve phytoremediation in heavily contaminated soil. For instance, *Serratia* spp., isolated from cadmium-contaminated soils, has been shown to improve the efficiency of phytoremediation by altering the physicochemical properties of the soil. Therefore, a comprehensive investigation of the structure and function of rhizosphere microbial communities is crucial for evaluating the quality of contaminated agricultural soils. Under HM stress, microbes either die due to the toxicity caused by the metals or survive and thrive by employing various resistance mechanisms against them. HM ions help protect the internal bacterial cells, and the formation of a biofilm on *Pseudomonas aeruginosa* increases its resistance to Cu, Pb, and Zn.[20,21]

While numerous studies have investigated the effectiveness of *V. zizanioides* in removing contaminants from soils and groundwater,[22,23] there is a notable lack of research on the biological interactions between plants and microorganisms in the context of HM phytoremediation. Recent studies have begun to explore these interactions, demonstrating that combining plants with microorganisms can enhance phytoremediation efficiency. Specifically, *Serratia* spp. has been shown to significantly improve cadmium accumulation in *V. zizanioides*.[24] Furthermore, research into microbial diversity under HM stress has shown that microbes either survive through resistance mechanisms or perish due to metal toxicity.[25] Ng *et al.*[26] modified the HM phytoremediation using *V. zizanioides* by ethylenediaminetetraacetic acid addition into the soil and ranked metal accumulation as follows: Zinc >>> Copper > Lead >> Cadmium. Since microorganisms promote most biogeochemical cycles on the Earth, their role is not negligible to the ecosystems.[27]

In addition to plant leaves or roots, soil microorganisms are crucial in phytoremediation.[25] The existing studies focus on investigating the phytoremediation process rather than biological interactions.[28-30] By investigating the impact of two grasses, *V. zizanioides* and *Juncus effusus* L., on the wetland bacterial and archaeal diversity, Long *et al.*[31] revealed that archaea faced decreasing abundance with increasing plant bacterial diversity. In another study, ecotoxicological impacts of Cd on the soil microorganisms were studied through polymerase chain reaction (PCR) denaturing gradient gel technique, showing that bacteria, fungi, and actinomycete are sensitive to Cd.[32]

The research to date has tended to focus on phytoremediation process rather than biological interactions.[28] Overall, there is a lack of comprehensive research thoroughly investigating soil biodiversity in the context of HM phytoremediation. To address this gap, this study primarily aims to examine the impact of Cd phytoremediation on microbial variation in soils assessed using next-generation sequencing (NGS)

to identify the key bacteria that are crucial for the remediation process.

2. Materials and methods

2.1. Soil preparation and plant material

Soil samples were taken from Chitgar Forest Park, Tehran, Iran, and were transferred to the laboratory. According to the soil taxonomy, the samples were classified as typic haplocambids. The samples were air-dried at room temperature; a 2 mm mesh screen was used to sieve the samples. In addition, the soil texture type was defined using a hydrometer test, and soil electrical conductivity, cation-exchange capacity, pH, total organic carbon, CaCO3, and elements[33] were measured according to standard methods[34] (Table 1).

$Cd(NO_3)_2$ solution was applied as a single dose, at concentrations of 20 and 60 mg/kg soil, with the control group (0 mg/kg) consisting of soil without metal addition. Table 2 presents the treatment plan for various soil samples. All experiments involving these treatments were replicated 3 times. All soil samples were maintained under field capacity moisture conditions for 3 weeks. Each pot contained 2 kg of soil. Eight seeds were planted in each pot. After 10 days, five unhealthy seedlings were eliminated. The pots were weighed and irrigated at intervals of 24 – 48 h. The plants were harvested once the growing season was completed.

Table 1. Chemical and physical characteristics of substrates used in the study

Sand	Silt	N	EC	pH	P	K	Zn	Mn	Fe
(%)					(Ds/m)			(mg/kg)	
27	53	0.09	62.3	7.8	18.9	940	0.63	5.43	3.53

Table 2. Experimental treatments

Sample abbreviation	Treatment name
B	Clean soil, no Cd, and no *V. zizanioides* plants (negative control)
V	Clean soil in the presence of *V. zizanioides* plants (positive control)
Cd20	Soil with 20 mg/kg Cd+ *V. zizanioides* plants
Cd60	Soil with 60 mg/kg Cd+ *V. zizanioides* plants

Abbreviation: *V. zizanioides*: *Vetiveria zizanioides*; B: Clean soil without *Vetiveria zizanioides*; V: Clean soil in the presence of *V. zizanioides*; Cd20: Cd-contaminated soil (20 mg/kg); Cd60: Cd-contaminated soil (60 mg/kg).

2.2. Plant sampling and analysis

2.2.1. Leaves and roots dry weight measurement

Leaf and root samples were dried at 70°C for 48 h and subsequently weighed.

2.2.2. HM leaching and analytical process

After harvesting, the leaves and roots of *V. zizanioides* were carefully washed with deionized water to remove any surface contaminants. The washed plant material was then dried at 70°C for 48 h to ensure complete moisture removal. Once dried, the plant tissues were finely ground to a homogeneous powder to facilitate efficient digestion and analysis. For metal analysis, the samples were digested in a mixture of concentrated nitric acid (HNO_3) and hydrogen peroxide (H_2O_2) in order to break down the plant matrix and release the metals into solution. This step was crucial to ensure that the metals of interest were fully extracted from the plant material. The digestates were then filtered and diluted with deionized water as needed. Finally, metal concentrations in the resulting solutions were determined using (furnace atomic absorption spectrometry; model 603 Perkin-Elmer, PerkinElmer, Inc., USA). This technique was chosen for its sensitivity and precision in measuring trace metal concentrations.

2.3. Soil microbial community analysis

2.3.1. DNA extraction

Microbial DNA from the total soil samples (Table 1) was extracted using the NucleoSpin® Microbial DNA Isolation Kit (Macherey-Nagel, Germany) following the manufacturer's instructions. The quality of the extracted DNA was assessed using Nano-drop ultraviolet-Vis's spectrophotometer (Thermo Fisher Scientific, USA) as previously reported by Yang *et al.*[9] Then, agarose gel electrophoresis (1%) was applied to study the structural integrity of the DNA molecules. DNA from the soil samples was utilized to analyze bacterial diversity through 16S rRNA amplicon sequencing.

2.3.2. Illumina sequencing data analysis

In the present study, the impact of Cd-phytoremediation by *V. zizanioides* grass on the soil microbial diversity was investigated using NGS. The 16S protocol was designed to amplify both bacteria and archaea using paired-end 16S community sequencing on the Illumina platform. PCR amplification was performed following standard procedures, using primers with barcodes: 515F (GTGCCAGCMGCCGCGGTAA) and 806R (GGACTACHVGGGTWTCTAAT), which target the V4 region of the 16S rRNA. Subsequently, sequencing

libraries were prepared using the TruSeq DNA PCR-Free Sample Prep Kit (Illumina, USA) following the manufacturer's guidelines. The quality of the library was assessed using the Qubit 2.0 Fluorometer (Thermo Scientific) and the Agilent Bioanalyzer 2100 system. Finally, the library was sequenced on the Illumina HiSeq 2500 platform, generating 250 bp paired-end reads (Beijing Genomics Institute, China).

2.3.3. Statistical and bioinformatics analysis

In addition, the sequences were aligned and compared with those in the gene database using the basic local alignment search tool program (National Center for Biotechnology Information) for identification. Strains with 97% similarity or more in sequence were identified as identical. To calculate alpha diversity, species diversity complexity was analyzed using several indices, including Chao 1, ACE, Shannon, and Simpson, with QIIME (V. 1.7.0). The results were visualized using R software (V. 2.15.3). Furthermore, beta diversity was evaluated using both weighted and unweighted UniFrac distances, analyzed with QIIME (V. 1.7.0). Principal coordinate analysis (PCoA) was also employed to visualize and identify differences between the samples based on the beta diversity distance matrix.

3. Results

3.1. Responses and plant growth

Empirical studies have indicated that Cd exerts a substantial influence on plant growth. As illustrated in Figures 1 and 2, *V. zizanioides* dry weight was dramatically reduced by increasing soil contaminant concentration. The leaves' weight was lower than 19 g for the contaminated soil, whereas it was measured up to 27 g for the clean samples. In addition, the same trend was observed for the roots weight, reaching 2.7, 1.92, 1.56, and 1.41 g for the B, V, Cd20, and Cd60 samples, respectively.

3.2. Phytoremediation potential of *Vetiveria*

Leaf necrosis and discoloration are common indicators of HM toxicity (Figure 3). Cadmium accumulation in *V. zizanioides* was measured by extracting HM elements from the leaves and roots. The results indicated that this plant demonstrates promising potential for Cd phytoremediation, with Cd metal concentrations exceeding 600 mg/kg DW in the leaves and more than 400 mg/kg DW in the roots (Figures 4 and 5).

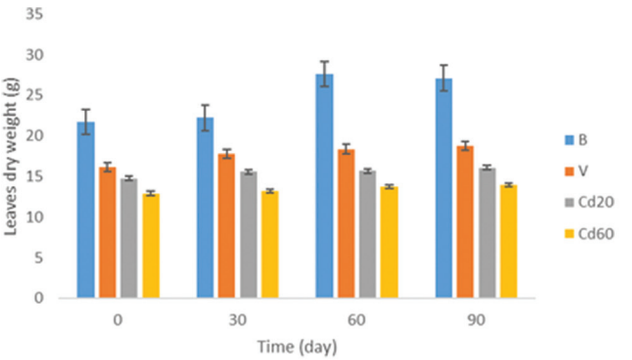

Figure 1. Dry weight of leaves of *Vetiveria zizanioides* grass during exposure time. Data points and error bars represent mean±SD of three replicates (*n*=3). Soil treatment definitions: B=Clean soil without *V. zizanioides*; V=Clean soil in the presence of *V. zizanioides*; Cd20=Cd-contaminated soil (20 mg/kg); Cd60: Cd-contaminated soil (60 mg/kg)

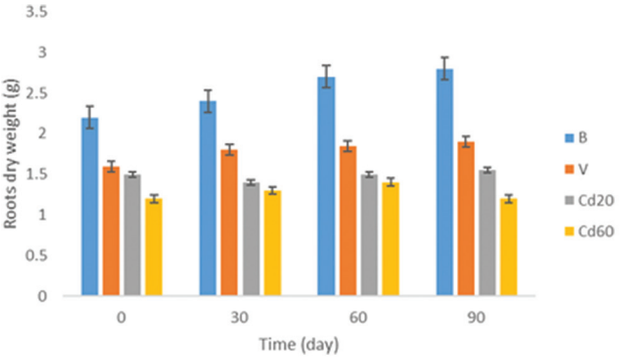

Figure 2. Dry weight of roots of *Vetiveria zizanioides* grass during the exposure time. Data points and error bars represent mean±SD of three replicates (*n*=3). Soil treatment definitions: B: Clean soil without *V. zizanioides*; V: Clean soil in the presence of *V. zizanioides*; Cd20: Cd-contaminated soil (20 mg/kg); Cd60: Cd-contaminated soil (60 mg/kg)

3.3. Impacts of HMs on the soil microorganisms

To investigate the relationships between soil microorganisms and plant roots, NGS was utilized to identify the bacteria species involved in phytoremediation. All effective reads were clustered into operational taxonomic units (OTUs) based on 97% DNA sequence similarity to facilitate analysis of soil microbial diversity. By comparing the number of OTUs, we revealed that the number of microorganisms were enriched in the presence of *V. zizanioides* grass. Increasing the contaminant concentration from 20 to

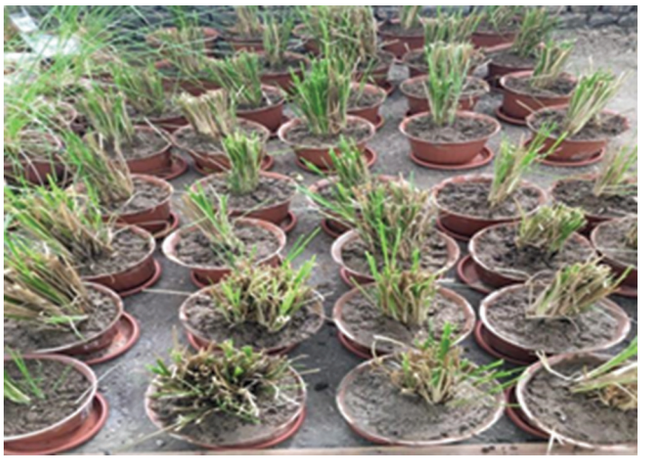

Figure 3. Morphological symptoms in *Vetiveria zizanioides* plants exposed to Cd contamination

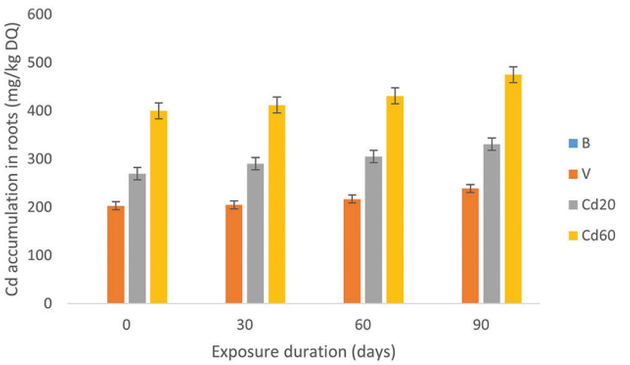

Figure 4. Heavy metal (Cd) accumulation in the roots of *Vetiveria zizanioides* grass across different metal exposure duration. Data points and error bars represent mean±SD of three replicates (*n*=3). Soil treatment definitions: B: Clean soil without *V. zizanioides*; V: Clean soil in the presence of *V. zizanioides*; Cd20: Cd-contaminated soil (20 mg/kg); Cd60: Cd-contaminated soil (60 mg/kg)

60 mg/kg of soil noticeably reduced the microbial count (Figure 6).

3.4. Soil microbial community structure

Community analysis was applied to estimate the impacts of HM contamination on the soil microbial community structure during the phytoremediation process through *V. zizanioides* grass. The results, presented in Figure 7A, demonstrated that exposing the soil samples to Cd results in microbial destruction at the genus level. *Sphingomonas* was identified as the strongest genus against Cd. Furthermore, it was revealed that planting *V. zizanioides* grass remarkably changes the soil microbiome. Considerable results were

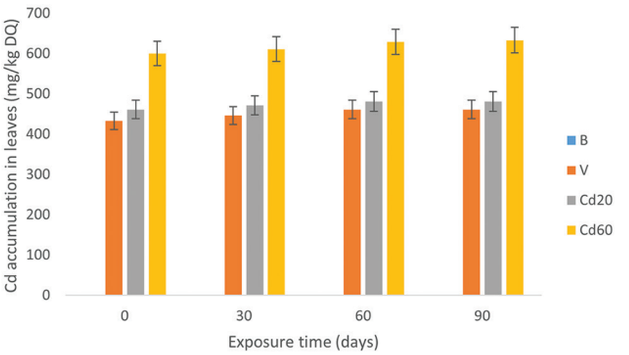

Figure 5. Heavy metal (Cd) accumulation in leaves of *Vetiveria zizanioides* grass across different metal exposure duration. Data points and error bars represent mean±SD of three replicates (*n*=3). Different letters in the same color indicate significant difference determined by analysis of variance followed by the least significant difference test ($p<0.05$). Soil treatment definitions: B: Clean soil without *V. zizanioides*; V: Clean soil in the presence of *V. zizanioides*; Cd20: Cd-contaminated soil (20 mg/kg); Cd60: Cd-contaminated soil (60 mg/kg)

additionally observed at the phylum level. Relative abundance of *Actinobacteria* was dramatically reduced from 0.39 in sample B to 0.03, 0.07, and 0.05 in samples V, Cd20, and Cd60, respectively. As illustrated in Figure 7B, Cd relatively removed *Firmicutes* from the soil; meanwhile, it had no significant impact on *Acidobacteria*, *Bacteriodetes*, *Gammatimonadete*, *Ghloroflexi,* and *Verrucomicrobia*.

3.4.1. Alpha diversity analysis

Alpha diversity analysis was used to measure species richness, which refers to the number of different species present. The results showed significantly increasing observed species in soil by Vetiveri culture, which raised from 1223 to 1864 (Table 3). The addition of contaminant (20 mg/kg) into soil resulted in slight species reduction, whereas it dramatically reduced to 1620 at 60 mg/kg Cd contamination.

Studying the species evenness by Shannon, Chao1, and ACE indexes, the Cd20 sample showed a relatively higher index, while the Simpson index did not show any considerable changes. It can be concluded that the species were present in all four samples, with the highest abundance of microorganisms observed at the same level in the Cd20 sample. Taken together, the results indicate that all the studied indices are more responsive

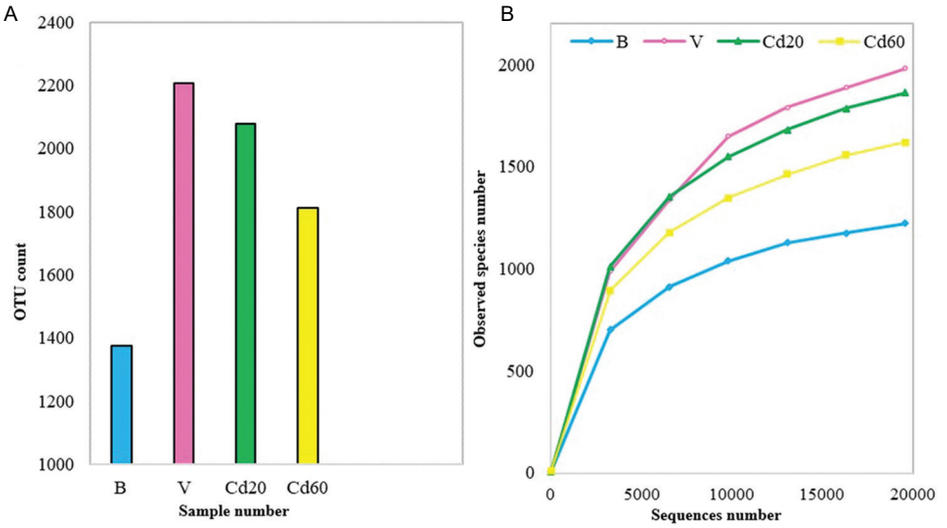

Figure 6. Soil microbial diversity under different treatment. (A) Over-the-counters count and (B) observed species number for the different soil sample types, The bacterial genus *Sphingomonas* is represented by purple bars in (A) belonging to the *Phylum Pseudomonatota*. This Phylum is synonym with *Phylum Proteobacteria* (B); (B: Clean soil without *Vetiveria zizanioides* planting; V: Clean soil in the presence of *V. zizanioides*; Cd20: Cadmium contaminated soil [20 mg/kg]; Cd60: Cadmium contaminated soil [60 mg/kg])

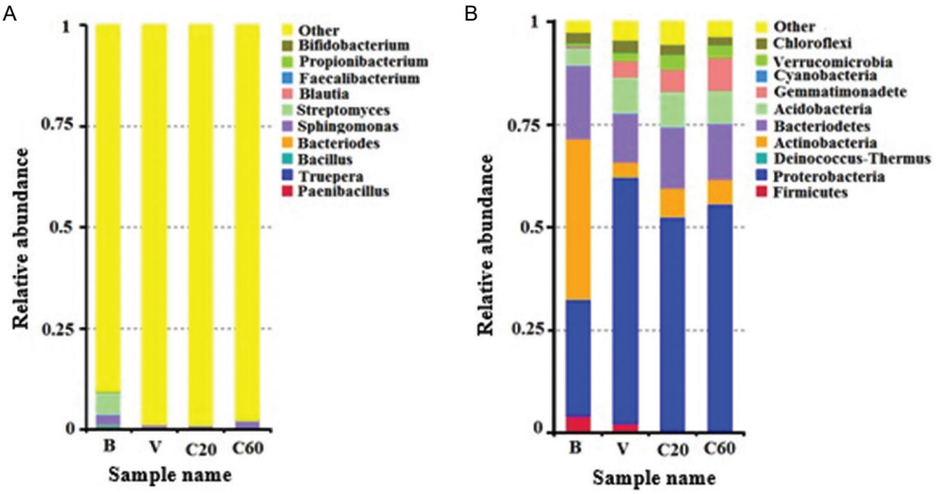

Figure 7. Species relative abundance at genus level (A) and phylum level (B). The bacterial genus *Sphingomonas* belongs to the *Pseudomonatota* phylum, which is synonymous with the *Proteobacteria* phylum. Soil treatment definitions: B: Clean soil without *Vetiveria zizanioides*; V: Clean soil in the presence of *V. zizanioides*; Cd20: Cd-contaminated soil (20 mg/kg); Cd60: Cd-contaminated soil (60 mg/kg)

Table 3. Indices of alpha diversity

Sample	Observed species	Shannon	Simpson	Chao1	ACE
B	1223	8.501	0.993	1410.789	1359.89
V	1864	9.395	0.996	2107.594	2130.127
Cd20	1853	9.473	0.997	2203.743	2164.503
Cd60	1620	9.231	0.996	1800.555	1865.044

Soil treatment definitions: B: Clean soil without *Vetiveria zizanioides*; V: Clean soil in the presence of *V. zizanioides*; Cd20: Cd-contaminated soil (20 mg/kg); Cd60: Cd-contaminated soil (60 mg/kg).

to microbial community evenness than to community richness.

3.4.2. Beta diversity analysis

PCoA was used to investigate differences in microbial community composition. Beta diversity analysis, accounting for 40.49% and 18.77% of the total variation in PC1 and PC2, respectively (Figure 8A), supported the results of the alpha diversity analysis. These findings showed that the microbial community structure of the blank sample was significantly different from that of the *V. zizanioides*-planted soils. The most exciting part of the results was the *V. zizanioides* grass controlling the negative impacts of HM on microbial diversity.

As shown in Figure 8B, the Cd20, Cd60, and V samples were distinct from the blank sample, indicating lower richness compared to the B sample. The results from unweighted UniFrac PCoA were consistent with those from the weighted UniFrac analysis, further supporting the findings from the alpha diversity analysis.

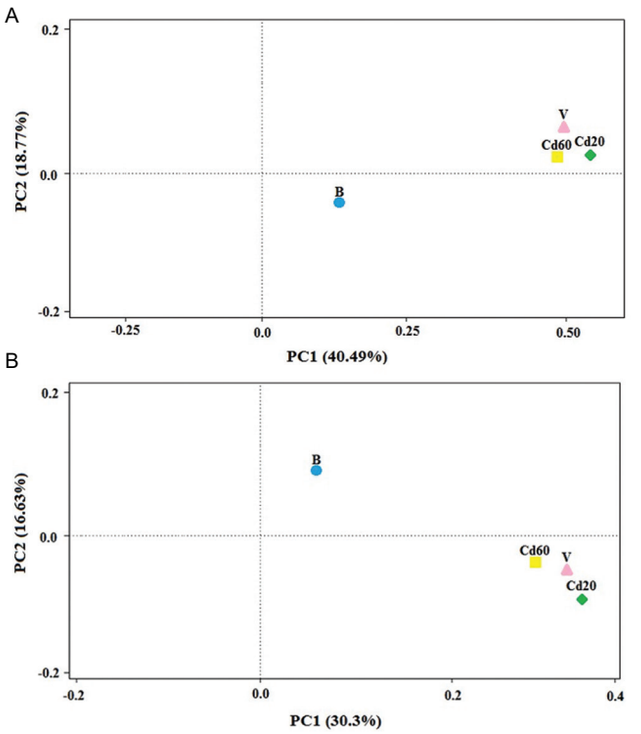

Figure 8. Two-dimensional principal coordinate analysis (PCoA) of the samples: (A) Weighted UniFrac and (B) Unweighted UniFrac PCoA. Soil treatment definitions: B: Clean soil without *Vetiveria zizanioides*; V: Clean soil in the presence of *V. zizanioides*; Cd20: Cd-contaminated soil (20 mg/kg); Cd60: Cd-contaminated soil (60 mg/kg)

4. Discussion

The results indicated that Cd in the solution had a negative impact on the dry weight of *V. Zizanioides* leaves and roots. It can be concluded that *V. zizanioides* is unable to grow effectively at high concentrations of Cd, as previously demonstrated by Liu *et al.*[35] They reported that when the Cd concentrations were >7.5 mg/L, the plant biomass decreased as Cd concentration in solution increased for both the roots and shoots. A similar pattern of reduced growth due to Cd toxicity has been observed in other species, such as *Brassica juncea* (L.) Czem, which showed a significant decrease in growth at Cd concentrations above 10 mg/L.[36] In contrast, Aibibu *et al.*[37] reported that a low concentration of Cd in the solution caused an increase in chlorophyll levels, root activity, and biomass accumulation in *V. zizanioides* after 15 days, with a 2.2% increase compared to the control group. Other studies on *Cicer arietinum* (chickpea) found no significant growth improvement in response to Cd exposure, highlighting species-specific responses to mental stress.[38] These contrasting findings highlight the varying effects of Cd at different concentrations on *V. zizanioides* growth.

Cadmium accumulation in the roots and leaves of plants can be more pronounced in those grown in contaminated soil compared to plants grown in non-contaminated soil. Yu *et al.*[39] indicated that at low cadmium concentrations (<3 mg/L), the stem tissue of *V. zizanioides* can utilize the osmosis of organic substances, such as carbohydrates and amino acids, to enhance cadmium tolerance. Interestingly, similar behavior was noted in *Helianthus annuus* (sunflower), which exhibited a stronger tolerance to Cd when root uptake was supported by osmotic adjustment mechanisms.[40] Cd accumulation in leaves did not show any considerable increase, while in roots, it was slightly increased over the experimental period. In further research, Phusantisampan *et al.*[41] stated that roots are more prone to Cd accumulation than leaves in *V. zizanioides* grass, a finding consistent with the observations for *Dittrichia viscosa*, which is also noted for efficient Cd uptake through root systems.[42]

This mechanism was observed not only in *V. zizanioides* but also in other plant-associated microbes, such as those in *C. arietinum* L., which showed increased glutathione synthesis in response to metal stress.[38] In line with this, our observation of microbial destruction at the genus level in *Actinobacteria* and *Sphingomonas* under cadmium exposure further highlights the detrimental impact of

Cd on soil microbial communities. Interestingly, the population of *Proteobacteria* was found to increase in the presence of *V. zizanioides*, indicating a potential synergy between these bacteria and the plant, similar to findings by Calcagnile *et al.*[43] for *Salix* species, which also demonstrated an increase in *Proteobacteria* under Cd stress. This finding is consistent with Long *et al.*[31] who reported that *Proteobacteria* was the dominant bacterial group in soil planted with *V. zizanioides*.

In contrast to *V. zizanioides*, *Populus* species have been found to boost the microbial diversity of beneficial fungi and bacteria in Cd-contaminated soils, a mechanism that contributes to improved bioremediation efficiency.[44] Similarly, the cultivation of *Populus* species resulted in a significant increase in beneficial microbial activity, leading to improved phytoremediation potential.[45] While the findings for *V. zizanioides* indicate that Cd negatively impacts plant growth and microbial diversity, investigations on other species like *Populus*, *Salix*, and *C. arietinum* provide additional insights into the complex interactions between plants, microbes, and HMs. Future studies should continue exploring a broader range of species to better understand the full potential of phytoremediation and bioremediation processes.

On the other hand, extrapolating results from laboratory or greenhouse experiments to field conditions is a challenging task, especially in the context of HM remediation. Controlled environments, such as pot cultures, provide valuable insights but fail to replicate the complexities of natural ecosystems, where factors such as soil heterogeneity, microbial diversity, and environmental variability influence remediation processes. Studies have shown that while laboratory conditions can demonstrate the potential for phytoremediation, field studies are crucial to account for the unpredictable variables present in natural settings.[46,47] These factors include soil type, climatic conditions, and the interaction of plant species with the environment, which can significantly affect the efficiency of HM removal.[48] Furthermore, the presence in the soil of different species of the same HM, like in the case of As, might reduce the ability of the plants due to the toxicity of the different species.[49] Therefore, for a comprehensive understanding of phytoremediation potential, it is essential to conduct field trials that incorporate these natural variables.

The management of Cd-contaminated plants and soil, particularly regarding root disposal and the prevention of soil re-contamination, have been reviewed and explained by several scientific sources and studies, as follows:

(i) Root extraction and disposal. It is recommended that if feasible, the root system of the plant should be completely removed to prevent the re-release of Cd into the environment. The roots should then be disposed of properly, for instance, by incineration at high temperatures or burial in hazardous waste landfills to ensure that Cd does not leach into other areas (Phytoremediation Resource Guide, 1999).[50]

(ii) Soil remediation after root removal. After root extraction, the soil can be treated using methods like soil washing, bioremediation with microorganisms, or the addition of amendments (e.g., biochar, compost) that can immobilize the residual Cd and reduce its bioavailability. This ensures that the remaining Cd in the soil does not become accessible to plants.[51]

(iii) Long-term monitoring. Even after root extraction and soil treatment, continuous monitoring of Cd levels in the soil is essential. Periodic soil testing will help determine if any Cd remains or if additional remediation is required to ensure soil health and prevent re-contamination. Completely removing the root system is ideal to prevent re-contamination, but if this is not possible, treating the soil and monitoring it over time for cadmium levels should be prioritized to ensure long-term soil safety.

5. Conclusion

In the present study, the effect of *V. zizanioides* on the Cd-contaminated soil microbial structure was investigated. First, the plant growth on the different Cd concentration was studied by measuring the leaves and roots dry weight. Then, *V. zizanioides* grass potential in HM removal from soil was analyzed. Finally, the impact of *V. zizanioides* grass and Cd-contamination on the microbial structure of soil was studied by NGS. The results proved that HM contamination destroys the soil biodiversity. Planting *V. zizanioides* enriches the soil microbiome and helps to reduce the negative impacts of contaminants on the microorganisms. In conclusion, the combination uses of phytoremediation and bioremediation (stimulation of the native microorganisms) provides a more efficient approach to addressing soil contamination. Although analyzing the physicochemical properties and elemental content of the soil after the experiment would have provided valuable insights, we recommend that future studies include this aspect to gain a more comprehensive understanding of the phytoremediation process.

Acknowledgments

None.

Funding

The authors extend our gratitude to the personnel of the Research Institute of Petroleum Industry, Iran, for assisting us in this research project. (Project No. 33481249).

Conflict of interest

The authors declare that there is no conflict of interest.

Author contributions

Conceptualization: Ebrahim Alaei
Formal analysis: Ebrahim Alaei
Methodology: Aida Abdali Dehdezi, Ebrahim Alaei
Writing – original draft: All authors
Writing – review & editing: All authors

Availability of data

Data is available from the corresponding author upon reasonable request.

References

1. Bhavya P, Madasseri S, Gowthamchand NJ, Anil S. Soil contamination and remediation. In: *Modern Approaches in Soil Science*. 2nd ed., Vol. 2. Haryana: Stella International Publication; 2024.
2. Debonne N, Van Vliet J, Metternicht G, Verburg P. Agency shifts in agricultural land governance and their implications for land degradation neutrality. *Glob Environ Change*. 2021;66:102221. doi: 10.1016/j.gloenvcha.2020.102221
3. Bernardino CA, Mahler CF, Alvarenga P, *et al*. Recent advances in phytoremediation of soil contaminated by industrial waste: A roadmap to a safer environment. In: *Bioremediation of Industrial Waste and Environmental Safety*. Germany: Springer; 2019. p. 207-21.
4. Zhang Z, Wang X, Jiang H. Sunflower (*Helianthus annuus*) and its role in Cd uptake and remediation. *Environ Sci Pollut Res Int*. 2019;26(3):3055-3064. doi: 10.1007/s11356-018-3801-9
5. Shaw DR, Dussan J. Mathematical modeling of toxic metal uptake and efflux pump in metal-resistant bacterium *Bacillus cereus* isolated from heavy crude oil. *Water Air Soil Pollut*. 2015;226(4):2385. doi: 10.1007/s11270-015-2385-7
6. Gondal MA, Aldakheel RK, Almessiere MA, *et al*. Determination of heavy metals in cancerous and healthy colon tissues using laser-induced breakdown spectroscopy and cross-validation with ICP-AES method. *J Pharm Biomed Anal*. 2020;183:113153. doi: 10.1016/j.jpba.2020.113153
7. Abdel-Shafy IH, Mansour SM. A review on polycyclic aromatic hydrocarbons: Source, environmental impact, effect on human health and remediation. *Egypt J Pet*. 2016;25:107-123. doi: 10.1016/j.ejpe.2015.03.011
8. Han X, Tianyi C, Sun T. *Study on Heavy Metal Pollution Characteristics and Its Health Risk Assessment From Sludge of Sewage Treatment Plants in Industrial Parks* [Preprint]; 2020. doi: 10.21203/rs.3.rs-34745/v1
9. Yang X, Liu L, Tan W, Liu C, Dang Z, Qiu G. Remediation of heavy metal contaminated soils by organic acid extraction and electrochemical adsorption. *Environ Pollut*. 2020;264:114745. doi: 10.1016/j.envpol.2020.114745
10. Abdin Y, Adel U, Yong SK, Yiu Fai T, Al-Wabel M. Competitive sorption and availability of coexisting heavy metals in mining-contaminated soil: Contrasting effects of mesquite and fishbone biochars. *Environ Res*. 2020;181:108846. doi: 10.1016/j.envres.2019.108846
11. Akhtar FZ, Archana KM, Krishnaswamy VG, Rajagopal R. Remediation of heavy metals (Cr, Zn) using physical, chemical and biological methods: A novel approach. *SN Appl Sci*. 2020;2:1918. doi: 10.1007/s42452-019-1918-x
12. Haq S, Bhatti AA, Dar ZA, Bhat SA. Phytoremediation of heavy metals: An eco-friendly and sustainable approach. In: Hakeem KR, Bhat SA, Qadri H, editors. *Bioremediation and Biotechnology, Sustainable Approaches to Pollution Degradation*. Germany: Springer; 2020. p. 215-231. doi: 10.1007/978-3-030-35691-0_10
13. Muthusaravanan S, Sivarajasekar N, Vivek JS. Research updates on heavy metal phytoremediation: Enhancements, efficient post-harvesting strategies and economic opportunities. In: Inamuddin, Ahamed MI, Lichtfouse E, editors. *Environmental Chemistry for a Sustainable World*. Germany: Springer; 2020. p. 191-222. doi: 10.1007/978-3-030-17724-9_9
14. Farraji H, Robinson B, Mohajeri P, Abedi T. Phytoremediation: Green technology for improving aquatic and terrestrial environments. *Nippon J Environ Sci*. 2021;1:1002. doi: 10.46266/njes.1002
15. Wani KA, Sofi ZM, Malik JA, Wani JA. Phytoremediation of heavy metals using *Salix* (willows). In: Hakeem KR, Bhat SA, Qadri H, editors. *Bioremediation and Biotechnology*. Cham: Springer; 2020. p. 161-174.

doi: 10.1007/978-3-030-40333-1_9
16. Manoj SR, Karthik C, Kadirvelu K. Understanding the molecular mechanisms for the enhanced phytoremediation of heavy metals through plant growth-promoting rhizobacteria: A review. *J Environ Manage*. 2020;254:109779. doi: 10.1016/j.jenvman.2019.109779
17. Awa SH, Hadibarata T. Removal of heavy metals in contaminated soil by phytoremediation mechanism: A review. *Water Air Soil Pollut*. 2020;231(2):47.
18. Almeida A, Ribeiro C, Carvalho F, *et al*. Phytoremediation potential of *Vetiveria zizanioides* and *Oryza sativa* for nitrate and organic substance removal in vertical flow constructed wetlands. *Ecol Eng*. 2019;138:19-27. doi: 10.1016/j.ecoleng.2019.06.020
19. Chen HM, Zheng CR, Tu C, Shen ZG. Chemical methods and phytoremediation of soil contaminated with heavy metals. *Chemosphere*. 2000;41:229-234. doi: 10.1016/s0045-6535(99)00415-4
20. Bhati T, Gupta R, Yadav N, *et al*. Assessment of bioremediation potential of *Cellulosimicrobium* sp. for treatment of multiple heavy metals. *Microbiol Biotechnol Lett*. 2019;47:269-277. doi: 10.4014/mbl.1808.08006
21. Tang H, Xiang G, Xiao W, Yang Z, Zhao B. Microbial mediated remediation of heavy metals toxicity: Mechanisms and future prospects. *Front Plant Sci*. 2024;15:1420408. doi: 10.3389/fpls.2024.1420408
22. Abdallah RS, Arief R, Yanuwiadi B. Phytoremediation of lead-contaminated soil using vetiver grass (*Vetiveria zizanioides* L.). *J Exp Life Sci*. 2019;9:54-59. doi: 10.21776/ub.jels.2019.009.01.09
23. Kiamarsi Z, Kafi M, Soleimani M, Nezami A, Lutts S. Conjunction of *Vetiveria zizanioides* L. and oil-degrading bacteria as a promising technique for remediation of crude oil-contaminated soils. *J Clean Prod*. 2020;253:119719. doi: 10.1016/j.jclepro.2019.119719
24. Liu H, Xie Y, Li J, *et al*. Effect of Serratia sp. K3 combined with organic materials on cadmium migration in soil-*Vetiveria zizanioides* L. system and bacterial community in contaminated soil. *Chemosphere*. 2020;242:125164. doi: 10.1016/j.chemosphere.2019.125164
25. Thijs S, Sillen W, Weyens N, Vangronsveld J. Phytoremediation: State-of-the-art and a key role for the plant microbiome in future trends and research prospects. *Int J Phytoremediation*. 2016;19(1):23-38. doi: 10.1080/15226514.2016.1216076
26. Ng YS, Shen ZG, Li XD. Modification of heavy metal phytoremediation using *Vetiveria zizanioides* by EDTA addition into soil. *Environ Pollut*. 2004;128(1-2):73-84. doi: 10.1016/j.envpol.2003.08.011
27. Martínez-Espinosa RM. Microorganisms and their metabolic capabilities in the context of the biogeochemical nitrogen cycle at extreme environments. *Int J Mol Sci*. 2020;21(12):4228. doi: 10.3390/ijms21124228
28. Effendi H, Bagus W, Utomo A, Pratiwi NT. Ammonia and orthophosphate removal of tilapia cultivation wastewater with *Vetiveria zizanioides*. *J King Saud Univ Sci.* 2018;32:207-212. doi: 10.1016/j.jksus.2018.04.018
29. Shah V, Daverey A. Phytoremediation: A multidisciplinary approach to clean up heavy metal-contaminated soil. *Environ Technol Innov*. 2020;18:100774. doi: 10.1016/j.eti.2020.100774
30. Borralho T, Gago D, Almeida A. Application of floating beds of macrophytes (*Vetiveria zizanioides* and *Phragmites australis*) for heavy metal removal in Água Forte Stream (Alentejo-Portugal). *J Ecol Eng*. 2020;21:153-163. doi: 10.12911/22998993/118285
31. Long Y, Yi H, Chen S, *et al*. Influences of plant type on bacterial and archaeal communities in constructed wetlands treating polluted river water. *Environ Sci Pollut Res Int*. 2016;23(19):19570-19579. doi: 10.1007/s11356-016-7166-3
32. Pan J, Yu L. Effects of Cd or/and Pb on soil enzyme activities and microbial community structure. *Ecol Eng*. 2011;37(11):1889-1894. doi: 10.1016/j.ecoleng.2011.07.002
33. Salman S, Salman A, Zeid SA, Seleem EM, Abdel-Hafiz MA. Soil characterization and heavy metal pollution assessment in Orabi farms, El Obour, Egypt. *Bull Natl Res Cent*. 2019;43(1):82. doi: 10.1186/s42269-019-0082-1
34. Parvin T, Salilih MF, Ishetu AI. Microbes used as a tool for bioremediation of heavy metal from the environment. *Cogent Food Agric*. 2020;6(1):1783174. doi: 10.1080/23311932.2020.1783174
35. Liu Y, Nuza'aiti A, Zeng G, *et al*. Cadmium accumulation in *Vetiveria zizanioides* and its effects on growth, physiological and biochemical characters. *Bioresour Technol*. 2010;101(17):6297-6303. doi: 10.1016/j.biortech.2010.03.02
36. Rana MS, Meena VS, Kour A. *Brassica juncea* for Cd removal: A comparative study. *J Environ Manage*. 2021;289:112537. doi: 10.1016/j.jenvman.2021.112537
37. Aibibu N, Liu Y, Zeng G, *et al*. Cadmium accumulation in *Vetiveria zizanioides* and its effects on growth, physiological and biochemical characters. *Bioresour Technol*. 2010;101:6297-6303. doi: 10.1016/j.biortech.2010.03.028
38. Gohari S, Ghaffari H, Asadi A. Mechanisms of heavy metal tolerance in *Cicer arietinum* under Cd stress. *Environ Toxicol Chem*. 2020;39(1):124-133.
39. Yu SH, Deng HP, Zhang B, *et al*. Physiological response of *Vetiveria zizanioides* to cadmium stress revealed by Fourier transform infrared spectroscopy. *Spectrochim Acta A Mol Biomol Spectrosc*. 2017;55(3):157-165.

doi: 10.1080/00387010.2017.1355321
40. Zheng S, Wang Q, Yuan Y, Sun W. Human health risk assessment of heavy metals in soil and food crops in the Pearl River Delta urban agglomeration of China. *Food Chem*. 2020;316:126213. doi: 10.1016/j.foodchem.2020.126213
41. Phusantisampan T, Meeinkuirt W, Saengwilai P, Pichtel J, Chaiyarat R. Phytostabilization potential of two ecotypes of *Vetiveria zizanioides* in cadmium-contaminated soils: Greenhouse and field experiments. *Environ Sci Pollut Res Int*. 2016;23(20):20027-20038. doi: 10.1007/s11356-016-7229-5
42. Anglana C, Capaci P, Barozzi F, *et al*. *Dittrichia viscosa* selection strategy based on stress produces stable clonal lines for phytoremediation applications. *Plants (Basel)*. 2023;12(13):2499. doi: 10.3390/plants12132499
43. Calcagnile M, Tredici SM, Talà A, Alifano P. Bacterial semiochemicals and transkingdom interactions with insects and plants. *Insects*. 2019;10(12):441. doi: 10.3390/insects10120441
44. Lorenz N, Hintemann T, Kramarewa T. Response of microbial activity and microbial community composition in soils to long-term arsenic and cadmium exposure. *Soil Biol Biochem*. 2006;38(6):1430-1437. doi: 10.1016/j.soilbio.2005.10.020
45. Wang L, Liu S, Li J, Li S. Effects of several organic fertilizers on heavy metal passivation in Cd-contaminated gray-purple soil. *Front Environ Sci*. 2022;10:895646. doi: 10.3389/fenvs.2022.895646
46. Zhou Q, Zhang J, Wang X, Li F. Field applications of phytoremediation for heavy metal-contaminated soils. *Environ Sci Pollut Res Int*. 2020;27(4):3721-3732. doi: 10.1007/s11356-019-07243-3
47. Singh P, Prasad SM. Phytoremediation of heavy metals: Concepts, methods, and applications. *Environ Monit Assess*. 2019;191(1):30. doi: 10.1007/s10661-018-7159-x
48. Ali H, Khan E, Sajad MA. Phytoremediation of heavy metals-concepts and applications. *Chem Eng J*. 2013;226:396-404. doi: 10.1016/j.chemosphere.2013.01.075
49. Pischke E, Barozzi F, Colina Blanco AE, *et al*. Dimethylmonothioarsenate is highly toxic for plants and readily translocated to shoots. *Environ Sci Technol*. 2022;56(14):10072-10083. doi: 10.1021/acs.est.2c01206
50. United States Environmental Protection Agency. (1999). *Phytoremediation Resource Guide* (EPA 542-B-99-003). Office of Solid Waste and Emergency Response.
51. Mahajan P, Kaushal J. Role of phytoremediation in reducing cadmium toxicity in soil and water. *J Toxicol.* 2018;2018:4864365. doi: 10.1155/2018/4864365

Asian Journal of Water, Environment and Pollution. Vol. 22, No. 2 (2025), pp. 43-50.
doi: 10.36922/ajwep.8196

ORIGINAL RESEARCH ARTICLE

Method validation and its application to gas chromatography-mass spectrometry analysis of dimethyl methylphosphonate in OPCW proficiency testing

Faris Rudi[1,2], Nor Kartini Abu Bakar[1]*, Noor Azilah Mohd Kasim[3], Mohd Nor Faiz Norrahim[4]*, and Wan Elyn Amira Wan Adnan[2]

[1]Department of Chemistry, Faculty of Science, Universiti Malaya, Kuala Lumpur, Malaysia
[2]Science and Technology Research Institute for Defence (STRIDE), Ministry of Defence, Kajang, Selangor, Malaysia
[3]Department of Chemistry and Biology, Center for Defence Foundation Studies, Universiti Pertahanan Nasional Malaysia, Kem Perdana Sungai Besi, Kuala Lumpur, Malaysia
[4]Research Center for Chemical Defence, Universiti Pertahanan Nasional Malaysia, Kem Perdana Sungai Besi, Kuala Lumpur, Malaysia
***Corresponding authors:** Nor Kartini Abu Bakar (kartini@um.edu.my), Mohd Nor Faiz Norrahim (faiz@upnm.edu.my)

Received: December 25, 2024; Revised: February 15, 2025; Accepted: February 19, 2025; Published online: March 27, 2025

Abstract: The detection and identification of chemical warfare agents (CWAs) are critical to safeguarding global security, as these toxic substances pose significant threats to human health and the environment. Effective monitoring and control of CWAs are essential for compliance with the Chemical Weapons Convention. Contamination of water sources with CWAs or their degradation products can have long-lasting ecological and public health implications. Dimethyl methylphosphonate (DMMP), a chemical simulant with structural similarities to hazardous organophosphorus agents, was selected for this study due to its relevance in proficiency testing (PT) and method validation. Here, we present the development and validation of a gas chromatography-mass spectrometry technique for the determination of DMMP. The QuEChERS extraction method was utilized to enhance sample preparation efficiency. The results obtained from the validated method revealed excellent linearity ($R^2 = 0.9998$), a low limit of detection of 0.0167 ppm, and high accuracy and precision, with recovery values between 95.7% and 97.3%, and low relative standard deviations at 3.5% for intraday and 3.7% for interday. The method was successfully applied in an Organisation for the Prohibition of Chemical Weapons PT, achieving a recovery value of 95.6% for DMMP. These results demonstrate the reliability of the method, underscoring its potential for use in international efforts to monitor and control CWAs, thereby preventing their misuse.

Keywords: Chemical warfare agents; OPCW proficiency testing; QuEChERS; Dimethyl methylphosphonate

1. Introduction

Chemical warfare agents (CWAs) include highly toxic chemicals and their pre-cursors specifically designed to inflict death, incapacitation, or severe harm upon individuals. Consequently, their use has been a serious concern for global security over a century.[1] The intentional deployment of chlorine gas during World War I (1914 – 1918) marks the historical commencement of large-scale chemical warfare, with devastating effects.[2] Throughout the 20th century and into the modern era, the world has witnessed the terrifying consequences of

CWAs in numerous incidents. The 1994 Tokyo subway sarin attack, orchestrated by the Aum Shinrikyo cult, killed 12 people, permanently harmed thousands, and left a deep psychological impact on the survivors.[3,4] Similarly, the 2017 assassination of Kim Jong-nam at Kuala Lumpur International Airport (KLIA 2) using the nerve agent VX highlighted the continuous threat CWAs pose even in civilian spaces.[3,4]

CWAs are highly toxic and have thus been included under the category of Weapons of Mass Destruction due to their great potential for mass casualties and devastating impacts on human health and the environment. These agents are designed to incapacitate, injure, or kill, and their exposure might lead to symptoms from respiratory distress, seizures, paralysis to even death, depending on the agent and level of exposure of the organisms.[1] The most toxic CWAs include highly potent inhibitors of acetylcholinesterase, such as nerve agents, such as sarin and VX, which build up acetylcholine at synapses and result in lethal respiratory failure. For example, VX is lethal even at a dermal dose of 6 – 10 mg, with death following in minutes if left untreated.[5]

In response to these threats, the international community has established stringent measures to control and eliminate CWAs. The Chemical Weapons Convention (CWC), which came into force on April 29, 1997, is a landmark treaty administered by the Organisation for the Prohibition of Chemical Weapons (OPCW). The CWC mandates the prohibition of the development, production, acquisition, stockpiling, and use of chemical weapons. As of 2020, 193 countries, representing over 98% of the global population, have ratified the treaty, reinforcing its status as one of the most universally adhered to disarmament treaties.

Despite these international agreements, ensuring compliance and preventing the illegal use of CWAs remains a critical challenge. The OPCW plays a pivotal role in overseeing compliance with the CWC through its Designated Laboratories (DLs), which are responsible for the off-site analysis of CWC-related chemicals obtained during Challenge Inspections or Alleged Use Investigations. These laboratories must demonstrate their ability to accurately detect and identify CWAs in complex matrices by participating in OPCW proficiency testing (PT), a rigorous interlaboratory testing regime conducted twice a year.[6] Participation in OPCW PT is crucial for laboratories seeking or maintaining DL status, as it evaluates their ability to perform accurate and reliable CWAs analysis.

CWAs are normally classified based on their chemical nature and physiological action. Some of the major groups include nerve agents, blister agents, blood agents, and choking agents. Nerve agents such as sarin (GB), soman (GD), tabun (GA), and VX, which belong to the group of organophosphorus compounds that work through irreversible inhibition of acetylcholinesterase, cause respiratory failure and eventual death.[7-9] These are highly toxic agents, and for that reason, direct experimentation with this chemical has huge safety and regulatory concerns. Therefore, developing analytical methods requires structural simulants as they share key physiochemical properties with CWAs but significantly pose a lower risk.[10-12]

Dimethyl methylphosphonate (DMMP) is an organophosphorus compound commonly used as a simulant for CWAs in OPCW PT. Figure 1 shows the chemical structure of the DMMP. A major component of the nerve agent simulants is DMMP, a surrogate compound that replicates the chemical properties of nerve agents such as sarin and soman. Although it represents the class of highly toxic organic compounds, DMMP has a relatively low toxicity but is structurally similar to sarin.[13] DMMP has been employed as a spiking agent in several OPCW PT rounds, including the 52nd OPCW PT, making it a relevant and practical choice for this research. The growing body of research on novel sample preparation and analytical techniques for CWAS detection is evident in the increasing number of scientific publications in this field. Over the past 20 years, an average of 140 scientific outputs per year has focused on the detection and analysis of CWAs, reflecting the continuous advancement in this field.

OPCW PT samples often include a variety of materials, such as water, soil, and organic matrices, spiked with low concentrations of CWAs or chemicals related to the CWC. These tests require precise sample preparation and analysis, as spiked analytes are frequently present in trace amounts and mixed with complex matrices that are deliberately designed to interfere with detection. Laboratories must use at least two independent analytical methods – one of which must be a spectrometric method – to ensure reliable identification. Analytical methods such as gas chromatography-mass spectrometry (GC-MS), combined with advanced extraction techniques,

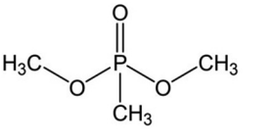

Figure 1. Chemical structure of dimethyl methylphosphonate

play a central role in this process.[14,15] Water bodies contaminated with CWAs or related compounds, such as DMMP, pose complex analytical challenges. These contaminants often occur in trace amounts and are accompanied by matrix interferences, requiring robust and sensitive analytical techniques.

Historically, liquid-liquid extraction (LLE) has been the most widely used sample preparation technique in OPCW PT. This classical method relies on the partitioning of analytes between two immiscible solvents with different polarities, which isolates the target compounds from the sample matrix.[16] For non-polar and semi-polar CWAs, dichloromethane is commonly employed as the extraction solvent. However, advancements in sample preparation methods have led to the development of alternative techniques such as single-drop microextraction, dispersive LLE, and solid-supported LLE, which offer enhanced precision and reliability.[17]

In recent years, interest has grown in the application of the Quick, Easy, Cheap, Effective, Rugged, and Safe (QuEChERS) method, which was originally developed for the analysis of pesticide residues in food products.[18] QuEChERS has gained popularity due to its simplicity and efficiency, making it an attractive alternative for sample preparation in various fields. Despite its widespread use for pesticide analysis, QuEChERS has not yet been extensively applied to the analysis of CWAs or OPCW PT samples. The QuEChERS technique was chosen in this study since it is simple, low in solvent consumption, and entails minimal sample handling, thereby increasing reproducibility.[19] As compared to traditional methods, such as LLE or solid phase extraction (SPE), QuEChERS achieves superior recovery with less matrix effect.[14] This is particularly beneficial in OPCW PT, where CWAs or their simulants are most found in complex and challenging matrices. Given the structural similarities between certain pesticides (*e.g.*, organophosphorus compounds) and CWAs, such as sarin, soman, and VX, adapting the QuEChERS method for CWAs analysis could offer significant benefits.[19] This study focuses on the adaptation and validation of the QuEChERS methodology for the analysis of DMMP for the 52nd OPCW PT.

This study aims to contribute to this expanding knowledge base by evaluating the performance of the QuEChERS method for DMMP detection, with a focus on key performance parameters such as selectivity, limit of detection (LOD), limit of quantification (LOQ), accuracy, precision, and specificity. In this study, DMMP serves as the reference standard for evaluating the QuEChERS method's performance in OPCW PT, a novel approach that has not been extensively explored in CWAS-related research. This method has the potential to streamline sample preparation, reduce costs, and enhance the accuracy of CWAS analysis, offering significant contributions to international efforts to prevent the use of chemical weapons.

2. Materials and methods

2.1. Reagents and materials

DMMP, utilized as the reference standard, was acquired from Thermo Scientific. Acetonitrile (ACN), toluene, hexane, and sodium chloride (NaCl) were sourced from Merck, while magnesium sulfate anhydrous ($MgSO_4$) and acetic acid were obtained from J.T. Baker Chemical Company. C_7-C_{30} saturated alkanes and fatty acid methyl ester (FAME) diesel was purchased from Sigma-Aldrich. All chemicals were of analytical grade, and ultrapure water was used throughout the experiments. The real sample analyzed in this study was obtained from the 52nd OPCW PT, where DMMP was included in the spiking list.

2.2. Methods

2.2.1. Sample preparation method

For sample preparation, 1 mL of the 52nd OPCW PT sample was added to a centrifuge tube and mixed with 500 µL of ACN (1% acetic acid). The tube was capped and placed in a freezer at −18°C for 15 min. Following this, 1.5 g of $MgSO_4$ and 0.75 g of NaCl were added to the mixture, which was shaken vigorously for 1 min. The mixture was then centrifuged at 4400 rpm under cooling at 5°C for 5 min. Subsequently, 600 µL of the upper layer was transferred into a vial containing 0.2 g of $MgSO_4$. The vial was shaken and centrifuged again at 4400 rpm under cooling for 2 min. Finally, the extract was transferred into a gas chromatography (GC) vial for analysis. Figure 2 shows the flow process of sample preparation used in this study.

2.2.2. Gas chromatography-mass spectrometry analysis

DMMP residues were determined using a 5975 Series Agilent GC-MS (Agilent Technologies, USA), equipped with an autosampler and employing splitless injection. The column used was HP-5MS Ultra Inert (Agilent Technologies, USA), measuring 30 m in length, with a 0.25 mm internal diameter and a film thickness of 0.25 µm. The oven temperature was initially set at 200°C for 2 min, then ramped to 290°C at a rate of

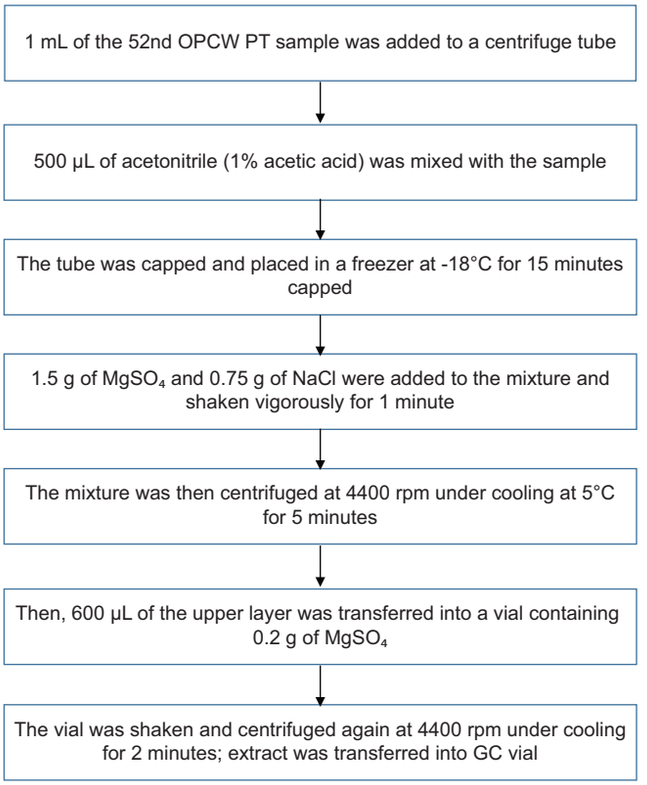

Figure 2. Flow process of sample preparation method
Abbreviations: GC: Gas chromatography; OPCW: Organisation for the Prohibition of Chemical Weapons; PT: Proficiency testing.

15°C/min, holding for an additional 4 min. Three ions were selected from DMMP for analysis: m/z 125, m/z 79, and m/z 47. The highest relative abundance ion (m/z 125) was designated as the quantifier ion, while m/z 79 and m/z 47 served as confirmation qualifier ions.

2.3. Method validation

2.3.1. Linearity study and calibration curve

To evaluate the linearity of the DMMP response, a series of standard solutions ranging from 1 ppm to 25 ppm were prepared in water. The 1 – 25 ppm concentration range was chosen in alignment with existing literature that determines exposure levels and detection limits for organophosphorus agents in environmental and forensic applications.[20,21] The concentration range chosen falls within the possible contamination scenario faced during OPCW PT and expresses confidence that the method is sufficient for trace-level detection in challenging matrices. In addition, toxicity studies have shown that acute exposure to organophosphorus at levels within this concentration range can produce mild-to-severe physiological effects, highlighting the need for accurate and sensitive analytical techniques.

The method's linearity was assessed by plotting the instrument response against the concentration of DMMP. A linear regression analysis of the calibration curve provided the coefficient of determination (R^2), indicating how well the data fit a linear model.

2.3.2. Specificity

The specificity of the method was assessed by introducing hydrocarbons and diesel into the sample matrix, as these are commonly encountered in OPCW PT samples. This validation is critical, as poor sample extraction can result in the loss of the target analyte, adversely affecting the accuracy of the analysis.

2.3.3. LOD and LOQ

The LOD and LOQ were determined using standard solutions at low concentrations. The LOD was defined as the concentration that produced a signal approximately three times the baseline noise, while the LOQ was the concentration that produced a signal roughly ten times the noise level.

2.3.4. Accuracy and precision

The method's accuracy was validated by spiking known concentrations of DMMP (1 ppm, 10 ppm, and 25 ppm) in triplicate. The percent recovery for each concentration was calculated to evaluate accuracy. Precision was assessed by evaluating method repeatability (intraday) and reproducibility (interday). Repeatability was performed by measuring triplicate spiking concentrations at 5 ppm and 15 ppm of DMMP within a single day, while reproducibility involved repeated measurements on different days. The relative standard deviation (RSD) was calculated for both intra- and inter-day assessments.

3. Results and discussion

The overall analysis method using GC-MS and QuEChERS methodology for the screening and detection of CWAS in the 52nd OPCW PT was successfully optimized. A validated GC-MS technique for identifying DMMP in OPCW PT samples performed well across all main analytical parameters. The method showed excellent linearity (R^2 = 0.9998) with LOD and LOQ values of 0.0167 ppm and 0.0557 ppm, respectively. These values indicate the method's sensitivity, important in PT where analytes are present in trace amounts.

3.1. Linearity, LOD and LOQ

The calibration curve was obtained by injecting a standard DMMP in concentrations of 1 ppm, 5 ppm, 10 ppm, 15 ppm, 20 ppm, and 25 ppm. The slopes and intercept of this equation were 179400.45 and −66927.88. The correlation coefficients (R^2) for this equation were 0.9998 indicating a strong and excellent linear relationship. The LOD for this method validation was 0.0167 ppm while the LOQ was 0.0557 ppm.

The sensitivity of this method with a LOD of 0.0167 ppm aligns with the past studies for CWAS detection where Sassolini *et al.*[16] used LLE with GC-MS and obtained an LOD of 0.05 ppm for organophosphorus compounds. Similarly, Konopski *et al.*[6] determined that the LOD for nerve agents in a method validation study was 0.02 ppm. In this regard, the approach presented herein performs better in terms of detection, indicating the benefits of QuEChERS as an extraction method. The reduced LOD value not only improved the limits of detection for CWAS simulants, such as DMMP, but it also increased the method's applicability in real-world environmental samples for trace-level CWAS detection.

In this study, the linearity ($R^2 = 0.9998$) is consistent with previously proven methodologies in this field. Dubey *et al.*[14] used GC-MS to detect CWAs and found an R^2 value of 0.9997 for nerve agents, indicating that the study's results matched recognized methodologies. This near-perfect linearity provides consistent quantification of DMMP across a wide concentration range, which is critical in PT.

3.2. Accuracy and precision

The accuracy and precision of the method were assessed based on recovery and repeatability, which are crucial indicators of the method's reliability in determining DMMP. The results are summarized in Table 1. The recovery rates ranged from 95.7% to 97.3%, and the %RSD was <10%, demonstrating that the method meets the required criteria for accuracy and precision. The repeatability and reproducibility were performed with spiking concentrations of 5 and 15 ppm of DMMP within a day and on different days. The results were tabulated in Table 2 with the percentage of RSD below 5% indicating a good analytical method.

The precision of this method, demonstrated by an RSD of <10%, is a key factor in assessing its reliability for repeated applications, such as PT. Dubey *et al.*[14] reported RSD values in the range of 8 – 10% for nerve agent detection. In contrast, this study achieved an RSD of <5%, highlighting the method's excellent reproducibility and robustness, particularly for use with complex samples containing high matrix interference.

Among the important findings in the present study is applying the QuEChERS extraction method, which conventionally is applied for pesticide residue analysis. Although QuEChERS has seldom been applied in the context of CWAs detection, the results of this study have proved better performance, exceeding the conventional approaches to extraction such as LLE and SPE, which have been considered the gold standard in CWAs analysis. The simplicity and efficiency of QuEChERS are the main advantages of this technique with few steps, less solvent used than LLE, and shorter processing times than SPE. Anastassiades *et al.*[18] originally developed the QuEChERS method for pesticide analysis, but its adaptation for the detection of DMMP suggests it could potentially be applied to other CWAS. The study by Antonijevic *et al.*,[19] which used a traditional conventional method, such as LLE, found high solvent consumption and longer extraction times. This, in contrast, can be avoided by using the QuEChERS approach. Moreover, the recovery rates for this study (95.7 – 97.3%) are higher compared to earlier studies. Pragney and Saradhi[17] successfully reported a recovery rate of 88 – 92% for organophosphorus agents with the SPE technique.

3.3. Specificity

The specificity of the method was evaluated by preparing a solution containing 10 ppm of DMMP, 10 ppm of C_7-C_{30} saturated alkanes, and 10 ppm of FAME diesel. This solution was prepared in triplicate to ensure reproducibility and precision. The analytical results indicated that the methodology achieved a DMMP extraction accuracy of 96.2%, reflecting its high level of analytical performance and reliability.

Table 1. Accuracy of the proposed method

Analyte	Spiked concentration (ppm)	Detected concentration (ppm)	Recovery (%)	RSD (%)
DMMP	1	0.957	95.7	6.2
	10	9.73	97.3	3.4
	25	24.175	96.7	4.1

Abbreviation: RSD: Relative standard deviation.

The identification of DMMP in the presence of interfering chemicals, such as hydrocarbons and diesel, which are typically introduced to PT samples to challenge the analytical process, provided the last evidence of the method's specificity. Indeed, recent research by Sassolini *et al*.[16] and Konopski *et al*.[6] indicated that achieving specificity in such complex matrices was challenging for LLE; in fact, lower accuracy was seen when contaminants were present in the sample. In contrast, the QuEChERS approach demonstrated exceptional resilience in this investigation, even when there is significant matrix interference, by offering high recoveries and accuracies at 96.2%.

Table 2. Accuracy of the proposed method

Analyte	Intraday precision RSD (%)		Interday precision RSD (%)	
	5 ppm	15 ppm	5 ppm	15 ppm
DMMP	4.2	3.5	4.8	3.7

Abbreviation: RSD: Relative standard deviation.

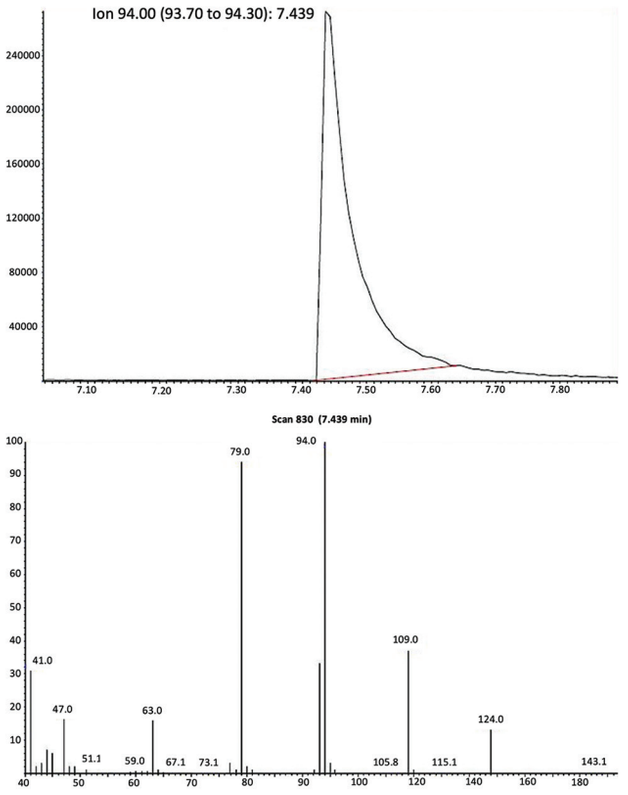

Figure 3. Extracted ion chromatogram of DMMP (top) and mass spectra of DMMP (bottom)
Abbreviation: DMMP: Dimethyl methylphosphonate

3.4. Real sample analysis

The proposed method of validation was used for a real sample, which was the OPCW 52nd PT sample. From the preliminary report by OPCW, DMMP was one of the spiking chemicals for sample 525 with a concentration of 5 ppm. The proposed method was able to extract and qualitatively detect DMMP in sample 525 with an accuracy of 95.6%. The extracted ion chromatogram and mass fragmentation of DMMP are shown in Figure 3.

4. Conclusion

The validation and application of the GC-MS method for analyzing CWC-related compounds, DMMP, in the context of OPCW PT, have proven highly successful. The study demonstrated that the validated approach, utilizing the QuEChERS extraction methodology, is both reliable and effective for detecting CWAs-related compounds. The method exhibited a remarkable linearity with a correlation coefficient of R^2 = 0.9998, indicating an excellent linear response across the studied concentration range. Furthermore, the low LOD at 0.0167 ppm and LOQ at 0.0557 ppm confirm the method's sensitivity for detecting low concentrations in complex matrices. The application of this validated method to an authentic sample from the 52nd OPCW PT resulted in a recovery rate of 95.6% for DMMP, demonstrating the method's efficiency and robustness. This approach not only meets the stringent requirements for OPCW PT but also enhances the analytical capabilities for the detection of CWC-related compounds. Consequently, it contributes significantly to ongoing global non-proliferation efforts, reinforcing the importance of reliable methodologies in the monitoring and control of chemical weapons. The future work will focus on further validation using actual G-series nerve agents in collaboration with an OPCW DL. This would provide a direct comparison between DMMP and real CWAs, ensuring the method's applicability in real-world scenarios.

Acknowledgments

The authors would like to thank the Department of Chemistry, Universiti Malaya, for the vital facilities and support throughout this study. We would like to acknowledge Universiti Pertahanan Nasional Malaysia (UPNM) for the great opportunity to cooperate and for the important contributions. Special thanks go to the Science and Technology Research Institute for

Defence (STRIDE), Ministry of Defence, Malaysia, for assistance and support.

Funding

None.

Conflict of interest

The authors declare that there is no conflict of interest.

Author contributions

Conceptualization: Faris Rudi, Nor Kartini Abu Bakar, and Noor Azilah Mohd Kasim

Investigation: Faris Rudi, Nor Kartini Abu Bakar, and Noor Azilah Mohd Kasim

Methodology: Faris Rudi and Wan Elyn Amira Wan Adnan

Writing – original draft: Faris Rudi, Nor Kartini Abu Bakar, Mohd Nor Faiz Norrrahim, and Wan Elyn Amira Wan Adnan

Writing – review & editing: All authors

Availability of data

Not applicable.

References

1. Meng WQ, Sedgwick AC, Kwon N, *et al*. Fluorescent probes for the detection of chemical warfare agents. *Chem Soc Rev*. 2023;52(2):601-662. doi: 10.1039/D2CS00650B
2. Fitzgerald G. Chemical warfare and medical response during world war I. *Am J Public Health*. 2008;98:611-625. doi: 10.2105/AJPH.2007.11930
3. Mohd Rudi MF, Hussein N, Mohd Kamel S, Aziz N. Decontamination of chemical warfare agent by nanocomposite adsorbent: A GC-MS study. *Defence S T Tech Bull*. 2021;14:12-19.
4. Tu AT. The use of VX as a terrorist agent: action by Aum Shinrikyo of Japan and the death of Kim Jong-Nam in Malaysia: four case studies. *Glob Secur Health Sci Policy*. 2020;5(1):48-56. doi: 10.1080/23779497.2020.1801352
5. Ranjan A, Jindal T. Toxicology of organophosphate poisoning in human. In: *Toxicology of Organophosphate Poisoning: New Insights*. Germany: Springer International Publishing; 2022. p. 27-43. doi: 10.1007/978-3-030-79128-5_2
6. Konopski L, Liu P, Wuryani W, Sliwakowski M. OPCW Proficiency test: A practical approach also for interlaboratory test on detection and identification of pesticides in environmental matrices. *ScientificWorldJournal*. 2014;2014:542357. doi: 10.1155/2014/542357
7. Labaška M, Gál M, Mackuľak T, *et al*. Neutralizing the threat: A comprehensive review of chemical warfare agent decontamination strategies. *J Environ Chem Eng*. 2024;12(6):114243. doi: 10.1016/j.jece.2024.114243
8. Ganesan K, Raza SK, Vijayaraghavan R. Chemical warfare agents. *J Pharm Bioallied Sci*. 2010;2(3):166-178. doi: 10.4103/0975-7406.68498
9. Delfino R, Ribeiro T, Figueroa-Villar J. Organophosphorus compounds as chemical warfare agents: A review. *J Braz Chem Soc*. 2009;20:407-428. doi: 10.1590/S0103-50532009000300003
10. James T, Collins S, Marczylo T. Identification of novel simulants for toxic industrial chemicals and chemical warfare agents for human decontamination studies: A systematic review and categorisation of physicochemical characteristics. *Int J Environ Res Public Health*. 2021;18:8681. doi: 10.3390/ijerph18168681
11. Tuccitto N, Spitaleri L, Li Destri G, Pappalardo A, Gulino A, Trusso Sfrazzetto G. Supramolecular sensing of a chemical warfare agents simulant by functionalized carbon nanoparticles. *Molecules*. 2020;25(23):5731. doi: 10.3390/molecules25235731
12. Puglisi R, Mineo PG, Pappalardo A, Gulino A, Trusso Sfrazzetto G. Supramolecular detection of a nerve agent simulant by fluorescent Zn–Salen oligomer receptors. *Molecules*. 2019;24(11):2160. doi: 10.3390/molecules24112160
13. Saya L, Ratandeep, Arya B, *et al*. Recent advances in sensing toxic nerve agents through DMMP model simulant using diverse nanomaterials-based chemical sensors. *Talanta*. 2024;272:125785. doi: 10.1016/j.talanta.2024.125785
14. Dubey V, Velikeloth S, Sliwakowski M, Mallard G. Official proficiency tests of the organisation for the prohibition of chemical weapons: Current status and future directions. *Accredit Qual Assur*. 2009;14(8):431-437. doi: 10.1007/s00769-009-0520-0
15. Mohd Rudi MF, Aziz N, Hussein N, Zahari N, Bakar SA, Ismail S. Identification of spiking chemicals related to the chemical weapons Convention in water sample during an interlaboratory competency test. *Defence S T Tech Bull*. 2018;11:317-330.
16. Sassolini A, Malizia A, D'Amico F, *et al*. Comparison of three sample preparation methods for analyis of chemical warfare agent simulants in water. *Malay J Anal Sci*. 2015;19:603-610.
17. Pragney D, Vijaya Saradhi UV. Sample-preparation techniques for the analysis of chemical-warfare agents and related degradation products. *TrAC Trends Anal*

Chem. 2012;37:73-82.
doi: 10.1016/j.trac.2012.03.007

18. Anastassiades M, Lehotay SJ, Štajnbaher D, Schenck FJ. Fast and easy multiresidue method employing acetonitrile extraction/partitioning and "dispersive solid-phase extraction" for the determination of pesticide residues in produce. *J AOAC Int*. 2003;86(2):412-431.
doi: 10.1093/jaoac/86.2.412
19. Antonijevic E, Musilek K, Kuca K, Djukic-Cosic D, Vucinic S, Antonijevic B. Therapeutic and reactivating efficacy of oximes K027 and K203 against a direct acetylcholinesterase inhibitor. *Neurotoxicology*. 2016;55:33-39.
doi: 10.1016/j.neuro.2016.05.006
20. Hu N, Wang Y, Chai J, *et al*. Gas sensor based on p-phenylenediamine reduced graphene oxide. *Sens Actuat B Chem*. 2012;163(1):107-114.
doi: 10.1016/j.snb.2012.01.016
21. Wu G, Zhang D, Xu W, *et al*. Highly cross-linked epoxy coating for barring organophosphate chemical warfare agent permeation. *ACS Omega*. 2022;7(14):12354-12364.
doi: 10.1021/acsomega.2c00915

Asian Journal of Water, Environment and Pollution. Vol. 22, No. 2 (2025), pp. 51-63.
doi: 10.36922/AJWEP025040020

ORIGINAL RESEARCH ARTICLE

Groundwater contamination with heavy metals: A case study in Hebron, Palestine

Waseem Al-Tamimi[1]*, Fadoua Hamzaoui-Azaza[2], Marwan Ghanem[3], and Rachida Bouhlila[1]

[1]Modeling Hydraulic and Environmental Laboratory, National Engineering School of Tunis (ENIT), University of Tunis El Manar, Campus Farhat Hached El Manar, Tunis, Tunisia
[2]Laboratory of Sedimentary Basins and Petroleum Geology (SBPG), Geology Department, Faculty of Sciences of Tunis, University of Tunis El Manar, Tunis, Tunisia
[3]Department of Geography, GeoInformatics Programme, Birzeit University, Ramallah, West Bank, Palestine
***Corresponding author:** Waseem Al-Tamimi (waseem.altamimi@enit.utm.tn)

Received: January 22, 2025; Revised: March 3, 2025; Accepted: March 6, 2025; Published Online: April 3, 2025

Abstract: The study aims to identify seasonal fluctuations in groundwater quality concerning heavy metal contamination. Specifically, it assesses heavy metal concentrations in groundwater in Wadi Al-Samen, evaluates its suitability for drinking purposes, and compares these levels with the World Health Organization standards. Groundwater samples were collected from 20 wells over two seasons and analyzed for 16 trace elements using atomic absorption spectrometry. The metals analyzed include barium, molybdenum, iron, cobalt, cadmium, chromium, boron, lithium, aluminum, arsenic, manganese, nickel, copper, zinc, lead, and selenium. Results showed that four samples exceeded the permissible limits for barium and lithium in both seasons, three samples exceeded the recommended zinc limits in both seasons, 17 samples exceeded the permissible selenium limit in the dry season, and 15 in the wet season, while one sample exceeded the recommended copper limit in both seasons. The heavy metal pollution index (HPI) and metal index (MI) were used to assess contamination levels. HPI values exhibited significant spatial variations, with recorded values of 17.2 in the dry season and 11.99 in the wet season, both below the critical threshold of 100. Groundwater quality was classified as poor in the Al-Hejreh well and very poor in the Al-Fawwar1 well, rendering it unsuitable for drinking. MI results indicated moderate heavy metal contamination, with mean MI values of 2.3 in the dry season and 2.2 in the wet season. The heavy metals detected in the study area were categorized into toxic elements, alkaline earth metals, alkali metals, transition metals, other metallic elements, and non-metallic elements. This research highlights groundwater contamination in Wadi Al-Samen and underscores the need for mitigation measures to reduce health risks for local residents.

Keywords: Heavy metals; Heavy metal pollution index; Metal index; Wadi Al-Samen

1. Introduction

Environmentally friendly wastewater management is a major challenge for developing countries, including the West Bank in Palestine. Heavy metal contamination from untreated sewage discharges is an escalating concern due to its possible risks to human health.[1] Assessing groundwater quality is crucial for water management, as both agricultural and industrial activities can negatively affect groundwater resources.[2] Heavy metals in groundwater, even in small amounts, are undesirable due to their toxicity to both human health

and ecosystems.[3,4] Heavy metals tend to bioaccumulate, leading to progressively higher concentrations in organisms over time.[5] In recent years, the use of heavy metals in agriculture and industry has increased.[6] When consumed through contaminated drinking water, these substances can have detrimental effects on human health.[4] Industrial expansion has further increased human exposure to heavy metals.[7] Among the most common heavy metals associated with human poisoning are lead (Pb), arsenic (As), manganese (Mn), cadmium (Cd), nickel (Ni), chromium (Cr), and copper (Cu). Bioaccumulation of heavy metals in the human body leads to toxic effects on various tissues and cells.[8] Acute and chronic toxic effects can result in serious complications, including nervous system disorders, gastrointestinal and renal dysfunction, blood vessel damage, skin lesions, immune system dysfunction, birth defects, and cancer.[9,10]

Lead toxicity has significant adverse effects on the human body, particularly on the neurological, renal, and reproductive systems.[11,12] The kidneys are the primary organs affected, with lead exposure leading to nephropathy and renal failure.[13] As the primary route of lead excretion, the kidneys play a crucial role in detoxification.[12] Lead exposure can also result in developmental abnormalities, including intellectual impairments in children and behavioral disturbances.[14] Children are particularly vulnerable to lead poisoning due to their increased exposure to lead-laden dust and a higher susceptibility to permanent neurological damage compared to adults.[15] Chronic lead toxicity is associated with encephalopathy, peripheral neuropathy, central nervous disorders, and anemia.[16]

Arsenic exposure poses significant health risks, affecting many parts of the human body.[17] It has been linked to gastrointestinal and hepatic disorders, vascular diseases, and cardiovascular and respiratory complications. Chronic arsenic poisoning is closely linked to skin, lung, and bladder cancer. Long-term exposure to arsenic through drinking water can cause cancer in these organs in a dose-dependent manner.[12] High levels of arsenic exposure can also lead to neurological disorders, including peripheral neuropathy.[18] In addition, cognitive impairment in both children and adults has been associated with arsenic toxicity. Clinical manifestations of chronic arsenic toxicity include perforation of the nasal septum, respiratory cancer, and peripheral neuropathy, as well as dermatological conditions and increased cancer risk.[16]

Chronic exposure to increased manganese levels has been associated with Central and Peripheral Neuropathies while Nickel toxicity has been linked to an increased risk of cancer and dermatological conditions.[16]

Cadmium toxicity primarily affects the respiratory system, with inhalation leading to flu-like symptoms. Prolonged exposure through smoke inhalation has been associated with chronic obstructive pulmonary disease and chronic bronchitis. Lung cancer is one of the most likely diseases if we consider that cadmium causes cancer. Cadmium is also a known carcinogen, with lung cancer being a significant health risk.[12] Ingesting cadmium-contaminated food or drinking water can adversely impact the gastrointestinal tract, leading to renal toxicity and kidney damage. Chronic cadmium exposure is also associated with itai-itai disease[13] and an increased risk of cardiovascular disease.[12] Clinical manifestations of chronic cadmium toxicity include proteinuria, glucosuria, osteomalacia, aminoaciduria, and emphysema while those of chromium toxicity include ulcers, perforation of nasal septum, and respiratory cancer.

Some heavy metals, such as chromium and nickel, have been linked to cancer in exposed human populations. Long-term inhalation of chromium can irritate the respiratory system, increasing lung sensitivity and the risk of lung cancer. The health effects of chromium poisoning extend to respiratory, skin, gastrointestinal, cardiovascular, and reproductive toxicity, as well as an elevated risk of cancer. Dermal contact with toxic chromium compounds can result in skin ulcers and dermatitis.[12] High levels of copper exposure can destroy red blood cells, which in turn leads to anemia. Excessive copper accumulation may also cause liver toxicity, which, at extreme doses, can be fatal.[16]

The presence of these metals in water represents a significant environmental concern, threatening both aquatic ecosystems and public health.[19] Elevated levels of heavy metals, including arsenic, cadmium, manganese, iron (Fe), copper, mercury (Hg), zinc (Zn), chromium, and selenium (Se), pose significant risks to human health, especially to children.[20] Industrial discharges, especially from tanneries, have caused a substantial rise in heavy metal concentrations in water and soil worldwide.[21-23] The presence of heavy metals in groundwater is controlled by both natural and human-made factors.[24] Natural factors include soil leaching, mineral weathering, aquifer type, water infiltration quality, and residence time. Anthropogenic sources primarily stem from industrial and household wastewater, soil contamination, urban stormwater,

surface runoff, landfill leachate, agricultural fertilizers and pesticides, as well as mining activities.[24,25]

In Hebron, major sources of water pollution include nearby disposal sites, wastewater from settlements, exposed sewage, runoff from wastewater and leachate pits, landfill sites, industrial activities, livestock waste, and the continuous burning of plastic and other waste.[26] While two-thirds of Hebron City is connected to a sewage network, the remaining communities use household cesspools (percolation pits) for sewage disposal, posing significant environmental risks to groundwater and surrounding ecosystems.[27]

Monitoring and evaluating water contamination has become an essential field of research due to the significant impact of water pollution on aquatic life and humans. Some metals, such as iron, copper, zinc, and manganese, are vital nutrients for the physiological and biochemical functioning of plants, animals, and humans. However, these metals can be harmful at higher concentrations. On the other hand, non-essential elements, such as lead, cadmium, and arsenic are harmful even at low concentrations when present in groundwater. These metals do not biodegrade and tend to build up in the environment, bioaccumulating through the food chain and posing serious risks to human health and ecosystems.[28-30]

The heavy metal pollution index (HPI) serves as an important tool for evaluating the overall contamination of both groundwater and surface water.[24,30] It provides a quantitative measure of water quality concerning heavy metal pollution.[31-33] Factors, such as excessive pesticide use, improper waste disposal, and the release of untreated industrial wastewater into streams contribute to the decline in groundwater quality.[34] Ensuring access to safe drinking water is a key challenge in many developing regions, including the West Bank in Palestine.[35] Over recent decades, the demand for clean drinking water has increased, yet supply and water quality remain inadequate. Consequently, many Palestinian families rely on groundwater wells and hand-dug wells as their primary water sources for both drinking and household purposes. Those living near untreated sewage sites may be unaware of the health risks posed by contaminated groundwater.

This study aims to detect seasonal changes in groundwater quality concerning heavy metal contamination. It specifically examines heavy metal concentrations in groundwater from Wadi Al-Samen, evaluates their suitability for drinking, and compares the findings with World Health Organization (WHO) standards.

2. Materials and methods

2.1. Study area

The Wadi Al-Samen area is situated in Hebron, in the southern part of the West Bank, approximately 36 km south of Jerusalem (Figure 1). The climate of Hebron is influenced by the Mediterranean Sea, resulting in a semi-arid climate classification. Winters are the primary rainy season, with precipitation varying from heavy to light. The annual average rainfall in Hebron Governorate is around 540 mm, with roughly 75% occurring between November and March. The estimated annual average rainfall in Wadi al-Samen is 492 mm.[26]

Hebron's topography is characterized by mountainous terrain with elevations exceeding 1,000 m above sea level, leading to frequent freezing temperatures during winter. The average minimum monthly temperature is approximately 3°C. Relative humidity in the western part of Hebron Governorate ranges from 55% to 60%, with a similar range observed in the mountainous areas of Hebron. Household and industrial waste is discharged directly into wadis without treatment, including into Wadi al-Samen.

In 2021, the average flow of wastewater through the Hebron Municipality network was approximately

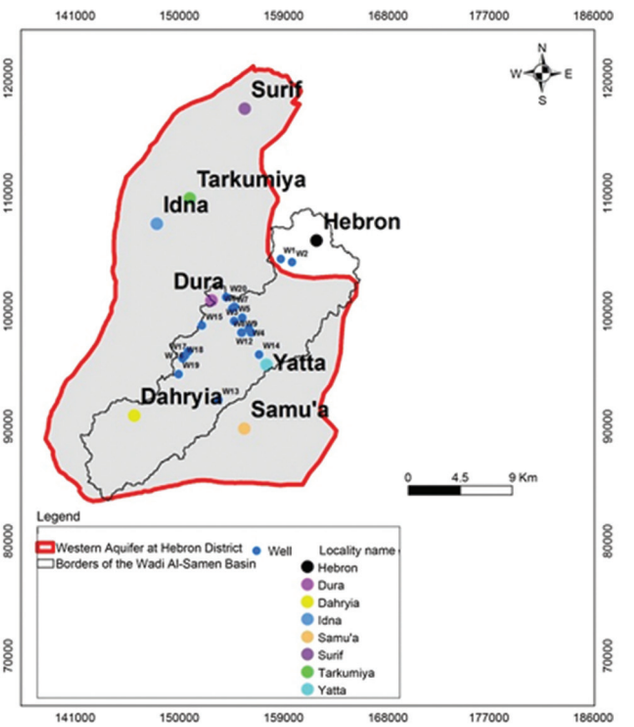

Figure 1. Geographical location of sample wells in the Hebron Governorate, Wadi Al-Saman Basin. The numbers at the borders represent the Palestinian coordinate system in West Bank.

444 m³/h (10,660 m³/day). This flow is projected to increase to 15,200 m³/day by 2027. In other parts of the Wadi al-Samen Basin, cesspits are commonly used for sanitation. The contents of the cesspits are often discharged indiscriminately into the environment, leading to potential contamination.

The area lacks comprehensive geological studies, which presents challenges in identifying geological features, comprehending tectonic processes, and defining the structural framework of the aquifer system. According to Zaarir[36] and Al-Tamimi,[37] the Hebron study area (Figure 2) is primarily composed of sedimentary carbonate rocks dating from the Albian to the Eocene periods, with quaternary alluvial deposits covering much of the surface. The primary aquifers in Hebron and the surrounding area consist of the following formations:

1. Aptian to Albian (Kobar Formation). Found in northern Hebron, west of Halhoul town, this formation primarily consists of limestone, marl, and marly limestone, with occasional marl-limestone intercalations. Thickness ranges from 30 m to 50 m.
2. Albian (Lower Beit Khail Formation). Composed of well-bedded, fine-crystalline, and highly karstic limestone, this formation also includes intermediate marl layers that increase in thickness downward, reaching depths between 120 m and 280 m.
3. Lower Middle Cenomanian (Yatta Formation). Consisting of fine- to medium-crystalline dolomite and limestone, this yellowish-brown formation occasionally includes marly limestone, which is often enriched with fossilized fauna. Thickness ranges from 50 m to 130 m.
4. Upper Middle Cenomanian (Hebron Formation). This formation includes hard, massive dolomite or limestone, typical of the Hebron area. It is highly karstic, with thickness ranging between 20 m and 120 m.
5. Upper Cenomanian (Bethlehem Formation). Rich in faunal content, this formation consists of limestone, dolomite, and chalky limestone with marl, with thickness ranging between 80 m and 270 m.
6. Upper Cenomanian (Turonian-Jerusalem Formation). Comprising limestone and dolomite, this formation covers 36.4% of the study area, ranking second in spatial extent within the study basin. Its thickness ranges from 90 m to 130 m.
7. Senonian (Abu Dis Formation). This formation is made up of chalks, chert, and marl, and it extends across the southern part of the basin. The chalk is typically white, covering approximately 0.7% of the basin, with thickness ranging from 0 m to 450 m.
8. Quaternary (Modern Deposits). This layer consists of alluvial deposits and unconsolidated sediments, such as clay, silt, gravel, and conglomerate, found on the valley floors. Thickness can reach tens of meters, and the red color of the alluvium is attributed to its limestone origin.

2.2. Field sampling and laboratory methods

Groundwater samples were collected in September 2019 and May 2020 to represent both dry and wet seasons.

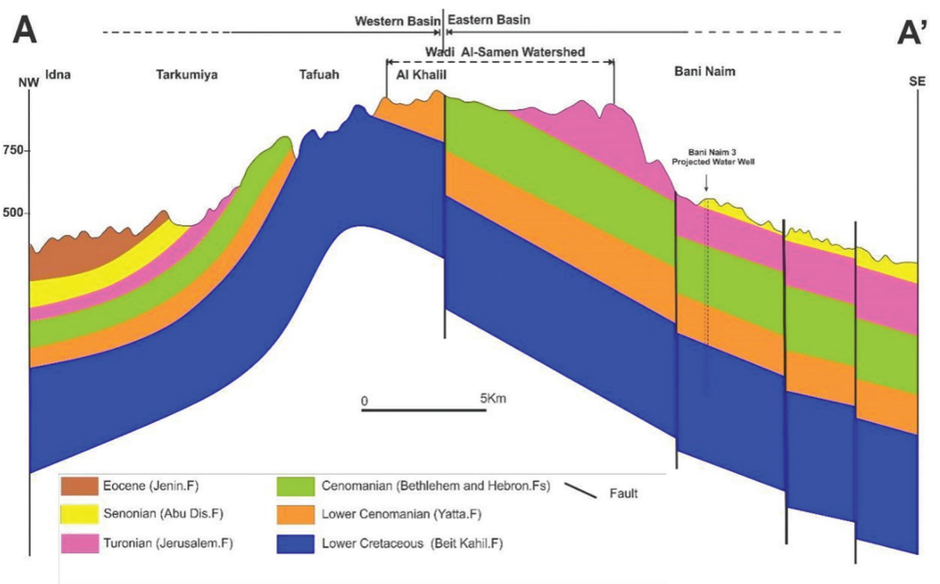

Figure 2. Geology of study area

Note: A, A' : Cross section from A(NW) to A'(SE). Abbreviations: F: Formation; NW: North West; SE: South East.

A total of 20 groundwater samples were gathered from 20 different locations. Each sample was collected in separate polypropylene bottles (Sigma, Germany) that had been pre-conditioned and acid-washed. These samples were then filtered and treated with concentrated nitric acid (Sigma, Germany) to lower the pH below 2.0, preventing precipitation and minimizing adsorption onto the walls of the container.

Before filling, each bottle was thoroughly washed three to five times with groundwater from the sampling site to ensure integrity. An atomic absorption spectrophotometer (PerkinElemer, USA) was used to measure the concentrations of heavy metals in the acidified filtrates.

2.3. HPI measurement

The HPI is a quantitative tool used to assess the combined impact of individual heavy metals on the overall quality of drinking water.[38] Ranging from 0 to 1, the HPI rating presents the relative significance of each quality parameter, and its deviation from the recommended standard (Si).[39-41]

The HPI was calculated following these steps: first, the weight of each parameter (Wi) was calculated; then the quality rating (Qi) for each heavy metal was determined; finally, the sub-indices were summed to obtain the overall index.

The Wi of each parameter (i) was determined using Equation I.

$$Wi = K/Si \quad \text{(I)}$$

Where Wi denotes the unit weight, Si is the recommended standard for the i-th parameter, and K is the proportionality constant.

The Qi for each metal was calculated using Equation II.

$$Qi = 100\ Vi/Si \quad \text{(II)}$$

Where Qi represents the sub-index for the i-th parameter, Vi is the measured value of the i-th parameter (in µg/L), and Si is the standard or permissible limit for the i-th parameter.

The HPI value, which indicates the overall quality of the drinking water in relation to heavy metals, was calculated using Equation III and Equation IV.

$$HPI = \frac{\sum_{i=1}^{n} Wi, Qi}{\sum_{i=1}^{n} Wi} \quad \text{(III)}$$

$$Qi = \sum i \frac{Mi(-)Ii}{Si - Ii} \times 100 \quad \text{(IV)}$$

Where Qi and Wi represent the sub-index and unit weight of the i-th parameter, respectively; n denotes the number of parameters considered; Mi, Ii, and Si correspond to the monitored values, the ideal value, and the standard values of the i-th parameter, respectively; − denotes the numerical difference between values, without considering the algebraic sign.

The metal quality index (MQI) serves as an early warning threshold, where a value below one is the threshold of warning. MQI was calculated using Equation V.

$$MQI = \sum_{i=1}^{n} \frac{Mi}{Si} \quad \text{(V)}$$

Where n denotes the number of parameters considered; Mi and Si correspond to the monitored values, the standard values of the i-th parameter, respectively.

The HPI categorizes water quality into three levels: low (HPI <100), threshold risk (HPI = 100), and high (HPI >100). When HPI exceeds 100, the water is deemed unsuitable for drinking. The HPI values for the dry and wet seasons are presented in Tables 1 and 2. [42-44]

In addition, the heavy metal evaluation index (HEI) was used to assess the quality of the water, specifically targeting heavy metal contamination.[31] The HEI was determined using Equation VI.

$$HEI = \sum_{i=1}^{n} \frac{Hc}{Hmac} \quad \text{(VI)}$$

Table 1. Water quality scale based on the heavy metal pollution index (HPI)[42]

HPI (%)	Water quality
0 – 24	Excellent
25 – 49	Good
50 – 74	Poor
75 – 100	Very poor
>100	Unfit for drinking

Table 2. Water quality classification using metal index (MI)[43,44]

MI	Characteristic	Class
<0.3	Very pure	I
0.3 – 1.0	Pure	II
1.0 – 2.0	Slightly affected	III
2.0 – 4.0	Moderately affected	IV
4.0 – 6.0	Strongly affected	V
>6.0	Seriously affected	VI

Where Hc and Hmac represent the monitored values and the maximum allowable concentration for the i-th parameter, respectively.

The HEI was classified into three categories: Low (HEI <10), medium (HEI = 10 – 20), and high (HEI >20). Higher HPI values correlate with increased health risks. The critical HPI threshold is typically set at 100, as shown in Table 1.[40,42]

2.4. Metal index (MI)

The MI offers a single value that encapsulates the contamination levels of the study area. An MI value exceeding one indicates a threshold warning, suggesting significant water quality degradation due to heavy metal concentrations exceeding the Maximum Allowable Concentration (MAC).[45]

The MI was calculated using Equation VII, as described by Tamasi and Cini.[46]

$$MI = \sum_{i=1}^{n} \frac{ci}{(MAC)i} \quad \text{(VII)}$$

Where MI is the MI, Ci refers to the concentration of each element in the solution, MACi is the maximum permissible concentration for each element, and the subscript i denotes the i-th sample.

The classification of water quality based on the MI is presented in Table 2.[43,44]

3. Results and discussion

3.1. HPI

The mean concentrations of 16 heavy metals were examined for both the dry and wet seasons, showing notable variations in metal concentrations across the different sampling locations. The concentrations of molybdenum (Mo), iron, cobalt, cadmium, chromium, boron, aluminum (Al), arsenic, manganese, nickel, copper, and lead were observed to be within the maximum allowable limits set by the WHO drinking water standards (2011). Based on their concentration levels and relative abundance, the metals were ranked in the following order: Se >Ba >Li >Zn >Cu.

The HPI was calculated using the mean concentrations of the 16 heavy metals. The overall HPI for Wadi Al-Samen was 17.2 during the dry season, significantly below the critical threshold of 100, indicating that the area is not severely polluted by heavy metals.

The highest HPI values were recorded at Al-Fawwar1 (89.73), Al-Hejreh (69.55), and Al-Fawwar2 (42.39) during the dry season, and at Al-Alaqa Al-Foqa (62.60), Abdo (44.47), and Khursa (41.53) during the wet season (Figure 3). These elevated values are likely attributed to domestic sewage discharge and the interaction between rock and water.

The lowest HPI values during the dry season were recorded in Karaza (3.40), Rihia (3.76), Al-Alaqa Al-Foqa (4.05), Omran1, Omran2, Omran3 (4.3), Ein-Qashqalah (4.39), Abdo (4.43), and Bi'r al-Wad (5.12). During the wet season, low HPI values were observed at Samu'a (3.03), Rihia (3.31), Omran1 (3.83), Ein-Qashqalah (3.84), Omran2 (3.90), Al-Fawwar1 (4.05), and Omran3 (4.08) (Figure 3). These lower HPI values suggest the diluting effect of rainwater seepage and percolation.

3.2. MI value

The MI for Wadi Al-Samen was found to be 2.3 in the dry season and 2.2 in the wet season. According to the classification by Lyulko *et al.* (2001)[43] and Caerio *et al*. (2005),[44] these values indicate moderate contamination by heavy metals. The findings align with the classification scale presented in Table 2,[43,44] confirming that water in Wadi Al-Samen is moderately impacted by heavy metal pollution in both seasons.

3.3. Groundwater contamination based on different groups of heavy metals

3.3.1. Toxic elements (lead and arsenic)

Lead is a highly toxic heavy metal naturally occurring in the Earth's crust and distributed across various environmental compartments. Due to its persistence and strong adsorption to soil particles, lead contamination remains a significant concern.[47] Human activities can contribute to elevated lead levels in natural water bodies.[48,49] The WHO[50] has set the permissible limit for lead in drinking water at 0.01 mg/L. Consumption of groundwater contaminated with lead can elevate blood lead levels in humans.[49]

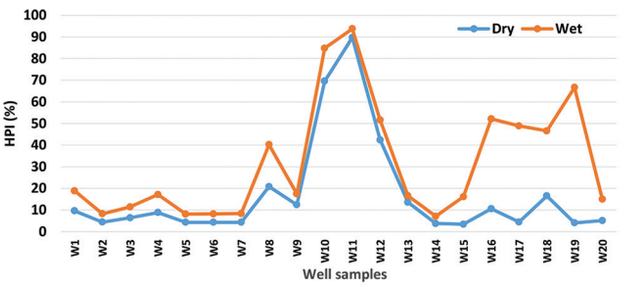

Figure 3. Seasonal variations in heavy metal pollution index (HPI). Data are presented as actual values of 20 samples.

The maximum lead concentration recorded in Wadi Al-Samen during the dry season was 0.003 mg/L, with an average of 0.00025 mg/L. In the wet season, lead concentrations ranged from 0 to 0.001 mg/L, with an average of 0.0001 mg/L. None of the 20 analyzed samples exceeded the WHO limit.

Arsenic contamination in groundwater is also a global concern, as it affects millions of people worldwide.[3,51,52] In the study area, arsenic compounds are commonly utilized in the leather tanning process, which can contribute to arsenic contamination. Prolonged exposure to arsenic in drinking water can cause severe health problems, such as cancer, skin lesions, cardiovascular diseases, and diabetes.[52] Inorganic arsenic compounds – known for their high toxicity—pose a greater risk than organic arsenic compounds typically found in seafood.[53]

The WHO (2011)[50] permissible arsenic concentration in drinking water is 0.01 mg/L. In Wadi Al-Samen, the maximum arsenic concentration during the dry season was 0.009 mg/L, with an average of 0.0009 mg/L. During the wet season, arsenic concentration ranged from 0 to 0.008 mg/L, with an average of 0.00075 mg/L. Out of twenty analyzed samples, no arsenic concentration levels higher than the allowable limit were recorded.

3.3.2. Alkaline Earth metal (barium)

Barium (Ba) contamination in surface and groundwater is primarily caused by leaching and erosion from sedimentary rocks. In addition, human activities, such as the excessive use of agricultural fertilizers contribute to elevated barium levels.

The WHO (2011)[50] permissible limit for barium in drinking water is 0.7 mg/L. In Wadi Al-Samen, the maximum barium concentration observed during the dry season was 150.7 mg/L, with an average of 21.80 mg/L. During the wet season, barium concentrations ranged from 0.014 to 148.79 mg/L, with an average of 21.32 mg/L.

Out of 20 analyzed samples, four exceeded the permissible barium limit in both seasons, (Figure 4). The elevated barium levels in these samples are primarily attributed to human activities, particularly the intensive use of agricultural fertilizers, as these samples were collected from agricultural areas.

3.3.3. Alkali metal (lithium)

Lithium (Li) is an alkali metal that occurs naturally in minerals, groundwater, and surface water as a monovalent cation.[54] It enters groundwater primarily through water-mineral interactions.[54] Lithium is widely

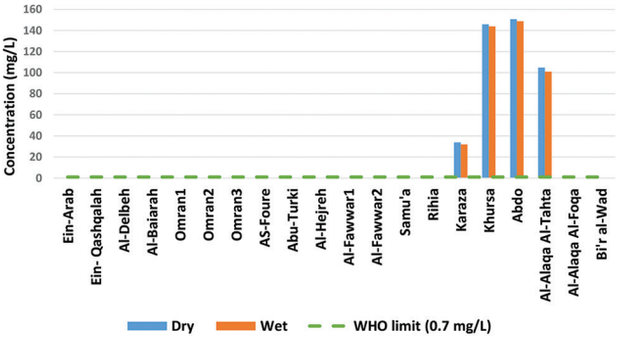

Figure 4. Barium concentrations in samples from two sampling rounds. Data are presented as actual values.

used in energy storage (Li-ion rechargeable batteries account for approximately 70% of global lithium consumption), ceramics, glass, and lubricating grease.[55] Lithium is also used pharmaceutically to treat bipolar disorder, and studies have linked its occurrence in drinking water to human health outcomes.[54] At low levels, lithium may provide behavioral benefits and function as a nutritionally essential trace element.[56] Studies have indicated that the human and environmental toxicity of lithium is low.[57-60] Lithium exposure has also been associated with lower rates of mental health disorders.[56] However, some studies suggest possible adverse effects, such as associations with autism and thyroid hormone disruption.[61]

The allowable level of lithium (Li) in drinking water is 0.70 mg/L, based on the WHO (2011) standard.[50] In Wadi Al-Samen, the maximum recorded lithium concentration during the dry season was 13.55 mg/L with an average of 1.79 mg/L. In the wet season, lithium concentration ranged from 0 to 12.99 mg/L, with an average of 1.68 mg/L.

In a study by Al-Zaarir,[36] lithium concentrations in samples from Al-Alaqa Al-Foqa and Al-Alaqa Al-Tahta exceeded permissible limits during both seasons. The study also indicated that other samples, including those from Abdo, Khursa, and Karaza, surpassed the recommended lithium concentration limits, suggesting a potential long-term risk of increasing lithium contamination. Out of 20 analyzed samples, four exceeded permissible limits in both seasons (Figure 5). The elevated lithium levels in these groundwater samples are likely linked to human activities, including waste burning, accumulation of used car parts, and improper disposal of batteries. Notably, 0.2% of collected samples exceeded the maximum permissible lithium concentration in both the dry and wet seasons, suggesting a persistent low-level contamination risk.

3.3.4. Transition metals (nickel, cobalt, manganese, and molybdenum)

Nickel, cobalt, and manganese concentrations in the study area were all within the allowable limits established by the WHO[60]: 0.07 mg/L for nickel, 0.005 mg/L for cobalt, and 0.4 mg/L for manganese.

The maximum recorded cobalt concentration in Wadi Al-Samen during the dry season was 0.002 mg/L, with an average of 0.00035 mg/L. In the wet season, cobalt concentrations ranged from zero to 0.002 mg/L, with an average of 0.003 mg/L.

The maximum manganese concentration observed in the dry season was 0.053 mg/L, with an average of 0.00415 mg/L. During the wet season, manganese concentrations ranged from zero to 0.052 mg/L, with an average of 0.0039 mg/L. None of the 20 samples analyzed exceeded the permissible limits for nickel, cobalt, or manganese.

Molybdenum (Mo) typically occurs at low concentrations in groundwater, but elevated levels can be indicative of anthropogenic contamination.[62] The WHO[50] permissible level of molybdenum is 0.07 mg/L. In Wadi Al-Samen, the maximum recorded molybdenum concentration during the dry season was 0.003 mg/L, with an average of 0.0008 mg/L. During the wet season, molybdenum concentrations ranged from zero to 0.002 mg/L, with an average of 0.0006 mg/L.

3.3.5. Metallic elements (copper, cadmium, zinc, iron, and chromium)

Zinc is an essential trace element found in many foods and drinking water, typically in the form of salt or organic complexes. A zinc deficiency can lead to health issues, such as dwarfism, dermatitis, and loss of taste. However, the presence of lead, mercury, and cadmium in groundwater can pose significant health risks to humans and the environment. High chromium concentrations in groundwater are associated with health issues, such as nasal septum ulceration and dermatitis.[63,64]

Copper is an ancient metal valued for its antibacterial properties and is essential for hemoglobin production.[65] It can enter water sources through mining, the use of copper utensils, plumbing, and various industrial activities. Although beneficial in trace amounts, excessive levels of copper can be toxic. Copper from food differs chemically from the form found in water. Prolonged storage of water in copper containers can increase its concentration and pose potential health risks.[66] High copper exposure may lead to gastrointestinal issues, liver toxicity, neurological problems, Wlison's disease, Alzheimer's disease, childhood liver cirrhosis, and mental illnesses.[67-71]

The WHO (2011)[50] sets the permissible level of copper in drinking water at 2 mg/L. During the dry season in Wadi Al-Samen, the concentration of copper ranged from 0 to 7.88 mg/L, with a mean value of 0.40 mg/L. In the wet season, the concentration of copper ranged from 0 to 7.62 mg/L, with an average of 0.38 mg/L. Out of 20 samples analyzed, one exceeded the permissible limit in both seasons (Figure 6). High copper concentrations in the Karaza well are likely due to plumbing corrosion, mining, and other human activities. Copper concentrations tend to decrease in winter, possibly due to increased water flow diluting its levels. Factors influencing copper corrosion include moderate alkalinity (pH: 7.9 – 8.2), water retention time in copper pipes, and temperature.[65]

Zinc is widely used in corrosion-resistant alloys, brass, galvanized steel, iron products, rubber production, and as a white pigment in zinc oxide.[72] Excessive zinc in the environment can be harmful, potentially affecting aquatic ecosystems.[73] Drinking water with zinc levels

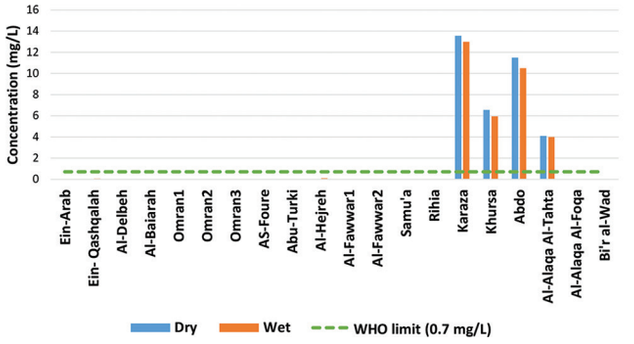

Figure 5. Lithium concentrations in samples from two sampling rounds. Data are presented as actual values of 20 samples.

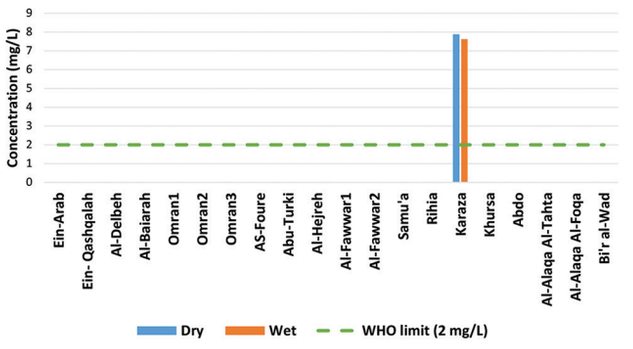

Figure 6. Copper concentrations in samples from two sampling rounds. Data are presented as actual values.

above 3 mg/L may have an undesirable astringent taste, opalescent appearance, and form a greasy film when boiled.[73] High zinc intake can cause fever, nausea, vomiting, stomach cramps, and diarrhea, along with gastric erosion and gastrointestinal disorders.[72]

A study by Al-Zaarir[36] indicated that copper, barium, or zinc levels did not exceed the permissible limits for groundwater samples. The permissible level of zinc is 3 mg/L, as established by the WHO.[50] The concentrations of zinc in the dry season ranged from zero to 7.42 mg/L, with an average of 1.04 mg/L. Out of 20 analyzed samples, 3 samples exceeded the permissible limits in both seasons (Figure 7). Elevated zinc levels in Karaza, Abdo, and Al-Alaqa Al-Tahta wells are likely due to the burning of wires and cables to retrieve copper. This highlights the need for proper waste management to protect human health and the environment.

Cadmium was not detected in significant concentrations in either season. The WHO[50] permissible level for cadmium is 0.003 mg/L.

Iron was detected in 0.1% of the groundwater sample. The WHO[50] permissible level of iron in drinking water is 2 mg/L. In Wadi Al-Samen, the maximum recorded iron concentration during the dry season was 0.143 mg/L, with an average of 0.0167 mg/L.

No samples exceeded the permissible limit for chromium concentrations. The maximum chromium concentration in the dry season was 0.001 mg/L, with an average of 0.00005 mg/L. Chromium was not detected during the wet season in any of the study locations. The WHO[50] permissible level of chromium is 0.05 mg/L.

3.3.6. Non-metallic elements (boron, selenium, and aluminum)

The WHO[50] permissible level of boron in drinking water is 2.4 mg/L. Long-term human exposure to boron compounds can cause gastrointestinal irritation. Boron typically enters water sources through industrial and domestic effluents.

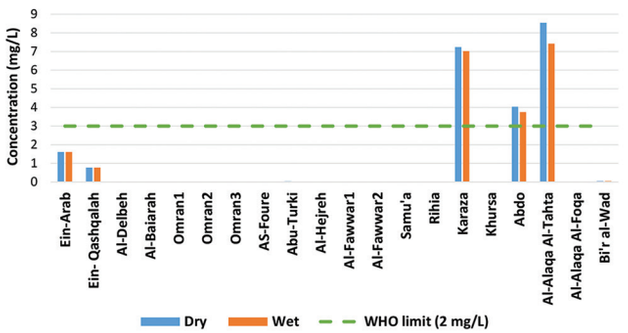

Figure 7. Zinc concentrations in samples from two sampling rounds. Data are presented as actual values.

In Wadi Al-Samen, the maximum boron (B) concentration during the dry season was 0.051 mg/L, with an average of 0.0215 mg/L. In the wet season, boron concentrations ranged from zero to 0.048 mg/L, with an average of 0.019 mg/L. No boron levels exceeded the permissible limits in either season.

Selenium (Se) is a naturally occurring element found in rocks, soil, plants, and water. Public health standards for safe selenium levels in drinking water vary widely, but the WHO[50] recommends a permissible level of 0.04 mg/L. Selenium can enter groundwater through the weathering of selenium-rich rocks and soil, often leaching into groundwater due to irrigation and rainfall.[74] While small amounts of selenium are beneficial, excessive levels can be toxic. Potential health effects associated with selenium overexposure include hair and fingernail loss, as well as numbness in the fingers and toes.[7]

In this study, selenium concentrations during the dry season ranged from 0.018 to 0.64 mg/L, with an average of 0.10 mg/L. The maximum selenium concentration in the wet season was 0.062 mg/L, with an average of 0.047 mg/L. Higher-than-permissible selenium levels were observed in 0.85% of samples in the dry season and 0.75% in the wet season.

The WHO[50] permissible level of aluminum in drinking water is 0.9 mg/L. The maximum aluminum concentration in Wadi Al-Samen during the dry season was 0.084 mg/L, with an average of 0.03 mg/L. The concentration of aluminum during the wet season ranged from 0 to 0.081 mg/L, with an average of 0.03 mg/L. None of the 20 analyzed samples exceeded the permissible limit of aluminum. Chemical processes such as carbonate/phosphate dissolution, oxidation/reduction reactions, along with agricultural practices (e.g., fertilizer application and irrigation) are likely contributors to groundwater self-pollution, as observed in Al-Zarqa Amman Basin in Jordan.[75]

Historically, these wells were considered clean; however, increasing contamination from human activities, industrial waste, sewage, and excessive groundwater pumping has degraded water quality. A study by Zaarir[36] reported no exceedance of threshold limits for copper, zinc, and barium in groundwater wells in the study area.

4. Conclusion

Wadi Al-Saman is a crucial groundwater recharge source for the Western Basin, which flows toward the

Mediterranean Sea. However, it is heavily polluted by wastewater from domestic and industrial activities in the Hebron area. This contamination is concerning, as elements such as lithium, zinc, barium, and copper originate primarily from anthropogenic sources, including industrial activities, municipal sewage, domestic wastes, and industrial discharges, all of which increase their concentrations in groundwater.

Water serves as the primary medium through which trace elements enter the environment, and the HPI effectively characterizes groundwater pollution in this region. The overall HPI for Wadi Al-Samen was found to be 17.2 in the dry season and 11.99 in the wet season, both below the critical threshold of 100. The MI was 2.3 in the dry season and 2.2 in the wet season, indicating moderate contamination. Groundwater was classified as poor in the Al-Hejreh well (W10) and very poor in the Al-Fawwar1 well (W11), rendering it unsuitable for drinking. The concentrations of barium, lithium, zinc, copper, and se exceeded permissible limits in some samples, signaling a potential threat to water resources in the Wadi Al-Samen area that necessitates immediate attention from the Palestinian local administration and the Water Authority.

This finding highlights the urgent need for wastewater treatment in major human settlements to prevent hazardous chemicals from polluting water bodies. Expanding the sampling network, increasing seasonal sampling frequency, and incorporating advanced geochemical analyses to differentiate between natural and anthropogenic contamination sources would enhance the robustness of future studies. In addition, evaluating the efficiency of existing wastewater treatment facilities and proposing targeted remediation measures would strengthen the study's practical impact on water resource management and policy development.

Our study underscores the importance of coordinated efforts by the Water Authority, Hebron Municipality, and other responsible agencies to implement biological and chemical wastewater treatment in Wadi Al-Samen. We also recommend the rapid rehabilitation and construction of a wastewater treatment plant to improve water quality in the region, safeguard public health, and protect aquatic ecosystems.

Acknowledgments

The authors are grateful thanks to the Palestinian and Tunisian Higher Education and Scientific Research ministries as well as the University of El Manar in Tunisia for their support. Thanks goes also to the Laboratory of Hydraulic and Environmental Engineering (GHE) at the National School of Tunisian Engineers in El Manar University.

Funding

None.

Conflict of interest

The authors declare they have no competing interests.

Author contributions

Conceptualization: Rachida Bouhalila, Marwan Ghanem
Formal analysis: Waseem Al-Tamimi, Marwan Ghanem
Investigation: Fadoua Hamzaoui-Azaza, Waseem Al-Tamimi
Methodology: Waseem Al-Tamimi
Writing – original draft: Waseem Al-Tamimi
Writing – review & editing: Rachida Bouhalila, Fadoua Hamzaoui-Azaza

Availability of data

Data are available from the corresponding author upon reasonable request.

Further disclosure

The research is part of the Ph.D thesis of Waseem Tamimi at the University of Tunis El Manar in Tunisia.

References

1. Al-Khuzaie MM, Abdul Maulud KN, Wan Mohtar WH, Yaseen MZ. Assessment of untreated wastewater pollution and heavy metal contamination in the Euphrates river. *Environ Pollut Bioavail*. 2023;36(1):2292110. doi: 10.1080/26395940.2023.2292110
2. Kana AA. Heavy metal assessment of groundwater quality in part of Karu, Central Nigeria. *Water Pract Technol*. 2022;17(9):1802-1817. doi: 10.2166/wpt.2022.102
3. Brindha K, Paul R, Walter J, Tan ML, Singh, MK. Trace metals contamination in groundwater and implications on human health: Comprehensive assessment using hydrogeochemical and geostatistical methods. *Environ Geochem Health*. 2020;42:3819-3839. doi: 10.1007/s10653-020-00637-9
4. Khalid S, Shahid M, Natasha SAH, *et al*, Heavy metal contamination and exposure risk assessment via drinking

groundwater in Vehari, Pakistan. *Environ Sci Pollut Res*. 2020;27:39852-39864.
doi: 10.1007/s11356-020-10106-6
5. Verma R, Dwivedi P. Heavy metal water pollution-A case study. *Recent Res Sci Technol*. 2013;5(5):98-99.
6. Witkowska D, Słowik J, Chilicka K. Heavy metals and human health: Possible exposure pathways and the competition for protein binding sites. *Molecules*. 2021;26(19):6060.
doi: 10.3390/molecules26196060
7. Ali Khan MM, Umar R, Lateh H. Study of trace elements in groundwater of Western Uttar Pradesh, India. *Sci. Res. Essays*. 2010;5(20):3175-3182.
8. Ali H, Khan E, Ilahi I. Environmental chemistry and ecotoxicology of hazardous heavy metals: Environmental persistence, toxicity, and bioaccumulation. *J Chem*. 2019;2019:6730305.
doi: 10.1155/2019/6730305
9. Balali-Mood M, Naseri K, Tahergorabi Z, Khazdair MR, Sadeghi M. Toxic mechanisms of five heavy metals: Mercury, lead, chromium, cadmium, and arsenic. *Front Pharmacol*. 2021;12:643972.
doi: 10.3389/fphar.2021.643972
10. Jaishankar M, Tseten T, Anbalagan N, Mathew, BB, Beeregowda KN. Toxicity, mechanism and health effects of some heavy metals. *Interdiscip Toxicol*. 2014;7(2):60-72.
doi: 10.2478/intox-2014-0009
11. Collin MS, Venkatraman SK, Vijayakumar N, *et al*., Bioaccumulation of lead (Pb) and its effects on human: A review. *J Hazard Mater Adv*. 2022;7:100094.
doi: 10.1016/j.hazadv.2022.100094
12. Jomova K, Alomar SY, Nepovimova E, Kuca K, Valko M. Heavy metals: Toxicity and human health effects. *Arch Toxicol*. 2025;99(1):153-209.
doi: 10.1007/s00204-024-03903-2
13. Mitra S, Chakraborty AJ, Tareq AM, *et al.,* Impact of heavy metals on the environment and human health: Novel therapeutic insights to counter the toxicity. *J King Saud Univ Sci*. 2022;34(3):101865.
doi: 10.1016/j.jksus.2022.101865
14. Hou S, Yuan L, Jin P, *et al*, A clinical study of the effects of lead poisoning on the intelligence and neurobehavioral abilities of children. *Theor Biol Med Model*. 2013;10:13.
doi: 10.1186/1742-4682-10-13
15. Loh N, Loh HP, Wang LK, Wang MHS. Health effects and control of toxic lead in the environment. In: Wang L, Wang MH, Hung YT, Shammas N, editors. *Handbook of Environmental Engineering.* Volume: Natural resources and control processes. 2016. p. 17.
doi: 10.1007/978-3-319-26800-2_5
16. Mahurpawar M. Effect of heavy metals on human health. *Int J Res Granthaalayah*. 2015;530(516):1-7.
doi: 10.29121/granthaalayah.v3.i9SE.2015.3282.
17. Toxicological Profile for Arsenic. Atlanta, GA: Agency for Toxic Substances and Disease Registry (ATSDR); 2007. Available from: https://www.atsdr.cdc.gov/toxprofiles/tp2.pdf [Last accessed on 2025 Feb 24.
18. Uede K, Furukawa F. Skin manifestations in acute arsenic poisoning from the Wakayama curry-poisoning incident. *Br J Dermatol*. 2003;149(4):757-762.
doi: 10.1046/j.1365-2133.2003.05511.x
19. Di Duca F, Montuori P, De Rosa E, *et al*. Assessing heavy metals in the Sele river estuary: An overview of pollution indices in Southern Italy. *Toxics*. 2024;12(1):38.
doi: 10.3390/toxics12010038
20. Troudi N, Tzoraki O, Hamzaoui-Azaza F, Melki F, Zammouri M. Estimating adults and children's potential health risks to heavy metals in water through ingestion and dermal contact in a rural area, Northern Tunisia. *Environ Sci Pollut Res Int*. 2022;29(37):56792-56813.
doi: 10.1007/s11356-022-19667-0
21. Sadeghi H, Fazlzadeh M, Zarei A, Mahvi AH, Nazmara S. Spatial distribution and contamination of heavy metals in surface water, groundwater and topsoil surrounding Moghan's tannery site in Ardabil, Iran. *Int J Environ Anal Chem*. 2020;102(5):1049-1059.
doi: 10.1080/03067319.2020.1730342
22. Shaibur MR. Heavy metals in chrome-tanned shaving of the tannery industry are a potential hazard to the environment of Bangladesh. *Case Stud Chem Environ Eng*. 2023;7:100281.
doi: 10.1016/J.CSCEE.2022.100281.
23. Angon PB, Islam MS, Shreejana KC, *et al*. Sources, effects and present perspectives of heavy metals contamination: Soil, plants and human food chain. *Heliyon*. 2024;10(7):e28357.
doi: 10.1016/j.heliyon.2024.e28357
24. Abdullah JE. Quality assessment for Shatt Al-Arab river using heavy metal pollution index and metal index. *J Environ Earth Sci*. 2013;3(5):114-120.
25. Abadi HT, Alemayehu T, Berhe BA. Heavy metal's pollution health risk assessment and source appraisal of groundwater and surface water in Irob catchment, Tigray, Northern Ethiopia. *Appl Water Sci*. 2024;14:201.
doi: 10.1007/s13201-024-02237-9
26. PWA [Palestinian Water Authority. *Annual Status Report on Water Resources, Water Supply, and Wastewater in the Occupied State of Palestine*. Palestinian Water Authority; 2012.
27. Abu Dayyeh Q. *Introduction to Water Poverty and Social Crisis in Hebron District Palestine*. France: OpenEdition Books; 2009. p. 111-119.
doi: 10.4000/books.irdeditions.4815
28. Kar D, Sur P, Mandal SK, Saha T, Kole RK. Assessment of heavy metal pollution in surface water. International *Int J Environ Sci Technol*. 2008;5:119-124.
doi: 10.1007/BF03326004
29. Nair IV, Singh K, Arumugam M, Gangadhar K, Clarson D. Trace metal quality of Meenachil River

at Kottayam, Kerala (India) by principal component analysis. *World Appl Sci J*. 2010;9(10):1100-1107.
30. Nalawade PM, Bholay AD, Mule MB. Assessment of groundwater and surface water quality indices for heavy metals nearby area of Parli thermal power plant. *Univ J Environm Res Technol*. 2012;2(1):47-51.
31. Mohan SV, Nithila P, Reddy SJ. Estimation of heavy metals in drinking water and development of heavy metal pollution index. *J Environ Sci Health Part A.* 1996;A-31:283-289. doi: 10.1080/10934529609376357
32. Prasad B, Kumari P, Bano S, Kumari S. Ground water quality evaluation near mining area and development of heavy metal pollution index. *Appl Water Sci*. 2014;4:11-17. doi: 10.1007/s13201-013-0126-x
33. Sarhat AR, Al-Obaidi BS. Assessment of heavy metal pollution in Sirwan River by heavy metal pollution index (HPI) and metal index (MI). *Water Conserv Sci Eng*. 2023;8:12. doi: 10.1007/s41101-023-00187-y
34. Lemessa F, Simane B, Seyoum A, Gebresenbet G. Assessment of the impact of industrial wastewater on the water quality of rivers around the Bole Lemi industrial park (BLIP), Ethiopia. *Sustainability*. 2023;15(5):4290. doi: 10.3390/su15054290
35. Daghara A, Al-Khatib IA, Al-Jabari M. Quality of drinking water from springs in Palestine: West bank as a case study. *J Environ Public Health*. 2019;2019:8631732. doi: 10.1155/2019/8631732
36. Zaarir M. Pollution *Effects of the Wastewater Flow on the Groundwater Quality in Wadi-Samen Catchment / Hebron/Palestine*. Master Thesis. Palestine: Institute of Environmental and Water Studies at Birzeit University; 2017. Available from: http://hdl.handle.net/20.500.11889/5774 [Last accessed on 2025 Mar 07.
37. Al-Tamimi W, Hamzaoui-Azaza F, Ghanem, M, Bouhalila, R. Hydro-geochemistry and application of water quality index (WQI) for ground water quality assessment, Wadi Al-Samen-Hebron-West Bank. *J Water Resour Protect*. 2023;15:481-508. doi: 10.4236/jwarp.2023.1510027
38. Dey M, Akter A, Islam S, *et al*. Assessment of contamination level, pollution risk and source apportionment of heavy metals in the Halda River water, Bangladesh. *Heliyon*. 2021;7(12):e08625. doi: 10.1016/j.heliyon.2021.e08625
39. Reza R, Singh G, Jain Manish K. Application of heavy metal pollution index for ground water quality assessment in Angul district of Orissa, India. *Int J Res Chem Environ*. 2011;1(2):118-122.
40. Prasad B, Mondal KK. The impact of filling an abandoned open cast mine with fly ash on ground water quality: A case study. *Mine Water Environ*. 2008;27:40-45. doi: 10.1007/s10230-007-0021-5
41. Prasad B, Kumari S. Heavy metal pollution index of ground water of an abandoned open cast mine filled with fly ash: A case study. *Mine Water Environ*. 2008;27(4):265-267.
42. Rao Q, Sun Z, Tian L, Li J, Sun W, Sun W. Assessment of arsenic and heavy metal pollution and ecological risk in inshore sediments of the Yellow River estuary, China. *Stoch Environ Res Risk Assess*. 2018;32:2889-2902. doi: 10.1007/s00477-018-1588-z
43. Lyulko I, Ambalova T, Vasiljeva T. *To Integrated Water Quality Assessment in Latvia, Paper presented at the International Workshop on Information for Sustainable Water Management.* MTM (Monitoring Tailor-Made) III, Nunspeet, Netherlands; 2001. p. 449-452.
44. Caerio S, Costa MH, Ramos TB, *et al*. Assessing heavy metal contamination in Sado Estuary sediment: An index analysis approach. *Ecol Indic*. 2005;5:155-169. doi: 10.1016/j.ecolind.2005.02.001
45. El-Degwy AA, Negm NA, El-Tabl AS, Goher ME. Assessment of heavy metal pollution in water and its effect on Nile tilapia (*Oreochromis niloticus*) in Mediterranean Lakes: A case study at Mariout Lake. *Appl Water Sci*. 2023;13:50. doi: 10.1007/s13201-022-01858-2
46. Tamasi G, Cini R. Heavy metals in drinking waters from Mount Amiata (Tuscany, Italy). Possible risks from arsenic for public health in the Province of Siena. *Sci Total Environ*. 2004;327(1-3):41-51. doi: 10.1016/j.scitotenv.2003.10.011
47. Sanders T, Liu Y, Buchner V, Tchounwou PB. Neurotoxic effects and biomarkers of lead exposure: A review. *Rev Environ Health*. 2009;24(1):15-45. doi: 10.1515/reveh.2009.24.1.15
48. Goel PK. *Water Pollution Causes Effect and Control*. Karnataka: New Age International Publishers; 1997. p. 269.
49. Ren YS, Ilyas M, Xu RZ, Ahmad W, Wang R, Hamad H. Concentrations of lead in groundwater and human blood in the population of Palosai, a Rural Area in Pakistan: Human exposure and risk assessment. *Adsorp Sci Technol*. 2022;2022:8341279. doi: 10.1155/2022/8341279
50. WHO[WorldHealthOrganization.*GuidelinesforDrinking Water Quality*. 4th ed. Geneva, Switzerland: World Health Organization; 2011. p. 564. Available from: http://apps.who.int/iris/bitstream/10665/44584/1/9789241548151_eng.pdf [Last accessed on 2025 Mar 07.
51. Katiyar P, Yadu B, Korram J, Satnami ML, Kumar M, Keshavkant S. Titanium nanoparticles attenuates arsenic toxicity by up-regulating expressions of defensive genes in *Vigna radiata* L. *J Environ Sci (China)*. 2020;92:18-27. doi: 10.1016/j.jes.2020.02.013
52. Sarkar S, Blaney LM, Gupta A, Ghosh D, Sengupta AK. Arsenic removal from groundwater and its safe containment in a rural environment: Validation

of a sustainable approach. *Environ Sci Technol*. 2008;42(12):4268-4273.
doi: 10.1021/es702556t

53. Kanel SR, Das TK, Varma RS, *et al*. Arsenic contamination in groundwater: Geochemical basis of treatment technologies. *ACS Environ Au*. 2023;3(3):135-152.
doi: 10.1021/acsenvironau.2c00053
54. Lindsey BD, Belitz K, Cravotta CA 3rd, Toccalino PL, Dubrovsky NM. Lithium in groundwater used for drinking-water supply in the United States. *Sci Total Environ.* 2021;767:144691.
doi: 10.1016/j.scitotenv.2020.144691
55. Dugamin EJM, Richard A, Cathelineau M, Boiron MC, Despinois F, Brisset A. Groundwater in sedimentary basins as potential lithium resource: A global prospective study. *Sci Rep*. 2021;11(1):21091.
doi: 10.1038/s41598-021-99912-7
56. Schrauzer GN, Shrestha KP. Lithium in drinking water and the incidences of crimes, suicides, and arrests related to drug addictions. *Biol Trace Elem Res*. 1990;25(2):105-113.
doi: 10.1007/BF02990271
57. Aral H, Vecchio-Sadus A. Toxicity of lithium to humans and the environment--a literature review. *Ecotoxicol Environ Saf*. 2008;70(3):349-356.
doi: 10.1016/j.ecoenv.2008.02.026
58. Hamstra SI, Roy BD, Tiidus P, *et al*. Beyond its psychiatric use: The benefits of low-dose Lithium appenementation. *Curr Neuropharmacol*. 2023;21(4):891-910.
doi: 10.2174/1570159X20666220302151224
59. Oruch R, Elderbi MA, Khattab HA, Pryme IF, Lund A. Lithium: A review of pharmacology, clinical uses, and toxicity. *Eur J Pharmacol*. 2014;740:464-473.
doi: 10.1016/j.ejphar.2014.06.042
60. Quiroz JA, Gould TD, Manji HK. Molecular effects of lithium. *Mol Interv*. 2004;4(5):259-272.
doi: 10.1124/mi.4.5.6
61. Lombard MA, Brown EE, Saftner DM, *et al*. Estimating lithium concentrations in groundwater used as drinking water for the conterminous United States. *Environ Sci Technol*. 2024;58(2):1255-1264.
doi: 10.1021/acs.est.3c03315
62. Harkness JS, Darrah TH, Moore MT, *et al*. Naturally occurring versus anthropogenic sources of elevated molybdenum in groundwater: Evidence for geogenic contamination from Southeast Wisconsin, United States. *Environ Sci Technol*. 2017;51(21):12190-12199.
doi: 10.1021/acs.est.7b03716
63. Singh KP, Bhayana N. Geochemistry of groundwater of Ludhiana area, Punjab with special reference to its use for India. *Geol Cong*. 1986:579-594.
64. Wilbur S, Abadin H, Fay M, *et al*. Toxicological profile for chromium. Atlanta, GA: Agency for Toxic Substances and Disease Registry (US); 2012. Available from: https://www.atsdr.cdc.gov/toxprofiles/tp7.pdf [Last accessed on 2025 Feb 24.
65. Sonon L, Kissel D, Vendrell P, Hitchcock R. *Copper Levels in Drinking Water from Private Household Wells in Major Provinces*. Georgia Water Resources Conference, University of Georgia. Athens, Georgia: Institute of Ecology, the University of Georgia; 2006.
66. Manne R, Kumaradoss MM, Iska RSR, Devarajan A, Mekala N. Water quality and risk assessment of copper content in drinking water stored in copper container. *Appl Water Sci*. 2022;12(3):27.
doi: 10.1007/s13201-021-01542-x
67. Asokan K, Vivekanand PA, Muniraj S. An eco-friendly method to remove copper ion from drinking water by using homemade bio-adsorbent in tip-tea-bag. *Mater Today Proc*. 2021;36:883-885.
doi: 10.1016/j.matpr.2020.07.023
68. Buchanan SD, Diseker RA 3rd, Sinks T, Olson DR, Daniel J, Flodman T. Copper in drinking water, Nebraska, 1994. *Int J Occup Environ Health*. 1999;5(4):256-261.
doi: 10.1179/oeh.1999.5.4.256
69. Fewtrell L, Kay D, Jones F, Baker A, Mowat A. Copper in drinking water--an investigation into possible health effects. *Public Health*. 1996;110(3):175-177.
doi: 10.1016/s0033-3506(96)80072-2
70. WHO [World Health Organization. *Guidelines for Drinking Water Quality*. 2nd ed., Vol. 1. Geneva, Switzerland: World Health Organization; 1993.
71. Larous S, Meniai AH, Lehocine MB. Experimental study of the removal of copper from aqueous solutions by adsorption using sawdust. *Desalination*. 2005;185:483-490.
doi: 10.1016/j.desal.2005.03.090
72. Sankhla SM, Rajeev K, Prasad L. Zinc impurity in drinking water and its toxic effect on human health. *Indian Internet J Forensic Med Toxicol*. 2019;17(4):84.
doi: 10.5958/0974-4487.2019.00015.4
73. WHO [World Health Organization. *Zinc in Drinking-Water*. Background Document For Development of WHO Guidelines for Drinking-water Quality. 2nd ed. Vol. 2. [Health Criteria and Other Supporting Information Geneva: World Health Organization; 2003.
74. Dhillon KS, Dhillon SK. Selenium in groundwater and its contribution towards daily dietary Se intake under different hydrogeological zones of Punjab, India. *J Hydrol*. 2016;553:615-626.
doi: 10.1016/j.jhydrol.2015.12.016
75. Kuisi MA, Abdel-Fattah A. Groundwater vulnerability to selenium in semi-arid environments: Amman Zarqa Basin, Jordan. *Environ Geochem Health*. 2010;32(2):107-128.
doi: 10.1007/s10653-009-9269-y

ACCSCIENCE PUBLISHING

Asian Journal of Water, Environment and Pollution. Vol. 22, No. 2 (2025), pp. 64-86.
doi: 10.36922/AJWEP025040019

ORIGINAL RESEARCH ARTICLE

Geospatial flood modeling and risk assessment of floodplain villages along the Barak River, Northeast India

Shanku Ghosh and Chakkaravarthi Prakasam*

Department of Geography, School of Earth Sciences, Assam University Diphu Campus, Karbi Anglong, Assam, India
***Corresponding author:** Chakkaravarthi Prakasam (cprakasam@gmail.com)

Received: January 22, 2025; 1st revised: March 4, 2025; 2nd revised: March 15, 2024; Accepted: March 17, 2025; Published Online: April 4, 2025

Abstract: Floods are events where areas or lands become submerged due to an excessive volume of water, leading to various impacts, such as human casualties; property damage; and social, economic, and environmental losses. This study aims to investigate the factors influencing flood hazard modeling using statistical models (e.g., frequency ratio, Shannon entropy) to identify flood-prone areas and assess the flood risk in villages within the Barak River basin for effective flood management. Among the states in India, Assam, Bihar, Uttar Pradesh, and West Bengal are among those that are highly affected by floods. In Assam, the Barak and Brahmaputra River valleys are particularly vulnerable to flooding, with Barak Valley being extremely prone to flood following monsoonal downpours and breaches in river embankment. This study's findings reveal that the entire Barak River floodplain (Barak Valley) exhibits high to very high flood susceptibility. All districts within Barak Valley show more than 50% of their area as flood-prone, with Karimganj district having the highest flood susceptibility, as 70% of its area is in the very high-risk category, which is the highest among the districts. A total of 866 villages in the study area are highly vulnerable to floods, accounting for 46% of the villages in the region. These villages are mostly located along the riverbanks and low-lying areas surrounding water bodies. These findings emphasize the need for targeted flood management strategies such as forecasting, early warning systems, and land use planning in these villages.

Keywords: Flood hazard; Vulnerability; Exposure risk assessment; Statistical models; Barak River basin

1. Introduction

Global flood risk is a significant concern, with studies showing an increasing trend in flood risk worldwide due to climate change.[1-3] High-income countries, including Singapore, Japan, Luxembourg, and South Korea, are among the most at-risk nations, with a slow but steady rise in flood risk projected under different scenarios.[1] Vulnerability to floods is influenced by exposure, sensitivity, and coping capacity, with spatial disparities between continents highlighting Asia and Europe as high-risk areas.[4] To address the challenges of flood risk assessment in developing regions, we need to map flood hazard, vulnerability, and risk, enabling reliable assessments and strengthening resilience worldwide.[5] Among the different types of disasters, floods are the single largest disaster, causing 21% of total disaster deaths, 13.46% of injuries, 46.73% of the disaster-affected population, and 24.38% of worldwide disaster economic damage.[6] Asia is home to a disproportionate share of 73% of the global flood-risk population. Within Asia, South Asia bears the brunt of flood impacts, with 39% of the continent's flood-affected population residing there, followed by Southeast and East Asia with 30% and 20%, respectively.[7] Globally, India is the second most flood-affected country next to China.[8]

India's climate is characterized by highly unpredictable monsoon rainfall. The country is home to numerous large and small rivers, and prolonged heavy downpours often lead to widespread flooding. India is a global hotspot for flooding. According to the Central Water Commission's 2010 data, roughly 40 million hectares of Indian land are susceptible to inundation, making it the world's second most flood-prone country. Annually, an average of 7.6 million hectares bears the brunt of these floods. Between 1953 and 2009, these floods inflicted a staggering economic toll of approximately 200 billion dollars in damages while tragically claiming the lives of nearly 92,000 people.[9] Flood damage in India varies across states. Bihar, West Bengal, Orissa, Assam, Andhra Pradesh, and Gujarat are highly affected by flooding. In 2018, Kerala faced severe floods, with extensive damage to property, infrastructure, and agriculture, costing approximately Rs. 3000 crores for rebuilding efforts.[10] Maharashtra, particularly districts such as Mumbai, Palghar, Thane, Raigad, Satara, Sangli, Pune, and Kolhapaur, experienced significant flood events in 2019 due to extremely heavy rainfall, emphasizing the importance of mitigation and adaptation strategies.[11] Among all the states in India, 10 states account for 46% of the country's floods, with Uttar Pradesh and Bihar constituting the highest proportion. Notably, 55% of Bihar's geographical area is affected by floods, followed by Assam (50%), Uttar Pradesh (37%), and West Bengal (32%). Physiographically, Assam is primarily divided into two main drainage systems: the Barak Valley and the Brahmaputra Valley. Both river valleys are highly prone to flooding, which is closely linked to the monsoon season. The formation of the monsoonal trough in the hilly and plateaus of Assam leads to huge downpours, resulting in excess accumulation of monsoonal rainfall in the rivers and subsequent flooding in plain areas. Major flooding events in Assam have been a recurring and devastating natural disaster, impacting both life and property in the region. The Brahmaputra River, along with extreme rainfall events in the Arunachal Himalaya, contributes significantly to floods in Assam.[12,13] Dhemaji district[14] and Majuli Island[15] are particularly notable as the worst flood-affected areas in Assam, with a significant portion of land being inundated during flood events. The southwest monsoon of 2019 brought heavy rainfall, leading to severe flooding in Assam, affecting millions of people and causing substantial damage to life and property.[16] These events underscore the urgent need for improved flood forecasting models and effective flood hazard management strategies in Assam to mitigate the impact of such disasters in the future.

The present study focuses on the Barak River, which is highly flood-prone. Each year, during the monsoon season, it inundates the downstream floodplains and causes damage in the Cachar, Karimganj, and Hailakandi districts of Assam. The study aims to develop Barak River flood hazard models and risk assessments for the flood-affected villages.

Modeling and mapping flood hazard zones are essential to flood disaster management. Flood hazard modeling methods are classified into three categories: empirical, physical, and physically-based models. The different types of empirical models are statistical, multi-criteria decision-making (MCDM), and machine learning/artificial intelligence. Among the different MCDM models, the analytic hierarchy process (AHP) is the most extensively applied and well-known for flood hazard mapping. Other notable models in this field include the frequency ratio (FR), Shannon entropy, and weight of evidence. According to Mudashiru *et al*.,[17] the application of empirical models in flood hazard mapping has increased by 35% from 2000 to 2019.[17] The shift from labor-intensive manual flood risk assessment technologies to high-tech digital methods has enhanced risk assessment accuracy.[18] The advent of different modern software, like Geographic Information System (GIS), in the 21st century, has increased the application of modeling approaches in flood research, drawing considerable attention from flood researchers. Remote sensing applications have enhanced the resolution and utilization of models in flood risk assessment and susceptibility mapping. The integration of remote sensing data with GIS, combined with various hydrologic and hydrodynamic models, has enabled flood hazard, risk, and vulnerability mapping.[19]

2. Study area

The Barak River basin of India is the focus of the present research (Figure 1). The Barak River, originating from Manipur, flows through Assam and further downstream through Bangladesh, ultimately emptying into the Bay of Bengal. The river basin area spans several states in India, including Meghalaya, Nagaland, Tripura, Manipur, Mizoram, and Assam. After passing through the Cahar district of Assam, the river enters Bangladesh, and in certain places, it demarcates the boundary between India and Bangladesh. Physiographically, the Barak River basin is surrounded by hilly terrains on three sides: (i) the northern side is bordered by the North Cachar

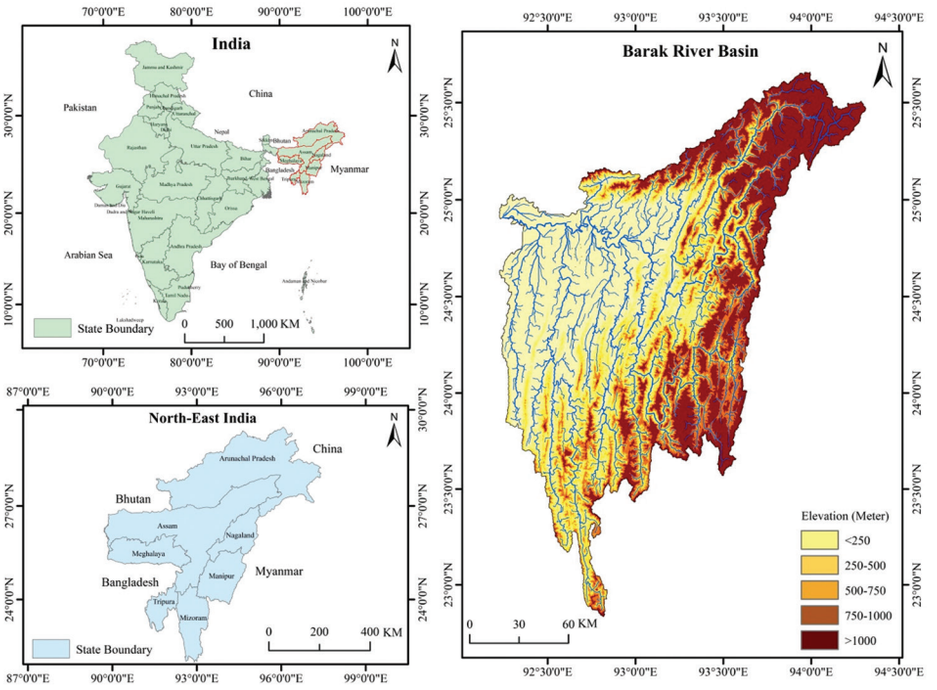

Figure 1. The study area map

Hills, (ii) the north-eastern and eastern sides are defined by the Naga and Barail ranges, and (iii) the southern and south-eastern sides are composed of Mizo hills.

The central, eastern, and Bangladesh parts of the basin are floodplains of the river, which are highly flood-prone. Flooding is a recurring event in the Barak River floodplain; each year during monsoon season, large areas get inundated by river floods, causing significant property and crop damage and disrupting the communication system. Major floods occurred in the study area in 1991, 1994, 1996, 2004, and 2009.[20] Floods in the Barak River basin are frequent and severely impact the Barak Valley of Assam, which comprises three districts: Cachar, Karimganj, and Halikandi, with a total geographical area of 6,922 km^2. Silchar, the second largest city of Assam, is located in the Cachar district along the banks of the Barak River. Barak Valley is one of the most densely populated regions of Assam, with a population of 1,736,617. Cachar is the second-most populated district, while Karimganj and Hailakandi have populations of 1,228,686 and 659,296, respectively. These populations are spread across 2,307 villages and town areas.[21,22]

3. Methodology

Figure 2 shows the methodological flowchart. Eight flood conditioning factors – drainage density, drainage frequency, topographic wetness index (TWI), slope, elevation, distance from the river, distance from the road, and geology – were used for the analysis. Secondary data were utilized to prepare all the model input layers. The training and validation flood points were drawn from the National Remote Sensing Centre generated flood inundation maps of 14th July 2022 flood. The area under the curve (AUC) method validated the generated maps. After the preparation of the input layers, input parameter weights were calculated for both Shannon's entropy and FR models. In the second stage, after delineating flood hazard-susceptible areas, the flood risk of the hazard-susceptible villages was studied. For risk assessment, village boundaries, and associated parameter data were derived using the Census of India 2011. Weights were assigned to four indicators for exposure assessment: village-level elevation, river length, normalized difference vegetation index (NDVI), and normalized difference water index (NDWI) using the AHP method. Similarly, weightages were assigned to six indicators – population density, household density, child population (0 – 6 years), illiteracy rate, marginal workers, and agricultural workers – for assessing the vulnerability of the villages. In the final stage, the risk index of the villages was derived by combining both the exposure and vulnerability indices.

3.1. Shannon's entropy model

Entropy measures each system's instability, abnormality, and unbalanced behavior.[23] The theory

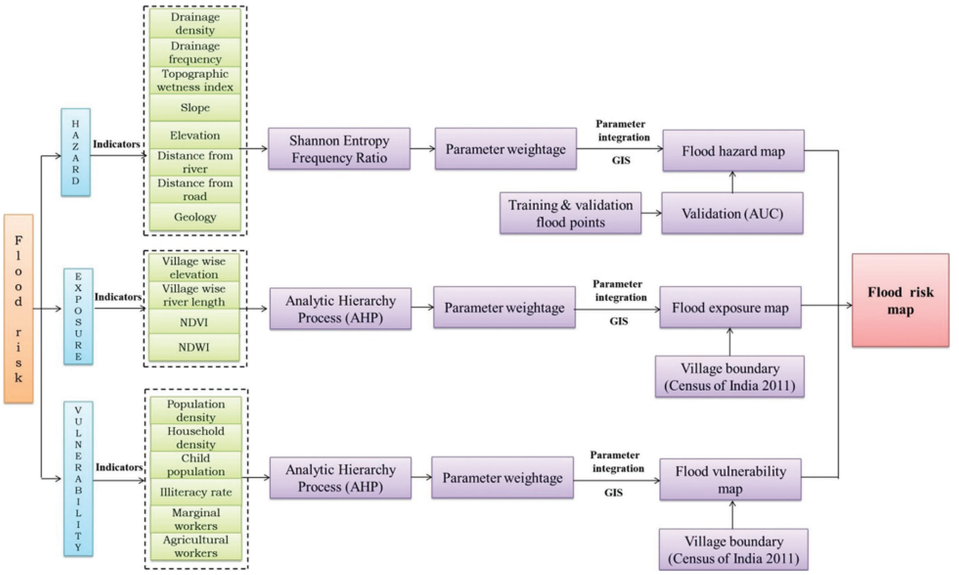

Figure 2. The methodological flowchart

Abbreviations: AUC: Area under the curve; GIS: Geographic Information System; NDVI: Normalized difference vegetation index; NDWI: Normalized difference water index.

was first introduced by Stefan-Boltzmann, with Shannon formalizing the numerical induction in 1948. Shannon later expanded the model into information theory, building upon the Boltzmann theorem.[24] The entropy model is extensively applied for risk and hazard assessments to calculate weighted indices of natural hazards and prioritize influencing factors.[25] The entropy weights of all indicators and the final susceptibility were determined using the following equations. Entropy weights were calculated for all indicators, and subsequent susceptibility zone maps were created using the following procedures and formulas.

(i) Step 1: Normalize the value of each indicator to calculate index weight using Equation I.

$$y_{ij} = \frac{X_{ij}}{\sum_{i=0}^{m} X_{ij}}, 0 \le y_{ij} \le 1 \quad \text{(I)}$$

where, y_{ij} is the specific gravity value for each X_{ij}, and m is the number of evaluation objects. X_{ij} is derived from the FR value, and i represents a class of j flood conditioning factor.

(ii) Step 2: Define entropy for each indicator j using Equation II.

$$e_{j=-k} \sum_{i=1}^{m} y_{ij} \ln y_{ij} \quad \text{(II)}$$

where e_j is the entropy value. The coefficient k is determined by the sample size (number of evaluating objects), m, using Equation III.

$$k = \frac{1}{\ln m} \quad \text{(III)}$$

The information utility value for each indicator h_j is derived from Equation IV.

$$h_j = 1 - e_j \quad \text{(IV)}$$

(iii) Step 3: Calculate the entropy weight of each indicator using Equation V.

$$w_j = \frac{h_j}{\sum_{j=1}^{n} h_j} \quad \text{(V)}$$

where w_j is the weight of the ith indicators, and n is the number of attribute indicators.

(iv) Step 4: Define the flood susceptibility mapping using Equation VI.

$$FSI = \sum_{j=1}^{n} w_j \, Nor\left(F_j\right) \quad \text{(VI)}$$

where FSI is the degree of flood susceptibility index, w_j stands for the weight of each indicator and $Nor\left(F_j\right)$ is the normalized rate for each flood indicator.

3.2. FR

The FR model is a bivariate statistical method commonly used in hazard and disaster susceptibility analysis. Its simplicity and effectiveness in predicting flood likelihood make it a popular choice for estimating hazard likelihood. The model calculates the likelihood of future flood occurrence by analyzing the distribution of past flood events across various factors.[26] This model suggests that the importance of a specific factor in predicting flood occurrence is directly corresponding to the ratio of its class within the controlling factor. The FSI for a pixel is determined by summing the flood frequencies of all factors associated with that pixel.[27] The model estimates pixel-wise flood potential by pixel-wise FR of all factors, which is calculated as an equation.

$$FR_{ij} = \frac{Lc}{Lt} / \frac{Af}{At} \quad \text{(VII)}$$

The FR of the factor classes has been calculated using Equation VII, where *Lc* indicates the training flood location in i^{th} class of flood conditioning factor *j*, *Lt* is the total number of training flood points, *Af* is the area or pixel number in the i^{th} class of *j* flood conditioning factor, and *At* is the total pixel count or area of the *j* factor.

3.3. Receiver operating characteristics curve

The AUC is used to validate or examine the capability of a model to predict the probability of occurrence of hazards and disasters. The receiver operating characteristics curve (ROC) is the tradeoff between false positive and accurate positive rates along the X and Y axes.[28] Plotting the sensitivity, quantification of the successful and non-successful events, and 1-specificity on the abscissa and ordinates are the key aspects of it.[29,30] The value of the AUC curve varies between 0.5 and 1.0; a value between 0.9 and 1.0 indicates excellent success or prediction rate, 0.8 – 0.9 indicates very good, 0.7 – 0.8 indicates good, 0.6 – 0.7 indicates moderate, and <0.6 indicates weak prediction rate of the model.[26,31] The AUC equation is presented in Equation VIII,

$$AUC = \frac{\Sigma TP + \Sigma TN}{P + N} \quad \text{(VIII)}$$

where *TP* or true positive is the flood pixels and *TN* or true negative is the non-flood pixels. *P* is the flood point sum, and *N* is the number of non-flood points.

4. Results and discussion

4.1. Flood hazard conditioning factors

4.1.1. Drainage density

Drainage density refers to the length of the channels in a drainage basin divided by the basin's total area.[32] It is considered one of the most important parameters of fluvial landscape evolution under the influence of rivers. Consequently, there is a positive correlation between drainage density and flooding. As a result, the likelihood of flooding increases with higher stream network density.[33] As shown in Figure 3, the drainage density of the study area has been categorized into five classes based on its spatial pattern, which reveals that all the drainage density classes have almost similar pixel counts. A positive correlation was noticed between the drainage density classes and their FRs. The very high drainage density class had the highest FR (47.93%) and vice versa. The floodplains of the Barak River basin have high (0.3 – 0.4) to very high (>0.4) drainage density, which defines its higher susceptibility to flooding.

4.1.2. Elevation

Elevation is a primary determinant of flood vulnerability. Studies have shown that elevation is the most influential variable in flood occurrence, with lower elevations correlating to a higher likelihood of inundation.[23] The analysis shows a considerable variation in elevation from mountains to floodplains of the Barak River basin. Figure 3 represents the elevation map of the study area, where the entire Barak River basin is classified into five elevation zones. The highest proportion (33.04%) of the study area topography has elevations <250 m, followed by very high (>1.000), which represents 21.82% of the study area. The very low elevated areas of the Barak River basin have 100% FRs, which indicates the flood occurrence in the study area and is bounded in the low elevated regions.

4.1.3. Slope

The slope is a measure of how steeply a line or surface inclines. It is calculated as the change in height relative to the horizontal distance and expressed as a percentage or angle. It significantly influences surface runoff and water infiltration into the ground, which makes it a crucial factor in studying and predicting flood occurrence.[27] Figure 3 shows the slope map of the Barak River basin, which has been categorized into five classes. The hilly surrounding regions have high (20 – 25°) to very high (>25°) slopes, and the

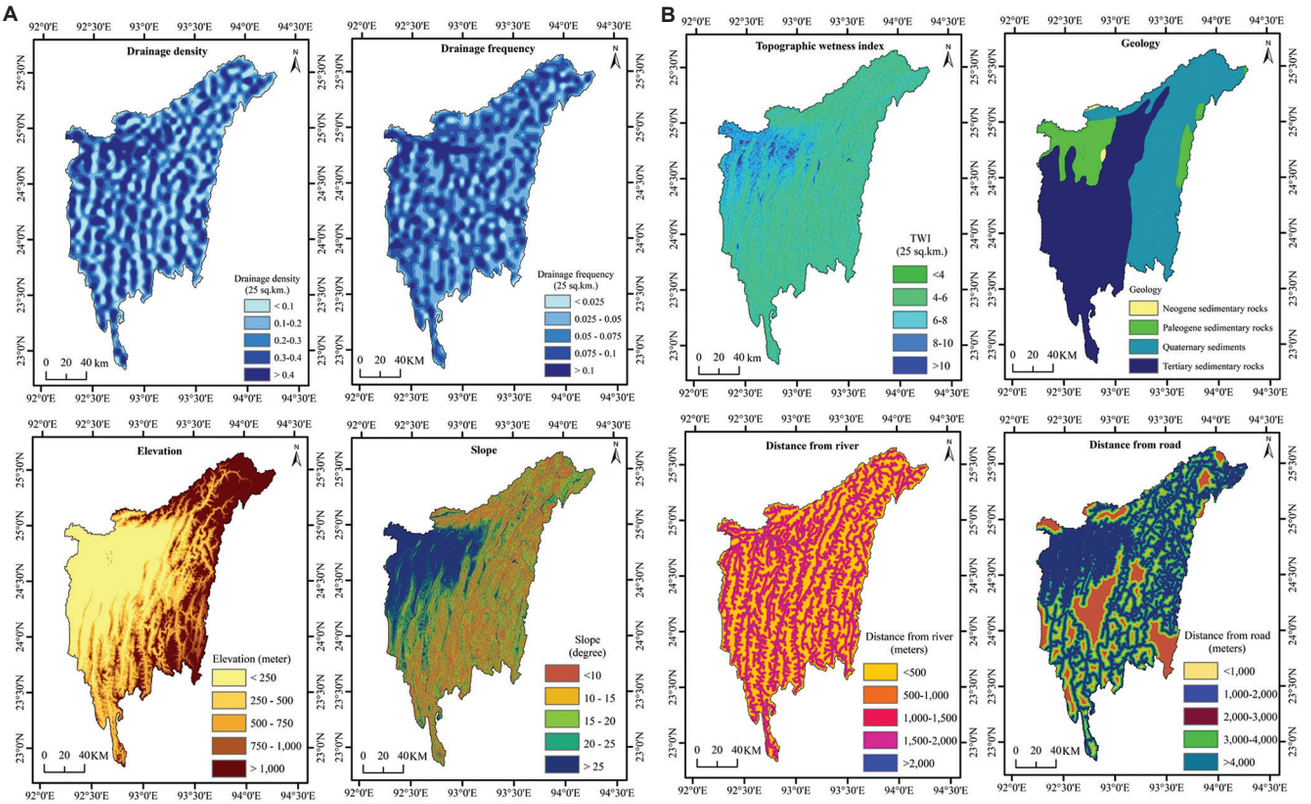

Figure 3. (A and B) Flood conditioning parameters

floodplains have a slope <10°. The calculated FR of different slope classes reveals that pixels with very low (<10°) slope values are highly susceptible to flood inundation.

4.1.4. Drainage frequency

Drainage frequency is the number of stream segments per unit area.[32] Various factors significantly influence stream frequency, including rock type, terrain ruggedness, slope steepness, rainfall patterns, subsurface material properties, vegetation cover, and drainage density. A higher stream frequency is generally associated with a denser drainage network. This indicates a landscape actively shaped by erosion and fluvial processes. Consequently, areas with high stream frequencies often exhibit a greater risk of flooding due to increased sediment load and reduced infiltration. However, these regions may also possess higher groundwater potential due to increased percolation.[34] The study area has been classified into five drainage frequency zones. FR analysis indicates a positive relationship between drainage frequency and flood susceptibility. Regions with high drainage frequencies exhibit a higher probability of flood occurrence.

4.1.5. TWI

The TWI is an effective parameter for measuring long-term moisture availability in topography. It quantifies the effect of local topography on runoff and overland flow generation.[35] The area's TWI provides insights into two key factors: terrain shape and hydrological conditions. This index quantifies the water content of each grid cell within the study area. Essentially, TWI highlights the variations in water saturation across a region.[33] Hence, it effectively contributes to flood occurrence. As shown in the TWI map, the water body surrounding areas and the downstream floodplains have high to very high moisture saturation. The class-wise FR is higher in areas with moisture-saturated TWI zones. As the TWI decreases, the class FR also decreases.

4.1.6. Geology

The geological characteristics of a region play a crucial role in determining flood hazards. Factors such as the rocks' infiltration and permeability are closely related and influence flood potential. Geology is also essential for reconstructing past flood occurrences.[4] The study area geology map has been extracted from the United States Geological Survey geology map of South Asia. The study area consists of four

Table 1. Assigning weights to the parameters and subclasses using the frequency ratio model

Class name/description	Pixel count	Percentage (%)	Number of floods	% of the number of floods	Frequency ratio	Rf	Rf (%)	Min (Rf)	Max (Rf)	Max–min (Rf)	(Max-min) Min Rf	Pr
Drainage density												
<0.1	5,312,800	15.75	5	4.13	0.26	0.05	5					
0.1 – 0.2	6,752,868	20.02	5	4.13	0.21	0.04	4					
0.2 – 0.3	7,788,913	23.09	22	18.18	0.79	0.16	16					
0.3 – 0.4	6,950,116	20.60	31	25.62	1.24	0.26	26					
>0.4	6,926,391	20.53	58	47.93	2.33	0.48	48					
Sum					4.83			0.04	0.48	0.44	0.19	2.35
Drainage frequency												
<0.025	1,803,030	5.35	1	0.83	0.15	0.03	3					
0.025 – 0.05	7,767,919	23.03	13	10.74	0.47	0.09	9					
0.05 – 0.075	9,156,685	27.15	24	19.83	0.73	0.14	14					
0.075 – 0.1	9,714,041	28.80	28	23.14	0.80	0.16	16					
>0.1	5,289,412	15.68	55	45.45	2.90	0.57	57					
Sum					5.05			0.03	0.57	0.54	0.19	2.86
Topographic wetness index												
<4.0	1,405,762	4.17	0	0	0	0	0					
4.0 – 6.0	17,854,614	52.92	8	6.61	0.12	0.02	2					
6.0 – 8.0	8,712,863	25.83	52	42.98	1.66	0.22	22					
8.0 – 10.0	3,314,004	9.82	34	28.10	2.86	0.37	37					
>10.0	2,449,204	7.26	27	22.31	3.07	0.40	40					
Sum					7.72			0	0.40	0.40	0.19	2.09
Slope												
<10	9,296,726	27.56	119	98.35	3.57	0.97	97					
10 – 15	4,477,825	13.27	1	0.83	0.06	0.02	2					
15 – 20	5,027,928	14.90	1	0.83	0.06	0.02	2					
20 – 25	5,033,950	14.92	0	0	0.00	0.00	0					
>25	9,900,018	29.35	0	0	0.00	0.00	0					
Sum					3.69			0.00	0.97	0.97	0.19	5.10

(Cont'd...)

doi: 10.36922/AJWEP025040019

Table 1. ***(Continued)***

Class name/description	Pixel count	Percentage (%)	Number of floods	% of the number of floods	Frequency ratio	Rf	Rf (%)	Min (Rf)	Max (Rf)	Max–min (Rf)	(Max-min) Min Rf	Pr
Geology												
Neogene sedimentary rock	16,390,344	48.59	47	38.84	0.80	0.04	4					
Paleogene sedimentary rock	13,106,647	38.86	0	0.00	0.00	0.00	0					
Quaternary sediments	4,126,165	12.23	69	57.02	4.66	0.25	25					
Tertiary sedimentary rock	107,931	0.32	5	4.13	12.91	0.70	70					
Sum					18.38			0.00	0.70	0.70	0.19	3.70
Distance from road												
<1000	17,186,661	50.95	119	98.35	1.93	0.96	96					
1000 – 2000	6,918,887	20.51	2	1.65	0.08	0.04	4					
2000 – 3000	3,760,359	11.15	0	0	0	0	0					
3000 – 4000	2,113,104	6.26	0	0	0	0	0					
>4000	3,752,077	11.12	0	0	0	0	0					
Sum					2.01			0	0.96	0.96	0.19	5.05
Distance from river												
<500	1,827,179	5.42	10	8.26	1.53	0.26	26					
500 – 1000	6,529,764	19.36	29	23.97	1.24	0.21	21					
1000 – 1500	7,023,579	20.82	38	31.40	1.51	0.26	26					
1500 – 2000	6,069,805	17.99	25	20.66	1.15	0.20	20					
>2000	12,280,761	36.41	19	15.70	0.43	0.07	7					
Sum					5.85			0.07	0.26	0.19	0.19	0.98
Elevation												
<250	11,146,025	33.04	121	100	3.03	1	100					
250 – 500	5,200,503	15.42	0	0	0	0	0					
500 – 750	5,330,397	15.80	0	0	0	0	0					
750 – 1000	4,699,604	13.93	0	0	0	0	0					
>1000	7,359,918	21.82	0	0	0	0	0					
Sum					3.03			0	1	1	0.19	5.26

Abbreviations: Pr: Final parameter weightage; Rf: Frequency ratio.

doi: 10.36922/AJWEP025040019

major geological formations: (i) Neogene sedimentary rock, (ii) Paleogene sedimentary rock, (iii) quaternary sediments, and (iv) tertiary sedimentary rock. Notably, 48.59% and 38.86% of the Barak River basin have Neogene and Paleogene sedimentary rock formations, respectively. Neogene sedimentary rock is found along the middle, eastern, and southern parts, and the quaternary sediments are found throughout the floodplains of the Barak River. The FR distribution (Tables 1 and 2) reveals that a significant proportion of past flood events have occurred in the regions composed of Neogene sedimentary rocks and quaternary sediments.

4.1.7. Distance from road

The distance from a road is a significant parameter in assessing flood risk. Due to their impervious nature, roads reduce the absorption of rainwater into the ground, contributing to increased runoff and potential flooding.[27] In addition, they may act like artificial barriers in surface runoff flow. Road network defines the connectivity and accessibility of any particular area. Occurrence of any hazard and disaster damages road connectivity, which makes any area inaccessible during the disastrous events. This makes the distance from the road an essential

Table 2. Assigning weights to the parameters and subclasses using Shannon's entropy model

Class name/description	Pixel count	Percentage (%)	Number of floods	% of the number of floods	Frequency ratio	SE			
						Pij	*Ej*	*h=1-e$_j$*	*Wj*
Drainage density								0.199	0.05
<0.1	5,312,800	15.75	5	4.13	0.26	0.05	−0.07		
0.1 – 0.2	6,752,868	20.02	5	4.13	0.21	0.04	−0.06		
0.2 – 0.3	7,788,913	23.09	22	18.18	0.79	0.16	−0.13		
0.3 – 0.4	6,950,116	20.60	31	25.62	1.24	0.26	−0.15		
>0.4	6,926,391	20.53	58	47.93	2.33	0.48	−0.15		
Sum					4.83	1.00	0.801		
Drainage frequency								0.244	0.06
<0.025	1,803,030	5.35	1	0.83	0.15	0.03	−0.05		
0.025 – 0.05	7,767,919	23.03	13	10.74	0.47	0.09	−0.1		
0.05 – 0.075	9,156,685	27.15	24	19.83	0.73	0.14	−0.12		
0.075 – 0.1	9,714,041	28.80	28	23.14	0.80	0.16	−0.13		
>0.1	5,289,412	15.68	55	45.45	2.90	0.57	−0.14		
Sum					5.05	1.00	0.756		
Topographic wetness index								0.297	0.07
<4.0	1,405,762	4.17	0	0.00	0.00	0	0		
4.0 – 6.0	17,854,614	52.92	8	6.61	0.12	0.02	−0.03		
6.0 – 8.0	8,712,863	25.83	52	42.98	1.66	0.22	−0.14		
8.0 – 10.0	3,314,004	9.82	34	28.10	2.86	0.37	−0.16		
>10.0	2,449,204	7.26	27	22.31	3.07	0.40	−0.16		
Sum					7.72	1	0.703		
Slope								0.898	0.22
<10	9,296,726	27.56	119	98.35	3.57	0.97	−0.01		
10_15	4,477,825	13.27	1	0.83	0.06	0.02	−0.03		
15 – 20	5,027,928	14.90	1	0.83	0.06	0.02	−0.03		
20 – 25	5,033,950	14.92	0	0.00	0.00	0.00	0		
>25	9,900,018	29.35	0	0.00	0.00	0.00	0		
Sum					3.69	1.00	0.102		

(Cont'd...)

Table 2. ***(Continued)***

Class name/description	Pixel count	Percentage (%)	Number of floods	% of the number of floods	Frequency ratio	SE			
						Pij	*Ej*	*h=1-e$_j$*	*Wj*
Geology								0.472	0.12
Neogene sedimentary rock	16,390,344	48.59	47	38.84	0.80	0.04	−0.06		
Paleogene sedimentary rock	13,106,647	38.86	0	0.00	0.00	0.00	0		
Quaternary sediments	4,126,165	12.23	69	57.02	4.66	0.25	−0.15		
Tertiary sedimentary rock	107,931	0.32	5	4.13	12.91	0.70	−0.11		
Sum					18.38	1.00	0.528		
Distance from road								0.896	0.22
<1000	17,186,661	50.95	119	98.35	1.93	0.96	−0.02		
1000 – 2000	6,918,887	20.51	2	1.65	0.08	0.04	−0.06		
2000 – 3000	3,760,359	11.15	0	0.00	0.00	0	0		
3000 – 4000	2,113,104	6.26	0	0.00	0.00	0	0		
>4000	3,752,077	11.12	0	0.00	0.00	0	0		
Sum					2.01	1.00	0.104		
Distance from river								0.043	0.01
<500	1,827,179	5.42	10	8.26	1.53	0.26	−0.15		
500 – 1000	6,529,764	19.36	29	23.97	1.24	0.21	−0.14		
1000 – 1500	7,023,579	20.82	38	31.40	1.51	0.26	−0.15		
1500 – 2000	6,069,805	17.99	25	20.66	1.15	0.20	−0.14		
>2000	12,280,761	36.41	19	15.70	0.43	0.07	−0.08		
Sum					5.85	1.00	0.957		
Elevation								1	0.25
<250	11,146,025	33.04	121	100.00	3.03	1	0		
250 – 500	5,200,503	15.42	0	0.00	0.00	0	0		
500 – 750	5,330,397	15.80	0	0.00	0.00	0	0		
750 – 1000	4,699,604	13.93	0	0.00	0.00	0	0		
>1000	7,359,918	21.82	0	0.00	0.00	0	0		
Sum					3.03	1	0		

Abbreviation: SE: Shannon's entropy.

parameter of flood damage. The road distance layer of the study has been delineated on both sides of roads using the Euclidean distance method in GIS.

4.1.8. Distance from river

The distance from a river is a key factor in determining the severity and reach of a flood. Areas closer to the river are generally at greater risk of more intense flooding and a wider spread of floodwater.[27] According to Wang *et al*.,[36] globally, a trend of relocating away from flood-inundated areas was observed in 53% of countries from 2000 to 2018, which ultimately resulted in a reduction in flood exposure, fatalities, and displacement.[36] The Shuttle Radar Topography Mission with a digital elevation model was used for stream extraction. The distance from the river was delineated on both sides of vectorized streams using the Euclidean distance method in GIS.

4.2. Flood hazard analysis and validation

Flood susceptibility maps were created using GIS (Figure 4). These maps were based on the relative importance of different flood conditioning factors, as determined by FR and Shannon entropy analyses. An FSI was calculated by combining information from all identified flood-inducing factors. Higher FSI values indicate a greater likelihood of flooding, while lower values suggest a lower risk. To categorize flood risk, the

Table 3. Class-wise area distribution of different flood susceptibility classes

Flood susceptibility	Frequency ratio model	Frequency ratio	Shannon entropy model	Shannon entropy
Very low	9,268.80	33	9,272.72	33
Low	10,338.74	37	10,458.77	38
Moderate	2,968.71	11	2,052.30	7
High	2,292.23	8	1,438.42	5
Very high	2,874.20	10	4,520.47	16
	2,7742.68	100.00	27,742.68	100.00

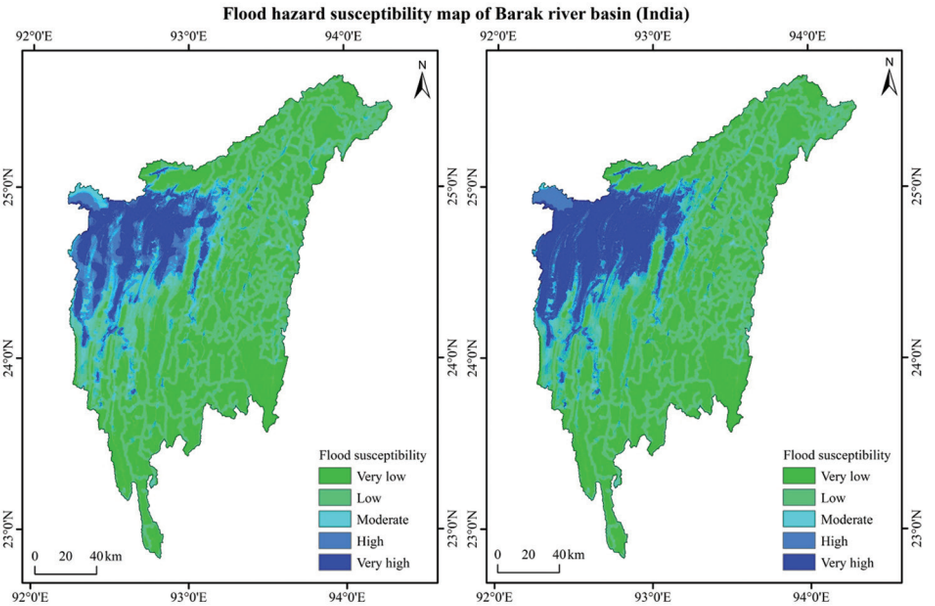

Figure 4. Flood susceptibility maps showing (A) frequency ratio and (B) Shannon's entropy

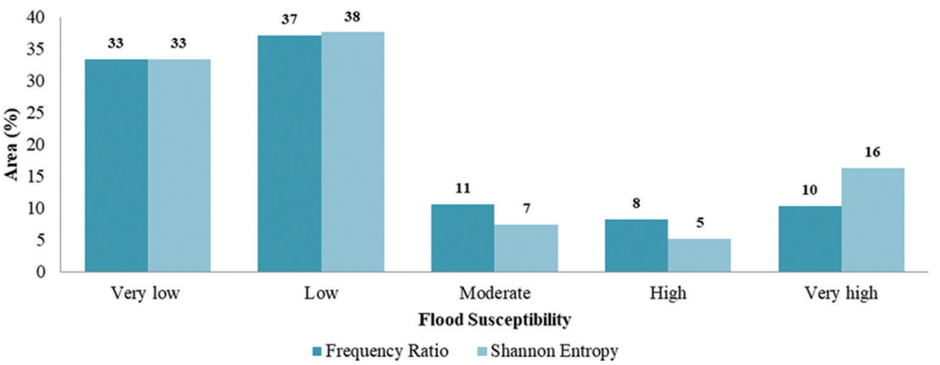

Figure 5. The area distribution of different flood susceptibility classes

study area was classified into five susceptibility zones based on FSI values. According to Table 3 and Figure 5, both the hazard maps indicate that around 70% of study areas have low to very low susceptibility to floods, around 10% are moderately susceptible, and around 20% are highly and very highly flood-susceptible.

The Barak Valley in Assam, a region of significant concern, is highly vulnerable to flooding. The lower floodplain of the Barak River basin, covering a total of 4,513.42 km^2, is at high risk. This area, which includes the districts of Cachar, Karimganj, and Hailakandi, is particularly susceptible to floods. According to

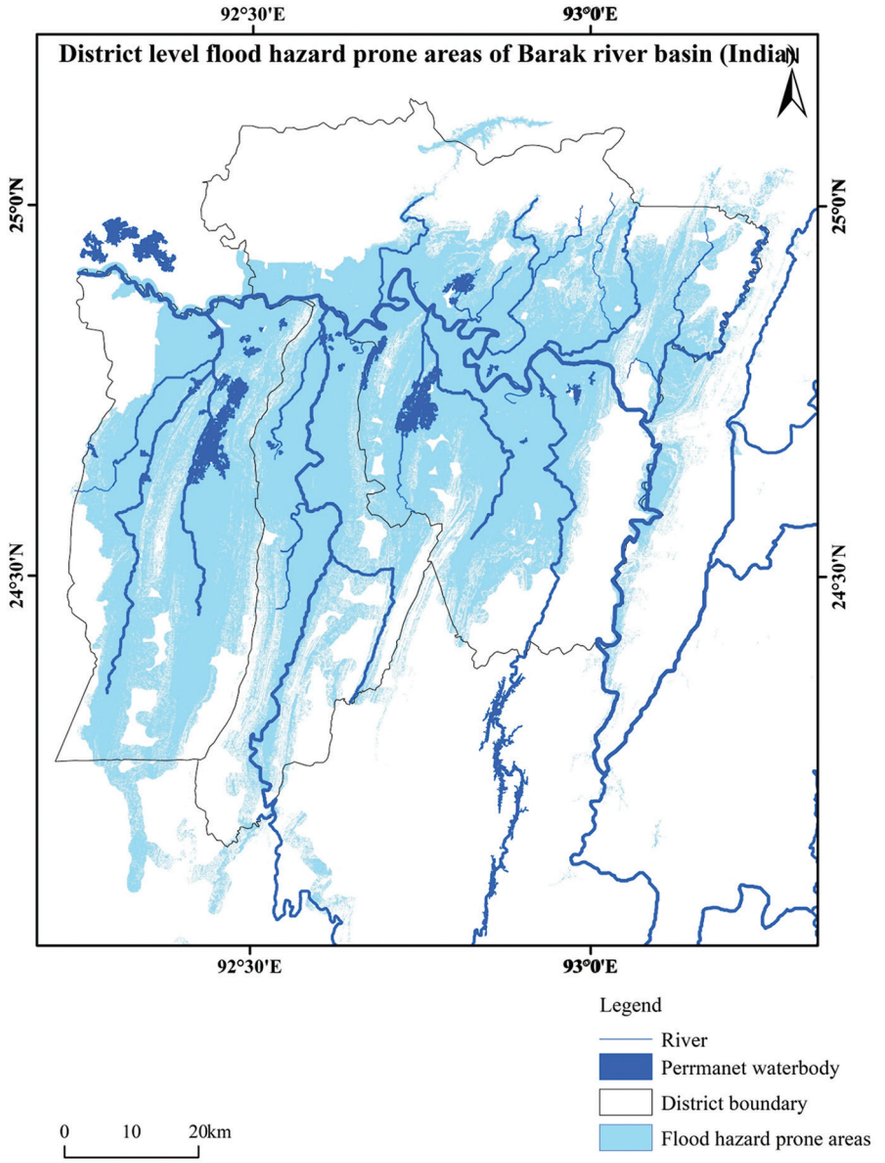

Figure 6. Flood-prone areas of the lower Barak River basin

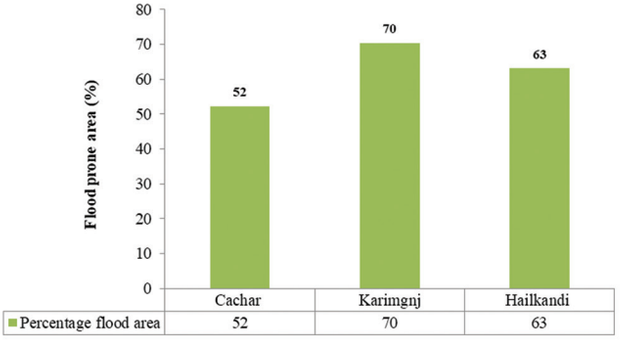

Figure 7. District-wise flood susceptibility area distribution

the generated flood maps (Figure 6), the districts of Cachar, Karimganj, and Hailakandi have 1,973.37, 1,273.27, and 840.88 km^2, respectively, classified as very highly flood-prone. In terms of percentage (Figure 7), Karimganj is the most vulnerable, with 70% of its area affected, followed by Hailakandi at 63% and Cachar at 52%.

A validation process is essential for assessing the accuracy of the generated flood hazard susceptibility maps. The present study utilized the AUC method to assess the accuracy of the maps. A total of 200 flood points were sourced from IRS-published maps of

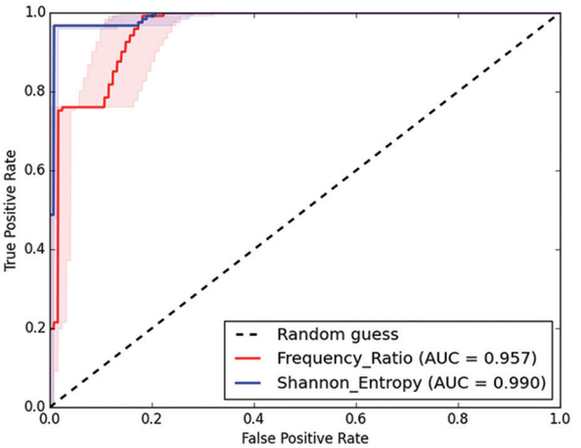

Figure 8. The area under the curve of generated flood hazard maps

different flood events. Of these, 80 points served as training points to correlate with conditioning factors, and 120 points were utilized for validation. As shown in Figure 8, the AUC values for the FR and Shannon's entropy models were calculated as 0.957 and 0.99, respectively, indicating acceptable performance for both in predicting flood hazard susceptibility. However, the entropy model demonstrated superior accuracy to the FR model, as evidenced by its higher AUC value.

4.3. Flood vulnerability assessment

Vulnerability refers to how likely people are to be harmed by natural disasters, accidents, or economic downturns. This harm can be physical, social, or economic.[37] It encompasses the potential for loss of life, property damage, and disruption of livelihoods. The flood vulnerability index provides a simplified measure of harm susceptibility through physical, social, and economic factors. It helps to identify the potential flood-vulnerable areas and can direct future mitigation and adaptation strategies.[38] Vulnerability can be classified as social vulnerability, economic vulnerability, physical vulnerability, and environmental vulnerability. Physical vulnerability includes infrastructure and agricultural activity; social vulnerability includes children, women, old, disabled people, refugees, and livestock; and economic vulnerability is related to economic losses related to hazards and disasters. The scale of flood vulnerability and its potential to turn into a disaster is determined by the value of the receptors or the exposed materials that may be affected by flooding events. This possibility of greater flood damage and losses is often exacerbated by illegal encroachment or occupation of river floodplains.[39] Flood vulnerability of certain regions is a function of exposure to flood susceptibility, adaptive capacity, and elements at risk.[40,41] In the present context, six variables – population density, household density, child population, illiteracy rate, marginal worker, and agricultural worker – were considered at the village level based on the 2011 Census of India. Weights were assigned depending on the level of significance (Table 4). The spatial distribution of vulnerability indicators is represented in Figure 9. The highest weights were assigned to the villages with high household density, high population density, high illiteracy rate, and a high number of marginal and agricultural workers who are directly affected by flooding events. The derived vulnerability map (Figure 10) inferred that 461 villages were highly vulnerable, whereas 485 villages were very highly vulnerable. These villages represent a socio-economically disadvantaged status with a high population, household density, high child population, high number of marginal workers, and illiteracy rate. In contrast, 330 villages were moderately vulnerable, and 310 villages had very low vulnerability, whereas 308 villages had low vulnerability, which depicts improved prevailing socio-economic status compared to previous villages.

4.4. Flood exposure assessment

Exposure is the potentiality of loss of life, resources, and commodities due to external hazardous or disastrous events.[37] The exposure index reflects the places that may be adversely affected and the factors in the environment that will affect floods.[42] In the present study, four variables (Figure 11) – village-river length, village-level elevation, NDVI, and NDWI – were considered for exposure assessment at the village level and assigned appropriate weights. The highest weightages (Table 5) were assigned to the villages with low elevation and villages with high drainage length, high NDWI, and low NDVI, as they are highly exposed to flooding. Flood exposure (Figure 12) in the study area has been scaled into five classes (very high, high, moderate, low, and very low). It is inferred from the exposure map that 530 and 283 villages of the study area have very low and low exposure, respectively; 179 villages are moderately exposed, while 561 and 340 villages are highly and very highly exposed to floods, respectively. These highly exposed villages are situated in the lowest elevated river valleys within the study area.

Table 4. The significant weightage of the vulnerability indicators

Parameters	Normalized AHP weightage (%)	Sub-classes	Functional relation	Rank
Population density	32.35	<200	Direct	1
		200 – 400		2
		400 – 600		3
		600 – 800		4
		>800		5
Household density	24.31	<50	Direct	1
		50 – 100		2
		100 – 150		3
		150 – 200		4
		>200		5
Population (0 – 6)	17.5	<100	Direct	1
		100 – 200		2
		200 – 300		3
		300 – 400		4
		>400		5
Illiteracy rate	12	<15	Direct	1
		15 – 25		2
		25 – 35		3
		35 – 45		4
		>45		5
Agricultural worker	8.12	<50	Direct	1
		50 – 100		2
		100 – 150		3
		150 – 200		4
		>200		5
Marginal worker	5.72	<40	Direct	1
		40 – 80		2
		80 – 120		3
		120 – 160		4
		>160		5

Abbreviation: AHP: Analytic hierarchy process.

4.5. Flood risk assessment

Disaster risk has been defined as the probability of disaster occurrence and its projected future damage or how badly it can affect any society. Disaster risk assessment is an essential step to being prepared and ready to act before a disaster strikes.[43] The term flood risk on different occasions has been elaborated similarly, emphasizing various elements by different scientists,[44] as shown in Equations IX to XIII.

$$\text{Risk} = \text{Hazard} \times \text{Vulnerability} \quad \text{(IX)}$$

$$\text{Risk} = \text{Impact of hazard} \times \text{Elements at risk} \times \text{Vulnerability of elements at risk} \quad \text{(X)}$$

$$\text{Risk} = \text{Hazard} \times \text{Vulnerability} \times \text{Value (of the threatened area)/preparedness} \quad \text{(XI)}$$

$$\text{Risk} = \text{Probability} \times \text{Consequences} \quad \text{(XII)}$$

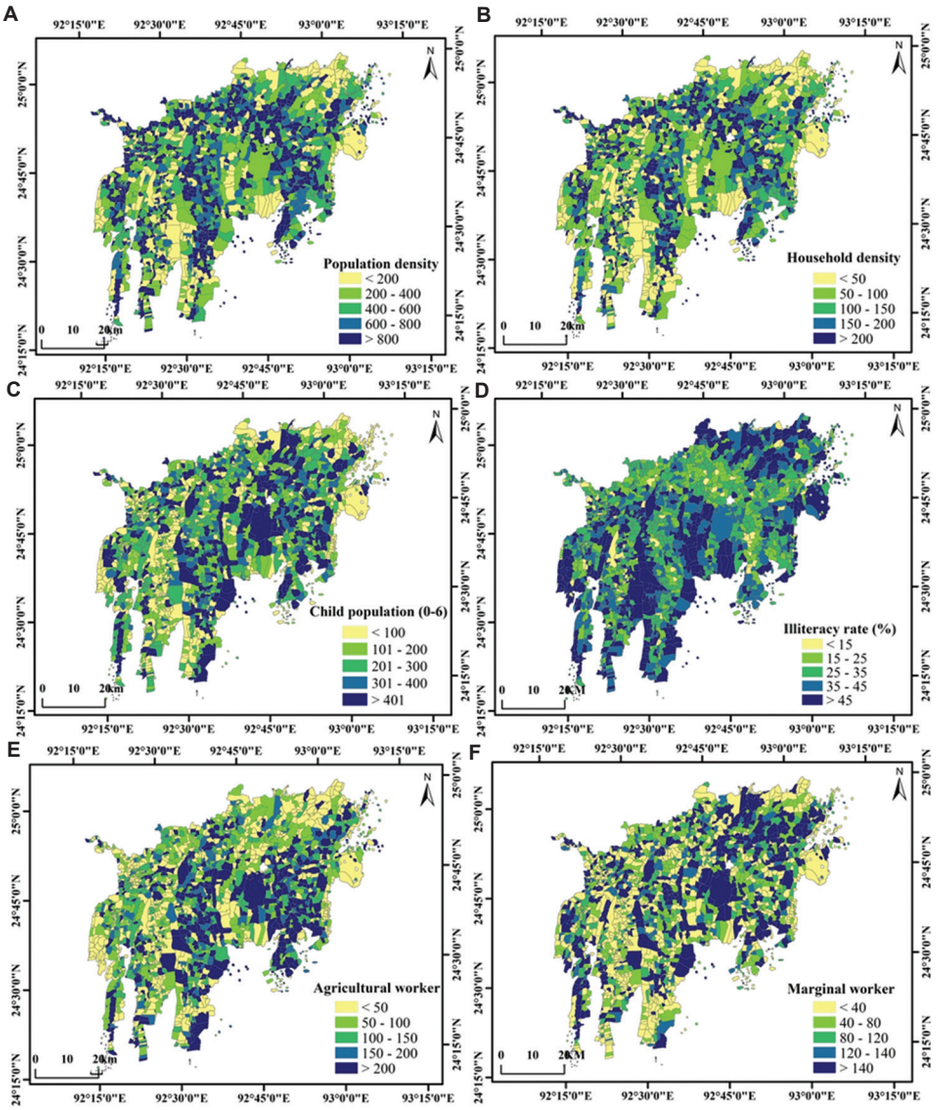

Figure 9. The vulnerability indicators showing the (A) population density, (B) household density, (C) child population, (D) illiteracy rate, (E) agricultural worker, and (F) marginal worker of the Barak River floodplain

$$\text{Risk} = \text{Hazard} \times \text{Consequences} \quad \text{(XIII)}$$

The present study combines the exposure and vulnerability index to derive the flood risk of Barak River floodplain villages. The risk map (Figure 13) is classified into five categories (very high, high, moderate, low, and very low) based on the risk level. It is inferred that among the total number of villages (Figure 14), 388 and 476 Barak River floodplain villages are at very high and high flood risk, 369 villages are at moderate risk, and 343 and 318 villages are at low and very low risk, respectively. It has been observed that 45.61% of severely flood risk-prone villages are located along the main tributary banks of the Barak River, confined with the lowest elevation and high soil moisture saturation. At the same time, 661 least risk-prone villages, which are unaffected by flood events, are located at high elevations relative to the previous villages. As elevation increases toward the surrounding hills, both the elevation and flood risk decrease, contributing to the lower flood vulnerability of these villages.

4.6. Discussion

Floods, a leading global natural disaster, cause substantial damage to life and property. This study

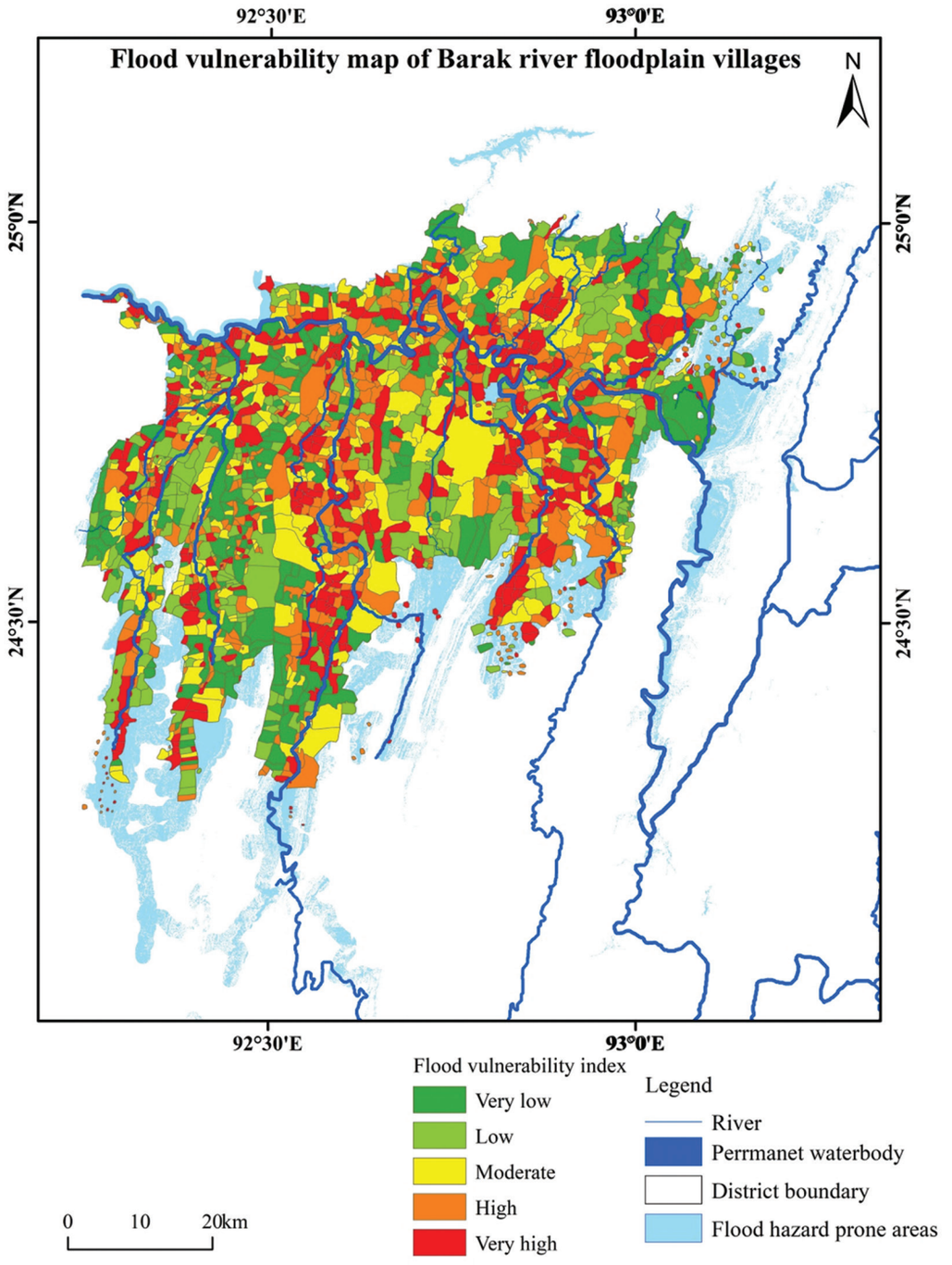

Figure 10. The vulnerability index of Barak River floodplain villages

delineates the flood-susceptible areas and assesses the risk to villages of the Barak River basin. Barak Valley of Assam is densely populated and is highly prone to flooding, which makes it essential to identify areas at risk for effective disaster management strategies. Flood modeling and susceptibility mapping are crucial for assessing vulnerability and developing mitigation plans. Factors, including topography, geology, hydrology, and landforms, contribute to flood occurrence within a river basin. To delineate the flood hazard-prone areas, several factors, such as drainage density, drainage frequency, TWI, slope, elevation, distance from rivers, distance from roads, and geology, were analyzed. The findings of the study indicate that areas below 250 m in elevation and slopes <10° are at high flood risk. In addition, regions with dense drainage networks, frequent

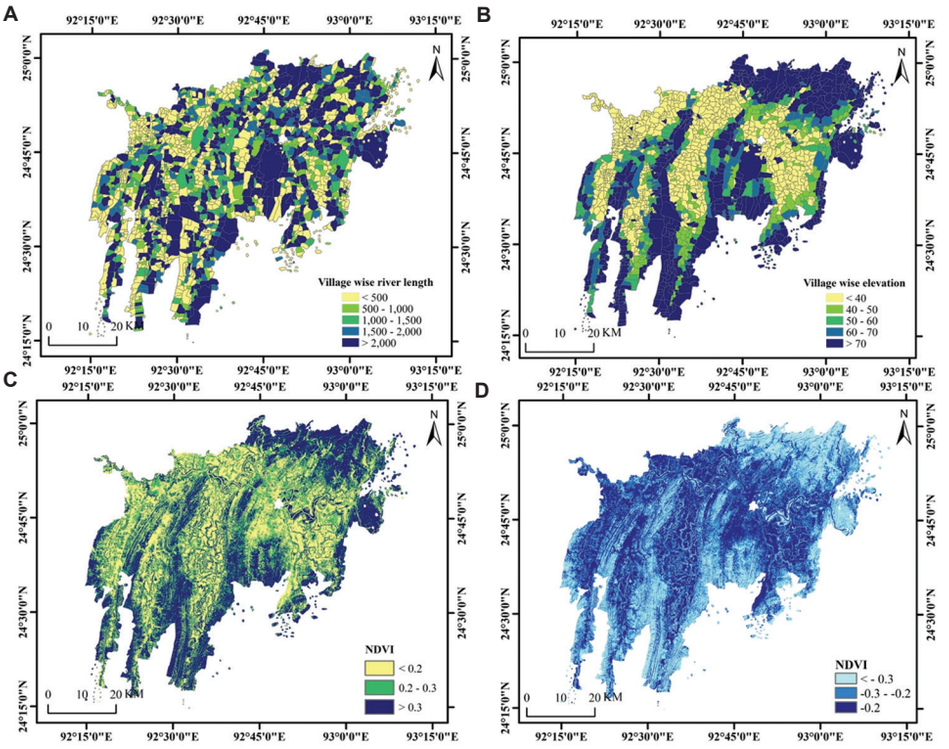

Figure 11. The exposure indicators showing the (A) village river length, (B) village elevation, (C) normalized difference vegetation index, and (D) normalized difference water index

Table 5. The significant weights of the exposure indicators

Parameters	Normalized AHP weightage (%)	Sub-classes	Functional relation	Rank
Village elevation	44.22	<40	Direct	1
		40 – 50		2
		50 – 60		3
		60 – 70		4
		>70		5
Village-wise river length	23.68	<500	Inverse	5
		500 – 1000		4
		1000 – 1500		3
		1500 – 2000		2
		>2000		1
NDWI	17.34	<−0.3	Inverse	3
		−0.3 – −0.2		2
		>−0.2		1
NDVI	13.76	<0.2	Direct	1
		0.2 – 0.3		2
		>0.3		3

Abbreviation: AHP: Analytic hierarchy process; NDVI: Normalized difference vegetation index; NDWI: Normalized difference water index.

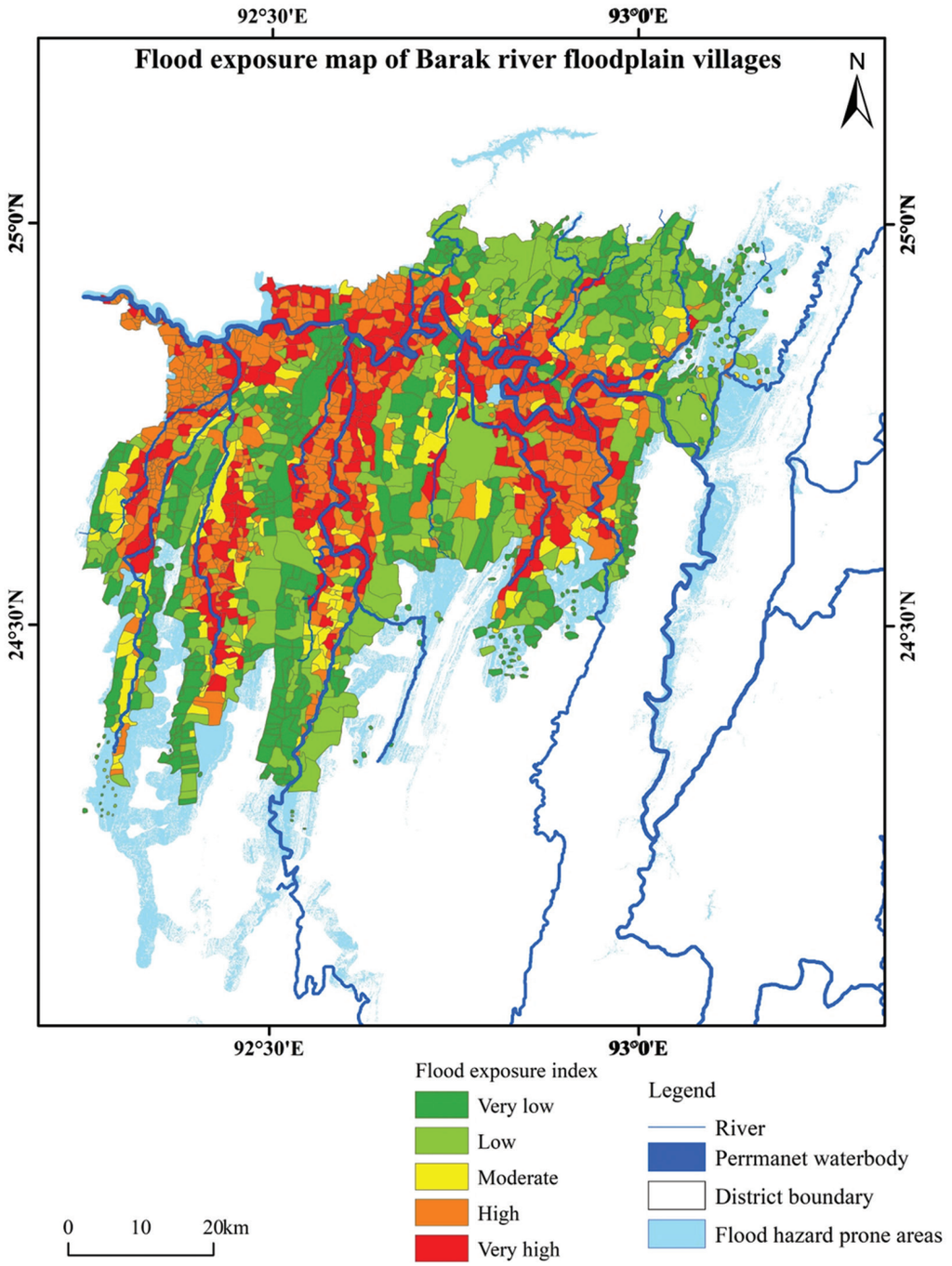

Figure 12. The exposure index of Barak River floodplain villages

watercourses, and proximity to rivers or roads are more likely to experience flooding.

After investigating all the factors, it was found that most of the very highly susceptible areas are concentrated in the eastern and central floodplain of the river. It can be attributed to prevailing factors, such as low elevation, flat plain topography, high topographic and soil moisture content, low slope, and nearby river locations. It makes the area highly flood-susceptible compared to other parts of the study area. According to the FR and entropy model, 18.62 and 21.48% of the basin area have high and very high flood susceptibility, respectively, concentrated in the Barak Valley of Assam (Barak River floodplain). Among the districts, Cachar district has a 1973.37 km² area susceptible to floods, which is the highest among the districts. Karimganj

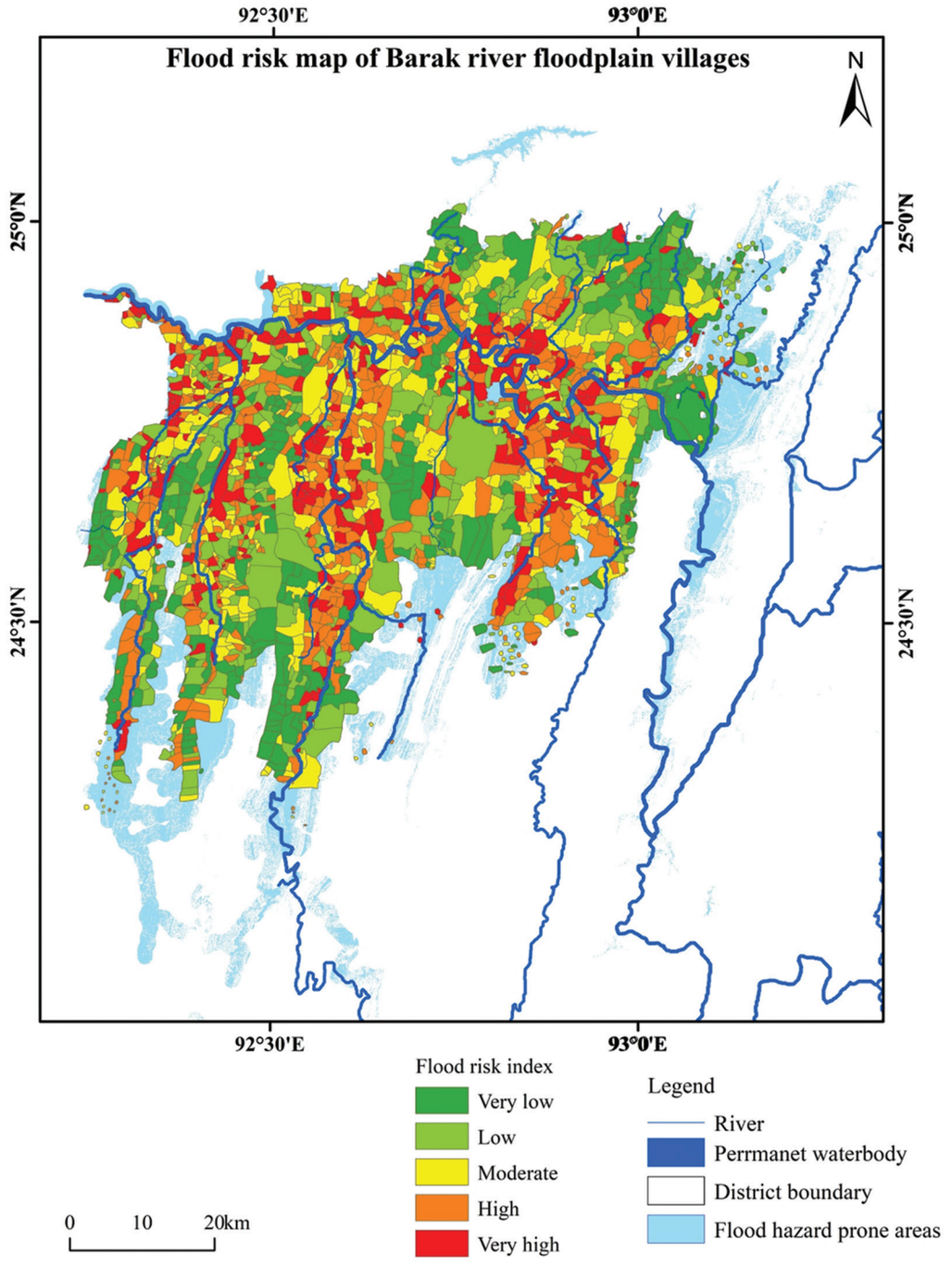

Figure 13. The risk index of Barak River floodplain villages

district, on the other hand, has approximately 70% of its area classified as highly susceptible to floods.

Further study has been carried out to assess the risk of hazard-prone villages and towns. Before risk assessment was conducted, flood vulnerability and flood exposure of the villages were studied. Results of the study revealed that 47.62% of villages are extremely exposed to floods, and these villages are located along the lowest elevated corridors and river banks. Notably, 49.95% of the villages are vulnerable to floods, and these villages are characterized by a socio-economically disadvantaged status. Furthermore, 45.62% of villages are severely prone to flooding, combining both exposure and vulnerability factors. Figure 15 shows the field pictures of Barak Valley flood-affected areas, and Table 6 shows flood damages that occurred at different

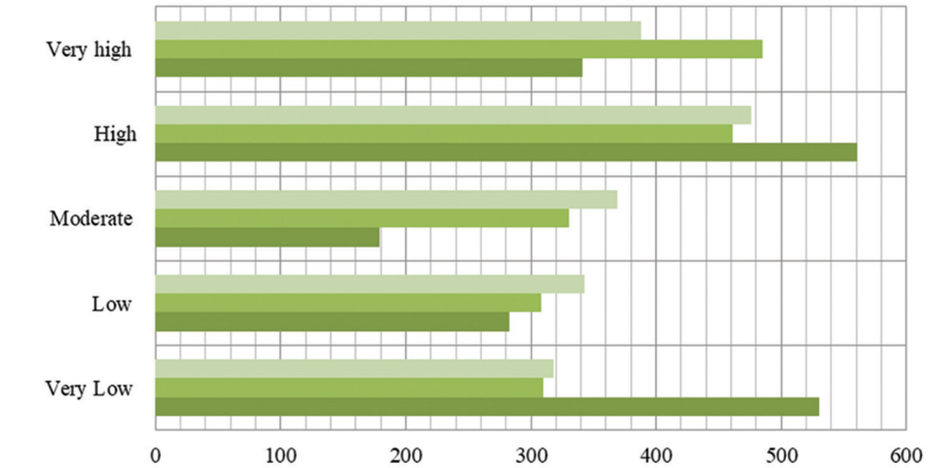

	Very Low	Low	Moderate	High	Very high
Risk	318	343	369	476	388
Vulnerability	310	308	330	461	485
Exposure	530	283	179	561	341

Figure 14. The number of villages with flood exposure, vulnerability, and risk

Figure 15. Field photos of the Barak Valley flood. Image taken by the authors.

times in Barak Valley districts. The data were sourced from the Assam Flood Memorandum 2015 – 2023. The 2022 destructive Assam flood caused great damage in the study area, where 1741 villages and almost 2 million people were affected by the 2022 Barak River flood. In total, 12,809 hectares of agricultural land were inundated, resulting in 56 human fatalities, over 100,000 damaged homes, and additional losses. This was followed by the 2018 flood, which impacted 667 villages, inundated 8,118.62 hectares of agricultural

Table 6. Flood damages in Barak River floodplain districts

District	Flood damage	2015	2016	2017	2018	2019	2022	2023
Cachar	Villages affected	-	-	-	188	55	826	02
	Population affected	5,458		-	-	19,048	1,434,750	565
	Total agricultural land affected (in Ha.)	13,716	0	1,585	1,016	45	8,618	0
	Human life lost	01	-	-	13	-	45	0
	Livestock Assam	-	-	-	-	-	5,211	0
	House damages	01	147	-	53	-	81,544	0
Karimganj	Villages affected	-	-	-	314	55	729	02
	Population affected	18,800	-	-	-	44,048	308,581	214
	Total agricultural land affected (in Ha.)	10,639	1,202	480	2,489.3	595	774	0
	Human life lost	-	-	02	08	-	08	0
	Livestock Assam	-	-	-	-	-	717	0
	House damages	-	2,562	-	-	-	8,518	0
Hailakandi	Villages affected	-	-	-	235	91	186	-
	Population affected	-	-	-	-	4,860	256,019	-
	Total agricultural land affected (in Ha.)	14,725	0	204	4,613.32	1,165	3,417	0
	Human life lost	-	-	-	02	-	03	0
	Livestock Assam	-	-	-	-	-	39	0
	House damages	-	0	-	407	-	28,364	0

land, caused 23 causalities, and damaged 460 houses. The data highlight that flooding and associated damages occur annually in the study area, making floods in the Barak River floodplain a common destructive disaster event. This underscores the need for better planning and management to reduce flood risks and enhance resilience for local communities.

5. Conclusion

Flood susceptibility modeling is a widely used approach in flood management strategies. Researchers often use statistical methods to create flood risk maps. Two popular statistical models, Shannon's entropy and FR, are known for their accuracy and have been utilized in the present study. This study aimed to produce a detailed flood risk map for the study area using geospatial technology. The goal is to identify high-risk zones and develop strategies to protect these areas from future floods. The present study generated flood susceptibility maps by combining eight conditioning factors and model weights. The FR model identified 29.32% of the study area as flood-prone, with 10.36% classified as very high, 8.26% as high, and 10.7% as moderate risk. Similarly, the entropy model indicated 28.88% of the basin as flood-prone, with 16.29% very high, 5.18% high, and 7.4% moderate risk. Both models consistently highlighted the lower Barak River floodplain as a critical flood-prone area. High AUC values (0.95 and 0.99, respectively) confirm the models' reliability, indicating solid predictive performance. Elevation, slope, road network, and road distance emerged as the region's primary factors influencing flood susceptibility. These findings can inform effective flood management strategies to minimize impacts.

Flood risk analysis of the Barak River floodplain villages shows that 866 villages are severely risk-prone to floods, which represents almost 2 million (1,878,366) population which are highly vulnerable, exposed, and risk-prone to floods. These villages are located along the low elevated banks of the Barak River and its tributaries. They are characterized by a high population, household density, a high number of marginal agricultural workers, and a high child population. For better flood management in these areas, specific planning, like flood forecasting, early warning, and floodplain land use planning, should be emphasized.

Acknowledgments

None.

Funding

This study is supported by the University Grant Commission (UGC), India, under the UGC-JRF fellowship (Student ID: 200510423613).

Conflict of interest

The authors declare that they have no competing interests.

Author contributions

Conceptualization: Shanku Ghosh
Formal analysis: Shanku Ghosh
Investigation: Chakkaravarthi Prakasam
Methodology: Chakkaravarthi Prakasam
Writing – original draft: Shanku Ghosh
Writing – review & editing: Chakkaravarthi Prakasam

Availability of data

The study was conducted mainly using secondary data, all of which are publicly available.

References

1. Glas H, Rocabado I, Huysentruyt S, *et al*. Flood risk mapping worldwide: A flexible methodology and toolbox. *Water*. 2019;11:2371. doi: 10.3390/w11112371
2. Rehman S, Hasan Mohd SU, Rai AK, Rahaman MH, Avtar R, Sajjad H. Integrated approach for spatial flood susceptibility assessment in Bhagirathi sub-basin, India using entropy information theory and geospatial technology. *Risk Anal*. 2022;42:2765-2780. doi: 10.1111/risa.13887
3. Duan Y, Xiong J, Cheng W, *et al*. Assessment and spatiotemporal analysis of global flood vulnerability in 2005-2020. *Int J Disast Risk Reduct*. 2022;80:103201. doi: 10.1016/j.ijdrr.2022.103201
4. Adi Prasojo O, Hurst MD, Williams RD, Naylor LA, Toney J. Slowing down the tidal flood wave is the key to reducing tidal flood risk in estuaries worldwide. In: *European Geosciences Union General Assembly*; 2024. doi: 10.5194/egusphere-egu24-17737
5. Duan Y. *Global Projections of Flood Risk Under Climate Change (No. EGU24-7030)*. Copernicus Meetings; 2024.
6. Antwi-Agyakwa KT, Afenyo MK, Angnuureng DB. Know to predict, forecast to warn: A review of flood risk prediction tools. *Water*. 2023;15(3):427. doi: 10.3390/w15030427
7. Di Baldassarre G, Montanari A, Lins H, Koutsoyiannis D, Brandimarte L, Blöschl G. Flood fatalities in Africa: From diagnosis to mitigation. *Geophys Res Lett*. 2010;37(22):1-5. doi: 10.1029/2010gl045467
8. Gupta L, Dixit J. A GIS-based flood risk mapping of Assam, India, using the MCDA-AHP approach at the regional and administrative level. *Geocarto Int*. 2022;37(26):1-33. doi: 10.1080/10106049.2022.2060329
9. Sarkar D, Mondal P. Flood vulnerability mapping using frequency ratio (FR) model: A case study on Kulik river basin, Indo-Bangladesh Barind region. *Appl Water Sci*. 2019;10(1):17. doi: 10.1007/s13201-019-1102-x
10. Devanand MR, Kundapura S. Flood inundation mapping of harangi river Basin, Kodagu, using GIS techniques and HEC-RAS Model. In: *Lecture Notes in Civil Engineering*. Singapore: Springer; 2020. p. 665-678. doi: 10.1007/978-981-15-6828-2_50
11. Mishra AK, Meera MS, Nagaraju V. Exploring extreme flood events of a western state of India during monsoon season of 2019 from space. *Mausam*. 2023;75(1):245-248. doi: 10.54302/mausam.v75i1.3568
12. Das S, Das T. Flood, livelihood, and community resilience: A study from Barak Valley region of Assam in Northeast India. In: *International Handbook of Disaster Research*. Singapore: Springer; 2022. p. 1-14. doi: 10.1007/978-981-16-8800-3_63-1
13. Gogoi PP, Vinoj V, Phukon P. Role of meteorology and local orography on a flood event in the Lower Subansiri Basin and post-flood changes to land use and land cover. *Curr Sci*. 2020;118:778-785. doi: 10.18520/cs/v118/i5/778-785
14. Das K, Simhachalam A, Bora AK. *Application of Geospatial Technology in Seasonal Flood Hazard Event in Dhemaji District of Assam*. Singapore: Springer; 2022. p. 247-269. doi: 10.1007/978-3-031-15501-7_10
15. Longkumer W, Kannan H. Between floods and climate change: Revisiting the mishing community of Majuli Island, Northeast India. *Asian J Water Environ Pollut*. 2024;21(2):57-64. doi: 10.3233/ajw240022
16. Mishra AK, Meer MS, Nagaraju V. Satellite-based monitoring of recent heavy flooding over north-eastern states of India in July 2019. *Nat Hazards*. 2019;97(3):1407-1412. doi: 10.1007/s11069-019-03707-z
17. Mudashiru RB, Sabtu N, Abustan I, Balogun W. Flood hazard mapping methods: A review. *J Hydrol*. 2021;603:126846. doi: 10.1016/j.jhydrol.2021.126846
18. Sargentis GF, Iliopoulou T, Ioannidis R, *et al*. Technological advances in flood risk assessment and related operational practices since the 1970s: A case study in the Pikrodafni river of Attica. *Water*. 2025;17(1):112. doi: 10.3390/w17010112
19. Morante-Carballo F, Montalván-Burbano N,

Arias-Hidalgo M, Domínguez-Granda L, Apolo-Masache B, Carrión-Mero P. Flood models: An exploratory analysis and research trends. *Water*. 2022;14(16):2488. doi: 10.3390/w14162488
20. Das P, Dey NB. Socio-economic vulnerability in a flood affected village of Barak valley, Assam, India. *Asia Pac J Soc Sci*. 2011;3:110-123.
21. Assam Flood Handbook. *Flood Memorandum to the Ministry of Home Affairs Government of India on Assam Floods – 2022.* Government of Assam; 2022.
22. Statistical Handbook of Assam. *Statistical Handbook Assam 2021*. Directorate of Economics and Statistics Government of Assam, Guwahati; 2021.
23. Islam S, Tahir M, Parveen S. GIS-based flood susceptibility mapping of the lower Bagmati basin in Bihar, using Shannon's entropy model. *Model Earth Syst Environ*. 2022;8:1-15. doi: 10.1007/s40808-021-01283-5
24. Sarkar D, Saha S, Mondal P. GIS-based frequency ratio and Shannon's entropy techniques for flood vulnerability assessment in Patna district, Central Bihar, India. *Int J Environ Sci Technol*. 2021;19(9):8911-8932. doi: 10.1007/s13762-021-03627-1
25. Al-Hinai H, Abdalla R. Mapping coastal flood susceptible areas using Shannon's entropy model: The case of Muscat governorate, Oman. *ISPRS Int J GeoInform*. 2021;10(4):252. doi: 10.3390/ijgi10040252
26. Chowdhury S. Flash flood susceptibility mapping of North-East depression of Bangladesh using different GIS based bivariate statistical models. *Watershed Ecol Environ*. 2024;6:26-40. doi: 10.1016/j.wsee.2023.12.002
27. Arora A, Pandey M, Siddiqui MA, Hong H, Mishra VN. Spatial flood susceptibility prediction in Middle Ganga Plain: Comparison of frequency ratio and Shannon's entropy models. *Geoc Int*. 2019;36(18):2085-2116. doi: 10.1080/10106049.2019.1687594
28. Pourghasemi HR, Kariminejad N, Amiri M, *et al*. Assessing and mapping multi-hazard risk susceptibility using a machine learning technique. *Sci Rep.* 2020;10(1):3203. doi: 10.1038/s41598-020-60191-3
29. Pourghasemi HR, Rahmati O. Prediction of the landslide susceptibility: Which algorithm, which precision? *CATENA*. 2018;162:177-192. doi: 10.1016/j.catena.2017.11.022
30. Malik S, Pal SC, Arabameri A, *et al*. GIS-based statistical model for the prediction of flood hazard susceptibility. *Environ Dev Sustain*. 2021;23(11):16713-16743. doi: 10.1007/s10668-021-01377-1
31. Yesilnacar EK. *The Application of Computational Intelligence to Landslide Susceptibility Mapping in Turkey.* Australia: University of Melbourne; 2005. p. 200.
32. Horton RE. Erosional development of streams and their drainage basins; hydrophysical approach to quantitative morphology. *Geol Soc Am Bull*. 1945;56:275-370. doi: 10.1130/0016-7606(1945)56[275:EDOSAT]2.0.CO;2
33. Chetia L, Paul SK. Spatial assessment of flood susceptibility in Assam, India: A comparative study of frequency ratio and shannon's entropy models. *J Indian Soc Remote Sens*. 2024;52(2):343-358. doi: 10.1007/s12524-023-01798-7
34. Abdo HG. Evolving a total-evaluation map of flash flood hazard for hydro-prioritization based on geohydromorphometric parameters and GIS–RS manner in Al-Hussain river basin, Tartous, Syria. *Nat Hazards*. 2020;104:681-703. doi: 10.1007/s11069-020-04186-3
35. Pourali SH, Arrowsmith C, Chrisman N, Matkan AA, Mitchell D. Topography wetness index application in flood-risk-based land use planning. *Appl Spat Anal Policy*. 2014;9(1):39-54.} doi: 10.1007/s12061-014-9130-2
36. Wang N, Sun F, Demetris Koutsoyiannis, *et al*. How can changes in the human-flood distance mitigate flood fatalities and displacements? *Geophys Res Lett*. 2023;50(20):1-9. doi: 10.1029/2023gl105064
37. UNISDR. *Terminology on Disaster Risk Reduction (DRR).* Geneva, Switzerland: UNISDR; 2009b.
38. Giannakidou CH, Diakoulaki D, Memos CD. Implementing a flood vulnerability index in urban coastal areas with industrial activity. *Nat Hazards*. 2019;97(1):99-120. doi: 10.1007/s11069-019-03629-w
39. Birkmann J. Measuring vulnerability to promote disaster-resilient societies: Conceptual frameworks and definitions. In: *Measuring Vulnerability to Natural Hazards: Towards Disaster Resilient Societies*. Vol. 1. New York: United Nations University Press; 2006. p. 3-7.
40. Scheuer S, Haase D, Meyer V. Exploring multicriteria flood vulnerability by integrating economic, social and ecological dimensions of flood risk and coping capacity: From a starting point view towards an end point view of vulnerability. *Nat Hazards*. 2010;58(2):731-751. doi: 10.1007/s11069-010-9666-7
41. Sharma SV, Sarathi Roy P, Chakravarthi V, Srinivasa Rao G. Flood risk assessment using multi-criteria analysis: A case study from Kopili River Basin, Assam, India. *Geomat Nat Hazards Risk*. 2017;9(1):79-93. doi: 10.1080/19475705.2017.1408705
42. Bin L, Xu K, Pan H, Zhuang Y, Shen R. Urban flood risk assessment characterizing the relationship among hazard, exposure, and vulnerability. *Environ Sci Pollut Res*. 2023;30(36):86463-86477. doi: 10.1007/s11356-023-28578-7
43. Jaiswal R, Donahue J, Reilly MJ. Disaster risk management. In: *Ciottone's Disaster Medicine*. Netherlands: Elsevier Inc. 2016. p. 167-177. doi: 10.1016/B978-0-323-28665-7.00028-5
44. Tariq MA, Farooq R, van de Giesen N. A Critical review of flood risk management and the selection of suitable measures. *Appl Sci*. 2020;10(23):8752. doi: 10.3390/app10238752

Asian Journal of Water, Environment and Pollution. Vol. 22, No. 2 (2025), pp. 87-96.
doi: 10.36922/AJWEP025060037

ORIGINAL RESEARCH ARTICLE

Assessment of surface water quality impacted by upstream artisanal mining in Prek Te area, Cambodia

Vibol Sao[1]*, Chan Oeurn Chey[2], Socheata Korng[2], Eang Chorney[1], and Kyoung-Woong Kim[3]

[1]Department of Environmental Engineering, Faculty of Engineering, Royal University of Phnom Penh, Phnom Penh, Cambodia
[2]Chemistry Program, Graduate School of Sciences, Royal University of Phnom Penh, Phnom Penh, Cambodia
[3]Department of Environment and Energy Engineering, Gwangju Institute of Science and Technology, Gwangju, Republic of Korea
***Corresponding author:** Vibol Sao (vibol.sao@rupp.edu.kh)

Received: February 7, 2025; 1st revised: March 2, 2025; 2nd revised: March 4, 2024; Accepted: March 14, 2025; Published Online: April 4, 2025

Abstract: Mining activities can significantly impact water quality by introducing various contaminants into water sources. The purpose of this study is to assess heavy metal concentrations and other elemental contaminants in water from the Prek Te area across two seasons and evaluate the potential health risks associated with drinking contaminated water. Surface water samples were collected twice in 2023: from March 5 – 11 (dry season) to October 20 – 26 (rainy season). A total of 21 surface water samples were collected from different locations along the Prek Te area. On-site measurements included pH, electrical conductivity, dissolved oxygen, and total dissolved solids, while laboratory analyses determined arsenic (As), chromium, nickel (Ni), copper, zinc, cadmium, and lead concentrations using inductively coupled plasma mass spectrometry. The results indicated that most parameters were within the World Health Organization guidelines and Cambodia Drinking Water Quality Standards, except for As and Ni. During the rainy season, the highest As concentration was 58.1 μg/L, followed by 22.0 μg/L and 10.8 μg/L. Health risk assessments revealed that the hazard index and hazard quotient for children exceeded 1, indicating potential non-carcinogenic health risks. In addition, children exhibited the highest lifetime cancer risk for As ($>1.8 \times 10^{-1}$), followed by women ($>1.2 \times 10^{-1}$) and men ($>1 \times 10^{-1}$). These findings suggest that children are more vulnerable to health risks associated with drinking contaminated water compared to adults. To ensure safe drinking water for communities along the Prek Te area, an urgent monitoring program and appropriate water treatment measures—particularly to remove As contamination—are recommended.

Keywords: Cambodia; Artisanal gold mining; Heavy metals; Health risk; Prek Te area

1. Introduction

Mondulkiri, Cambodia's largest province, is located in the eastern region of the country and shares borders with Vietnam to the east and south, Kratie Province to the west, Stung Treng Province to the northwest, and Ratanakiri Province to the north. Despite its vast land area, Mondulkiri has the lowest population density in Cambodia. The province is known not only for its potential to attract tourists but also for its abundant mineral resources, including gold deposits. However, gold mining in Mondulkiri is predominantly small-scale,

commonly referred to as artisanal gold mining, which is typically carried out by individuals, families, or small community groups using rudimentary technology and traditional extraction methods. Artisanal gold mining is a major environmental concern due to inefficient and often nonexistent pollution control measures during mineral extraction and processing.[1] Most artisanal gold mining operations take place near water bodies such as rivers and streams, which facilitate the acquisition of alluvial ores and provide water for operational needs.[2] However, runoff from mining activities can degrade water quality by introducing contaminants through processes such as cleaning, dewatering, and acid rock drainage.[3] Among human activities, mining poses a significant threat to surface water quality, particularly affecting rivers, streams, lakes, and rainfall-dependent water sources.[4]

Despite its environmental challenges, artisanal gold mining has made a substantial financial contribution to rural communities by generating income from mineral resources.[5] The Cambodian government recognizes mining as a strategic sector for economic growth, given the country's diverse mineral resources, including gold, copper (Cu), and other base metals, which have the potential to boost economic development if effectively explored and managed.[6] Mining has both positive and negative effects on the environment and society. While it contributes to infrastructure development, economic growth, job creation, and social programs, it also poses severe risks to freshwater ecosystems. These risks include contamination from mine effluent discharge, seepage from tailings and waste rock impoundments, and water-intensive ore processing techniques. The release of hazardous chemicals into rivers, streams, and lakes as a result of mining operations has deteriorated water quality and threatened aquatic life. Consequently, rural communities relying on these water sources face significant health risks.[7]

A combination of factors, including increased sedimentation and its correlation with toxic contaminants such as arsenic (As) and mercury (Hg), further degrades water quality downstream of gold mining activities.[8] Among the most evident risks associated with artisanal mining is the high potential for miners to sustain bodily injuries.[9] The rise in artisanal gold mining has also led to a greater reliance on chemical-based techniques for gold processing and recovery, especially those involving cyanide and Hg, both of which pose serious environmental and public health hazards.[10]

Furthermore, gold mining operations can significantly elevate the concentrations of heavy metals associated with gold deposits, including Cu, zinc (Zn), As, cadmium (Cd), Hg, and lead (Pb), in the surrounding environment. This contamination affects soil, sediments, surface water, and groundwater, posing serious risks to human and animal health.[11] Due to their high mobility and persistence, these heavy metals can be easily dispersed, absorbed by plants and animals, and bioaccumulated in humans through the food chain.[12]

This study aims to:

(i) Evaluate the levels of heavy metals and other elemental contaminants in drinking water sources in the Prek Te area throughout the year, in accordance with the Cambodian Drinking Water Quality Standard (CDWQS)[13] and the World Health Organization (WHO) drinking water quality guidelines.[14]

(ii) Assess the non-carcinogenic and carcinogenic health risks posed by selected trace elements in drinking water sources.

2. Materials and methods

2.1. Study area

This cross-sectional survey involved the sampling of surface water along Prek Te, a tributary of the Mekong River, extending from Chong Phlah Commune, Keo Seima District, Mondulkiri Province, to Sangkat Roka Kandal, Kratie City, Kratie Province (Figure 1). Cambodia experiences two distinct seasons: the dry season (November–April) and the rainy season (May–October). During the dry season, temperatures can reach up to 40°C in April, whereas in the rainy season, temperatures drop to around 22°C, with high humidity.

The water level in Prek Te is significantly impacted by the flow of the Mekong River. During the rainy season, the water level can exceed 10 m, whereas in the dry season, it typically ranges from 1 to 3 m.

2.2. Samples collection

Surface water quality sampling was conducted twice: the first from March 5 to 11, 2023 (dry season), and the second from October 20 to 26, 2023 (rainy season). A total of 21 surface water samples were collected from different locations along Prek Te. Sampling locations were selected based on accessibility, as some sites were situated in dense forest areas with no access routes. The distance between sampling locations ranged from 5 to 10 km, covering a total stretch of 145 km. The first sampling site was located at an artisanal mining site, while the final site (21st location) was at the confluence

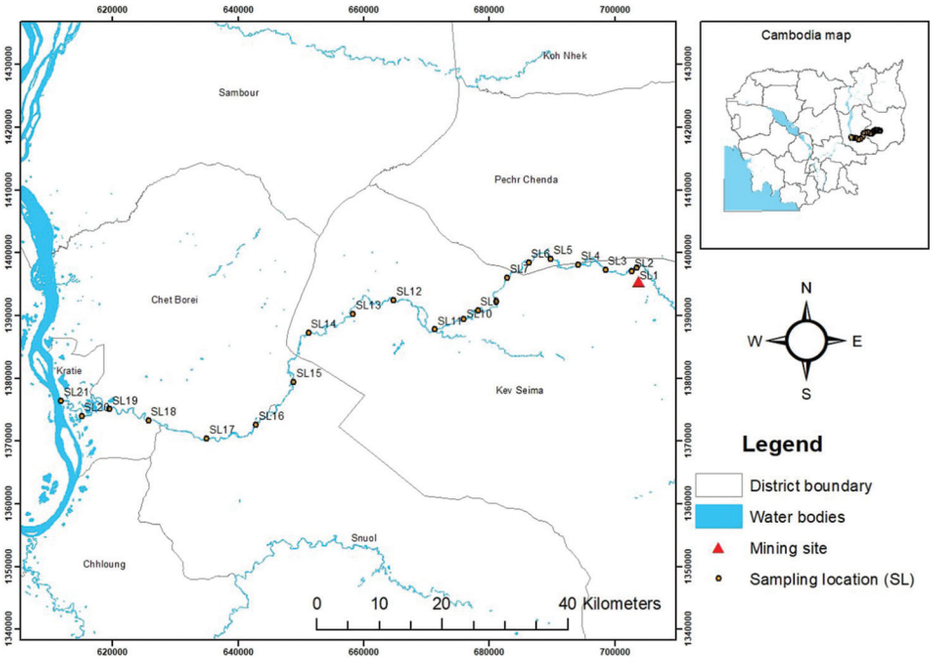

Figure 1. Map of surface water sampling locations

of Prek Te and the Mekong River. Surface water samples were collected at a depth of approximately 0 – 30 cm.[15] Sterilized polytetrafluoroethylene bottles were used to store 100 mL of each water sample. To preserve the samples, nitric acid (HNO_3) was added, and they were stored in an ice box during field sampling. Subsequently, the samples were transferred to a refrigerator set at 4°C for storage until analysis for As, chromium (Cr), Ni, Cu, Zn, Cd, and Pb.[16]

Physicochemical parameters were measured on-site at each sampling location. pH was measured using a HANNA pH/ORP meter HI98191 (HANNA, Italy), while electrical conductivity (EC) and total dissolved solids (TDS) were determined using a HANNA Conductivity/TDS/Salinity meter HI 98192 (HANNA, Italy). In addition, dissolved oxygen (DO) was measured with a HANNA HI 9147 meter (HANNA, Italy).

2.3. Samples preparation and analysis

Prior to instrumental analysis, filtration was carried out to evaluate the dissolved fraction of the water samples. Sartorius filter papers (0.45 µm pore size) were used for filtration, and 50 mL of filtered water was extracted for analysis.

Filtering water samples is a standard procedure that enhances precision, sensitivity, and reliability in analytical measurements. It minimizes instrument blockages, reduces contamination, improves analytical sensitivity, and guarantees consistency in the detection of heavy metals and trace elements in water samples. The concentrations of As, Cr, Ni, Cu, Zn, Cd, and Pb were determined using an inductively coupled plasma mass spectrometry (ICP-MS; 8990 GC System, Agilent, United States). Calibration standards of 1 µg/L, 5 µg/L, 10 µg/L, 20 µg/L, 50 µg/L, and 100 µg/L were prepared from a stock multielement standard solution for ICP (Sigma-Aldrich, Switzerland) in 2% HNO_3.

For quality control, a certified reference material (CRM), River Thames water (LGC6019, LGC Standards, United Kingdom), was used to ensure accuracy and precision in the measurements. After every 10 sample analyses, the CRM sample was run to verify the ICP-MS accuracy. If the recovery rate fell outside the recommended range (80 – 120%), a new calibration curve was applied before further analysis.

2.4. Health risk assessment

Health risk assessment is a systematic process used to evaluate the potential adverse health effects resulting from exposure to environmental hazards. It is a widely adopted tool used by regulatory agencies, health organizations, and industries to ensure that activities such as mining, manufacturing, and waste disposal do not pose significant health risks to human populations. In this study, water samples from residential areas along Prek Te were analyzed to assess lifetime cancer risk

(LCR) and non-carcinogenic health risks associated with heavy metal exposure.

The non-carcinogenic risk was determined using Equations I–II:[17]

$$ADD = \frac{C \times IR \times EF \times ED}{BW \times AT} \quad \text{(I)}$$

$$HQ = \frac{ADD}{RfD} \quad \text{(II)}$$

Where *HQ* is the hazard quotient (HQ < 1 suggests unlikely adverse health effects, while HQ > 1 indicates a higher probability of adverse health effects[18]), *ADD* is the average daily dose (mg/kg/day), *C* is the average concentration of heavy metals in water, *IR* is the ingestion rate of drinking water per capita, *EF* is exposure frequency, *ED* is exposure duration, *BW* is body weight, and *AT* is averaging time, calculated as *ED* × 365.[19] Table 1 shows the summary of exposure assumptions used to calculate the health risk assessment.

The hazard index (HI), which represents the combined risk from multiple substances, is given by:

$$HI = \sum HQ = \frac{ADD_1}{RfD_1} + \frac{ADD_2}{RfD_2} + \ldots + \frac{ADD_i}{RfD_i} \quad \text{(III)}$$

Where HI > 1 suggests that the combined exposure to multiple contaminants may cause non-carcinogenic effects.

The LCR was estimated using Equations IV and V:

$$LCR = LADD \times CSF \quad \text{(IV)}$$

$$LADD = \frac{CW \times IR \times EF \times ED}{BW \times AT} \quad \text{(V)}$$

Where LCR > 10^{-4} is deemed an unacceptable risk, while an acceptable range falls between 10^{-6} and 10^{-4}. Lifetime average daily dose is calculated similarly to ADD, except for AT. AT for carcinogenic risk is set as 70 years, equivalent to 25,550 days.

Table 2 presents the reference dose (RfD) and cancer slope factor used in the health risk assessment.

2.5. Statistical analysis

Statistical analyses were performed using SPSS for Windows (version 21). The Mann–Whitney U test was used to determine whether there were significant differences in water quality between the dry and rainy seasons along the Prek Te area.

Table 1. Summary of exposure assumptions used for health risk assessment

Risk exposure factors	Unit	Values		
		Men	Women	Children
Ingestion rate	L/day	2	2	1
Exposure frequency	Days/year	365	365	365
Exposure duration	Years	20	20	20
Average time (AT) for non-carcinogenic	Day	7.300	7.300	7.300
AT for carcinogenic	Day	25,550	25,550	25,550
Average body weight	Kg	70	60	20

Table 2. Summary of RfD and CSF used for health risk assessment[17] and[20]

Parameters	Unit	RfD/CSF factors	
		RfD	CSF
Arsenic	mg/kg/day	3×10^{-4}	1.5
Copper	mg/kg/day	4×10^{-2}	NA
Chromium	mg/kg/day	3×10^{-3}	NA
Cadmium	mg/kg/day	5×10^{-4}	NA
Lead	mg/kg/day	3.5×10^{-3}	NA
Zinc	mg/kg/day	3×10^{-1}	NA
Nickel	mg/kg/day	2×10^{-2}	NA

Abbreviations: CSF: Cancer slope factor; NA: Not applicable; RfD: Oral reference dose; USEPA: United States Environmental Protection Agency.

3. Results and discussion

3.1. Water quality in dry and rainy seasons

Table 3 summarizes the water quality parameters observed during the dry and rainy seasons. Surface water is essential for ecological, commercial, drinking, irrigation, and societal purposes, encompassing rivers, lakes, streams, canals, ponds, wetlands, and reservoirs. However, mining activities can significantly impact water quality by disturbing soil and rock, leading to increased erosion and sedimentation in nearby water sources.[21] Contaminated sediment can degrade water quality by smothering aquatic habitats, reducing light penetration, and diminishing water clarity. In addition, sediment particles can act as carriers for contaminants such as heavy metals.

Table 3. Summary of water quality in dry and rainy seasons along Prek Te

Parameters	Dry season (*n*=21)				Rainy season (*n*=21)				CDWQS	WHO
	Mean	Min	Max	SD	Mean	Min	Max	SD		
pH	6.64	6.0	7.20	0.33	7.41	6.9	7.70	0.21	6.5 – 8.5	6.5 – 8.5
DO (mg/L)	5.58	4.07	6.47	0.68	6.40	5.38	7.17	0.62	-	-
EC (µS/cm)	95.5	32.8	589	129	92.6	56.1	142	22.6	-	-
TDS (mg/L)	5.58	4.07	6.47	0.68	6.40	5.39	7.17	0.62	800	1000
As (µg/L)	1.23	0.92	2.88	0.42	8.53	1.01	58.1	12.1	50	10
Cu (µg/L)	1.06	0.78	2.82	0.43	26.5	17.6	34.7	4.64	1000	2000
Cr (µg/L)	0.40	0.29	1.05	0.16	1.63	0.16	11.5	2.44	50	50
Cd (µg/L)	ND	ND	ND	ND	0.04	0.03	0.07	0.01	3	3
Pb (µg/L)	0.28	0.22	0.64	0.09	0.42	0.22	1.32	0.26	10	10
Zn (µg/L)	1.18	0.81	3.20	0.52	84.8	10.6	356	91.07	3000	5000
Ni (µg/L)	0.36	0.27	0.88	0.13	8.30	1.51	45.8	11.5	20	70

Abbreviations: As: Arsenic; CDWQS: Cambodian Drinking Water Quality Standard; Cu: Copper; Cd: Cadmium; Cr: Chromium; DO: Dissolved oxygen; EC: Electrical conductivity; ND: Non-detected; Ni: Nickel; Pb: Lead; SD: Standard deviation; TDS: Total dissolved solid; WHO: World Health Organization; Zn: Zinc.

The analytical results reveal that, except for As and Ni, most quality parameters were within the WHO guidelines and the CDWQS. During the rainy season, the highest As concentration among all sampling locations was 58.1 µg/L at Sampling Location 1, followed by 21.96 µg/L at Sampling Location 2 and 10.8 µg/L at Sampling Location 3. The concentration at Sampling Location 1 exceeded both the CDWQS limit (50 µg/L) and the WHO guideline (10 µg/L), while the concentrations at Sampling Locations 2 and 3 exceeded only the WHO guideline. These sampling locations are in proximity to the mining site. However, the mean As concentration across all sampling locations was 8.5 ± 12.1 µg/L, which remains below both CDWQS and WHO limits. In contrast, during the dry season, all trace element concentrations were below both CDWQS and WHO limits, likely due to the absence of mining runoff.

During the rainy season, the highest Ni concentration among all sampling locations was 45.8 µg/L at Sampling Location 1, followed by 25.4 µg/L at Sampling Location 2, 24.4 µg/L at Sampling Location 3, and 23.8 µg/L at Sampling Location 4. These values exceeded the CDWQS limit of 20 µg/L but remained below the WHO guideline of 70 µg/L. However, the mean Ni concentration across all sampling locations was 8.30 ± 11.5 µg/L.

Arsenic and Ni are naturally occurring elements found in various minerals, including sulfide ores, which are frequently targeted in mining operations for commodities such as gold, Cu, and Pb-Zn.[22,23] A previous study reported As concentrations of up to 15.3 mg/L near a mining site, with levels decreasing downstream.[1] In the present study, trace element concentrations were lower in the dry season compared to the rainy season, indicating improved water quality during the dry season. Increased runoff during the rainy season likely mobilizes contaminants from mining tailings or other sources, transporting them into nearby water sources. Conversely, the dry season is characterized by reduced precipitation and runoff, limiting pollutant transport and resulting in improved water quality.

Similar trends have been observed in other mining-affected regions. For instance, a study conducted in Wonogiri, an artisanal gold mining area in Indonesia, reported elevated heavy metal concentrations both at mining sites and in surrounding communities.[24] The levels of heavy metals such as As, Pb, and Cd have increased in artisanal mining communities, surpassing naturally occurring background levels.[25] Populations residing downstream, where metals have been inappropriately disposed of, as well as those living in close proximity to mining sites, face increased exposure to these contaminants through drinking water and food consumption.

To mitigate these environmental and public health risks, stringent laws or regulations should be enacted to prevent small-scale illegal mining and protect water quality. Effective implementation of these regulations requires targeted training and educational initiatives for miners and other pertinent stakeholders.

3.2. Influence of seasonal impact on water quality

Table 4 presents the influence of seasonal impact on water quality along Prek Te. Statistical analysis indicates that all measured parameters, including pH, DO, EC, TDS, and the concentrations of As, Cu, Cr, Cd, Pb, Zn, and Ni, exhibited significant differences (p<0.05) between the rainy and dry seasons. A p<0.05 suggests that the likelihood of these differences occurring by chance is <5%, providing strong evidence of seasonal impact on water quality.

The observed significant differences suggest that seasonal factors (rainy and dry seasons), such as variations in precipitation and hydrological conditions, influence water quality. During the rainy season, increased precipitation leads to higher runoff, which transports pollutants into water bodies, leading to elevated concentrations of dissolved metal and other contaminants. Seasonal variations in water quality are critical considerations for effective water resource management and environmental protection.

In addition, seasonal fluctuations in river flow, particularly under the influence of the monsoon, may contribute to variations in water quality.[26] Increased rainfall during the rainy season can result in higher discharge rates and greater transport of total suspended solids, thereby affecting the overall water quality of the Mekong River.[27] These seasonal variations can have detrimental effects on the water quality.[28]

3.3. Human health risk assessment

3.3.1. Non-carcinogenic risk assessment

Non-carcinogenic risk assessment is a critical process in environmental health used to evaluate the potential adverse health effects of exposure to chemical substances that do not cause cancer. This assessment typically focuses on risks such as organ damage, developmental toxicity, and neurological effects. The process integrates data from exposure assessment and dose-response analysis to estimate the potential risks associated with chemical exposure through drinking water.

A key metric in non-carcinogenic risk assessment is the HQ, which is calculated by dividing the estimated exposure dose by the RfD. HQ > 1 indicates a potential risk of adverse health effects, whereas HQ < 1 suggests that non-carcinogenic health risks are unlikely.[29] The human health risk assessment was conducted for three demographic groups: men, women, and children. The non-carcinogenic risk was calculated based on ADD and the frequency of water consumption. Table 5 presents the non-carcinogenic risk calculations for the dry season, while Table 6 provides the corresponding values for the rainy season. During the dry season, the HQ levels for As, Cu, Cr, Cd, Pb, Zn, and Ni remained below 1 across all groups, indicating that drinking water posed no potential non-carcinogenic health risks. In contrast, in the rainy season, the HQ of As exceeded 1 for children, indicating potential non-carcinogenic risks associated with As in their drinking water. Notably, children exhibited higher HQ values compared to women and men, highlighting their increased vulnerability to water contaminants.

Further analysis revealed that HQ values for As exceeded 1 at Sampling Locations 1, 2, and 3 across all groups, suggesting that drinking water from these

Table 4. Influence of seasonal impact on water quality along Prek Te

Parameters	Dry season (n=21)				Rainy season (n=21)				Mann–Whitney U test (p-value)
	Mean	Min	Max	SD	Mean	Min	Max	SD	
pH	6.64	6.0	7.20	0.33	7.41	6.90	7.70	0.21	0.001*
DO (mg/L)	5.58	4.07	6.47	0.68	6.40	5.38	7.17	0.62	0.001*
EC (µS/cm)	95.5	32.8	589	128	92.6	56.1	142.5	22.6	0.001*
TDS (mg/L)	5.58	4.07	6.47	0.68	6.40	5.39	7.17	0.62	0.001*
As (µg/L)	1.23	0.92	2.88	0.42	8.53	1.01	58.1	12.1	0.001*
Cu (µg/L)	1.06	0.78	2.82	0.43	26.5	17.6	34.7	4.64	0.001*
Cr (µg/L)	0.4	0.29	1.05	0.16	1.63	0.16	11.5	2.44	0.001*
Cd (µg/L)	ND	ND	ND	ND	0.04	0.03	0.07	0.01	0.001*
Pb (µg/L)	0.28	0.22	0.64	0.09	0.42	0.22	1.32	0.26	0.005*
Zn (µg/L)	1.18	0.81	3.20	0.52	84.8	10.6	356	91.1	0.001*
Ni (µg/L)	0.36	0.27	0.88	0.13	8.30	1.51	45.8	11.5	0.001*

Note: *Significant difference at p<0.05.

Abbreviations: As: Arsenic; Cu: Copper; Cd: Cadmium; Cr: Chromium; DO: Dissolved oxygen; EC: Electrical conductivity; ND: Non-detected; Ni: Nickel; Pb: Lead; SD: Standard deviation; TDS: Total dissolved solid; Zn: Zinc.

Table 5. Non-carcinogenic risk assessment for the dry season

Parameters	Dry season (*n*=21)						
	Mean concentration (µg/L)	Men		Women		Children	
		ADD	HQ	ADD	HQ	ADD	HQ
As	1.23	0.04	0.12	0.04	014	0.06	0.21
Cu	1.06	0.03	0.00	0.03	0.00	0.05	0.00
Cr	0.40	0.01	0.00	0.01	0.00	0.02	0.01
Cd	ND	0.00	0.00	0.00	0.00	0.00	0.00
Pb	0.28	0.01	0.00	0.01	0.00	0.01	0.00
Zn	1.18	0.03	0.00	0.04	0.00	0.06	0.00
Ni	0.36	0.01	0.00	0.01	0.00	0.02	0.00

Abbreviations: ADD: Average daily dose; As: Arsenic; Cu: Copper; Cd: Cadmium; Cr: Chromium; HQ: Hazard quotient; ND: Non-detected; Ni: Nickel; Pb: Lead; Zn: Zinc.

Table 6. Non-carcinogenic risk assessment for the rainy season

Parameters	Rainy Season (*n*=21)						
	Mean concentration (µg/L)	Men		Women		Children	
		ADD	HQ	ADD	HQ	ADD	HQ
As	8.53	0.24	0.81	0.28	0.95	0.43	1.42
Cu	26.5	0.76	0.02	0.88	0.02	1.33	0.03
Cr	1.63	0.05	0.01	0.05	0.02	0.08	0.03
Cd	0.04	0.00	0.00	0.00	0.00	0.00	0.00
Pb	0.42	0.01	0.00	0.01	0.00	0.02	0.01
Zn	84.8	2.42	0.01	2.83	0.01	4.24	0.01
Ni	8.30	0.24	0.01	0.28	0.01	0.41	0.02

Abbreviations: ADD: Average daily dose; As: Arsenic; Cu: Copper; Cd: Cadmium; Cr: Chromium; HQ: Hazard quotient; ND: Non-detected; Ni: Nickel; Pb: Lead; Zn: Zinc.

locations may pose non-carcinogenic health risks. Multiple studies have confirmed that children are more susceptible to contaminants in drinking water than adults.[30-32]

Figure 2 illustrates the HI, which represents the cumulative non-carcinogenic risk from combined chemical contaminants across different seasons for males, women, and children. During the rainy season, HI values exceeded 1 for children and women, indicating potential non-carcinogenic risks associated with the drinking water of Prek Te. In contrast, during the dry season, HI values remained below 1 for all groups, suggesting no significant non-carcinogenic risks from drinking water consumption.

Similarly, elevated HI values (>1) were observed among children, women, and men in various drinking water sources within the Tonle Sap Great Lake basin.[33] In addition, oral HI values for both adults and children exceeded the safe thresholds (HI > 1), classifying them within a high-risk category for non-carcinogenic impact.[34]

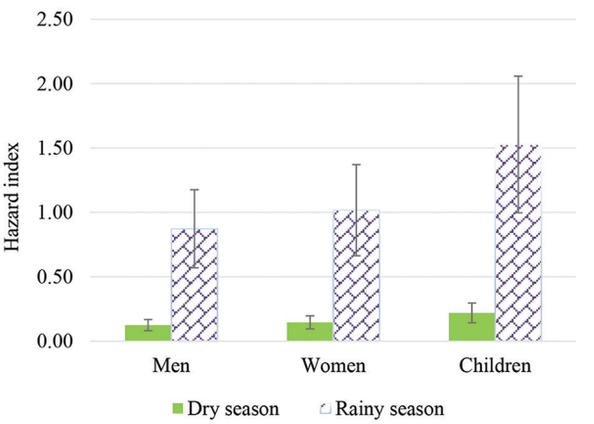

Figure 2. Hazard index of combined chemical contaminants in drinking water across different seasons for men, women, and children

Table 7. Carcinogenic risk assessment (arsenic exposure) for the dry and rainy seasons in Prek Te

Season	Mean concentration (µg/L)	Men		Women		Children	
		LADD	LCR	LADD	LCR	LADD	LCR
Dry Season (*n*=21)	1.235	1.0×10^{-2}	1.5×10^{-2}	1.2×10^{-2}	1.8×10^{-2}	1.8×10^{-2}	2.6×10^{-2}
Rainy Season (*n*=21)	8.531	6.9×10^{-2}	1×10^{-1}	8.1×10^{-2}	1.2×10^{-1}	1.2×10^{-1}	1.8×10^{-1}

Abbreviations: As: Arsenic; LADD: Lifetime average daily dose; LCR: Lifetime cancer risk.

3.3.2. Carcinogenic risk assessment

The carcinogenic risks associated with drinking water during the rainy and dry seasons are presented in Table 7. The LCR of As for men, women, and children in the dry season was calculated as 1.5×10^{-2}, 1.8×10^{-2}, and 2.6×10^{-2}, respectively. These values indicate that for every 10,000 individuals exposed to As in drinking water over their lifetime, approximately 150, 180, and 260 cases of cancer may develop in men, women, and children, respectively.

In the rainy season, the LCR of As increased to 1×10^{-1}, 1.2×10^{-1}, and 1.8×10^{-1} for men, women, and children, respectively. These values indicate that for every 100 exposed individuals, approximately 10, 12, and 18 cases of cancer could be expected due to As contamination in drinking water. The United States Environmental Protection Agency does not classify several metals—including Cu, Cr, Cd, Pb, Zn, and Ni—as carcinogenic through oral exposure. However, LCR values are essential for assessing As-related risks among different demographic groups. Higher LCR values indicate an increased risk of developing cancer from As exposure, highlighting the need for effective mitigation strategies to minimize exposure, especially among vulnerable populations such as children.

Inorganic arsenic is one of the most prevalent chemical contaminants in drinking water worldwide and is a confirmed human carcinogen.[35] Prolonged exposure to low concentrations of heavy metals may lead to the development of various cancers years after initial exposure.[36] Contaminated drinking water containing heavy metals (Pb, Cr, Cd, and Ni) has been associated with an increased risk of cancer in humans.[37] Given that As concentrations in drinking water exceeded acceptable limits, particularly for children, urgent interventions are necessary to mitigate public health risks.[38]

4. Conclusion

This study investigated the seasonal variations in surface water quality and the associated human health risks due to chemical contamination from upstream artisanal mining activities along Prek Te. The analytical results revealed that most water quality parameters complied with the WHO guidelines and CDWQS, except for As and Ni.

Arsenic concentrations reached a maximum of 58.1 µg/L, exceeding both the CDWQS limits of 50 µg/L and the WHO guideline of 10 µg/L. Additional recorded values of 21.9 µg/L and 10.8 µg/L also surpassed the WHO guideline. Ni concentrations were found at a maximum of 45.8 µg/L, with other recorded values of 25.4 µg/L, 24.4 µg/L, and 23.8 µg/L. These concentrations exceeded the CDWQS limit of 20 µg/L but remained below the WHO guideline of 70 µg/L. Contaminant concentrations were generally lower in the dry season compared to the rainy season, indicating better water quality during the dry season.

Statistical analysis revealed a significant seasonal difference ($p<0.05$) in all assessed water quality parameters, including pH, DO, EC, TDS, As, Cu, Cr, Cd, Pb, Zn, and Ni. The health risk assessment indicated that residents along Prek Te are exposed to chemical contaminants primarily through the drinking water pathway. HQ and HI values were higher in children than in women and men, indicating that children are more susceptible to non-carcinogenic risks from waterborne contaminants. Furthermore, LCR analysis showed that children face a higher risk of As-related health effects compared to adults. These findings highlight the urgent need for a regular water quality monitoring program. In addition, the implementation of appropriate drinking water treatment methods, particularly for As removal, is critical to ensuring safe drinking water for residents in the Prek Te area.

Acknowledgments

The authors would like to extend our heartfelt gratitude to the Soil Environmental Laboratory, Department of Environment and Energy Engineering (DEEE), Gwangju Institute of Science and Technology (GIST) for generously providing the facilities and instrument necessary for conducting the water samples analysis. Their support and access to advanced analytical instruments are essential in ensuring the accuracy and reliability of our results.

Funding

This study was supported by the Korea International Cooperation Agency (KOICA) and the Gwangju Institute of Science and Technology (GIST), Republic of Korea, under the Project for Establishment of Environmental Engineering in RUPP to Foster the Human Resources of Higher Education in Cambodia.

Conflict of interest

The authors declare there is no conflict of interest.

Author contributions

Conceptualization: Chan Oeurn Chey
Formal analysis: Socheata Korng
Investigation: Eang Chorney
Methodology: Vibol Sao
Writing – original draft: Vibol Sao
Writing – review & editing: Kyoung-Woong Kim

Availability of data

All relevant data are included in the paper.

References

1. Tum S, Toda K, Matsui T, *et al.* Seasonal effects of natural attenuation on drainage contamination from artisanal gold mining, Cambodia: Implication for passive treatment. *Sci Total Environ*. 2022;806:150398. doi: 10.1016/j.scitotenv.2021.150398
2. Bruno DE, Ruban DA, Tiess G, *et al*. Artisanal and small-scale gold mining, meandering tropical rivers, and geological heritage: Evidence from Brazil and Indonesia. *Sci Total Environ*. 2020;715:136907. doi: 10.1016/j.scitotenv.2020.136907
3. Macdonald K, Lund M, Blanchette M. *Impacts of Artisanal small-scale Gold Mining on Water Quality of a Tropical River (Surow River, Ghana). In: Conference: International Mine Water Association*; 2015. p. 21-24.
4. WHO. World Health Statistics, Monitoring Health for SDG. Geneva: World Health Organization; 2019.
5. Zvarivadza T. Artisanal and small-scale mining as a challenge and possible contributor to sustainable development. *Resour Policy*. 2018;56:49-58. doi: 10.1016/j.resourpol.2018.01.009
6. Fong-Sam Y. The Mineral Industry of Cambodia. *Minerals Yearbook, Volume III: Asia and the Pacific: Area Reports: International*; 2012.
7. Armah FA, Quansah R, Luginaah I. A systematic review of heavy metals of anthropogenic origin in environmental media and biota in the context of gold mining in Ghana. *Int Sch Res Notics*. 2014;2014:252148. doi: 10.1155/2014/252148
8. Barcelos DA, Pontes FV, da Silva FA, Castro DC, Dos Anjos NO, Castilhos ZC. Gold mining tailing: Environmental availability of metals and human health risk assessment. *J Hazard Mater*. 2020;397:122721. doi: 10.1016/j.jhazmat.2020.122721
9. Ajith MM, Ghosh AK, Jansz J. Risk factors for the number of sustained injuries in artisanal and small-scale mining operation. *Saf Health Work*. 2020;11(1):50-60. doi: 10.1016/j.shaw.2020.01.001
10. Bose-O'Reilly S, Drasch G, Beinhoff C, *et al*. Health assessment of artisanal gold miners in Indonesia. *Sci Total Environ*. 2010;408(4):713-725. doi: 10.1016/j.scitotenv.2009.10.070
11. Ncube-Phiri S, Mucherera B, Ncube A. Artisanal small-scale mining: Potential ecological disaster in Mzingwane District, Zimbabwe. *Jàmbá*. 2015;7(1):158.
12. Gibb H, O'Leary KG. Mercury exposure and health impacts among individuals in the artisanal and small-scale gold mining community: A comprehensive review. *Environ Health Perspect*. 2014;122(7):667-672. doi: 10.1289/ehp.1307864
13. MIME. Drinking Water Quality Standard. *Ministry of Industry, Mine and Energy, Phnom Penh, Cambodia*; 2004.
14. WHO. *Guideline for Drinking Water Quality*. 4th ed., Vol. 1. Geneva, Switzerland: World Health Organization; 2011.
15. Houri A, El Jeblawi SW. Water quality assessment of Lebanese coastal rivers during dry season and pollution load into the Mediterranean Sea. *J Water Health*. 2007;5(4):615-623. doi: 10.2166/wh.2007.047
16. Sghiouer FE, Nahli A, Bouka H, Chlaida M. Assessment of the bacteriological and physicochemical water quality of the Inaouene and Larbaa Rivers (Taza, Morocco). *AJWEP.* 2024;21(6):249-259. doi: 10.3233/ajw240093
17. US EPA. *Exposure Factors Handbook: 2009 Update. EPA/600/R-09*/052A. United States: US EPA; 2009.
18. Watts RJ. *Hazardous Wastes: Sources, Pathways, Receptors*. New York: John Wiley & Sons; 1998.
19. Mesdaghinia A, Nasseri S, Hadi M. Assessment of carcinogenic risk and non-carcinogenic hazard quotient of chromium in bottled drinking waters in Iran. *IJHE*. 2016;9:347-358.
20. Maleki A, Jari H. Evaluation of drinking water quality and non-carcinogenic and carcinogenic risk assessment of heavy metals in rural areas of Kurdistan, Iran. *Environ Technol Innov*. 2021;23:101668. doi: 10.1016/j.eti.2021.101668
21. Nuryanty CD, Riani E, Abidin Z, Sutjahjo SH, Riyadi A. Mercury contamination from artisanal

small-scale gold mining activities in Simpenan District, Sukabumi Regency, West Java, Indonesia. *AJWEP.* 2024;21(4):83-89.
doi: 10.3233/ajw240049

22. Tabelin CB, Silwamba M, Paglinawan FC, *et al.* Solid-phase partitioning and release-retention mechanisms of copper, lead, zinc and arsenic in soils impacted by artisanal and small-scale gold mining (ASGM) activities. *Chemosphere*. 2020;260:127574.
doi: 10.1016/j.chemosphere.2020.127574
23. Gonnelli C, Renella G. Chromium and nickel. *Heavy Metals in Soils: Trace Metals and Metalloids in Soils and their Bioavailability*. Berlin: Springer; 2013. p. 313-333.
24. Nurcholis M, Yudiantoro DF, Haryanto D, Mirzam A. Heavy metals distribution in the artisanal gold mining area in Wonogiri. *Indones J Geogr*. 2017;49(2):133-144.
25. Obiri S, Yeboah PO, Osae S, *et al*. Human health risk assessment of artisanal miners exposed to toxic chemicals in water and sediments in the Prestea Huni Valley District of Ghana. *Int J Environ Res Public Health*. 2016;13(1):139.
doi: 10.3390/ijerph13010139
26. Chea R, Grenouillet G, Lek S. Evidence of water quality degradation in lower Mekong basin revealed by self-organizing map. *PLoS One*. 2016;11(1):e0145527.
doi: 10.5061/dryad.51021
27. Prathumratana L, Sthiannopkao S, Kim KW. The relationship of climatic and hydrological parameters to surface water quality in the lower Mekong River. *Environ Int*. 2008;34(6):860-866.
doi: 10.1016/j.envint.2007.10.011
28. Sharma R, Kumar A, Singh N, Sharma K. Impact of seasonal variation on water quality of Hindon River: Physicochemical and biological analysis. *SN Appl Sci*. 2021;3:1-11.
doi: 10.1007/s42452-020-03986-3
29. Preonty NEJ, Hassan MN, Reza AHMS, Rasel MIA, Mahim MMA, Jannat MFT. Pollution and health risk assessment of heavy metals in surface water of the industrial region in Gazipur, Bangladesh. *Environ Chem Ecotoxicol*. 2025;7:527-538.
doi: 10.1016/j.enceco.2025.02.014
30. Sao V, Chey CO, Sriv T, *et al.* Assessing drinking water quality and health risks of contaminants in the coastal areas of Cambodia. *J Water Health*. 2023;21(2):224-234.
doi: 10.2166/wh.2023.215
31. Xiao Y, Yin S, Hao Q, Gu X, Pei Q, Zhang Y. Hydrogeochemical appraisal of groundwater quality and health risk in a near-suburb area of North China. *J Water Supply Res Technol*. 2020;69(1):55-69.
doi: 10.2166/aqua.2019.101
32. Varol S, Şekerci M. Hydrogeochemistry, water quality and health risk assessment of water resources contaminated by agricultural activities in Korkuteli (Antalya, Turkey) district center. *J Water Health*. 2018;16(4):574-599.
doi: 10.2166/wh.2018.003
33. Phan K, Hoeng S, Phin S, *et al.* Chemical risks in drinking water of inhabitants in the basin of the Tonle Sap Great Lake. *J Water Health*. 2023;21(12):1908-1921.
doi: 10.2166/wh.2023.236
34. Sayed FA, Eid MH, El-Sherbeeny AM, Abdel-Gawad GI, Mohamed EA, Abukhadra MR. Environmental and health risk assessment of polycyclic aromatic hydrocarbons and toxic elements in the red sea using Monte Carlo simulation. *Sci Rep.* 2025;15(1):4122.
35. Taiwo A, Olujimi O, Bamgbose O, Arowolo T. Surface water quality monitoring in Nigeria: Situational analysis and future management strategy. In: *Water Quality Monitoring and Assessment*. Vol. 13. London: Intechopen; 2012. p. 301-320.
36. Luvhimbi N, Tshitangano T, Mabunda J, Olaniyi F, Edokpayi J. Water quality assessment and evaluation of human health risk of drinking water from source to point of use at Thulamela municipality, Limpopo Province. *Sci Rep.* 2022;12(1):6059.
37. Mohammadi AA, Zarei A, Majidi S, *et al*. Carcinogenic and non-carcinogenic health risk assessment of heavy metals in drinking water of Khorramabad, Iran. *MethodsX*. 2019;6:1642-1651.
doi: 10.1016/j.mex.2019.07.017
38. Cao S, Duan X, Zhao X, *et al.* Health risks from the exposure of children to As, Se, Pb and other heavy metals near the largest coking plant in China. *Sci Total Environ*. 2014;472:1001-1009.
doi: 10.1016/j.scitotenv.2013.11.124

ACCSCIENCE PUBLISHING

Asian Journal of Water, Environment and Pollution. Vol. 22, No. 2 (2025), pp. 97-113.
doi: 10.36922/ajwep.8381

ORIGINAL RESEARCH ARTICLE

Integrated modeling of socioeconomic and hydrological factors for adaptive drought response in the Kowsar Dam basin, Iran

Ali Ghasemi, Seyed Nematollah Mosavi*, and Bahaeddin Najafi

Department of Agricultural Economics, Marvdasht Branch, Islamic Azad University, Marvdasht, Iran
***Corresponding author:** Seyed Nematollah Mosavi (seyed_1978mo@yahoo.com)

Received: January 3, 2025; 1st revised: February 26, 2025; 2nd revised: March 7, 2025; 3rd revised: March 15, 2025; Accepted: March 17, 2025; Published online: April 4, 2025

Abstract: The agricultural sector faces major challenges from increasing droughts and declining water resources, especially in arid and semi-arid areas. The present study aims to simulate the effects of drought on socioeconomic, hydrological, and adaptive behavioral parameters at the basin level to identify drought-vulnerable areas and improve agricultural sector management under drought conditions. This study integrates water evaluation and planning, positive mathematical programming, and theory of planned behavior models to analyze hydrological, socioeconomic, and behavioral systems, respectively, under drought scenarios. To implement this integrated model, the Kowsar Dam basin in Iran was selected as the study area. The results showed that droughts significantly reduce crop yields, increase unmet water demand, alter cultivation patterns, and lower farmers' profits, all driven by reduced rainfall, higher temperatures, and shrinking water resources. Attitudes, norms, and perceived control explained 74.1% of behavioral intention and 58.6% of farmers' drought responses. Therefore, influencing psychological parameters can help foster the acceptance of drought adaptation strategies at the basin level. In conclusion, this integrated framework serves as a valuable tool for identifying drought-vulnerable areas and designing effective policies and interventions for drought management.

Keywords: Drought modeling; Drought-vulnerable regions; Integrated modeling; Climate resilience; Behavioral adaptation

1. Introduction

Climate change is increasing the frequency of droughts, posing significant challenges to agriculture and the environment.[1-3] Drought, a complex natural event, impacts large geographical areas and populations, reducing water resources in arid and semi-arid regions and exacerbating issues like land-use changes.[4-7] Water scarcity is a critical global issue, with declining surface and groundwater resources intensifying environmental pressures and conflicts among users, particularly in agriculture.[8-12] Farmers are directly affected by drought-induced declines in agricultural productivity, making them a key focus of drought impact studies.[13] Agriculture accounts for 70% of global water usage and 50% of habitable land, with rising food demand further straining water supplies, especially in arid regions.[14]

Drought poses a growing threat to global agriculture, particularly in arid regions like Iran, where water scarcity has reached critical levels.[15-17] From 1960 to 2005, Iran's temperatures rose by 2.5 – 5°C, and its annual rainfall of 400 billion m^3 lost 270 billion m^3 to

evaporation, reducing agricultural output and increasing food demand gaps.[18-22] Investigating the impacts of drought is essential for managing risks and mitigating water depletion in agriculture, particularly in water-scarce regions.

Hydrological assessments at the basin level typically use criteria like water availability, demand reliability, and unmet demand.[12,21,23,24] For instance, Nazari[21] predicted reduced water resources in Iranian rivers under the A1 climate scenario (2015 – 2030), while Mirzaei and Zibaei[12] studied the impact of climate change on water availability and crop requirements in the Halil River basin. Studies also evaluate the effects of drought on water requirements and crop yields.[25-29] For instance, Ashofteh *et al*.[25] found that alfalfa, potato, and corn crops would require more water, while wheat and barley would require less in Azerbaijan (2026 – 2032). Valizadeh *et al.*[29] projected over 10% decline in wheat yield in Sistan Baluchistan under the A2 scenario.

While biophysical and hydrological modeling dominate drought impact assessments,[30-33] socioeconomic impacts are often overlooked.[34,35] Integrated modeling frameworks that combine technical-agronomic, hydrological, and socioeconomic dimensions can simulate climate scenarios and policy impacts, optimizing socioeconomic benefits.[12,35-37] However, these models often fail to account for human behavioral responses to climate impacts.

Adaptation strategies are crucial for sustaining rural households during droughts,[38] yet prior studies have underemphasized their importance.[39] For example, Chathuranika *et al.*[40] discussed adaptive strategies for water scarcity in Uzbekistan, highlighting the agricultural technology of mulching as a suitable adaptation. Asif Khan *et al.*[41] proposed forest conservation policies as a specialized adaptive strategy to address climate change challenges. Barua *et al.*[42] demonstrated that the adoption of adaptation practices to reduce field salinity could effectively address climate change issues. However, farmers' lack of effective adaptation knowledge underscores the need for clearer strategies.[43] Recent research identifies factors influencing adaptation strategy use[44,45] and assesses the adaptive capacity of rural households.[46,47] Adaptive capacity refers to the ability of a system to adjust to climate variability and extremes, mitigate potential damages, seize opportunities, or cope with consequences. Psychological and contextual factors shape adaptive behaviors, influencing individuals' actions.[48,49] The present study focuses on analyzing farmers' intentions and behaviors toward adopting adaptive strategies to cope with drought.

The novelty of this research lies in the integration of the water evaluation and planning (WEAP), positive mathematical programming (PMP), and theory of planned behavior (TPB) models to comprehensively analyze drought impacts on hydrological, socioeconomic, and behavioral parameters at the basin level. The WEAP model is used for hydrological modeling to assess crop yields, water requirements, water availability, and unmet demand, while the PMP model enables socio-economic optimization to evaluate changes in farmers' gross margins and cultivation patterns. The TPB model is applied for behavioral analysis to understand farmers' intentions and adaptive behaviors under drought conditions. This integrated approach advances existing research by providing a holistic framework that combines hydrological, economic, and psychological perspectives, offering deeper insights into drought vulnerability and adaptation strategies. The study investigates the effects of decreasing precipitation, increasing temperatures, and changes in water resources on these parameters. Following the overview of the study area and methodology, the results of the drought impacts are presented, followed by conclusions and practical recommendations.

2. Materials and methods

2.1. Study area

To achieve the objectives outlined above, the sub-basin of Kowsar Dam in Kohgiluyeh and Boyer-Ahmad province in Iran, including the areas of Bashet, Gachsaran, and Choram (covering 4,710, 3,018, and 3,376 hectares, respectively), was chosen as the study area (Figure 1). An analysis of climatic data on temperature and precipitation across the studied watershed indicates the following:

(i) The long-term trend shows a decrease in precipitation, while the average temperature is increasing.
(ii) Projections for the next 10 years suggest a 21% decrease in precipitation and a 1°C increase in temperature.
(iii) The average annual runoff has declined to 100 million m^3 in the last 5 years.

As a result, the region has experienced successive droughts in recent years, a decline in the amount of rainfall, inefficient water usage patterns, and high per capita water consumption, all of which have exacerbated water stress and contributed to the water shortage in this region.[50,51]

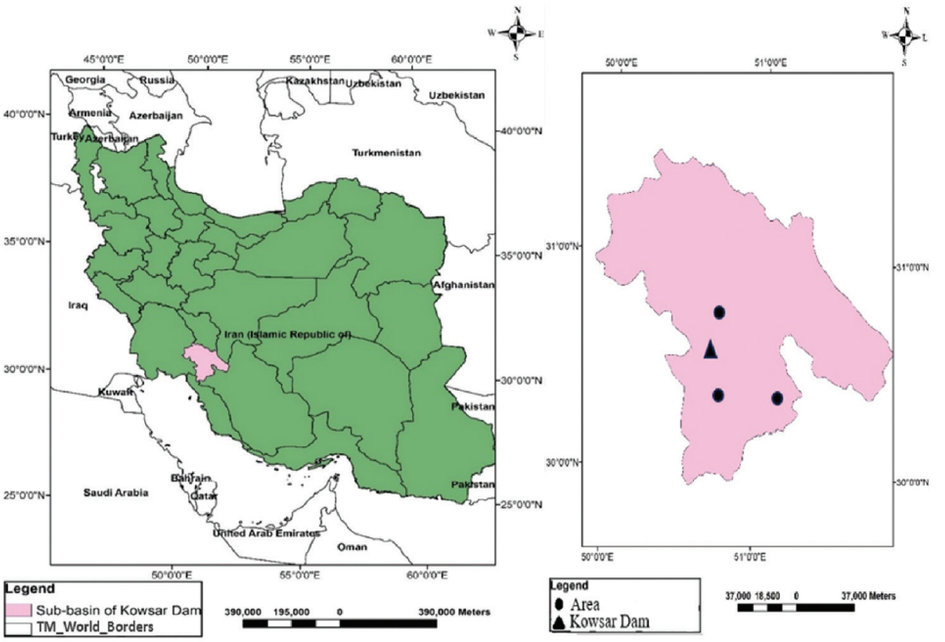

Figure 1. Location of the sub-basin of Kowsar Dam in Iran

2.2. Methodology

Figure 2 illustrates the conceptual framework for analyzing the impacts of drought in the study area through four interconnected steps:

(i) Hydrological simulation: The process begins with hydrological simulation using the WEAP model, where drought scenarios are defined. In addition, the MABIA plugin in the WEAP tool is used to assess the impacts of these drought scenarios on crop yields and water requirements.[12,24]

(ii) Economic analysis: The PMP model is applied to evaluate the economic impacts on farmers under drought scenarios.[36]

(iii) Behavioral analysis: The TPB model is used to analyze farmers' intentions and behaviors regarding the acceptance of adaptive strategies to cope with drought.[6,44,52]

2.2.1. WEAP model

The WEAP model is a useful and practical tool for planning and evaluating water resources, based on the fundamental principle of water balance. It considers various sub-basins, water demand sectors, infrastructure, and water transfer channels, all of which are interrelated.[53] The water balance and the interaction of elements used to measure hydrological functions in the basin are illustrated in Figure 3.

To simulate the hydrology of the Koosar Dam sub-basin, a network of water demand and supply nodes, along with land use in different areas of the sub-basin, is presented in Figure 4.

In this model, empirical functions were used for each agricultural unit to describe and simulate evaporation and transpiration, runoff, changes in soil moisture, baseflow trends to the river, and deep infiltration into groundwater.[54]

2.2.2. MABIA plugin

The MABIA method available in the WEAP software is an effective tool to simulate variables such as transpiration, evaporation, irrigation requirements and planning, crop growth, and yield. This method provides daily simulations, including units for estimating evapotranspiration and soil water capacity. It is important to note that this model was implemented using a plugin in WEAP. The MABIA method simulates water requirements and crop yields, allowing users to evaluate the impacts of climate change and water availability on crop growth. However, this method does not account for the impacts of carbon dioxide pollution on crops.[35] This limitation prevents the simulation and evaluation of environmental issues arising from different scenarios within the WEAP software and the MABIA plugin.

2.2.3. Equations for WEAP model functionality

The WEAP model solves the water mass balance equation for each demand node (*DS*) and link in the

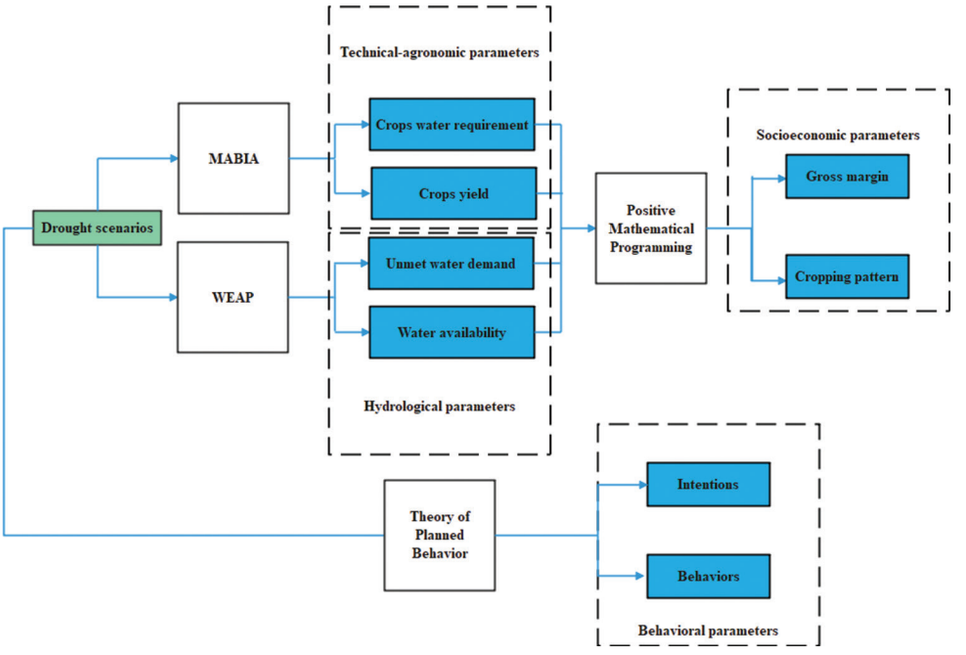

Figure 2. Conceptual framework for analyzing the impacts of drought
Abbreviation: WEAP: Water evaluation and planning.

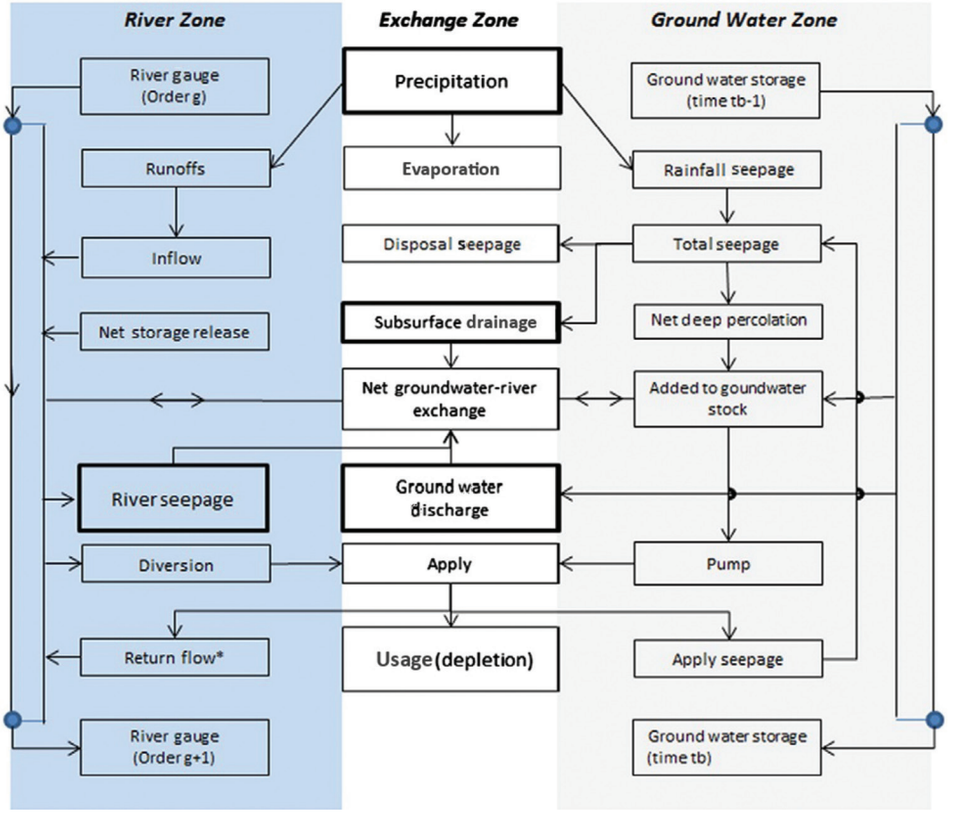

Figure 3. Water balance and interaction of elements

system over time steps. Water is distributed to meet the needs of consumers and the downstream flow, based on the priority of demands, the superiority of the source (*Src*), the mass balance equation, and other constraints.

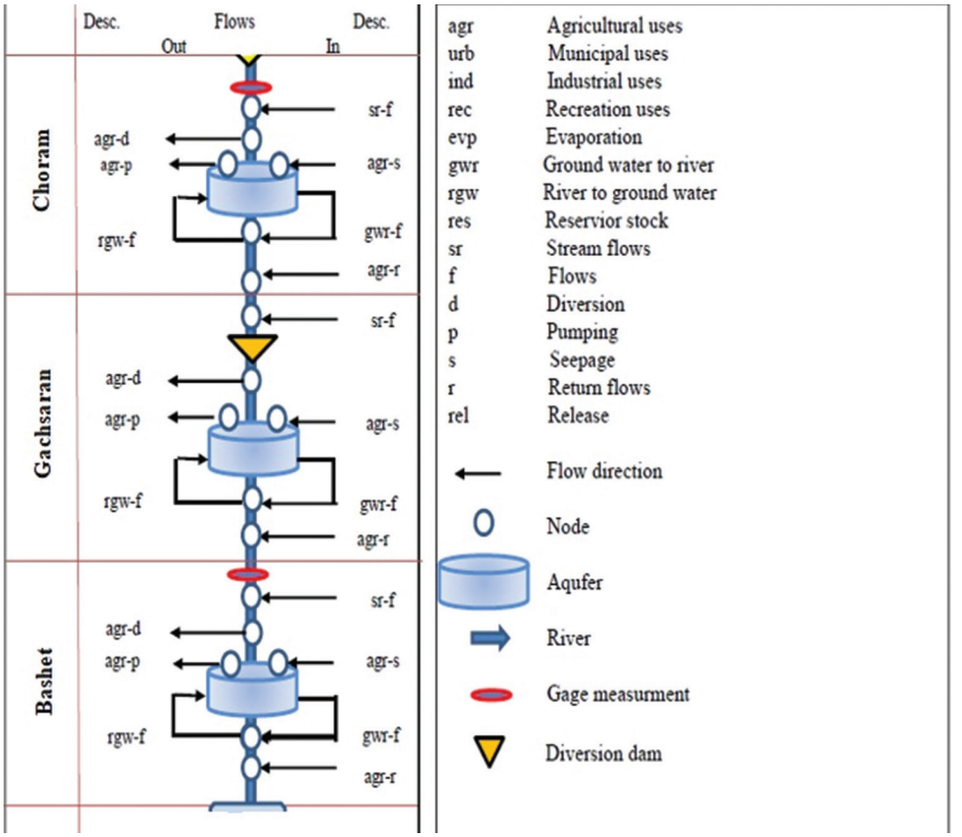

Figure 4. Network of water demand and supply nodes, along with land use

(i) Annual demand calculation

Annual demand (*AD*) at a *DS* is the sum of demands from its basic branches (*Br*):

$$AD_{DS} = \sum_{Br} (TAL_{Br} \times WUR_{Br}) \quad \text{(I)}$$

Where *TAL* represents the total activity level (for example, in the agricultural sector, the total activity level refers to the total area under crop cultivation), and *WUR* is the water use rate.

(ii) Resource demand calculation

Resource demand (*MSR*) adjusts annual demand (*MD*) for reuse, storage, and losses:

$$MSR_{DS} = \frac{MD_{DS,m} \times (1 - RR_{DS}) \times (1 - DSMS_{DS})}{1 - LR_{DS}} \quad \text{(II)}$$

Where *RR* is the reuse rate, *DSMS* is the annual storage at the *DS*, and *LR* is the loss rate.

(iii) Water flow transmission

If *DS* is the demand node and *Src* is the water source, the equation is:

$$I = \sum_{Src} TLO_{Src,DS} \quad \text{(III)}$$

Where *I* denotes input, and *TLO* stands for transmission link outflow. The equations for the water flow transmission link are defined as:

$$TLO_{Src,DS} = TLI_{Src,DS} - TLL_{Src,DS} \quad \text{(IV)}$$

$$TLL_{Src,DS} = (TLLfs_{Src,DS} + TLLtG_{Src,DS}) \times TLI_{Src,DS}$$

$$TLI_{Src,DS} \leq MFV_{Src,DS}$$

$$TLO_{Src,DS} \leq MFP_{Src,DS} \times SR_{Src,DS}$$

Where *TLO* denotes the outflow of the transmission link, *TLI* refers to the inflow of the transmission link, *TLL* is the water loss in the transmission link, *TLLfs* represents the water loss of the transmission link from the system, *TLLtG* refers to the water loss of the transmission link transferring to groundwater, *MFV* is the maximum flow volume, *MFP* represents the maximum flow percentage, and *SR* denotes the resource equipment.

(iv) Resource discharge calculation

Output flow (*O*) from an *Src*:

$$O_{Src} = DO_{Src} + \sum_{DS} TLI_{Src,DS} \quad \text{(V)}$$

Where *DO* represents the downstream output flow. This equation was solved using the following constraint, where *AfR* refers to the available *Src*.

$$O_{Src} \leq SAfR_{Src} \quad \text{(VI)}$$

2.3. PMP model

In the present study, the effects of drought on the socioeconomic status of farmers in the study area were investigated using the PMP model. The advantage of this model lies in its ability to provide a more detailed analysis of the impact of policies at the farm level. In addition to its application in the agricultural sector, the model is used in the water resource management sector to analyze policies concerning irrigation water demand and supply. A key aspect of the PMP model is determining the level of spatial aggregation to define the domain of the model. Once this level is established, instead of analyzing policies over a broad range, a combination of regional attributes is used with smaller datasets, allowing the policies to be explored at the specified regional level. Furthermore, the impacts of spatial aggregation enhance the PMP model by enabling it to predict the effects of policies based on partial data collected from the studied regions. The optimization model is an economic model in the form of a PMP method, which aims to maximize the gross margin of farmers using the following equation:

$$\max Z_1 = \sum_g \sum_i p_i.y_{i,g}.X_{i,g} - \sum_g \sum_i tc_{i,g}.X_{i,g} - \sum_g \sum_i wp.(nw_{i,g}/ef).X_{i,g} \quad \text{(VII)}$$

Equation VII expresses the gross margin function, where the model parameters are defined as follows: p_i is the price per unit of crop *i* (dollar/hectare); $y_{i,g}$ is the yield of crop *i* in region *g* per unit area (Ton/hectare); $tc_{i,g}$ is the production cost, excluding water costs, for crop *i* in region *g* per unit area (dollar/hectare); *wp* is the price of each unit of water applied (dollar/m^3); $nw_{i,g}$ is the net water consumption of crop *i* in region *g* in the unit area (m^3/hectare); ef is the efficiency of irrigation technology in the region (between 0 and 1). The decision variable $X_{i,g}$ represents the area under crop cultivation *i* in region *g*, and Z_1 is the economic objective variable for the basin. The objective function is maximized and subjected to resource constraints and calibration.

$$\text{St: } \sum_i a_{i,g,j} X_{i,g} \leq b_{g,j} \; \forall g,j \; [\lambda^1] \quad \text{(VIII)}$$

$$\text{St: } \sum_i EW_{i,g} X_{i,g} \leq TWUg \; \forall g \; [\lambda^1] \quad \text{(IX)}$$

$$X_{i,g} \leq \tilde{X}_{i,g} + \varepsilon \qquad \forall g,i \quad \left[\lambda^2\right] \quad \text{(X)}$$

$$X_{i,g} \geq 0 \; \forall g,I \quad \text{(XI)}$$

Equations VIII and IX define the system limitations, including constraints on other production inputs as well as constraints on water input. $a_{i,g,j}$ denotes the technical coefficients of inputs, excluding water *j*, for crops *i* in region *g*, $b_{g,j}$ represents the inventory of input resources, excluding water, $TEW_{i,g}$ is the water applied to crops in region *g* ($TEW_{i,g}=nw_{i,g}$/ef), TWU_g refers to the amount of water available in region *g* (m^3). Moreover, Equation X represents the calibration constraints of the model, where $\tilde{X}_{i,g}$ refers to the cultivated area of crops in the base year.

Howitt[55] and Heckelei[56] demonstrated that the vector of dual values of λ^2, related to calibration constraints, represents various types of model specification errors, data errors, cointegration errors, risk behavior, and price expectations. In the calibration of an ascending non-linear cost function, the dual vector of λ^2 is interpreted as a differential marginal cost vector, denoting the cost vector *c*, and the marginal and real cost of producing the *i*-th observed activity. In the second step, the dual values of the first step are employed to estimate the parameters of the non-linear objective function.

In other words, dual values are employed in this step to calibrate the parameters of the non-linear objective function. This allows the activity levels observed in the baseline period to be reproduced by the non-linear model without the calibration constraints.[55] In this step, any non-linear function that satisfies the desired conditions can be used for calibration.[56] As such, the quadratic cost function is utilized to calibrate the model as follows. The variable cost function includes a quadratic function, as shown in Equation XII:

$$C^v{}_i = \sum_g \left(TEW_{i,g}.wp\right) + \sum_g tc_{i,g} = d'x + \frac{1}{2}x'Qx \quad \text{(XII)}$$

In this function, *d* is the vector ($n\times1$) of the parameters of the linear component of the cost function, while *Q* is the positive semi-definite, symmetric matrix with dimensions ($n\times n$) of the parameters of the quadratic component of the cost function. In this context, Howitt[55] indicated that the variable marginal cost vector *MC* of the above cost function is equal to the total of the accounting cost vector *c* and the differential marginal cost vector λ^2.

$$MC_i = \frac{\partial C^v{}_i(x)}{\partial x} = d + Qx = c + \lambda^2 \quad \text{(XIII)}$$

The approach proposed by Heckelei and Britz[57] was utilized to estimate the parameters of the proposed cost

function. In this method, it is assumed that the observed accounting cost vector of each activity C is equal to the average cost of the quadratic variable cost function for each crop. Therefore, the values of the vector parameters d and the diagonal elements of the matrix Q are obtained using Equation XIX:

$$q_{ii} = \frac{2\lambda^2{}_i}{\tilde{x}_i} \quad , \; d_i = c_i - \lambda^2{}_i \tag{XIX}$$

Where d is the linear component of the cost function, and q_{ii} is the diagonal element of the cost function. In the third step of the PMP method, the estimated functions of the previous step are investigated into the objective function of the problem. Then, a non-linear programming model is generated, similar to the initial problem, but without the calibration constraints and with the inclusion of other system constraints. The non-linear objective function was developed as shown in Equation XV:

$$Maximize \;\; Z = \sum_g \sum_i \left(P_i \; y_{i,g}\right) * X_{i,g} - \sum_g \sum_i (d_i + (\sum_g \sum_{ii} (q_{ii} * X_{i,g})) * X_{i,g}) \tag{XV}$$

The parameters of this model, including prices, water required for crops, available water, cost of inputs, and crop yields were obtained from the Regional Water Company of Kohgiluyeh and Boyer-Ahmad,[51] the Jihad Agriculture Organization in the Kohgiluyeh and Boyer-Ahmad province, and a sample of 351 farmers.

2.4. TPB model

The TPB model predicts desired behavior by examining an individual's behavioral intention. Behavioral intention is influenced by attitudes, subjective norms, and perceived behavioral control. TPB is one of the most common and powerful models for predicting human social behavior. In this study, the target population consisted of farmers in the sub-basin of Kowsar Dam, located in Kohgiluyeh and Boyer-Ahmad province, Iran. Data for this section of the study were collected in early 2023 through face-to-face interviews using a questionnaire. A sample of farmers in the sub-basin was selected, with the sample size determined based on the population and using Morgan and Krejcie's table. This resulted in 351 farmers being chosen through simple random sampling. A pilot test, involving 50 respondents, was conducted to ensure the readability and clarity of the questionnaires. Before each interview, participants were informed about data protection measures, and both verbal and written consent were obtained.

To prepare the questionnaire, we conducted a literature review on drought adaptation and the TPB model, especially within the context of Iran. Previous studies were extensively consulted to identify items that accurately measured the variables of the research model. Interviewees were selected from the sub-basin of Kowsar Dam to facilitate communication with the farmers and provide the necessary background training. Table 1 presents the items from the theories examined in the questionnaire. To assess the reliability and validity of the items, the following measures were used: Average variance extracted (AVE), Cronbach's alpha coefficient, and composite reliability (CR). In addition, first-order confirmatory factor analysis (λ) was used to evaluate the model's fit validity. The factor loadings (λ) for all items were above 0.6 and statistically significant (p<0.01). Therefore, the selected items for measuring the components of the model were deemed both appropriately chosen and accurately measured. The values for AVE, CR, and α were calculated to be >0.6, 0.8, and 0.8, respectively (Table 1). Therefore, all latent variables of the proposed model demonstrated suitable validity and reliability.

2.5. Statistical analysis

To simulate the hydrological effects of drought, the WEAP software was used, and the PEST tool employed for simulation validation. The GAMS software, coupled with the CONOPT4 solver, was utilized to model the PMP. For data analysis in the TPB model, SPSS was used for descriptive statistics, while Smart Partial Least Squares software was used for inferential statistics. In this study, structural equation modeling (SEM) was applied for modeling and statistical analysis.[65] SEM methods quantitatively assess the confirmation or rejection of theoretical models.[66] These methods combine aspects of factor analysis and multiple regression analysis, allowing researchers to test the relationships between observed variables (measurable) and latent variables (theoretical constructs). The partial least squares technique, a third-generation SEM method, was used to examine the relationships between latent variables measured by observed variables.[65] One of the main reasons for choosing this method is its comprehensive capability to test the proposed theories in a study.[65]

Table 1. Survey items

Constructs	Measurement item	λ	*t*	Reliability and validity statistics	Sources
Sources	Att1: Living in the rural is enjoyable even in the presence of drought	0.601	6.834	AVE: 0.601 CR: 0.830 α: 0.804	38,47,52,58
	Att2: My adaptation to drought has great value for the community	13.145	0.773		
	Att3: My adaptation to drought is very necessary	10.206	0.711		
	Att4: My adaptation to drought is completely rational	10.039	0.702		
	Att5: My adaptation to drought is beneficial	8.255	0.643		
Subjective norms	Sn1: If I adapt to drought, my friends, relatives and neighbors will approve my actions	19.185	0.818	AVE: 0.712 CR: 0.884 α: 0.827	38,47,59,60
	Sn2: If I adapt to drought, the people who are important to me will approve my actions	18.746	0.809		
	Sn3: If I adapt to drought, the society will approve my actions	25.342	0.853		
	Sn4: Rural community expects me to continue my activities even in the presence of drought.	11.950	0.754		
Perceived behavior control	Pbc1: I have the knowledge, and ability to adapt to drought	10.860	0.733	AVE: 0.688 CR: 0.855 α: 0.822	47,61-63
	Pbc2: I have the necessary skills to implement adaptation strategies	9.128	0.685		
	Pbc3: I want to adapt to drought	13.726	0.782		
Intentions	Int1: I'd like to stay in the rural despite the drought	26.840	0.885	AVE: 0.760 CR: 0.906 α: 0.883	38,64
	Int2: I'd like to engage in drought adaptation programs	28.105	0.897		
	Int3: I plan to engage in drought adaptation programs	15.897	0.792		
Behavior	B1: I stay in the rural despite the drought and implement drought adaptation strategies	10.926	0.728	AVE: 0.632 CR: 0.850 α: 0.817	

Notes: Response scale (1 – 5): Strongly disagree–Strongly agree; α=Cronbach's alpha. Abbreviations: Att: Attitude; AVE: Average variance extracted; B: Behavior; CR: Composite Reliability; Int: Intention; Pbc: Perceived behavior control; Sn: Subjective norms.

3. Results and discussion

3.1. Validation assessment of hydrological simulation

The PEST tool was used to assess the performance of the WEAP model. It allows users to automatically compare the model's results with real-world data and adjust the model's settings to enhance its accuracy. This tool used water flow data from hydrometric stations to evaluate the accuracy of the model's simulations and calibration. Specifically, the average monthly water inflow data from the Khairabad and Pulflor hydrometric stations (2011 – 2020) were compared with the model's simulated water flow output for the area upstream of these stations. The results are shown in Figures 5 and 6. A comparison of the model's simulated water flow with the actual water inflow at the Khairabad and Pulflor stations in 2011 indicates that the model performs with high accuracy. This is evident as the simulated outflow from the land upstream of the stations closely matched the actual inflow observed at the stations.

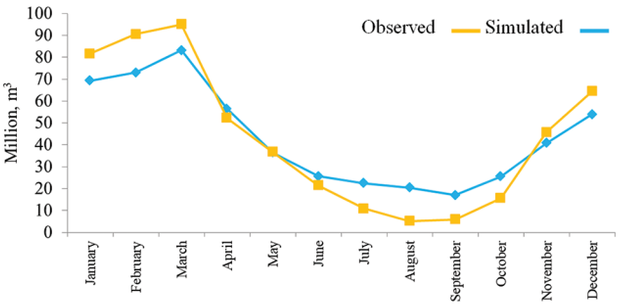

Figure 5. Comparison of observed and simulated inflow at the Khairabad hydrometric station

3.2. Technical-agronomic impacts of drought scenarios

Two drought scenarios were created for this study. The first scenario involved a decrease in rainfall and an increase in temperature. The second scenario included a decrease in rainfall, an increase in temperature, and a reduction in the amount of water available in the basin (based on climate data from 2013 to 2020). The impacts of these scenarios on crop yields and water requirements are shown in Tables 2 and 3.

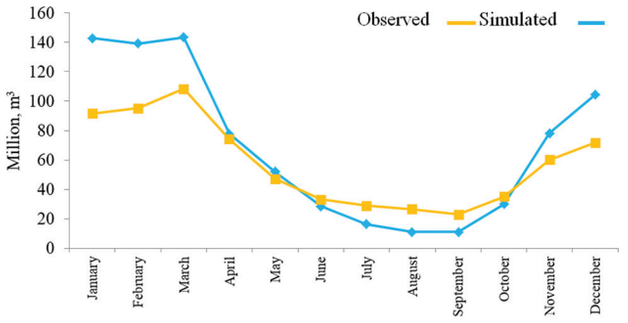

Figure 6. Comparison of observed and simulated inflow at the Pulflor hydrometric station

Table 2 demonstrates that, under the first drought scenario (reduced rainfall and higher temperatures), the average yield of all crops in the Bashet, Gachsaran, and Choram regions will decrease. In the Bashet region, wheat crops will experience the largest yield reduction, while tomato and rice crops will see the smallest reductions. In the Gachsaran region, the yield reduction will range from 0.6% to over 4% across all crops, with corn and wheat being the most affected, while cucumber and bean crops will be the least affected.

Table 2. Effects of drought scenarios on the average yield of crops (kg/hectare) in different regions during the 2011 – 2030 period

Area	Crops	Reference	Scenario 1 (percent changes)	Scenario 2 (percent changes)
Bashet	Seed maize	11,233	10,930 (−2.7)	10,250 (−8.8)
	Barley	1,895	1,869 (−1.4)	1,792 (−5.4)
	Bean	2,037	2,008 (−1.4)	1,847 (−6.4)
	Cucumber	23,234	22,921 (−1.3)	21,064 (−9.3)
	Pea	3,100	3,055 (−1.4)	2,931 (−5.4)
	Rice	6,645	6,568 (−1.1)	5,571 (−16.2)
	Tomato	37,093	36,671 (−1.1)	32,594 (−12.1)
	Watermelon	46,832	45,821 (−2.2)	41,142 (−12.1)
	Wheat	6,992	6,565 (−6.1)	6,428 (−8.1)
Gachsaran	Seed maize	9,637	9,195 (−4.6)	8,779 (−8.9)
	Barley	3,100	3,014 (−2.8)	2,995 (−3.4)
	Bean	1,791	1,775 (−0.9)	1,699 (−5.1)
	Cucumber	20,941	20,798 (−0.7)	19,144 (−8.6)
	Pea	1,364	1,349 (−1.1)	1,294 (−5.1)
	Rice	4,224	4,155 (−1.6)	3,699 (−12.4)
	Tomato	27,263	26,975 (−1.1)	24,196 (−11.2)
	Watermelon	37,463	36,814 (−1.7)	33,312 (−11.1)
	Wheat	5,587	5,336 (−4.5)	5,165 (−7.6)
Choram	Barley	4,775	4,548 (−4.8)	4,495 (−5.9)
	Bean	1,069	1,039 (−2.8)	976 (−8.7)
	Cucumber	19,689	18,955 (−3.7)	17,954 (−8.8)
	Pea	1,730	1,706 (−1.4)	1,626 (−6.0)
	Rice	7,790	7,513 (−3.6)	6,456 (−17.1)
	Tomato	22,423	22,142 (−1.3)	19,364 (−13.6)
	Watermelon	21,155	20,703 (−2.1)	18,595 (−12.1)
	Wheat	3,980	3,702 (−7.0)	3,646 (−8.4)

Table 3. Effects of drought scenarios on the net water requirement (m^3/hectare) of crops in different regions during the 2011 – 2030 period

Area	Crops	Reference	Scenario 1 (percent changes)	Scenario 2 (percent changes)
Bashet	Seed maize	11,082	11,530 (+4.0)	11,577 (+4.5)
	Barley	4,344	4,452 (+2.5)	4,455 (+2.6)
	Bean	7,793	8,192 (+5.1)	8,207 (+5.3)
	Cucumber	7,582	7,946 (+4.8)	8,015 (+5.7)
	Pea	4,278	4,591 (+7.3)	4,618 (+7.9)
	Rice	11,022	11,669 (+5.9)	11,972 (+8.6)
	Tomato	10,555	10,896 (+3.2)	11,350 (+7.5)
	Watermelon	9,551	9,866 (+3.3)	10,062 (+5.4)
	Wheat	4,849	5,198 (+7.2)	5,209 (+7.4)
Gachsaran	Seed maize	10,915	11,338 (+3.9)	11,400 (+4.4)
	Barley	3,292	3,359 (+2.0)	3,361 (+2.1)
	Bean	7,316	7,580 (+3.6)	7,590 (+3.7)
	Cucumber	7,457	7,796 (+4.5)	7,865 (+5.5)
	Pea	4,168	4,460 (+7.0)	4,473 (+7.3)
	Rice	10,738	11,425 (+6.4)	11,940 (+11.2)
	Tomato	10,437	10,756 (+3.0)	11,116 (+6.5)
	Watermelon	9,392	9,795 (+4.3)	10,087 (+7.4)
	Wheat	4,686	5,028 (+7.3)	5,044 (+7.6)
Choram	Seed maize	9,768	10,310 (+5.5)	10,336 (+5.8)
	Barley	3,127	3,305 (+5.7)	3,306 (+5.7)
	Bean	7,544	8,077 (+7.0)	8,112 (+7.5)
	Cucumber	8,356	8,952 (+7.1)	9,070 (+8.5)
	Pea	4,049	4,310 (+6.5)	4,324 (+6.8)
	Rice	11,037	11,557 (+4.7)	11,727 (+6.3)
	Tomato	10,310	10,601 (+2.8)	10,684 (+3.6)
	Watermelon	9,229	9,604 (+4.0)	9,667 (+4.7)
	Wheat	4,559	4,904 (+7.5)	4,915 (+7.8)

In the Choram region, wheat and barley crops will experience the biggest yield reduction, while tomato and pea crops will see the smallest reductions. The percentage of yield reduction in this region was also higher (>2%) compared to the other regions. Overall, the yield reduction for most crops due to the first drought scenario in the Kowsar Dam basin is relatively small. This suggests that drought conditions, driven by less rain and higher temperatures, do not significantly impact production in the area. Wheat, however, is more sensitive to changes in rainfall and temperature than other crops.[35] Table 2 also shows that under the second drought scenario (less rainfall, higher temperatures, and decreased water availability), rice, tomato, and watermelon crops will experience the largest yield reductions. The yield reduction for all crops exceeded 5% compared to normal conditions, indicating that the second drought scenario had a greater negative impact on crop yields than the first scenario. Comparing both scenarios, it can be concluded that the yield reduction of rice, tomato, and watermelon crops is greater than for other crops due to the reduced water availability. These crops require more irrigation water than crops like barley and wheat; hence, the decrease in available water had a more significant impact on their yield. In contrast, crops like wheat and barley, which rely more on rainfall, were less affected by reduced water availability. Therefore, simulating drought conditions through reduced rainfall and increased temperatures had a more pronounced effect on the yield of these crops than on others.

Table 3 shows that wheat and pea crops are more sensitive to decreased rainfall and increased temperature, as they need more irrigation water compared to other crops under the first drought scenario. Overall, reduced rainfall and higher temperatures increased the need for irrigation water for crops in the basin.[12,35] The results also indicate that the highest reduction in yield and the greatest increase in irrigation water needs were observed for wheat crops due to the decrease in rainfall and the rise in temperature in the Kowsar Dam basin. This reinforces the fact that wheat crops are more dependent on rainfall and temperature than other crops.[35] Furthermore, the simulation results suggest that the percentage changes in irrigation water requirements were not significantly different between the two drought scenarios, except for rice crops. Therefore, reducing the amount of available water did not have a significant negative impact on irrigation water needs for most crops, except for rice. Similarly, it can be concluded that the reduction in available water has a greater negative impact on crop yield compared to the decrease in the amount of rainfall. Nevertheless, the impact on irrigation water requirements was noticeably different. Moreover, the decrease in rainfall and the increase in temperature showed a more significant negative impact on irrigation water needs for the crops in the basin compared to the decrease in the amount of available water.

3.3. Hydrological impacts of drought scenario

After describing the impacts of reduced rainfall, higher temperatures, and limited water availability on crop yields and water needs, the effects of drought on the water situation of the basin were analyzed. The unmet water demand, defined as the difference between water demand and water supply, serves as an indicator of the basin's water situation. The greater the disparity between water demand and the amount of water supplied, the higher the unmet demand; and vice versa. The unmet water demand in different regions of the basin during the 2011 – 2030 period was studied under both normal conditions and drought conditions (reduced rainfall, higher temperatures, and reduced water availability). The unmet water demand for the Bashet, Gachsaran, and Choram regions was simulated under the second drought scenario, as depicted in Figures 7-9.

Figure 7 shows that the unmet water demand is higher under the drought scenario than under normal conditions. Under normal conditions, the unmet water demand exceeded 60 million m^3, while under drought conditions, it fluctuated around 85 million m^3. This indicates that drought will significantly affect

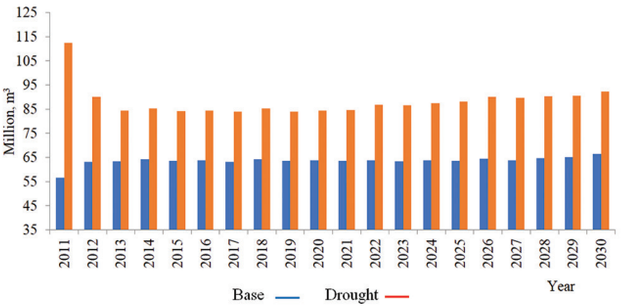

Figure 7. Unmet water demand for the agricultural units in Bashet under the second drought scenario

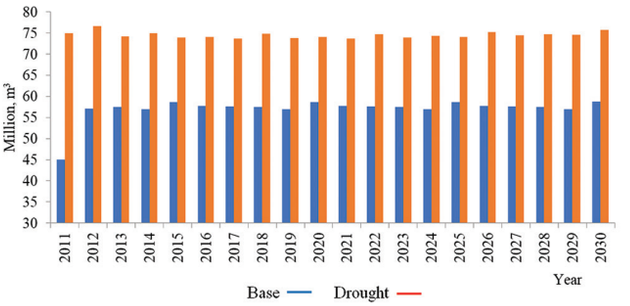

Figure 8. Unmet water demand for the agricultural units in Gachsaran under the second drought scenario

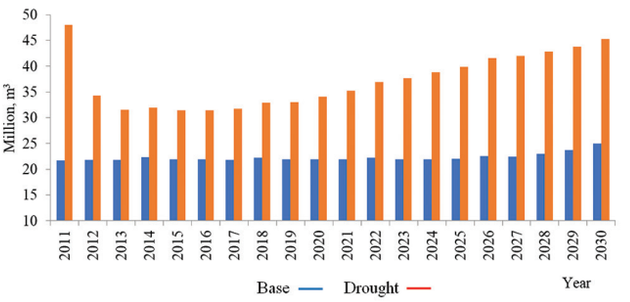

Figure 9. Unmet water demand for the agricultural units in Choram under the second drought scenario

the agricultural areas of the Bashet region, making it more difficult to meet their water needs in the future. The results further suggest that by the end of 2030, the unmet water demand for agricultural areas in this region will surpass 92 million m^3. In 2030, about 38% of the water demand of agricultural areas will remain unmet under drought conditions, which constitutes a significant shortfall. Thus, it can be concluded that, during a drought, the areas in this region will face substantial problems in meeting their water demands.

Figure 8 illustrates that the average unmet water demand during drought conditions in the Gachsaran

region is approximately 74 million m^3, which is lower than that of the Bashet region. By the end of 2030, the unmet water demand for Gachsaran's agricultural areas will reach about 75 million m^3. This represents roughly 28% of the total water demand for agricultural areas in the region. In other words, more than 28% of the water demand in Gachsaran's agricultural areas will go unmet in 2030 under drought conditions. Nevertheless, this region is expected to experience more favorable conditions compared to the agricultural areas of the Bashet region.

As shown in Figure 9, the unmet water demand in the Choram agricultural area started to increase after a sharp decrease in 2018. This upward trend will result in the unmet water demand for agricultural areas in this region exceeding 45 million m^3 by the end of the simulation period (2030). By 2030, more than 81% of the water demand in the Choram region's agricultural areas will remain unmet under drought conditions. It can therefore be concluded that the water supply situation for agricultural areas downstream of the basin will be highly unfavorable over the next 30 years under drought conditions.

3.4. Socioeconomic impacts of drought scenario

The outputs of the simulation of crop yields, water needs, and water availability, both with and without drought scenarios in the Kowsar Dam basin, were used as inputs for the PMP model. The PMP model was then run for typical farms in all three regions, both with and without the proposed drought scenarios, and the results are shown in Figure 10. A typical farm in each region is a hypothetical representation of an average farm, including factors such as the cultivated area, cropping pattern, soil quality, crop yield, the percentage of farms with access to water resources, and the use of modern irrigation technologies. To assess the economic impacts of drought, only the impacts of the second drought scenario were considered, which involved a simultaneous decrease in rainfall, an increase in temperature, and a reduction in available water resources. Figure 10 shows that the gross margin of typical farms in all areas under the Kowsar Dam basin declines due to drought. Among the regions studied, the Choram region experienced the largest decrease in gross margin, with the typical farm's gross margin falling from 520 to 275 per hectare, a reduction of about 47%. The differing results across regions highlight the dynamics and the multi-level vulnerability of these areas, a phenomenon that has been observed in other studies.[12,35,67,68] At the basin level, drought resulted in a reduction of more than 32% in the gross margin of farmers in the Kowsar Dam basin.

To better understand the economic impacts of drought, the cropping pattern under the drought scenario (reduced rainfall, higher temperatures, and limited water availability) is provided in Table 4 for the entire Kowsar Dam basin. The drought scenario resulted in a 21% reduction in the area dedicated to rice and wheat cultivation compared to the normal scenario. Other crops remained unaffected. As a result, the total cultivated area in the Kowsar Dam basin decreased by approximately 15% due to drought. This reduction negatively impacts farmers' welfare and food security in the studied areas. An analysis of farm-level decision-making showed that crop pattern changes do not fully capture the potential for farm-level adaptation to mitigate the harmful effects of drought.[67]

3.5. Analysis of farmers' behavior in dealing with drought

The SEM was examined using appropriate indicators, and the results were presented in Table 5.

The outcomes of the ultimate influence of variables on farmers' behavior are displayed in Figure 11. The

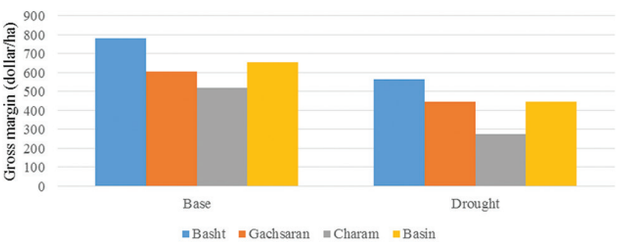

Figure 10. Impacts of the second drought scenario on the gross margin (dollar/hectare) of representative farms in the Kowsar Dam basin

Table 4. Effects of the second drought scenario on the cultivation pattern (hectares)

Crops	Reference	Scenario 2 (percent changes)
Seed maize	1,485	1,485 (0.0)
Barley	500	500 (0.0)
Bean	88	88 (0.0)
Cucumber	60	60 (0.0)
Pea	97	97 (0.0)
Rice	1,296	1,023 (−21.1)
Tomato	41	41 (0.0)
Watermelon	657	657 (0.0)
Wheat	6,880	5,449 (−20.8)
Basin	11,104	9,400 (−15.3)

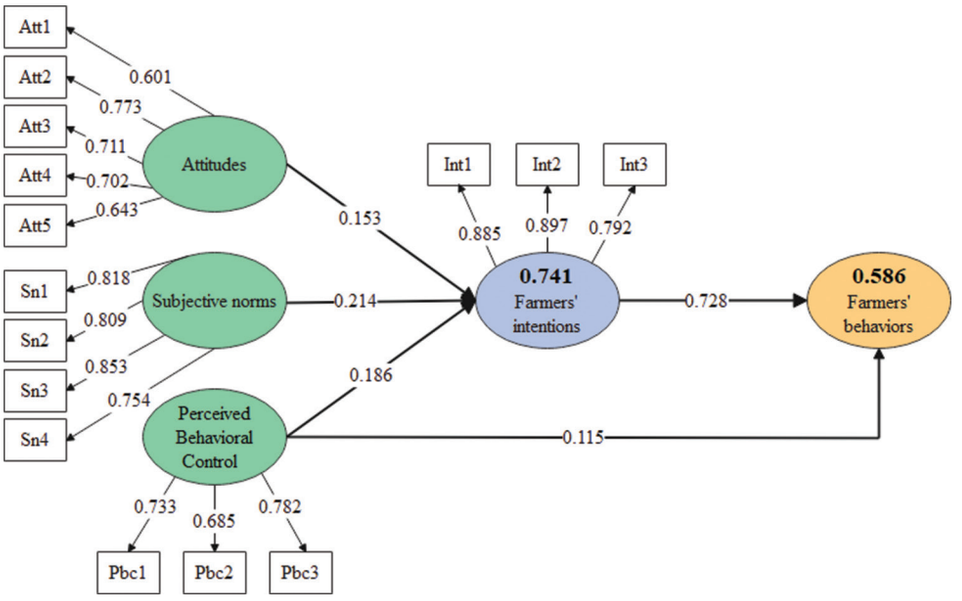

Figure 11. Theory of planned behavior model with standardized path coe□cients
Abbreviations: Att: Attention; Int: Intention; Pbc: Perceived behavior control; Sn: Subjective norm.

Table 5. Summary of fit goodness indices for the structural equation modeling

Fit index	SRMR	D-G1	D-G2	D-G2	RMS-Theta
Suggested value	<0.1	>0.05	>0.05	>0.90	≤0.11
TPB	0.07	0.628	0.733	0.96	0.06

Abbreviations: D-G: Degrees of freedom adjustment index; NFI: Normed fit index; RMS: Root mean square; SRMR: Standardized root mean square residual; TPB: Theory of planned behavior.

Table 6. Results of structural equation modeling

Hypothesis	γ	*t*	Result
Att→Intention	0.153	2.293	Confirm
Sn→Intention	0.214	2.524	Confirm
Pbc→Intention	0.186	2.423	Confirm
Pbc→Behavior	0.115	2.091	Confirm
Int→Behavior	0.728	8.862	Confirm

Abbreviations: Att: Attention; Int: Intention; Pbc: Perceived behavior control; Sn: Subjective norm.

findings demonstrated that the TPB model accounts for 74.1% of behavioral intentions and 58.6% of farmers' behavior. Behavioral intention measures the relative strength of a person's intention to perform a specific behavior. In addition, the results of SEM are outlined in Table 6. The results suggest that farmers' behavioral intentions are distinctly and significantly influenced by the three variables: Attitude, subjective norm, and perceived behavior control. Moreover, farmers' intentions had a direct and significant impact on their behaviors. These findings indicate that the TPB model is highly effective in examining farmers' behavior in the Kowsar Dam sub-basin concerning drought adaptation.

According to the results, farmers' attitudes significantly and positively influence their behavioral intentions. This positive and significant impact of attitudes on farmers' behavioral intentions has been consistently observed in various studies focusing on adaptive behavior in response to environmental challenges.[44,57] Consequently, it can be inferred that farmers with favorable attitudes and mindsets toward drought adaptation strategies are more likely to remain in rural areas and adapt to drought conditions.

The positive and significant impact of the subjective norm variable indicates that positive feedback from peers and influential community figures can enhance farmers' intentions to stay in rural areas and adopt drought adaptation strategies. This positive and significant influence of the subjective norm on farmers' behavioral intentions in addressing environmental challenges has also been supported by research conducted by Savari and Moradi[38] and Savari and Khaleghi.[60]

The positive and significant effect of the perceived behavior control variable on farmers' intentions and behaviors was clearly evident. Therefore, individuals with high self-confidence who believe in their ability to participate in drought-adaptive activities are more

likely to engage in these activities, a conclusion that is also supported by additional studies.[44,64,69]

4. Conclusion

Investigating the impacts of drought on technical-agronomic parameters (e.g., crop yields and water requirements), hydrological parameters (e.g., unmet water demand), economic parameters (e.g., cropping patterns and farmers' gross margins), and psychological parameters (e.g., intentions, attitudes, subjective norms, and perceived behavioral control) provide critical insights for policymakers in arid and semi-arid regions. This study utilized an integrated approach, combining the WEAP model with the MABIA extension, PMP, and TPB models, to identify vulnerable areas across technical, hydrological, socioeconomic, and psychological dimensions. The main conclusions drawn from this study are as follows:

(i) Crop yield: Drought significantly reduces crop yields (3–18% under Scenario 2 [decreased rainfall, increased temperature, and reduced water resources]). The Choram region is the most vulnerable, with the highest productivity losses.
(ii) Water requirements: The net water requirement for crops increases (2–8% under Scenario 1 [decreased rainfall and increased temperature]). However, under Scenario 2, water-intensive crops show only a slight increase in water demand.
(iii) Hydrological impacts: Drought increases unmet water demand across the basin, with the most significant impact in the Choram region.
(iv) Socioeconomic impacts: Farmers' gross margins per hectare decline significantly, highlighting the adverse economic effects of drought.
(v) Behavioral insights: The TPB model demonstrates that fostering positive attitudes, promoting supportive community norms, and enhancing farmers' self-confidence can increase their willingness to adopt drought-adaptation strategies.

To mitigate the impacts of drought, policymakers should prioritize the implementation of adaptive strategies, including:

(i) Water management: Invest in efficient irrigation technologies and water-saving practices to address unmet water demand, especially in vulnerable regions like Choram.
(ii) Crop diversification: Promote drought-resistant crops and diversify cropping patterns to reduce dependency on water-intensive crops.
(iii) Economic support: Provide financial incentives and subsidies to farmers to offset reduced gross margins and encourage the adoption of adaptive practices.
(iv) Capacity building: Enhance farmers' awareness and skills through training programs to improve their ability to implement drought-adaptation strategies.
(v) Community engagement: Foster positive attitudes and social norms by leveraging local leaders and community networks to encourage collective action against drought.

The limitations of the present study include the lack of necessary information for simulating the environmental impacts of drought, which could facilitate a more integrated analysis of drought effects in future studies.

Acknowledgments

We would like to express our sincere appreciation to Islamic Azad University, Marvdasht Branch, for their support.

Funding

None.

Conflict of interest

The authors declare that they have no known competing interests.

Author contributions

Conceptualization: Seyed Nematollah Mosavi
Formal analysis: Seyed Nematollah Mosavi, Bahaedin Najafi
Investigation: Ali Ghasemi, Seyed Nematollah Mosavi
Methodology: Ali Ghasemi, Seyed Nematollah Mosavi
Writing – original draft: Ali Ghasemi
Writing – review & editing: Seyed Nematollah Mosavi, Bahaedin Najafi

Availability of data

The data are available on request from the corresponding author.

References

1. Ado AM, Leshan J, Savadogo P, Bo L, Shah AA. Farmers' awareness and perception of climate change impacts: Case study of Aguie district in Niger. *Environ*

Dev Sustain. 2019;21(6):2963-2977.
doi: 10.1007/s10668-018-0173-4

2. Mirzaei A, Azarm H, Yazdanpanah M, Najafabadi MM. Socio-economic, social-capital, and psychological characteristics and climate change adaptive behavior of farmers in Iran. *Clim Res.* 2022;87:1-12.
doi: 10.3354/cr01683
3. Udmale P, Ichikawa Y, Manandhar S, Ishidaira H, Kiem AS. Farmers' perception of drought impacts, local adaptation and administrative mitigation measures in Maharashtra State, India. *Int J Disaster Risk Reduct.* 2014;10:250-269.
doi: 10.1016/j.ijdrr.2014.09.011
4. Bento VA, Gouveia CM, DaCamara CC, Trigo IF. A climatological assessment of drought impact on vegetation health index. *Agric For Meteorol.* 2018;259:286-295.
doi: 10.1016/j.agrformet.2018.05.014
5. Ngondjeb YD. Agriculture and climate change in Cameroon: An assessment of impacts and adaptation options. *Afr J Sci Technol Innov Dev.* 2013;5(1):85-94.
doi: 10.1080/20421338.2013.782151
6. Pakmehr S, Yazdanpanah M, Baradaran M. How collective efficacy makes a difference in responses to water shortage due to climate change in southwest Iran. *Land Use Policy.* 2020;99:104798.
doi: 10.1016/j.landusepol.2020.104798
7. Wilhite DA, Svoboda MD, Hayes MJ. Understanding the complex impacts of drought: A key to enhancing drought mitigation and preparedness. *Water Resour Manag.* 2007;21(5):763-774.
doi: 10.1007/s11269-006-9076-5
8. Eliasson J. The rising pressure of global water shortages. *Nature.* 2015;517(7532):6.
doi: 10.1038/517006a
9. Li M, Fu Q, Singh VP, Ma M, Liu X. An intuitionistic fuzzy multi-objective non-linear programming model for sustainable irrigation water allocation under the combination of dry and wet conditions. *J Hydrol.* 2017;555:80-94.
doi: 10.1016/j.jhydrol.2017.09.055
10. Lu H, Li J, Ren L, Chen Y. Optimal groundwater security management policies by control of inexact health risks under dual uncertainty in slope factors. *Chemosphere.* 2018;198:161-173.
doi: 10.1016/j.chemosphere.2018.01.121
11. Mirzaei A, Azarm H, Naghavi S. Optimization of cropping pattern under seasonal fluctuations of surface water using multistage stochastic programming. *Water Supply.* 2022;22(6):5716-5728.
doi: 10.2166/ws.2022.224
12. Mirzaei A, Zibaei M. Water conflict management between agriculture and wetland under climate change: Application of economic-hydrological-behavioral modelling. *Water Resour Manag.* 2021;35(1):1-21.
doi: 10.1007/s11269-020-02703-4
13. Edwards, B., Gray, M., Hunter, B. The social and economic impacts of drought. *Aust J Soc Issues.* 2019;54(1):22-31.
doi: 10.1002/ajs4.52
14. Bruinsma J. *World Agriculture: Towards 2015/2030: An FAO Perspective.* UK: Routledge; 2017.
15. Hadizadeh F, Allahyari MS, Damalas CA, Yazdani MR. Integrated management of agricultural water resources among paddy farmers in Northern Iran. *Agric Water Manag.* 2018;200:19-26.
doi: 10.1016/j.agwat.2017.12.031
16. Mardani Najafabadi M, Mirzaei A, Azarm H, Nikmehr S. Managing water supply and demand to achieve economic and environmental objectives: Application of mathematical programming and ANFIS models. *Water Resour Manag.* 2022;36(9):3007-3027.
doi: 10.1007/s11269-022-03178-1
17. Yazdanpanah M, Forouzani M., Abdeshahi A, Jafari A. Investigating the effect of moral norm and self-identity on the intention toward water conservation among Iranian young adults. *Water Policy.* 2016;18(1):73-90.
doi: 10.2166/wp.2015.031
18. D'Odorico P, Carr J, Dalin C, *et al*. Global virtual water trade and the hydrological cycle: Patterns, drivers, and socio-environmental impacts. *Environ Res Lett.* 2019;14(5):053001.
doi: 10.1088/1748-9326/ab05f4
19. Khalili D. Challenges facing water resources management under drought conditions in Iran. *Strateg Res J Agric Sci Nat Resour.* 2016;1(2):149-164.
doi: 10.22047/SRJASNR.2016.110542
20. National Climate Change Office. *Iran Second National Communication to UNFCC.* National Climate Change Office at the Department of Environment on Behalf of the Government of the Islamic Republic of Iran; 2010.
21. Nazari MR. The economic impacts of climate change on Iranian agricultural sector. In: *Technical Workshop of Investigating Climate Change Related Challenges and Implementing the United Nations Framework Convention on Climate Change in Iran, Tehran*; 2015. (In Persian)
22. Sadeghi SH, Moghadam ES, Delavar M, Zarghami M. Application of water-energy-food nexus approach for designating optimal agricultural management pattern at a watershed scale. *Agric Water Manag.* 2020;233:106071.
doi: 10.1016/j.agwat.2020.106071
23. Ashraf Vaghefi S, Mousavi SJ, Abbaspour KC, Srinivasan R, Yang H. Analyses of the impact of climate change on water resources components, drought and wheat yield in semiarid regions: Karkheh River Basin in Iran. *Hydrol Processes.* 2014;28(4):2018-2032.
doi: 10.1002/hyp.9747
24. Mirzaei A, Zibaei M. Investigation of adaptation strategies for agricultural water resources management under climate change in Halil-rud river basin. *J Agric*

Econ Dev. 2021;34(4):397-419. (In Persian)
25. Ashofteh PS, Bozorg Haddad O, Massah Bavani A. Impact of climate change on water requirement of Aidoghmoush irrigation network. In: *21st International Congress on Irrigation and Drainage.* New Delhi: International Commission on Irrigation and Drainage; 2011. (In Persian)
26. Maddah V, Soltani A, Zeinali E, Bannayan Aval M. Simulating climate change impacts on wheat production in Gorgan, Iran. *Bull Environ Pharmacol Life Sci.* 2015;4:58-67.
27. Moradi R, Koocheki A, Nassiri Mahallati M. Adaptation of maize to climate change impacts in Iran. *Mitig Adapt Strateg Glob Chang.* 2014;19(8):1223-1238. doi: 10.1007/s11027-013-9470-2
28. Nassiri M, Koocheki A, Kamali GA, Shahandeh H. Potential impact of climate change on rainfed wheat production in Iran. *Arch Agron Soil Sci.* 2006;52(1):113-124. doi: 10.1080/03650340600560053
29. Valizadeh J, Ziaei SM, Mazloumzadeh SM. Assessing climate change impacts on wheat production (a case study). *J Saudi Soc Agric Sci.* 2014;13(2):107-115. doi: 10.1016/j.jssas.2013.02.002
30. Moriondo M, Bindi M, Zbigniew W, *et al*. Impact and adaptation opportunities for European agriculture in response to climatic change and variability. *Mitig Adapt Strateg Glob Chang.* 2010;15(7):657-679. doi: 10.1007/s11027-010-9219-0
31. Ventrella D, Charfeddine M, Moriondo M, Rinaldi M, Bindi M. Agronomic adaptation strategies under climate change for winter durum wheat and tomato in southern Italy: Irrigation and nitrogen fertilization. *Reg Environ Chang.* 2012;12(3):407-419. doi: 10.1007/s10113-011-0256-3
32. Joyce BA, Mehta VK, Purkey DR, Dale LL, Hanemann M. Modifying agricultural water management to adapt to climate change in California's central valley. *Clim Chang.* 2011;109:299-316. doi: 10.1007/s10584-011-0335-y
33. Rochdane S, Reichert B, Messouli M, Babqiqi A, Khebiza MY. Climate change impacts on water supply and demand in Rheraya Watershed (Morocco), with potential adaptation strategies. *Water.* 2012;4:28-44. doi: 10.3390/w4010028
34. Blanco-Gutierrez I, Varela-Ortega C, Purkey DR. Integrated assessment of policy interventions for promoting sustainable irrigation in semi-arid environments: A hydro-economic modeling approach. *J Environ Manag.* 2013;128:144-160. doi: 10.1016/j.jenvman.2013.04.037
35. Esteve P, Varela-Ortega C, Gutierrez I, Downing TE. A hydro-economic model for the assessment of climate change impacts and adaptation in irrigated agriculture. *Ecol Econ.* 2015;120:49-58. doi: 10.1016/j.ecolecon.2015.09.017
36. Forni LG, Medellin-Azuara J, Tansey M, *et al*. Integrating complex economic and hydrologic planning models: An application for drought under climate change analysis. *Water Resour Econ.* 2016;16:15-27. doi: 10.1016/j.wre.2016.10.002
37. Kavand H, Ziaee S, Mardani Najafabadi M. Assessing the consequences of internalization of the side effects of water pollution on the quantitative and qualitative management of Zayandehroud basin. *J Agric Econ Dev.* 2020;34(3):341-356. (In Persian)
38. Savari M, Moradi M. Explaining cognitive factors influencing farmers' intention towards livability in drought conditions in Hendijan County. *Geogr Environ Plan.* 2020;30(4):139-160.
39. Khanal U, Wilson C, Hoang VN, Lee B. Farmers' adaptation to climate change, its determinants and impacts on rice yield in Nepal. *Ecol Econ.* 2018;144:139-147. doi: 10.1016/j.ecolecon.2017.08.006
40. Chathuranika I, Khaniya B, Neupane K, *et al*. Implementation of water-saving agro-technologies and irrigation methods in agriculture of Uzbekistan on a large scale as an urgent issue. *Sustain Water Resour Manag.* 2022;8:155. doi: 10.1007/s40899-022-00746-6
41. Asif Khan M, Khalid Anser M, Usman B, *et al*. Decoding carbon sequestration: the impact of agriculture, conservation policies, climate, and land use. *Asian J Water Environ Pollut.* 2025;2025;025050027. doi: 10.36922/AJWEP025050027
42. Barua P, Rahman SH, Eslamian S. Adaptation practices by the farmers for reduction of salinisation problem in the paddy fields of South-Eastern coast of Bangladesh. *Asian J Water Environ Pollut.* 2022;19(6):37-44. doi: 10.3233/AJW220086
43. Quandt A, Neufeldt H, McCabe JT. The role of agroforestry in building livelihood resilience to floods and drought in semiarid Kenya. *Ecol Soc.* 2017;22(3):10. doi: 10.5751/ES-09461-220310
44. Pakmehr S, Yazdanpanah M, Baradaran M. Explaining farmers' response to climate change-induced water stress through cognitive theory of stress: An Iranian perspective. *Environ Dev Sustain.* 2021;23(4):5776-5793. doi: 10.1007/s10668-020-00846-3
45. Zobeidi T, Yazdanpanah M, Komendantova N, Sieber S, Loehr K. Factors affecting smallholder farmers' technical and non-technical adaptation responses to drought in Iran. *J Environ Manag.* 2021;298:113552. doi: 10.1016/j.jenvman.2021.113552
46. Zarafshani K, Maleki T, Keshavarz M. Assessing the vulnerability of farm families towards drought in Kermanshah province, Iran. *GeoJournal.* 2020;85:823-836. doi: 10.1007/s10708-019-09994-0
47. Zobeidi T, Yaghoubi J, Yazdanpanah M. Exploring the

motivational roots of farmers' adaptation to climate change induced water stress through incentives or norms. *Sci Rep.* 2022;12(1):15208.
doi: 10.1038/s41598-022-19384-1

48. Callejas Moncaleano DC, Pande S, Rietveld L. Water use efficiency: A review of contextual and behavioral factors. *Front Water.* 2021;3:685650.
doi: 10.3389/frwa.2021.685650
49. Khoshnodifar Z, Karimi H, Ataei P. Mechanisms to change farmers' drought adaptation behaviors in Sistan and Baluchistan Province, Iran. *Front Sustain Food Syst.* 2023;7:1121254.
doi: 10.3389/fsufs.2023.1121254
50. Layani G, Bakhshoodeh M. Water security in Kowsar Dam basin under climate variability: Application of system dynamics approach. *Agric Econ (Karaj).* 2019;13(1):47-72.
doi: 10.22034/IAES.2019.98544.1649
51. Regional Water Company of Kohgiluyeh and Boyer-Ahmad. *Comprehensive Reports of Water Resources of Kowsar Basin*; 2019. (In Persian)
52. Luís S, Lima ML, Roseta-Palma C, *et al*. Psychosocial drivers for change: Understanding and promoting stakeholder engagement in local adaptation to climate change in three European Mediterranean case studies. *J Environ Manag.* 2018;223:165-174.
doi: 10.1016/j.jenvman.2018.06.020
53. Yates D, Sieber J, Purkey D, Huber-Lee A. WEAP21 - a demand-, priority-, and preference-driven water planning model. Part 1: Model characteristics. *Water Int.* 2005;30(4):487-500.
doi: 10.1080/02508060508691893
54. Sieber J, Purkey D. *WEAP, Water Evaluation and Planning System. User Guide.* Sweden: Stockholm Environment Institute, U.S. Center; 2011.
55. Howitt R. Positive mathematical programming. *Am J Agric Econ.* 1995;77:329-342.
56. Heckelei T. *Calibration and Estimation of Programming Models for Agricultural Supply Analysis.* PhD thesis. Germany: University of Bonn; 2002.
57. Heckelei T, Britz W. Positive mathematical programming with multiple data points: A cross-sectional estimation procedure. *Cahiers Econ Sociol Rural.* 2000;57:27-50.
doi: 10.3406/reae.2000.1649
58. Greaves M, Zibarras LD, Stride C. Using the theory of planned behavior to explore environmental behavioral intentions in the workplace. *J Environ Psychol.* 2013;34:109-120.
doi: 10.1016/j.jenvp.2013.02.003
59. Azarm H, Bakhshoodeh M, Zibaei M, Nasrnia F. Incorporating land use changes and pastoralists' behavior in sustainable rangeland management: Evidence from Iran. *Rangeland Ecol Manag.* 2022;80:48-60.
doi: 10.1016/j.rama.2021.09.009
60. Savari M, Khaleghi B. Application of the extended theory of planned behavior in predicting the behavioral intentions of Iranian local communities toward forest conservation. *Front Psychol.* 2023;14:1121396.
doi: 10.3389/fpsyg.2023.1121396
61. De Leeuw A, Valois P, Ajzen I, Schmidt P. Using the theory of planned behavior to identify key beliefs underlying pro-environmental behavior in high-school students: Implications for educational interventions. *J Environ Psychol.* 2015;42:128-138.
doi: 10.1016/j.jenvp.2015.03.005
62. Han H. The norm activation model and theory-broadening: Individuals' decision-making on environmentally-responsible convention attendance. *J Environ Psychol.* 2014;40:462-471.
doi: 10.1016/j.jenvp.2014.10.006
63. Zhang L, Ruiz-Menjivar J, Luo B, Liang Z, Swisher ME. Predicting climate change mitigation and adaptation behaviors in agricultural production: A comparison of the theory of planned behavior and the Value-Belief-Norm Theory. *J Environ Psychol.* 2020;68:101408.
doi: 10.1016/j.jenvp.2020.101408
64. Yazdanpanah M, Forouzani M. Application of the theory of planned behaviour to predict Iranian students' intention to purchase organic food. *J Clean Prod.* 2015;107:342-352.
doi: 10.1016/j.jclepro.2015.02.071
65. Hair JF, Hult GTM, Ringle CM, Sarstedt M, Thiele KO. Mirror, mirror on the wall: A comparative evaluation of composite-based structural equation modeling methods. *J Acad Mark Sci.* 2017;45:616-632.
doi: 10.1007/s11747-017-0517-x
66. Khoshmaram M, Shiri N, Shinnar RS, Savari M. Environmental support and entrepreneurial behavior among Iranian farmers: The mediating roles of social and human capital. *J Small Bus Manag.* 2020;58(5):1064-1088.
doi: 10.1111/jsbm.12501
67. Reidsma P, Ewert F, Lansink AO, Leemans R. Adaptation to climate change and climate variability in European agriculture: The importance of farm level responses. *Eur J Agron.* 2010;32:91-102.
doi: 10.1016/j.eja.2009.06.003
68. Westerhoff L, Smit B. The rains are disappointing us: Dynamic vulnerability and adaptation to multiple stressors in the Afram Plains, Ghana. *Mitig Adapt Strateg Glob Chang.* 2008;14:317-337.
doi: 10.1007/s11027-008-9166-1
69. Yaghoubi J, Yazdanpanah M, Komendantova N. Iranian agriculture advisors' perception and intention toward biofuel: Green way toward energy security, rural development and climate change mitigation. *Renew Energy.* 2019;130:452-459.
doi: 10.1016/j.renene.2018.06.081

Asian Journal of Water, Environment and Pollution. Vol. 22, No. 2 (2025), pp. 114-124.
doi: 10.36922/AJWEP025060033

ORIGINAL RESEARCH ARTICLE

Utilization of treated wastewater from sewage treatment plants as a replacement for potable water in concrete mix

Jitin Vasudeva, Mrunmyee Manjari Sahoo*, and Jaspreet Singh
School of Civil Engineering, Lovely Professional University, Kapurthala, Punjab, India
***Corresponding author:** Mrunmyee Manjari Sahoo (Mrunmayee.23405@lpu.co.in)

Received: February 3, 2025; 1st revised: March 15, 2025; 2nd revised: March 22, 2025; Accepted: March 24, 2025; Published Online: April 15, 2025

Abstract: With only 0.5% of Earth's water being potable and increasing demand driven by urbanization and construction, there is an urgent need to identify sustainable alternatives to freshwater for concrete production. This study examines the use of purified sewage water from a 10 million liters-per-day sewage treatment plant at Bambianwali, which employs sequential batch reactor technology, as a substitute for potable water in concrete mixing. An extensive analysis was conducted over a 3-year period (2021 – 2023) to evaluate the suitability of treated sewage water for concrete production. Water quality parameters analyzed included pH, temperature, total suspended solids, chemical oxygen demand, biological oxygen demand, fecal coliform, and total Kjeldahl nitrogen. Plain cement concrete cubes were prepared and tested for compressive strength using three different water mixtures: 100% potable water, a 60:40 mixture of primary treated wastewater and potable water, and a 60:40 mixture of secondary treated wastewater and potable water. After 28 days of curing, the concrete cubes prepared with secondary treated wastewater in a ratio of 60:40 achieved a characteristic strength of 22.03 N/mm^2, compared to 23.96 N/mm^2 for cubes made with 100% potable water. In contrast, cubes made with primary treated wastewater showed a reduced strength of 17.30 N/mm^2. These findings indicate that secondary treated sewage water can serve as a feasible substitute for potable water in concrete mixing, though the compressive strength of resulting concrete may vary depending on the extent of treatment applied to the water.

Keywords: Sewage water; Concrete production; pH; Temperature; Total suspended solids; Chemical oxygen demand; Biological oxygen demand; Fecal coliform

1. Introduction

The phrase "elixir of life" aptly describes water. Although water covers over 71% of the Earth's surface, only 3% of it is categorized as freshwater. Of this small fraction, roughly 80% is locked in polar ice caps and remains inaccessible. As a result, only approximately 0.5% of the Earth's water is considered potable and safe for human consumption.[1]

Over the past century, global water scarcity has become a critical issue, driven by factors such as overcrowding, urbanization, pollution, climate change, inadequate freshwater management, and environmental degradation.[2] In parallel, water plays an important role in the production of cement-based materials, such as paste, mortar, and concrete.[3] Concrete is produced by combining water with inert ingredients (coarse and fine particles) and binding agents (Portland cement

or asphalt). Globally, the concrete industry consumes almost one trillion gallons of water annually.[4]

While an adequate water supply is essential to generate a workable concrete mix that can be properly mixed, placed, compacted, and finished, using less water generally results in superior concrete with improved strength characteristics.[5] Water is also required for various concrete-related processes, including aggregate washing, cleaning of batching plants, and rinsing of concrete mixer trucks.[6]

Cement-based materials can be produced using any potable water, provided it contains no harmful levels of acids, salts, alkalis, oils, sugar, or organic compounds.[7] Water that is highly alkaline or acidic, contains algae, or has elevated chloride concentrations[8] should be avoided, as it can negatively impact the setting, hardening, and strength development of concrete.

Due to the increasing scarcity of potable water, the search for alternative sources has gained momentum.[9] Potential substitutes often contain higher concentrations of dissolved chemicals and suspended particulates and include sources such as saltwater, treated industrial wastewater, treated sewage wastewater, wastewater from carwash service stations, runoff from ready-mix concrete plants, and wastewater from stone-cutting operations.[10] When adequately treated, all of these water resources have been shown to produce concrete with acceptable strength and durability.[6] Water usage in the construction industry is nearly proportional to concrete production.[7] As a result, using partially or fully treated wastewater in concrete manufacturing could reduce the demand for potable water and lower the cost associated with wastewater treatment.[11] Despite environmental and public health concerns, wastewater continues to be used in concrete applications in various regions. Treated sewage wastewater refers to domestic, municipal, and industrial wastewater that has undergone treatment to remove all pollutants and suspended particles before discharge into the environment.[12] Producing such treated effluent requires a combination of physical, chemical, and biological treatment processes to ensure compliance with environmental safety standards.[13] A by-product of this process is sewage sludge, a semi-solid waste that requires further treatment before it can be safely disposed of on land.[12]

Reclaimed water, often referred to as recycled water, is wastewater that has been treated to remove suspended and solid particles. It has a wide range of applications, such as irrigation, concrete production, groundwater replenishment, and landscaping.[14] Sludge generated during this process is often mixed with biowaste to produce compost, which is widely used in agriculture.[15] In some cases, reclaimed wastewater can even be used to cultivate spirulina.[16]

This study focuses on the use of recycled wastewater in the production and curing of concrete. In addition to environmental benefits, the use of treated wastewater in concrete manufacturing may offer financial advantages. By introducing the construction industry—a constantly expanding sector in most economies – as a key consumer of treated wastewater, investment in wastewater treatment and reuse technologies can be further incentivized.[17,18] The current research aims to:

- Investigate the potential applications of various wastewater sources, including treated industrial and sewage water, for use in the production and curing of concrete.
- Evaluate the durability and strength of concrete structures when treated wastewater is used in place of potable water.
- Analyze the economic benefits of employing sewage treatment plants (STPs) in concrete manufacturing, particularly in reducing potable water consumption and sewage water treatment costs.
- Assess the potential health risks and environmental impacts associated with the use of treated wastewater in concrete construction.
- Explore the potential for expanding treated wastewater markets and investment opportunities by targeting the construction sector as a major consumer.

2. Materials and methods

This study was based on the characterization of wastewater and the evaluation of concrete prepared using treated wastewater as a replacement for potable water. The primary materials investigated were treated wastewater and concrete, both of which underwent detailed laboratory analysis.

2.1. Sampling

To ensure high quality and strict compliance with environmental standards, treated sewage water samples were collected daily from the outlet of 10 million liters-per-day (MLD) STP in Bambianwali. These samples underwent comprehensive and rigorous laboratory analysis to determine critical parameters, such as pH, total suspended solids (TSS), chemical (COD) and biological oxygen demand (BOD), and the concentrations of key nutrients such as sulfate, chloride, sodium, nitrate, and fecal coliform (F. coli) (Figure 1 & 2).

2.2. Concrete cube sampling and curing

Concrete was prepared by mixing cement with samples of both primary and secondary treated wastewater. The fresh concrete was then cast into standard molds. These molds were subsequently cured in water for 7, 14, and 28 days. After each curing period, the concrete cubes were tested to evaluate their physical and mechanical properties.

2.3. Analysis of concrete cubes

To evaluate the properties of cement concrete, various laboratory tests were performed. The parameters tested and the associated test methods are listed in Table 1.

To prepare the concrete samples, treated wastewater obtained from the 10 MLD STP at Bambianwali was mixed with potable water in the following ratios:

(i) 100% potable water
(ii) 60:40 mixture of primary treated domestic wastewater (mechanical) and potable water
(iii) 60:40 mixture of secondary treated domestic wastewater (biological) and potable water.

Concrete cubes were cast using each water combination and subsequently tested to assess their properties.

3. Results and discussion

This section presents a comprehensive analysis of the wastewater samples collected over a 3-year period from the outlet of the 10 MLD STP at Bambianwali. It also includes a performance assessment of concrete cubes prepared using potable water, primary treated wastewater, and secondary treated wastewater.

3.1. Analysis of treated sewage water parameters (April 2021 – March 2022)

3.1.1. pH

The pH values of the treated wastewater from the 10 MLD STP at Bambianwali (Figure 3) were monitored monthly and exhibited consistent results throughout the year. In April, the mean pH was 7.15, closely aligning with the median of 7.16, indicating slightly alkaline conditions. May recorded a mean and median of 7.18, indicating stable pH levels. In June, the mean pH was 7.16, and the median was 7.17, maintaining the same trend. A slight decrease was observed in July, with both mean and median values at 7.13. In August, the mean was 7.15, and the median was 7.16, while in September, both values stood at 7.14. In October, the mean was 7.13, with a median of 7.14. November showed a slight increase, with a mean of 7.17 and a median of 7.13. Finally, in December, the mean pH was 7.13, and the median was 7.14. Overall, the pH values remained within a narrow range, demonstrating effective treatment and consistent effluent quality. The complete pH values for the 31-months period (April 2021 to October 2023) are presented in Figure 4.

Table 1. Tests conducted for concrete property analysis

Serial no.	Parameter	Test performed
1	Workability	Slump test
2	Compressive strength	Load test

3.1.2. Temperature

Figure 5 presents the monthly mean and median temperatures over the 3-year study period, including April 2021 – March 2022. In April, the mean temperature was 26.82°C, with a slightly higher median of 27.355°C. Temperatures increased in May, reaching a mean of 28.09°C and a median of 28.22°C. This upward trend continued in June (mean: 28.66°C; median: 28.81°C) and July (mean: 28.80°C; median: 28.90°C). The highest temperatures were recorded in August, with a mean of 29.42°C and a median of 29.35°C. A gradual decline began in September (mean: 28.46°C; median: 28.62°C), followed by a more noticeable decrease in October (mean and median: 27.00°C). Cooling continued through November (mean: 25.93°C; median: 26.10°C), and reached the lowest values in December (mean: 20.68°C; median: 20.29°C). A slight increase was observed in January (mean: 21.14°C; median: 21.19°C), with further increases in February (mean: 21.39°C; median: 20.94°C) and March (mean: 23.29°C; median: 23.11°C). Overall, the data exhibit a clear seasonal pattern, with peak temperatures in the summer and lower values in the winter, consistent with the regional climate.

3.1.3. TSS

Figure 6 illustrates the monthly mean and median values of TSS for April 2021 – March 2022, highlighting trends in water quality. The mean TSS values ranged from 16.42 to 17.14 mg/L, with the lowest observed in November and the highest in December. Median values were relatively stable around 17 mg/L, except in August, where a drop to 16.5 mg/L indicated a slight decline in central tendency. In other months – April, May, June, July, September, and October – the median remained stable (17 mg/L),

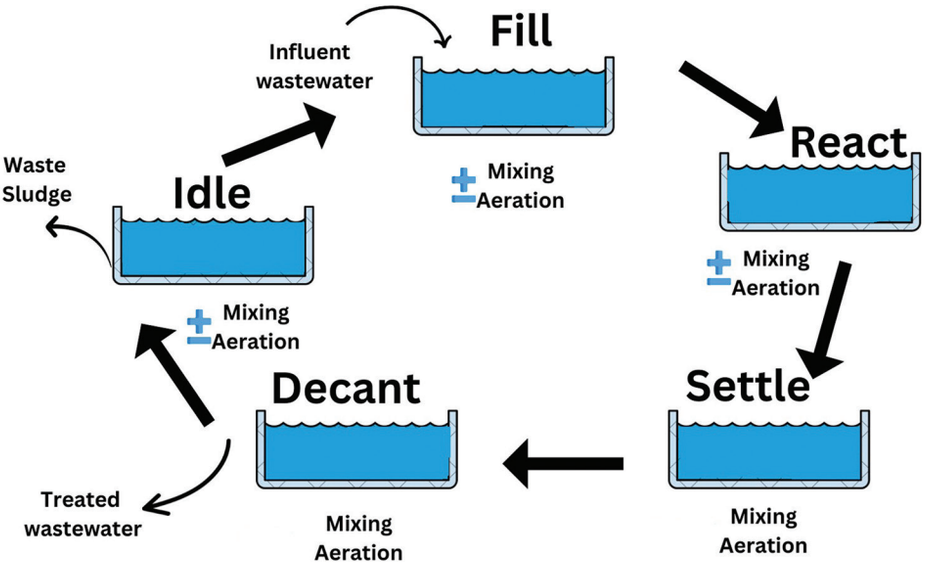

Figure 1. Phases of sequencing batch reactor operational cycle

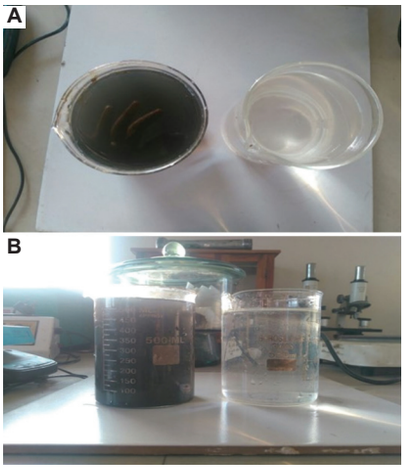

Figure 2. (A and B) Represent both Inlet and Outlet samples from the 10 million liters-per-day sewage treatment plant at Bambianwali, Jalandhar

Figure 3. Sequencing batch reactor basin of the 10 mL/day sewage treatment plant at Bambianwali, Jalandhar, during the aeration and filling phase

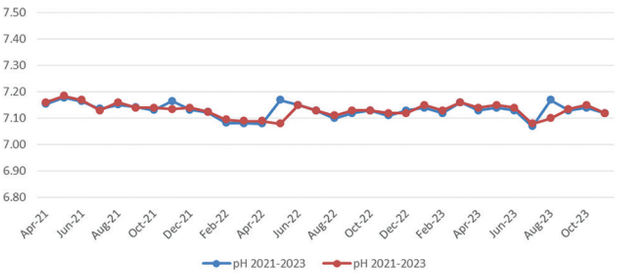

Figure 4. pH values of treated wastewater from the 10 million liters-per-day sewage treatment plant at Bambianwali (2021 – 2023)

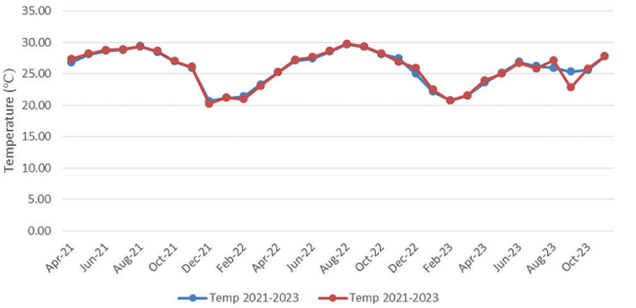

Figure 5. Temperature (Temp) values of treated wastewater from the 10 million liters-per-day sewage treatment plant at Bambianwali (2021 – 2023)

suggesting consistent water quality despite minor fluctuations in mean values. These TSS measurements are important for environmental monitoring, regulatory compliance, and water resources management.

3.1.4. Chemical oxygen demand

Figure 7 presents the monthly mean and median COD

levels in wastewater used for cement production from April 2021 to March 2022, in reference to water transport standards. The mean COD values consistently ranged from 38 to 41 mg/L, indicating a stable central tendency across most months. COD is an important parameter for assessing the concentration of organic pollutants in wastewater, particularly in evaluating its suitability for industrial reuse, such as cement production. Maintaining COD levels within regulatory limits helps environmental degradation and ensures compliance with quality standards. The data reveal monthly fluctuations in COD levels and serve as a basis for informed environmental management decisions.

3.1.5. BOD

Figure 8 presents the monthly BOD values from April 2021 – March 2022. BOD levels ranged from a low of 7.0 mg/L in December to a high of 7.54 mg/L in October. Median BOD values remained relatively consistent between 7 mg/L and 8 mg/L across the study period, reflecting overall stability in organic pollutant load. July exhibited a median BOD of 8.0 mg/L, indicating a typical seasonal peak. BOD is a key indicator of organic contamination and plays a critical role in evaluating water quality, regulatory compliance, and environmental management. These monthly data highlight seasonal trends in BOD and offer insights for ongoing water quality monitoring and management.

3.1.6. F. coli

Figure 9 summarizes the monthly F. coli counts from April 2021 – March 2022, which are used to assess water quality, particularly in relation to potable water and public health standards. The mean F. coli counts ranged from 542.5 colony-forming units (CFU)/100 mL in December to 642.5 CFU/100 mL in June, indicating seasonal variability in bacterial contamination. Median values followed a similar trend, ranging from 540 CFU/100 mL in December to 645 CFU/100 mL in June. July recorded a median count of 595 CFU/100 mL, indicating heightened microbial presence during that period. F. coli levels are crucial indicators of potential waterborne health risks and are essential for environmental monitoring and regulatory compliance. The data highlight monthly fluctuations in F. coli levels and inform public health interventions aimed at safeguarding water quality year-round.

3.1.7. Total Kjeldahl nitrogen (TKN)

Figure 10 presents the monthly concentrations of TKN

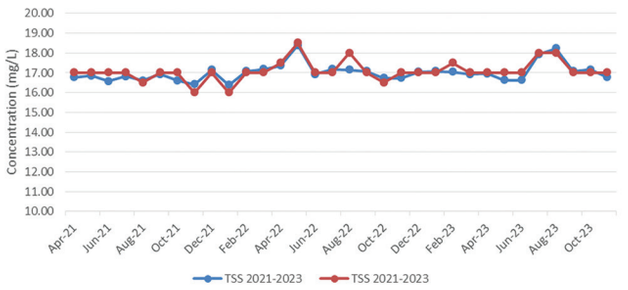

Figure 6. Total suspended solid values of treated wastewater from the 10 million liters-per-day sewage treatment plant at Bambianwali (2021 – 2023)

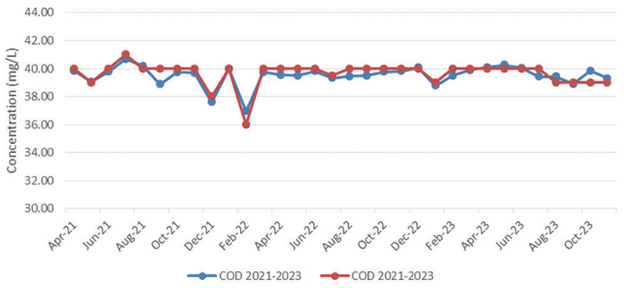

Figure 7. Chemical oxygen demand values of treated wastewater from the 10 million liters-per-day sewage treatment plant at Bambianwali (2021 – 2023)

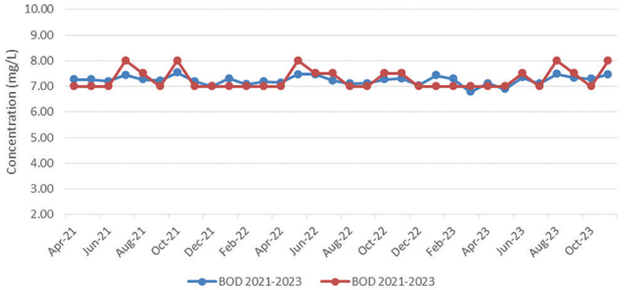

Figure 8. Biochemical oxygen demand (BOD) values of treated wastewater from the 10 million liters-per-day sewage treatment plant at Bambianwali (2021 – 2023)

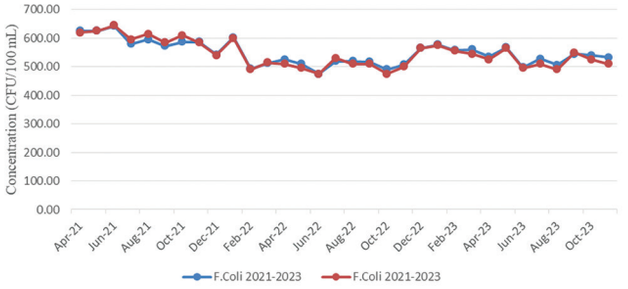

Figure 9. Fecal coliform values of treated wastewater from the 10 million liters-per-day sewage treatment plant at Bambianwali (2021 – 2023)

from April 2021 – March 2022. TKN is commonly used in water quality assessment and environmental monitoring as an indicator of nitrogen pollution. The mean and median TKN values ranged from 2.25 mg/L in May to 3.5 mg/L in December, showing notable variation across the year. Median TKN concentrations ranged from 2.0 mg/L in May to 3.5 mg/L in both June and September, indicating significant monthly trends. In July and November, TKN concentrations were 2.5 mg/L, reflecting relative stability in those months. These measurements are important for assessing nitrogen loading in water bodies, and can inform environmental policies and strategies for maintaining water quality standards. The data highlight monthly fluctuations in TKN, offering insights into seasonal variation in nitrogen levels over the 12-month period.

3.2. Analysis of treated sewage water parameters (April 2022 – March 2023)

3.2.1. pH

The pH values from April 2022 to March 2023 show slight fluctuations, as indicated by the mean and median values. The mean of pH in April was 7.08, and the median was 7.09. This was slightly higher in May, with mean of 7.17 and median was 7.08. In June, the mean fell slightly to 7.15, although the median was also 7.15. A more notable improvement occurred in July, with mean value as 7.13 and a median of 7.13, and even further improved in August with the values of mean and median as 7.10 and 7.11 respectively. In September the pH values increased again, with mean as 7.12 and median as 7.13. This rise continued in October, with an mean of 7.13 and median also as 7.13. Finally, November pH levels dropped slightly to mean of 7.11 and a median of 7.12. The similar range was observed from December 2022 to March 2023. Overall, the data show small changes in pH levels over the period of 12 months, with values generally staying around a neutral pH of 7.

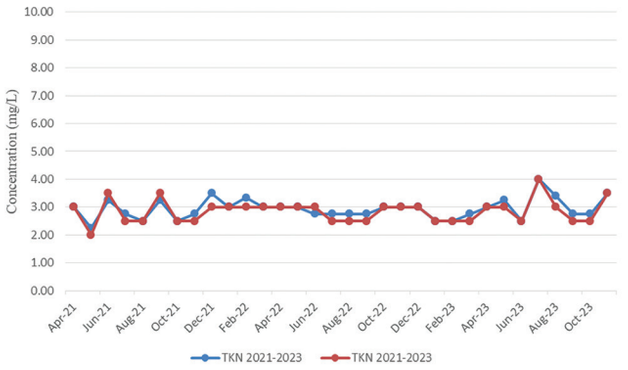

Figure 10. Total Kjeldahl nitrogen values of treated wastewater from the 10 million liters-per-day sewage treatment plant at Bambianwali (2021 – 2023)

3.2.2. Temperature

Figure 5 presents the monthly temperatures of treated sewage water over a 1-year period (April 2022 – March 2023). These data are important for assessing the suitability of sewage reuse in cement production, particularly from environmental and operational perspectives. Temperatures ranged from 20.71°C in February to 29.8°C in August, with a peak of 28.64°C recorded in July. Seasonal temperature fluctuations can affect sludge properties and influence the performance of cement manufacturing processes. The data highlight the importance of controlling temperature fluctuations throughout the year to ensure efficient sludge handling, consistent cement quality, and environmentally sustainable operations.

3.2.3. TSS

Figure 6 illustrates the monthly variation of TSS concentrations from April 2022 – March 2023, reflecting the quality of treated wastewater used in cement production. Mean TSS concentrations ranged from 16.73 mg/L in October to 18.38 mg/L in May, indicating seasonal variation in suspended solids. Median TSS values also fluctuated, ranging from 16.5 mg/L in October to 18.5 mg/L in May, with relatively stable levels of 17.5 mg/L in February and August. Monitoring TSS is critical for determining the suitability of wastewater in industrial processes, including cement production, and for ensuring compliance with environmental regulations. These data offer valuable insights into seasonal trends and help guide effective environmental management in industrial processes.

3.2.4. Chemical oxygen demand

Figure 7 shows the monthly COD values of treated wastewater from April 2022 – March 2023. COD is a key indicator of organic pollutant load and is essential in evaluating the environmental suitability of wastewater for reuse in cement production. Most months showed relatively consistent COD values around 40 mg/L, indicating a stable central tendency. A slight decrease to approximately 39 mg/L was observed in February.

3.2.5. BOD

Figure 8 presents the monthly BOD levels from April 2022 – March 2023. These values are relevant for assessing the suitability of treated sewage water

for cement production, particularly with respect to environmental regulations and water quality standards. Mean BOD values ranged from a low of 6.78 mg/L in March to a high of 7.47 mg/L in May and June, indicating moderate fluctuations in organic pollutant levels. Median BOD values followed a similar trend, ranging from 7.00 mg/L in April and December to 7.50 mg/L in June, July, October, and November, suggesting a generally consistent trend with occasional peaks.

3.2.6. F. coli

Figure 9 shows the monthly mean and median of F. coli concentrations from April 2022 – March 2023. These measurements are important for assessing microbial contamination and determining whether treated wastewater meets environmental and public health standards for industrial reuse. The mean F. coli count in April was 525 CFU/100 mL, with a median of 510, indicating a moderate bacterial load. In May and June, the means decreased to 510 CFU/100 mL and 475 CFU/100 mL, respectively, indicating a temporary reduction in bacterial contamination. A slight increase occurred in July, followed by relatively stable values in August (520 CFU/100 mL) and September (517.5 CFU/100 mL), with medians consistently around 510 CFU/100 mL. October shows a slight decrease, with a mean of 490 and a median of 475 CFU/100 mL. In contrast, November and December recorded increases, with mean values of 507.5 and 565 CFU/100 mL, respectively. January and February showed the highest levels, with means of 577.5 and 557.5 CFU/100 mL, and medians of 575 and 555 CFU/100 mL, respectively – indicating elevated bacterial contamination during winter.

3.2.7. TKN

Figure 10 provides the monthly mean and median concentrations of TKN from April 2022 – March 2023. These values are relevant for assessing nitrogen levels in wastewater and its potential environmental impact when reused in cement production. TKN concentrations remained relatively stable throughout the year, generally ranging between 2.5 and 3.0 mg/L. The mean values were consistently close to 3.0 mg/L from April to November and again from December to March, with slight decreases observed in January, February, and March. Median TKN values followed a similar trend, with TKN concentrations remaining around 3 mg/L for most of the year. However, in July, August, and September, the median values dropped slightly to 2.5 mg/L, indicating minor seasonal variation. Overall, the data suggest a relatively stable nitrogen profile in treated sewage water, with only limited fluctuation.

3.3. Analysis of treated sewage water parameters (April – November 2023)

3.3.1. pH

Figure 4 displays the monthly mean and median pH values from April to November 2023. The pH values show minor fluctuations throughout the period, generally remaining close to neutral. In April, the mean and median pH were 7.13 and 7.14, respectively. May showed a slight increase, with values of 7.14 (mean) and 7.15 (median). In June, both the mean and median slightly declined to 7.13 and 7.14, respectively, with July recording a mean of 7.07 and a median of 7.08, and August showing values of 7.07 (mean) and 7.09 (median). In September, both the mean and median increased again to 7.13. This upward trend continued in October with mean and median values of 7.14 and 7.15, respectively. November recorded a slight drop to 7.12 for both mean and median. Overall, the data indicate minor monthly variations in pH, with values consistently near neutral.

3.3.2. Temperature

Figure 5 presents the monthly mean and median temperatures of treated sewage water from April to November 2023. In April, the mean temperature was 23.57°C, with a mean of 23.96°C. Temperatures rose in May, reaching 25.16°C (mean) and 24.99°C (median), and continued to increase in June to 26.86°C and 26.73°C, respectively. A slight decrease occurred in July, with temperatures of 26.24°C (mean) and 25.86°C (median). August showed mean and median temperatures of 25.92°C and 27.15°C, respectively, indicating an unusual spike. September recorded a slight decline, with a mean of 25.33°C and a sharp decline in the median to 22.81°C. October temperatures stabilized at 25.62°C (mean) and 25.82°C (median). November recorded the highest temperatures of the period, with both mean and median at 27.80°C. These data suggest fluctuations in temperature stability, particularly in August and September, where deviations from the overall trend were more pronounced.

3.3.3. TSS

Figure 6 presents the monthly mean and median values of TSS in treated sewage water from April to November 2023. In April, the mean TSS was 16.96 mg/L, with a median of 17 mg/L. In May, the mean slightly decreased to 16.63 mg/L, while the median remained stable at 17 mg/L. June recorded

a mean TSS of 16.62 mg/L, with the median again at 17 mg/L. A significant increase occurred in July, where the mean rose to 17.94 mg/L and the median to 18 mg/L. August continued this upward trend, with a mean of 18.23 mg/L and a median of 18 mg/L. In September, the mean decreased to 17.07 mg/L, and in October, the mean was 17.16 mg/L while the median returned to 17 mg/L. Finally, in November, the mean TSS was 16.77 mg/L, with the median still at 17 mg/L. Overall, while minor fluctuations were observed, the TSS values consistently hovered around 17 mg/L, with July and August showing slightly elevated levels (18 mg/L).

3.3.4. Chemical oxygen demand

Figure 7 presents the monthly mean and median values of COD in treated sewage water from April to November 2023. In April, the mean COD was 40.08 mg/L, and the median was 40 mg/L. A slight increase was recorded in May, with the mean rising to 40.26 mg/L, while the median remained unchanged. In June, values remained stable at 40.04 mg/L (mean) and 40 mg/L (median). A sharp decrease occurred in July, with the mean dropping to 39.42 mg/L and the median to 39 mg/L. In August, the mean further decreased to 39 mg/L, while the median remained stable at 39 mg/L. September showed a continued decrease, with a mean of 38.9 mg/L and a median of 39 mg/L. In October, the mean increased slightly to 39.84 mg/L, with the median remaining unchanged at 39 mg/L. Finally, in November, the mean and median values were 39.3 mg/L and 39 mg/L, respectively. These results indicate a gradual downward trend in COD levels over the study period, with relatively low variation in median values compared to the mean.

3.3.5. Biochemical oxygen demand

Figure 8 presents the monthly mean and median values of BOD from April to November 2023, showing generally stable trends with minor fluctuations. In April, the mean BOD was 7.12 mg/L and the median was 7.00 mg/L. In May, the mean slightly decreased to 6.89 mg/L, while the median remained stable at 7.00 mg/L. In June, the mean increased to 7.35 mg/L and the median rose to 7.5 mg/L. July recorded a slight decrease, with the mean dropping to 7.10 mg/L and the median returning to 7.00 mg/L. A noticeable increase occurred in August, with the mean reaching 7.48 mg/L and the median increasing to 8.00 mg/L. In September, the mean was 7.33 mg/L, and the median remained at 7.5 mg/L. October saw the mean drop slightly to 7.29 mg/L, while the median returned to 7.00 mg/L. Overall, the BOD values remained fairly consistent, with a peak observed in August and November.

3.3.6. F. coli

Figure 9 presents the monthly and median values of F. coli concentrations from April to November 2023. In April, the mean was 535 CFU/100 mL and the median was 525 CFU/100 mL. Both values increased sharply in May, with the mean reaching 567.5 CFU/100 mL and the median 565 CFU/100 mL. In June, values decreased to 497.5 CFU/100 mL (mean) and 495 CFU/100 mL (median). In September, the mean was 550 CFU/100 mL. In October, the mean slightly decreased to 540 CFU/100 mL, while the median settled at 525 CFU/100 mL. In November, both values decreased further, with the mean at 532.5 CFU/100 mL and the median at 510 CFU/100 mL. These data indicate general fluctuations in F. coli concentrations, with peaks occurring from May to September and relatively lower levels in June – August.

3.3.7. TKN

Figure 10 presents monthly variations in TKN concentrations from April to November 2023. In April, both the median and median TKN values were 3.0 mg/L. In May, the mean increased slightly to 3.25 mg/L, while the median remained at 3.0 mg/L. In June, both values decreased to 2.5 mg/L. July recorded the highest TKN values of the study period, with both the mean and median at 4.00 mg/L. In August, the mean decreased to 3.4 mg/L, while the median dropped to 3.0 mg/L. In September and October, the mean was 2.75 mg/L, and the median was 2.5 mg/L. Finally, in November, both values rose again to 3.5 mg/L. Overall, the TKN levels showed general stability, with moderate fluctuations and a peak observed in July.

3.4. Concrete mixed with 100% potable water

Concrete cubes were prepared using a mixture of cement, sand, and aggregate, combined with 100% potable water. The mixture was poured into 150 mm cube molds and manually mixed. After curing, a load test was performed to obtain baseline strength for comparison in future tests (Figure 11 and Table 2).

3.5. Concrete mixed with primary treated wastewater and potable water (60:40 ratio)

Concrete cubes were prepared by combining cement, sand, aggregate, and a mixture of 60% primary treated wastewater and 40% potable water. The mixture was

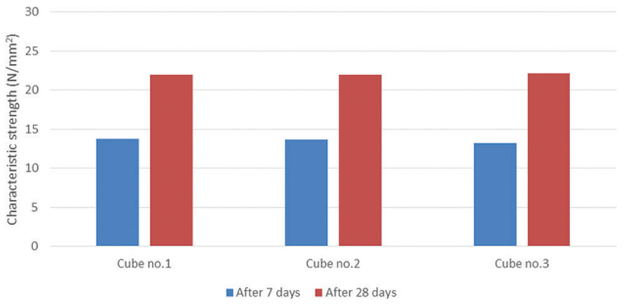

Figure 11. Characteristic strength of concrete mixed with 100% potable water

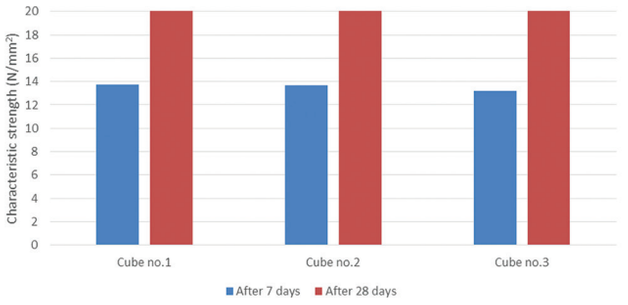

Figure 12. Characteristic strength of concrete mixed with primary treated wastewater and potable water (60:40 ratio)

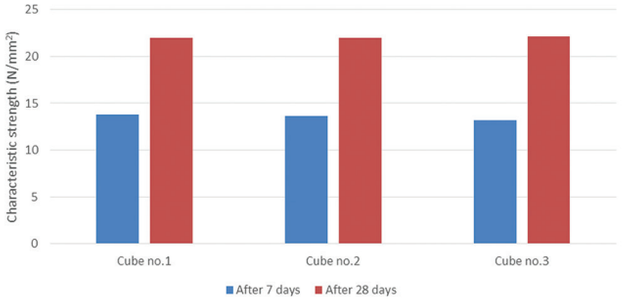

Figure 13. Characteristic strength of concrete mixed with secondary treated wastewater and potable water (60:40 ratio)

poured into a 150 mm cube mold and subsequently subjected to a load test. To facilitate interpretation of the results, a bar chart was created (Figure 12 and Table 3).

3.6. Concrete mixed with secondary treated wastewater and potable water (60:40 ratio)

Concrete cubes were prepared by mixing cement, sand, aggregate, and a water blend consisting of 60% secondary treated wastewater and 40% potable water. The mixture was poured into 150 mm cube molds and subjected to load testing. The results were visualized using a bar chart (Figure 13 and Table 4).

Table 2. Strength of concrete mixed with 100% potable water

Characteristic strength of concrete (N/mm²)	After 7 days	After 28 days
Cube no. 1	13.11	23.75
Cube no. 2	13.91	24.28
Cube no. 3	13.77	23.85

Table 3. Strength of concrete mixed with primary treated wastewater and potable water (60:40 ratio)

Characteristic strength of concrete (N/mm²)	After 7 days	After 28 days
Cube no. 1	13.77	17.00
Cube no. 2	13.77	17.22
Cube no. 3	13.44	17.66

Table 4. Strength of concrete mixed with secondary treated wastewater and potable water (60:40 ratio)

Characteristic strength of concrete (N/mm²)	After 7 days	After 28 days
Cube no. 1	13.77	21.99
Cube no. 2	13.66	22.00
Cube no. 3	13.22	22.11

3.7. Economic consideration

According to the mix design for M-20 grade concrete, approximately 142 L of water is required per 1 cubic meter (cum) of concrete. The primary rationale for introducing treated sewage water is to reduce the consumption of potable water and promote sustainability. By replacing 60% of the required water, approximately 85 L of potable water can be saved per 1 cum of concrete. As the current commercial rate of Rs 20/1,000 L, this results in a saving of Rs 1.70/cum. Therefore, for 1,000 cum of concrete produced, 85 kL of potable water can be saved – resulting in a total cost saving of approximately Rs 1,700. This approach not only supports economic efficiency but also conserves vital freshwater resources for future generations, especially given the rising cost of water treatment and distribution.

4. Conclusion

The study showcases that treated sewage water from the STP at Bambianwali can efficiently substitute potable water in concrete production, thereby supporting

sustainable water management practices. Continuous water quality monitoring over a 3-year period confirms the reliability of the treated sewage water for industrial uses. Concrete cubes mixed with secondary treated wastewater demonstrated strength comparable to those mixed with potable water, suggesting its viability as an alternative in concrete mixing. This strategy not only conserves potable water but also encourages the reuse of treated wastewater, in line with broader environmental sustainability goals. This practice could result in water savings of approximately 85 L/1 cum of concrete, translating to a cost saving of approximately Rs 1,700/1,000 cum of concrete. This approach can play a crucial role in ensuring the availability of potable water for future generations, especially given the rising cost associated with its treatment and distribution. Future research should prioritize the examination of the long-term durability and performance of concrete produced with treated sewage water to fully establish its suitability for widespread use in the construction industry.

Acknowledgments

None.

Funding

None.

Conflict of interest

The authors declare no conflicts of interest.

Author contributions

Conceptualization: All authors
Formal analysis: Jitin Vasudeva
Investigation: Jitin Vasudeva
Methodology: All authors
Writing – original draft: Jitin Vasudeva
Writing – review & editing: All authors

Availability of data

The data this article are available from the corresponding author upon reasonable request.

References

1. Micheal A, Salam HA. Reliability of using secondary and tertiary treated wastewater in concrete mixing and curing. *Environ Dev Sustain*. 2024;26:31657-31676. doi: 10.1007/s10668-024-04613-6
2. Hamada HM, Shi J, Abed F, Al Jawahery MS, Majdi A, Yousif ST. Recycling solid waste to produce eco-friendly ultra-high performance concrete: A review of durability, microstructure and environment characteristics. *Sci Total Environ*. 2023;876:162804-162804. doi: 10.1016/j.scitotenv.2023.162804
3. Maroušek J, Marouškova A, Zoubek T, Bartoš P. Economic impacts of soil fertility degradation by traces of iron from drinking water treatment. *Environ Dev Sustain*. 2021;24:1-10. doi: 10.1007/s10668-021-01636-1
4. Gokulanathan V, Arun K, Priyadharshini P. Fresh and hardened properties of five non-potable water mixed and cured concrete: A comprehensive review. *Construct Build Mater*. 2021;309:125089. doi: 10.1016/j.conbuildmat.2021.125089
5. Mangi SA, Makhija A, Raza MS, Khahro SH, Jhatial AA. *A Comprehensive Review on Effects of Seawater on Engineering Properties of Concrete*. California: Silicon Publishing Inc.; 2020. doi: 10.1007/s12633-020-00724-7
6. Maroušek J, Marouškova A. Economic considerations on nutrient utilization in wastewater management. *Energies*. 2021;14(12):3468. doi: 10.3390/en14123468
7. Akbari M, Loganathan N, Tavakolian H, Mardani A, Štreimikienė D. The dynamic effects of micro-structural shocks on private investment behaviour. *Acta Mont Slov*. 2021;26(1):1-17. doi: 10.46544/AMS.v26i1.01
8. Pavolová H, Bakalár T, Kyšeľa K, Klimek M, Hajduová Z, Zawada M. The analysis of investment into industries based on portfolio managers. *Acta Mont Slov*. 2021;(26):161-170. doi: 10.46544/ams.v26i1.14
9. Varshney H, Khan RA, Khan IK. Sustainable use of different wastewater in concrete construction: A review. *J Build Eng*. 2021;41:102411. doi: 10.1016/j.jobe.2021.10241
10. Hassani MS, Asadollahfardi G, Saghravani SF, Jafari S, Peighambarzadeh FS. The difference in chloride ion diffusion coefficient of concrete made with drinking water and wastewater. *Construct Build Mater*. 2020;231:117182-117182. doi: 10.1016/j.conbuildmat.2019.117182
11. Govindarajan ND, None Anubama S, Arun N, None Arun G. Utilization of reclaimed sewage water in concrete. *Int J Eng Res*. 2020;9(2). doi: 10.17577/ijertv9is020347
12. Liu Y, Zhuge Y, Chow CW, *et al*. Utilization of drinking water treatment sludge in concrete paving blocks: Microstructural analysis, durability and leaching properties. *J Environ Manag*. 2020;262:110352. doi: 10.1016/j.jenvman.2020.110352

13. Ghrair AM, Heath A, Paine K, Al Kronz M. Waste wash-water recycling in ready mix concrete plants. *Environments*. 2020;7(12):108. doi: 10.3390/environments7120108
14. Roychand R, Kumar Pramanik B, Zhang G, Setunge S. Recycling steel slag from municipal wastewater treatment plants into concrete applications-a step towards circular economy. *Resour Conserv Recycl*. 2020;152:104533. doi: 10.1016/j.resconrec.2019.104533
15. He X, Zheng Z, Ma M, *et al*. New treatment technology: The use of wet-milling concrete slurry waste to substitute cement. *J Clean Prod*. 2020;242:118347-118347. doi: 10.1016/jjclepro.2019.118347
16. Asadollahfardi G, Mahdavi AR. The feasibility of using treated industrial wastewater to produce concrete. *Struct Concrete*. 2018;20(1):123-132. doi: 10.1002/suco.201700255
17. Crini G, Lichtfouse E. Advantages and disadvantages of techniques used for wastewater treatment. *Environ Chem Lett*. 2018;17. doi: 10.1007/s10311-018-0785-9
18. Al-Joulani MA. Effect of using tertiary treated wastewater from nablus wastewater treatment plant (NWWTP), on some properties of concrete. *Int J Innov Technol Explor Eng*. 2019;8(11):2460-2466. doi: 10.35940/ijitee.k1709.0981119

ACCSCIENCE PUBLISHING

Asian Journal of Water, Environment and Pollution. Vol. 22, No. 2 (2025), pp. 125-139.
doi: 10.36922/AJWEP025060032

ORIGINAL RESEARCH ARTICLE

Natural radioactivity and radiation risks of soils in Ali Al-Sharqi and Kumait, Iraq

Zahraa A. Ismail AL-Sudani[1]*, Sawsan Sherif[2], and Mazin Mohammed[3]

[1]Department of Physics, College of Science, University of Misan, Misan, Iraq
[2]Department of Physics, College of Education for Pure Sciences, University of Basrah, Basrah, Iraq
[3]Radiation Protection Center, Ministry of Environment, Baghdad, Iraq
***Corresponding author**: Zahraa A. Ismail AL-Sudani (zahraaismail@uomisan.edu.iq)

Received: February 3, 2025; 1st revised: March 10, 2025; 2nd revised: March 23, 2025; 3rd revised: March 30, 2025; Accepted: March 31, 2025; Published online: April 16, 2025

Abstract: Humans are subjected to natural radiation from external sources, such as radionuclides on Earth and cosmic radiation, as well as internal radiation from radionuclides integrated into the body. Radionuclide intake occurs mostly through the ingestion of food and water, as well as inhalation. The natural radioactivity in the soils of Ali Al-Sharqi and Kumait, two cities in Misan province, Iraq, were measured. The soil samples were collected from 47 Ali Al-Sharqi and Kumait areas, and levels of natural radionuclide were analyzed using a high-purity germanium detector. The average activity concentrations of radionuclides, radium-226, thorium-232, and potassium-40, were found to be 15.1 ± 2.5, 14.7 ± 2.4, and 180.8 ± 7.9 Bq/kg, respectively, for Ali Al-Sharqi. In Kumait, the corresponding values were 13.6 ± 2.1, 17.2 ± 2.4, and 193.6 ± 8.6 Bq/kg, respectively. Radiation risk parameters were also evaluated for both cities. The average radium equivalent activities for Ali Al-Sharqi and Kumait were 50.2 Bq/kg and 53.2 Bq/kg, respectively. Internal and external hazard indices were 0.2 and 0.1, while the gamma level index was 0.2 in both cities. In Ali Al-Sharqi, the absorbed gamma dose rates in the air (D_{in}, D_{out}, and D_{tot}) were 44.8, 23.5, and 68.3 nGy/h, the annual effective dose equivalents ($AEDE_{in}$, $AEDE_{out}$, and $AEDE_{tot}$) were 0.2, 0.02, and 0.2 mSv/y, the excess lifetime cancer risks ($ELCR_{in}$, $ELCR_{out}$, and $ELCR_{tot}$) were 0.8×10^{-3}, 0.1×10^{-3}, and 0.9×10^{-3}, and the annual gonadal dose equivalent was 165.3 μSv/y. In Kumait, the corresponding values were 47.2, 24.8, and 72 nGy/h, 0.2, 0.03, and 0.3 mSv/y, 0.8×10^{-3}, 0.1×10^{-3}, and 0.9×10^{-3}, and 175 μSv/y, respectively. These findings indicate that the measured levels of radioactivity and health hazard parameters in both cities were below the global average values reported by the United Nations Scientific Committee on the Effects of Atomic Radiation. Therefore, the natural radioactivity in the soils of the investigated areas does not pose a health risk to the public.

Keywords: Soil; Radionuclides; High-purity germanium; Dose rate; Ali Al-Sharqi.

1. Introduction

Radiation in the environment originates from two sources: natural and artificial. Natural radiation includes both cosmic and terrestrial components, while artificial radiation arises from nuclear weapon testing and nuclear accidents.[1] Cosmic radiation, which comes from cosmic rays, varies in intensity based on latitude and elevation. Natural terrestrial radiation in the Earth's crust is primarily caused by the decay of uranium-238, thorium-232 (^{232}Th), and potassium-40 (^{40}K). The concentration of natural radioactive materials in the soils

is not uniform and varies according to the types of rocks from which they originate.[2-4] Natural radiation accounts for roughly 87% of human radiation exposure, with the remaining exposure stemming from artificial sources.[5] It is crucial for individuals to be aware of the radiation risks posed by both natural and artificial radioactive sources. For example, radon gas and its decay products in soil, sediment, and building materials can lead to internal radiation exposure that harms the respiratory system.[6] Long-term exposure to both uranium and radium through inhalation can cause many health effects, including bone, cranial, and nasal tumors, due to radium exposure. On the other hand, exposure to thorium may lead to leukemia and hepatic, pancreatic, lung, skeletal, and kidney cancers.[7] Consequently, quantitative information on the distribution of radioactive materials in various parts of the world is essential for protecting human life from radiation exposure.[8] Numerous studies have been conducted worldwide to measure the levels of radionuclides in soil specimens and the radiation risks in Amman, Aqaba (Jordan),[9] Rize (Turkey),[10] Upper Egypt,[11] southwest of Nigeria,[12] North Lebanon,[13] Sicily (Italy),[14] Port Said (Egypt),[15] Tongliao (China),[16] Pshdar (Iraqi-Kurdistan),[17] Shabwah and Hadramout (Yemen),[18] Wassit (Iraq)[19] Kirkuk (Iraq),[20] Mounana (Gabon),[21] Rio de Janeiro (Brazil),[22] Kuwait,[23] North Waziristan (Pakistan)[24]; and (Taghdoua) Saudi Arabia.[25] However, the level of radioactivity in the cities of Ali Al-Sharqi and Kumait is unknown. This study is crucial as it aims to assess the radiation exposure levels in these cities. By measuring activity concentrations of radionuclides (radium-226 [^{226}Ra], ^{232}Th, and ^{40}K) in soil samples of Ali Al-Sharqi and Kumait cities using a high-purity germanium (HPGe) detector, the radiological hazard parameters were evaluated. These include radium equivalent activity (Ra_{eq}), internal and external hazard indices (H_{in} and H_{ex}), gamma level index (Iγ), absorbed gamma dose rates (D_{in}, D_{out}, and D_{tot}), annual effective dose equivalents ($AEDE_{in}$, $AEDE_{out}$, and $AEDE_{tot}$), excess lifetime cancer risks ($ELCR_{in}$, $ELCR_{out}$, and $ELCR_{tot}$), and annual gonadal dose equivalent (AGDE). The results of this study will provide baseline data for Ali Al-Sharqi and Kumait, which can serve as a foundation for future research in the region.

2. Materials and methods

2.1. The study area

The study area included the cities of Ali Al-Sharqi and Kumait, located in Misan province, Iraq. Ali Al-Sharqi is situated in the northeastern and northwestern parts of the Misan, between latitudes 32°4′0″and 32°16′0″N and longitudes 46°44′0″and 46°52′0″E. The city covers an area of 1,513 km^2 and had a population of 30,000, as of 2014. Kumait, located in the northwestern part of Misan province, lies between latitudes 31°56′00″ and 32°4′0″N and longitudes 46°44′0″and 46°56′0″E. It has an area of 1,554 km^2, with a population of 46,000 as of 2014.

2.2. Collection and preparation of samples

A total of 47 soil samples were collected (24 samples from Ali Al-Sharqi and 23 samples from Kumait). Each sample was collected from a 0 to 5 cm depth of the soil's surface at a predetermined location, as shown in Figure 1. The location coordinates were determined using an eTrex Vista HCX Global Positioning System with part number 20233 (Garmin, United States), as listed in Tables 1 and 2 and shown in Figures 2 and 3. The collected soil samples were placed in clean zip-lock bags, each labeled with a distinct code for identification. The samples were then transported to the lab for preparation. The samples were thoroughly mixed and sieved through a 75-μm mesh (200 mm × 50 mm) with the part number 60132000075 and serial number 03008399 (Retsch, Germany). The sieved samples were dried in a Herfy-28L electric oven (Denik Company, Korea) at 80°C for 2 h to eliminate moisture from the soil, followed by weighing. The samples were transferred into 500 mL Marinelli polyethylene beakers (GA-MA, United States), sealed with plastic tape to avoid the leakage of airborne radionuclides, and left to rest for 4 weeks. This waiting period allowed the daughter products to reach radioactive secular equilibrium with their parent isotopes (^{226}Ra and radon-222) before being analyzed using a gamma spectrometer.[26]

2.3. Analyzing samples and assessment of activity concentrations

The naturally occurring radionuclides in the soils were measured utilizing a gamma spectrometer system

Figure 1. Soil samples collection

Table 1. Natural radioactivity in soil specimens of Ali Al-Sharqi

Sample code	Sample location	Coordinates of location (GPS)		Radionuclide activity concentrations (Bq/kg)		
		Latitude (N)	Longitude (E)	^{226}Ra±S.D.	^{232}Th±S.D.	^{40}K±S.D.
S_1	Al-Saaeidia	32° 14×48.9″	46° 43×58.6″	16.7±2.8	17.5±3	158.9±8
S_2	Abd Al-Khan	32° 14×45.3″	46° 43×06.1″	8.7±1.6	14.6±1.9	198.1±8.3
S_3	Al-Akhua	32° 14×20.8″	46° 42×39.1″	13.2±2.4	14.2±2.6	169.8±6.8
S_4	Palestine	32° 13×48.5″	46° 41×57.4″	13.1±2.3	13.2±2.4	178.4±7.8
S_5	Al-Shiyahina	32° 13×01.3″	46° 41×24.8″	12.9±2.5	17.2±2.8	193.4±8.8
S_6	Al-Karima	32° 11×31.4″	46° 41×09.7″	16.1±3.3	17.5±2.6	175.7±7.4
S_7	Al-Hikma	32° 11×10.1″	46° 43×04.4″	12.9±2.1	17.2±2.5	179.2±9.6
S_8	Al-Shahid Hikma	32° 10×59.6″	46° 42×49.6″	13.4±2.8	12.4±2.4	178.5±5.8
S_9	Al-Awadi	32° 10×25.7″	46° 43×40.0″	13.2±2.5	14.1±2.3	182.2±9.1
S_{10}	Al-Duwayjat	32° 08×19.8″	46° 43×06.1″	15.1±2.7	16.8±2.3	189.6±7.9
S_{11}	Al-Jabha (Jabbar Mankhi)	32° 07×30.7″	46° 43×24.3″	11.9±3.2	15.4±2.4	189.5±7.9
S_{12}	Ramadan	32° 07×26.9″	46° 43×46.9″	13.5±2.7	14.8±1.6	179.7±8.6
S_{13}	Al-Huda	32° 07×06.6″	46° 44×23.6″	15.9±1.8	15.4±2.9	172.8±7.9
S_{14}	Al-Salam	32° 07×16.0″	46° 43×48.0″	33.9±3.4	17.4±2.7	163.2±8.4
S_{15}	Al-Muealimin	32° 07×05.8″	46° 44×17.9″	21.5±2.5	8.3±2.9	172.8±8.7
S_{16}	Al-Sadrayn	32° 06×54.7″	46° 44×14.4″	18.6±2.1	13.1±1.8	169.4±8.7
S_{17}	Fateh (Abu Amid Al-Husseini)	32° 06×43.2″	46° 43×52.3″	16.7±2.5	11.4±2.2	201.3±8.7
S_{18}	Al-Banda	32° 06×03.8″	46° 45×19.6″	10.9±2.6	14.4±2.4	179.8±6.5
S_{19}	Al-Muhsiniyyah	32° 05×37.6″	46° 46×14.2″	8.9±1.5	16.3±2.8	192.2±7.9
S_{20}	Al-Madlul	32° 04×26.5″	46° 47×24.1″	11.9±1.9	16.3±2.4	179.8±6.7
S_{21}	Al-Jayazina	32° 04×16.9″	46° 47×40.0″	17±2.1	11.8±1.9	201.6±8.3
S_{22}	Zawiat Al-Eadala	32° 04×16.6″	46° 51×20.5″	13.2±2.4	13.8±2.1	181.6±8.2
S_{23}	Al-Eadala	32° 04×48.0″	46° 51×57.5″	11.2±1.9	15.3±1.7	179.5±5.8
S_{24}	Al-Shahmania	32° 04×13.1″	46° 52×30.2″	22.4±3.6	16.4±2.3	172.3±7.5
Minimum				8.7±1.6	8.3±2.9	158.9±8
Maximum				33.9±3.4	17.5±3	201.6±8.3
Mean value±standard deviation				15.1±2.5	14.7±2.4	180.8±7.9
World average (UNSCEAR[1])				35	30	400

Abbreviations: GPS: Global positioning system; ^{40}K: Potassium-40; ^{226}Ra: Radium-226; S.D.: Standard deviation; ^{232}Th: Thorium-232; UNSCEAR: United Nations Scientific Committee on the Effects of Atomic Radiation.

consisting of a P-type HPGe coaxial detector, model GC4020, number 10025 (Canberra, United States). This detector has a constant relative efficiency of 40% and a resolution at full-width half maximum of 2 keV at the 1,332 keV gamma line of ^{60}Co. A crystal diameter of 62.2 mm was operated under a high voltage bias of +3,000 V (DC). The detector was covered with a 12 cm thick lead shield to minimize the background radioactivity from its surrounding environment. All samples' gamma spectra were analyzed using Canberra Genie-2000 version 3.1 software, which includes peak search, nuclide identification and activity, and uncertainty calculation modules. The energy and relative efficiency calibrations of the detector were performed using a standard multi-gamma source with certificate number 1035-SE-40524-16, type CBSS 2, serial number 280616 – 1597016 (Czech Metrology Institute, Czech Republic). This source contains 12 radionuclides, including ^{241}Am (59.54 keV), ^{109}Cd (88.3 keV), ^{139}Ce (165.85 keV), ^{57}Co (122.06 and

Table 2. Natural radioactivity in soil specimens of Kumait

Sample code	Sample location	Coordinates of location (GPS)		Radionuclide activity concentrations (Bq/kg)		
		Latitude (N)	Longitude (E)	^{226}Ra±S.D.	^{232}Th±S.D.	^{40}K±S.D.
S_1	Shaltag Aeur	32° 03×58.4″	46° 48×57.4″	19.5±2.8	19.7±2.8	197.4±8.3
S_2	Hamid Mutashar	32° 03×55.8″	46° 49×10.7″	15.8±2.7	26.6±3.6	221.3±11.5
S_3	Al-Makayin	32° 03×51.5″	46° 47×38.2″	11.7±2.2	17.3±1.9	194.7±11.2
S_4	Manati-Syid	32° 03×38.0″	46° 50×39.5″	12.5±1.7	9.7±1.9	156.7±6.2
S_5	Khalaf Al-Alwan	32° 03×07.3″	46° 53×20.4″	17.5±2.8	19.4±2.7	295.2±9.4
S_6	Al- Bedouins	32° 02×59.4″	46° 50×01.1″	14.8±1.9	18.5±2.4	183.5±8.2
S_7	Al- Ziyadat	32° 03×22.3″	46° 47×13.9″	17.2±2.7	7.2±1.6	185.7±9.4
S_8	Al-Hussein	32° 02×27.8″	46° 52×13.6″	14.5±2.1	17.4±2.8	184.7±8.4
S_9	Al-Buckmer	32° 02×16.0″	46° 47×13.3″	13.4±2.7	21.7±2.4	231.7±11.6
S_{10}	Al-Shuhadaa	32° 01×58.3″	46° 52×07.2″	13.6±2.7	15.3±2.5	179.5±6.7
S_{11}	Al-Zahraa	32° 01×58.0″	46° 53×04.6″	9.6±1.7	11.6±1.8	203.4±11.2
S_{12}	Al-Bithunuan	32° 01×34.9″	46° 48×31.1″	7.8±1.9	17.7±2.8	188.5±8.3
S_{13}	Al-Dujaila	32° 01×17.2″	46° 44×09.8″	11.2±1.3	14.6±2.2	185.7±7.5
S_{14}	Al-Sumud	32° 01×00.7″	46° 53×51.3″	13.5±2.3	13.5±1.8	192.5±7.8
S_{15}	Amer Shehaza	32° 00×25.5″	46° 51×07.5″	10.6±1.3	18.2±2.7	189.4±7.5
S_{16}	Abd-Al	31° 59×39.3″	46° 54×39.2″	13.4±1.3	16.6±2.1	179.4±6.3
S_{17}	Al-Jidiya	31° 58×46.8″	46° 48×58.2″	14.5±2.6	9.3±1.4	138.4±6.3
S_{18}	Al- Suwayediiyn	31° 58×22.9″	46° 48×34.8″	10.9±1.8	16.7±2.3	179.2±6
S_{19}	Al-Kolbe	31° 57×54.3″	46° 47×43.5″	4.6±1.4	12.7±2.2	182.4±7.2
S_{20}	Saad River	31° 57×20.6″	46° 55×50.5″	9.5±1.4	18.5±2.7	216.5±9.7
S_{21}	Al-Bueli	31° 55×40.1″	46° 54×40.5″	12.8±2.1	16.9±2.5	179.4±6.9
S_{22}	Al- Jaibeen	31° 54×51.5″	46° 55×38.5″	16.4±2.2	28.7±3.2	194.8±11.4
S_{23}	Al-Safha	31° 54×00.6″	46° 56×31.2″	27.6±2.6	29.5±2.8	192.9±11.7
Minimum				4.6±1.4	7.2±1.6	138.4±6.3
Maximum				27.6±2.6	29.5±2.8	295.2±9.4
Mean value±standard deviation				13.6±2.1	17.2±2.4	193.6±8.6
World average (UNSCEAR[1])				35	30	400

Abbreviations: GPS: Global positioning system; ^{40}K: Potassium-40; ^{226}Ra: Radium-226; S.D.: Standard deviation; ^{232}Th: Thorium-232; UNSCEAR: United nations scientific committee on the effects of atomic radiation.

136.47 keV), ^{60}Co (1,173.24 and 1,332.5) keV, ^{137}Cs (661.66 keV), ^{113}Sn (391.69 keV), ^{85}Sr (514 keV), ^{88}Y (898.02 and 1,836.08 keV), ^{51}Cr (320 keV), ^{54}Mn (834.8 keV), and ^{65}Zn (1,116 keV) in the energy range of 59.54 keV to 1,836.08 keV with a mass of 441.0 g, density of 0.98 ± 0.01 g/cm^3, and a volume of 450.0 ± 4.5 cm^3. For ^{226}Ra activity calculation, the gamma-ray peaks of ^{214}Pb at 295.2 and 351.9 keV, and ^{214}Bi at 609.3, 1,120.3, and 1,764.5 keV were used under equilibrium conditions. For ^{232}Th activities, the gamma-ray energy peaks of ^{212}Pb at 238.6 keV, ^{228}Ac at 338.4, 463, 911.2, 964.6, and 969.0 keV, and ^{208}Tl at 583.2 and 860.6 keV were analyzed. The peak energy of 1,460.80 keV was utilized to determine the concentration of ^{40}K.[27] The instrument MEFFTRAN was selected to determine the true coincidence summing correction and self-absorption correction. The program uses Genie 2,000 to determine self-absorption and genuine chance summation corrections. The input data consist of the material composition of the detection, measuring instrument, and the sample. The bulk density of the material, the chemical formulations of any elements or compounds (e.g., SiO_2, Ge, H_2O), and the quantity of each (in weight percent) were inputted into the program. The tool generated a file containing the material attenuation coefficients for various gamma radiation

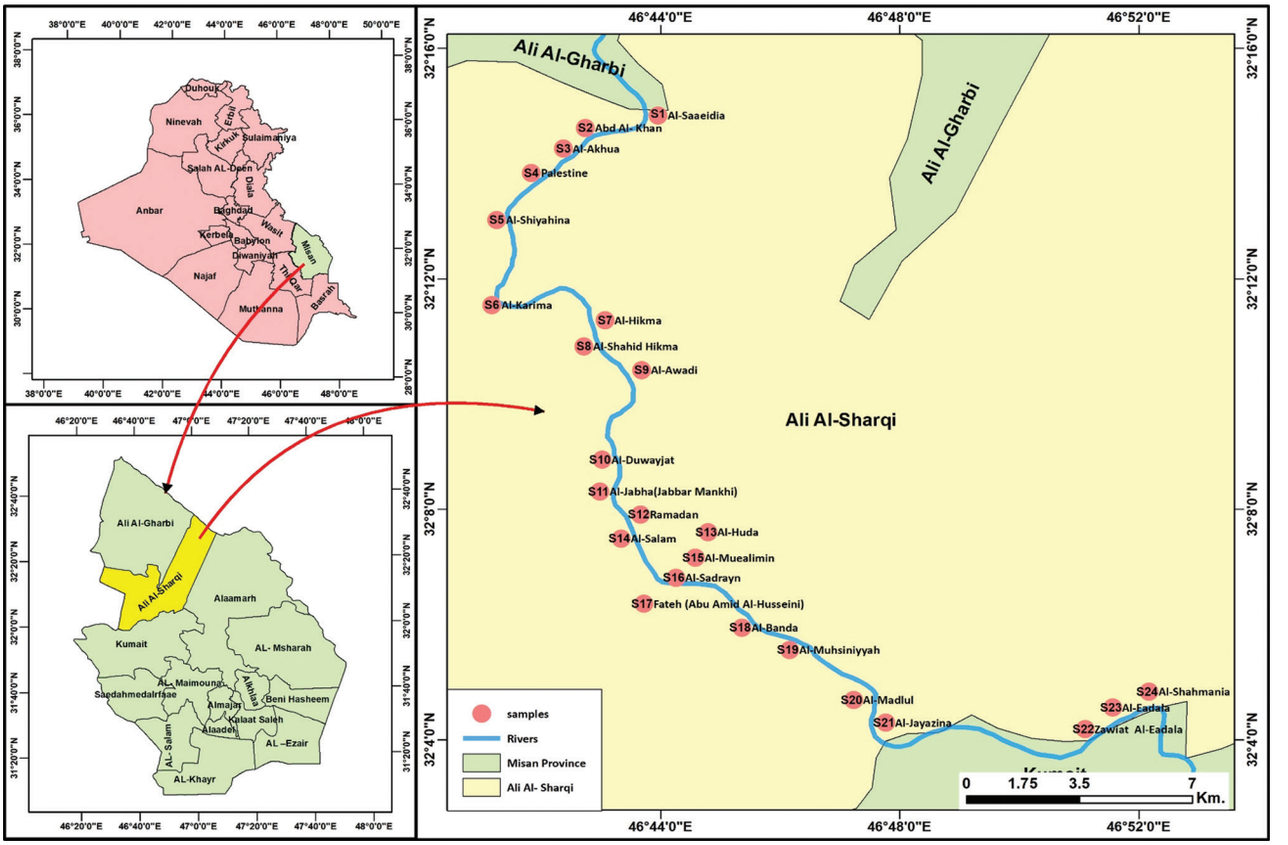

Figure 2. Soil sample locations in Ali Al-Sharqi city

energies and a file containing the parameters provided. In addition, the detector's parameters and the measuring geometry were established. The detector is composed of specific materials and has specific measurements, as indicated by the manufacturer's documentation. The shape of the measurement is determined by the position of the monitor and sample with one another, as well as the material and dimensions of the measuring vessel. A 0.5 L cylindrical polypropylene measure container was placed directly on the detector head. The efficiency of the detector, the material of the calibration reference, and the material of the tested sample are other factors considered when determining the amount of gamma radiation absorbed by the sample and how to account for self-absorption at specific radiation energies. Soil samples were placed sequentially on the detector and counted for 3,600 s. The efficiency and minimum detectable activity for radionuclides ^{226}Ra, ^{232}Th, and ^{40}K in soil were determined (Table 3).

The background distribution that resulted from natural radionuclides in the areas surrounding the detector was also measured by counting an empty Marinelli beaker the same way the samples were prepared in the laboratory. After calculating and subtracting the background, activity concentrations (A) of ^{226}Ra, ^{232}Th, and ^{40}K in each sample were computed using Equation I,[27]

$$A\left(\frac{Bq}{kg}\right) = \frac{A_n}{\varepsilon\, p_{\gamma}\, M\, t} \quad \text{(I)}$$

Where A_n is the net count rate under the full energy peaks, ε is the detector efficiency at the specified energy, Pγ is the absolute transition probability, M is the sample mass (kg), and t is the counting time (second).

2.4. Evaluation of radiation health risk parameters

Radiation risk parameters were evaluated to obtain relevant information on the radiation health status of the research areas.

2.4.1. Radium equivalent activity

The radium equivalent activity is a very useful guideline in organizing the safety standards in radiation protection for humans, and it was calculated using Equation II.[28,29] It is assumed that 370 Bq/kg of ^{226}Ra, 259 Bq/kg of ^{232}Th, and 4,810 Bq/kg of ^{40}K produce the same gamma-ray dose rate,

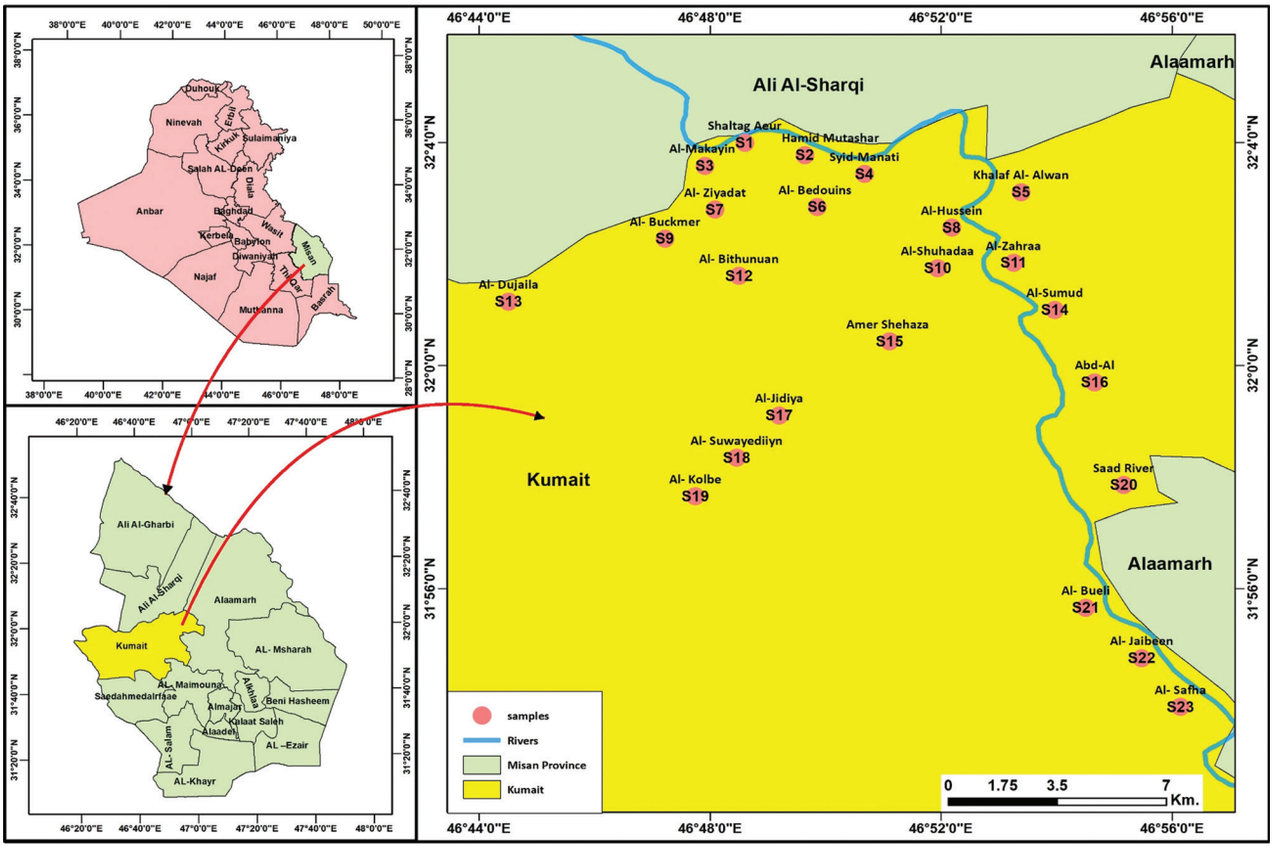

Figure 3. Soil sample locations in Kumait city

Table 3. The efficiency and minimum detectable activity for radium-226, thorium-232, and potassium-40

Nuclide	Efficiency	Minimum detectable activity (Bq/kg)
Radium-226	0.06103	1.831
Thorium-232	0.01142	2.632
Potassium-40	0.0113	2.79

$$Ra_{eq} = A_{Ra} + (1.43 \times A_{Th}) + (0.077 \times A_k) \quad \text{(II)}$$

Where A_{Ra}, A_{Th}, and A_K are the activity concentrations of ^{226}Ra, ^{232}Th, and ^{40}K in Bq/kg, respectively.

2.4.2. Hazard index

To account for the hazards associated with the external and internal exposure of the radiation emanating from ^{226}Ra, ^{232}Th, and ^{40}K in the studied soil samples, the internal hazard index (H_{in}) and external hazard index (H_{ex}) were determined using Equations III and IV.[30-32]

$$H_{in} = \frac{A_{Ra}}{185} + \frac{A_{Th}}{259} + \frac{A_K}{4810} \quad \text{(III)}$$

$$H_{ex} = \frac{A_{Ra}}{370} + \frac{A_{Th}}{259} + \frac{A_K}{4810} \quad \text{(IV)}$$

The prime objective of H_{in} and H_{ex} is to limit the radiation dose to a dose equivalent limit of 1 mSv/year. Thus, their values must be less than unity (i.e. ≤1) for the radiation hazards to be negligible.

2.4.3. Gamma index

The radioactivity level index (I_γ) can be used to estimate the gamma-radiation hazard levels, typically those associated with natural radionuclides, and it was evaluated using Equation V.[33,34]

$$I_\gamma = \frac{A_{Ra}}{300} + \frac{A_{Th}}{200} + \frac{A_K}{3000} \quad \text{(V)}$$

The value of Iγ must be less than unity to keep the radiation hazard insignificant.

2.4.4. Absorbed dose rate

The absorbed dose rate in the air is measured one meter above the ground surface and is used to express the radiation dose received in the open air. This parameter is critical for evaluating radiation risk. The indoor,

outdoor, and total absorbed gamma dose rates (D_{in}, D_{out}, and D_{tot}) were computed using Equations VI-VIII.[35,36]

$$D_{in}\left(\frac{nGy}{h}\right)=\left(0.92\times A_{Ra}\right)+\left(1.1\times A_{Th}\right)+\left(0.081\times A_{K}\right) \quad \text{(VI)}$$

$$D_{out}\left(\frac{nGy}{h}\right)=\left(0.462\times A_{Ra}\right)+\left(0.604\times A_{Th}\right)+\left(0.0417\times A_{K}\right) \quad \text{(VII)}$$

$$D_{tot}\left(\frac{nGy}{h}\right)=D_{in}+D_{out} \quad \text{(VIII)}$$

2.4.5. AEDE

To estimate the AEDE, one has to consider the conversion coefficient 0.7 Sv/Gy, which is used to convert the absorbed rate in the air to human effective dose equivalent with indoor and outdoor occupancy of 80 and 20%, respectively. The indoor, outdoor, and total annual effective dose rates ($AEDE_{in}$, $AEDE_{out}$, and $AEDE_{tot}$) were determined using Equations IX-XI,[37-39]

$$AEDE_{in}\left(\frac{mSv}{y}\right)=D_{in}\left(\frac{nGy}{h}\right)\times 0.7\left(\frac{Sv}{Gy}\right)\times 0.8\times 8760\frac{h}{y}\times 10^{-6} \quad \text{(IX)}$$

$$AEDE_{out}\left(\frac{mSv}{y}\right)=D_{out}\left(\frac{nGy}{h}\right)\times 0.7\left(\frac{Sv}{Gy}\right)\times 0.2\times 8760\frac{h}{y}\times 10^{-6} \quad \text{(X)}$$

$$AEDE_{tot}\left(\frac{mSv}{y}\right)=AEDE_{in}+AEDE_{out} \quad \text{(XI)}$$

2.4.6. ELCR

ELCR is used in radiation protection assessment to predict the probability of individuals' cancer development over a lifetime due to low radiation exposure levels. Based on the calculated values of annual effective dose rates, the indoor, outdoor, and total lifetime cancer risks ($ELCR_{in}$, $ELCR_{out}$, and $ELCR_{tot}$) were calculated using the Equations XII-XIV,[7,40,41]

$$ELCR_{in}=AEDE_{in}\left(\frac{mSv}{y}\right)\times DL\times RF \quad \text{(XII)}$$

$$ELCR_{out}=AEDE_{out}\left(\frac{mSv}{y}\right)\times DL\times RF \quad \text{(XIII)}$$

$$ELCR_{tot}=ELCR_{in}+ELCR_{out} \quad \text{(XIV)}$$

Where DL is the duration of life (70 years), and RF is the risk factor (The International Commission on Radiological Protection 60 uses values of 0.05 Sv^{-1} for the public).

2.4.7. AGDE

Radiation can have various effects on living organisms. These effects may kill a cell, cause it to change, or not affect the DNA. The United Nations Scientific Committee on the Effects of Atomic Radiation (UNSCEAR) primarily focuses on the gonads, active bone marrow, and the cells on the bone surface when assessing radiation impacts. Equation XV was used to calculate the AGDE resulting from the radiation emitted by ^{226}Ra, ^{232}Th, and ^{40}K[42,43] to determine the radiation risk to these tissues.

$$AGDE\left(\frac{\mu Sv}{y}\right)=\left(3.09\times A_{Ra}\right)+\left(4.18\times A_{Th}\right)+\left(0.314\times A_{K}\right) \quad \text{(XV)}$$

3. Results and discussion

3.1. Activity concentrations of radionuclides

The results of activity concentrations of ^{226}Ra, ^{232}Th, and ^{40}K in the soils of Ali Al-Sharqi and Kumait cities are presented in Tables 1 and 2.

The activity concentrations of ^{226}Ra, ^{232}Th, and ^{40}K in Ali Al-Sharqi varied from 8.7 ± 1.6 (S_2) to 33.9 ± 3.4 (S_{14}) Bq/kg, 8.3 ± 2.9 (S_{15}) to 17.5 ± 3 (S_1) Bq/kg, and 158.9 ± 8 (S_1) to 201.6 ± 8.3 (S_{21}) Bq/kg with an average value of 15.1 ± 2.5 Bq/kg, 14.7 ± 2.4 Bq/kg, and 180.8 ± 7.9 Bq/kg, respectively (Table 1). In Kumait, the activity concentrations of related radionuclides were varied from 4.6 ± 1.4 (S_{19}) to 27.6 ± 2.6 (S_{23}) Bq/kg, 7.2 ± 1.6 (S_7) to 29.5 ± 2.8 (S_{23}) Bq/kg, and 138.4 ± 6.3 (S_{17}) to 295.2 ± 9.4 (S_5) Bq/kg with an average value of 13.6 ± 2.1 Bq/kg, 17.2 ± 2.4 Bq/kg, and 193.6 ± 8.6 Bq/kg, respectively, for ^{226}Ra, ^{232}Th, and ^{40}K (Table 2).

It can be noted from Tables 1 and 2 that the mean activity concentrations of ^{226}Ra in Ali Al-Sharqi soil were higher than in Kumait. In comparison, the mean activity concentrations of ^{232}Th and ^{40}K in Kumait soil were higher than in Ali Al-Sharqi.

The findings indicate that average values of ^{226}Ra, ^{232}Th, and ^{40}K in Ali Al-Sharqi and Kumait soil samples are below the global average of 35, 30, and 400 Bq/kg, respectively.[44] For this study, a coverage

factor of $k = 2$ was selected for the uncertainty analysis, corresponding to a confidence level of approximately 95%.

3.2. Comparison of the natural radioactivity results

The average activity concentrations of natural radionuclides in soil specimens of the research areas (Ali Al-Sharqi and Kumait) were compared with identical measurements conducted in the world and Iraq, as demonstrated in Table 4.

The mean concentration of ^{226}Ra is lower than other reported values. The average activity of ^{232}Th is higher than China (Guangyao), Saudi Arabia (Dammam), and Kuwait and Iraq (Al-Sadr) but lower than Algeria (Setif), Nigeria (southwestern region), Malaysia (Peninsular Malaysia), Pakistan (Waziristan), Yemen (Sana'a), Iran (Ramsar and Mahallat), Turkey (Samsun), Jordan (northern highlands), Iraq (Erbil), Iraq (Wassit), Iraq (Thi-Qar), and Iraq (Abu Al Khasib).[45-51] Furthermore, the mean activity for ^{40}K is lower than in these previous studies.

3.3. Radiological hazard

Tables 5 and 6 show the radiological risk parameters obtained from soil samples in the study areas.

The levels of Ra_{eq} ranged from 44.8 (S_2) to 71.3 (S_{14}) Bq/kg with an average of 50.2 ± 5.7 Bq/kg in Ali Al-Sharqi (Table 5) and from 36.8 (S_{19}) to 84.6 (S_{23}) Bq/kg with an average of 53.2 ± 12.1 Bq/kg in Kumait (Table 6). All values of Ra_{eq} were lower than the worldwide average value of 370 Bq/kg.[1]

The values of H_{in} varied from 0.1 (S_2) to 0.3 (S_{14}) with an average of 0.2 ± 0.02 in Ali Al-Sharqi (Table 5) and from 0.1 (S_4, S_{11}, S_{12}, S_{17}, and S_{19}) to 0.3 (S_{23}) with an average of 0.2 ± 0.04 in Kumait (Table 6). Whereas values of H_{ex} varied from 0.1 ($S_{1–13}$ and $S_{15–23}$) to 0.2 (S_{14} and S_{24}) with an average of 0.1 ± 0.01 in Ali Al-Sharqi (Table 5) and from 0.09 (S_{19}) to 0.2 (S_1, S_2, S_5, S_9, S_{22}, and S_{23}) with an average of 0.1 ± 0.03 in Kumait (Table 6). All these values of H_{in} and H_{ex} were less than the value of global values.[1]

The levels of Iγ varied from 0.2 ($S_{1–13}$ and $S_{15–24}$) to 0.3 (S_{14}) with an average of 0.2 ± 0.01 in Ali Al-Sharqi

Table 4. Mean activity concentrations of ^{226}Ra, ^{232}Th, and ^{40}K in the present study compared to literature values

Country	Mean activity concentration (Bq/kg)			References
	^{226}Ra	^{232}Th	^{40}K	
Guangyao, China	26.8	8.87	453.81	Wang and Ye[42]
Setif, Algeria	47	33	329	Boukhenfouf and Boucenna[45]
Southwestern region, Nigeria	54.5	91.1	286.5	Ajayi[12]
Peninsular Malaysia	57	68	427	Almayahi *et al*.[46]
Waziristan, Pakistan	69.5	123.68	453.60	Khan *et al*.[24]
Sana'a, Yemen	48.2	41.7	939.1	Harb *et al*.[47]
Dammam, Saudi Arabia	16.73	10.40	419.78	Al-Ghamdi[43]
Kuwait	16.99	12.70	333.20	Bajoga *et al*.[23]
Ramsar and Mahallat, Iran	24.3	25.8	457.7	Kardan *et al*.[48]
Samsun, Turkey	19	22	521	Tufan and Bostancı[49]
Jordan	42.5	26.7	291.1	Al-Hamarneh and Awadallah[50]
Erbil, Iraq	25.61	20.15	326.64	Hussein[51]
Al-Sadr, Iraq	15.35	13.31	351.39	Al-Alawy *et al*.[44]
Wassit, Iraq	19.420	18.487	204.266	Nafee *et al*.[18]
Thi-Qar, Iraq	29.2	22.7	304.6	Najam *et al*.[19]
Abu Al Khasib, Iraq	58.44	19.38	321.76	Mohammed and Ahmed[39]
World average	35	30	400	UNSCEAR[1]
Ali Al- Sharqi, Iraq	15.1	14.7	180.8	Present study
Kumait, Iraq	13.6	17.2	193.6	

Abbreviations: ^{40}K: Potassium-40; ^{226}Ra: Radium-226; ^{232}Th: Thorium-232; UNSCEAR: United nations scientific committee on the effects of atomic radiation.

Table 5. Radiological risk indices in Ali Al-Sharqi soil samples

Sample code	Radiation hazard indices													
	Ra_{eq} (Bq/kg)	H_{in}	H_{ex}	Iγ	D_{in} (nGy/h)	D_{out} (nGy/h)	D_{tot} (nGy/h)	AED_{Ein} (mSv/y)	$AEDE_{out}$ (mSv/y)	$AEDE_{tot}$ (mSv/y)	$ELCR_{in}$ ($\times10^{-3}$)	$ELCR_{out}$ ($\times10^{-3}$)	ELCRtot ($\times10^{-3}$)	AGDE (μSv/y)
S_1	54	0.2	0.1	0.2	47.5	24.9	72.4	0.2	0.03	0.23	0.8	0.1	0.9	174.6
S_2	44.8	0.1	0.1	0.2	40.1	21.1	61.2	0.2	0.02	0.22	0.7	0.09	0.79	150.1
S_3	46.6	0.2	0.1	0.2	41.5	21.8	63.3	0.2	0.02	0.22	0.7	0.09	0.79	153.5
S_4	45.7	0.2	0.1	0.2	41	21.5	62.5	0.2	0.02	0.22	0.7	0.09	0.79	151.7
S_5	52.4	0.2	0.1	0.2	46.5	24.4	70.9	0.2	0.02	0.22	0.8	0.1	0.9	172.5
S_6	54.7	0.2	0.1	0.2	48.3	25.3	73.6	0.2	0.03	0.23	0.8	0.1	0.9	178.1
S_7	51.3	0.2	0.1	0.2	45.3	23.8	69.1	0.2	0.02	0.22	0.8	0.1	0.9	168
S_8	44.9	0.2	0.1	0.2	40.4	21.1	61.5	0.2	0.02	0.22	0.7	0.09	0.79	149.3
S_9	47.4	0.2	0.1	0.2	42.4	22.2	64.6	0.2	0.02	0.22	0.7	0.09	0.79	156.9
S_{10}	53.7	0.2	0.1	0.2	47.7	25	72.7	0.2	0.03	0.23	0.8	0.1	0.9	176.4
S_{11}	48.5	0.2	0.1	0.2	43.2	22.7	65.9	0.2	0.02	0.22	0.7	0.09	0.79	160.6
S_{12}	48.5	0.2	0.1	0.2	43.3	22.7	66	0.2	0.02	0.22	0.7	0.09	0.79	160
S_{13}	51.2	0.2	0.1	0.2	45.6	23.9	69.5	0.2	0.02	0.22	0.8	0.1	0.9	167.8
S_{14}	71.3	0.3	0.2	0.3	63.5	33	96.5	0.3	0.04	0.34	1.1	0.14	1.24	228.7
S_{15}	46.7	0.2	0.1	0.2	42.9	22.2	65.1	0.2	0.02	0.22	0.7	0.09	0.79	155.4
S_{16}	50.4	0.2	0.1	0.2	45.2	23.6	68.8	0.2	0.02	0.22	0.8	0.1	0.9	165.4
S_{17}	48.5	0.2	0.1	0.2	44.2	23	67.2	0.2	0.02	0.22	0.8	0.09	0.89	162.5
S_{18}	45.3	0.2	0.1	0.2	40.4	21.2	61.6	0.2	0.02	0.22	0.7	0.09	0.79	150.3
S_{19}	47	0.2	0.1	0.2	41.7	22	63.7	0.2	0.02	0.22	0.7	0.09	0.79	156
S_{20}	49.1	0.2	0.1	0.2	43.4	22.8	66.2	0.2	0.02	0.22	0.7	0.09	0.79	161.4
S_{21}	49.4	0.2	0.1	0.2	44.9	23.4	68.3	0.2	0.02	0.22	0.8	0.1	0.9	165.2
S_{22}	46.9	0.2	0.1	0.2	42	22	64	0.2	0.02	0.22	0.7	0.09	0.79	155.5
S_{23}	46.9	0.2	0.1	0.2	41.7	21.9	63.6	0.2	0.02	0.22	0.7	0.09	0.79	154.9
S_{24}	59.1	0.2	0.2	0.2	52.6	27.4	80	0.3	0.03	0.33	0.9	0.11	1.01	191.9
Minimum	44.8	0.1	0.1	0.2	40.1	21.1	61.2	0.2	0.02	0.22	0.7	0.09	0.79	149.3
Maximum	71.3	0.3	0.2	0.3	63.5	33	96.5	0.3	0.04	0.34	1.1	0.14	1.24	228.7
Mean value±standard deviation	50.2±5.7	0.2±0.02	0.1±0.01	0.2±0.01	44.8±5	23.5±2.6	68.3±7.5	0.2±0.02	0.02±0.003	0.2±0.03	0.8±0.08	0.1±0.01	0.9±0.09	165.3±17.1
World average (UNSCEAR[1])	370	≤1	≤1	≤1	84	59	143	0.41	0.07	0.48	1.16	0.29	1.45	300

Abbreviations: AEDE: Annual effective dose equivalents; AGDE: Annual gonadal dose equivalent; D: Absorbed gamma dose rates; ECLR: Excess lifetime cancer risk; H_{ex}: External hazard index; H_{in}: Internal hazard index; $_{in}$: Internal; $_{out}$: External; Raeq: Radium equivalent activity; $_{tot}$: Total; UNSCEAR: United Nations Scientific Committee on the Effects of Atomic Radiation.

doi: 10.36922/AJWEP025060032

Table 6. Radiological risk indices in Kumait soil samples

Sample code	Radiation hazard indices													
	R_{aeq} (Bq/kg)	H_{in}	H_{ex}	Iγ	D_{in} (nGy/h)	D_{out} (nGy/h)	D_{tot} (nGy/h)	$AEDE_{in}$ (mSv/y)	$AEDE_{out}$ (mSv/y)	$AEDE_{tot}$ (mSv/y)	$ELCR_{in}$ ($\times10^{-3}$)	$ELCR_{out}$ ($\times10^{-3}$)	$ELCR_{tot}$ ($\times10^{-3}$)	AGDE (μSv/y)
S_1	62.9	0.2	0.2	0.2	55.6	29.1	84.7	0.3	0.03	0.33	1	0.1	1.1	204.6
S_2	70.9	0.2	0.2	0.3	61.7	32.6	94.3	0.3	0.03	0.33	1.1	0.1	1.2	229.5
S_3	51.4	0.2	0.1	0.2	45.6	24	69.6	0.2	0.02	0.22	0.8	0.1	0.9	169.6
S_4	38.4	0.1	0.1	0.1	34.9	18.2	53.1	0.2	0.02	0.22	0.6	0.07	0.67	128.4
S_5	68	0.2	0.2	0.3	61.4	32.1	93.5	0.3	0.03	0.33	1.1	0.1	1.2	227.9
S_6	55.4	0.2	0.1	0.2	48.8	25.7	74.5	0.2	0.03	0.23	0.8	0.1	0.9	180.7
S_7	41.8	0.2	0.1	0.2	38.8	20	58.8	0.2	0.02	0.22	0.7	0.08	0.78	141.6
S_8	53.6	0.2	0.1	0.2	47.4	24.9	72.3	0.2	0.03	0.23	0.8	0.1	0.9	175.5
S_9	62.3	0.2	0.2	0.2	55	29	84	0.3	0.03	0.33	0.9	0.1	1	204.9
S_{10}	49.3	0.2	0.1	0.2	43.9	23	66.9	0.2	0.02	0.22	0.8	0.09	0.89	162.3
S_{11}	41.8	0.1	0.1	0.2	38.1	19.9	58	0.2	0.02	0.22	0.7	0.08	0.78	142
S_{12}	47.6	0.1	0.1	0.2	41.9	22.2	64.1	0.2	0.02	0.22	0.7	0.09	0.79	157.3
S_{13}	46.4	0.2	0.1	0.2	41.4	21.7	63.1	0.2	0.02	0.22	0.7	0.09	0.79	153.9
S_{14}	47.6	0.2	0.1	0.2	42.9	22.4	65.3	0.2	0.02	0.22	0.7	0.09	0.79	158.6
S_{15}	51.2	0.2	0.1	0.2	45.1	23.8	68.9	0.2	0.02	0.22	0.8	0.1	0.9	168.3
S_{16}	51	0.2	0.1	0.2	45.1	23.7	68.8	0.2	0.02	0.22	0.8	0.1	0.9	167.1
S_{17}	38.5	0.1	0.1	0.1	34.8	18.1	52.9	0.2	0.02	0.22	0.6	0.07	0.67	127.1
S_{18}	48.6	0.2	0.1	0.2	42.9	22.6	65.5	0.2	0.02	0.22	0.7	0.09	0.79	159.8
S_{19}	36.8	0.1	0.09	0.1	33	17.4	50.4	0.2	0.02	0.22	0.6	0.07	0.67	124.6
S_{20}	52.6	0.2	0.1	0.2	46.6	24.6	71.2	0.2	0.03	0.23	0.8	0.1	0.9	174.7
S_{21}	50.8	0.2	0.1	0.2	44.9	23.6	68.5	0.2	0.02	0.22	0.8	0.1	0.9	166.5
S_{22}	72.4	0.2	0.2	0.3	62.4	33	95.4	0.3	0.04	0.34	1.1	0.1	1.2	231.8
S_{23}	84.6	0.3	0.2	0.3	73.5	38.6	112.1	0.4	0.04	0.44	1.3	0.2	1.5	269.2
Minimum	36.8	0.1	0.09	0.1	33	17.4	50.4	0.2	0.02	0.22	0.6	0.07	0.67	124.6
Maximum	84.6	0.3	0.2	0.3	73.5	38.6	112.1	0.4	0.04	0.44	1.3	0.2	1.5	269.2
Mean value±standard deviation	53.2±12.1	0.2±0.04	0.1±0.03	0.2±0.04	47.2±10.1	24.8±5.4	72±15.5	0.2±0.04	0.03±0.006	0.3±0.06	0.8±0.2	0.1±0.02	0.9±0.2	175±37.2
World average (UNSCEAR[1])	370	≤1	≤1	≤1	84	59	143	0.41	0.07	0.48	1.16	0.29	1.45	300

Abbreviations: AEDE: Annual effective dose equivalents; AGDE: Annual gonadal dose equivalent; D: Absorbed gamma dose rates; ECLR: Excess lifetime cancer risk; H_{ex}: External hazard index; H_{in}: Internal hazard index; $_{in}$: Internal; $_{out}$: External; Raeq: Radium equivalent activity; $_{tot}$: Total; UNSCEAR: United Nations Scientific Committee on the Effects of Atomic Radiation.

Table 7. Radiological hazard indices in the investigated soil samples compared to literature values

Country	Radiological hazard indices											References
	R_{aeq} (Bq/kg)	H_{in}	H_{ex}	Iγ	D_{in} (nGy/h)	D_{out} (nGy/h)	$AEDE_{in}$ (mSv/y)	$AEDE_{out}$ (mSv/y)	$ELCR_{in}$ ($\times10^{-3}$)	$ELCR_{out}$ ($\times10^{-3}$)	AGDE (μSv/y)	
Sicily, Italy	72	-	-	-	-	34	0.32	0.04	-	-	-	Lanzo *et al.*[14]
Mounana, Gabon	2,928.75	15.51	7.92	-	-	1,352.76	9.30	1.66	-	-	-	Mouandza *et al.*[21]
Uttara Kannada, India	140.74	0.48	0.38	0.51	-	64.84	0.32	0.08	-	1.59	478.8	Suresh *et al.*[32]
Punjab, Pakistan	179.26	0.642	0.482	-	-	85.045	0.417	0.105	-	-	-	Rahman *et al.*[4]
Shabwah and Hadramout, Yemen	94.73	-	0.26	0.36		46.50	-	0.031	-	-	-	Nafee *et al.*[18]
Taghdoua, Saudi Arabia	-	-	-	-	70	37	0.3	0.1	1.3	0.2	-	Aydarous *et al.*[25]
Fars, Iran	-		-	-		32.6	0.189	0.039	-	-	-	Faghihi *et al.*[53]
Bolu, Turkey	62.8	-	0.2	0.2	-	29.9	-	0.036	-	0.13	209.7	Dizman *et al.*[27]
Ma'an, Jordan	94.21	0.41	0.25	-	-	37.15	-	0.045	-	-	-	Saleh and Shaye[55]
Tulkarem, Palestine	72	0.3	0.21	0.55	-	35.5	-	0.044	-	-	-	Thabaynehxx
Pshdar, Iraq	69.83	0.227	0.200	-	-	33.26	-	0.040	-	-	-	Muhammad *et al.*[54]
Kirkuk, Iraq	81.182	0.286	0.210	0.603	-	38.618	0.189	0.048	-	-	-	Taqi *et al.*[20]
Baghdad, Iraq	74.383	0.248	0.206	0.577	-	36.320	0.178	0.045	-	-	-	Mohammed *et al.*[39]
Al-Sadr, Iraq	61.434	0.208	0.166	-	57.974	29.535	0.285	0.037	0.997	0.128	-	Al-Alawy *et al.*[44]
Ad Dayr, Iraq	-	-	-	-	91.72	46.16	0.45	0.06	1.48	0.19	-	Mohammed and Ahmed[38]
World average	370	1≥	1≥	≤1	84	59	0.41	0.07	1.16	0.29	300	UNSCEAR[1]
Ali Al- Sharqi, Iraq	50.2	0.2	0.1	0.2	44.8	23.5	0.2	0.02	0.8	0.1	165.3	Present study
Kumait, Iraq	53.2	0.2	0.1	0.2	47.2	24.8	0.2	0.03	0.8	0.1	175	

Note: Refers to not available.

Abbreviations: AEDE: Annual effective dose equivalents; AGDE: Annual gonadal dose equivalent; D: Absorbed gamma dose rates; ECLR: Excess lifetime cancer risk; H_{ex}: External hazard index; H_{in}: Internal hazard index; $_{in}$: Internal; $_{out}$: External; Raeq: Radium equivalent activity; tot: Total; UNSCEAR: United Nations Scientific Committee on the Effects of Atomic Radiation.

doi: 10.36922/AJWEP025060032

(Table 5) and from 0.1 (S_4, S_{17}, and S_{19}) to 0.3 (S_2, S_5, S_{22}, and S_{23}) with an average of 0.2 ± 0.04 in Kumait (Table 6). The determined values of Iγ were below global values.[1]

The levels of D_{in} ranged from 40.1 (S_2) to 63.5 (S_{14}) nGy/h with an average of 44.8 ± 5 nGy/h in Ali Al-Sharqi (Table 5) and from 33 (S_{19}) to 73.5 (S_{23}) nGy/h with an average of 47.2 ± 10.1 nGy/h in Kumait (Table 6). D_{out} values ranged from 21.1 (S_2 and S_8) to 33 (S_{14}) nGy/h with an average of 23.5 ± 2.6 nGy/h in Ali Al-Sharqi (Table 5) and from 17.4 (S_{19}) to 38.6 (S_{23}) nGy/h with an average of 24.8 ± 5.4 nGy/h in Kumait (Table 6). Furthermore, the values of D_{tot} ranged from 61.2 (S_2) to 96.5 (S_{14}) nGy/h with an average of 68.3 ± 7.5 nGy/h in Ali Al-Sharqi (Table 5) and from 50.4 (S_{19}) to 112.1 (S_{23}) nGy/h with an average of 72 ± 15.5 nGy/h in Kumait (Table 6). These computed air-absorbed dose rates were below the world average of 84 nGy/h, 59 nGy/h, and 143 nGy/h, respectively, for D_{in}, D_{out}, and D_{tot}.[1]

The $AEDE_{in}$ values varied from 0.2 ($S_{1–13}$ and $S_{15–23}$) to 0.3 (S_{14} and S_{24}) mSv/y with a mean of 0.2 ± 0.02 mSv/y in Ali Al-Sharqi (Table 5) and from 0.2 (S_3, S_4, $S_{6–8}$, and $S_{10–21}$) to 0.4 (S_{23}) mSv/y with a mean value of 0.2 ± 0.04 mSv/y in Kumait (Table 6). $AEDE_{out}$ values varied from 0.02 ($S_{2–5}$, $S_{7–9}$, $S_{11–13}$, and $S_{15–23}$) to 0.04 (S_{14}) mSv/y with a mean value of 0.02 ± 0.003 mSv/y in Ali Al-Sharqi (Table 5) and from 0.02 (S_3, S_4, S_7, $S_{10–20}$, and S_{21}) to 0.04 (S_{22} and S_{23}) mSv/y with a mean value of 0.03 ± 0.006 mSv/y in Kumait (Table 6). In addition, $AEDE_{tot}$ values varied from 0.22 ($S_{2–5}$, $S_{7–9}$, $S_{11–13}$, and $S_{15–23}$) to 0.34 (S_{14}) mSv/y with a mean value of 0.2 ± 0.03 mSv/y in Ali Al-Sharqi (Table 5) and from 0.22 (S_3, S_4, S_7, $S_{10–19}$, and S_{21}) to 0.44 (S_{23}) mSv/y with a mean value of 0.3 ± 0.06 mSv/y in Kumait (Table 6). The estimated values of AEDE were lower than the worldwide average values of 0.41 mSv/y, 0.07 mSv/y, and 0.48 mSv/y, respectively, for $AEDE_{in}$, $AEDE_{out}$, and $AEDE_{tot}$.[1]

The levels of $ELCR_{in}$ ranged from 0.7×10^{-3} ($S_{2–4}$, S_8, S_9, S_{11}, S_{12}, S_{15}, $S_{18–20}$, S_{22}, and S_{23}) to 1.1×10^{-3} (S_{14}) with an average of $(0.8 \pm 0.08) \times 10^{-3}$ in Ali Al-Sharqi (Table 5) and from 0.6×10^{-3} (S_4, S_{17}, and S_{19}) to 1.3×10^{-3} (S_{23}) with an average of $(0.8 \pm 0.2) \times 10^{-3}$ in Kumait (Table 6). $ELCR_{out}$ values ranged from 0.09×10^{-3} ($S_{2–4}$, S_8, S_9, S_{11}, S_{12}, S_{15}, $S_{17–20}$, S_{22}, and S_{23}) to 0.14×10^{-3} (S_{14}) with an average of $(0.1 \pm 0.01) \times 10^{-3}$ in Ali Al-Sharqi (Table 5) and from 0.07×10^{-3} (S_4, S_{17}, and S_{19}) to 0.2×10^{-3} (S_{23}) with an average of $(0.1 \pm 0.02) \times 10^{-3}$ in Kumait (Table 6). Moreover, $ELCR_{tot}$ values varied from 0.79×10^{-3} ($S_{2–4}$, S_8, S_9, S_{11}, S_{12}, S_{14}, S_{15}, $S_{18–20}$, S_{22}, and S_{23}) to 1.24×10^{-3} (S_{14}) with an average of $(0.9 \pm 0.09) \times 10^{-3}$ in Ali Al-Sharqi (Table 5) and from 0.67×10^{-3} (S_4, S_{17}, and S_{19}) to 1.5×10^{-3} (S_{23}) with an average of $(0.9 \pm 0.2) \times 10^{-3}$ in Kumait (Table 6). The evaluated values of ELCRs were below the worldwide average of 1.16×10^{-3}, 0.29×10^{-3}, and 1.45×10^{-3}, respectively, for $ELCR_{in}$, $ELCR_{out}$, and $ELCR_{tot}$.[1]

The levels of AGDE varied from 149.3 (S_8) to 228.7 (S_{14}) μSv/y with a mean value of 165.3 ± 17.1 μSv/y in Ali Al-Sharqi (Table 5) and from 124.6 (S_{19}) to 269.2 (S_{23}) μSv/y with a mean value of 175 ± 37.2 μSv/y in Kumait (Table 6). These AGDE values were less than the worldwide average value of 300 μSv/y.[1]

Based on the above outcomes, it can be concluded that the mean values of the radiological risk parameters in the soil of the research areas were below the globally recommended levels. Therefore, there are no potential health risks to the general public in Ali Al-Sharqi and Kumait, and the radiation levels remain in normal ranges.

3.4. Comparison of radiological hazard indices of the soil of the current study with identical research

The average radiological risk indices obtained from the soils of the research areas were compared with those obtained from other regions in the world and Iraq, as shown in Table 7.

The mean values for Ra_{eq}, H_{in}, H_{ex}, Iγ, D_{in}, D_{out}, $AEDE_{in}$, $AEDE_{out}$, $ELCR_{in,}$ $ELCR_{out}$, and AGDE in the present study are generally lower than those reported in previous studies. However, the mean value of $AEDE_{in}$ in Ali Al-Sharqi and Kumait exceeds that observed in Iran (Fars),[19] Iraq (Kirkuk),[19] and Iraq (Baghdad).[53] In addition, the mean value of Iγ in Ali Al-Sharqi and Kumait is comparable to those observed in Turkey (Bolu).[52]

4. Conclusion

Natural radionuclides of ^{226}Ra, ^{232}Th, and ^{40}K were measured in soil specimens from two cities, Ali Al-Sharqi and Kumait, utilizing an HPGe detector. The average concentrations of these radionuclides for Ali Al-Sharqi were 15.1 Bq/kg for ^{226}Ra, 14.7 Bq/kg for ^{232}Th, and 180.8 Bq/kg for ^{40}K. In Kumait, the respective concentrations were 13.6, 17.2, and 193.6 Bq/kg for ^{226}Ra, ^{232}Th, and ^{40}K, respectively. These concentrations were all below the internationally recommended limits reported by UNSCEAR in 2,000. Based on the measured activity concentrations in soil, the radiological parameters, including Ra_{eq}, H_{in} and H_{ex}, Iγ, D_{in}, D_{out}, and D_{tot}, $AEDE_{in}$, $AEDE_{out}$, and $AEDE_{tot}$, $ELCR_{in}$, $ELCR_{out}$,

and $ELCR_{tot}$, and AGDE were calculated. The mean values for radiological risk parameters in the study areas were below the globally recommended safety values reported by UNSCEAR in 2,000.

Consequently, natural radioactivity measurements indicate that Ali Al-Sharqi and Kumait soils are considered radiologically safe and do not pose any health risks to the public. Furthermore, the findings of this study provide valuable baseline data that can support the development of maps for naturally occurring radioactivity, aiding in future soil radiological environmental monitoring effects.

Acknowledgments

The authors would like to thank the Iraqi Ministry of Environment for their continuous support.

Funding

None.

Conflict of interest

The authors declare that they have no competing interests.

Author contributions

Conceptualization: Zahraa A. Ismail AL-Sudani
Formal analysis: All authors
Investigation: Zahraa A. Ismail AL-Sudani, Sawsan Sherif
Methodology: All authors
Writing – original draft: Zahraa A. Ismail AL-Sudani, Sawsan Sherif
Writing – review & editing: Zahraa A. Ismail AL-Sudani

Availability of data

The datasets used and analyzed during the current study are available from the corresponding author upon reasonable request.

References

1. UNSCEAR. Effects of Ionizing Radiation. New York: United Nations; 2000. p. 453-487.
2. Banerjee KS, Guin R, Gutierrez-Villanueva JL, Charro ME, Sengupta D. Variation in u-238 and th-232 enrichment in u-mineralized zone and geological controls on their spatial distribution, Singhbhum shear zone of India. *J Environ Earth Sci*. 2012;65:2103-2110. doi: 10.1007/s12665-011-1191-9
3. Otansev P, Karahan G, Kam E, Barut I, Taskin H. Assessment of natural radioactivity concentrations and gamma dose rate levels in Kayseri, Turkey. *Radiat Prot Dosimetry*. 2012;148(2):227-236. doi: 10.1093/rpd/ncr023
4. Rahman S, Matiullah MF, Rafique M, Anwar J, Ziafat M. Measurement of naturally occurring/fallout radioactive elements and assessment of annual effective dose in soil samples collected from four districts of the Punjab province, Pakistan. *J Radioanal Nucl Chem.* 2011;287(2):647-655. doi: 10.1007/s10967-010-0819-7
5. Kassa MK, Deressu TT. Measurement of natural radioactivity levels and evaluation of radiological hazard risks in areas of eastern coastline sediments of Lake Hawassa in Ethiopia's Sidama Region. *J Phys.* 2023;9(4):1819-1837. doi: 10.22059/poll.2023.357027.1843
6. Hameed PS, Pillai GS, Satheeshkumar G, Mathiyarasu R. Measurement of gamma radiation from rocks used as building material in Tiruchirappalli District, Tamil Nadu, India. *J Radiat Nucl Chem.* 2014;300:1081-1088. doi: 10.1007/s10967-014-3033-1
7. Ramasamy V, Suresh G, Meenakshisundaram V, Ponnusamy V. Horizontal and vertical characterization of radionuclides and minerals in river sediments. *Appl Radiat Isot.* 2011;69(1):184-195. doi: 10.1016/j.apradiso.2010.07.020
8. Rani A, Singh S. Natural radioactivity levels in soil samples from some areas of Himachal Pradesh, India using γ-ray spectrometry. *Atmos Environ*. 2005;39(34):6306-6314. doi: 10.1016/j.atmosenv.2005.07.050
9. Al-Jundi J, Al-Bataina B, Abu-Rukah Y, Shehadeh HM. Natural radioactivity concentrations in soil samples along the Amman Aqaba Highway, Jordan. *Radiol Meas.* 2003;36(1-6):555-560. doi: 10.1016/S1350-4487(03)00202-6
10. Kurnaz A, Küçükömeroğlu B, Keser R, *et al.* Determination of radioactivity levels and hazards of soil and sediment samples in Fırtına Valley (Rize, Turkey). *Appl Radiat Isot.* 2007;65(11):1281-1289. doi: 10.1016/j.apradiso.2007.06.001
11. Harb SRM, Din KS, Abbady AE, Mohamed AEE, Michel R. Measurements of natural radionuclides in soil samples from Upper Egypt. *Nucl Sci Technol*. 2008;19(5):302-307. doi: 10.1016/S1001-8042(09)60008-7
12. Ajayi OS. Measurement of activity concentrations of ^{40}K, ^{226}Ra and ^{232}Th for assessment of radiation hazards from soils of the SouthWestern region of Nigeria. *Radiat Environ Biophys*. 2009;48:323-332. doi: 10.1007/s00411-009-0225-0

13. El Samad O, Baydoun R, Nsouli B, Darwish T. Determination of natural and artificial radioactivity in soil at North Lebanon province. *J Environ Radioact*. 2013;125:36-39.
doi: 10.1016/j.jenvrad.2013.02.010
14. Lanzo G, Rizzo S, Tomarchio E. A radiometric and petrographic approach to risk assessment at alte madonie mounts region (Sicily, Italy). *Radiat Prot Dosimetry.* 2014;158(4):427-434.
doi: 10.1093/rpd/nct245
15. Attia TE, Shendi EH, Shehata MA. Assessment of natural and artificial radioactivity levels and radiation hazards and their relation to heavy metals in the industrial area of port said city, Egypt. *Environ Sci Pollut Res Int.* 2015;22:3082-3097.
doi: 10.1007/s11356-014-3453-z
16. Haribala, Hu B, Wang C, *et al*. Assessment of radioactive materials and heavy metals in the surface soil around uranium mining area of Tongliao, China. *Ecotoxicol Environ Saf.* 2016;130:185-192.
doi: 10.1016/j.ecoenv.2016.04.002
17. Mustafa MI, Yazici NA, Mangur PH. The investigation of terrestrial radioactivity in soil samples around pshdar region in Iraqi-Kurdistan. *Zanco J Pure Appl Sci*. 2016;28(6):13-20.
doi: 10.21271/ZJPAS.28.6.3
18. Nafee S, Al-Othmany D, Hamidalddin S, Al-Zahrani J, Alharbi W, Barashed H. Measurement of gamma emitting radionuclides for assessment, environmental hazards of radiation in rock and soil samples of Shabwah and Hadramout regions, Yemen. *J Geosci Environ Protect*. 2017;5(5):66-75.
doi: 10.4236/gep.2017.55005
19. Najam LA, Salim KM, Khalid HT. Evaluation of natural radioactivity of soil samples from different regions of wassit governorate. *Pollution*. 2017;3(1):47-53.
doi: 10.7508/pj.2017.01.006
20. Taqi AH, Shaker AM, Battawy AA. Natural radioactivity assessment in soil samples from Kirkuk city of Iraq using HPGe detector. *Int J Radiat Res*. 2018;16(4):455-463.
doi: 10.18869/acadpub.ijrr.16.4.455
21. Mouandza SYL, Moubissi AB, Abiama PE, Ekogo TB, Ben-Bolie GH. Study of natural radioactivity to assess of radiation hazards from soil samples collected from Mounana in South-East of Gabon. *Int J Radiat Res.* 2018;16(4):443-453.
doi: 10.18869/acadpub.ijrr.16.4.443
22. Ribeiro FCA, Silva JIR, Lima ESA, Do Amaral Sobrinho NMB, Perez DV, Lauria DC. Natural radioactivity in soils of the state of Rio de Janeiro (Brazil): Radiological characterization and relationships to geological formation, soil types and soil properties. *J Environ Res*. 2018;182:34-43.
doi: 10.1016/j.jenvrad.2017.11.017
23. Bajoga AD, Al-Dabbous AN, Abdullahi AS, Alazemi NA, Bachama YD, Alaswad SO. Evaluation of elemental concentrations of uranium, thorium and potassium in top soils from Kuwait. *Nucl Eng Environ Technol*. 2019;51(6):1638-1649.
doi: 10.1016/j.net.2019.04.021
24. Khan UI, Qin Z, Xie T, *et al.* Evaluation of health hazards from radionuclides in soil and rocks of North Waziristan, Pakistan. *Int J Radiat Res.* 2020;18(2):243-253.
doi: 10.18869/acadpub.ijrr.18.2.243
25. Aydarous AS, Zeghib S, Abdullahi S, Al-Subaie H. Radiological hazard assessment and sensitivity analysis for soil samples in Taghdoua area of Ranyah, Saudi Arabia. *J Radiol Res Appl Sci.* 2022;15(2):119-128.
doi: 10.1016/j.jrras.2022.05.006
26. De Regge P, Burns K, Danesi PR. The IAEA programme and perspectives for environmental radionuclide monitoring and preparation of reference materials. *Czech J Phys*. 1999;49:237-245.
doi: 10.1007/s10582-999-0032-5
27. Dizman S, Görür FK, Keser R, Görür O. The assessment of radioactivity and radiological hazards in soils of Bolu province, Turkey. *Environ Forensics*. 2019;20(3):211-218.
doi: 10.1080/15275922.2019.1629129
28. Beretka J, Mathew PJ. Natural radioactivity of Australian building materials, industrial wastes and by-products. *Health Phys*. 1985;48(1):87-95.
doi: 10.1097/00004032-198501000-00007
29. Smail JM, Ahmad ST, Mansour HH. Estimation of the natural radioactivity levels in the soil along the Little Zab River, Kurdistan Region in Iraq. *J Radiol Nucl Chem.* 2022;331(1-10):119-128.
doi: 10.1007/s10967-021-08064-5
30. Krieger RJ. Radioactivity of construction materials. *World J Nucl Sci Technol.* 1981;47(8):468-473.
doi: 10.1016/S0160-3450(16)31258-2
31. Yadav M, Rawat M, Dangwal A, Prasad M, Gusain GS, Ramola RC. Levels and effects of natural radionuclides in soil samples of Garhwal Himalaya. *J Radioanal Nucl Chem*. 2014;302:869-873.
doi: 10.1007/s10967-014-3277-9
32. Mountford PJ, Temperton DH. Recommendations of the international commission on radiological protection (ICRP) 1990. *Eur J Nucl Med*. 1992;19:77-79.
doi: 10.1007/BF00184120
33. Suresh S, Rangaswamy DR, Sannappa J, Dongre S, Srinivasa E, Rajesh S. Estimation of natural radioactivity and assessment of radiation hazard indices in soil samples of Uttara Kannada district, Karnataka, India. *J Radiat Nucl Chem.* 2022;331(4):1869-1879.
doi: 10.1007/s10967-021-08145-5
34. European Commission. *Radiological Protection Principles Concerning the Natural Radioactivity of Building Materials*. Radiation Protection No. 112. Luxembourg: Publications of the European

Communities; 1999.
35. Temelli UE. Determination of natural radioactivity levels of concrete core and cements in Eskisehir Area. *Fresenius Environ Bull*. 2018;27:2717-2723.
36. Asaduzzaman K, Khandaker MU, Amin YM, Bradley DA. Natural radioactivity levels and radiological assessment of decorative building materials in Bangladesh. *Indoor Built Environ*. 2016;25(3):541-550. doi: 10.1177/1420326X14562048
37. Ravisankar R, Chandramohan J, Chandrasekaran A, *et al.* Assessments of radioactivity concentration of natural radionuclides and radiological hazard indices in sediment samples from the East coast of Tamilnadu, India with statistical approach. *Mar Pollut Bull*. 2015;97(1-2):419-430. doi: 10.1016/j.marpolbul.2015.05.058
38. Sukumaran Chettiar Rajamma S, Abraham S, Panakal John J. Gamma radiation profile of the high background radiation area along southwest coastal India and its neighbourhood. *Pollution*. 2023;9(4):1867-1879. doi: 10.22059/poll.2023.360416.1937
39. Mohammed RS, Ahmed RS. Estimation of excess lifetime cancer risk and radiation hazard indices in Southern Iraq. *Environ Earth Sci*. 2017;76:303. doi: 10.1007/s12665-017-6616-7
40. Ugbede FO, Okoye ONN, Akpolile AF, Oladele BB. Baseline radioactivity in the soil of evangel take-off campus, evangel university, Nigeria, and its associated health risks. *Chem Africa*. 2021;4(3):703-713. doi: 10.1007/s42250-021-00254-8
41. Agar O, Boztosun I, Korkmaz ME, Özmen SF. Measurement of radioactivity levels and assessment of radioactivity hazards of soil samples in Karaman, Turkey. *Radiat Prot Dosimetry*. 2014;162(4):630-637. doi: 10.1093/rpd/ncu027
42. Wang Z, Ye Y. Assessment of soil radioactivity levels and radiation hazards in Guangyao Village, South China. *J Radiochem Nucl Chem*. 2021;329:679-693. doi: 10.1007/s10967-021-07818-5
43. Al-Ghamdi AH. Health risk assessment of natural background radiation in the soil of Eastern Province, Saudi Arabia. *J Radiat Res Sci.* 2019;12(1):219-225. doi: 10.1080/16878507.2019.1637045
44. Al-Alawy IT, Taher WI, Mzher OA. Soil radioactivity levels, radiation hazard assessment and cancer risk in Al-Sadr City, Baghdad Governorate, Iraq. *Int J Radiat Res*. 2023;21(2):293-298.
45. Boukhenfouf W, Boucenna A. The radioactivity measurements in soils and fertilizers using gamma spectrometry technique. *J Environ Radioact.* 2011;102(4):336-339. doi: 10.1016/j.jenvrad.2011.01.006
46. Almayahi BA, Tajuddin AA, Jaafar MS. Radiation hazard indices of soil and water samples in Northern Malaysian Peninsula. *Appl Radiat Isot*. 2012;70(11):2652-2660. doi: 10.1016/j.apradiso.2012.07.021
47. Harb S, El-Kamel AEH, Abbady AEB, Saleh EE, El-Mageed AI. Specific activities of natural rocks and soils at quaternary intraplate volcanism north of Sana'a, Yemen. *J Med Pharmacol*. 2012;37(1):54-60. doi: 10.4103/0971-6203.92721
48. Kardan MR, Fathabdi N, Attarilar A, *et al*. A national survey of natural radionuclides in soils and terrestrial radiation exposure in Iran. *J Environ Radioact*. 2017;178:168-176. doi: 10.1016/j.jenvrad.2017.08.010
49. Tufan MÇ, Bostancı S. Radioactivity concentrations in soil and dose assessment for Samsun City Centre, Turkey. *Radiat Prot Dosimetry*. 2012;151(3):532-536. doi: 10.1093/rpd/ncs034
50. Al-Hamarneh IF, Awadallah MI. Soil radioactivity levels and radiation hazard assessment in the highlands of northern Jordan. *Radiat Meas.* 2009;44(1):102-110. doi: 10.1016/j.radmeas.2008.11.005
51. Hussein ZA. Assessment of natural radioactivity levels and radiation hazards for soil samples used in Erbil Governorate, Iraqi Kurdistan. *ARO Sci J Koya Univ*. 2019;7(1):34-39. doi: 10.14500/aro.10471
52. Mohammed NA, Ebrahiem SA. Radioactivity levels of ^{238}U, ^{234}Th, ^{40}K and ^{137}C in the soil surface of selected regions from Baghdad Governorate. J Nucl Eng Sci. 2020;14(1):15-27. doi: 10.1504/ijnest.2020.108794
53. Faghihi R, Mehdizadeh S, Sina S. Natural and artificial radioactivity distribution in soil of Fars Province, Iran. *Radiat Prot Dosimetry*. 2011;145(1):66-74. doi: 10.1093/rpd/ncq367
54. Muhammed MI, Najim Y, Mangur P. The Investigation of Terrestrial Radioactivity in Soil Samples around Pshdar Region in Iraqi-Kurdistan. *ZANCO J Pure and Appl Sci*. 2016;28(6):13-20.
55. Saleh, H, Shayeb MA. Natural radioactivity distribution of southern part of jordan (Maan) Soil. Ann Nucl Energy. 2014;65:184-9. doi: 10.1016/j.anucene.2013.10.042

ACCSCIENCE PUBLISHING

Asian Journal of Water, Environment and Pollution. Vol. 22, No. 2 (2025), pp. 140-151.
doi: 10.36922/AJWEP025090057

ORIGINAL RESEARCH ARTICLE

Water scarcity in Asian nations and the path to resilience

Muhammad Khalid Anser[1], Muhammad Zaheer Akhtar[2], Syed Tahir Hussain Shah[3], Muhammad Azhar Khan[2], and Khalid Zaman[2]*

[1]Department of Economics, Faculty of Economics and Administrative Sciences, Recep Tayyip Erdoğan University, Rize, Türkiye
[2]Department of Economics, Faculty of Social and Administrative Sciences, The University of Haripur, Haripur, Khyber Pakhtunkhwa, Pakistan
[3]Department of Economics, Faculty of Social Sciences and Humanities, University of Wah, Wah Cantonment, Punjab, Pakistan
***Corresponding author:** Khalid Zaman (khalid.zaman@uoh.edu.pk)

Received: February 25, 2025; 1st revised: February 25, 2025; 2nd revised: March 15, 2025; 3rd revised: March 27, 2025; Accepted: March 28, 2025; Published online: April 16, 2025

Abstract: Water, the most essential component for life and ecological balance, is scarce worldwide, particularly in underprivileged countries. This research uses panel data from 39 Asian nations spanning from 1996 to 2022 to examine the impact of water scarcity (WS) on climate change, socioeconomic issues, governance instability, food production, and sustainable groundwater planning. The generalized method of moments estimator results reveal that government effectiveness, regulatory quality, and crop production reduce WS by 17.581%, 55.049%, and 0.171%, respectively. In contrast, agricultural land degradation, renewable energy demand, and climate funding exacerbate WS by 0.001%, 1.551%, and 10.397%, respectively. The study underscores the importance of effective governance and climate financing in securing Asia's water future.

Keywords: Water stress; Climate risk; Governance; Climate financing; Population growth; Renewable energy demand; Asian economies

1. Introduction

Water, as the most crucial component and a vital resource, plays a pivotal role in sustaining human life and maintaining ecological equilibrium on a global scale. It is irrefutable that survival for any living organism is impossible without water.[1] Despite covering 71% of the Earth's surface, only a small fraction – approximately 2.5% – is fresh and usable for human consumption.[2] Moreover, the increasing demand for water, driven by population growth (POPG), has led to over a third of the world facing various water scarcity (WS) challenges. This alarming trend of WS has become a major global issue, particularly affecting underprivileged nations, which remain vulnerable if swift and effective measures are not implemented.[3] Water insecurity primarily affects developing countries, often exacerbated by ineffective policies and management. In the context of the ever-changing global ecosystem, climate change has emerged as the most pressing environmental concern of the Anthropocene age, driven primarily by the escalating use of fossil fuels since industrialization. Consequently, the impacts of climate change on freshwater ecosystems and water supplies are expected to be among the key challenges faced by nations in the 21st century.[4]

The interconnections between climate change, WS, and various socioeconomic issues – such as political strife, food security, and sustainable groundwater planning – pose serious global challenges. Agriculture, the cornerstone of many Asian economies, is particularly affected by WS, which in turn impacts food production, livelihoods, and economic growth.[5] In addition, rising sea levels and groundwater depletion threaten coastal areas and drinking water supplies, potentially leading to increased risks of poverty, hunger, and waterborne diseases. Recognizing the urgency and importance of addressing WS, global attention has focused on water access, allocation, and management, as these are fundamental for both human and ecosystem health. Achieving some of the Sustainable Development Goals requires access to sufficient and safe water.[6] Nevertheless, in certain countries, especially those under dictatorships, strict water restrictions may be imposed to control the populace, exacerbating WS for vulnerable individuals. To mitigate this, appropriate regulations and stringent laws must be enacted, and governments must initiate water-related projects and awareness programs to promote water conservation and prevent over-exploitation of water resources.[7] With growing concerns over climate change and the need for sustainable practices, efforts should be directed toward making the energy sector and water management more eco-friendly. Moreover, good governance, rule of law, anti-corruption measures, and accountability are essential for improving water resource management and streamlining the energy sector.[8]

The present study identifies key research questions to be addressed through detailed empirical testing. First, it explores the potential of integrated governance strategies in mitigating WS, focusing on institutional factors that contribute to ineffective water resource management. Second, it examines the relationship between the use of renewable energy sources and WS in Asia, considering the interdependencies between water, energy, food, and ecosystems. Third, the study investigates the effects of POPG on WS, acknowledging that a growing population impacts water demand, consumption habits, and overall water availability.

While the literature on water-related issues is extensive, there is limited research on how governance indicators, climate policy, and food security measures can reduce water stress.[9,10] This study uses the generalized method of moments (GMM) estimator with panel data from 39 Asian nations, spanning 1996 to 2022, to identify causal links between climate adaptation techniques in water management, agricultural sustainability, and governance quality. This distinction sets this study apart in the field. In addition, the present study quantifies how climate funding and efficient governance may influence water stress, with implications for policy, especially for national and international organizations designing efficient water management systems.

2. Literature review

The present study draws on resource dependency theory and institutional theory. According to resource dependency theory,[11] systems and organizations must rely on external resources to remain robust and sustainable. This theory emphasizes the importance of adaptive resource management in the context of WS, highlighting how renewable energy, agriculture, and government policies affect resource viability. Institutional theory[12] examines how social and organizational standards affect behavior. This perspective is useful for evaluating governance and policy frameworks aimed at providing long-term solutions to WS. In recent years, research on resource reliance and WS management has increased significantly. Ahmad *et al*.[13] examined how resource reliance and external economic constraints impact the adoption of renewable energy in developing countries, with their findings indicating that these adjustments led to reduced water usage. Anser *et al*.[14] stressed the necessity of institutional frameworks for sustainable agriculture as a means of alleviating environmental stress. These findings support the theory that strong institutional frameworks and resource-reliance management may mitigate WS. Research on institutional quality and environmental policy illuminates the significance of governance in sustainable resource management. Strong leadership is critical for improving environmental policy implementation, thereby reducing resource loss and enhancing sustainability.[15]

The present study applies institutional theory to examine how effective governance mediates the relationship between renewable energy adoption and agricultural sustainability in the context of water constraints. Rao *et al*.[16] examined how institutional reforms could accelerate the adoption of renewable energy and the role of governance in addressing resource limitations. Their research investigates the widespread use of renewable energy sources to reduce water stress. Malla *et al*.[17] found that renewable energy sources help minimize water consumption in power generation, particularly in water-scarce regions. Yang and Solangi[18] stressed the necessity for coordinated conservation measures, focusing on the intersection of renewable energy, WS, and sustainable agriculture.

Du Plessis[19] notes that South Africa is among the regions experiencing significant water stress, with global water shortages projected by 2050. The study advocates for water policy reforms, expanding monitoring networks, and fostering water diplomacy among stakeholders to effectively address these challenges. Scanlon *et al*.[20] considered the interconnection between groundwater and surface water while analyzing trends in water resource development. Their study revealed substantial variations in total water storage across regions over the past century, with climate variability and human activities, particularly irrigation, significantly influencing these changes. They recommended the implementation of diverse management techniques to enhance water resource resilience.

Richter[21] assessed water use in 28 utilities serving 23 million people reliant on rivers. Despite a 24% increase in population, over half of the cities reduced per capita water use. However, water consumption in the Colorado River Basin increased by 1%. Suna *et al*.[22] highlighted the worsening water availability in India due to climate change, which is negatively impacting agriculture and rural livelihoods. Effective irrigation management was emphasized as a solution to these challenges. Liu *et al*.[23] quantified agricultural WS in China using the agricultural WS index (AWSI), noting that climate change could increase the value of the AWSI, especially in Inner Mongolia. They suggested improving irrigation efficiency as a potential solution.

Harik *et al*.[24] used agent-based modeling (ABM) to predict farmers' decisions under potential WS scenarios induced by climate change. Their study found that farmers primarily adopted adaptive actions, such as switching crops or seeking alternative water sources, under low-to-moderate water constraints. However, severe water shortages led many farmers to cease farming, urbanize their lands, or leave them fallow. Including social influences in the ABM reduced adaptability, resulting in increased land selling or abandonment in response to WS. Essaber *et al*.[25] focused on climate project funding in Egypt, Morocco, and Tunisia. They identified local and international funding sources and advocated for an integrated financing approach involving all actors to effectively combat climate change. Cao *et al*.[26] introduced a methodology to analyze the Virtual Water Footprint in Chinese provinces, highlighting strategies for reducing agricultural water footprints and alleviating national water stress. Moursy *et al*.[27] compared drip and surface irrigation in the Nile Delta, finding drip irrigation to be more effective in water use and conservation across various crops. Fang *et al*.[28] examined the water footprint and virtual water trade of Belt and Road Initiative (BRI) nations, noting that economic and population expansion has led to an increased water footprint. The study emphasized the importance of collaboration on water resource management to address WS challenges within the BRI.

Based on the existing literature, the present study proposes several hypotheses related to WS and governance challenges in Asian countries:

H_1: Government regulatory quality (RQ) and effectiveness are crucial in mitigating climate risks and addressing WS challenges in Asian countries.

H_2: Mitigating climate hazards and resolving water shortages in Asia can be achieved through the implementation of renewable energy sources and climate funding initiatives.

H_3: Increasing populations, unsustainable agricultural practices, and land degradation exacerbate drought conditions in Asia.

This research aims to illuminate the region's water deficit and sustainable water resource management issues by evaluating these hypotheses.

While there is considerable research on the economic factors, governance, and WS in Asian nations, there remains a gap in the literature concerning the effectiveness of specific government initiatives in this context.[29,30] Previous studies have outlined the high-level role of governance but have not sufficiently explored how governance can mitigate climate change and address water shortages.[31,32] In addition, early studies have overlooked the potential of renewable energy to alleviate WS.[33,34] Renewable energy technologies may improve water availability and usage, yet the literature has not adequately addressed this relationship.[35,36]

For sustainable resource management, it is important to explore the relationship between renewable energy consumption (REC) and water shortages in Asia. While climate funds have been mentioned, their usage and effectiveness in solving water shortages have not been fully examined.[37,38] A detailed review of the impact and efficiency of climate funding in mitigating water shortages would significantly contribute to the field. Moreover, the interconnectedness of water shortages, POPG, crop yields, and agricultural land degradation (AGLD) requires further investigation. Understanding how these factors influence water availability and consumption patterns is essential for developing sustainable water resource management strategies.

3. Data and methodology

The present study adopts a methodological approach designed to ensure the replicability and clarity of the research techniques. To address endogeneity issues frequently encountered in environmental and resource management research, the analysis employs dynamic panel data with the GMM estimator. GMM is particularly well-suited to capturing dynamic relationships, as it accounts for unobserved heterogeneity, lagged dependent variables, and instrumental effects. Recent studies by Arellano and Bond[39], Blundell and Bond[40] confirm the effectiveness of this method for panel data analysis. In line with this approach, the following section details the variables employed in the model:

(i). Dependent variable

- WS (indicating climate risk): Measured as water productivity – total gross domestic product (GDP) (constant 2015 US$) per m^3 of total freshwater withdrawal – sourced from the World Development Indicators.[41]

(ii). Independent variables

- RQ: Captures the government's ability to establish and enforce robust policies and regulations that support private sector development. Values range from −2.5 to 2.5, expressed in standard normally distributed units, obtained from the World Governance Indicators[42]
- Government effectiveness (GEF): Reflects the quality of public services, civil service independence from political influences, and the quality of policy formulation and implementation. Also expressed in standard normally distributed units (−2.5 to 2.5), sourced from the World Governance Indicators.[42]

(iii). Controlled variables

- REC: The share of renewable energy in total final energy consumption, sourced from the World Development Indicators[41]
- POPG: Measured as the annual percentage change in population, sourced from the World Development Indicators[41]
- AGLD: Represented by the percentage of land area designated for agriculture, sourced from the World Development Indicators[41]
- Climate financing (CLF): Constructed using principal component analysis, this index incorporates weighted components of foreign direct investment inflows, REC, carbon damages, and trademark application (direct resident) expenditure. The method is adapted from Khan *et al*.,[43] with data sourced from the World Development Indicators.[41]

The study focuses on 39 Asian countries as the unit of analysis, chosen from a total of 48 countries in the region based on data availability. The panel dataset spans 26 years, covering the period from 1996 to 2022. The countries are categorized into subregions as follows:

- Eastern Asia: China, Japan, Mongolia, North Korea, and South Korea
- Southern Asia: Afghanistan, Bangladesh, Bhutan, India, Iran, Maldives, Nepal, Pakistan, and Sri Lanka.
- South-Eastern Asia: Brunei Darussalam, Cambodia, Indonesia, Laos, Myanmar, Malaysia, Philippines, Singapore, Thailand, Timor-Leste, and Vietnam
- Western Asia: Armenia, Bahrain, Cyprus, Georgia, Jordan, Iraq, Israel, Kuwait, Lebanon, Oman, Qatar, Saudi Arabia, Syria, State of Palestine, Turkey, United Arab Emirates, and Yemen
- Central Asia: Azerbaijan, Kyrgyzstan, Kazakhstan, Tajikistan, Turkmenistan, Uzbekistan.

The study utilizes a regression model to explore the relationship between governance indicators and water governance across Asia. This model, referred to as the Good Governance and Water Resources Model or the Water Governance Model, is grounded in theoretical relationships established in the present research. It aims to examine how governance indicators influence water governance practices in the region. The model is specified as follows:

$$WS_t = \propto_0 + \propto_1 WS_{t-1} + \propto_2 GEF_t + \propto_3 RQ_t + \propto_4 REC_t + \propto_5 POPG_t + \propto_6 CROP_t + \propto_7 AGLD_t + \propto_8 CLF_t + \mu_t \quad \text{(I)}$$

Where WS, GEF, RQ, REC, POPG, AGLD, and CLF retain their previously defined meanings, and crop production (CROP) denotes CROP.

Dynamic GMM is frequently applied by economists for parameter estimation in changing panel data simulations.[39] It proves particularly valuable in addressing challenges such as unobserved heterogeneity, endogeneity, and serial correlation within panel datasets. A commonly used variant is the two-step differenced GMM estimator, which involves differencing the data to eliminate individual-specific effects and generate valid instruments for accurate estimation. This estimator operates in two phases. In the first phase, data differencing removes time-invariant unobserved heterogeneity, thereby mitigating endogeneity concerns. In the second phase, the system

of equations is estimated using the GMM framework, incorporating instruments derived from the differenced data to ensure robust parameter estimates.

4. Results

Table 1 presents descriptive statistics for selected Asian countries from 1996 to 2022. The mean WS level across these countries was 43.751 m^3 of total freshwater withdrawal per constant 2015 US$ of GDP, with considerable variability, as indicated by a standard deviation of 114.613. GEF and RQ exhibited overall negative evaluations, with mean indices of −0.036 and −0.112, respectively, reflecting diverse governance performances across the region. REC accounted for an average of 25.223% of GDP, highlighting a regional commitment to sustainability. POPG averaged 1.597%, while CROP recorded an average index of 87.603, suggesting variability in agricultural productivity.

The percentage of land area designated for agriculture (AGLD) averaged 400,195.4, with large variability indicated by a standard deviation of 945,180.9. CLF had a mean index of 0.0003, reflecting relatively low financial support for climate-related projects, yet with the potential for notable fluctuations (standard deviation: 1.183).

The kurtosis coefficients offer additional insights into variable distributions. Leptokurtic distributions have heavier tails and sharper peaks compared to a normal distribution, whereas platykurtic distributions exhibit flatter peaks and lighter tails. The high kurtosis value of 34.634 for WS indicates significant heterogeneity and substantial variability across Asian nations. GEF and RQ have kurtosis values of 2.977 and 2.951, respectively, suggesting distributions that are approximately normal, with moderate variability. In contrast, REC, with a kurtosis of 2.679, demonstrates a platykurtic distribution, signifying lower variability. The POPG kurtosis of 6.108 indicates a leptokurtic distribution characterized by limited variability but heavier tails. CROP shows a modestly peaked distribution, with a kurtosis of 4.031, exhibiting minor variability in agricultural output. AGLD, with a kurtosis of 18.688, displays a strongly leptokurtic distribution, indicating significant variability likely driven by diverse regional land-use patterns. CLF, with a kurtosis of 3.217, suggests a distribution that is approximately normal with somewhat pronounced tails. Collectively, these results illustrate the diverse distributional characteristics of the variables examined across the investigated sites, enhancing the understanding of their statistical behavior. The analysis presented in Table 2 employs a two-step GMM dynamic panel data approach to investigate the factors influencing WS governance in selected Asian countries.

The study finds that GEF has a significant negative impact on WS governance. Specifically, a 1% improvement in GEF leads to a substantial 17.581% reduction in WS issues. This suggests that nations with stronger governance systems are better equipped to manage water shortages and promote sustainable water resource management. Similarly, the coefficient of RQ also exhibits a significant and negative impact on WS governance. A 1% enhancement in RQ results in a remarkable 55.049% reduction in WS issues. This finding suggests that fragmented water resource institutions – often stemming from poor inter-agency coordination – hinder the efficient management of

Table 1. Descriptive statistics

Methods	WS	GEF	RQ	REC	POPG	CROP	AGLD	CLF
Mean	43.751	−0.036	−0.112	25.223	1.597	87.603	400195.4	0.0003
Maximum	996.803	2.436	2.260	96.041	7.349	203.570	5290386	4.689
Minimum	0.196	−2.307	−2.344	0.0005	−3.6296	19.210	6.600	−3.086
Std. Dev.	114.613	0.870	0.878	29.704	1.279	27.439	945180.9	1.183
CV	261.966	−2416.670	−783.929	117.765	80.087	31.321	236.179	394333.3
Skewness	5.220	0.501	0.116	1.020	0.859	0.148	3.806	0.242
Kurtosis	34.634	2.977	2.951	2.679	6.108	4.031	18.688	3.217

Source: Author's estimate. CV: Coefficient of variation; Skewness measures the asymmetry of distribution: a value of 0 indicates symmetry, while positive and negative values indicate right- and left-skewed distributions, respectively; Kurtosis values >3 indicate heavy-tailed distributions, <3 indicate light-tailed, a normal distribution has a kurtosis of 3.
Abbreviations: AGLD: Agricultural land degradation; CLF: Climate financing; CROP: Crop production; GEF: Government effectiveness; POPG: Population growth; REC: Renewable energy consumption; RQ: Regulatory quality; Std. Dev.: Standard deviation; WS: Water scarcity.

Table 2. Panel two-step generalized method of moment estimates

Variables	Coefficient	S.E.	*t*-statistic	Prob.
WS(−1)	0.878	0.0008	991.661	0.000
Governance indicators (used as explanatory variables)				
GEF	−17.581	0.180	−97.388	0.000
RQ	−55.049	0.162	−339.306	0.000
Macroeconomic variables (used as controlled variables)				
REC	1.551	0.098	15.721	0.000
POPG	−5.172	0.059	−87.506	0.000
CROP	−0.171	0.003	−55.549	0.000
AGLD	0.0006	3.3×10^{-05}	18.527	0.000
CLF	10.397	0.152	68.164	0.000
Effect specification				
Cross-section fixed (first differences)				
Mean dependent variable	1.869	Std. Dev. dependent variable		19.386
S.E. of regression	28.265	Sum squared residual		708,669.5
J-statistic	27.795	Instrument rank		40
Probability (*J*-statistic)	0.679			

Source: Author's estimate.
Abbreviations: AGLD: Agricultural land degradation; CLF: Climate financing; CROP: Crop production; GEF: Government effectiveness; POPG: Population growth; Prob.: Probability; REC: Renewable energy consumption; RQ: Regulatory quality; Std. Dev.: Standard deviation; S.E.: Standard error; WS: Water scarcity.

water resources. This research also finds that renewable energy sources have a notable beneficial effect on water shortage management. A 1% increase in REC leads to a 1.551% reduction in WS issues, highlighting the potential of renewable energy to support sustainable water resource management. Consistent with previous studies, these results are encouraging: Areas facing water shortage can benefit from integrating renewable energy sources. One major advantage of this shift is reduced reliance on water-intensive energy production techniques such as coal-fired power plants and nuclear reactors. Transitioning to renewable energy can reduce a country's water footprint in the energy sector, freeing up water for other essential uses.

The coefficient for POPG indicates a significant negative impact on WS governance. Specifically, a 1% increase in POPG corresponds to a 5.172% reduction in WS issues. This finding suggests that, in some contexts, POPG may drive improvements in water infrastructure or governance, although further investigation is needed to clarify this dynamic. The coefficient of CROP also shows a significant negative impact on WS governance. A 1% increase in CROP is associated with a 0.171% decline in WS issues. However, the study warns that agricultural WS may worsen in regions experiencing soil desiccation and reduced precipitation due to global warming, ultimately affecting crop yields. Conversely, the coefficient for AGLD significantly influences water shortage governance. For every 1% increase in AGLD, water shortage problems rise by 0.0006%. This underscores the need for more effective water management in agriculture. Degraded soil retains less water and results in higher runoff and lower groundwater recharge, reducing the availability of farmable water and threatening farmers' livelihoods. As AGLD directly contributes to water shortages, governments should implement strategies to improve water retention in soils and prevent further land degradation. Sustainable land management strategies, such as soil conservation, afforestation, and reforestation, are essential in this regard. The coefficient for CLF shows a significant positive impact on WS governance. A 1% increase in CLF leads to a 10.397% rise in WS issues. This result highlights the influence of climate change – particularly the growing risks of droughts and weather variability – on water availability. Table 3 presents the results of the Arellano–Bond serial correlation test for the first and second lagged terms.

Table 3. Arellano–Bond serial correlation estimates

Test order	m-statistic	Rho	S.E. (rho)	Prob.
AR (1)	−0.006	−306886.996	48696645.623	0.995
AR (2)	NA	11900.195	NA	NA

Source: Author's estimate.
Abbreviations: AR: Autocorrelation; Prob.: Probability; S.E.: Standard error.

The GMM methodology employs the Arellano–Bond tests for autocorrelation (AR) (1) and AR (2) serial correlation to assess model validity. Under the null hypothesis of no autocorrelation, the test results indicate that the AR(1) probability value is 0.995. Therefore, at the 5% significance level, the null hypothesis is not rejected, confirming the absence of first-order autocorrelation in the model.

5. Discussion

Integrating water pollution control with water resource planning is recommended to ensure water resource management that is both socially and economically beneficial.[44] Improved WS regulation can yield long-term economic benefits. When government agencies fail to coordinate water resource management effectively, institutions may become fragmented. This fragmentation can lead to wasted resources, conflicting strategies, and unnecessary duplication of efforts, leading to inefficient water management.

Streamlining water resource planning and eliminating legislative inefficiencies can help nations improve both water consumption and cost management.[45] Disjointed water resource institutions may also deter businesses and investors. Inconsistent policies and regulatory uncertainty can restrict investment in water-dependent industries, ultimately slowing economic growth. By contrast, a more efficient governmental response to water shortages can produce positive financial impacts.

First, improved water governance can optimize water use across sectors such as agriculture, manufacturing, and domestic consumption. Efficient resource utilization enhances productivity and supports overall economic growth.[46] Second, better water shortage management may stabilize the economy and attract greater investment. Businesses are more likely to invest in regions where water resources are reliable, contributing to job creation and broader economic development. Investments in renewable energy also support innovation, economic growth, and resilience to external shocks. Countries with energy security are better positioned to manage their water resources effectively.[47]

As the global population continues to grow, intelligent water resource management becomes increasingly crucial. To meet rising demand, nations must prioritize water balance – ensuring that water supply aligns with consumption needs. This includes strategies such as optimizing agricultural irrigation, promoting water reuse, and encouraging conservation practices. These approaches help reduce water waste and improve efficiency, thereby aiding efforts to meet population-driven water demand.[48]

The condition of global water supplies is directly tied to population trends. As water sources come under increasing stress, protecting both human health and ecosystems requires a strong emphasis on maintaining water quality. Adequate wastewater treatment and pollution control are especially important in densely populated regions that are more vulnerable to contamination.[49] Sustaining a growing population demands adequate water resources for agriculture, domestic use, and industrial activity. However, uncontrolled POPG can lead to the overexploitation of water resources, aquifer depletion, and ecosystem degradation. Comprehensive land reforms are therefore essential to ensuring a sustainable water supply in the face of continued population pressure. Such reforms should include proper land-use planning to strategically allocate land among agricultural, industrial, and urban uses.[50] Promoting sustainable, water-efficient agriculture and incorporating water-sensitive design into urban planning are key strategies for effective long-term water resources management.

The impact of CROP on WS governance is closely tied to the agricultural sector, which is a major water consumer in many countries. As CROP increases, so does the demand for irrigation water. This rising need places additional pressure on water supplies, particularly in arid regions. The cultivation of crops can exacerbate water shortage; therefore, nations must prioritize environmentally sustainable farming practices. Adopting water-saving irrigation methods – such as drip irrigation – can assist in optimizing water consumption and reducing water wastage.[51] Agricultural planning and crop selection based on local water availability and climatic conditions can further enhance water-use efficiency. Environmentally, agricultural production has significant implications for WS governance. In regions already experiencing soil desiccation and severe WS due to global warming and decreasing precipitation,

increased agricultural water demand may worsen the situation. This could jeopardize food security and the livelihoods of vulnerable populations by reducing agricultural yields. To address these challenges, climate-resilient agricultural practices are essential. Farmers should adopt drought-resistant crop varieties, improve soil health through sustainable agricultural practices, and invest in upgraded water storage and harvesting systems.[52]

Advanced agriculture offers a solution by reducing waste of water, fertilizers, and pesticides through the use of technology. Tools such as soil moisture sensors, automated irrigation systems, and satellite imagery enable precise irrigation, thereby enhancing water conservation and agricultural productivity. Techniques such as drip irrigation, rainwater collecting, and other advanced systems can significantly reduce water loss and improve water-use efficiency. Degraded soil causes sedimentation and the deterioration of water quality – issues that may negatively affect aquatic ecosystems and human health.[53] Addressing these concerns requires land restoration and protection. Sustainable land management practices aimed at rehabilitating degraded lands can improve soil health, increase water retention, boost agricultural productivity, and enhance water availability. Investments in farmer training and agricultural extension services are also critical for disseminating best practices and building capacity in water-efficient agriculture. In addition, governments should improve the monitoring and enforcement of regulations against illegal land clearing and deforestation to mitigate AGLD and reduce the risk of water shortages.

Long-term environmental changes and catastrophic events pose serious threats to ecosystems and increase pressure on water demand. To mitigate the impacts of climate change on water resources, projects and initiatives must be adequately funded. Investment in climate-resilient infrastructure – particularly water storage and distribution systems – can help manage the effects of shifting weather patterns and fluctuating water supply. CLF can also support the development of technologies aimed at improving water efficiency and reducing waste.[54] Changes in precipitation patterns, prolonged droughts, and more intense weather events directly affect water supplies. These changes not only affect the quantity and quality of water but also endanger ecosystems, biodiversity, and human livelihoods. CLF plays a critical role in safeguarding water resources and natural ecosystems from climate variability.[55] In addition, climate change adaptation and mitigation strategies may be more effective when coordinated across neighboring nations that share transboundary water resources.

This study presents several limitations that highlight directions for future research. First, the analysis covers 39 Asian countries from 1996 to 2022; however, the absence of comprehensive data may have excluded relevant factors that could have enhanced the findings. Due to inconsistencies in reporting across countries, several socioeconomic and environmental aspects of WS may have been overlooked. Future studies should incorporate larger and more detailed datasets, including information on national water regulations and governance systems, to improve the robustness of the results. Although this study employs GMM to address endogeneity, it may not fully capture all dynamic changes in water management and governance over time. Alternative econometric models, such as spatial models or dynamic panel threshold models, could offer deeper insights into the complex interactions among variables.

This research primarily focuses on governance indicators, climate-related factors, and economic variables affecting water shortage. However, future studies could incorporate additional dimensions, such as technology innovation, institutional capacity, and localized water management practices. Future research may also examine how renewable energy integration, advanced irrigation technologies, and water conservation strategies contribute to reducing global water stress. To improve the granularity of findings, future analyses should consider subnational or city-level data, offering a better understanding of localized water governance issues and solutions. In addition, examining the long-term effects of climate adaptation policies on sustainable water resource management would be valuable, particularly given the current study's emphasis on CLF in addressing water shortages. Expanding the dataset to include other water-stressed regions outside Asia would enhance the generalizability of findings and allow for cross-regional comparisons of policy effectiveness.

6. Conclusion and policy recommendations

The present study analyzes key drivers of water shortage governance – specifically, GEF, RQ, REC, POPG, CROP, AGLD, and CLF – across 39 Asian countries from 1996 to 2022. The findings reveal the complex dynamics between GEF, CLF, and agricultural practices in shaping WS outcomes. The results suggest that

renewable energy adoption can reduce water shortages and promote sustainability in resource-constrained countries. Governance quality emerged as a critical factor, highlighting the importance of strong institutional frameworks in effective resource management. CLF was also found to support water adaptation strategies. In the agricultural sector, sustainable practices – including crop diversity and environmentally responsible land use – can mitigate water shortages and improve resilience.

The use of dynamic panel data analysis provides new insights into how these variables interact over time, filling a gap in the literature and offering practical recommendations for policymakers. The study emphasizes the need for integrated solutions to WS. By merging empirical evidence with theoretical perspectives, it contributes to both academic understanding and real-world policy applications for countries striving to balance sustainable development with effective resource management.

This research advances academic discourse by highlighting the importance of interdisciplinary approaches to global water issues. It offers significant theoretical and practical contributions by integrating renewable energy, agricultural approaches, and governance indicators into a unified analytical framework, thereby enhancing scholarly knowledge on resource management. The study's findings are also relevant for policymakers and practitioners working to address water shortages through research. The study concludes that cross-sector collaboration is essential for achieving long-term sustainability. It identifies key drivers and solutions that can support effective water governance in the face of climate and resource pressures.

The following policy recommendations are proposed for Asian economies to mitigate climate-related risks through a water governance approach:

(i) Implement immediate measures to enhance water governance frameworks by fostering collaboration among governments, stakeholders, and communities. Establish transparent and efficient water management systems to optimize water allocation and utilization

(ii) Encourage the rapid adoption of renewable energy sources, such as solar and wind power, to reduce reliance on water-intensive energy production. This transition will alleviate pressure on water resources and contribute to sustainable development

(iii) Develop pricing strategies that incentivize responsible water consumption across industrial, agricultural, and domestic sectors. Such mechanisms can promote water conservation and reduce wasteful practices

(iv) Launch public awareness campaigns to educate citizens about water conservation practices, efficient water usage, and the importance of preserving water resources. An informed public can play an active role in reducing water demand and managing scarcity

(v) Develop and implement immediate drought management plans in water-stressed regions. These plans should include measures to mitigate the impact of droughts on agriculture, communities, and ecosystems.

Acknowledgments

None.

Funding

None.

Conflict of interest

The authors declare no conflicts of interest.

Author contributions

Conceptualization: Muhammad Khalid Anser, Muhammad Zaheer Akhtar, Khalid Zaman
Formal analysis: All authors
Investigation: Muhammad Khalid Anser, Muhammad Zaheer Akhtar
Methodology: Muhammad Khalid Anser, Muhammad Zaheer Akhtar, Syed Tahir Hussain Shah
Writing – original draft: All authors
Writing – review & editing: All authors

Availability of data

The data used in this study are freely available from the World Development Indicators and the World Governance Indicators, both published by the World Bank (https://databank.worldbank.org/source/world-development-indicators).

References

1. Azimov U, Avezova N. Sustainable small-scale hydropower solutions in central Asian countries for local and cross-border energy/water supply. *Renew Sustain Energy Rev.* 2022;167:112726. doi: 10.1016/j.rser.2022.112726

2. Ngene BU, Nwafor CO, Bamigboye GO, Ogbiye AS, Ogundare JO, Akpan VE. Assessment of water resources development and exploitation in Nigeria: A review of integrated water resources management approach. *Heliyon*. 2021;7(1):e05955. doi: 10.1016/j.heliyon.2021.e05955
3. Rosmadi HS, Ahmed MF, Mokhtar MB, Lim CK. Reviewing challenges of flood risk management in Malaysia. *Water.* 2023;15(13):2390. doi: 10.3390/w15132390
4. Dalstein F, Naqvi A. 21st-century water withdrawal decoupling: A pathway to a more water-wise world? *Water Resour Econ*. 2022;38:100197. doi: 10.1016/j.wre.2022.100197
5. Katimbo A, Rudnick DR, DeJonge KC, *et al.* Crop water stress index computation approaches and their sensitivity to soil water dynamics. *Agric Water Manag.* 2022;266:107575. doi: 10.1016/j.agwat.2022.107575
6. Sadoff CW, Borgomeo E, Uhlenbrook S. Rethinking water for SDG 6. *Nat Sustain*. 2020;3(5):346-347. doi: 10.1038/s41893-020-0530-9
7. Chakkaravarthy DN, Balakrishnan T. Water scarcity-challenging the future. *Int J Agric Environ Biotechnol*. 2019;12(3):187-193. doi: 10.30954/0974-1712.08.2019.2
8. Sadaoui N, Zabat L, Sekrafi H, Abid M. The moderating role of natural resources between governance and CO_2 emissions: Evidence from MENA countries. *Energy Environ*. 2024;35(3):1597-1615. doi: 10.1177/0958305X221141389
9. Mfarrej MFB. Exploring the nexus between climate change, water scarcity, and security dynamics in the Middle East and North Africa. *Next Res.* 2025;2(1):100168. doi: 10.1016/j.nexres.2025.100168
10. Dzvene AR, Zhou L, Slayi M, Dirwai TL. A scoping review on challenges and measures for climate change in arid and semi-arid agri-food systems. *Discov Sustain*. 2025;6(1):151. doi: 10.1007/s43621-025-00945-z
11. Pfeffer J, Salancik GR. External control of organizations: A resource dependence perspective. *Organ Behav.* 2015;2:355-370. doi: 10.4324/9781315702001
12. Scott WR. Institutional theory: Contributing to a theoretical research program. In: Smith KG, Hitt MA, editors. *Great Minds in Management: The Process of Theory Development*. Oxford UK: Oxford University Press. Available from: https://www.researchgate.net/publication/265348080 [Last accessed on 2024 Oct 12].
13. Ahmad M, Peng T, Awan A, Ahmed Z. Policy framework considering resource curse, renewable energy transition, and institutional issues: Fostering sustainable development and sustainable natural resource consumption practices. *Resour Policy*. 2023;86:104173. doi: 10.1016/j.resourpol.2023.104173
14. Anser MK, Yousaf SU, Usman B, *et al.* Beyond climate change: Examining the role of environmental justice, agricultural mechanization, and social expenditures in alleviating rural poverty. *Sustain Futures.* 2023;6:100130. doi: 10.1016/j.sftr.2023.100130
15. Ullah S, Luo R, Nadeem M, Cifuentes-Faura J. Advancing sustainable growth and energy transition in the United States through the lens of green energy innovations, natural resources and environmental policy. *Resour Policy*. 2023;85:103848. doi: 10.1016/j.resourpol.2023.103848
16. Rao A, Kumar S, Karim S. Accelerating renewables: Unveiling the role of green energy markets. *Appl Energy.* 2024;366:123286. doi: 10.1016/j.apenergy.2024.123286
17. Malla FA, Grover S, Hussain A, *et al.* Water footprints in power generation: Challenges and strategies for a sustainable environment. *Curr Dir Water Scarcity Res.* 2024;8:149-162. doi: 10.1016/B978-0-443-23631-0.00010-8
18. Yang Z, Solangi YA. Analyzing the relationship between natural resource management, environmental protection, and agricultural economics for sustainable development in China. *J Clean Prod*. 2024;450:141862. doi: 10.1016/j.jclepro.2024.141862
19. Du Plessis A. Water resources from a global perspective. In: *South Africa's Water Predicament: Freshwater's Unceasing Decline*. Cham: Springer International Publishers; 2023. p. 1-25.
20. Scanlon BR, Fakhreddine S, Rateb A, *et al.* Global water resources and the role of groundwater in a resilient water future. *Nat Rev Earth Environ.* 2023;4(2):87-101. doi: 10.1038/s43017-022-00378-6
21. Richter BD. Decoupling urban water use from population growth in the Colorado River Basin. *J Water Resour Plan Manag.* 2023;149(2):04022082. doi: 10.1061/JWRMD5.WRENG-588
22. Suna T, Kumari A, Paramaguru PK, Kushwaha NL. Enhancing agricultural water productivity using deficit irrigation practices in water-scarce regions. In: *Enhancing Resilience of Dryland Agriculture Under Changing Climate: Interdisciplinary and Convergence Approaches*. Singapore: Springer Nature Singapore; 2023. p. 177-206.
23. Liu J, Fu Z, Liu W. Impacts of precipitation variations on agricultural water scarcity under historical and future climate change. *J Hydrol*. 2023;617:128999. doi: 10.1016/j.jhydrol.2022.128999
24. Harik G, Alameddine I, Zurayk R, El-Fadel M. An integrated socio-economic agent-based modeling framework towards assessing farmers' decision making under water scarcity and varying utility functions. *J Environ Manage*. 2023;329:117055.

doi: 10.1016/j.jenvman.2022.117055
25. Essaber S, Essayem A, Baccouche I. Catalyzing climate finance for climate actions in MENA countries: A holistic view of Egypt, Morocco, and Tunisia. In: *Digital Economy, Energy and Sustainability: Opportunities and Challenges*. Cham: Springer International Publishers; 2023. p. 55-63.
26. Cao X, Bao Y, Li Y, Li J, Wu M. Unravelling the effects of crop blue, green and grey virtual water flows on regional agricultural water footprint and scarcity. *Agric Water Manag*. 2023;278:108165. doi: 10.1016/j.agwat.2023.108165
27. Moursy MAM, ElFetyany M, Meleha AMI, El-Bialy MA. Productivity and profitability of modern irrigation methods through the application of on-farm drip irrigation on some crops in the Northern Nile Delta of Egypt. *Alex Eng J*. 2023;62:349-356. doi: 10.1016/j.aej.2022.06.063
28. Fang K, He J, Liu Q, *et al.* Water footprint of nations amplified by scarcity in the belt and road initiative. *Heliyon*. 2023;9(1):e12957. doi: 10.1016/j.heliyon.2023.e12957
29. Barati AA, Pour MD, Sardooei MA. Water crisis in Iran: A system dynamics approach on water, energy, food, land, and climate (WEFLC) nexus. *Sci Total Environ.* 2023;882:163549. doi: 10.1016/j.scitotenv.2023.163549
30. Beker BA, Kansal ML. Complexities of the urban drinking water systems in Ethiopia and possible interventions for sustainability. *Environ Dev Sustain*. 2024;26(2):4629-4659. doi: 10.1007/s10668-022-02901-7
31. Gharib AA, Blumberg J, Manning DT, Goemans C, Arabi M. Assessment of vulnerability to water shortage in semi-arid river basins: The value of demand reduction and storage capacity. *Sci Total Environ*. 2023;871:161964. doi: 10.1016/j.scitotenv.2023.161964
32. Tsakiris GP, Loucks DP. Adaptive water resources management under climate change: An introduction. *Water Resour Manag*. 2023;37:2221-2233. doi: 10.1007/s11269-023-03518-9
33. Grzegorzek M, Wartalska K, Kaźmierczak B. Review of water treatment methods with a focus on energy consumption. *Int Commun Heat Mass Transf*. 2023;143:106674. doi: 10.1016/j.icheatmasstransfer.2023.106674
34. Hassan Q, Al-Hitmi M, Tabar VS, Zuhair A, Salman HM, Jaszczur M. Middle East energy consumption and potential renewable sources: An overview. *Clean Eng Technol*. 2023;12:100599. doi: 10.1016/j.clet.2023.100599
35. Abu-Rayash A, Dincer I. Development of an integrated model for environmentally and economically sustainable and smart cities. *Sustain Energy Technol Assessments.* 2024;73:104096. doi: 10.1016/j.seta.2024.104096
36. Wang J, Li W, Haq SU, Shahbaz P. Adoption of renewable energy technology on farms for sustainable and efficient production: Exploring the role of entrepreneurial orientation, farmer perception and government policies. *Sustainability.* 2023;15(7):5611. doi: 10.3390/su15075611
37. Kuhl L, Shinn JE, Arango-Quiroga J, Ahmed I, Rahman MF. The liberal limits to transformation in the Green Climate Fund. *Clim Dev.* 2024;16(9):826-837. doi: 10.1080/17565529.2023.2235318
38. Lazaro LLB, Grangeia CS, Santos L, Giatti LL. What is green finance, after all?-Exploring definitions and their implications under the Brazilian biofuel policy (RenovaBio). *J Clim Finance.* 2023;2:100009. doi: 10.1016/j.jclimf.2023.100009
39. Arellano M, Bond S. Some tests of specification for panel data: Monte Carlo evidence and an application to employment equations. *Rev Econ Stud.* 1991;58(2):277-297. doi: 10.2307/2297968
40. Blundell R, Bond S. Initial conditions and moment restrictions in dynamic panel data models. *J Econom*. 1998;87(1):115-143. doi: 10.1016/S0304-4076(98)00009-8
41. World Bank. World Development Indicators (WDI). Washington, DC; 2022. Available from: https://databank.worldbank.org/source/world-development-indicators [Last accessed on 2024 Sep 05].
42. World Bank. World Governance Indicators (WGI). Washington, DC; 2022. Available from: https://databank.worldbank.org/source/worldwide-governance-indicators [Last accessed on 2024 Sep 05].
43. Khan A, Khan B, Khan G. Dynamic effects of energy aid in energy transition under the moderating role of the government's regulatory quality. *Sustain Futures.* 2024;8:100247. doi: 10.1016/j.sftr.2024.100247
44. Yang C, Menz C, Fraga H, *et al*. Assessing the grapevine crop water stress indicator over the flowering-veraison phase and the potential yield loss rate in important European wine regions. *Agric Water Manag.* 2022;261:107349. doi: 10.1016/j.agwat.2021.107349
45. Zhang CY, Oki T. Water pricing reform for sustainable water resources management in China's agricultural sector. *Agric Water Manag.* 2023;275:108045. doi: 10.1016/j.agwat.2022.108045
46. Dziedzic M, Gomes PR, Angilella M, *et al.* International circular economy strategies and their impacts on agricultural water use. *Clean Eng Technol.* 2022;8:100504. doi: 10.1016/j.clet.2022.100504
47. Tehrani MM, Akhtari M, Kasaeian A, Rad MAV, Toopshekan A, Motlagh MS. Techno-economic

investigation of a hybrid biomass renewable energy system to achieve the goals of SDG-17 in deprived areas of Iran. *Energy Convers Manag.* 2023;291:117319. doi: 10.1016/j.enconman.2023.117319

48. Trang TT, Bush SR, Van Leeuwen J. Enhancing institutional capacity in a centralized state: The case of industrial water use efficiency in Vietnam. *J Ind Ecol.* 2023;27(1):210-222. doi: 10.1111/jiec.13367
49. Zhan J, Wu Z. Effects of liquor production wastewater discharge on water quality and health risks in the Chishui River Basin, Southwest China. *J Clean Prod.* 2023;418:138136. doi: 10.1016/j.jclepro.2023.138136
50. Subekti R, Sulistiyono A, Maharani DP, Dewi IGAGS. The urgency of the legal strategy of abandoned-land use through the formation of land bank in Indonesia. *Cogent Soc Sci.* 2023;9(1):2239050. doi: 10.1080/23311886.2023.2239050
51. Xiao Y, Sun C, Wang D, Li H, Guo W. Analysis of hotspots in subsurface drip irrigation research using CiteSpace. *Agriculture.* 2023;13(7):1463. doi: 10.3390/agriculture13071463
52. Alkhalidi A, Assaf MN, Alkaylani H, Halaweh G, Salcedo FP. Integrated innovative technique to assess and prioritize risks associated with drought: Impacts, measures/strategies, and actions, global study. *Int J Disaster Risk Reduct.* 2023;94:103800. doi: 10.1016/j.ijdrr.2023.103800
53. Rashmi I, Karthika KS, Roy T, *et al*. Soil erosion and sediments: A source of contamination and impact on agriculture productivity. In: Naeem M, Bremont JF, Ansari AA, Gill SS, editors. *Agrochemicals in Soil and Environment*. Singapore: Springer; 2022.
54. Shishlov I, Censkowsky P. Definitions and accounting of climate finance: Between divergence and constructive ambiguity. *Clim Policy.* 2022;22(6):798-816. doi: 10.1080/14693062.2022.2080634
55. Saeed S, Makhdum MSA, Anwar S, Yaseen MR. Climate change vulnerability, adaptation, and feedback hypothesis: A comparison of lower-middle, upper-middle, and high-income countries. *Sustainability.* 2023;15(5):4145. doi: 10.3390/su15054145

Asian Journal of Water, Environment and Pollution. Vol. 22, No. 2 (2025), pp. 152-167.
doi: 10.36922/ajwep.8393

ORIGINAL RESEARCH ARTICLE

An enhanced renewable energy integration system with improved power system stability

Vemireddy Suryanarayana Reddy* and Busireddy Hemanth Kumar

Department of Electrical and Electronics Engineering, School of Engineering, Mohan Babu University, Tirupati, Andhra Pradesh, India

(This article belongs to the *Special Issue: Renewable Energy Systems and Strategies in Smart Grids and Smart Cities Development*)

***Corresponding author:** Vemireddy Suryanarayana Reddy (Vemireddysnr@gmail.com)

Received: January 3, 2025; 1st revised: February 26, 2025; 2nd revised: March 22, 2025; Accepted: March 24, 2025; Published online: April 17, 2025

Abstract: The utilization of renewable energy sources for energy transition is gaining significant popularity due to pollution control and other environmental benefits. To move toward green energy generation, the integration of renewable energy sources with the existing conventional grid plays a key role. The performance of a modern interconnected power system, particularly with a high penetration of renewable energy sources, is significantly impacted by power system oscillations. Flexible Alternating Current Transmission System (FACTS) devices are recommended to improve control framework performance, and the power system stabilizer is the customary controller for damping such oscillations. FACTS offer a powerful strategy as they can control transport voltage, transmission line impedance, and power flows. This paper presents an efficient control scheme that combines four FACTS controllers: the static VAR compensator for controlling reactive power in control frameworks, the unified power flow controller for managing active and reactive power flows on transmission lines, the static synchronous compensator for maintaining system voltage stability, and the static synchronous series compensator for controlling transmission line impedance. To address the challenges posed by the variability of renewable energy sources such as wind and solar, the ant colony optimization algorithm is employed to optimally tune the controllers' parameters. By generating controlled voltage and interfacing with the transmission line, these controllers enhance system stability, even under fluctuating renewable energy inputs. The IEEE 30-Bus system was used for simulation and control design, demonstrating the effectiveness of this approach in damping inter-area oscillations and improving the stability and resilience of a renewable-energy-integrated power system.

Keywords: Renewable energy sources; Pollution control; Integration of renewable energy; Ant colony optimization algorithm; Power stability

1. Introduction

The rise in energy consumption, the expansion of industry, and the connectivity of large systems with numerous producing units have all contributed to the emergence of challenges in the functioning of power systems, especially stability concerns. The growing demand for electric energy has caused substantial difficulties in the way of transmission lines, and the capacity of these lines cannot be expanded simply by adding more generating facilities or transmission lines.[1,2] A power system's stability and proper functioning are

affected by low-frequency oscillations (LFO), as these oscillations can cause significant system deviations that might lead to instability and impact system security. Damping interarea oscillations is challenging, as they are common in interconnected power systems.[3,4] On the other hand, nearby mode, which is confined to the frequency range of 0.1 – 0.8 Hz and arises from interfacing one generator with the rest of the control framework, typically occurs within a frequency range of 0.7 – 2.0 Hz. Local oscillations occur between 0.8 Hz and 2.0 Hz in frequency, whereas interarea oscillations, characterized by generators in different areas vibrating at frequencies ranging from 0.2 Hz to 0.8 Hz, are a more significant concern. Interarea oscillations are riskier to the reliability of the electrical system due to poor damping factors.[5-7] Periodic disturbances can lead to forced oscillations, whose amplitude is inversely linked to the damping of the system, and these oscillations decay rapidly when the disturbance source is removed. Numerous approaches for reducing forced oscillations have been proposed, given these characteristics. An established technique for reducing oscillations is the power system stabilizer (PSS). Recent advancements in the implementation process of Flexible Alternating Current Transmission Systems (FACTS) have improved the mitigation of these oscillations. Various power system control concerns have been frequently solved using FACTS devices.[8-10] FACTS provide efficient control strategies to enhance the flow of power on current transmission lines. Due to the high-speed control capability of their power electronics components, FACTS devices have become common in the power sector.[11-13] FACTS controllers play a significant role in improving the reliability of power systems. The system's steady-state operations, including voltage control, power flow management, and the enhancement of transfer capability, have mostly been addressed by FACTS devices. Among several series of power electronics-based FACTS controllers, the best options for enhancing power oscillation damping are the static synchronous compensator (STATCOM), static synchronous series compensator (SSSC), unified power flow controller (UPFC), and static VAR compensator (SVC).[14,15] Numerous researchers have proposed alternative methods for developing damping controllers based on FACTS devices. The following section includes recent studies relevant to the intended research. In a study by Fathollahi *et al.*,[16] the sine cosine algorithm (SCA) – a population-based stochastic metaheuristic optimization method – was explained. This algorithm's main goal was to fine-tune the settings of a PSS to efficiently attenuate electromechanical oscillations in a single machine connected to a large power supply. To discover the optimal PSS parameter values, the SCA was utilized to frame the optimization problem in terms of minimizing the objective function. However, the design issue was considered an optimization problem, and the choice factors were the controllers' parameters. The PSS-UPFC approach was developed to enhance the dynamic stability of power systems, as introduced in Therattil *et al.*[17] The Ant Lion Optimization technique was used to optimize the design of the PSS and UPFC.

2. Survey of literature

In 1988, Hingorani and Guygyi introduced the concept of FACTS controllers.[1] FACTS commonly refers to the use of high-power semiconductor gadgets to direct numerous electrical factors and parameters, including receptive and dynamic control, stage points, voltage, impedance, and power flows. Since then, numerous studies have been conducted in this area, utilizing FACTS devices to enhance control in transmission frameworks. Various modeling techniques have been applied to model the UPFC.[2-4] In their articles on the susceptance and termination point models of the SVC,[5,6] Bian, Ramey, and Nelson,[2] as well as Sen and Stacey[3] examined methods to improve control framework stability. The optimal placement of the SVC using fuzzy logic and particle swarm optimization (PSO) algorithms was studied by Reddy and Babu.[7] In this study, the SVC was modeled as a device injecting reactive power at the bus to which it was connected, with its optimal location determined using the fuzzy technique. The full power injection model and the corresponding Jacobian matrix elements were modified in the Newton Raphson (NR) approach for load flow investigations by Metavural and Mehmattumay.[8] This research derived the power injection equations for the UPFC. Using load flow calculations, Chengaiah and Marutheswar [[9] presented a study on UPFC control setup. In their paper, Kumar and Nagaraju[10] discussed how to minimize transmission network losses using the UPFC in load flow analyses. This research used the Hale network, incorporated the UPFC power injection model, and examined power flows for various UPFC control parameter values. A differential algorithm for UPFC loss reduction through optimal location and UPFC control parameter adjustment was proposed by Vanitha and Sudhakaran.[11] This study compared the UPFC genetic algorithm with differential evolution. del Valle *et al.*[12] described the

PSO method in detail for optimal allocation and sizing of the UPFC. To ascertain the influence of the position and size of each UPFC unit, this study tested various power system load conditions and evaluated the optimal way to set PSO parameters.

In a study by Guha *et al.*,[18] a metaheuristic optimization method was presented to enhance the stability of the power system using a supplementary damping controller with the SSSC. The method utilized two control channels, phase, and magnitude, to enhance stability and resistance under various operating conditions. For the optimization process, the authors employed a multi-objective approach based on weighted factor summation. Meanwhile, Saidi[19] introduced a hybrid control method for multi-area, multi-machine power systems incorporating FACTS devices using non-linear modeling. The method aimed to dampen interarea oscillations and maximize the utilization of the UPFC. *Shehata et al.*[20] utilized PSO-adaptive neuro-fuzzy inference system (ANFIS) models to estimate the PSS parameters for single-machine infinite bus systems, both with and without the UPFC. They applied the ANFIS model, combining fuzzy logic and neural networks, to model the complexities of these systems. In addition, they employed the PSO algorithm, a metaheuristic optimization technique, to find the optimal solution for the problem. In Khawaja *et al.*,[21] a hybrid optimization-based SSSC controller was developed to address power oscillations in power transmission systems. The introduced controller was designed to optimize the parameters of the SSSC damping controller through a hybrid differential evolution-PSO optimization algorithm. In Behzadpoor *et al.*,[22] developed a hybrid optimization technique called hybrid controlled series compensator-pattern search, combining the chaotic SCA and pattern search for the coordinated design of PSSs and SVC-based controllers.

Due to the erratic power supply from renewable energy sources, effective management is necessary to maximize their potential. In this context, a hybrid energy storage system is required. Combining hybrid energy storage devices with renewable energy sources can improve power management in a direct current (DC) microgrid. This study suggests the optimal hybrid energy storage solution for a DC microgrid using proportional-integral (PI) controllers to efficiently utilize renewable energy sources. The PSO method was used in this model to determine the optimal PI controller. A 72 W DC microgrid system was considered to verify the efficacy of the proposed optimal PI controller.[1]

3. Research method

The four FACTS controllers proposed in this study were applied to AC power system networks. An ant colony optimization (ACO) approach was used to enhance performance, reduce oscillations, and increase power system stability.

3.1. FACTS controller

The term "FACTS" refers to a group of power electronics-based devices that enhance the controllability and stability of power systems, as well as their capacity to transmit electricity. The purpose of using FACTS tools is to improve the initial swing, effectively dampen oscillations, and aid in system stabilization in the event of a major failure.[23,24] Examples include STATCOM, SSSC, UPFC, and SVC. These devices offer an additional method of improving LFO by including supplemental damping controllers, which have been effectively utilized to increase the transient stability margin.

The basic design of FACTS on a transmission line is shown in Figure 1. The network status can be quickly controlled by the FACTs controllers. For effective management of transmission line power, FACTS controllers can be used to precisely adjust the relative phase angle between two control areas. This facilitates active power exchange across the transmission line and helps stabilize frequency variations. By reducing oscillations in a disrupted system through carefully regulated controller damping, transient stability may be attained. The key benefit of incorporating FACTS into a power system is the enhancement of system stability and reliability by regulating the system's power flow and providing sufficient power oscillation damping. Therefore, in the following section, we describe the model of the aforementioned FACTS controllers.

3.1.1. SVC model

The SVC is a member of the FACTS family of shunt devices. It comprises an FC-TCR type, in which a

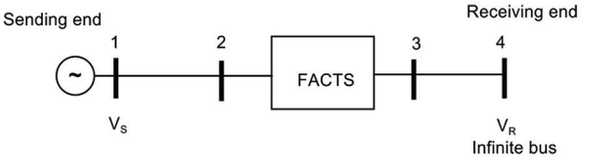

Figure 1. A general block layout displaying the transmission FACTS device

Abbreviations: V_R: Receiving end voltage; V_S: Sending end voltage; FACTS: Flexible Alternating Current Transmission System.

permanent capacitor and a thyristor-controlled reactor are connected in parallel. SVC can also be used to reduce LFO by controlling the reference voltage with an additional signal. SVC is primarily utilized to increase voltage stability in electrical systems.[25,26] Figure 2 depicts the basic schematic circuit of the SVC.

The SVC's control system can be described using the following first-order model for the purpose of dynamic simulation:

$$B_{SVC} = \frac{1}{K_{SVC}}\left(T_{SVC}\left(-U_{t_SVC} + U_{ref_SVC} + V_{SVC}\right) - B_{SVC}\right) \quad \text{(I)}$$

where,
U_{ref_SVC} is the reference voltage of the SVC,
V_{t_SVC} is the bus voltage of the SVC,
B_{SVC} is the equivalent substance of SVC,
V_{SVC} is the control input to the SVC,
T_{SVC} is the gain and time constant of the SVC.

3.1.2. UPFC model

The most widely used and adaptable FACTS device is the UPFC, utilizing electrical components to regulate power flow on power networks. The UPFC can reduce oscillations in a power system and control the voltage, impedance, and phase angle simultaneously or independently.[27] As shown in Figure 3, the UPFC comprises a shunt controller and a series controller, both of which are connected through a shared DC bus.

The UPFC consists of two converters, as shown in Figure 3, each connected to the system in series through an insertion transformer. To accommodate the shared DC voltage, a DC connection, along with a capacitor bank, links the two converters. The UPFC can simultaneously or independently regulate the line phase angle, voltage, and impedance. The series and shunt converters use a voltage source converter (VSC), which is connected to the coupled transformer's secondary side. The current value of the bus to which the shunt converter is connected can be managed using the reactive power from the conversion device. The complex power flow can be managed through a transmission line by controlling the series converter.

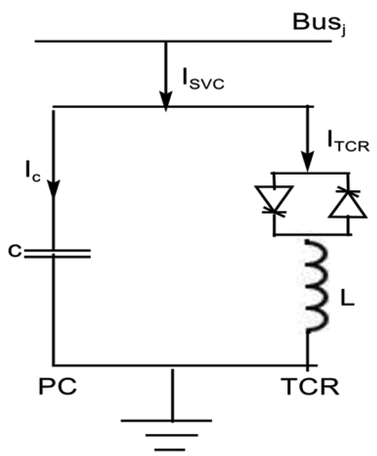

Figure 2. Static VAR compensator model
Abbreviations: Bus$_j$: Bus node *j*; I_c: Capacitor current; I_{SVC}: Static VAR compensator current; I_{TCR}: Thyristor-controlled reactor current; L: Inductor; PC: Point of coupling; TCR: Thyristor-controlled reactor.

3.1.3. STATCOM model

A shunt-coupled FACTS component used as a variable voltage source is called a STATCOM. By adjusting the magnitude and phase angle of the injected voltage source in a steady state, it can either inject or absorb reactive power. It typically consists of a pairing transformer, a capacitor, and a VSC.[28] Although STATCOMs may be used to control other system variables, shunt-linked FACTS devices are mostly employed to adjust the bus voltage magnitude. The basic STATCOM model circuit is depicted in Figure 4.

The required reactive power in either direction is provided by installing the STATCOM at the proper position. The direction of the voltage supplied by the VSC of the STATCOM determines whether reactive power is absorbed or delivered at the utility bus. In addition, the voltage difference between the utility bus and the converter terminal is a factor. Therefore, STATCOMs are primarily utilized for maintaining voltage, improving transient stability, and increasing damping.

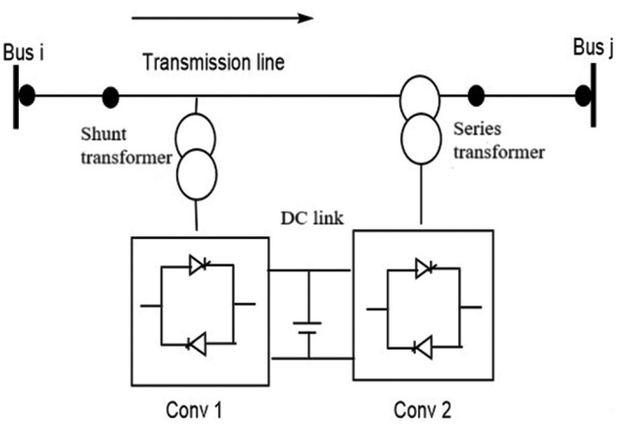

Figure 3. Basic schematic of the unified power flow controller
Abbreviations: Conv: Converter; DC: Direct current.

3.1.4. SSSC model

The SSSC, a series converter, injects a voltage into the line in parallel with the line flow. It can be used to manage the power flow in the system. An SSSC is a series-connected capacitor consisting of a VSC, diode, and DC link capacitor, coupled to the transmission line through a coupling transformer, as shown in Figure 5. This device can provide several compensations by injecting a controllable voltage into the line, thereby altering the transmission line impedance.[29] The SSSC enables both reactive and active power exchange with the power system, allowing the flow of both types of power to be controlled.

Compared to the thyristor-controlled series compensator (TCSC), the SSSC has the benefit of eliminating the capacitance and inductance of reactors and capacitors. In addition, it is symmetrically proficient in both capacitive and inductive modes. Each of these FACTS devices has its own control system. Innovative methods and strategies have successfully been employed to control power systems, increase the capacity and reliability of electrical power transmission, and maintain system stability. The controllers are expanding the available power transmission capacity to deliver more efficient and stable electricity coefficients, thereby strengthening the system. The parameter settings of the abovementioned controllers must be adjusted due to the optimization challenges they face. The performance of FACTS controllers in dampening oscillations in power systems is greatly improved by optimization techniques. They allow for fine-tuning control settings, accounting for complex system dynamics, responding to changing conditions, and maximizing the overall responsiveness of FACTS devices to effectively reduce oscillation issues and maintain grid stability. In our proposed system, FACTS device tuning is optimized using ACO, a swarm-based optimization technique.

4. Optimization technique

This section outlines the specifics of the ACO algorithm applied to the coordinated parameter-tuning architecture of the STATCOM, SSSC, UPFC, and SVC controllers. ACO, a probabilistic method for addressing computing issues, can speed up finding a suitable path through a network. The method was initially proposed by Macro Doriso in his 1992 doctoral thesis. The initial algorithm was created using the concept of the ant colony's search for food in relation to a food supply. Ants begin the food search by wandering randomly throughout the nest.[30,31] Once they locate a food source, they transport small quantities of food to their nest. When traveling back, they deposit a chemical pheromone, which is influenced by the characteristics of the ants and the food source.

The pheromone trail left by ants when they migrate from one location to another is followed by others. Ants are more likely to follow the trail with the highest concentration of pheromones. In doing so, they effectively mark the trail, making it easier to be recognized and followed by other ants. Subsequent ants can then choose the shortest path among several options. The parametric random decision rules govern the sequential decision-making process that generates the solution. The learning of the parameters, which the decision policy depends on, forms the foundation of

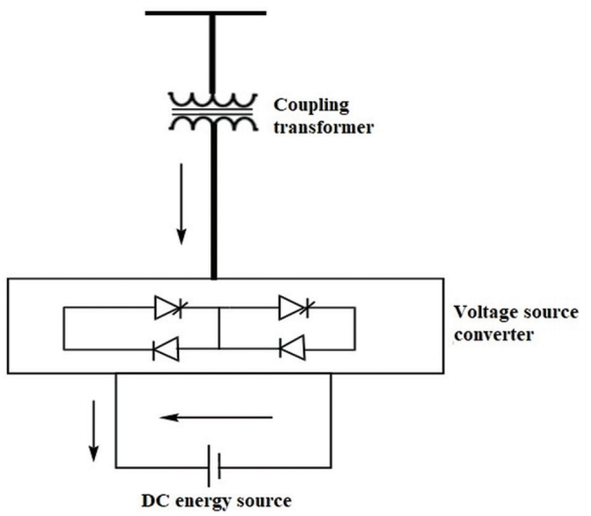

Figure 4. Circuit for the static synchronous compensator

Abbreviation: DC: Direct current.

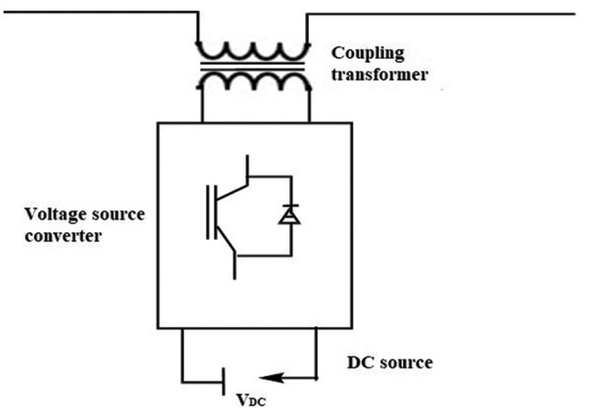

Figure 5. Static synchronous series compensator model

Abbreviation: DC: Direct current.

the ACO algorithm. To effectively mitigate oscillatory behavior and ensure stable grid operation, the ACO algorithm has the ability to dynamically adjust and optimize control settings in real-time.

Table 1 displays the ACO parameters and their corresponding values, which are used to modify the settings of the FACTS controllers. The fundamental process of ACO has been represented into four essential phases:

(i) Initialization
(ii) Probabilistic ant movement
(iii) Update of pheromones
(iv) Stopping condition.

First stage – initialization: The goal is to identify the shortest route between two points at the nodes of the solution space, with the ant colony initially established randomly. Initialization considers the pheromone concentration at the boundaries, the suggested value, and the ant's choice.

Second stage – probabilistic ant movement: At each step of the process, ants make decisions to discover a satisfactory solution based on a probabilistic strategy that depends on the statistical data and pheromone values. The probability of an ant moving from point A to point B is given by:

$$P^{k}{}_{ab}(t) = \frac{\left[\pi_{ab}(t)\right]^{\alpha}\left[\eta_{ab}\right]^{\beta}}{\sum_{k \in allowed_k}\left[\pi_{ak}(t)\right]^{\alpha}\left[\eta_{ak}\right]^{\beta}} \quad \text{(II)}$$

where,

P^{k}_{ab} represents the probability of moving from area A to B,

τ is the pheromone,

η is a heuristic value.

The constant parameters α and β control the influence of pheromones versus the heuristic value. After visiting each node, the next visit or iteration is chosen based on probability.

Table 1. Parameters of ACO and their values

ACO parameters	Value
Iteration nn	100
Number of ants	50
α	0.8
β	0.2
Evaporation rate	0.9
Number of parameters	4
Number of nodes	200

Abbreviation: ACO: Ant colony optimization.

Third stage – pheromone updating: Once all ants have found a solution, each ant deposits a pheromone (τ_{ab}) on the trail. The pheromone is now updated according to Equation III:

$$\pi_{ab}(t)=(1-\rho)\tau_{ab}(t)+\Delta\tau_{ab}(t) \quad \text{(III)}$$

Pheromone evaporation is applied to prevent faulty convergence and improper judgments, where ρ is the pheromone evaporation rate ($0 < \rho \leq 1$), and $\Delta\tau_{ab}(t)$ is given by Equation IV:

$$\Delta\tau_{ab}(t) = \sum_{k=1}^{NA}\Delta\tau^{k}_{ab}(t) \quad \text{(IV)}$$

where NA represents the total count of ants and $\Delta\tau_{ab}(t)$ is the quantity of pheromone left by k ants at the nodes i and j, calculated as follows:

$\Delta\tau_{ab}(t) = L^{Q}_{k}$, if the k-th ant uses nodes a and b in its tour; otherwise, the entire tour length represented by the k-th ant is L_k, and Q is a constant.

Fourth stage – stopping condition: Ants examine each path, considering the viability and cost of each tour. If the minimal stopping condition is satisfied, the program terminates. Otherwise, it returns to Stage 2 and continues searching for the best solution, disregarding the number of repetitions.

4.1. FACTS controllers with ACO algorithm

The ACO algorithm continuously tracks system dynamics, evaluates controller behavior, and modifies control parameters. This adaptability ensures that the dampening capabilities of the power system remain effective across a range of conditions. The ACO's job is to find the path between the starting point and the endpoint that minimizes time while being the most optimal solution.

4.1.1. ACO algorithm

A population of m ants (solutions) is generated at random to start the process. Each ant k (k = 1, 2., m) denotes a solution string, in which a chosen value is assigned to each variable. Following the performance index, the ant is then graded. To provide the best potential solution, the pheromone concentration on every path (variable value) is modified as follows:

Every arc is given a specific amount of pheromone at the beginning of the search. When an ant k reaches node i, it follows a pheromone trail to calculate the likelihood that node j will be selected as the next node.

The probability of an ant moving from node i to node j is given by:

$$P_{i,j} = \frac{(\tau_{i,j}^{\alpha})(\eta_{i,j}^{\beta})}{\sum(\tau_{i,j}^{\alpha})(\eta_{i,j}^{\beta})} \quad \text{(V)}$$

where,

$\tau_{i,j}$ is the total amount of pheromone between nodes i and j,

α is the parameter controlling the impact of τ, i, j,

$\eta_{i,j}$ is the desirability of nodes i and j (usually $1/d_{i,j}$),

β controls the impact of $\eta_{i,j}$.

The pheromone value varies as the arc (i,j) is crossed, following the equation:

$$\tau_{i,j} = (1-\rho)\tau_{i,j} + \Delta\tau_{i,j} \quad \text{(VI)}$$

where,

ρ is the rate of pheromone evaporation,

$\Delta\tau_{i,j}$ stands for the amount of pheromone deposited.

The hit-trial approach is used to initialize the gain parameters of the alternating current FACTS controllers, whereas ACO selects the optimal values. The gain values of the four FACTS controllers in ACO depend on the locations of the ants. An update in the ant's position causes the associated gain values of the alternating current FACTS controllers to be updated accordingly. For each updated gain value, the entire model is executed, and the resulting deviations in rotor angle, angular speed, and generator voltages – regarded as the objective function – are recorded. The gain that minimizes the objective function the most, or the gain that results in the smallest deviations in rotor angle, angular speed, and generator voltage across all four machines, is chosen as the final FACTS gain once each iteration has been completed.

5. Results and discussion

This section verifies the performance of the FACTS controllers on the IEEE-30 bus system constructed using MATrix LABoratory/SIMULINK. The main objective of this work was to examine these FACTS devices within the IEEE-30 bus system and assess their performance. To reduce oscillations, FACTS devices such as STATCOM, SSSC, UPFC, and SVC are used. This section discusses the efficacy of FACTS controllers in dampening oscillations both with and without the use of the ACO algorithm.

5.1. IEEE-30 bus system with multiple FACTS devices

The IEEE 30-bus system is a widely used benchmark for power system analysis, integrating multiple energy sources such as thermal generators, wind power, small hydro, and photovoltaic arrays. To enhance power system stability and efficiency, FACTS controllers are strategically placed at weak buses and transmission lines. The optimal locations for FACTS device installation are identified based on system stability analysis.[32,33] SVCs are employed to regulate reactive power distribution among buses, while SSSCs adjust transmission line impedance to control real power flow. UPFCs improve voltage regulation and power flow capacity in transmission lines, whereas STATCOMs stabilize voltages and mitigate oscillations. By positioning FACTS devices at weak lines and buses, the system effectively manages reactive power flow, prevents transmission line overloads, and enhances overall grid reliability. Figure 6 illustrates the architecture of the IEEE-30 bus system with FACTS controllers.

The IEEE-30 bus system, incorporating renewable energy sources such as wind, solar, and small hydro, consisted of six generators and 41 transmission lines. The integration of these renewable sources introduced voltage fluctuations and power flow variations, necessitating the strategic placement of FACTS controllers for enhanced stability. Branch 15 was identified as an optimal location for an SSSC based on the L_{mn} sensitivity index, helping to regulate real power flow amid varying renewable generations. Similarly, buses 26 and 29 experienced significant voltage variations due to fluctuating renewable outputs, as indicated by the Fast Voltage Stability Index (FVSI). To mitigate these instabilities, an SVC was installed on bus 29. Voltage fluctuations caused by variable renewable power injection were detected by the voltage sensitivity

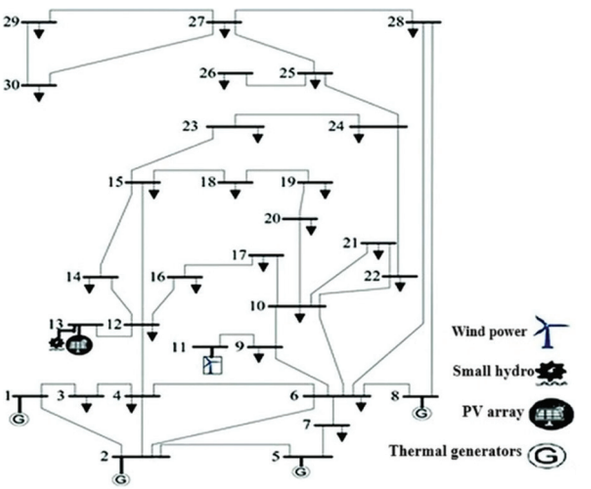

Figure 6. IEEE-30 bus system
Abbreviation: PV: Photovoltaic.

factor (VSF), leading to the placement of a STATCOM at bus 24 for voltage stabilization. In addition, as lines 4, 7, and 9 – connecting buses 3 to 4, 4 to 6, and 6 to 7 – experienced high active power variations due to the intermittent nature of renewable generation, a UPFC was installed at bus 6 to regulate voltage magnitude and phase angles, ensuring efficient power distribution across the grid. This strategic deployment of FACTS controllers helped maintain power system stability, improved voltage profiles, and enhanced the reliability of renewable energy integration into the IEEE-30 bus network.

5.1.1 L_{mn}

L_{mn}, a line stability metric, is based on the concept of power flow across a single line. The line index L_{mn} can take a maximum value of 1 and a minimum value of 0. L_{mn} values near 1 indicate that a line is approaching its instability point. The origin of the L_{mn} is given by:

$$L_{mn} = \frac{4XQ_r}{\left[V_s \sin(\theta - \delta)\right]^2} \quad \text{(VII)}$$

where V_s is the sending end voltage, Q_r is the receiving end's reactive power, X represents the line reactance, and θ and δ correspond to the phase angles of the sending and receiving buses, respectively.

5.1.2. Fast Stability Index

The line stability index FVSI is based on the understanding of power flow through a single line. The stability index of the linked line is calculated using the following equation:

$$FSI = \frac{4Z^2Q_r}{V_s^2 X} \quad \text{(VIII)}$$

FVSI values near 1 indicate that the line is approaching the point of instability. If the value exceeds unity, the system will fail, and a sudden voltage drop will occur in one of the buses connected to the line. The system's weakest bus can also be identified using this index.

5.1.3. Voltage Sensitivity Index

Many utilities employ sensitivity factors as indices to identify voltage stability issues and develop appropriate solutions to correct the voltage. These indices generate QV curves to predict generator voltage control issues, which can be described as:

$$VSF_i = \frac{dv}{dq}; \quad \text{(IX)}$$

In this case, VSF is used. A high value of VSF that eventually changes sign is an indication of an "unstable" voltage control state. A high level of sensitivity means that even minor changes in loading can result in significant variations in voltage magnitude, signaling bus fragility.

5.2. Results of simulations under various loading scenarios

Examining the impact of the different loading conditions on the system's efficiency is important, as the operational load is constantly changing. The various power system states, including speed deviation (Δω), angle deviation, and rotor angle, were utilized by the base case system, FACTS devices, and FACTS with the ACO system. For comparison, three distinct situations were taken into account: normal, lighter, and heavy loading conditions.

5.2.1. Results from simulation under normal operating conditions

To evaluate the effectiveness of the ACO-based FACTS controllers compared to the base case system, a simulation under typical loading conditions was conducted. According to the following data, the oscillations in the base case system were unable to dampen oscillations.

Table 2 presents the power system states under normal operating conditions, highlighting the impact

Table 2. Performance of the power system under typical operating conditions

Power system states	Overshoot			Settling time (s)		
	Base case	FACTS only	FACTS with ACO	Base case	FACTS only	FACTS with ACO
Δω	0.0185	0.0181	0.0155	25	9.2	3.12
Δδ	−2.014	−2.016	−1.83	25	11.15	2.98
δ	2.32	2.11	1.97	14	4.27	2.45

Notes: Δω: Speed deviation; Δδ: Rotor angle deviation; δ: Voltage stability.
Abbreviations: ACO: Ant colony optimization; FACTS: Flexible Alternating Current Transmission System.

of FACTS controllers with and without ACO. The table compares the overshoot and settling time for Δω, rotor angle deviation (Δδ), and voltage stability (δ) across three cases: the base case (no FACTS controllers), FACTS only, and FACTS with ACO. The results showed that the ACO-optimized FACTS controllers significantly enhance the system's stability by reducing both overshoot and settling time.

For overshoot, the ACO-FACTS system achieved the lowest values, indicating better stability. For instance, the overshoot in Δω reduced to 0.0155 pu with ACO-FACTS compared to 0.0185 pu in the base case and 0.0181 pu with FACTS only. Similarly, Δδ overshoot decreased to -1.83 rad with ACO-FACTS, showcasing improved stability compared to -2.014 rad in the base case and -2.016 rad with FACTS only. δ also improved, with the overshoot reducing to 1.97 in the ACO-FACTS scenario, compared to 2.32 in the base case and 2.11 with FACTS only. The settling time values further demonstrate the effectiveness of ACO-FACTS controllers. The settling time for Δω decreased to 3.12 s with ACO-FACTS, a substantial improvement from 25 s in the base case and 9.2 s with FACTS only. Similarly, Δδ and δ settled faster with ACO-FACTS, achieving 2.98 and 2.45 s, respectively, compared to the longer settling times in the base and FACTS-only cases. These results indicate that the ACO-FACTS combination enhances the power system's dynamic response by reducing overshoot and expediting stabilization, ultimately improving overall reliability and performance.

The speed variations exhibited by the base case, FACTS only, and FACTS with ACO are shown in Figure 7 under typical operating conditions. Due to minimal generator oscillation, the maximum overshoot for the FACTS-only and ACO-based FACTS, ranged from 0.09% to 7.25%, with the settling time for both ranging from 47.25 to 81.56%. The system's Δδ under typical operating conditions is shown in Figure 8.

In the first scenario, the rotor angle variation was oscillatory and took a long time to improve power system stability, even if the system dampened the LFO since the FACTS controllers were synchronized with the ACO. When the power was changed, the system became unstable, and the angle deviations were exposed to further changes. The rotor angle under normal loads is shown in Figure 8 for both the base case and the ACO with the FACTS scenario. The settling

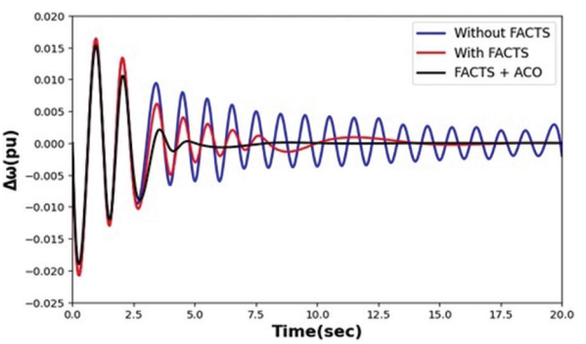

Figure 7. Rotor speed deviation with FACTS, without FACTS, and FACTS + ACO under normal loading conditions

Abbreviations: ACO: Ant colony optimization; FACTS: Flexible Alternating Current Transmission System.

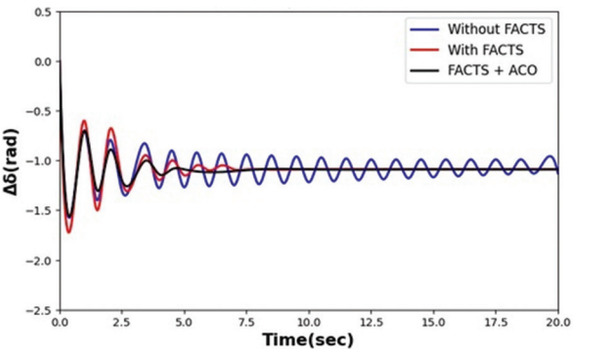

Figure 8. Rotor angle deviation under normal loading conditions with FACTS, without FACTS, and with FACTS + ACO

Abbreviations: ACO: Ant colony optimization; FACTS: Flexible Alternating Current Transmission System.

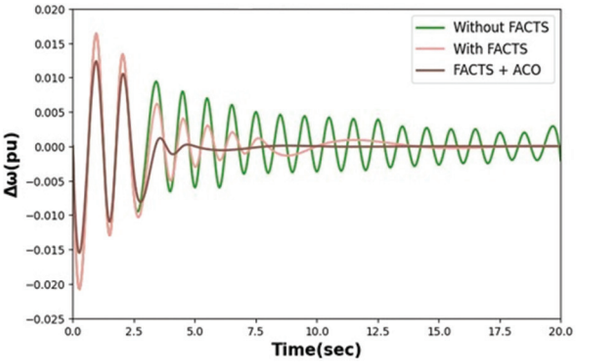

Figure 9. Rotor speed deviation with FACTS, without FACTS, and FACTS + ACO under heavy loading conditions

Abbreviations: ACO: Ant colony optimization; FACTS: Flexible Alternating Current Transmission System.

Table 3. Performance of the power system under demanding operating conditions

Power system states	Overshoot			Settling time (s)		
	Base case	FACTS only	FACTS with ACO	Base case	FACTS only	FACTS with ACO
Δω	0.0175	0.0171	0.0153	25	9.4	3.54
Δδ	−2.06	−2.01	−1.76	25	10.7	2.86
δ	2.27	2.5	1.92	10.3	4.19	2.32

Notes: Δω: Speed deviation; Δδ: Rotor angle deviation; δ: Voltage stability.
Abbreviations: ACO: Ant colony optimization; FACTS: Flexible Alternating Current Transmission System.

times for the FACTS and FACTS-ACO were 62.83 and 88.39%, respectively, and the largest overshoot was 0.15% and 13.75%. The ACO-based FACTS controllers successfully stabilized the system under the existing disturbance, in contrast to the base case.

5.2.2. Results from simulation under heavy operating conditions

The ACO with FACTS controllers was selected for a rapid load increment to generate a disturbance under demanding operating conditions. The power system's performance under these conditions is displayed in Table 3. Table 3 showcases the system's behavior under demanding operating conditions, comparing the base case, FACTS only, and FACTS with ACO tuning. The table evaluates the system's stability based on overshoot and settling time metrics. In terms of overshoot, the ACO-optimized FACTS controllers demonstrated improved performance. For angular Δω, the overshoot reduced from 0.0175 pu in the base case to 0.0171 pu with FACTS, and further decreased to 0.0153 pu with ACO, indicating better speed stability. Similarly, Δδ overshoot decreased from -2.06 rad in the base case to -2.01 rad with FACTS and further improved to -1.76 rad with ACO tuning, enhancing rotor stability. The δ also benefited from ACO optimization, decreasing from 2.27 in the base case to 1.92 with ACO, showcasing better voltage regulation.

Regarding settling time, ACO-optimized FACTS controllers significantly enhanced system responsiveness. The Δω settling time improved from 25 s in the base case to 9.4 s with FACTS, and further reduced to 3.54 s with ACO, ensuring faster stabilization. Similarly, the Δδ settling time decreased from 25 s to 10.7 s with FACTS and further improved to 2.86 s with ACO, indicating quicker system recovery. The δ settling time also reduced significantly from 10.3 s in the base case to 2.32 s with ACO, demonstrating enhanced voltage stability. These improvements in rotor speed deviation under heavy loading are depicted in Figure 9, which illustrates the enhanced damping performance achieved through ACO-optimized FACTS controllers. Overall, Table 3 highlights the effectiveness of ACO-optimized FACTS controllers in improving the power system's stability under demanding conditions by reducing both overshoot and settling time, resulting in faster stabilization and better voltage regulation.

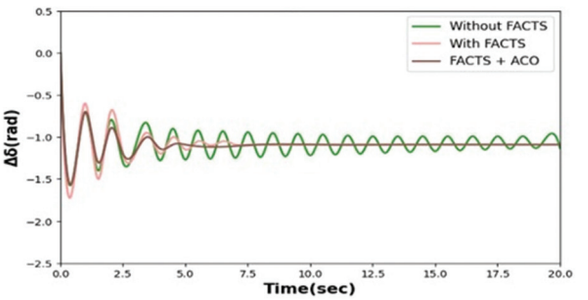

Figure 10. Rotor angle deviation with FACTS, without FACTS, and FACTS + ACO under heavy loading conditions
Abbreviations: ACO: Ant colony optimization; FACTS: Flexible Alternating Current Transmission System.

The system's angle deviation oscillated in the base case, but when ACO-based FACTS controllers were applied, the oscillations were reduced, and a steady state was reached. As a result, adopting ACO-based FACTS damping controllers efficiently increased power system stability. The system achieved a steady state when a change in the rotor angle was converted into a negative change. The Δδ for the FACTS controllers and the base case with the ACO under heavy loading conditions are shown in Figure 10.

The device exhibited interarea oscillation depending on angle stability. After reaching a maximum value, the oscillation started to decline as the system returned to its normal value. The settling time for FACTS was 65.3%, and the settling time for ACO-based FACTS was 87.2%.

Table 4. Performance of the power system under light operating conditions

Power system states	Overshoot			Settling time (s)		
	Base case	FACTS only	FACTS with ACO	Base Case	FACTS only	FACTS with ACO
Δω	0.0169	0.0166	0.0144	25	9.45	3.16
Δδ	−2.01	−1.95	−1.62	25	7.07	3.02
δ	2.09	2.01	1.87	9.36	3.59	2.16

Notes: Δω = Speed deviation; Δδ = Rotor angle deviation; δ: Voltage stability
Abbreviations: ACO: Ant colony optimization; FACTS: Flexible Alternating Current Transmission System.

5.2.3. Results from simulation under lighter operating conditions

A disturbance is assumed to occur when the load changes quickly. The overshoot and settling time under lighter operating conditions are shown in Table 4. Table 4 presents the power system performance during light operation conditions, highlighting the impact of FACTS controllers with and without ACO. The table compares the overshoot and settling time for Δω, Δδ, and δ across three scenarios: the base case (without FACTS controllers), FACTS only, and FACTS with ACO. The results demonstrate that ACO-optimized FACTS controllers significantly enhanced the system's stability by reducing overshoot and improving settling time, even under light operating conditions. In terms of overshoot, the ACO-FACTS system achieved the lowest values, indicating better stability. For Δω, the overshoot reduced to 0.0144 pu with ACO-FACTS, compared to 0.0169 pu in the base case and 0.0166 pu with FACTS only. Similarly, the Δδ overshoot decreased to -1.62 rad with ACO-FACTS, which is lower than -2.01 in the base case and -1.95 with FACTS only. δ also showed improvement, with the overshoot reducing to 1.87 in the ACO-FACTS case, compared to 2.09 in the base case and 2.01 with FACTS only.

For settling time, the ACO-FACTS system again demonstrated superior performance. The settling time for Δω decreased to 3.16 s with ACO-FACTS, a significant improvement over 25 s in the base case and 9.45 s with FACTS only. Similarly, Δδ and δ settled faster with ACO-FACTS, achieving 3.02 s and 2.16 s, respectively, compared to the longer settling times in the base and FACTS-only cases.

These results confirm that the ACO-optimized FACTS controllers effectively enhance the power system's performance during lighter operating conditions by minimizing overshoot, improving settling time, and providing better voltage regulation and oscillation damping, ultimately ensuring more stable and reliable system operation.

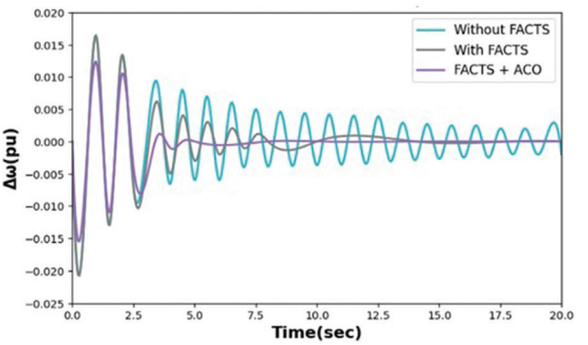

Figure 11. Deviation of rotor speed with FACTS, without FACTS, and FACTS + ACO, under light operating conditions

Abbreviations: ACO: Ant colony optimization; FACTS: Flexible Alternating Current Transmission System.

For the base case, FACTS only, and FACTS-ACO, the generator's disturbance caused a maximum overshoot of Δω that changed from 0.0169, 0.0166, and 0.0144 pu, with settling times of 25, 9.45, and 3.16 s, respectively, as shown in Figure 11. In general, the proposed system's Δω exhibited better damping when compared to the base case and the FACTS-only device.

Even though the angle reached its normal value, the device became unstable when Δδ was subjected to a change, as this also exposed the active power to a change. The rotor angles for the base case and the FACTS controllers with ACO are shown in Figure 12 under light loading conditions.

With the base case, FACTS only, and FACTS with ACO, Δδ were approximately 2.09, 2.01, and 1.87 rad, respectively. In general, the suggested system exhibits improved damping behavior under light loading conditions, enhancing power system stability. The gain in power system stability is generally reduced by a longer settling period. As a result, the simulation findings show that the damping controllers can be fine-tuned to demonstrate their superiority over the base case system's insufficient sizing.

5.2.4. Calculation of Performance Indices

To enhance system design or model a flexible system, the current focus was on emphasizing the robustness of the developed controllers. In this regard, three additional performance indices – integral of time absolute error (ITAE), integral of square error (ISE), and integral of absolute error (IAE) – are also considered to analyze the performance consistency of the tuned controller, in addition to the confined objective function. The following three performance indices can be listed in the following order:

$$\text{ISE}=\int_0^{t_{sim}}\left\{(\Delta fi)^2+(\Delta P_{tiei-j})^2\right\}dt \quad \text{(X)}$$

$$\text{IAE}=\int_0^{t_{sim}}\left\{\left|\Delta fi\right|+\left|\Delta P_{tiei-j}\right|\right\}dt \quad \text{(XI)}$$

$$\text{ITAE}=\int_0^{t_{sim}}\left\{\left|\Delta fi\right|+\left|\Delta P_{tiei-j}\right|\right\}tdt \quad \text{(XII)}$$

With the proposed system, the ISE, IAE, and ITAE values were around 0.0003, 0.0353, and 0.6786. Over time, the oscillations became less apparent, especially in conditions with longer delays, which was why FACTS controllers were created. Rotor speed variations in the instance of d=180 ms practically came to an end at time t=3.5 ms. However, it can be shown that the fluctuations persisted throughout the experiment for d=0 ms. This was achieved by designing the ACO-based FACTS controllers for the delay scenarios. The ACO-based FACTS controllers have effectively reduced system variations in rotor speed or frequency caused by the introduction of voltage power disturbances.

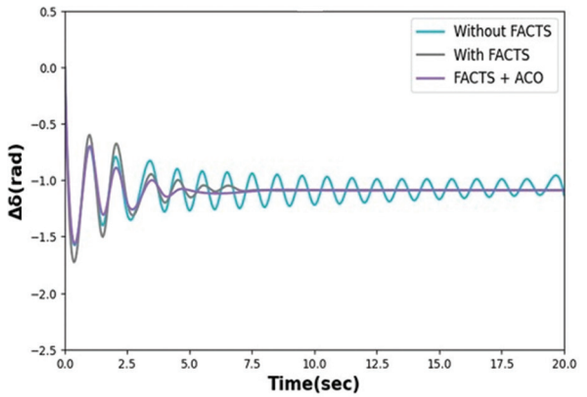

Figure 12. Rotor angle deviation with FACTS, without FACTS, and FACTS + ACO, under light operating conditions

Abbreviations: ACO: Ant colony optimization; FACTS: Flexible Alternating Current Transmission System.

Table 5 illustrates the overall active and reactive power loss with and without FACTS controllers for the ACO-based systems. The proposed approach achieved less power loss. Figure 13 compares the scenarios with and without FACTS controllers, showing that FACTS controllers yield the best outcomes and the most effective system responses.

Rotor speed variation can significantly affect damping oscillations, as shown in Figure 14 when comparing rotor Δω with and without FACTS controllers. Rotor speed was effectively managed by the FACTS controllers, which also reduced deviations.

Figure 14 illustrates the effectiveness of the proposed method. When a disturbance occurred, the system experienced sudden fluctuations in load and generator output. To prevent instability caused by these oscillations, the proposed system combined an effective ACO algorithm with FACTS controllers before regulating the rotor speed.

Figure 15 compares Δω for systems with and without the proposed ACO-based controller, showing improved system stability. The blue solid line (without ACO) displays larger oscillations and a longer settling time. In contrast, the red dashed line (with ACO) demonstrates faster damping and a reduced peak deviation. These findings indicate that the proposed controller effectively enhances system stability by minimizing oscillations and improving response time.

Figure 16 illustrates a plot of load angle deviation over time, comparing system behavior with and without the ACO method. The blue solid line (without ACO) shows larger oscillations and slower damping, indicating instability. In contrast, the red dashed line (with ACO) demonstrates smaller oscillations and faster convergence to stability. These findings confirm the effectiveness of the ACO method in enhancing system stability and improving dynamic performance.

Table 5. Total losses for IEEE-30 bus system

Power type	Without FACTS controllers	With FACTS controllers	FACTS with ACO
Total real power loss (pu)	0.1457	0.1195	0.0624
Total reactive power loss (pu)	0.2578	0.2356	0.1132

Abbreviations: ACO: Ant colony optimization; FACTS: Flexible Alternating Current Transmission System.

Figure 17 compares the control effort over time for systems with and without the ACO method. The blue solid line (without ACO) shows larger fluctuations and higher peaks, indicating increased control effort and instability. The red dashed line (with ACO) demonstrates reduced oscillations and smoother control effort, suggesting improved efficiency and stability. These results highlight the effectiveness of the ACO method in minimizing control effort while maintaining system performance.

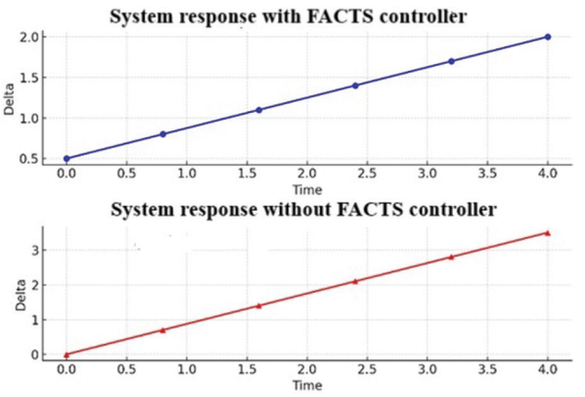

Figure 13. Comparison of systems with and without FACTS controllers
Abbreviation: FACTS: Flexible Alternating Current Transmission System.

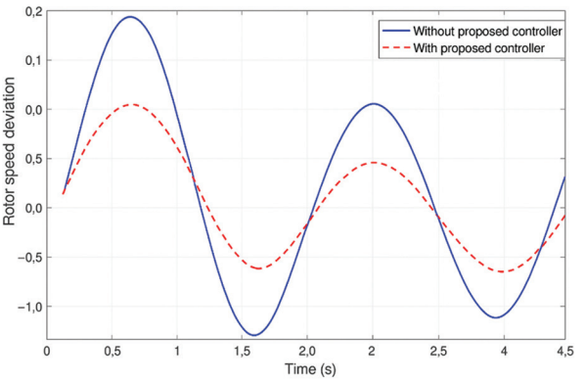

Figure 14. Rotor speed deviation without and with FACTS controller
Abbreviation: FACTS: Flexible Alternating Current Transmission System.

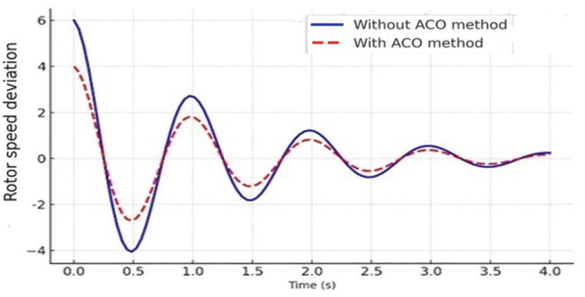

Figure 15. Rotor speed deviation with and without ACO
Abbreviation: ACO: Ant colony optimization.

Figure 18 compares the Δδ over time for two cases: without the ACO method (blue solid line) and with the ACO method (red dashed line). Without ACO, the rotor angle exhibits higher oscillations and a longer time to stabilize. In contrast, with ACO, oscillations are damped more rapidly, leading to a more stable and controlled response. These results confirm the improved performance of the ACO-based method in minimizing Δδ and achieving superior system stability.

Figure 19 highlights improvements in dynamic stability through the optimal synchronization of four FACTS controllers – SVC, STATCOM, SSSC, and UPFC – optimized using the ACO method. The performance is assessed by comparing damping

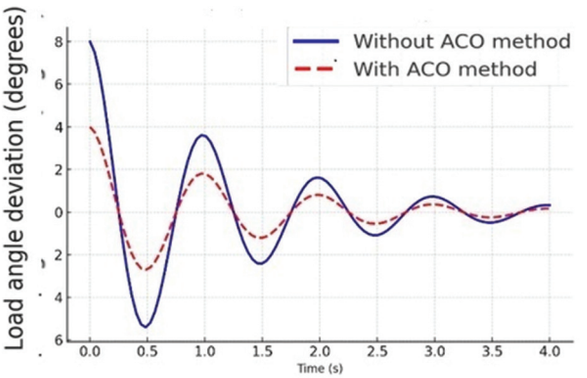

Figure 16. Load angle deviation over time
Abbreviation: ACO: Ant colony optimization.

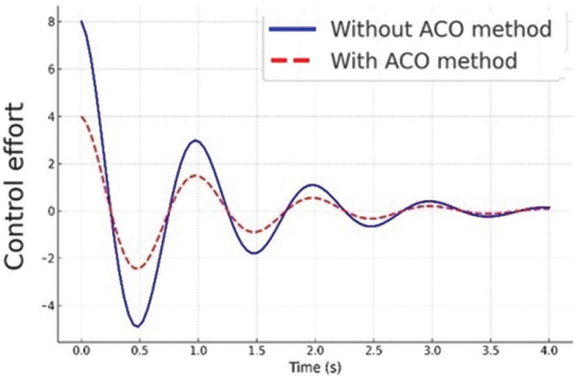

Figure 17. Control effort over time
Abbreviation: ACO: Ant colony optimization.

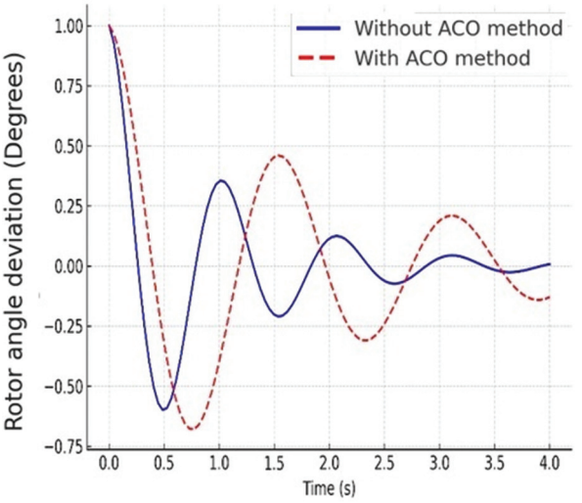

Figure 18. Rotor angle deviation over time
Abbreviation: ACO: Ant colony optimization.

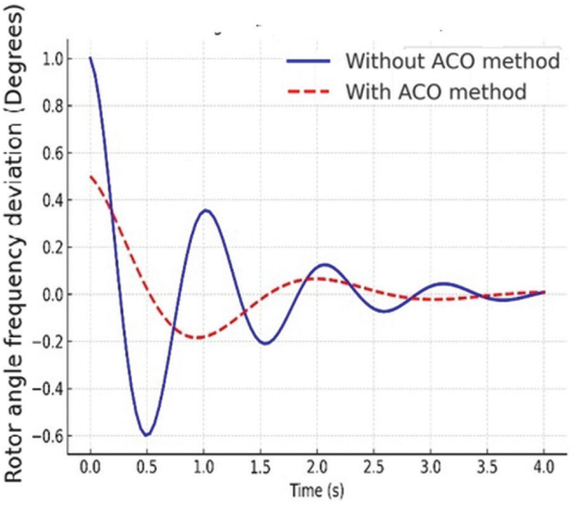

Figure 19. Rotor angular frequency deviation
Abbreviation: ACO: Ant colony optimization.

ratios, rotor angles, and time-domain responses of the recommended ACO technique against a baseline system under varying loading scenarios. Results demonstrate that the proposed ACO method effectively reduces LFO and improves the dynamic stability of power networks. In addition, the study includes the integration of intermittent renewable energy sources, such as solar and wind power, to assess their impact on system stability. The ACO-based FACTS controllers effectively mitigate the fluctuations introduced by renewable energy sources, ensuring smoother power system operation. These findings demonstrate that the proposed model is effective in resolving the issue of LFO in power systems. Simulation, modeling, and

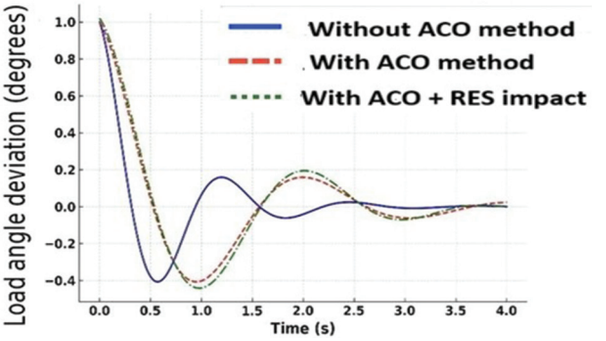

Figure 20. Rotor angle deviation with FACTS controllers and renewable energy integration
Abbreviations: ACO: Ant colony optimization; FACTS: Flexible Alternating Current Transmission System.

experimental validations were conducted using the IEEE 30-bus system, demonstrating its applicability to modern power grids with high penetration of renewable energy sources.

Figure 20 illustrates the impact of renewable energy integration on Δδ in a power system employing ACO-optimized FACTS controllers (SVC, STATCOM, SSSC, and UPFC). The comparison between systems with and without ACO-based FACTS controllers demonstrates their effectiveness in damping LFOs. With renewable energy sources integrated, the system exhibits improved stability, reduced deviations, and better synchronization, ensuring enhanced dynamic performance under varying loading conditions. These results validate the efficiency of ACO-based FACTS controllers in mitigating oscillations and enhancing power system stability.

6. Conclusion

This study introduces an optimized FACTS controller design incorporating ACO to enhance power system stability, with an additional focus on renewable energy integration. The results demonstrate that the ACO-based tuning method significantly improves system performance by reducing overshoot, shortening settling time, and enhancing voltage stability when compared to conventional controllers. As shown in Figure 17, the Δδ is significantly reduced when ACO-based FACTS controllers are combined with renewable energy integration. The deviation stabilizes more rapidly and exhibits reduced oscillations compared to the system without ACO, highlighting the beneficial impact of integrating renewable sources with optimized FACTS control.

Key contributions of this work include improved damping of interarea oscillations, more efficient power

flow management, and enhanced transient stability. For instance, under demanding operating conditions, the ACO-optimized FACTS controllers reduced the overshoot of Δω by approximately 12.5% and shortened the settling time by over 60% compared to conventional FACTS controllers. With renewable energy integration, the system's response time is further enhanced, and stability is maintained more effectively during fluctuations. Similarly, during light operation scenarios, δ overshoot decreased by 10%, showcasing enhanced stability and faster response. However, the proposed approach has certain limitations. The ACO algorithm requires considerable computational power, which may pose challenges for real-time applications. In addition, FACTS devices involve high installation and operational costs, making large-scale implementation subject to further cost-benefit analysis. Despite these limitations, the model's effectiveness was validated using the IEEE 30-bus test system – a widely recognized benchmark for real-world power grid simulations. FACTS controllers, such as STATCOM and UPFC, have been successfully deployed in large-scale wind farms and power grids, enhancing system stability and reliability. The proposed ACO-FACTS framework, combined with renewable energy integration, offers a robust solution for improving dynamic performance and mitigating stability issues in modern power systems. Innovative financing mechanisms to support large-scale deployment of renewable integration have also been recently explored.[34]

Acknowledgments

None.

Funding

None.

Conflict of interest

The authors declare no competing interests.

Author contributions

Conceptualization: Vemireddy Suryanarayana Reddy
Formal analysis: All authors
Investigation: Vemireddy Suryanarayana Reddy
Methodology: Vemireddy Suryanarayana Reddy
Writing – original draft: All authors
Writing – review & editing: All authors

Availability of data

The data supporting the findings of this study, including simulation results and controller parameters used in the IEEE 30-Bus system model, are available from the corresponding author upon reasonable request. Custom MATLAB/Simulink models and optimization methods developed for this research may also be shared to facilitate reproducibility and further investigation.

References

1. Hingorani NG. Flexible AC transmission system. *IEEE Spectr*. 1988;25(4):40-45.
2. Bian B, Ramey HJ, Nelson RM. Susceptance model of SVC for power flow analysis. *IEEE Trans Power Syst*. 1997;12(1):200-206.
3. Hussein NAK, Basel OM. Integrating renewable energy systems into urban planning for sustainable cities. *ESTIDAMAA*. 2024;82:15-21. doi: 10.70470/ESTIDAMAA/2024/003
4. Goel S, Jena B, Sharma R. A case study on optimal tilt angle and spacing for rooftop solar photovoltaic system at Bhubaneswar. *J Mod Technol.* 2024;121:121-131.
5. Solanke AV, Verma SK, Kumar S, Oyinna B, Okedu KE. MPPT for hybrid energy system using machine learning techniques. *J Mod Technol.* 2024;121:19-37.
6. Devarapalli R, Bhattacharyya B, Sinha NK, Dey B. Amended GWO approach based on multi-machine power system stability enhancement. *ISA Trans.* 2021;109:152-174. doi: 10.1016/j.isatra.2020.09.016
7. Reddy KS, Babu KR. Optimal SVC placement using fuzzy logic and PSO for improved voltage stability. *Electr Power Syst Res.* 2008;78(5):837-844.
8. Metavural S, Mehmattum O. A full power injection model for UPFC with modified Jacobian elements. *Int J Electr Power Energy Syst.* 2010;32(3):229-238.
9. Chengaiah M, Marutheswar K. Power flow control using unified power flow controller (UPFC). *J Electr Eng Technol.* 2011;5(2):256-262.
10. Kumar A, Nagaraju K. Minimization of transmission network losses using UPFC in power flow studies. *Int J Power Energy Syst.* 2012;29(3):189-196.
11. Vanitha R, Sudhakaran R. Differential evolution algorithm for UPFC optimal placement and loss reduction. *Energy Procedia.* 2012;14:1791-1796.
12. Del Valle Y, Venayagamoorthy GK, Mohagheghi S, Hernandez J, Harley RG. Particle swarm optimization: Basic concepts, variants and applications in power systems. *IEEE Trans Evol Comput.* 2008;12(2):171-195. doi: 10.1109/TEVC.2007.896686
13. Sreedivya KM, Jeyanthy PA, Devaraj D. Improved design of interval type-2 fuzzy based wide area power system stabilizer for inter-area oscillation damping.

Microprocess Microsyst. 2021;83:103957.
doi: 10.1016/j.micpro.2021.103957

14. Ghaedi S, Abazari S, Markadeh GA. Transient stability improvement of power system with UPFC control using transient energy function and sliding mode observer based on locally measurable information. Measurement. 2021;183:109842.
doi: 10.1016/j.measurement.2021.109842
15. Da Silva GS, de Oliveira EJ, de Oliveira LW, de Paula AN, Ferreira JS, Honorio LM. Load frequency control and tie-line damping via virtual synchronous generator. Int J Electr Power Energy Syst. 2021;132:107108.
doi: 10.1016/j.ijepes.2021.107108
16. Fathollahi A, Kargar A, Derakhshandeh SY. Enhancement of power system transient stability and voltage regulation performance with decentralized synergetic TCSC controller. Int J Electr Power Energy Syst. 2022;135:107533.
doi: 10.1016/j.ijepes.2021.107533
17. Therattil JP, Jose J, Prasannakumari PRN, *et al*. Hybrid control of a multi-area multi-machine power system with FACTS devices using non-linear modelling. IET Gener Transm Distrib. 2020;14(10):1993-2003.
doi: 10.1049/iet-gtd.2019.1165
18. Guha D, Roy PK, Banerjee S. Performance evolution of different controllers for frequency regulation of a hybrid energy power system employing chaotic crow search algorithm. ISA Trans. 2022;120:128-146.
doi: 10.1016/j.isatra.2021.03.017
19. Saidi AS. Impact of grid-tied photovoltaic systems on voltage stability of Tunisian distribution networks using dynamic reactive power control. Ain Shams Eng J. 2022;13(2):101537.
doi: 10.1016/j.asej.2021.06.023
20. Shehata AA, Tolba MA, El-Rifaie AM, Korovkin NV. Power system operation enhancement using a new hybrid methodology for optimal allocation of FACTS devices. Energy Rep. 2022;8:217-238.
doi: 10.1016/j.egyr.2021.11.24
21. Khawaja AW, Kamari NAM, Zainuri MAAM. Design of a damping controller using the SCA optimization technique for the improvement of small signal stability of a single machine connected to an infinite bus system. Energies. 2021;14(11):2996.
doi: 10.3390/en14112996
22. Behzadpoor S, Davoudkhani IF, Abdelaziz AY, Geem ZW, Hong J. Power system stability enhancement using robust FACTS-based stabilizer designed by a hybrid optimization algorithm. Energies. 2022;15(22):8754.
doi: 10.3390/en15228754
23. Pathan MIH, Rana MJ, Shahriar MS, Shafiullah M, Zahir MH, Ali A. Real-time LFO damping enhancement in electric networks employing PSO optimized ANFIS. Inventions. 2020;5(4):61.
doi: 10.3390/inventions5040061
24. Behera S, Barisal AK, Dhal N, Lal DK. Mitigation of power oscillations using hybrid DE-PSO optimization-based SSSC damping controller. J Electr Syst Inf Technol. 2019;6(1):1-17.
doi: 10.1186/s43067-019-0007-y
25. Solomon E, Khan B, Boulkaibet I, *et al*. Mitigating low-frequency oscillations and enhancing the dynamic stability of power system using optimal coordination of power system stabilizer and unified power flow controller. Sustainability. 2023;15(8):6980.
doi: 10.3390/su15086980
26. Mahadevan J, Rengaraj R, Bhuvanesh A. Application of multi-objective hybrid artificial bee colony with differential evolution algorithm for optimal placement of microprocessor based FACTS controllers. Microprocess Microsyst. 2021:104239.
doi: 10.1016/j.micpro.2021.104239
27. Kotsampopoulos P, Georgilakis P, Lagos DT, Kleftakis V, Hatziargyriou N. FACTS providing grid services: Applications and testing. Energies. 2019;12(13):2554.
doi: 10.3390/en12132554
28. Naderi E, Pourakbari-Kasmaei M, Abdi H. An efficient particle swarm optimization algorithm to solve optimal power flow problem integrated with FACTS devices. Appl Soft Comput. 2019;80:243-262.
doi: 10.1016/j.asoc.2019.04.012
29. Khamari D, Sahu RK, Gorripotu TS, Panda S. Automatic generation control of power system in deregulated environment using hybrid TLBO and pattern search technique. Ain Shams Eng J. 2020;11(3):553-573.
doi: 10.1016/j.asej.2019.10.012
30. Sahu PR, Hota PK, Panda S. Modified whale optimization algorithm for coordinated design of fuzzy lead-lag structure-based SSSC controller and power system stabilizer. Int Trans Electr Energy Syst. 2019;29(4):e2797.
doi: 10.1002/etep.2797
31. Lee Y, Song H. A reactive power compensation strategy for voltage stability challenges in the Korean power system with dynamic loads. Sustainability. 2019;11(2):326.
doi: 10.3390/su11020326
32. Ćalasan M, Konjić T, Kecojević K, Nikitović L. Optimal allocation of static var compensators in electric power systems. *Energies*. 2020;13(12):3219.
doi: 10.3390/en13123219
33. Zhang G, Hu W, Cao D, *et al*. A data-driven approach for designing STATCOM additional damping controller for wind farms. Int J Electr Power Energy Syst. 2020;117:105620.
doi: 10.1016/j.ijepes.2019.105620
34. Zhang Y, Su Y. Towards a sustainable future: Exploring innovative financing models for renewable energy. MEDAAD. 2024;2024:34-40.
doi: 10.70470/MEDAAD/2024/006

Asian Journal of Water, Environment and Pollution. Vol. 22, No. 2 (2025), pp. 168-183.
doi: 10.36922/ajwep.8499

ORIGINAL RESEARCH ARTICLE

Topographic and watershed analysis of Haditha Dam Basin using geographic information system and remote sensing for water management

Nabaa Isam Ali* and Salwan Sabbar Al-Hasnawi

Department of Remote Sensing, College of Remote Sensing and Geophysics, Al-Karkh University of Science, Baghdad, Iraq
***Corresponding author:** Nabaa Isam Ali (nabaa.isam@kus.edu.iq)

Received: January 10, 2025; 1st revised: February 21, 2025; 2nd revised: March 13, 2025; Accepted: March 27, 2025; Published online: April 23, 2025

Abstract: Water scarcity and inefficient water management are critical challenges, particularly in Iraq, because it faces significant challenges in managing its water resources due to increasing demand for water and climate change, which threatens water security. This study aims to promote sustainable water resource management practices in arid and semi-arid regions, focusing on the Haditha Dam Basin in Iraq. The topographic and hydrological characteristics of the basin were analyzed using geographic information systems and remote sensing techniques. The study relied on Sentinel-1/2 satellite data to classify land use and land cover (LULC) and create high-resolution digital elevation models (DEMs). Using ArcGIS Pro, several hydrological factors were analyzed, including slopes, flow directions, water accumulation, and sub-basin identification. Results revealed a marked topographic contrast between the northern and southern regions of the basin. The southern regions are characterized by flat areas that facilitate groundwater recharge, while the steep northern slopes lead to increased erosion and rapid surface runoff. Several sub-basins were identified, with the main basin accounting for approximately 40% of the total water input. These results are consistent with previous studies in arid and semi-arid regions, such as the Duhok Dam Basin in Iraq, where topographical features play a key role in hydrological response. Study limitations include DEM accuracy, which may not capture the fine details of small-scale flow characteristics due to their resolution (10 m). Furthermore, remote sensing cannot directly measure subsurface hydrology, requiring verification with field data or additional models. LULC classification is also affected by seasonal variations and spectral mixing, which may affect the accuracy of the results. Despite these challenges, the study provides valuable information for policymakers to improve water resource management in arid regions. It also provides a scientific basis for developing more effective flood control and reservoir management strategies, contributing to sustainable water resource planning.

Keywords: Watershed management; Hydrological analysis; Geographic information system; Digital elevation model; Terrain modeling

1. Introduction

Water is a key issue in Asia. Various non-natural factors have impacted the amount and quality of water in South Asia. Although the natural weathering process contributes to numerous water constituents, the increasing population pressure has made the water situation very critical in quantitative and qualitative terms due to natural effluents flowing into natural water bodies.[1] Water is necessary for drinking, sanitation,

agriculture, industry, and sustaining ecosystems and is vital for life. However, <1% of the world's water in rivers, lakes, wetlands, and aquifers is accessible and is under threat.[2-4]

Iraq and other countries rely heavily on their water bodies for their economy and human life. It is essential to develop strategic plans for water management to meet future requirements[5] due to the decrease in the quantities and degradation in the quality of the water reaching Iraq's borders with the Euphrates and Tigris rivers.[6] The Euphrates and Tigris Rivers are Iraq's two primary surface water sources,[7] and future predictions suggest that they will become scorched by 2040.[8] To overcome this problem, a prudent water management plan is to be adopted, and dams are to be constructed to form reservoirs.[9] The Haditha Dam reservoir in Anbar state, western Iraq, is a significant source of drinking water, irrigation, flood control, and hydropower generation.[10] Operations such as evaporation and leakage have resulted in the loss of a significant amount of surface water.

A reduction in the amount of water in both lakes is caused by several factors, including those related to the nature and quality of the water (water depth, water quality, volume, and shape of the area of surface water), as well as climatic factors (relative humidity, temperature, wind, and sun radiation).[11] For this reason, finding ways to retain and control the water lost is necessary. Thus, water resource management is critical to ensuring that water is utilized efficiently and conserved[12] while also increasing the amount of rainwater collected by the dam. One of the most essential methods is watershed management.

The dynamic practice of managing land, biota, water, and other resources in a particular area for social, ecological, and economic reasons is known as watershed management. It requires effective collaborations between researchers and practitioners, interdisciplinary work, and participatory water resource management decision-making[13] Water resources specialists have warned of the threats of proceeding low water levels within the Euphrates River, which has essentially influenced the conditions of the national water stores in the Anbar Governorate. Specialists uncovered that a present-day dam lake had been decreased to an insignificant waterway after water flow levels dropped to 150 m^3/s; in 2020, it was 1,200 m^3/s. For this reason, it is necessary to find ways to hold and control water and ensure that it is not lost and increase the amount of rainwater collected by the dam by using geographic information systems (GIS) to suggest redirecting the lost water to Lake Haditha to improve water availability. Several recent studies have confirmed that GIS and remote sensing (RS) can significantly improve water resources management in arid regions in addition to other techniques, such as land use land cover (LULC) classification. According to the LULC classification, vegetated regions help retain groundwater, whereas urban growth and impermeable surfaces worsen surface runoff. The report points out that 1.2 billion cubic meters of water are lost yearly due to evaporation and recommends specific management techniques, such as better flood mitigation planning, erosion control, and reservoir optimization.[14]

Wise management of water resources also requires adopting modern technologies such as hydrological modeling to address water challenges[15,16] and Mcdonnell[17] confirmed that ArcGIS Pro provides advanced capabilities for cartographic modeling and spatial analysis, making it an essential tool in environmental and hydrological studies. DeMers[18] also indicated that ArcGIS Pro features a modern user interface and advanced analytical capabilities, making it the first choice for GIS researchers. It features advanced analytical capabilities, such as hydrological network analysis and sub-basin identification, making it the ideal choice for complex studies.[19,20] Despite the progress in using RS and GIS techniques to analyze the characteristics of water basins, there is a lack of applied studies on water management in arid and semi-arid regions such as the Haditha Dam basin. Previous research has focused on analyzing changes in water bodies without providing practical solutions to reduce water loss. This study aims to fill this research gap through a detailed analysis of the topographic and hydrological characteristics of the Haditha Dam Basin using Sentinel-1 imagery and digital elevation models (DEM), focusing on the influence of slopes and watersheds on runoff and soil erosion, as well as land use analysis (LULC) and assessing their impact on groundwater storage. The study will also provide recommendations for improving water resource management, including enhancing water storage, flood control, and reducing water losses.

2. Literature review and aims of the study

2.1. Literature review

Hydrological modeling using RS and GIS techniques has witnessed significant developments in analyzing and evaluating water basins' morphometric and hydrological characteristics. For example, RS and GIS

techniques were used in the study of the Duhok Dam in Kurdistan Region to assess the changes in water surface area between 2001 and 2012, where satellite data (Landsat 7 ETM+) were analyzed using ENVI and ArcGIS programs, taking into account field and climatic data to ensure the accuracy of the results.[21] This study is consistent with other research, such as the study of the Varuna River Basin in India, which used RS to identify the best locations for groundwater recharge facilities based on slope, soil depth, and runoff assessment.[22]

The study of the Chilikot Basin in Ethiopia revealed that spectral data analysis and DEM help identify drainage patterns and topography, supporting water conservation initiatives.[23] In the Akero River Basin in India, manual and automated GIS techniques enabled accurate mapping of drainage networks and detailed morphological measurements.[24] Another study confirmed that integrating RS techniques with GIS enhances the ability to manage water resources sustainably in arid regions.[25] Patil and Kherde[26] also showed that integrating hydrological modeling and spatial analysis using GIS can provide effective solutions for water management in river basins.

These studies underscore the importance of integrating RS and GIS techniques into water resources management, as they provide practical tools for monitoring environmental changes, analyzing hydrological data, and making informed decisions in water basin management, which can be generalized to improve water management efficiency and sustainable water project planning. This study hopes to contribute to a deeper understanding of the hydrological characteristics of the Haditha Dam Basin and provide practical tools for improving water management in scarce areas, enhancing long-term environmental and economic benefits.

2.2. Aims of the study

This study has five aims:

(i) Analyze the topographic and hydrological characteristics of the Haditha Dam Basin using Sentinel-1 satellite images and DEM.
(ii) Identify topographic features such as slopes and water flow accumulation and their impact on water runoff and soil erosion.
(iii) Conduct LULC to assess their impact on water runoff and groundwater storage.
(iv) Identify sub-basins within the central basin and understand their contribution to water flow toward the reservoir.
(v) Provide recommendations for sustainable water resource management, including improving water storage, flood control, and reducing water loss.

3. Materials and research methods

3.1. Study area and hydrological characteristics

Haditha Dam is located at coordinates 34.30685°N and 42.27985°E in the western Iraqi Anbar Governorate. Built in 1987, the dam rises 57 meters above the riverbank to form Lake Haditha, a reservoir holding around 8.3 billion m^3 of water. The reservoir, which covers an area of around 500 km^2 at its whole operating water level of 147 meters, is an essential source of drinking water, agriculture, and hydroelectric power. The dam basin is around 10,000 km^2 and has a diverse topography, including valleys, hills, and plains. The Euphrates River feeds the reservoir, which has experienced substantial hydrological changes throughout time. Due to significant upstream dam building and rising water use, the river's annual flow has decreased over the past few decades from its historical estimate of about 30 billion m^3.[27] There are noticeable seasonal changes, with springtime peak flows caused by rain and snowmelt. After international water accords, recent estimates show that the Euphrates currently have flow rates that have, under some circumstances, increased from about 240 m^3/s to 450 m^3/s. At Haditha Dam, operational difficulties still exist despite this progress. Up to 3,000 m^3/s may be safely released by the structure, with forecasts of up to 4,000 m^3/s during extreme situations.

Different sub-catchments that define discrete drainage zones within the basin further define the research region. Targeted water management methods may be informed by an understanding of localized runoff patterns and water distribution, which is made possible by these sub-catchments, as shown in Figure 1.

3.2. Data

As presented previously,[30,31] satellite data have been used to estimate changes in water volume in lakes and reservoirs, providing a powerful tool for monitoring water resources.

Sentinel-1, as shown in Figure 2, provides radar images with a spatial resolution of 10 m with a revisit time of around 5 days obtained from the European Space Agency Copernicus program. The Sentinel-2 optical image provides multispectral data with a resolution of up to 10 m with a revisit time of around 5 days, obtained from the same program. DEMs were created using

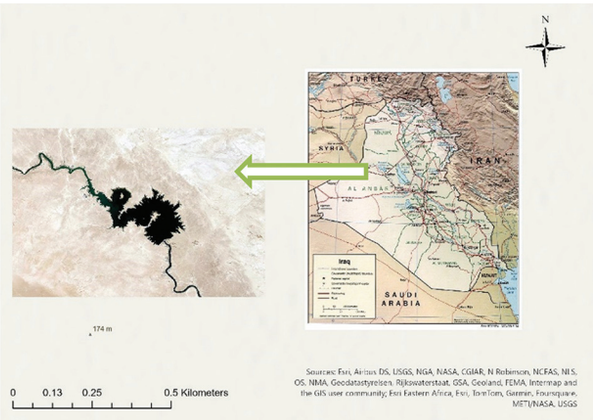

Figure 1. The study area (Haditha Lake)[28,29]

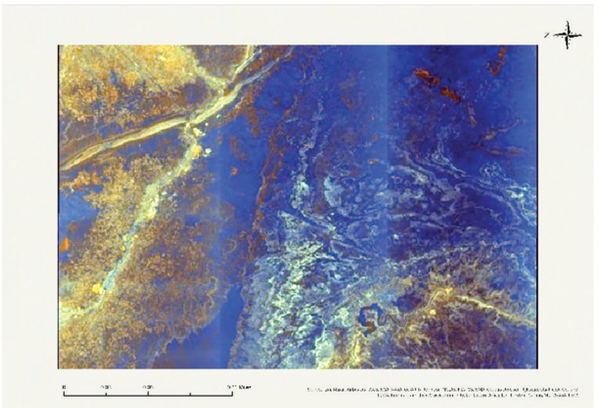

Figure 2. The Sentinel-1A (S1A_IW_GRDH) image of the study area. Scale bar: (0.11 miles)

interferometry processing of Sentinel-1 data. Due to its synthetic aperture radar (SAR) capabilities, Sentinel-1 is particularly well-suited for producing high-resolution DEMs, which are essential for precise topographic and hydrological analysis. The Sentinel-1 can collect data in all weather, including cloud cover and sunshine, unlike optical sensors like Sentinel-2 or Landsat 8, guaranteeing constant, dependable imagery throughout time. This is very useful for areas where weather or atmospheric circumstances could ordinarily make data collecting difficult. ArcGIS Pro was selected for this study because of its advanced hydrological modeling capabilities, excellent DEM processing accuracy, and smooth integration with RS data (Sentinel-1 & Sentinel-2). ArcGIS Pro offers stronger spatial tools, improved raster-based analysis, and more accurate watershed delineation than Quantum GIS and System for Automated Geoscientific Analyses.

The hydrological findings were verified using field data verification, comparisons with other GIS models (e.g., Hydrologic Engineering Center–Hydrologic Modeling System), and cross-referencing with topographic maps. These procedures demonstrated that ArcGIS Pro is the most suitable option for this study as it produces reliable and accurate hydrological outputs.

3.3. Methods

3.3.1. Sentinel-1 and -2 images pre-processing

The Sentinel-1 images were pre-processed using the Sentinel Application Platform (SNAP) software (version 11.0.0). The data can be utilized for generating DEMs through a series of pre-processing steps, including radiometric calibration to convert raw digital data into backscatter coefficients that reflect the physical properties of the surface, thermal noise removal to reduce or eliminate noise from the satellite's electronics, which can affect data quality, and terrain correction to correct distortions caused by terrain (such as mountains or valleys) that affect the angle of incidence of radar waves,[32] as shown in Figure 3.

The DEM was then used to conduct the topographic and watershed hydrologic analyses. The Sentinel-2 images were pre-processed using SNAP software, geometrically corrected to ensure accurate locations, and then rescaled to 10 m resolution to improve analysis and reduce unnecessary data. Spectral bands (2, 3, 4, and 8) are selected for vegetation studies, and the data are exported to GeoTiff format for LULC classification, as shown in Figure 4.

To manage satellite data uncertainties, Sentinel-1 SAR data guaranteed all-weather DEM production, whereas cloud-masked Sentinel-2 photos were utilized for LULC classification to reduce uncertainty. Radiometric/geometric adjustments in SNAP software decreased distortions, whereas interferometric methods (in SAR) increased terrain accuracy. Despite atmospheric or sensor restrictions, consistent hydrological analysis was ensured by resampling the data to a resolution of 10 m.

3.3.2. Topographic analysis

GIS techniques were used to analyze the terrain and identify erosion areas in the river basin, as in previous studies.[33,34] The slope, direction, curvature, and shading maps were created using ArcGIS Pro tools. These tools were used to analyze terrain features and their effect on water flow. Contour lines were created to visualize elevation changes and identify potential water flow paths, as shown in Figure 5. Terrain analysis tools play an important role in understanding and analyzing DEMs. The slope tool calculates the degree of slope, which is essential for erosion, drainage, and structural

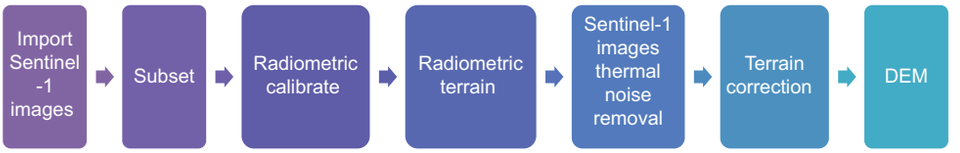

Figure 3. The flowchart of digital elevation model generation

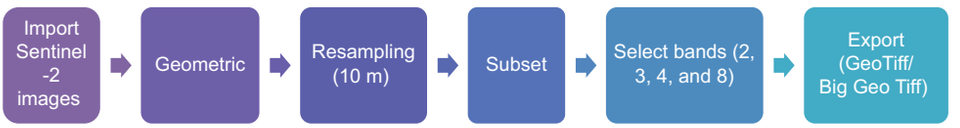

Figure 4. The flowchart of Sentinel-2 pre-processing

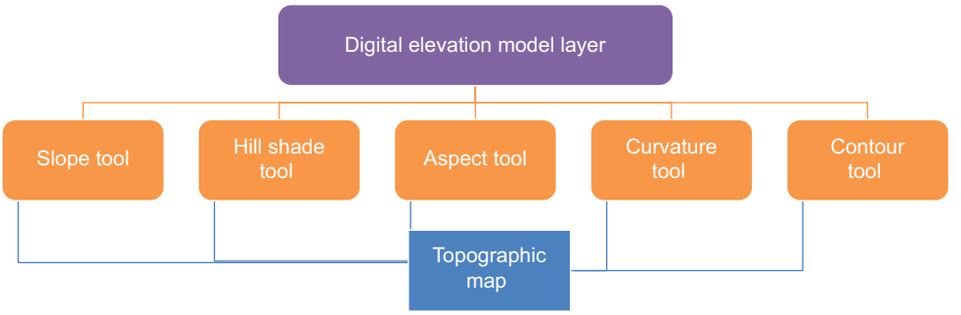

Figure 5. The flowchart of topographic analysis

planning studies, while the hill shade tool produces shade maps to improve terrain visualization. The aspect tool determines the direction of the slope, which is useful for solar radiation and microclimate studies. The curvature tool assesses concavity or convexity, which helps understand surface water flow and sediment transport, and the contour tool creates contour lines to simplify terrain representation on maps. These tools complement each other to provide a comprehensive view of terrain and environmental analysis.[35,36]

3.3.3. Watershed hydrological analysis

The GIS has been used to identify priorities in river basin management, as in previous studies.[37,38] GIS tools like the "fill," "flow direction," and "flow accumulation" functions are used to simulate water flow and model the natural movement of water over the terrain according to the topography and climate. Figure 6 shows the watersheds analysis using ArcGIS Pro, with a series of tools used to study and model the characteristics of watersheds through the following steps:

(i) Step 1. Preparing DEM datasets for hydrological analysis: The fill tool eliminated continuous flow routes and DEM depressions. The flow direction tool using the D8 method, which simulates water movement by allocating a direction to each cell based on the steepest descent, was used to calculate the flow direction.

(ii) Step 2. Analysis of flow accumulation: The number of upstream cells draining into each grid cell was calculated using the flow accumulation tool. Cells were categorized as belonging to a stream network based on a threshold; streams are generally defined as contributing areas of ≥1 km^2, which ensures that only hydrologically significant streams are considered, preventing small, non-permanent flow paths from skewing and not included in the analysis.

(iii) Step 3. Ordering and extracting stream networks: The Strahler Stream Order technique was used to classify the streams, helping differentiate major streams from minor tributaries and aiding in better hydrological interpretation. Higher-order streams are created when smaller tributaries combine; first-order streams are the smallest headwater channels. The raster stream network was transformed into vector format for additional analysis using the stream-to-feature tool.

(iv) Step 4. Delineation of watersheds: To increase the accuracy of the watershed boundaries, pour points (outlet sites) were manually modified using the snap pour point tool to match high-flow accumulation regions. The snap pour point modification reduces

watershed delineation mistakes brought on by limitations in DEM resolution. Individual sub-basins were created using the watershed tool, and their contributions to the Haditha Dam reservoir were examined.

The fill tool removed dips in the DEM to ensure flow continuity, the flow direction tool determined the direction of water flow for each cell, and the flow accumulation tool calculated the number of cells contributing to flow to define stream networks. Con tool was used to extract specific paths based on certain conditions, stream order tool classified streams hierarchically, and stream-to-feature converted point data to vectors. The contour tool created contour lines to visualize terrain, the basin identified individual basins, the snap pour point tool adjusted pour points to match the highest flow accumulation, and the watershed tool identified and delineated the watershed catchment areas based on pour points. These tools provided a comprehensive framework for understanding watershed dynamics and planning resource management.[39,40]

3.3.4. LULC classification

Remote sensing data have been used to monitor changes in land use, providing valuable insights for water resource management, as studied before.[41,42] Understanding LULC is important for hydrological and topographic analyses in drainage basins, as it affects runoff, groundwater recharge, and water quality. For example, deforestation increases erosion, harming water quality and reducing the basin's storage capacity.[43] LULC analysis also helps identify optimal areas for rainwater collection and storage, which promotes effective water resource management. For example, LULC analysis was used to study the impact of land use changes on river flows and flood risk in the Grand Ethiopian Renaissance Dam basin. In this study, LULCs were classified using the unsupervised classification method in ArcGIS Pro, resulting in four main categories: water, vegetation, urban areas, and soil, as shown in Figure 7.

4. Results

4.1. Sentinel-1 pre-processing

The DEM produced by the SNAP program following the pre-processing of the Sentinel-1 image is shown in Figure 8. Pre-processing is altering the original data table to create a new one, which includes using various techniques to change the data before latent vectors are extracted. Artificial intelligence devised a definition based on scientific data handling.[44]

4.2. Topographic analysis

4.2.1. Slope analysis

As shown in Figure 9, slope analysis using a DEM is a process that extracts information about the slope and the orientation of the terrain. The calculated slope value could be classified into different categories based on the calculated slope value. A map of the slope of the study area is based on an analysis of GIS data. Slope analysis relies on a DEM to measure the change in elevation across, while bodies or regions with very low slope values were represented by dark blue to purple. In addition, places with a moderate slope are indicated by yellow to orange hues, whereas areas with a high slope are indicated by red.[45] The light blue to green color indicates areas with low slopes. The terrain is

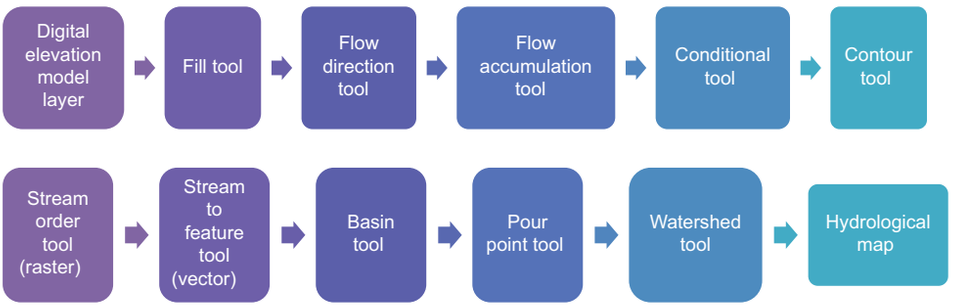

Figure 6. The flowchart of hydrological analysis

Figure 7. The flowchart of land use and land cover

flatter when the slope value is lower and steeper when the slope value is higher.

4.2.1.1. The slope's effect on water retention and flow

According to the slope study in Figure 9, steep slopes (>20°) predominate in the basin's northern parts, encouraging fast surface runoff and little water retention. On the other hand, the central and southern regions have slopes of <5°, which improve the potential for groundwater recharge by allowing for more water penetration and retention. Reservoir water quality and sedimentation rates are impacted by the high runoff from higher terrains, which also adds to erosion and sediment transport.

4.2.2. Hill shade map

The GIS software and the DEM analysis produced a hill shadow map of the research area. The map depicts the research area's landscape in three dimensions, and Figure 10 shows that it is not flat. The 0 represents fully shaded areas, indicating low illumination, often due to steep terrain facing away from the light source. The three-dimensional shadow map shows that it is used to create a three-dimensional effect, where the high areas appear as shaded areas, while the low areas appear as illuminated areas.[45]

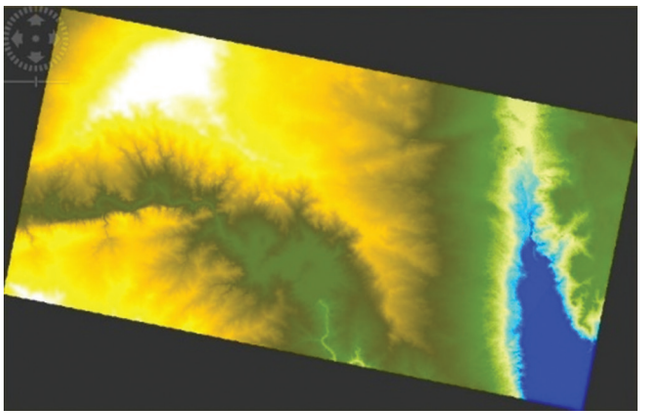

Figure 8. The Sentinel-1 to digital elevation model image

4.2.3. Aspect map analysis

An aspect-slope map simultaneously shows the aspect (direction) and degree (steepness) of the slope of a terrain (or other continuous surface). Aspect categories are represented by colors (red, orange, yellow, etc.). In addition, a text analysis technique that divides the textual material and describes its sentiment based on its constituent parts. It is essential that data analysis be simple and focused on the most important aspects of the data. Consequently, analysts can effectively respond to the present research questions without being too specific.[46]

The aspect map in Figure 11 shows the cells along the slope direction of the terrain research area. The largest regions in the study area are located in the east, northeast, and northwest, whereas the south, north, and southwest have smaller sections and a very small flat area. The map classifies the slopes according to their geographical directions. The key shows the distribution of colors associated with different directions, helping to understand how terrain interacts with natural factors such as sunlight, wind, and water flow.

4.2.4. Keynotes based on key

The yellow (east-facing slopes, 67.5° – 112.5°) represent slopes that receive sunlight in the morning, which makes them important for agriculture and for analyzing solar radiation. Yellow areas are visible on

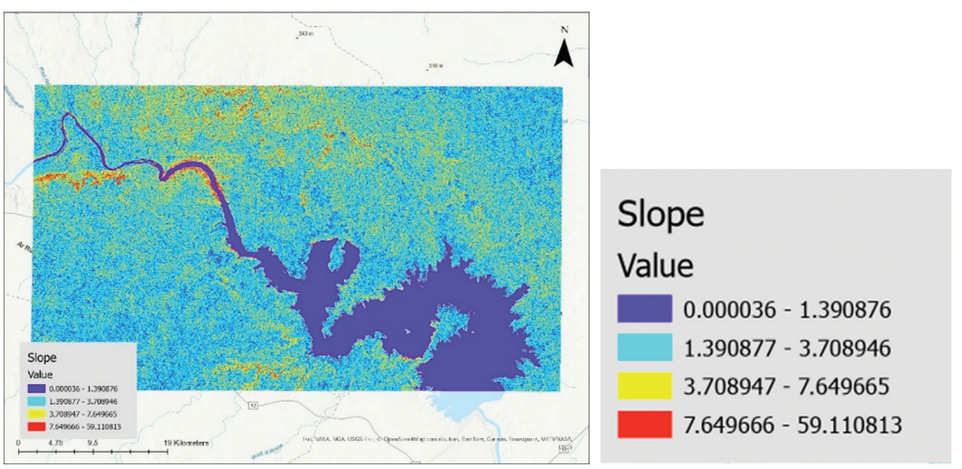

Figure 9. The slope map of the study area

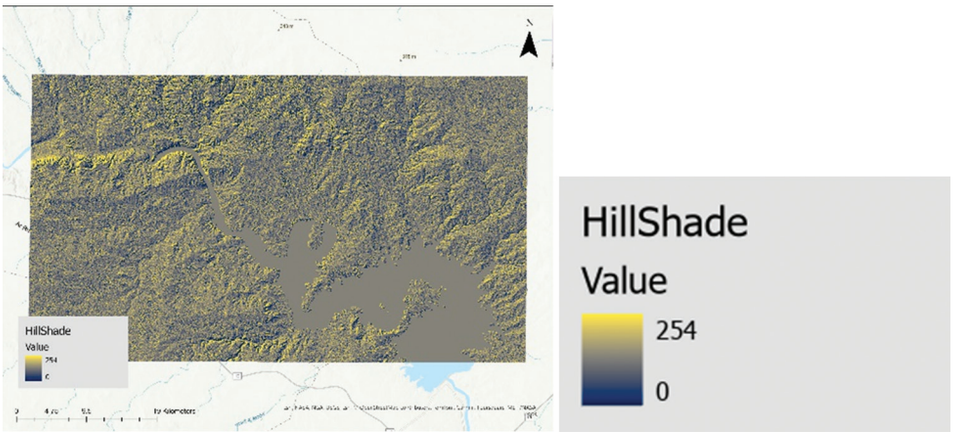

Figure 10. The hill shade map of the study area

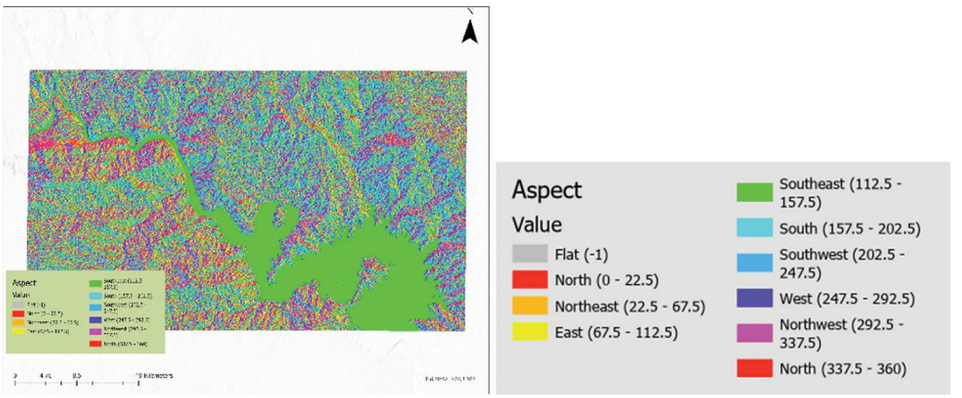

Figure 11. Aspect map of the study area

east-facing hills and slopes, indicating their distribution in the study area. The red (north-facing slopes, 337.5° – 360° and 0° – 22.5°) areas are concentrated on steep terrain, especially in valleys or areas protected from direct sunlight. The green (southeast-facing slopes, 112.5° – 157.5°) and light green (south-facing slopes, 157.5° – 202.5°) slopes are the most exposed to sunlight during the day, especially the southern slopes, which makes them warm and suitable for vegetation that needs sunlight. The sky blue (southwest-facing slopes, 202.5° – 247.5°) and blue (west-facing slopes, 247.5° – 292.5°) slopes that receive afternoon sunlight are often found on hills or valleys oriented west. The Violet (northwest-facing slopes, 292.5° – 337.5°) slopes are cool and shady, similar to the northern slopes, but may receive some indirect sunlight in the afternoon.

4.2.5. A curvature map

A map of the research area's curvature is displayed in Figure 12. A curvature map classifies the terrain according to the Earth's surface shape, with colored values in the legend signifying various terrain features.

This map is a tool for understanding slope characteristics and surface water flow dynamics.[47] Interpretation of colors and values in the image:

(i) Dark blue (values: −19.467 – 0.004) represents concave surfaces (negative curvature). These areas usually indicate valleys, drainage paths, or depressions where water collects. They are often in areas of lower elevations, where water and sediments are deposited.

(ii) Yellow (values: 0.005 – 6.236) represents surfaces that are almost flat or have a slight curvature. These often represent transitional areas between concave and convex areas and indicate a constant slope or planar areas. These areas may not induce significant water flow but support sediment deposition.

(iii) Green (values: 6.237 – 12.468) represents moderately convex surfaces. These areas are often mid-slope or gently rising terrain, which affects the direction of water flow without significantly accelerating runoff. These areas are widespread on the map, indicating widespread terrain with moderate inclination.

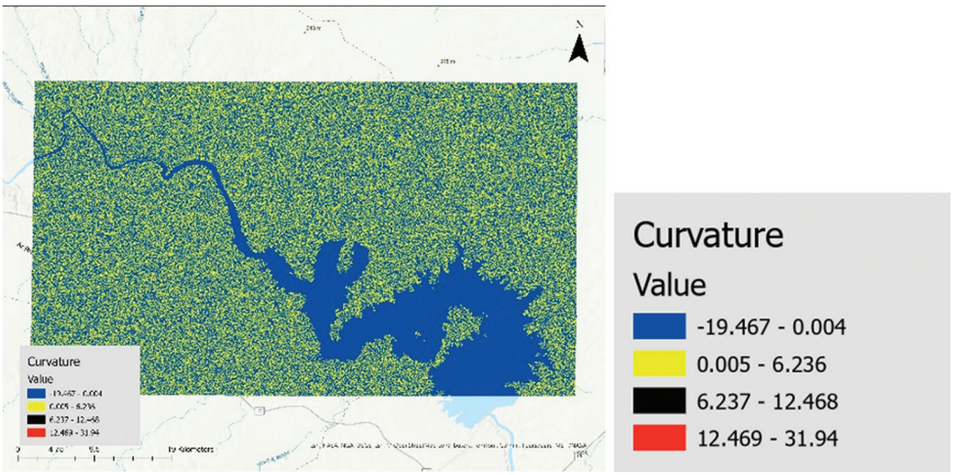

Figure 12. The curvature map of the study area

(iv) Red (values: 12.469 – 31.94) represents surfaces that are sharply convex (positive curvature). These areas represent peaks, ledges, or sharp ridges where water flow disperses. These areas are vulnerable to erosion because they represent the highest points in the landscape. The scattered red areas highlight the steeper hills and terrain features that direct water away from these locations.

4.2.5.1. Curvature's function in flow accumulation

Connecting convex aspects to flow dispersion and concave portions to water collecting zones, concave regions (negative curvature values) serve as water collecting zones, promoting retention and groundwater infiltration, according to the curvature map in Figure 12. On the other hand, convex topography (positive curvature values) promotes surface water dispersal, reducing buildup and raising the possibility of flash floods downstream.

4.3. Water flow analysis

4.3.1. Hydrological analysis

After filling the elevation holes, the DEM data are free of obstacles that may block the natural flow of water. As a result, the dataset becomes more accurate and representative of the natural terrain, facilitating flow analysis. The flow direction in each DEM cell represents the path the water is expected to take under the influence of gravity. This result helps determine the water flow paths from each point, making it easier to understand the pattern and direction of water movement. Figure 13 shows a map of the flow direction of the study area. This accumulated flow at each cell helps identify areas that collect large amounts of water that may turn into major rivers or valley paths.

4.3.2. The flow accumulation map

The flow accumulation map can locate rivers, natural waterways, and areas that may be subjected to surface runoff or water accumulation. In addition, Figure 14 shows a map of the flow accumulation of the study area. A runoff accumulation map shows the flowing water collected in each grid cell in a given area. These maps are typically used in hydrological model analysis to determine water flow directions and drainage patterns.

Based on the image provided, high values (light areas) are light or white areas that indicate high values of runoff accumulation. These areas typically represent rivers, streams, or places where water accumulates extensively due to surface flows. In contrast, low values (dark areas) indicate low runoff accumulation values. These areas may be hilltops, flat lands, or areas where water does not naturally collect. The median in the image shows that the values range from 0 (no runoff) to 2.39383×10^7 (maximum value of runoff accumulation). This wide range indicates a large discrepancy between high and low-flow areas.

4.3.3. The stream order map

The analysis results in a map of the stream order, where each stream is labeled according to its rank. First-order branches represent small streams that do not connect to any other branches. When two first-order branches meet, a second-order branch is formed, and the process continues for higher-order streams. Figure 15 shows a map of the stream order of the study area. The stream order map represents the hierarchical classification of streams based on their connectivity and structure within a watershed. A detailed analysis of the map can be found in Maarez and Jaber.[48]

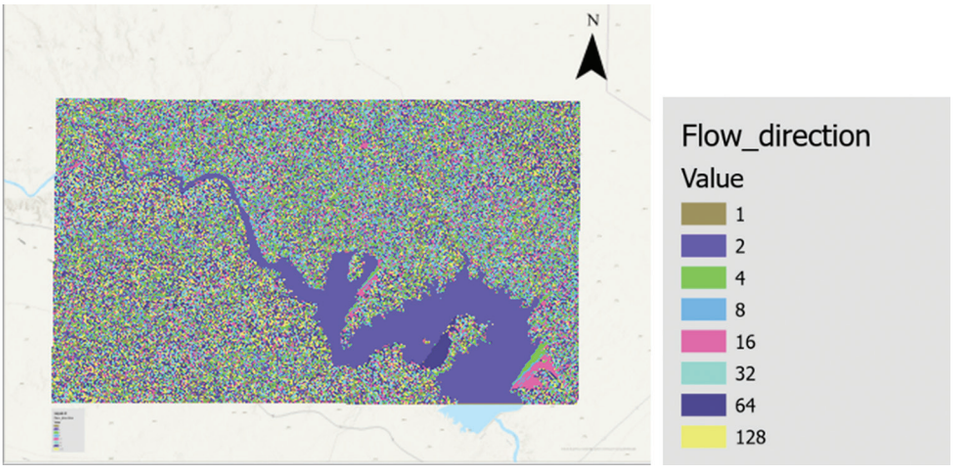

Figure 13. The flow direction map of the study area

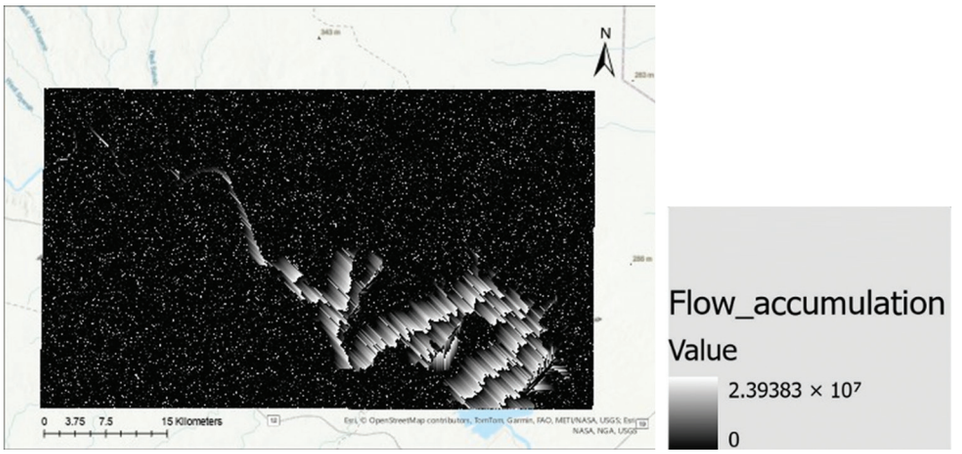

Figure 14. The flow accumulation map of the study area. Flow accumulation value: 2.39383 × 10^7.

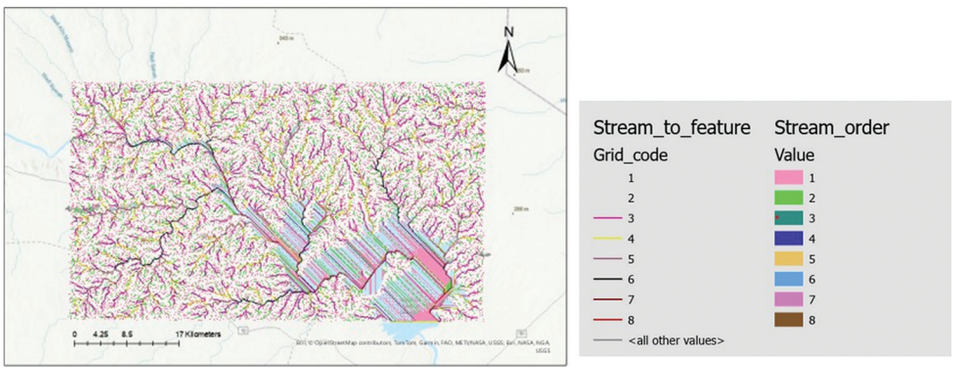

Figure 15. The stream order map of the study area

4.3.4. Watercourse analysis

An analysis of the watercourse classification patterns can be categorized into five key classifications.

(i) Hydrological classification. In this classification, the map uses Strahler's system to classify waterways based on their connections. In this system, class 1 (pink) represents small streams (upstream tributaries), which are the most widespread and numerous. Higher grades (2 – 8) represent confluence areas where small streams merge to form larger channels. The highest ranks represent significant rivers.

(ii) Water-way network patterns. The dendritic pattern shows a network that follows a tree pattern, common in areas with homogeneous geology and topography. This style promotes efficient water flow. Geometric patterns indicate areas that show straight or angular patterns, which may indicate geological influences such as faults or rock layers.

(iii) Color representation of ranks. The map uses color coding to represent different stream ranks. Pink color (first order) represents the smallest branches that form the basis of the drainage network, while colors from green to yellow (ranks 2 – 5) represent the intermediate ranks where the sewage pool begins. Blue to brown colors (ranks 6 – 8) represent major channels and larger rivers.

(iv) Rank distribution. Moving from lower to higher ranks shows water accumulation in the landscape, from highlands to plains. The lower ranks (pink) are more evenly distributed, while the higher ranks (blue and brown) are concentrated in valleys or plains.

(v) Hydrological insights. These insights can be further classified into three parameters. One of these parameters is discharge density, which indicates that a high density of first-order streams suggests high discharge. This typically reflects an area with high rainfall rates or impermeable surfaces. Second, hydrological connection indicates that higher-order sewer connectivity promotes efficient water transport, reducing the risk of local flooding. Finally, the map can help identify water basins. The map can define sub-basin boundaries, with higher-order streams defining the primary boundaries.

4.3.5. The watershed basin map

Figure 16 displays the watershed basin map of the Haditha Dam area. The image illustrates the division of aquariums, with each aquarium assigned a unique color and grid code. The legend in the image refers to the grid symbols representing basins or sub-regions. Geographic features are also highlighted, with large basins (such as the area in purple or green) representing major basins with extensive drainage. In contrast, small basins (such as in pink or cyan) represent smaller sub-basins. Several key points can be highlighted in the watershed basin map analysis:

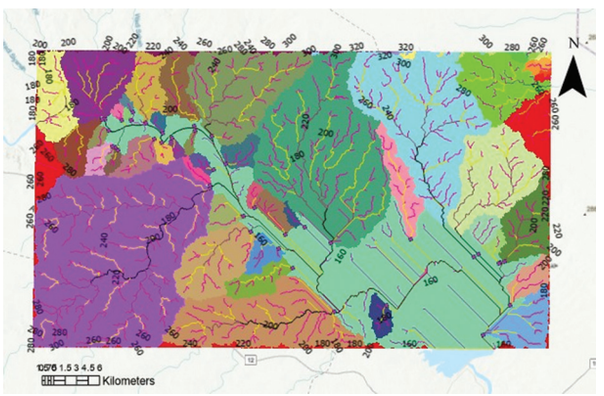

Figure 16. The watershed basin map of the Haditha Dam area

(i) Definition of water basins. The image contains multiple water basins extracted using flow direction and flow accumulation data. The apparent boundaries define hydrological breaks, with water flowing within each basin based on topography.

(ii) Distribution of basin sizes. Large basins may indicate areas with less steep terrain or areas where several small basins are clustered. Small ponds are frequently found in areas with local drainage or steep terrain.

(iii) Structural relationships between basins. Based on the picture, there is a gradation in the sizes of the basins, where large basins may contain several smaller sub-basins. This structure can be used in multi-scale hydrological studies such as flood management or water resources planning. Ponds of the same color in the picture represent separate watersheds or sub-basins. Each color indicates a unique watershed identified using flow accumulation and direction data. These basins are separated by water dividing lines, meaning all water within the one-colored area flows toward the same outlet or meeting point.

(iv) Contributions of watersheds and sub-basins to reservoir inflow. The watershed delineation discovered several sub-basins contributing to the Haditha Dam reservoir, as shown in Figure 16. The biggest sub-basin, which makes up about 40% of the study area, is a crucial hydrological contributor, directing water flow into the reservoir. Major drainage paths are located in the center and southern basin areas, directly feeding the reservoir, according to flow accumulation studies shown in Figure 14.

4.3.6. LULC classification

The watershed basin map of the Haditha Dam area, which displayed a map of the LULC research area, is shown in Figure 17. This map shows the result of unsupervised classification. There are four basic classes for the study area, which are: (i) Blue, representing areas containing the riverbed and reservoir of the Haditha Dam area,

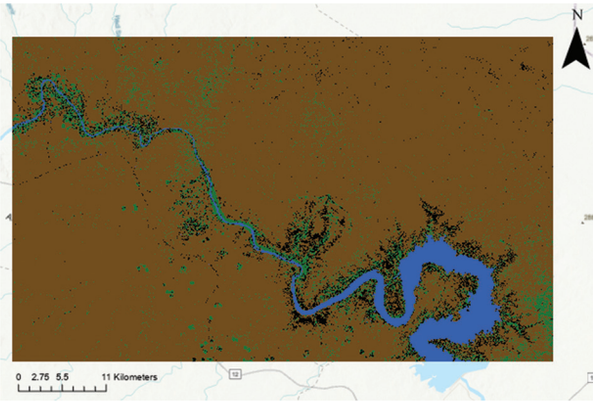

Figure 17. The land use and land cover map of the Haditha Dam area

(ii) brown, indicating bare land or dry soil, (iii) green, which includes areas of agricultural vegetation, and (iv) black, indicating urban areas or human structures.

These categories are considered the most important and have the most significant impact on water flow to the basin. Urban areas on the map can affect water flow in different ways. Urban areas or human structures increase surface runoff due to impermeable surfaces, reducing groundwater recharge and increasing the risk of flooding. Dark soils or natural depressions can act as temporary water storage areas, slowing the flow and limiting erosion and sediment transport to rivers and reservoirs, where forests enhance infiltration. Meshesha *et al*.[44] showed that changes in land use can significantly affect hydrological responses, especially in areas experiencing deforestation. Thus, the map provides essential data for understanding the natural and human factors that affect water flow, contributing to better water resource management and effective planning to reduce risks such as floods or water shortages.

4.3.7. Effects of terrain and land use on hydrological response

The interaction between various land cover types – such as vegetation, bare land, and urban areas – and topographical factors play a role in influencing groundwater recharge and discharge. According to the LULC classification in Figure 17, impermeable surfaces in urbanized regions increase surface runoff, which lowers infiltration capacity. In contrast, by permitting percolation into the soil, agricultural and vegetated areas – mostly found in flatter zones – improve groundwater recharge. The distribution of land cover and the topography features work together to retain water across the basin effectively.

5. Discussion

Topographic analysis revealed that the Haditha Dam basin is characterized by a mixture of flat plains and steep hills, with slopes ranging from 0° to 30°. The slope map Figure 9 shows that the steepest slopes are concentrated in the northern part of the basin, while the southern areas are mostly flat. This slope variation significantly impacts water flow and erosion, with steeper slopes experiencing faster runoff and higher erosion rates. Bright areas (high values) indicate slopes facing the light source, often north-facing slopes if the light comes from the south, while dark areas (lower values) represent shaded areas, such as valleys or steep slopes facing away from light or areas obscured by adjacent terrain. The image shows topographic details such as peaks, valleys, and plains, making it useful for visualizing the elevation and structure of the landscape.

The flow accumulation map Figure 14 indicates that most of the water flows toward the central and southern parts of the basin, where the reservoir is located. This pattern is consistent with the branched drainage network observed in the watercourse map Figure 15, which shows a hierarchical structure of watercourses converging into larger channels.

Several sub-basins were identified within the basin using the watersheds identification tool in Figure 16, with each basin contributing to the total water flow to the reservoir. The largest sub-basin covers about 40% of the basin area. It is located in the central region, characterized by moderate slopes and high flow accumulation. As pointed out by Shekhar and Pandey,[45] using RS and GIS techniques can help identify areas with high groundwater potential.

These results are consistent with previous studies on similar basins in arid regions, which highlighted the importance of slopes and flow accumulation in determining water availability and flood risk,[13,49]; they are also consistent with previous findings[46,50] that GIS-based hydrological modeling can provide accurate analysis of runoff response. However, this study provides more detailed insights into the specific characteristics of a modern dam basin, which can guide targeted water management strategies.

Compared to research in arid Areas, the study's findings are consistent with those of other dry and semi-arid areas, where topographical features significantly influence hydrological response. Research conducted in dry basins, such as the Duhok Dam Basin in Iraq and the Varuna River Basin in India, has also shown that flat terrain improves water retention and groundwater

recharge, whereas steep slopes speed up runoff and erosion.[34,45] In semi-arid areas of Ethiopia and North Africa, where impermeable surfaces decrease penetration and exacerbate flash floods, urbanization has also been linked to increased surface runoff, as seen in the Haditha Basin.[41] The work confirms earlier findings that hydrological modeling in dry locations with limited data requires RS and GIS approaches.[14] These parallels underline the necessity of terrain-based water management techniques in dry regions around the globe and support the findings' generalizability outside of the Haditha Basin.

There are several principal contributions from the findings of this paper. First, it provides scientific input for scholars and researchers. It shows how well Sentinel-1 SAR and Sentinel-2 optical data may be used for hydrological modeling in areas with limited data. It also enhances knowledge of runoff patterns, flow accumulation, and sub-basin hydrodynamics by offering a high-resolution DEM-based flow study. The findings suggest incorporating ground-based hydrological measurements for model validation and draw attention to the shortcomings of DEM-based flow analysis. Secondly, the findings act as policy-related results for decision-making and water resource managers. It highlights the need for reservoir optimization measures by identifying a water balance shortfall (153 m^3/s input vs. 200 m^3/s outflow) and large yearly evaporation losses (~1.2 billion m^3). It also supports evidence-based policy measures, such as those to manage watersheds to lessen sedimentation and erosion in Haditha Reservoir, sustainable drainage systems in urban development initiatives to reduce the danger of flooding, and schemes for groundwater recharge that use human-made infiltration basins in areas with high permeability. It also supports the integration of RS and GIS technology into national water governance systems.

Furthermore, the results provide engineering and real-world uses for engineers, urban planners, and hydrologists by offering ideas for flood reduction according to topography, with a focus on controlled water retention and slope management. The findings also identify areas with significant runoff risk and recommend using geospatial technologies to prepare for infrastructure resilience. In addition, it suggests that higher-resolution elevation models be included to improve topographic accuracy in hydrological evaluations and encourages the creation of a national water monitoring system based on GIS to enable real-time assessments of water resources. Policymakers, engineers, and researchers aiming to improve water security in arid and semi-arid regions might use this study as a decision-support tool by connecting scientific hydrological models with practical water management applications. Future research should concentrate on climate-driven impact assessments, hydrological model validation, and multi-source data integration to create more robust and adaptable water management plans.

5.1. Specific policy suggestions for water management organization

The following suggestions are specifically designed for government organizations, legislators, and water resource managers in charge of sustainable water governance in dry countries like Iraq to guarantee that the study's conclusions immediately influence water management policies:

(i) Improving erosion control and watershed management. The intervention is proposed to the Ministry of Agriculture and the Ministry of Water Resources. According to the study, the northern basin's steep slopes are a major cause of the Haditha Reservoir's fast runoff and sedimentation. The policy intervention that could be implemented is to reduce erosion and silt buildup in the reservoir by putting soil conservation measures like check dams, afforestation, and terracing into practice. Moreover, infiltration could be improved, and water loss could be reduced from surface runoff by encouraging the regeneration of vegetation cover in degraded regions. In addition, improving reservoir performance can minimize water loss.

(ii) For Iraq's water resources management authorities and dam operators. Significant evaporative losses (~1.2 billion m^3 yearly) and a water balance imbalance (inflow: 153 m^3/s, outflow: 200 m^3/s) were discovered by the investigation. Hence, to maximize water retention, it is suggested to use dynamic reservoir operating plans based on seasonal inflow trends and evaporation rates. To lower evaporation losses in the Haditha Dam, invest in artificial reservoir covers or floating solar panels.

(iii) Policies for urban planning to reduce the risk of flooding in which local governments and municipal planning authorities are the target audience. According to the LULC research, impermeable surfaces and urban growth raise the danger of flooding and runoff. Hence, new urban projects are suggested to have sustainable urban drainage systems, such as rainwater collection systems, green roofs, and permeable pavements. In addition,

to reduce flood damage in cities, main drainage canals should be designated as flood buffer zones.

(iv) Improving agricultural water management & groundwater recharge with the Departments of Water Resources and Irrigation as the target audience. The southern basin's flat regions were the best for groundwater recharging. Hence, to improve groundwater storage in agricultural areas, it is suggested that artificial recharge basins and infiltration ponds be built. Moreover, to minimize surface water loss, effective irrigation technology (such as drip irrigation and intelligent irrigation scheduling) can be used.

(v) Integrating RS and GIS into water governance. The Iraqi Ministry of Water Resources and Environmental Agencies is the intended audience. The study showed that hydrological models based on GIS offer useful information for planning water resources. Hence, real-time RS data are suggested to create a GIS-based National Water Monitoring System to monitor drought conditions, flood threats, and reservoir levels. It is also indicated to include RS and GIS capabilities in national disaster response and water distribution plans.

Despite the contributions of this study, there are several limitations. The main drawbacks of this study are the use of RS-based hydrological modeling, including topography misrepresentation, interpolation mistakes, and DEM resolution restrictions. Small-scale flow characteristics could be missed by the Sentinel-1 DEM (10 m resolution), which could result in inaccurate flow accumulation and direction. Furthermore, subsurface hydrology cannot be directly measured by RS; validation is done by field data or additional models. Seasonal variations and spectral mixing impact the accuracy of LULC categorization. Future research should use *in situ* hydrological data, higher-resolution DEMs, and sophisticated models like the soil and water assessment tool or the Hydrologic Engineering Center's Hydrologic Modeling System to increase accuracy.

6. Conclusion

To evaluate topography, watershed dynamics, and land use implications on water flow and retention, this study integrates RS and GIS-based hydrological modeling to provide a thorough geospatial analysis of the Haditha Dam Basin. The study's conclusions directly affect hydrological research, environmental planning, and the management of water resources in arid and semi-arid areas.

Acknowledgments

The authors would like to thank the support staff of the Remote Sensing Department at Al-Kharkh University of Science and the GIS Department at the Iraqi Geological Survey for their assistance.

Funding

None.

Conflict of interest

The authors declare no conflicts of interest.

Author contributions

Conceptualization: Nabaa Isam Ali
Data curation: Salwan Sabbar Al-Hasnawi
Formal analysis: Salwan Sabbar Al-Hasnawi
Investigation: All authors
Methodology: Nabaa Isam Ali
Writing – original draft: Nabaa Isam Ali
Writing – review & editing: Salwan Sabbar Al-Hasnawi

Availability of data

Data of this study are available from the corresponding author on reasonable request.

References

1. Subramanian V. Controlling factors in river water quality in Asia. In: *Surface and Sub-Surface Water in Asia - Issues and Perspectives*. Amsterdam: IOS Press; 2015.
doi: 10.3233/978-1-61499-540-1-1
2. Ranjith J, Rajeev H. Aqua check-water quality monitoring system. *Indian J Image Process Recognit*. 2023;3(3):1-5.
doi: 10.54105/IJIPR.B3910.043323
3. Lunegova IV, Tyts VV, Lopatin SA. Water and its importance for human life and health. *Pharm Formulas*. 2022;4(3):50-57.
doi: 10.17816/phf115210
4. Panhwar A, Abro R, Kandhro A, *et al.* Global water mapping, requirements, and concerns over water quality shortages. In: *Water Quality - New Perspectives*. Germany: BoD - Books on Demand; 2022.
doi: 10.5772/INTECHOPEN.108331
5. Jawad LA. Freshwater ecosystem conservation in Iraq: Recommendations for management. In: *Tigris and Euphrates Rivers: Their Environment from Headwaters to Mouth*. Germany: Springer Nature; 2021.

doi: 10.1007/978-3-030-57570-0-79
6. Abd El Mooty M, Kansoh R, Abdulhadi A. Challenges of water resources in Iraq. *Hydrol Curr Res*. 2016;7(4):260. doi: 10.4172/2157-7587.1000260
7. Aftan OA. The effect of lack of water resources on food security in Iraq. *J Juridical Polit Sci*. 2023;12(1):45-71. doi: 10.55716/jjps.2023.12.1.2
8. Choi YW, Eltahir EAB. Uncertainty in future projections of precipitation decline over mesopotamia. *J Clim*. 2023;36(4):1213-1228. doi: 10.1175/JCLI-D-22-0268.1
9. Goodwin D, Raffin M, Jeffrey P, Smith HM. Applying the water safety plan to water reuse: Towards a conceptual risk management framework. *Environ Sci Water Res Technol* (*Camb*). 2015;1(5):709-722. doi: 10.1039/C5EW00070J
10. Harlıoğlu M, Mustafa SOM, Batool Z. The present situation of the fisheries sector in Iraq: A critical review. *Çanakkale Onsekiz Mart Univ J Mar Sci Fish*. 2023;6(1):70-75. doi: 10.46384/JMSF.1216078
11. Suleiman A, Al-Karbouli E. *Hydrological Assessment of the Volume of Water Losses in Al-Habbaniyah Lake and Its Impact on the Tourism Activity of the Tourist City h Using Modern Geographical Technologies*. Available from: https://www.researchgate.net/publication/370691969 [Last accessed on 2024 May 16].
12. Ahmed MF, Alam L, Ta GC, Mohamed CAR, Mokhtar M. A review on the environmental pollution of langat river, Malaysia. *AJWEP.* 2016;13(4):25-31. doi: 10.3233/AJW-160035
13. Fu Y, He G, Zhao S, Jiang H. Research on watershed water ecological management and compensation based on evolutionary game. *Aqua Water Infrastruct Ecosyst Soc*. 2023;72(7):1164-1183. doi: 10.2166/aqua.2023.222
14. Khormi HM. Using GIS tools and data for hydrological modelling in Arid Areas: A literature review. *Egypt J Environ Change*. 2019;11(1):5-27. doi: 10.21608/EJEC.2019.96533
15. Al-Ansari N, Knutsson S. *Toward Prudent Management of Water Resources in Iraq Toward Prudent Management of Water Resources in Iraq Article Info*; 2011. Available from: https://www.researchgate.net/publication/228835253 [Last accessed on 2025 Apr 05].
16. Longley P. *Geographic Information Science and Systems*. Available from: https://www.wiley.com/en-us/geographic+information+science+and+systems%2c+4th+edition-p-9781119128458 [Last accessed on 2025 Feb 25].
17. Mcdonnell RA. *Principle of Geographic Information Systems*. 1998. Available from: https://www.researchgate.net/publication/37419765 [Last accessed on 2025 Feb 25].
18. Demers MN. *Fundamental Geographic Information System*. Available from: https://www.scribd.com/document/424758422/fundamentals-of-geographic-inf-systems [Last accessed on 2025 Feb 25].
19. Goodchild MF. Twenty years of progress: GIScience in 2010. *J Spatial Informat Sci*. 2010;1(2010):3-20. doi: 10.5311/JOSIS.2010.1.2
20. Hakim WL, Fadhillah MF, Won JS, Park YC, Lee CW. Advanced time-series inSAR analysis to estimate surface deformation and utilization of hybrid deep learning for susceptibility mapping in the Jakarta metropolitan region. *GISci Remote Sens*. 2025;62(1):2465349. doi: 10.1080/15481603.2025.2465349
21. Mustafa YT, Noori MJ. Satellite remote sensing and geographic information systems (GIS) to assess changes in the water level in the Duhok dam. *Int J Water Res Environ Eng.* 2013;5:351-359. doi: 10.5897/IJWREE2012.0402
22. Rai PK, Singh P, Mishra VN, Singh A, Sajan B, Shahi AP. Geospatial approach for quantitative drainage morphometric analysis of varuna river basin, India. *J Landsc Ecol*. 2020;12(2):1-25. doi: 10.2478/jlecol-2019-0007
23. Gebre T, Kibru T, Tesfaye S, Taye G. Analysis of watershed attributes for water resources management using GIS: The case of chelekot micro-Watershed, Tigray, Ethiopia. *J Geographic Informat System*. 2015;7(2):177-190. doi: 10.4236/jgis.2015.72015
24. Viswanadh GK, Reddy BR, Chandra GS, Giridhar MVSS. Integrated Watershed Management by Using Remote Sensing and Geographical Information System: A Case Study. *In: Proceedings of Two Day National Conference on Water, Environment and Society*. 2014. Available from: https://www.researchgate.net/publication/265908500-integrated-watershed-management-by-using-remote-sensing-and-geographical-information-system-a-case-study/citations [Last accessed on 2024 May 18].
25. Mukhtorov U, Kakhorov B, Khafizova Z, Murodova D, Egamberdiev R. Study of monitoring of water bodies using remote sensing data and GIS technologies (Talimarjan water reservoir). *IOP Conf Ser Earth Environ Sci*. 2024;1420:012007. doi: 10.1088/1755-1315/1420/1/012007
26. Patil G, Kherde R. Assessment of large river basin approaching gis and computation of simulation techniques using latest software. *Ecol Eng Environ Technol*. 2024;25(1):360-368. doi: 10.12912/27197050/175753
27. Mohammed KS, Erzaig AS. Hydrological assessment of the volume of water losses in Al-Habbaniyah Lake and its impact on the tourism activity of the tourist city h using modern geographical technologies. *J Univ Anbar Humanit.* 2022;2(3):237.
28. Enabling Peace in Iraq Center. *Climate Briefing - EPIC - Enabling Peace in Iraq Center* Enabling

Peace in Iraq Center. 2023. Available from: https://enablingpeace.org/climate-briefing [Last accessed on 2025 Mar 20].
29. Wikipedia Contributors. *Geography of Iraq - Wikipedia*. 2024. Available from: https://en.wikipedia.org/wiki/geography-of-iraq [Last accessed on 2025 Mar 20].
30. Duan Z, Bastiaanssen WGM. Estimating water volume variations in lakes and reservoirs from four operational satellite altimetry databases and satellite imagery data. *Remote Sens Environ*. 2013;134:403-416. doi: 10.1016/J.RSE.2013.03.010
31. Jain SK, Singh P, Seth SM. Assessment of sedimentation in Bhakra reservoir in the western Himalayan region using remotely sensed data. *Hydrol Sci J*. 2002;47(2):203-212. doi: 10.1080/02626660209492924
32. Li T, Zhang B, Cheng X, *et al.* Resolving fine-scale surface features on polar sea ice: A first assessment of UAS photogrammetry without ground control. *Remote Sens.* 2019;11(7):784. doi: 10.3390/RS11070784
33. *Application of GIS and Remote Sensing for Watershed Development Project - A Case Study - Geospatial World*. Available from: https://geospatialworld.net/article/application-of-gis-and-remote-sensing-for-watershed-development-project-a-case-study [Last accessed on 2025 Mar 12].
34. Agarwal R, Garg PK, Garg RD. Remote sensing and GIS based approach for identification of artificial recharge sites. *Water Resour Manage*. 2013;27(7):2671-2689. doi: 10.1007/S11269-013-0310-7
35. Wilson JP, Gallant JC. Terrain Analysis: Principles and Applications. John P, Wilson John C, Gallant Wilson JP, Gallant JC, editors. United States: John Wiley & Sons; 2000. p. 520. Available from: https://www.wiley.com/en-us/terrain+analysis%3a+principles+and+applications-p-9780471321880 [Last accessed on 2025 Feb 25].
36. Rhind DW, Green NPA. Design of a geographical information system for a heterogeneous scientific community. *Int J Geogr Inf System*. 1988;2(2):171-189. doi: 10.1080/02693798808927893
37. Kumar D, Dhaloiya A, Nain AS, Sharma MP, Singh A. Prioritization of watershed using remote sensing and geographic information system. *Sustainability* (*Switzerland*). 2021;13(16):9456. doi: 10.3390/SU13169456
38. Tiwari K, Goyal R, Sarkar A. GIS-based methodology for identification of suitable locations for rainwater harvesting structures. *Water Resour Manag*. 2018;32(5):1811-1825. doi: 10.1007/S11269-018-1905-9
39. Wang X, Xie H. A review on applications of remote sensing and geographic information systems (GIS) in water resources and flood risk management. *Water*. 2018;10(5):608. doi: 10.3390/W10050608
40. Tarboton DG. A new method for the determination of flow directions and upslope areas in grid digital elevation models. *Water Resour Res*. 1997;33(2):309-319. doi: 10.1029/96WR03137
41. Rawat JS, Kumar M. Monitoring land use/cover change using remote sensing and GIS techniques: A case study of Hawalbagh block, district Almora, Uttarakhand, India. *Egypt J Remote Sens Space Sci*. 2015;18(1):77-84. doi: 10.1016/J.EJRS.2015.02.002
42. Soundranayagam JP, Sivasubramanian P, Chandrasekar N, Durairaj KSP. An analysis of land use pattern in the industrial development city using high resolution satellite imagery. *J Geogr Sci*. 2011;21(1):79-88. doi: 10.1007/S11442-011-0830-0
43. Lu D, Weng Q. A survey of image classification methods and techniques for improving classification performance. *Int J Remote Sens*. 2007;28(5):823-870. doi: 10.1080/01431160600746456
44. Meshesha TM, Tsunekawa A, Haregeweyn N, *et al.* Agroecology-based land use/land cover change detection, prediction and its implications for land degradation: A case study in the upper blue Nile Basin. *Int Soil Water Conserv Res*. 2024;12(4):786-797. doi: 10.1016/j.iswcr.2024.02.002
45. Shekhar S, Pandey AC. Delineation of groundwater potential zone in hard rock terrain of India using remote sensing, geographical information system (GIS) and analytic hierarchy process (AHP) techniques. *Geocarto Int*. 2015;30(4):402-421. doi: 10.1080/10106049.2014.894584
46. Wang K, Davies EGR, Liu J. Integrated water resources management and modeling: A case study of Bow river basin, Canada. *J Clean Prod*. 2019;240:118242. doi: 10.1016/J.JCLEPRO.2019.118242
47. Jehanzeb M, Cheema M. *Remote Sensing and GIS Applications in Water Resources Management*. Available from: https://www.researchgate.net/publication/321966058 [Last accessed on 2025 Mar 12].
48. Maarez HG, Jaber HS. Topographic and hydrologic analyses using geographic information system (GIS): A case study of karbala City-Iraq. *E3S Web Conf*. 2021;318:10. doi: 10.1051/e3sconf/202131804006
49. Kalogirou E, Melillos G, Hadjimitsis D, Makri D. Sea Surface Temperature and Ocean Wind Speed Data in the Cyprus Region from Sentinel-3 Using Sentinel Application Platform (SNAP) and Arc GIS Pro. In: EGU General Assembly Conference Abstracts; 2023. p. 53- 67. Available from: https://ui.adsabs.harvard.edu/link_gateway/2023EGUGA..2516909K/doi:10.5194/egusphere-egu23-16909 [Last accessed 2024 Nov 14].
50. Masud MJ, Bastiaanssen WG. *Remote Sensing and GIS Applications in Water Resources Management. Water Resources Management*. 2017. p. 351-373. Available from: https://www.researchgate.net/publication/321966058_remote_sensing_and_gis_applications_in_water_resources_management [Last accessed on 2025 Mar 12].

Asian Journal of Water, Environment and Pollution. Vol. 22, No. 2 (2025), pp. 184-203.
doi: 10.36922/AJWEP025080049

ORIGINAL RESEARCH ARTICLE

Mitigating the impacts of climate change: A case study of the city of Tshwane, South Africa

Odirile Sefolo[1], Ilesanmi Daniyan[2]*, Kemlall Ramdass[3], Oluwatoyin Esther Akinbowale[4], and Humbulani Simon Phuluwa[5]

[1]Department of Industrial Engineering, Faculty of Engineering and the Built Environmen, Tshwane University of Technology, Pretoria, Gauteng, South Africa
[2]Department of Mechatronics Engineering, College of Engineering, Bells University of Technology, Ota, Ogun State, Nigeria
[3]Department of Industrial Engineering and Engineering Management, College of Science, Engineering and Technology, University of South Africa, Florida, Gauteng, South Africa
[4]Faculty of Economics and Finance, Tshwane University of Technology, Pretoria, Gauteng, South Africa
[5]Department of Industrial Engineering and Engineering Management, College of Science, Engineering and Technology, University of South Africa, Florida, Gauteng, South Africa
***Corresponding author:** Ilesanmi Daniyan (iadaniyan@bellsuniversity.edu.ng)

Received: February 19, 2025; 1st revised: March 12, 2025; 2nd revised: March 30, 2025; 3rd revised: April 3, 2025; 4th revised: April 3, 2025; Accepted: April 8, 2025; Published online: April 24, 2025

Abstract: Climate change poses a major global challenge which affects human health and livelihood, ecosystem, critical sectors and infrastructure among others. The objective of this research is to investigate and mitigate the impacts of climate change in the City of Tshwane. A combination of quantitative and case study approaches was employed, with datasets obtained from the South African Weather Service, the City of Tshwane, and the Auditor-General. The data were modeled using a combination of discrete event simulation and system dynamics within the AnyLogic (version 8.2.3) environment. The results showed an increase in climate trends from 1981 to 2022, suggesting a growing frequency of heat waves, heavier rainfall, and more frequent floods, among other phenomena. The study recommends the use of simulation approaches to assess the impacts of climate change on the city's infrastructure during the planning process. The findings can assist the City of Tshwane in planning for future climate scenarios, enabling stakeholders to develop sustainable strategies for climate change adaptation and mitigation, with the goal of creating a climate change-resilient city. If the suggested climate change policies are implemented, there would be a 15% annual decrease in extreme events (including excessive temperature, flooding, and drought), a 3% reduction in greenhouse gas emissions, and a 25% decrease in gross domestic product loss, alongside a 15% improvement in infrastructure performance.

Keywords: Adaptation; Climate change; Infrastructure; Simulation

1. Introduction

Climate change refers to changes in the average temperature and weather patterns of a region or the planet over time. The City of Tshwane recognizes climate change as a significant challenge, as failure to address its impacts over the years could have severe consequences.[1] Roads and stormwater infrastructures are

important for economic development, as they facilitate access to markets, local communities, and opportunities in South Africa. The impacts of climate change have an influence on the specifications for designing road and stormwater infrastructure. In the City of Tshwane, the service life of road and stormwater infrastructure is diminishing, and a large proportion of the City's budget is allocated to maintenance caused by climate change. The City of Tshwane Metropolitan Municipality was established on December 5, 2000, by merging several municipalities and councils that were previously part of the Pretoria regime and its surrounding areas.[2]

Infrastructure such as roads and drainage systems are essential elements of a reliable, effective, and functional transport system; without them, the economy cannot function. These infrastructures also impact public health, the economy, and disaster management policies. However, roads and stormwater infrastructure are simultaneously exposed to climate change and, in some cases, contribute to it. For example, construction activities in the road sector involve energy-intensive materials, such as bitumen (derived from fossil fuels), which contribute to carbon emissions.

The widespread flooding in South Africa in February 2023 resulted in the pronouncement of a national state of disaster in line with the Disaster Management Act. This followed significant flooding that affected homes, caused dam overflows, and damaged road infrastructure across the country.[3] The adverse effects of climate change in South Africa have resulted in considerable loss of life, damage to livelihoods, and a decline in the gross domestic product (GDP).[4,5]

There is growing concern about the vulnerability of infrastructure due to previous occurrences and the predicted increase in extreme weather events.[6-8] As a result, developing a flexible physical network solution is still challenging for engineers and designers.[9] Therefore, a modeling and simulation approach may be helpful in assessing the impacts of climate change in South Africa and exploring possible mitigation strategies.

Schweikert *et al.*[10] investigated the effect of climate change on road infrastructure in South Africa using a stressor-response approach. The study projected that the cost incurred due to climate change may range between 116.8 and 228.7 million United States dollars (USD) in the 2050s if no adaptation policy measures are implemented. However, with the implementation of adaptation policies, these costs could be reduced to 55.7 million USD. The policies include the construction of modern roads with secondary pavements. Dube and Nhamo,[11] whose findings align with those of Anekwe *et al.*,[12] identified a declining temperature trend in South Africa. Employing a mixed-methods research design, they investigated the impacts of climate change on the Kruger National Park in South Africa and found high inter-annual variability in rainfall, with an overall decreasing trend. This variability has led to increased costs related to environmental and wildlife management, as well as government expenditures. They also reported significant losses of flora and fauna and damage to key infrastructure within the park, attributing these impacts to climate-related events, such as floods, droughts, and extreme weather, highlighting the need for the development of adaptation measures. Chersich and Wright[13] investigated the impacts of climate change on the health sector in South Africa through a systematic literature review and found that, although various climate change policy frameworks exist in the country, only a few address the impacts of climate change on the health sector. The review also reported that while the country has established systems for forecasting extreme weather events, there is little evidence of adaptation measures. Botai *et al.*[14] examined the spatial-temporal variability of precipitation patterns in South Africa using satellite precipitation data from 1998 to 2015. The study indicated significant variation in precipitation across the country. For instance, the precipitation distribution was found to be uniform in the southern and central parts of South Africa, while the western and northeastern parts showed extreme irregularity. Between December to February, precipitation distribution was more uniform, while it was moderate between September and November, with extreme irregularity observed between June and August. The study by Jovanovic *et al.*[15] on evapotranspiration in South Africa revealed a slight reduction in evapotranspiration rates in South Africa from 2000 to 2012 in all climatic regions, except in the southern part of the country. This outcome corroborates Botai *et al.*'s[14] conclusion that the southern part of the country continues to experience more regular climatic conditions. Ndlovu and Demlie[16] investigated drought and rainfall patterns across the KwaZulu-Natal (KZN) province of South Africa over a period of 48 years (1970 – 2017). It was found that the frequency of drought is increasing, with rainfall frequency decreasing.

However, the results obtained by Orimoloye *et al.,*[17] who assessed drought conditions in South Africa using Terra MOD13Q1 data from the satellite in the Free State province, indicated that drought is less prevalent during the winter season but more severe in the summer in this region.

Climate change has significant negative impacts on the transport sector, especially road infrastructure,

exposing people to various risks. Some studies indicate that inadequate drainage systems are one of the major causes of the destruction of road and stormwater infrastructure.[18,19] Nevertheless, climate change also contributes significantly to the destruction of road and stormwater infrastructure, leading to increased rainfall intensity, flooding, and loss of ecosystems and biodiversity. The impact of climate change further extends to the destruction of runoff that reaches roads and drainage systems, thereby causing flooding of highways.[18] Another area of concern is the scarcity of water resources due to climate change and poor management.[20] Anekwe *et al.*[12] investigated the impacts of climate change variability on water resources in the Jozini municipality, South Africa, using conventional and machine learning approaches on precipitation and temperature datasets. The results indicated that variations in rainfall and temperature have serious consequences on water levels in the dam, negatively affecting water availability in the municipality. These findings may assist stakeholders in formulating and implementing policies to promote water availability, particularly in the construction of modern dams.

Ray[21] stated that climate change negatively affects Africa's economies, leading to a decline in GDP, loss of business and livelihoods, and increased investment in the repair of damaged infrastructure and the development of countermeasures.

The costs associated with infrastructure repair and recovery from heavy rainfall in Cape Town in 2011 exceeded rand (R) 20 million.[4] In 2022, the flooding in KZN resulted in the loss of 440 lives and the destruction of road infrastructure worth R5.6 billion.[5] Comins[5] noted that KZN would lose 1.8% of its annual GDP due to the flooding. Existing studies highlight the need for integrated climate impact modeling, as it allows for a detailed understanding of the interactions between climate change, human life, the physical environment, and socio-economic activities. These models also suggest possible adaptation and mitigation approaches that could help policymakers reduce risks and vulnerabilities.[22,23] Ciscar and Dowling[24] emphasized that existing integrated climate impact models have been implemented in only a few countries to capture a limited scope of climate change impacts, underscoring the need for empirical studies on the application of these models, especially in developing economies with increasing energy demands. Ciscar and Dowling[24] further pointed out that the effects of extreme weather events, such as floods, require more attention and the use of different modeling techniques to capture their impacts.

The use of system dynamics (SD) modeling for climate change simulations has also been reported. For example, Gohari *et al.*[25] employed the SD simulation technique to assess climate change adaptation strategies for water conservation in Iran. The study found that improvements in infrastructure, effective water management, and regulation of the ecosystem could reduce water stress in the country. Existing studies have also applied the SD technique to investigate the impacts of climate change on water resource systems and to model complex systems.[26-29]

Unlike the singular SD technique employed in previous studies,[25-29] the present research goes beyond using a single approach and demonstrates the applicability of an integrated modeling and simulation approach for investigating the impacts of climate change. This represents advancement in methodological approaches by enabling time- and cost-effective modeling and simulation of complex phenomena, such as the impact of climate change, which can facilitate better policy formulation and informed decision-making.

However, the combination of the discrete event simulation (DES) and SD to investigate climate change impacts has not been sufficiently reported in existing literature. Thus, the novelty of this study lies in its use of an integrated DES and SD approach to model and simulate climate change activities and mitigation strategies in South Africa (specifically the City of Tshwane) over the next 10 years. The findings of this study can assist the City of Tshwane in planning for future climate scenarios and enable stakeholders to develop sustainable means of climate change adaptation or mitigation in the pursuit of a climate-resilient city.

Although some studies have been conducted on the effects of climate change in South Africa, the investigation of its impacts using modeling and simulation approaches has not been sufficiently discussed. Thus, the objectives of this study are to investigate and mitigate the effects of climate change in South Africa, using the City of Tshwane as a case study, and to examine the impacts of climate change policy frameworks on the city's infrastructure management.

The following research questions underpin this study: (i) What are the potential climate change risks and possible mitigation strategies? (ii) What are the effects of climate change policy implementation on the city's infrastructure management? (iii) How can the impacts of climate change on roads and stormwater infrastructure in South Africa be effectively mitigated?

This research contributes to a better understanding of the impacts of climate change on roads and stormwater

infrastructure in South Africa infrastructure and offers insights into how to effectively mitigate these effects.

2. Methodology

2.1. Research design

The study is exploratory, quantitative, and descriptive in nature, aimed at gaining a deeper understanding of a persistent phenomenon. Climate change is considered a persistent challenge, and the exploratory aspect seeks to answer questions, address phenomena, or identify general principles to explain the phenomenon, utilizing the inductive method. In exploratory research, primary or secondary data are collected and organized for synthesis.[30] In this study, secondary data were collected and analyzed.

The quantitative method was employed because it allows for the representation of measured variables numerically in terms of amount, quantity, frequency, or rate. These variables' associations with other factors can be determined via systematic measurement and statistical analysis.[31,32]

Figure 1 shows the research methodology of the study and the steps followed during the research, summarizing the approach employed in the study. As discussed in the literature section, variables such as the amount of rainfall, GDP, greenhouse gas (GHG) emissions, extreme events, and infrastructure performance are related to climate change. Therefore, secondary quantitative data on these variables were collected and compared using regression graphs, Microsoft Excel, and AnyLogic software to answer the research questions.

The methods applied in this study quantified and analyzed variables to obtain results. These include:

(i) Inductive reasoning: Collection and analysis of historical data (temperature and rainfall) to identify trends related to climate change impacts and to draw conclusions.

(ii) Data collection: Historical quantitative datasets on rainfall, temperature, and capital expenditure on infrastructure in the City of Tshwane were obtained from the South African Weather Service (SAWS) and the City of Tshwane.

(iii) Data analysis: The datasets were analyzed using charts and pie charts to visualize the trends in temperature, rainfall, and the cost implications of climate change. In addition, the analysis explored how the absence of adaptation would impact the economy.

(iv) Modeling and simulation: A combination of DES and SD was employed to model and simulate the effects of variables classified as extreme events (such as GHG emissions, extreme temperatures, drought, rainfall, and flooding) on the city's road and stormwater infrastructure and GDP performance. These extreme events are considered the effects of climate change. The goal of the modeling and simulation was to ascertain the effects of these extreme events on the city's infrastructure and economic activities (reflected in the GDP) to facilitate appropriate policy recommendations for effective climate change mitigation and adaptation. Finally, conclusions were drawn, and recommendations were made to support climate change mitigation and adaptation efforts.

Figure 2 illustrates the conceptual framework, linking the key variables derived from the literature related to climate change. These variables include the amount of rainfall, GDP, the greenhouse effect, extreme events, and infrastructure performance. The major threats are the greenhouse effect and extreme events, such as rainfall, flooding, drought, and extreme temperatures.

2.2. Case study

For the purpose of this study, a case study was employed to gain an in-depth understanding of the complex issue of climate change impacts. Existing studies indicate the suitability of the case study approach for investigating multifaceted and complex issues, making it extensively applicable across different fields.[33,34] This approach allows researchers to explore and understand intricate issues by analyzing past reports or studies. It is considered a suitable research method, especially when a holistic, in-depth investigation is conducted. The case study method transcends quantitative statistical results

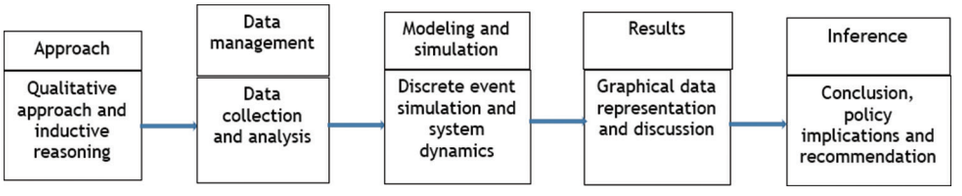

Figure 1. A comprehensive guide to the quantitative research methodology employed in this study

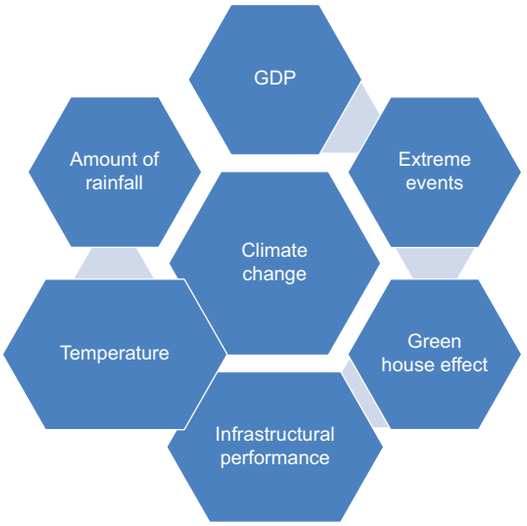

Figure 2. A conceptual framework linking the key variables derived from the literature
Abbreviation: GDP: Gross domestic product.

to provide insights that aid in understanding behavioral patterns from the perspective of the actors involved.[34-36] The City of Tshwane was chosen as the case study for this research. In this case study, the researchers examined the impact of climate change on the City's roads and stormwater infrastructure, and the findings were analyzed accordingly.

The study specifically investigated climate change events in the City of Tshwane, including the Mamelodi floods and Centurion floods.

At the beginning of the research, several observations were made, and field trips were conducted to assess the flood damage and the broader effects of climate change. Although the case study is limited to the City of Tshwane, it is important to note that areas outside the city also experience different climatic conditions.

2.3. The City of Tshwane context

The city is located at 25° 40'S, 28° 20'E in the Gauteng province of South Africa. It covers a total area of 6,299 km^2 and had a population of 4,040,315 as of 2022. Tshwane's road network consists of 60 roads, which are grouped into three classes: national routes, provincial roads, and municipal roads.[2] The stormwater drainage system, with a flow rate of 15.93 m^3/s, combines surface drainage from paved roads and underground pipe systems, with pipe sizes ranging from 1,500 mm by 1,200 mm to 1,800 mm to 1,800 mm. This system collects stormwater from the city and includes field inlets that are connected to the stormwater pipeline, which receives stormwater runoff. Outlet structures are constructed at the end of the stormwater pipeline to prevent erosion. The climate change policy proposes an increase in the capacity of the drainage system, with pipe sizes ranging from 2,100 mm in height by 3,800 mm in width to 3,600 mm by 3,800 mm, and a flow rate of 36.0 m^3/s. The city falls within the summer rainfall region of eastern South Africa, receiving an annual average rainfall of 670 mm.[37]

Figure 3 depicts maps of South Africa, Gauteng province, and the City of Tshwane.

2.4. Description of the datasets

Data were collected from the records of the City of Tshwane,[2] the SAWS,[37] and from grey literature.

Historical data may omit important factors, which can lead to inaccurate analysis and forecasts. Moreover, such data may be subjected to bias, incompleteness, and loss of relevance over time. To overcome these limitations, the researchers gathered data from multiple sources, such as the SAWS, the City of Tshwane, and grey literature, and analyzed the various datasets. Furthermore, critical thinking and the SD simulation approach were employed to provide some future insights and projections for the data analysis.

Figure 4 presents the average rainfall of the City of Tshwane from 1981 to 2022 (42 years), showing variations in rainfall patterns.[37] The line representing average rainfall indicates years of heavy rainfall, as well as periods of drought. For instance, since 2015, rainfall has been above average (except for 2018), causing flooding in some areas.

Figure 5 shows the average monthly rainfall in the City of Tshwane from 1981 to 2022. The plot reveals that high rainfall typically occurs between January and March, as well as in November and December. In contrast, April and October experience moderate rainfall, while May through September generally see low rainfall.

Table 1 presents the seasonal rainfall for the City of Tshwane's temperature. The highest rainfall occurs in summer, while the lowest is observed in winter.

Figure 6 presents the average temperatures in the City of Tshwane from 1981 to 2022.[37] The average temperature over the 12-month period from 1981 to 2022 is 18.78°C. Temperatures are typically lower in June and July, while January and December experience higher summer temperatures. As a result, the rainfall and temperature graphs exhibit nearly identical parabolic shapes.

Table 2 presents the minimum, maximum, and average temperatures on a seasonal basis.

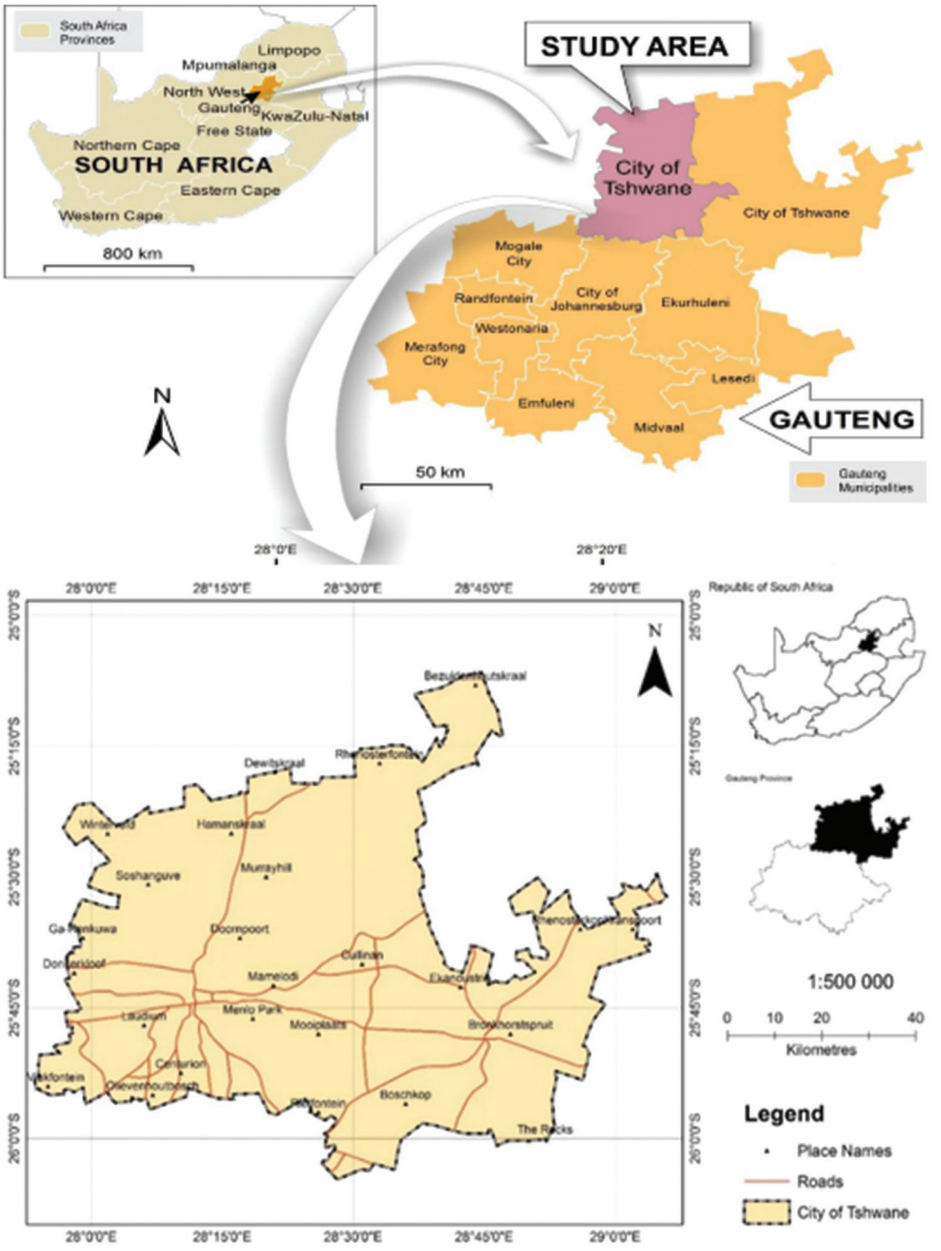

Figure 3. Maps showing South Africa, Gauteng province, and the City of Tshwane. Adapted from[38,39].

The average temperature from 1961 to 1990 (17.85°C) shown in Table 2 is lower than the average temperature from 1981 to 2022 (18.78°C), indicating a rising temperature trend. This increase contributes to global warming and climate change.

Datasets related to environmental variables, such as the GHG effect, the number of extreme events (including extreme temperatures, heavy rainfall, floods, and droughts), as well as the environmental variable of GDP loss, were obtained from the SAWS.[37] GDP loss here refers to the reduction in the total market value of products and services produced in the city due to the effects of climate change. In South Africa, rainfall is considered normal if the total amount is <75 mm, heavy if it exceeds 75 mm, and extreme if it exceeds 115 mm in a specific area on a given day.[40,41] A flood is considered a situation in which water overflows beyond the capacity of watercourses and drainage systems, thereby submerging dry land. The average temperatures in South Africa range from 15°C to 36°C in summer and −2°C–26°C in winter.[41] According to a South African government report on geography and climate,[42] the

country is relatively dry, with an annual average rainfall of about 464 mm, compared to the global average rainfall of 990 mm. In addition, according to Writer,[43] a drought in South Africa is defined as a period when an area experiences precipitation or rainfall lower than the average, characterized by a reduction in soil moisture and groundwater levels.

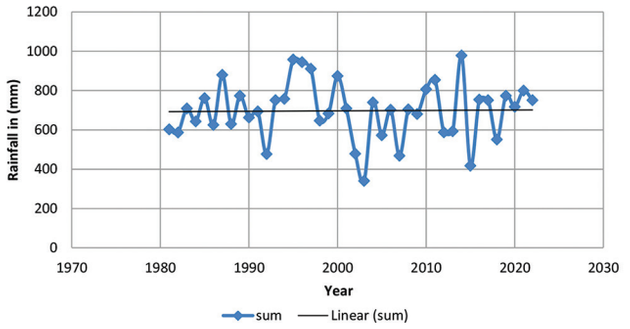

Figure 4. Average rainfall in the City of Tshwane from 1981 to 2022[37]

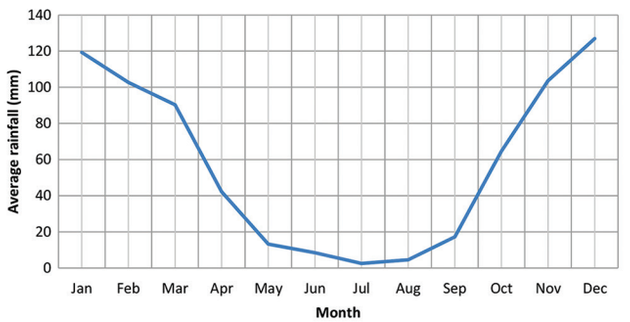

Figure 5. Average monthly rainfall in the City of Tshwane from 1981 to 2022[37]

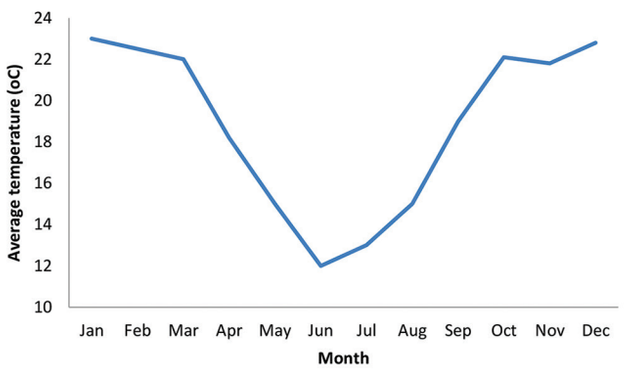

Figure 6. Average temperature variations in the City of Tshwane (from 1981 to 2022)[37]

2.5. Analysis, modeling, and simulation of the datasets

The data were analyzed descriptively as follows:

(i) Creating themes such as "evaluation of bias in the dataset," "annual rainfall in the City of Tshwane," and "modeling and simulation of the climate change and the mitigation strategy," and categorizing data accordingly.

(ii) Elaborating on the meaning and significance of these themes as they relate to climate change and its effect on road and stormwater infrastructure in the City of Tshwane.

(iii) Using graphs and plots, such as regression plots, pie charts, and simulation software, to interpret the data collected from the SAWS and the City of Tshwane on weather and climate change.

(iv) Utilizing regression analysis to compare the relationships between variables (GHG emissions and extreme events, GHG emissions and GDP loss, rainfall, and infrastructure performance). Regression analysis employs data from two variables to make future projections. This method will allow the City of Tshwane to develop specific strategies, enabling meaningful predictions regarding extreme events, loss of GDP, infrastructure performance, heavy rainfall, and increases in GHG emissions.

The consideration of GHG emissions as a variable stems from the fact that they may contribute to temperature increases. The more GHGs are emitted, the higher the likelihood of an increase in atmospheric temperature, as the gases trap heat, leading to global warming. Furthermore, as indicated in the literature, extreme events due to climate change can disrupt lives, businesses, and livelihoods, thereby resulting in a reduction in GDP.

AnyLogic software was used in the study because it is suitable for modeling and simulating events and business applications. AnyLogic simulation models enable engineers and managers to gain deeper insights and optimize complex systems and processes across various industries.[44] The AnyLogic modeling and simulation technique allows researchers to set the

Table 1. Average seasonal and annual rainfall (mm) in the City of Tshwane from 1961 to 1990

Variable	Winter	Spring	Summer	Autumn	Average
Rainfall (mm)	13	192	325	141	671

Source: City of Tshwane[2].

Table 2. Seasonal and annual daily temperatures in the City of Tshwane from 1961 to 1990

Temperature (°C)	Winter	Spring	Summer	Autumn	Average
Minimum	3.9	12.5	16.1	10.7	10.80
Maximum	20.5	26.5	28.2	24.6	24.90
Average	12.2	19.5	22.2	17.6	17.85

Source: City of Tshwane[2].

model's starting state and apply selected rules to simulate the evolution of the system over time.[45]

A combination of SD and DES was used in this study. The SD method is best known for its high level of abstraction, requiring few details, and is typically deterministic with continuous time modeling. Its coupled first-order differential equations are solved by numerical methods. In contrast, DES focuses on systems where a sequence of operations or tasks needs to be performed.[44,45]

The choice to combine SD and DES arose from the fact that SD offers an opportunity to precisely evaluate and model the impact of climate change on road and stormwater infrastructure. On the other hand, DES can be useful in the development and testing of new policies, as it helps understand how changes in systems (such as variation in weather conditions) can affect overall outcomes (such as the impact on road and stormwater infrastructure, as well as the proposed mitigation strategies). DES is a powerful and comprehensive paradigm capable of modeling almost any system that changes over time through events, provided these changes can be reasonably approximated within the events or important occurrences. Thus, the abstract simulation used in SD is more suited for long-term, strategic modeling and simulation.[44,45] Hence, the combination of SD and DES was found to be suitable for investigating and representing the impact of climate change on road and stormwater infrastructure, including the proposed mitigation strategies. The integrated approach enables the simulation of climate-related events, such as temperature changes, rainfall, and GHG emissions that occur at specific times. Meanwhile, SD enables these activities to be tracked continuously over time. DES focuses on understanding the changes in the state and events, while SD tracks the activities to capture the system's state at different points in time without any gaps.

The combined use of DES and SD modeling was carried out sequentially. DES was used to simulate the behavior of the City of Tshwane's stormwater infrastructure, representing two scenarios (with and without policy implementation). Thereafter, the models were used to predict the behavior over a 10-year period under the SD modeling framework.

Table 3. Parameters of the drainage system (with and without policy implementation)

Drainage parameter	Drainage system without policy intervention	Drainage system with policy intervention
Height (mm)	−1,800	−3,600
Width (mm)	−1,800	3,800
Designed flow rate (m^3/sec)	3	36.0

The methodology focuses on the development of two drainage system models: one based on the "business-as-usual" approach (i.e., without policy implementation) and the other incorporating dynamic factors, such as forecasted changes in environmental policies. These models are compared to the present drainage network design, which relies solely on historical data. The performances of the drainage systems are evaluated by comparing their designed flow rate values to the simulated flow rate values (expressed as percentages) to determine whether the systems operate within the expected range of design values, particularly in relation to flood occurrences, as assessed by the DES. Table 3 presents the parameters of the drainage system (with and without policy implementation) used for the DES.

The DES was conducted in four steps:

(i) Observation of the system's real dynamics. The model's input parameters comprise the following: the rainfall dataset (derived from Table 1), the temperature dataset (derived from Table 2), and the drainage system's parameters (Table 3). The model's outputs include the GHG effect, GDP loss, number of extreme events, and drainage system performance. The performance of the drainage systems was evaluated by comparing their designed flow rates with the simulated values to determine the lifespan and quality of roads and stormwater in the model.

(ii) Modeling the relationship between GDP loss and GHG emissions. The relationship between GDP

loss and GHG emissions was modeled using the equation derived from the regression graph (Equation I):

$$y = 0.0083x - 2.4587 \quad \text{(I)}$$

where y represents GDP loss (%) and x represents GHG emissions (expressed in tCO_2e).

(iii) Modeling the relationship between GHG emissions (x) and temperature (t). The relationship between GHG emissions and temperature was modeled and observed using Equation II:

$$x = 0.0254t - 6.5745 \quad \text{(II)}$$

where represents temperature (°C).

(iv) SD simulation. The important moments in the system's lifecycle were considered instantaneous, indivisible events. All changes in the system were associated with these climate events. The system was observed for 10 years into the future using the SD simulation.

The SD steps are summarized into five phases:

(i) Problem definition: This phase involves tracking climate events or activities (such as temperature, rainfall, and GHG emissions) and capturing the state of infrastructure performance and the average loss of GDP at different points in time without any gap over a period of 10 years. This phase helps to define and formulate the policies required to address the identified problem.

(ii) Dynamics hypothesis: In this phase, a theory is formulated regarding the emergence of the problem, and a causal loop diagram is created to provide insight into the causal relationships between variables. The causal loop diagram is then converted into a level and rate (stock and flow) diagram. For example, heavy rainfall causes flooding, while extreme weather events (such as an increase in temperature) lead to an increase in the emission of GHGs.

(iii) Formulation: This phase presents the equations that define the relationships between the variables, including the estimation of parameters and the determination of initial conditions (Table 4). The equations that define the relationships between the variables were obtained from regression analysis.

(iv) Testing: This phase involves validating the developed model by observing its behavior and determining whether the model behavior accurately represents real systems. The model's behavior and outputs were visualized over time to ensure consistency with real-world observations.

Table 4. Equations defining the relationship between the variables

Equation	Description
$\frac{\Delta Ait}{Ait} = git + \delta 1Tit + \delta 2Rit + \delta 3SPTit + \delta 4SPRit$	Economic Modeling Equation
$y=0.083x-2.4587$	GDP loss versus GHG emission
$y=0.025x-6.5745$	GHG emission versus temperature

Abbreviations: GDP: Gross domestic product; GHG: Greenhouse gas.

(v) Policy formulation and evaluation: In this phase, decisions are made regarding the redesign of the model or the adjustment values of parameter values to improve the performance of the system.

The DES and SD models were implemented in the AnyLogic software environment (version 8.2.3). The software employed the stock-and-flow diagram as the visual modeling language, with the input variable being the City of Tshwane's climate change policy. The model variables influenced by this policy included: (i) Average rainfall, (ii) infrastructure performance, (iii) average loss of GDP, (iv) GHG effects, and (v) the number of extreme weather events in the City of Tshwane.

The model was simulated using the policy implementation serving as a mitigation strategy. Multiple simulation runs were conducted, which resulted in improvements in GHG emissions and GDP performance. Two SD models were developed: the first, without climate change policy implementation (Figure 7), and the second, with policy implementation (Figure 8).

To assess the effect of climate change policy implementation in the SD model, the first model (Figure 7) was modified by incorporating a feedback loop and a policy parameter. This modification produced a scenario different from the one generated without the climate change policy implementation. The resulting scenario enabled an understanding of potential future conditions by evaluating simulated forecasts. The main objective of the scenario was to examine the impact of climate change policy on the performance of road and stormwater infrastructure, GHG emissions, amount of rainfall, and the number of extreme events, to effectively mitigate the impacts of climate change. The DES model advanced in increments of 0.5-time units to balance computational efficiency and simulation accuracy by

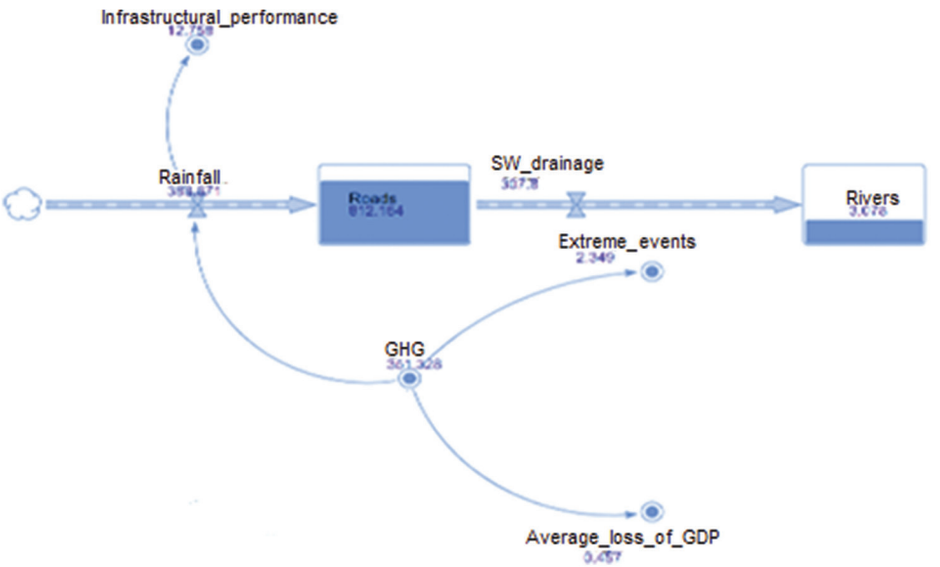

Figure 7. AnyLogic model depicting the scenario without policy implementation
Abbreviations: GDP: Gross Domestic Product; GHG: Greenhouse gas; SW: Surface water.

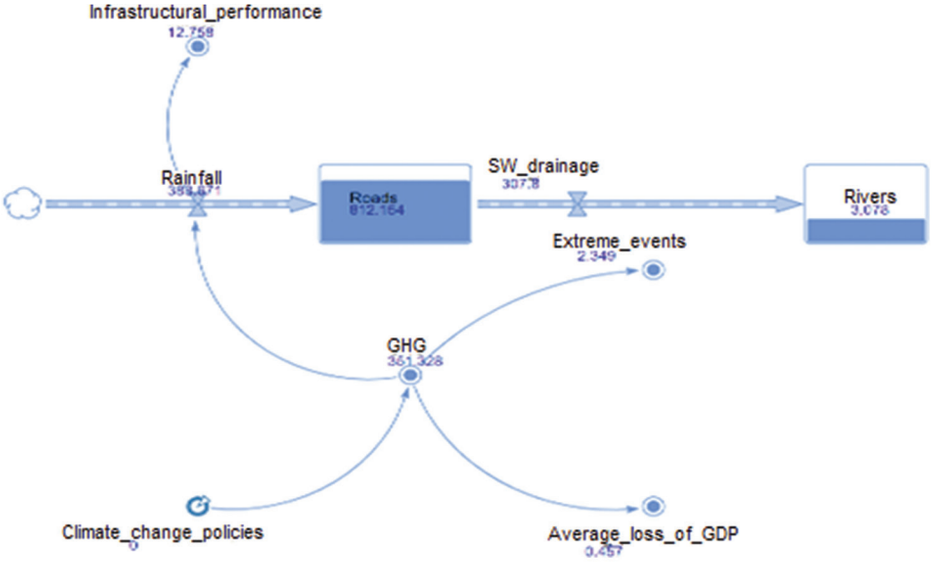

Figure 8. AnyLogic model depicting the scenario with policy implementation
Abbreviations: GDP: Gross domestic product; GHG: Greenhouse gas; SW: Surface water.

reducing approximation errors, while the SD model ran continuously. Overall, the combined DES and SD model required a total simulation time of 5.05 minutes.

The models simulated the temporal and spatial application of the climate change policy under two scenarios: Without policy implementation (Figure 7) and with policy implementation (Figure 8).

The South African climate change policy actions, as outlined in the Climate Change Act 2024,[46] aim to coordinate and integrate climate change responses. These actions align with the National Climate Change Response Policy, which emphasizes both adaptation and mitigation strategies over short-, medium-, and long-term horizons to support the transition to a low-carbon economy. This policy encompasses carbon taxation, smart agriculture, renewable energy initiatives, integrated resource plans, and the Just Energy Transition Partnership, among others.

The following are the assumptions underlying the DES and SD modeling and simulation:

(i) Discrete-time: The DES assumes that time progresses in discrete steps, with events occurring at specific points in time.
(ii) State change: The DES assumes that the system's state changes dynamically as events occur, and the system behavior is primarily driven by events.
(iii) Stochastic behavior: The DES model also assumes that the time between events, as well as the behavior of entities and resources, are subjected to random variability.
(iv) Aggregation: One of the assumptions in the SD model is that extreme events – including excessive temperature, flooding, and drought – are modeled as a single event or entity. This approach reduces the complexity of the model and reflects the interrelated nature of these variables. For instance, temperature can influence precipitation patterns, leading to either heavy rainfall (and flooding) or drought. High temperatures may increase the rate of evaporation, causing dry conditions and droughts, while also increasing the amount of atmospheric water vapor, which can intensify precipitation and lead to heavy rainfall and flooding. Given this cause-effect relationship between temperature, heavy rainfall, flooding, and drought, these variables were aggregated and modeled as a single event or entity.
(v) Continuous time: The SD assumes a continuous progression of time, representing modeling system changes as ongoing processes over time.
(vi) Closed system: The SD model is treated as a closed system, meaning that no external factors influence the system's behavior unless they are explicitly included in the model.

3. Results and discussion

3.1. Evaluation of bias in datasets

Harman's one-factor test was conducted to evaluate the presence of common bias. For the climate change dataset, the total variance extracted was 6.253, with the corresponding sum of squares accounting for 31.835% of the variance. Similarly, the financial dataset showed a total extraction of 6.850 and a sum of squares of 34.122%.

According to the rule of thumb, if the total variance extracted by one factor exceeds 50%, common method bias may be present. In this study, there is no evidence of such bias for both the rainfall and temperature datasets, as the total variance explained by one factor is below the 50% threshold—31.835% for rainfall and 34.122% for temperature.[31]

3.2. Descriptive statistics and analysis of variance

Table 5 presents the descriptive statistics for average monthly rainfall in the City of Tshwane from 1981 to 2022. Descriptive statistics are used to numerically describe and summarize the dataset. The mean represents the central tendency, that is, the rainfall, while the standard deviation measures the variations within the dataset. The large standard deviation values observed in Table 5 indicate significant variability in rainfall over the 42-year period (1981 – 2022). This variability may be attributed to the effects of climate change, as

Table 5. Descriptive statistics of average monthly rainfall in the City of Tshwane from 1981 to 2022

Month	*N*	Range	Minimum	Maximum	Sum	Mean		Standard deviation
						Statistic	Standard error	
January	42	457.00	8.00	465.00	5473.60	130.3238	11.14551	72.23114
February	42	331.50	20.90	352.40	4314.40	102.7238	10.37460	67.23511
March	42	317.80	0.10	317.90	3793.60	90.3238	10.65665	69.06299
April	42	133.20	0.00	133.20	1772.00	42.1905	4.87410	31.58779
May	42	87.60	0.00	87.60	552.50	13.1548	3.11226	20.16978
June	42	68.90	0.00	68.90	354.40	8.4381	2.07840	13.46959
July	42	30.30	0.00	30.30	105.60	2.5143	0.87653	5.68054
August	42	54.40	0.00	54.40	235.90	5.6167	1.58145	10.24900
September	42	116.10	0.00	116.10	740.10	17.6214	3.74341	24.26005
October	42	176.70	0.00	176.70	2711.40	64.5571	6.42257	41.62303
November	42	271.80	0.00	271.80	4352.40	103.6286	8.60268	55.75175
December	42	172.80	43.00	215.80	5332.10	126.9548	6.80836	44.12323

Table 6. Descriptive statistics of average yearly temperature in the City of Tshwane from 1981 to 2022

Variable	*N*	Range	Minimum	Maximum	Sum	Mean		Standard deviation
						Statistic	Standard error	
Rainfall	42	53.13	28.32	81.44	2439.84	58.0915	1.85334	12.01104

Table 7. Confidence interval and component variance for rainfall

Model	Standard deviation	Standard error	95% confidence interval for mean		Between-component variance
			Lower bound	Upper bound	
Fixed effects	6.10233	1.76159	35.5685	80.3348	-
Random effects	-	15.25579	23.9596	91.9437	2361.97017

Table 8. Analysis of variance results for rainfall

Comparison	Sum of squares	df	Mean square	*F*	Significance
Between groups	25960.395	10	2596.039	69.714	0.023
Within groups	37.238	1	37.238	-	-
Total	25997.633	11	-	-	-

it suggests significant fluctuations in monthly rainfall patterns over time.

Table 6 presents the descriptive statistics of average yearly temperature in the City of Tshwane from 1981 to 2022. The large standard deviation value (12.01104), indicates significant variations in the dataset. This finding further implies significant variation in the amount of rainfall over the 42-year period (1981 – 2022), which may be attributed to the effect of climate change.

A one-way analysis of variance was conducted using the *F*-distribution at a 95% confidence interval to determine whether the means of the temperature and rainfall differ significantly. In this analysis, average monthly rainfall (1981 – 2022) was taken as the dependent variable, while average monthly temperature over the same period was taken as the independent variable. The mean temperature for the 12 months (January – December) was 57.9517, which falls within the 95% confidence interval range, from a lower bound of 35.5685 to an upper bound of 80.3348.

The confidence interval for a mean provides a range of possible values for the population mean. As the confidence interval presented in Table 7 does not include zero, it suggests that the difference is statistically significant, and that the observed mean is a true reflection of the rainfall dataset. The "between-component variance" estimates the differences in average monthly rainfall, treating each month (January – December) as a group. The result indicates statistically significant variations in the average rainfall among the months, as indicated by the high component variance value (2,361.97017). This finding provides evidence of changing rainfall patterns across months during the 1981 – 2022 period, likely influenced by climate change. Table 8 presents the analysis of variance results. The F-value represents the ratio of between-group variance (temperature and rainfall) to within-group variance. A high F-value (69.714), as shown in Table 8, suggests a significant difference between the groups. Furthermore, the $p < 0.05$, (0.023), indicating that the variation in the pattern of average monthly temperature and rainfall in South Africa is statistically significant.

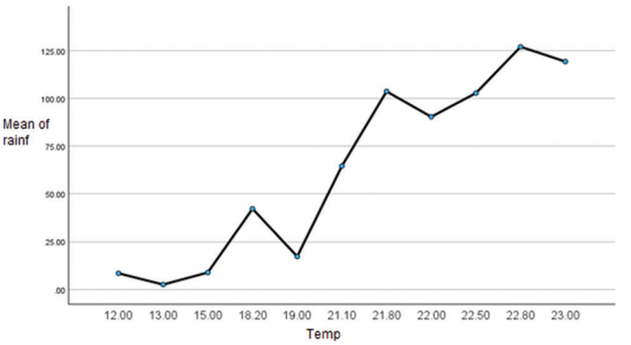

Figure 9. Mean plot for the temperature (temp) and rainfall (rainf) datasets

Figure 9 displays the mean plots used to visualize the differences between group means for temperature and rainfall. Each data point in the plot represents the mean of a specific group, further illustrating the existence

of statistically significant differences or variations between the groups. This finding is an indication that notable changes in temperature and rainfall patterns occurred during the study period, likely as a result of climate change.

3.3. Annual rainfall in the City of Tshwane

As shown in Figure 4 in Section 2.4 (rainfall data from 1981 to 2022 in the City of Tshwane), rainfall has not been uniform, leading to periods of droughts and floods.

Figure 10 illustrates the relationship between the annual rainfall and infrastructure performance. Equation III, derived from the regression graph, demonstrates that the relationship between rainfall and infrastructure performance is inversely proportional:

$$Y = -0.0923x + 48.632 \quad \text{(III)}$$

This indicates that as rainfall increases, the performance of infrastructure – specifically its durability and safety – decreases. The R-squared value for the regression line is 0.818, which is a statistical measure of how well the data fit the regression model (goodness of fit). A value closer to 1 indicates higher reliability of the regression equation, while a value closer to 0 indicates lower reliability.[31]

Figure 11 depicts the relationship between GDP loss and GHG emissions. Equation IV, derived from the regression graph, shows that the relationship between GDP loss and GHG emissions is directly proportional:

$$Y = 0.0083X - 2.4587 \quad \text{(IV)}$$

The R-squared value for the regression line is 0.878.

The forecast for GDP growth can be derived from the economic modeling Equation V.

$$\frac{\Delta Ait}{Ait} = git + \delta 1Tit + \delta 2Rit + \delta 3SPTit + \delta 4SPRit \quad \text{(V)}$$

where T is temperature, R represents rainfall, and the spatial effect terms (standard penetration test [SPT] and soil penetration resistance [SPR]) affect total factors and productivity exponentially.

From Equation V, two key parameters that directly influence climate change – namely, temperature and rainfall – are included in the economic modeling equation, along with the spatial effects terms (SPT and SPR).

The inclusion of these two variables (temperature and rainfall) in Equation III is due to their crucial role in influencing other variables and climate change. In other words, other variables may be indirectly determined by temperature and rainfall. For instance, temperature can serve as a variable to determine extreme events, such as heatwaves, while rainfall can be used to prevent extreme events, such as flooding, when its amount exceeds a certain threshold. Both temperature and rainfall can also impact infrastructure performance and GDP. For example, the lower the occurrence of extreme events due to excessive temperature and rainfall, the higher the infrastructure performance, assuming design and service requirements are met.

The inclusion of all six variables may result in a complex equation that could be challenging to resolve mathematically.

The results indicate that the effect of climate change on the South African economy is significant. This agrees with the findings of Ray,[21] who stated that climate change negatively affects African economies through GDP

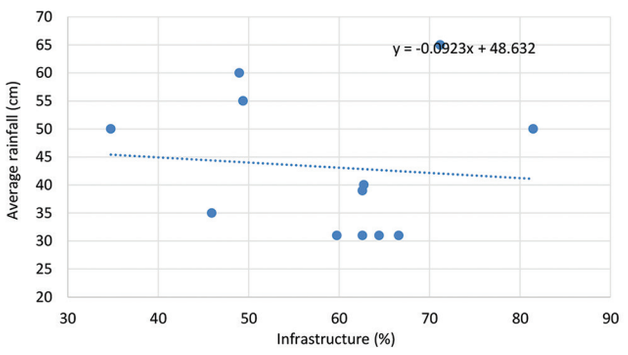

Figure 10. The relationship between rainfall data and infrastructure performance

Source: Functional relationship derived from the regression plot based on the data obtained from the South African Weather Service[37].

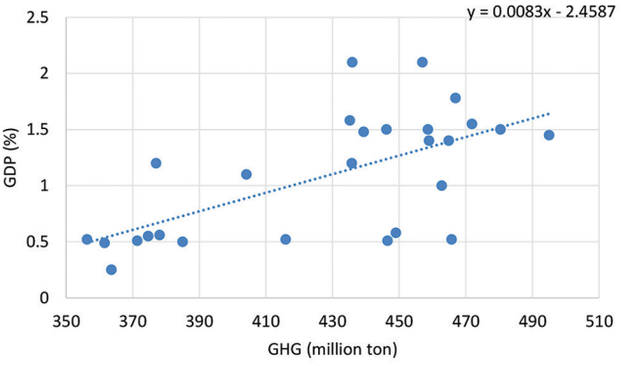

Figure 11. The relationship between gross domestic product loss and greenhouse gas emissions

Source: Functional relationship derived from the regression plot based on data obtained from the South African Weather Service[37].

decline, loss of business and livelihoods, and increased investment in repairing damaged infrastructure and developing countermeasures.

For example, the costs associated with infrastructure repair and recovery following heavy rainfall in Cape Town in 2011 exceeded R20 million.[4] In 2022, the KZN flooding resulted in the loss of 440 lives and the destruction of road infrastructure worth R5.6 billion. Comins[5] estimated that KZN would lose 1.8% of its annual GDP.

Figure 12 shows the relationship between GHG emission and temperature. Equation VI, derived from the regression graph, demonstrates that the relationship between GHG emissions and temperature is directly proportional. Higher temperatures increase the likelihood of GHG emissions. This may be due to higher temperatures accelerating the decomposition of organic matter, as increased microbial activities raise the concentration of carbon in the atmosphere. Furthermore, higher temperatures may drive an increased energy demand for cooling. In addition, higher air temperatures can hold more moisture, leading to greater amounts of trapped water vapor, which contributes to global warming. Similarly, lower temperatures may also lead to increased GHG emissions due to higher energy demand for heating, thereby resulting in carbon emissions resulting from increased energy consumption.

$$Y = 0.0254x - 6.5745 \quad \text{(VI)}$$

The R-squared value for the regression line shown in Figure 12 is 0.825. Given the R-squared values of the three regression models are close to 1, it implies that the regression models are highly reliable.[31]

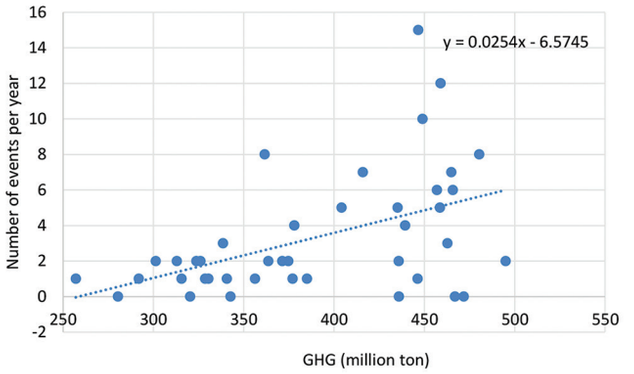

Figure 12. The relationship between greenhouse gas emissions and temperature

Source: Functional relationship derived from the regression plot based on data obtained from the South African Weather Service[37].

3.4. Modeling and simulation of climate change and mitigation strategies

Figure 13 illustrates the modeling and simulation of climate change and mitigation strategies for the next 10 years. The model's input variable was the climate change policy, which depends on how often it is reviewed and updated each year. The model variables included: (i) Average rainfall, (ii) infrastructure performance, (iii) average loss of GDP, (iv) GHG emissions, and (v) the number of extreme weather events in the City of Tshwane. Changes in the climate change policy affect the amount of GHG emissions, and the model then simulates the impact of average rainfall, infrastructure performance, and GDP loss as functions of GHG emissions. The green line represents infrastructure performance without the climate change policy, showing poor infrastructure performance. The blue line represents the number of extreme events due to an increase in GHG emissions. The orange line represents GDP loss resulting from GHG emissions, and the red line represents GHG emissions as a result of implementing the climate change policy. All these variables – GDP loss, GHG emissions, extreme events, and infrastructure performance – are controlled by the climate change policy. Without policy implementation, the model showed higher rainfall, decreased infrastructure performance, and more extreme events.

Figure 14 shows the results of implementing the climate change policy over the next 10 years. The model was tested multiple times by varying the number of times the climate change policy is updated and implemented each year. The more the climate change policy is implemented, the greater the decrease in GHG

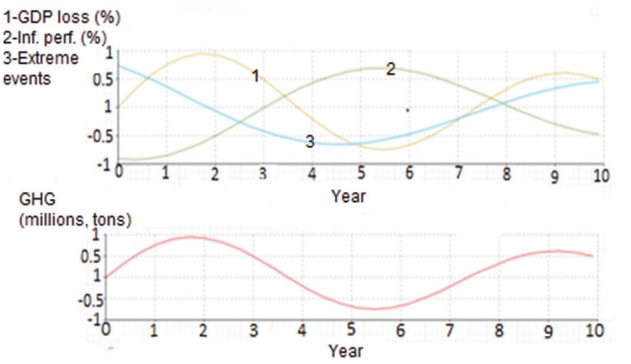

Figure 13. AnyLogic model of climate change mitigation

Abbreviations: GDP: Gross Domestic Product; GHG: Greenhouse gas; Inf. perf.: Infrastructure performance; No: Number.

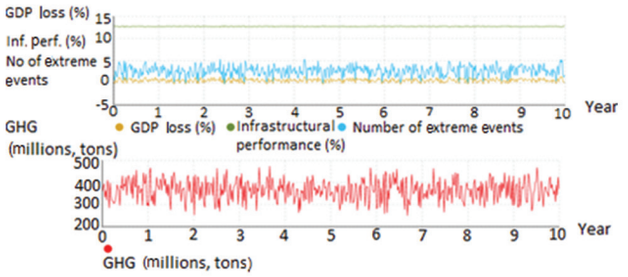

Figure 14. Mitigation results from the simulation model of climate change

Abbreviations: GDP: Gross Domestic Product; GHG: Greenhouse gas; Inf. perf.: Infrastructure performance; No: Number.

emissions, which positively impacts the reduction of the number of extreme weather events and lessens GDP loss. The green line represents infrastructure performance, which improved by 15%; the blue line represents the number of extreme events, which decreased by 15%; the orange line represents GDP loss, which improved by 25%; and the red line represents the amount of GHG emissions, which decreased by 3%.

Implementation of the climate change policy within the Department of Roads and Stormwater Infrastructure more than once a year could reduce the amount of GHG emissions, which would, in turn, reduce GDP loss due to fewer extreme weather events.

The modeling horizon was set for a period of 10 years. After running multiple simulations, where the frequency of climate change policy implementation was varied, the results showed a 15% decrease in climate trends, a 3% reduction in GHG emissions, a 25% decrease in GDP loss, and a 15% increase in infrastructure performance.

4. Discussion

During the period covered by this study, the City of Tshwane operated with an infrastructure budget of R33.038 billion (2018/2019).[2] The population of Tshwane continues to grow annually, with its growth rate exceeding that of Gauteng and South Africa as a whole.[47]

Based on the latest data, Tshwane's high population growth is primarily driven by urbanization, which is creating challenges, as people are building in high-risk areas. Tshwane is exposed to numerous hazards, such as wildfires, floods, droughts, and extreme temperatures. Climate change has a direct impact on the frequency and intensity of these climate hazards, while factors include population growth, urbanization, adaptation interventions, and land use planning play key roles in the number of residents and the vulnerability of infrastructure to these hazards.

The simulation conducted in this study was able to predict the situation over the next 10 years, considering whether or not the climate change policy is implemented.

The simulation results indicated a significant occurrence of extreme events, such as extreme temperatures, droughts, rainfall fluctuations, and GHG emissions, which had a notable negative impact on economic activities, as reflected in the city's GDP, especially when climate change policies were not implemented. However, with the implementation of climate change policies, the magnitude of these extreme events was reduced, resulting in a decrease in GDP loss. Hence, the climate change policy in the Gauteng Department of Roads and Stormwater Infrastructure should be implemented in every project. This approach could also be extended to the National Department of Roads and Stormwater Infrastructure to achieve better outcomes. It is critical for local government bodies to implement climate change policies to reduce the amount of GHG emissions.

The rainfall observed from 1981 to 2022 was not consistent; periods of heavy rainfall and droughts were experienced. The rainfall projections suggest more extreme climate trends in the future, including severe floods and droughts, if climate policies are not implemented. Anekwe *et al.*[12] also found that variations in rainfall and temperature have serious consequences for water resources in South Africa.

The findings of this study are supported by the works of Anekwe *et al.*[12] and Dube and Nhamo,[11] who noted significant variations in weather and temperature patterns in South Africa. Furthermore, Botai *et al.*[14] observed substantial variations in precipitation concentration across the country, while Ndlovu and Demlie[16] found an increasing frequency of droughts and a reduction in rainfall frequency in South Africa between 1970 and 2017 in the KZN province. However, a report from the University of Witwatersrand[48] indicated that flooding in Durban (KZN) has been catastrophic. This suggests that KZN alternates between two extreme events – drought and flooding. These extreme events of drought and flooding have been included in South Africa's climate risk profile, according to the World Bank Group,[49] further supporting the findings of this study. This underscores the need for timely intervention and the implementation of climate change policies.

According to the data gathered and analyzed, it is recommended that the road and stormwater

infrastructure be redesigned for effective climate change mitigation. Furthermore, simulation and modeling tools should be integrated into the planning and decision-making processes of climate adaptation plans and policy development. In this technology- and data-driven era, data is crucial for forecasting and decision-making,[50,51] especially rainfall data. Hence, rainfall data, runoff coefficients, and runoff data for the past three decades should be critically analyzed to identify trends in the area. This analysis will inform both structural and non-structural solutions for stormwater management in South Africa. At present, there is no climate change legislation in South Africa, as the draft climate change bill published in June 2018 has yet to be implemented. Thus, the implementation of South Africa's climate change laws and policies is strongly recommended. This recommendation aligns with the view of Averchenkova *et al.*,[52] who emphasized that, despite South Africa's sophisticated governance systems, the country faces challenges in implementing national climate policy.

The quality of the drainage system in the City of Tshwane also needs to be assessed. A reliable stormwater collection system should be designed with interlocking features, particularly for rural and urban areas that require protection from flooding, given the economic implications. Stormwater must be approached as a hazard, as it can damage road structures and other infrastructure. Effective management planning will require detailed information on how and where impacts will occur, as well as data on the cost and performance of stormwater management practices, such as green infrastructure strategies. At present, stormwater management in Tshwane mainly focuses on collecting runoff and directing it to nearby watercourses. This implies that the present design of the stormwater drainage system prioritizes flow management without sufficient consideration for environmental preservation. The stormwater collection system around the City of Tshwane is full of waste, grass, and untreated sewage due to lack of maintenance and population growth, highlighting the need for a redesign.

To address variations in rainfall patterns leading to drought, the country could adopt coping strategies such as water resource conservation and distribution techniques, modern irrigation facilities, and adjustments in cropping patterns to align with rainfall trends.[53,54] Furthermore, reservoirs with large capacities should be established in areas vulnerable to both floods and droughts to mitigate the impacts of these extreme weather events. Mechanisms can be developed to harvest the floodwater into reservoirs for storage during periods of heavy rainfall, which can then be used during droughts. This would offer multiple benefits, such as water storage, flood prevention, and drought mitigation.[55]

The findings of this study contribute to the body of knowledge by demonstrating the applicability of an integrated model for assessing the impacts of climate change. The study enhances the understanding of climate change impacts in South Africa, specifically the City of Tshwane. With the 10-year predictions of climate change and its potential effects (with or without the implementation of climate change policy), policymakers will be better positioned to prioritize climate change policy implementation and make informed decisions on developing effective adaptation and mitigation strategies.

5. Conclusion and recommendations

5.1. Conclusion

This study focused on assessing the impact of climate change on the City of Tshwane, South Africa. Based on the simulation results, the following conclusions are drawn:

(i) The effects of climate change – particularly flooding – have significant cost implications, leading to increased expenses for the development and repair of roads and stormwater infrastructure.

(ii) Rainfall dataset observed from 1981 to 2022 showed considerable variability, with periods of heavy rainfall and drought. Projections suggest more extreme climate trends in the future, including severe floods and droughts if climate change policies are not implemented.

(iii) Implementing climate change policies could lead to an annual improvement in GDP by 25%, a 3% reduction in GHG emissions, and a 15% increase in infrastructure performance.

The novel contribution of this study lies in the integration of the DES and SD models to investigate the impact of climate change on roads and stormwater infrastructure in the City of Tshwane, as well as to represent mitigation strategies over a 10-year period. Thus, the study contributes both methodologically and empirically by generating data related to climate change that can assist the relevant stakeholders in making informed decisions on its mitigation. The model could be further improved by incorporating factors, such as infrastructure maintenance, for which data is limited. There is also a lack of accurate, city-specific data on

GHG emissions, as existing figures are reported at the provincial level. Furthermore, quantitative data are needed on elements, such as the annual percentage or scorecard of infrastructure constructed, the extent and measurements of flood events, and a political stability index to better inform policy and infrastructure planning.

5.2. Policy implications

Effectively mitigating the impact of climate change on roads and stormwater infrastructure requires deliberate and sustained policy implementation. The following policy implications are proposed for consideration by relevant stakeholders:

(i) Increase public awareness and education on the impacts of climate change and promote individual, corporate, and governmental actions to mitigate its effects
(ii) Integrate climate change adaptation and mitigation strategies into national planning and development processes to ensure coherence across sectors
(iii) Strengthen coordination between subnational and national government plans aimed at climate change mitigation and adaptation
(iv) Encourage human capacity development in the areas of climate change policy analysis, formulation, and implementation
(v) Address resource constraints that hinder the development and implementation of effective climate change policies.

5.3. Limitations and directions for future study

This study is limited to the analysis and simulation of historical data on stormwater collection systems, road infrastructure, climate change, and financial datasets specific to the City of Tshwane. It does not consider the age-related issues within the lifecycle of road and stormwater infrastructure. The historical data used in this study may omit important factors, potentially leading to inaccuracies in the analysis and forecasting. Moreover, such data may be subjected to bias and incompleteness and may lose relevance over time. Although Harman's one-factor test was conducted to assess the presence of bias and to establish the reliability of the dataset, the use of primary data may offer greater accuracy and reliability due to its direct acquisition from original sources. Therefore, future works could benefit from the use of primary data and should also consider investigating the typical performance challenges associated with the lifecycle of road and stormwater infrastructure. In addition, further studies could explore the interactions between climate change and infrastructure lifecycle to provide a more comprehensive understanding of long-term infrastructure resilience and sustainability.

Acknowledgments

None.

Funding

None.

Conflict of interest

The authors declare no conflicts of interest.

Author contributions

Conceptualization: All authors
Formal analysis: All authors
Investigation: All authors
Methodology: All authors
Writing – original draft: All authors
Writing – review & editing: All authors

Availability of data

The data supporting the findings of this study are available from the corresponding author upon reasonable request.

References

1. Collins J. *Ascertaining Credibility in Research Surveys and Studies*. 2020. Available from: https://www.impactio.com/blog/ascertaining-credibility-in-research-surveys-and-studies [Last accessed on 2023 Mar 23].
2. City of Tshwane. *City Strategy and Organisational Performance Department the Draft Consolidated Audited Annual Report for the City of Tshwane and Its Entities for the End of the 2019/20 Financial Year Submitted in Terms of Section 127*(*2*) *of the Municipal Finance Management Act, 56 of 2003* (*MFMA*) *and Section 46 of the Municipal Systems Act, 32 of 2000* (*MSA*). 2021. Available from: https://lg.treasury.gov.za/supportingdocs/tsh/tsh_annual%20report%20draft_2022_y_20230123t130226z_mmasellom.pdf [Last accessed on 2022 Mar 17].
3. South African Government News Agency. *National Destructive Flooding Declared National State of Disaster Declared on Floods SA*. 2023. Available from: https://www.sanews.gov.za/south-africa/national-state-disaster-declared-floods [Last accessed on 2023 Mar 20].
4. Motsoere S. *Manufacturers Mood Darkens after Deadly*

South African Floods. Bloomberg; 2022. Available from: https://www.bloomberg.com/news/articles/2022-05-03/manufacturers-mood-darkens-after-deadly-south-african-floods [Last accessed on 2022 May 07].
5. Comins L. *KZN Flood Economic Impact Update. South Africa's Freight News*. 2022. Available from: https://www.freightnews.co.za/article/kzn-floods-economic-impact-update [Last accessed on 2022 May 06].
6. Chinowsky P, Paul S, Hayles C, Carolyn H, Schweikert A, Strzepek N. Climate change: Comparative impact on developing and developed countries. *Eng Proj Organ.* 2011;1(1):67-80. doi: 10.1080/21573727.2010.549608
7. Pijoos I. *Hundreds Rescued from Mamelodi Flooding, While the "Phanda Pusha Pay Entrepreneur" Keeps Feet Dry*. 2019. Available from: https://www.timeslive.co.za/news/south-africa/2019-12-10-hundreds-rescued-from-mamelodi-flooding-plus-watch-the-phanda-push-pay-hustler [Last accessed on 2022 May 07].
8. Le Roux A. *South African City Dwellers Frog in the Boiling Pot*. 2021. Available from: https://www.issafrica.org/iss-today/south-african-city-dwellers-frogs-in-the-boiling-pot [Last accessed on 2022 May 07].
9. Climate Report. 2015. Available from: https://nerc.ukri.org/research/partnerships/ride/lwec/report-card/infrastructure [Last accessed on 2021 May 13].
10. Schweikert A, Chinoswky A, Kwiatkowski KP, *et al*. Road infrastructure and climate change: Impacts and adaptations for South Africa. *J Infrastruct Syst*. 2014;21(3):0401404. doi: 10.1061/(ASCE)IS.1943-555X.0000235
11. Dube K, Nhamo G. Evidence and impact of climate change on South African national parks. Potential implications for tourism in the Kruger National Park. *Environ Dev.* 2020;33:100485. doi: 10.1016/j.envdev.2019.100485
12. Anekwe IMS, Zhou H, Makhathini MSM, Mkhize M. Investigating the Impact of Climate Change on Water Resources in Jozini Municipality, South Africa. In: *11th Annual International Conference on Sustainable Development* (*ICSD*). New York, USA, Columbia University Campus; 2023. p. 1-12.
13. Chersich MF, Wright CY. Climate change adaptation in South Africa: A case study on the role of the health sector. *Global Health.* 2019;15:22. doi: 10.1186/s12992-019-0466-x
14. Botai CM, Botai JO, Adeola AM. Spatial distribution of temporal precipitation contrasts in South Africa. *S Afr J Sci*. 2018;114(7-8):70-78. doi: 10.17159/sajs.2018/20170391
15. Jovanovic N, Mu Q, Bugan RDH, Zhao M. Dynamics of MODIS evapotranspiration in South Africa. *Water SA*. 2015;41(1):79-90. doi: 10.4314/wsa.v41i1.11
16. Ndlovu MS, Demlie M. Assessment of meteorological drought and wet conditions using two drought indices across KwaZulu-Natal Province, South Africa. *Atmosphere*. 2020;11(6):623. doi: 10.3390/atmos11060623
17. Orimoloye IR, Olusola OO, Belle JA. Satellite-based application in drought disaster assessment using terra MOD13Q1 data across Free State Province, South Africa. *J Environ Manag.* 2021;285:112112. doi: 10.1016/j.jenvman.2021.112112
18. Al-Ghadi SM, Mohtar WHM, Razali SFM, El-Shafie A. The practical influence of climate change on the performance of road stormwater drainage infrastructure. *J Eng.* 2020;2020:8582659. doi: 10.1155/2020/8582659
19. De Abreu VH, Santos AS, Monteiro TGM. Climate change impacts on the road transport infrastructure: A systematic review on adaptation measures. *Sustainability.* 2022;14:8864. doi: 10.3390/su14148864
20. Rentachintala LRNP, Reddy MGM, Mogapatra PK. Urban stormwater management for sustainable and resilient measures and practices: A review. *Water Sci Technol.* 2022;85(4):1120-1140. doi: 10.2166/wst.2022.017
21. Ray CA. *The Impact of Climate Change on Africa's Economies*. 2021. Available from: https://www.fpri.org/article/2021/10/the-impact-of-climate-change-on-africas-economies [Last accessed on 2022 Oct 29].
22. Baniya R, Regmi RK, Talchabhadel R, *et al*. Integrated modeling for assessing climate change impacts on water resources and hydropower potential in the Himalayas. *Theor Appl Climatol*. 2024;155:3993-4008. doi: 10.1007/s00704-024-04863-4
23. Van Beek L, Hajer M, Pelzer P, van Vuuren D, Cassen C. Anticipating futures through models: The rise of integrated assessment modelling in the climate science-policy interface since 1970. *Global Environ Change*. 2020;65:102191. doi: 10.1016/j.gloenvcha.2020.102191
24. Ciscar JC, Dowling P. Integrated assessment of climate impacts and adaptation in the energy sector. *Energy Econ.* 2014;46:531-538. doi: 10.1016/j.eneco.2014.07.003
25. Gohari A, Mirchi A, Madani K. System dynamics evaluation of climate change adaptation strategies for water resources management in central Iran. *Water Resour Manage*. 2017;31:1413-1134. doi: 10.1007/s11269-017-1575-z
26. Terzi S, Sušnik J, Schneiderbauer S, Torresan S, Critto A. Stochastic system dynamics modelling for climate change water scarcity assessment of a reservoir in the Italian Alps. *Nat Hazards Earth Syst Sci*. 2021;21:3519-3537. doi: 10.5194/nhess-21-3519-2021
27. Phan TD, Bertone E, Stewart RA. Critical review of system dynamics modelling applications for water

resources planning and management. *Clean Environ Syst.* 2021;2:100031.
doi: 10.1016/j.cesys.2021.100031

28. Hassanzadeh E, Zarghami M, Hassanzadeh Y. Determining the main factors in declining the Urmia Lake level by using system dynamics modeling. *Water Resour Manag.* 2012;26(1):129-145.
doi: 10.1007/s11269-011-9909-8
29. Xiao-Jun W, Jian-Yun Z, Jian-Hua W, *et al*. Climate change and water resources management in Tuwei river basin of Northwest China. *Mitig Adapt Strateg Glob Chang*. 2014;19(1):107-120.
doi: 10.1007/s11027-012-9430-2
30. Singh A. *An Introduction to Experimental and Exploratory Research*. 2021. Available from: https://papers.ssrn.com/sol3/papers.cfm?abstract_id=3789360 [Last accessed on 2023 Mar 12].
31. Podsakoff PM, MacKenzie SB, Lee JY, Podsakoff NP. Common method biases in behavioral research: A critical review of the literature and recommended remedies. *J Appl Psychol.* 2003;88(5):879-903.
doi: 10.1037/0021-9010.88.5.879
32. Rahaman MDS. The advantages and disadvantage of using quantitative and qualitative approaches and method in language testing and assessment research: A literature review. *J Educ Learn*. 2016;6(1):102-112.
doi: 10.5539/jel.v6n1p102
33. Somo G, Daniyan IA, Swanepoel J, Mpofu K. System dynamics modelling and simulation of computer control systems for steel ingot furnaces. *S Afr J Ind Eng.* 2023;34(4):116-131.
doi: 10.7166/34-4-2862
34. Crowe S, Vresswell K, Robertson A, Huby G, Avery A, Sheikh A. The case study approach. *BMC Med Res Methodol.* 2011;11:100.
doi: 10.1186/1471-2288-11-100
35. Akhtar I. Research design. In: *Research in Social Science: Interdisciplinary Perspective*. 1st ed. Kanpur, India: Social Research Foundation; 2016. p. 17.
36. Zainal Z. Case study as a research method. *J Kemanuisiaan Bil.* 2007;9(1):1-6.
37. South African Weather Service. *Annual Report*. 2021. Available from: https://www.weathersa.co.za/documents/corporate/annual%20state%20of%20the%20climate%202021_04042022114230.pdf [Last accessed on 2023 Mar 20].
38. Adeyemi A, Botai J, Ramoelo A, van der Merwe F, Tsela P. Effect of impervious surface area and vegetation changes on mean surface temperature over Tshwane metropolis, Gauteng Province, South Africa. *S Afr J Geomat.* 2015;4(4):351-368.
doi: 10.4314/sajg.v4i4.1
39. Magidi J, Ahmed F. Spatio-temporal variations of land surface temperature using landsat and MODIS: Case study of the city of Tshwane, South Africa. *S Afr J Geomat.* 2020;9(2):379-396.
doi: 10.4314/sajg.v9i2.25
40. McBride CM, Kruger AC, Dyson L. Changes in extreme daily rainfall characteristics in South Africa: 1921-2020. *Weather Clim Extrem.* 2022;38:100517.
doi: 10.1016/j.wace.2022.100517
41. World Bank Group. *South Africa Climatology*. 2021. Available from: https://climateknowledgeportal.worldbank.org/country/south-africa/climate-data-historical [Last accessed on 2025 Mar 28].
42. South African Government Report. *Geography and Climate*. 2025. Available from: https://www.gov.za/about-sa/geography-and-climate [Last accessed on 2025 Mar 28].
43. Writer S. *What is Drought and Why Is It an Increasing Issue in South Africa*. 2022. Available from: https://www.greeneconomyjournal.com/explainer/what-is-drought-and-why-is-it-an-increasing-issue-in-south-africa [Last accessed on 2025 Mar 28].
44. AnyLogic. *AnyLogic Simulation Software*. 2023. Available from: https://www.anylogic.com [Last accessed on 2023 Sep 16].
45. Daniyan IA, Mpofu K, Ramatsetse BI, Zeferino E, Monzambe G, Sekano E. Design and simulation of a flexible manufacturing system for manufacturing operations of railcar subassemblies. *Procedia Manuf.* 2021;54:112-117.
doi: 10.1016/j.promfg.2021.07.018
46. Government Gazette, Republic of South Africa. 2024. Available from: https://www.gov.za/sites/default/files/gcis_document/202407/50966climatechangeact222024.pdf [Last accessed on 2025 Apr 03].
47. STATS SA. *Midyear Population Estimates*. 2022. p. 1-50. Available from: https://www.statssa.gov.za/publications/P0302/P03022022.pdf [Last accessed on 2023 May 24].
48. University of Witwatersrand. *The 2022 Durban Floods Were the Most Catastrophic Yet Recorded in KwaZulu-Natal*. 2023. Available from: https://www.wits.ac.za/news/latest-news/general-news/2023/2023-04/the-2022-durban-floods-were-the-most-catastrophic-yet-recorded-in-kwazulu-natal.html [Last accessed on 2023 Apr 19].
49. World Bank Group. *Climate Risk Country Profile South Africa*. 2022. Available from: https://climateknowledgeportal.worldbank.org/sites/default/files/country-profiles/15932-wb_south%20africa%20country%20profile-web.pdf [Last accessed on 2022 Oct 29].
50. Ngepah J, Raoul C, Djemo T, Saba CH. Forecasting the economic growth impacts of climate change in South Africa in the 2030 and 2050 horizons. *Sustainability.* 2022;14:8299.
doi: 10.3390/su14148299
51. Dube K, Nhamo G, Chikodzi D. Flooding trends and their impacts on coastal communities of

Western Cape Province, South Africa. *GeoJournal.* 2022;87(4):453-468.
doi: 10.1007/s10708-021-10460-z

52. Averchenkova A, Gannon KE, Curran P. *Governance of Climate Change Policy: A Case Study of South Africa*. Policy Briefs & Reports. London: Grantham Research Institute on Climate Change and the Environment and Centre for Climate Change Economics and Policy, London School of Economics and Political Science; 2019. p. 18-35.
doi: 10.13140/RG.2.2.10021.04323
53. Gupta B, Aggarwal S, Jose MM. Long-term seasonal and annual rainfall trend analysis of Giridih District, Jharkhand, India. *Asian J Water Environ Pollut.* 2024;21(4):73-81.
doi: 10.3233/AJW240048
54. Sittichok K, Vongphet J, Seidou O. Predicted rainfall, surface runoff and water yield responses to climate change in the Phetchaburi River Basin, Thailand. *Asian J Water Environ Pollut.* 2022;19(3):1-13.
doi: 10.3233/AJW220033
55. Krishnaveni M, Arunya KG. Analysing micro-level rainfall trends: Implications for water conservation in Paravanar River Basin. *Asian J Water Environ Pollut.* 2024;21(5):1-14.
doi: 10.3233/AJW240054

ACCSCIENCE PUBLISHING

Asian Journal of Water, Environment and Pollution. Vol. 22, No. 2 (2025), pp. 204-215.
doi: 10.36922/AJWEP025080051

ORIGINAL RESEARCH ARTICLE

Wastewater treatment using recycled automobile tires

Liudmyla Melnik[1], Olha Rybalova[2]*, Olena Bryhada[2], Oleksii Ilinskyi[2], Anton Matsak[2]*, and Bohdan Tsymbal[2]

[1]Laboratory of Urban and Production Wastewater, Ukrainian Scientific Research Institute of Ecological Problems, Kharkiv, Ukraine

[2]Department of Occupational Hazard and Environmental Safety, Faculty of Public Safety and Management, National University of Civil Defence of Ukraine, Cherkasy, Ukraine

***Corresponding authors:** Olha Rybalova (olgarybalova@ukr.net); Anton Matsak (antonmatsak1984@gmail.com)

Received: February 21, 2025; 1st revised: March 14, 2025; 2nd revised: April 4, 2025; 3rd revised: April 13, 2025; Accepted: April 14, 2025; Published online: April 24, 2025

Abstract: This study explores a promising phytoremediation method for wastewater treatment using various filtering material types, including used automobile tires and construction waste. Developing an affordable, eco-friendly solution to minimize the release of untreated wastewater into natural water sources by utilizing industrial byproducts and waste materials is a critical challenge. This research focuses on the scientific understanding of implementing phytoremediation facilities that utilize construction debris and discarded automobile tires as filtering media for wastewater treatment. The proposed filter materials (waste tires and construction waste) demonstrated the following treatment effectiveness: ammonium – 40%; nitrates, nitrites, chemical oxygen demand (COD), and suspended solids – 70%; organic pollutants by COD and biological oxygen demand – 70% and 28.5%, respectively; chlorides – 20%; sulfates – 23%; total iron – 99%; surfactants – 28%; and overall disinfection efficiency of nearly 99%. These results confirm the effectiveness of the proposed filtering media in enhancing wastewater treatment through phytoremediation.

Keywords: Environmental hazard; Waste; Automobile tires; Utilization; Wastewater; Treatment facility; Purification processes

1. Introduction

One of the world's key environmental problems is the issue of car tire recycling. With the development of the automotive industry, the problem of recycling used tires is constantly growing. As the number of cars increases, so does the number of tires that need to be recycled. More than 1.5 million tons of car tires are used annually in the United States and more than 2 million tons in the European Union (EU).[1] Given the sharp increase in the number of cars in Ukraine – 202 cars per 1,000 inhabitants, totaling about 10 million units – there is an urgent issue of warehousing, storage, transportation, and processing of tens of millions of car tires annually.[2]

The storage of rubber waste is associated with the very long decomposition period of rubber under natural conditions. Worn tires are practically not subjected to natural degradation, and, as a result, require large space for storage and disposal. In landfills, tires can accumulate methane and other gases; they are flammable, posing risks of emergencies, fires, and pollution. When one ton of tires is burned, about 270 kg of soot and 450 kg of toxic substances are released into the atmosphere. Tire

dump fires can last for weeks, poisoning the surrounding area within a radius of 10 km.

Despite the emergence of new environmentally friendly methods of recycling tire waste, the problem of environmental pollution due to the storage of used car tires in landfills becomes more acute each year.[3]

This research proposes an environmentally and cost-effective method of wastewater treatment for small settlements using used car tires and construction waste as a filter nozzle, which will improve the state of aquatic ecosystems and increase waste disposal.

Surface water pollution and waste management are major environmental issues in many countries around the world. An evaluation of environmental risks related to the degradation of surface waters in Ukraine has revealed that the waterways within the Siversky Donets River basin are in the most critical state.[4] An analysis of the quality of water resources in the Kharkiv region (Ukraine) indicated that, in many aspects, they fail to comply with international and national standards.[5] In one study,[6] the discharge of wastewater into the Udy River was analyzed over the period from 1992 to 2016. The investigation into how natural and anthropogenic factors influence the ecological condition of the Udy River demonstrated that wastewater discharge, with a correlation coefficient of 0.75, represents a major contributor to surface water pollution. In addition, a multifactor correlation-regression analysis identified the natural and anthropogenic factors exerting the greatest influence on the hydrochemical characteristics of the Oskil River. The results of the research showed that the quality of water bodies is most affected by wastewater discharges and rising air temperatures, which indicates the need to reduce the load from industrial facilities and utilities.[6]

The problem of surface water pollution caused by discharges of untreated wastewater in small towns without sewerage networks is extremely acute and may lead to emergencies due to the epidemiological risk of increasing infectious diseases through recreational water use.

2. Materials and methods

2.1. Method background

The determination of the possibility of using phytoremediation facilities with the addition of used automobile tires as filtering nozzles for wastewater treatment has become the main focus and scientific novelty of this study.

The main objective of this research was to explore the potential of using phytoremediation systems with waste automobile tires as filtering materials for wastewater treatment.

The purpose of this study was to reduce the pollution of aquatic ecosystems by introducing phytoremediation technology for wastewater treatment using construction waste and used car tires as filter nozzles.

To achieve this goal, the following tasks were set:

(i) To analyze modern methods for the utilization of used car tires

(ii) To evaluate phytoremediation-based methods of wastewater treatment

(iii) To improve the wastewater treatment method through the use of construction waste and used car tires.

The technological process of wastewater treatment at such facilities occurs in two stages. First, mechanical and primary wastewater treatment takes place in septic tanks, where suspended solids are removed by sedimentation. The next stage involves an underground filter trench system, which may be gravel- or tunnel-based. The primary function of this trench is to create conditions for the development of a significant number of microorganisms throughout its volume. A biofilm – a mucus coating formed by specific microorganisms derived from wastewater – develops on the trench's filter material and participates in the biological treatment process.

Sewage, clarified and pre-treated in the settling tanks through the drip biofilter, enters the area of the underground filter in portions. The natural soil acts as a carrier for the immobilization of microflora. Given that the filter unit (composed of used car tires, basalt crumb, and gravel) is a porous material, a biofilm begins to form during the first 2 – 3 weeks of operation. Intensive mass transfer and the presence of oxygen in the water support the active development of microflora on the filter material, ensuring the completion of the deep biological purification process.

From the filtering trenches, treated water can either be discharged into the artificial groundwater recharge system (AGRS) or undergo further treatment at the facilities using phytoremediation technology, mainly involving shrub plantings on the surface (Figure 1).

Such structures are located around reservoirs, intercepting pollutant flows. These are either neutralized by natural biochemical processes in the dams and trenches or transferred to the underground

streams, where natural soil purification processes of contaminated water continue (Figure 1).

Most often, filter trenches are integrated with elements of AGRS. Their main purpose in this context is to divert purified water into aquifers through infiltration. A key function of the AGRS system is its barrier role – during short-term inflows of contaminated water, the AGRS system can prevent groundwater pollution. Water exiting the AGRS is typically of high quality, with almost complete retention of suspended solids and microorganisms, complete decomposition of pathogenic microorganisms, and overall improvement of other properties of water. Groundwater treated by AGRS systems usually meets hygienic standards for drinking water. In the AGRS system, the water temperature also stabilizes, aligning with natural groundwater temperatures.

The biochemical oxidation of pre-treated wastewater in the biofilter occurs in two phases as it seeps through the filter media: first, carbon and hydrogen are oxidized to produce carbon dioxide and water; then nitrogen is oxidized, initially forming nitrogen salts, and eventually nitrates (nitrification).

Figure 1. Filter trench in the zone of interception of polluted surface runoff

For each site, a treatment scheme was selected according to the construction conditions, terrain, and wastewater flow.

Settling tanks remain on the surface of the earth, and the area above the filter trenches can be used for landscaping (Figure 2).

Experimental studies of filtration and wastewater treatment processes were conducted under laboratory conditions using filtering phytoremediation facilities with specialized filtering nozzles.

As filtering materials, automobile tires with a directional tread pattern were used. The tire size used was 205/55 R16, where the profile width is 205 mm, the profile height is 55% of the width, and the inner diameter is 16 inches. The outer diameter for this size is approximately 630 mm, and the tire carcass is made of steel cord or polyester threads, ensuring strength and shape stability under high loads. The rubber compound consists of synthetic rubber with silica additives, allowing effective performance within a temperature range of −20°C – 40°C, as commonly used in summer or all-season tires. The tread depth initially measures 7 – 9 mm, with a minimum allowable depth of 1.6 mm.

The average lifespan of the tires used is 4 – 6 years or 40,000 – 60,000 km of mileage. Factors affecting tire quality include driving style, road conditions, and temperature variations.

Laboratory studies were conducted to evaluate the toxicity of tires in water-saturated soil. The data gathered indicate that tire samples containing rubber materials and metallic cords were not toxic to microorganisms.

Figure 2. Sewage treatment plants for individual houses using non-traditional materials operating in Ukraine (Tatarbunary Town Museum). (A-D) Stages of filter trench construction: (A) Arrangement of a septic tank; (B) Construction of a filter trench using available space; (C) Laying waste tires and geotextiles to prevent clogging; (D) Development of a recreational area on top of the filter trench.

Chemical and biological analyses were performed using standard methodologies.

The experiment lasted 6 months (from March 1 to August 31, 2024) under laboratory conditions, using a setup measuring 1 m × 0.5 m × 0.8 m, with a wastewater flow rate of 20 dm^3/day. The water first passed through a filtering layer of rubber granules (particle size 2 – 10 mm), which captured mechanical pollutants and adsorbed organic contaminants. It then reached the plant roots, which absorbed biogenic substances and facilitated biological treatment.

The filtrate analysis was performed on the day of sampling, with three replicates used to determine parameters such as suspended solids concentration, nitrates, phosphates, ammonium, chemical oxygen demand (COD), and biological oxygen demand (BOD_5).

2.2. Analysis of methods based on literature

2.2.1. Modern methods of used tire utilization

The rapid growth of the automotive industry, coupled with improvements in living standards, has resulted in a substantial increase in the production of car tires, which require proper disposal once they reach the end of their lifecycle.

Torosian and Chernyaev[7] investigated the environmental risks associated with car tires during their usage, assessing the extent of dust pollution and its effects on human health. They proposed a schematic for an international environmental safety control system designed to regulate tire usage. This system includes a procedural algorithm aimed at reducing risks associated with improper or disorganized tire disposal.

Shaker and Mohammed[8] presented various methods for recycling automotive waste – such as oils, tires, and glass – and discussed the economic feasibility of disposal and the potential of applying recycling processes in the city of Divaniya to reduce the amount and volume of waste.

Waste from car tires belongs to the category of waste subjected to industrial recycling. Thermal decomposition of polymer waste is one of the promising options for tire processing; however, it remains relatively expensive. In addition to incineration for energy purposes, tire waste can be mechanically processed – for example, by shredding – and used in road construction. While increasing fragmentation significantly improves functionality, it also raises operational costs, making the process less cost-effective. Of the total waste, 2 – 2.5 million tons of used tires were reprocessed in the EU, of which only 23% were reused. The remaining used car tires are not disposed of due to a lack of cost-effective disposal methods, which poses a significant environmental problem. Globally, efforts are underway to find solutions efficient solutions for tire utilization and to extend their safe operating lifespan. The most frequently discussed approaches in the literature for reducing the volume of used tire waste include: utilizing tires as fuel through energy recovery; shredding and repurposing the material for various applications; and modifying tire designs to enhance durability and prolong usability, such as through retreading or altering their chemical composition.[1]

Dębska *et al.*[9] documented the results of tests on epoxy solutions in which sand was replaced with granules made from used tires in amounts of 0, 20, 40, 60, 80, and 100% by volume. As the proportion of tire waste increased, the composite's strength parameters decreased. Nevertheless, the resulting material showed low water absorption and a low thermal conductivity coefficient. Using ADINA software, a numerical simulation of temperature distribution was conducted on a section of a building structure containing the modified rubber solution. The simulation results confirmed the composite's practical applicability due to its excellent thermal insulation properties.[9]

The use of rubber crumbs to modify road bitumen represents an environmentally sustainable solution for rubber waste management.[10] Enhancing the stability of rubber crumb-modified road asphalt mixtures is a critical environmental strategy for the future. Plewa[10] presented the findings of fatigue resistance tests conducted on asphalt concrete with asphalt rubber binders. The results demonstrated that mineral-rubber-asphalt mixtures exhibited improved functional properties compared to conventional mineral-asphalt mixtures.

Chen *et al.*[11] stated that used car tires have emerged as one of the fastest-growing types of solid waste in China. The paper examined the current recycling potential of pyrolysis, which is regarded as a promising technology for processing used tires. In addition, Chen *et al*. propose a novel pyrolysis method designed to overcome the limitations of existing tire recycling technologies and mitigate the growing tire waste crisis.

Pyrolysis is currently a modern technology used to recover fuel and soot from used tires. However, the detailed mechanisms of degradation and kinetics of tire pyrolysis remain under-researched. Shahi *et al.*[12] investigated the pyrolysis of the tread, sidewall, and inner liner of used light vehicle tires using thermogravimetric analysis. The degradation profiles of these tire components were predicted using different kinetic models.

In a study by Kuznetsov *et al*.,[13] the high potential for utilizing tires unsuitable for further use through pyrolysis and combustion of thermal decomposition products in coal-water fuel mixtures is demonstrated. It was found that adding pyrolysis products of liquid rubber to the structure of coal-water suspension leads to a significant acceleration of ignition processes. Based on experimental results, a new mathematical model was developed to describe the ignition process of highly inhomogeneous, multicomponent fuels.

In Vambol *et al.*'s research,[14] the authors used numerical simulations to demonstrate the feasibility of utilizing waste tires at high temperatures, followed by the methanation of fuel gases and the separation of multicomponent hydrocarbon mixtures to produce liquefied methane.

Nie *et al*.[15] highlight that hydrothermal gasification is a promising approach for recycling used tires. The hydrothermal gasification of spent tires was assessed through chemical equilibrium analysis combined with the response surface methodology. The study considered various parameters, including the subcritical temperature range (250 – 300°C), transition temperature range (350 – 400°C), supercritical temperature range (550 – 600°C), supercritical pressure (22.5 – 30.5 MPa), and raw material concentration (5 – 20 wt%). This investigation provides foundational data for the hydrothermal treatment of used tires. Meanwhile, Subatkevičienė *et al.*[16] proposed the use of car tire waste as sorbents for treating industrial wastewater containing petroleum products. Production of sorbents from shredded used tires reduces waste and protects water bodies from harmful pollutants. Experimental findings showed a cleaning efficiency ranging from 91.51% to 95.21%.

In a study by Sivaraman *et al*.,[17] a method for recycling used tires as an adsorbent to sequester hexavalent chromium from a simulated wastewater system is described. Leather and electroplating industry effluents often contain high concentrations of chromium, which is a toxic and mutagenic contaminant. The spent tire samples were activated with orthophosphoric acid and used for adsorption studies. The proposed method of using spent tire particles as adsorbents in the treatment of contaminated hexavalent chromium water provides valuable guidance for further research in the areas of dynamic adsorption and wastewater treatment.

The analysis of modern methods for the disposal of used car tires underscores the relevance and necessity of continued scientific research aimed at waste reduction and environmental protection.

2.2.2. Phytoremediation methods for wastewater treatment

Phytoremediation is an efficient and cost-effective biotechnology for the purification of water, soil, and air. It is based on the ability of plants and associated decomposer microorganisms to remove toxic substances from the environment or convert them into safe compounds.

Numerous studies by Ukrainian and international researchers have focused on the purifying properties of higher aquatic plants (HAP). These plants not only absorb dissolved substances from water but also serve as substrates for the growth of various microorganisms. These microorganisms contribute to the neutralization of a significant portion of pollutants discharged into natural water bodies through surface runoff, thereby enhancing the quality of aquatic ecosystems.[18,19]

Among the wide variety of macrophytes, the most commonly used species for wastewater treatment include common reed (*Phragmites australis* [Cav.] Trin ex Stend.), narrow-leaved cattail (*Typha angustifolia* L.), broad-leaved cattail (*Typha latifolia* L.), and lake bulrush (*Scirpus lacustris* L.), along with several other species. According to researchers, up to 450 kg of nitrogen, 180 kg of phosphorus, 220 kg of potassium, and 330 kg of chloride can be removed per hectare of reeds during the growing season.[19,20]

Air-water macrophytes (such as reeds, cattails, and others) enhance the gas regime of wetlands and waterlogged soils. In the oxygen-rich environment surrounding their fine roots, rhizosphere microorganisms proliferate in large numbers. These microorganisms play a key role in the aerobic decomposition of organic matter accumulated in silt deposits, facilitating the conversion of substances into more bioavailable forms such as nutrition. As a result, HAP stimulates self-purification processes and promotes air circulation within bottom sediments.[18] Research conducted by specialists at the Ukrainian Research Institute of Environmental Problems on the purification capacity of HAP led to the development of a method for using these plants in treatment systems such as Constructed Wetlands.[21] To date, more than 60 wastewater treatment projects in Ukraine have been designed based on this methodology.

Constructed Wetlands have been successfully implemented for the treatment of domestic wastewater in countries like the Netherlands, Japan, and China, as well as for the purification of contaminated surface runoff in Norway, Australia, and other nations, including Ukraine.[22]

In Ukraine, Constructed Wetlands treatment systems are referred to as bioengineered treatment plants (BTP). The operating principle of these systems is based on harnessing natural self-purification processes that occur within the filter layer, which serves as a substrate for the development of biogeocenoses of HAP. Table 1 provides an overview of the main purification systems that utilize phytoremediation.[23]

At present, several types of BTP have been developed, each with various treatment conditions and types of bioplateaus. Systems incorporating HAP are effectively employed for the additional purification of wastewater following traditional treatment methods. Bioplateau systems not only water-air HAP (such as reeds, cattails, bulrushes, and sedges) but also various types of submerged vegetation, including redwood, watercress, hornwort, and others.

The design characteristics and technological differences in the construction and operation of treatment facilities using HAP, similar to Constructed

Table 1. Comparative characteristics of purification systems using phytoremediation

Treatment system	Location	Application	Water movement	Treatment efficiency	Disadvantages
Botanical sites	Shallow water bodies	Primary and additional treatment of domestic and industrial wastewater	Horizontal (through HAP thickets)	Organic substances: Up to 97%; heavy metals: Up to 90%	(i) Efficiency depends on the season of the year (ii) Limited contact time between wastewater with HAP
Phytofiltration devices	Alluvial underwater ridges near rivers	Biomelioration of natural waters	Horizontal	Not specified	(i) Insignificant contact time between wastewater and HAP (ii) Possible leakage of treated water
Bio stands with HAP landings	Reservoirs with planted HAP	Primary and additional treatment of domestic wastewater	Horizontal (in water column)	N: 10 – 80%, chemical oxygen demand: Up to 90%; suspended solids: Up to 98%; petroleum products: Up to 60%; disinfection: up to 90%	(i) Low productivity (ii) Requires large areas of land (iii) Presence of stagnant zones (iv) Risk of recontamination
Artificial natural wetlands	Wetlands with artificial or natural embankments	Primary and additional treatment of domestic wastewater	Horizontal (through HAP thickets)	NH_4^{2-}: 30 – 60%; NO_3^-: 0 – 20%; biological oxygen demand (BOD_5): 50 – 70%	(i) Low controllability of cleaning processes (ii) Efficiency depends on the season of the year
Bioplato	Canals, rivers, lowlands, or upper ponds	Primary and additional treatment of domestic wastewater	Horizontal (through HAP thickets)	Ammonium nitrogen: 30 – 60%; NO_3^-: 10 – 20%; BOD: 50 – 70%; disinfection: up to 90%	(i) Requires large areas of land (ii) Efficiency depends on the season of the year

Abbreviations: HAP: Higher aquatic plants; N: Nitrogen; NH_4^{2-}: Ammonium; NO_3^-: Nitrates.

Wetlands, have led to a variety of terminological definitions. These include terms such as botanical sites (or hydrobotanical sites), filter ponds, biological ponds with HAP, filtration devices, artificial wetlands (or artificial swamps), bioplateaus, and bioengineering facilities for water quality regulation. A common feature across all these systems is the presence of biocenoses of HAP, which directly or indirectly influence the biological processes involved in water quality transformation (purification) and the engineering characteristics of the structures (e.g., specific structural elements, operational parameters).

Typically, in such systems, water passes through thickets of HAP or bog vegetation, partially through a soil layer, and is then removed from the site through drainage. The primary operational parameters of artificial wetlands include the filtration path length (ranging from 100 to 1,500 m) and the water flow velocity (requiring 6 – 10 days for passage). The effectiveness of these systems is evidenced by reductions in the concentrations of ammonium nitrogen (by 30 – 60%), nitrates (by 10 – 20%), and BOD_5 by 50 – 70%.[24]

To fully understand the potential of HAP, further research is needed to identify the most suitable phytoremediation technologies for treating contaminated wastewater.

To assess the efficiency of surface wastewater treatment after fires using the phytoremediation method, experimental studies were conducted using a model setup. The modeling of phytoremediation and infiltration processes was carried out in the laboratory of the Department of Labor Protection and Technogenic and Ecological Safety at the National University of Civil Defense of Ukraine.

Experimental results demonstrated the high effectiveness of using reeds and filter nozzles made from defibrated polyethylene terephthalate (PET) containers for stormwater treatment. The treatment efficiency reached 98.0% for suspended solids, 92.0% for BOD_5, 80.0% for petroleum products, and 90.0% for COD.[25]

2.2.3. Wastewater treatment method with used car tires

The problem of untreated wastewater remains particularly acute in small settlements lacking centralized sewerage networks. In many cases, insufficient attention has been given to wastewater treatment in these areas. Although aeration tanks, biofilters, or settling tanks were sometimes installed, issues related to their proper operation and ongoing maintenance were often left unaddressed. Some settlements still lack sewage treatment facilities altogether, even when a centralized water supply exists but no drainage system is in place.

At present, in numerous villages and even small towns, the volume of wastewater generated and the limited financial resources available for the operation of treatment facilities, such as funding for technical staff, electricity costs, and routine maintenance, have significantly decreased. As a result, most treatment facilities in such communities are either non-functional or used merely as reservoirs for wastewater storage before uncontrolled discharge into the environment.

This situation with water purification arises from two challenges: First, the unsuitability of existing (conventional) treatment technologies for small-scale applications, and second, the high cost of operating such systems. For example, aeration tanks, commonly used as treatment plants, require constant artificial support to maintain biodegradation processes. This includes aeration, the addition of microorganisms, electricity consumption, regular monitoring, and skilled maintenance. In addition, the operation of aeration tanks is affected by fluctuations in the flow rate and chemical composition of the water supplied for treatment. The maintenance of such structures is manageable for large cities with significant volumes of wastewater. However, in villages, wastewater volumes are typically low, and there are often no funds allocated for the operation of treatment facilities.

Typically, in small settlements, the consumption of wastewater ranges from 15 to 30 m3/day (in villages, the water supply usually serves several two- or three-story buildings, a school, or a hospital). In such conditions, the most promising solution is the creation of autonomous sewerage systems in the villages. However, establishing a closed drainage cycle requires an effective method for treating small volumes of wastewater. Among the various treatment options available for small volumes of wastewater, the market offers different types of bioprocessors. These systems are generally expensive to construct and operate, requiring the installation of prefabricated units, ongoing maintenance, and continuous servicing by the manufacturer. Unfortunately, the use of BTP is not always appropriate due to a number of limiting factors, such as terrain features, availability of free space, and other site-specific constraints. BTP is cost-effective primarily when wetlands are available or when they can use existing infrastructure from previous treatment facilities.

Recently, as an alternative to sewage treatment plants in settlements with small amounts of wastewater, the installation of autonomous sewage treatment plants

employing phytotechnologies for individual houses and residential areas has become increasingly widespread. These modern small-scale treatment plants include components such as sand and gravel filters, filtration fields, and, where necessary, AGRS. They are adapted to provide complete wastewater treatment of small volumes of wastewater in the absence of centralized sewerage networks.

The following treatment facilities typically consist of three units (Figure 3): The first is a two-section septic tank (zone A); the second includes sludge wells (zone B); and the third is the core biological treatment unit – underground filter trenches (zone C). The number and length of these trenches are calculated based on the volume and quality of wastewater, topography, and soil properties. If needed, the facility may also include a phytotechnology unit.

At present, there are several options for such treatment plants, which differ in the design of filter trenches. Grytsenko *et al*.[26] proposed the use of filter trenches for surface wastewater treatment, with the filter layer made of basalt crumb, where pollutants are adsorbed. The treated wastewater is then filtered through a sand layer into the lower strata. This application is particularly suitable for areas where the water supply depends on underground storage and where the groundwater level is critically high. In another study,[27] the method of surface wastewater treatment was further improved by utilizing PET granules and polyurethane foam granules as the filter layer. The application of PET waste packaging for treating stormwater and meltwater not only helps to reduce the anthropogenic influence on the environment but also increases the utilization of plastic waste.

To treat wastewater from small settlements or individual houses, we propose the use of drainage tunnels incorporating secondary materials (used car tires, basalt crumbs, gravel, etc.).

A large number of used tires are generated annually at enterprises across the country, providing an opportunity for their reuse, particularly as a building material for strengthening drainage canals and constructing facilities of this type.

Modern tires are complex structures composed of layers reinforced with metal or textile cords and tread. Only high-quality and environmentally friendly rubber compounds are used for the production of car tires, including natural rubber, synthetic rubber, carbon black, and lubricant. Rubber compounds make up over 80% of the total weight of a tire, while the remaining 20% consists of various reinforcing materials.

Toxicity tests of tires in wet soil were performed in the laboratory. The data obtained showed that tire samples containing rubber materials and metal cords were not toxic to microorganisms. Tire waste is classified as hazard class IV, that is, non-toxic, which supports its further secondary use in underground filter trenches.

3. Results and discussion

This experiment on wastewater treatment using phytoremediation facilities with filtering media (based on used automobile tires and construction materials) demonstrated high efficiency in removing various pollutants. Specifically, after 6 months of research, the treatment efficiency was as follows: total iron removal – 99% (the best result among hydrochemical indicators); suspended solids, COD, nitrates, and nitrites – 70% removal efficiency; other parameters showed varying degrees of treatment, ranging from 50% to 99%, with an overall disinfection efficiency of 99% (Table 2).

These results confirm the effectiveness of the proposed method, particularly in the removal of organic pollutants, biogenic substances, and toxic components.

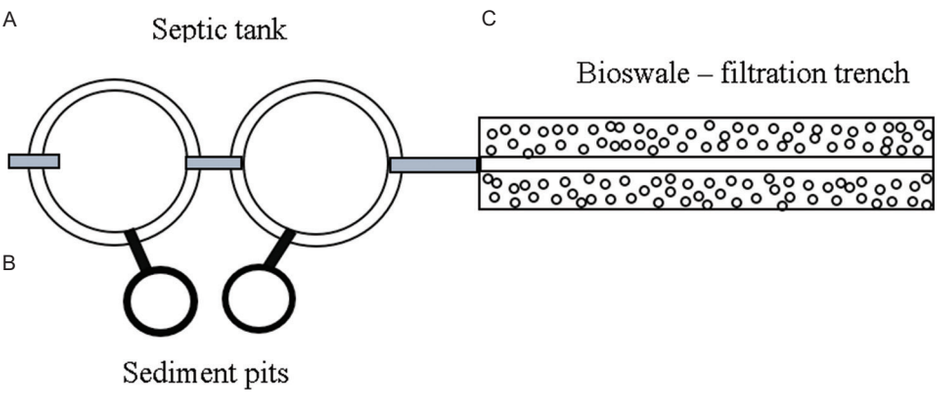

Figure 3. (A-C) Schematic of an autonomous treatment plant for individual houses and residential areas

Table 2. Efficiency of wastewater treatment by phytoremediation using used car tires

Ingredient name	Before treatment	After treatment	Treatment efficiency, %
Suspended substances, mg/dm^3	150	45	70
pH	8	Not determined	-
COD, mg O_2/dm^3	156	50	70
BOD_5, mg O_2/dm^3	70	50	28.5
Ammonium nitrogen, mg/dm^3	30	18	40
Nitrite, mg/dm^3	0.06	0.02	67
Nitrates, mg/dm^3	33.6	10	70.2
Chlorides, mg/dm^3	226.2	181	20
Sulfates, mg/dm^3	150	115	23
Iron, mg/dm^3	1.8	0,16	99
Surfactants, mg/dm^3	2.5	1,8	28
Total microbial amount, CFU/mL	8.8×10^5	1.0×10^3	99

Abbreviations: Abbreviations: BOD_5: Biological oxygen demand; CFU: Colony-forming units; COD: Chemical oxygen demand; O_2: Oxygen.

The efficiency of wastewater treatment is presented in Table 2.

It is important to highlight the role of filtering nozzles (2 – 10 mm) made from recycled automobile tires, which proved effective in the mechanical treatment of capturing suspended particles and adsorbing organic compounds. Rubber granules derived from tires possess a high adsorption capacity due to their porous structure, enabling them to efficiently retain petroleum products and heavy metals. Moreover, the use of construction materials (such as gravel or sand) in combination with rubber granules provided an additional filtration effect, further improving overall treatment quality.

Phytoremediation, with the usage of aquatic plants – common reed (*P. australis* [Cav.] Trin ex Stend.), narrow-leaf cattail (*T. angustifolia* L.), broadleaf cattail (*T. latifolia* L.), lake bulrush (*S. lacustris* L.), and other species – has proved their effectiveness with the removal of biogenic substances (nitrogen compounds) and organic pollutants. The plants actively absorbed nutrients from the water, while their root systems created favorable conditions for microorganism growth, facilitating the decomposition of organic compounds.

A remarkable result was the disinfection rate of 99%, demonstrating the combined effectiveness of filtration and biological plant activity in reducing the concentration of pathogenic microorganisms. However, it should be noted that treatment efficiency for certain components – such as ammonium nitrogen (40%), chloride ions (20%), sulfates (23%), and surfactants (28%) – remained relatively low. This may be attributed to the limited sorption capacity of the materials used in the filtering nozzles, as well as the high initial concentration of these substances in the incoming wastewater. To improve these results, the addition of supplementary sorbents, such as activated carbon or specialized mineral additives, could be considered.

The experiment also confirmed that the combination of phytoremediation and filtering media is a cost-effective and environmentally friendly technology. The use of waste automobile tires not only helps address the issue of waste disposal but also enables resource reuse, aligning with the principles of sustainable development. Moreover, this method can be easily adapted for local treatment facilities in small communities or industrial sites where access to large-scale treatment systems is limited. Overall, the experimental results demonstrate that the combined use of phytoremediation and filtering nozzles is a promising approach in the field of wastewater treatment.

It is worth mentioning that the implementation of autonomous treatment plants with elements of phytotechnology for small settlements is gaining popularity.

The introduction of autonomous treatment facilities, such as filter trenches, offers several advantages:

(i) No odors
(ii) No large land areas need to be allocated
(iii) No large sanitary protection zones are required
(iv) The possibility of creating separate treatment sections for individual buildings
(v) Independence from fluctuations in the volume and quality of wastewater.

For small cities, villages, or individual houses, a combination of several structures was used, each performing a specific function and contributing to improved water purification efficiency.

As the project did not include buildings, heating systems, water supply infrastructure, electrical equipment, or accommodation for service and laboratory staff, the overall development cost was lower compared to traditional treatment facilities with similar initial characteristics.

Such systems are specifically advantageous when sewage treatment plants are needed for individual users in rural areas or when the facility operates only seasonally, such as during the holiday period. During temporary surges in wastewater volume, additional phytotechnology treatment blocks can be employed to handle the overflow. In essence, such structures can be adapted to different living conditions and scenarios involving small volumes of wastewater. Facilities such as children's camps, sanatoriums, holiday homes, and recreational centers, which typically operate for up to 6 months a year, can effectively address their wastewater treatment needs using such phytotechnology-based systems.

4. Conclusion

Tire recycling is a critically important process for protecting both the environment and human health. The decomposition of tires takes about 100 years, as they are almost non-biodegradable.

The environmental and social harm caused by tire disposal in landfills, including the usage of large areas for unorganized (unauthorized) dumping and the risk of air pollution, highlights the urgent need for sustainable methods of reusing waste tires.

An analysis of the current waste management system in Ukraine has revealed significant shortcomings. Therefore, the use of waste car tires as a filter layer in wastewater treatment systems can simultaneously enhance the efficiency of industrial waste disposal and contribute to the protection of water bodies from contaminants.

The wastewater treatment efficiency of phytoremediation models with the filtering nozzles (made from used automobile tires and construction materials) was as follows: 40% for ammonium; 70% for nitrates, nitrites, COD, and suspended solids; 28.5% for BOD_5; 20% for chlorides; 23% for sulfates; 99% for total iron; 28% for surfactants, and 99% for overall disinfection. These results confirm the effectiveness of using this type of filtering media in wastewater treatment applications.

The economic benefits of the proposed method include several key factors: The simplicity of phytoremediation systems, the absence of complex engineering devices for controlling water levels or flow, the elimination of chemical or reagent use, and a reduced need for highly qualified personnel.

The environmental benefits are equally significant. Such systems can replicate natural riverine areas, using aquatic plants commonly found in floodplains. The development or expansion of such areas can intercept and treat wastewater before it enters rivers, without disrupting the natural conditions of the region. This approach effectively removes suspended solids, organic matter (including petroleum products), and pathogenic microorganisms, while also reducing overall water mineralization.

Acknowledgments

None.

Funding

None.

Conflict of interest

The authors declare no conflicts of interest.

Author contributions

Conceptualization: Liudmyla Melnik, Olha Rybalova
Formal analysis: Liudmyla Melnik, Olha Rybalova
Investigation: Liudmyla Melnik, Olena Bryhada, Bohdan Tsymbal
Methodology: Olena Bryhada, Oleksii Ilinskyi, Bohdan Tsymbal
Writing – original draft: Olha Rybalova, Anton Matsak
Writing – review & editing: Olha Rybalova, Anton Matsak

Availability of data

Data are openly available in a public repository that issues datasets with and without DOIs.

References

1. Szczucka-Lasota B, Węgrzyn T, Łazarz B, Kamińska JA. Tire pressure remote monitoring system reducing the

rubber waste. *Transp Res Part D Transp Environ.* 2021;98:102987.
doi: 10.1016/j.trd.2021.102987

2. Klimishnina M. State and prospects of development of tire recycling technologies and their environmental impact. *Technol Audit Prod Res*. 2016;6(2(32)): 57-63.
doi: 10.15587/2312-8372.2016.86810
3. Khudyakova T, Shmidt A, Shmidt S. Sustainable development of smart cities in the context of the implementation of the tire recycling program. *J Entrep Sustain Issues*. 2020;8(2):698-715.
doi: 10.9770/jesi.2020.8.2(42)
4. Rybalova O, Artemiev S, Sarapina M, *et al*. Development of methods for estimating the environmental risk of degradation of the surface water state. *Eastern-Europ J Enterprise Technol*. 2018;2:4-17.
doi: 10.15587/1729-4061.2018.127829
5. Loboichenko VM, Vasyukov AE, Tishakova TS. Investigations of mineralization of water bodies on the example of river waters of ukraine. *Asian J Water Environ Pollut*. 2017;14:37-41.
doi: 10.3233/AJW-170035
6. Vasenko A, Rybalova O, Kozlovskaya O. A study of significant factors affecting the quality of water in the oskil river (Ukraine). *Eastern-Europ J Enterprise Technol*. 2016;3:48-55.
doi: 10.15587/1729-4061.2016.72415
7. Torosian L, Chernyaev I. Method of creating control framework for environmental safety of car tires. *Transp Res Procedia*. 2020;50:689-697.
doi: 10.1016/j.trpro.2020.10.081
8. Shaker A, Mohammed F. Benefits and challenges of waste recycling, a field study in al-diwaniyah governorate. *Al-Qadisiyah J Agric Sci*. 2021;11(2):85-108.
doi: 10.33794/qjas.2021.170228
9. Dębska B, Lichołai L, Miąsik P. Assessment of the applicability of sustainable epoxy composites containing waste rubber aggregates in buildings. *Buildings*. 2019;9(2):31.
doi: 10.3390/buildings9020031
10. Plewa A. Use of crumb rubber from used car tires in mineral asphalt mixes. *Inż Ekol.* 2014;40:217-227.
doi: 10.12912/2081139X.84
11. Chen B, Zheng D, Xu R, *et al*. Disposal methods for used passenger car tires: One of the fastest growing solid wastes in China. *Green Energy Environ*. 2021;7:1298-1309.
doi: 10.1016/j.gee.2021.02.003
12. Shahi A, Dwivedi C, Manjare S. Experimental and theoretical investigation on pyrolysis of various sections of the waste tire and its components. *Chem Eng Res Design.* 2022;179:66-76.
doi: 10.1016/j.cherd.2021.12.022
13. Kuznetsov GV, Syrodoy SV, Purin MV, Zenkov AV, Gvozdyakov DV, Larionov KB. Justification of the possibility of car tires recycling as part of coal-water composites. *J Environ Chem Eng*. 2020;9(1):104741.
doi: 10.1016/j.jece.2020.104741
14. Vambol S, Vambol V, Kondratenko O, Koloskov V, Suchikova Y. Substantiation of expedience of application of high-temperature utilization of used tires for liquefied methane production. *J Achiev Mater Manuf Eng*. 2018;87:77-84.
doi: 10.5604/01.3001.0012.2830
15. Nie SQ, Chen MQ, Li QH. Evaluation on hydrothermal gasification of waste tires based on chemical equilibrium analysis. *Int J Hydrogen Energy*. 2021;47(3):1435-1448.
doi: 10.1016/j.ijhydene.2021.10.233
16. Subatkevičienė K, Tetsman I, Gargasas J. Research of wastewater treatment with sorbents. *Sci Future Lithuania*. 2019;11:1-6.
doi: 10.3846/mla.2019.7086
17. Sivaraman S, Anbuselvan NM, Venkatachalam P, Shanmugam SR, Selvasembian R. Waste tire particles as efficient materials towards hexavalent chromium removal: Characterisation, adsorption behaviour, equilibrium, and kinetic modelling. *Chemosphere.* 2022;295:133797.
doi: 10.1016/j.chemosphere.2022.133797
18. Rybalova O, Bryhada O, Ilinskyi O, Bondarenko O, Zolotarova S. Phytoremediation methods for wastewater treatment. *Dan Sci J.* 2020;41:10-13.
19. Hu H, Li X, Wu S, Yang C. Sustainable livestock wastewater treatment via phytoremediation: Current status and future perspectives. *Bioresour Technol*. 2020;315:123809.
doi: 10.1016/j.biortech.2020.123809
20. Wei W, Tong J, Hu BX. Study on ecological dynamic model for phytoremediation of farmland drainage water. *J Hydrol*. 2019;578:124026.
doi: 10.1016/j.jhydrol.2019.124026
21. Mahmedov VH, Zakharchenko MA. Manual for the use of water bioengineering methods for the treatment of non-mineralized contaminated waters of the agricultural sector of Ukraine. 1993; 20-24.
22. Matsak A, Tsytlishvili K, Rybalova O, Artemiev S, Romin A, Chynchyk O. Method of agricultural sewage water purification at troughs and a biosorption bioreactor. *Eastern Europ J Enterp Technol.* 2018;5(10(95)):15-24.
doi: 10.15587/1729-4061.2018.144138
23. Zakharchenko MA, Ryzhykova IA. *Perekhoplennia ta Ochyshchennia Poverkhnevoho Stoku za dopomohoiu Sporud Fitoremediatsii. In: V Mizhnarodna Naukovo-Praktychna Konferentsiia Ekolohichna bezpeka: Problemy i Shliakhy Vyrishennia: Zb. nauk. st. U 2-kh t.* Vol. 2; 2008. p. 298-303.
24. Akansha J, Nidheesh PV, Gopinath A, Anupama KV, Kumar MS. Treatment of dairy industry wastewater by combined aerated electrocoagulation and phytoremediation process. *Chemosphere*. 2020;

253:126652.
doi: 10.1016/j.chemosphere.2020.126652

25. Ilinskyi OV, Rybalova OV, Bryhada OV, Bondarenko OO, Artem'Iev SR. The green plant model use for the evaluation of effectiveness of phytoremediation methods in surface wastewater treatment. *Techno-ecological safety*. 2021;36-43.
doi: 10.52363/2522-1892.2021.1.6
26. Grytsenko A, Rybalova O, Matsak A, Artemiev S. Using of production wastes in stormwater drainage purification. *Mater Sci Forum.* 2020;1006:194-201.
doi: 10.4028/www.scientific.net/MSF.1006.194
27. Grytsenko A, Matsak A, Rybalova O, Bryhada O, Dadashov I. Use of PET granules for improving a surface runoff treatment. problems of emergency situations. Materials Technologies. *Mater Sci Forum.* 2021;1038:242-251.
doi: 10.4028/www.scientific.net/MSF.1038.242

ACCSCIENCE PUBLISHING

Our Journals

Organoid Research (OR) is an international, peer-reviewed journal dedicated to advancing the field of organoid science by publishing high-quality research articles, reviews, and perspectives. The journal focuses on studies that provide significant conceptual, experimental, and translational advances in the development and application of organoid technologies.

OR welcomes submissions spanning diverse areas of organoid science, including but not limited to stem cell biology, tissue engineering, regenerative medicine, disease modeling, and drug discovery. The journal encourages papers that explore bioengineered organoids, organoid-based systems biology, and the integration of organoids with clinical research. Special emphasis is placed on contributions that advance novel approaches to organoid development, including the use of cutting-edge bioengineering techniques, materiobiology, and integrative technologies such as artificial intelligence, high-throughput screening, and precision medicine. Additionally, the journal values research that delves into ethical considerations and challenges related to the clinical translation of organoid systems.

Advanced Neurology is a peer-reviewed and open-access journal that aims to publish and disseminate novel research in the breadth of neurology and neuroscience. The journal aims to advance our understanding in the nervous system and provide a platform to neuroscientists and physicians to showcase their findings in original fundamental and clinical research as well as to present new ideas that highlight the changes in the neurological clinical practice.

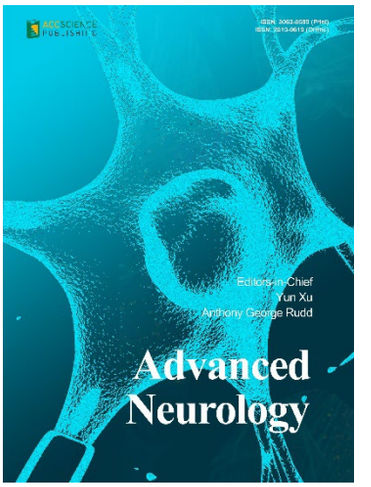

Advanced Neurology covers subject areas, including but not limited to the following:

- Neurological disorders
- Neurodegenerative disease
- Cerebrovascular disease
- Epilepsy and movement disorders
- Neuroimmune disease
- Neurological infections
- Muscle disease
- Molecular and cellular neuroscience
- Systems neuroscience
- Cognitive neuroscience
- Computational modeling of nervous system

Start a new journal

Write to us via email if you are interested to start a new journal with AccScience Publishing. Please attach your CV, professional profile page and a brief pitch proposal in your email. We shall inform you of our decision whether we are interested to collaborate in starting a new journal.

Contact: info@accscience.com

https://accscience.com/journal/AJWEP

ACCSCIENCE PUBLISHING

Contact
www.accscience.com
8 Burn Road, #15-03 Trivex, Singapore 369977
Email: editorial@accscience.com
Phone: +65 8182 1586